THE INFLUENCE OF SALTMARSH VEGETATION CANOPIES ON HYDRODYNAMICS IN THE INTERTIDAL ZONE

Rami Malki

A thesis submitted to Cardiff University in accordance with the requirements for the degree of Doctorate of Philosophy in the Division of Civil Engineering, Cardiff School of Engineering, Cardiff University.

October 2009

ProQuest LLC
789 East Eisenhower Parkway
P.O. Box 1346
Ann Arbor, MI 48106-1346

[*This page has been intentionally left blank*]

Abstract

Recent estimates of global sea level rise indicate mean values around 3.1 mm yr^{-1}. As a result, many coastlines face an increasing risk of coastal erosion, and the threat of flooding is becoming a major concern. Unfortunately, coastal defences can be very costly; with recent estimates as high as £5000 per metre length of seawall in the UK. There is a need to consider more economically feasible options, and by accounting for the ability of saltmarshes to absorb wave energy, reduce flow velocities and stabilise sediments, the costs of coastal defence structures may be significantly reduced. But first, an improved understanding of the implications of saltmarsh vegetation on hydrodynamics is fundamental to their inclusion in the design of coastal protection schemes. This includes the influence of saltmarsh vegetation on velocity and turbulence structures and the drag forces that arise due to the obstruction to the flow created by the vegetation.

Two contrasting areas of coastal saltmarsh were selected for the location of a field survey to identify typical field conditions, such as bed gradients, submergence levels, vegetation types and densities. The two sites differ in that the first was non-grazed, while the second was heavily grazed to assess the impact of sheep farming on vegetation characteristics. The vegetation species, stem densities and submergence levels observed during the field survey were used as a guideline for designing a series of laboratory experiments to investigate the impact of saltmarsh vegetation on hydrodynamics.

Uniform cylinder models are widely used to simulate vegetation canopies in hydrodynamic studies, yet the cylinder model can lead to an oversimplification of vegetation morphology. A comparison was made by conducting experiments under uniform flow conditions where uniform cylinder arrays and vegetation canopies were installed onto a flume bed at stem densities of 800, 1160 and 1850 stems m^{-2}. There were differences in velocity and turbulence structures through the two types of canopy. For the same stem density, the proportion of the total flow passing through the canopy region was approximately 10% greater for the uniform cylinder arrays. The foliage found in the upper part of vegetation canopies resulted in a considerably higher level of obstruction and contributed towards reducing velocities and Reynolds stresses within the canopy. Reynolds stress penetration depths were up to 15 times greater for the uniform cylinder arrays compared to the vegetation canopies.

Computational fluid dynamics models can be a useful tool for predicting the impact of saltmarsh vegetation on hydrodynamics for coastal management. Applying such models to vegetated flows requires knowledge of the drag coefficient to determine the drag term in the Navier-Stokes equations. However, in the absence of measured data, such models are often applied with the assumption that the drag coefficient is constant in value, and commonly used values include '1.0' and '1.2'. Such assumptions may be easily linked to the uniform cylinder model. However, drag coefficients calculated for Common Cordgrass ranged between 0.4 and 1.7. Values were dependent on numerous parameters, including the Reynolds number, the submergence level, the stem density and the maturity of the vegetation.

Instead of the traditional drag-force approach for determining canopy hydrodynamics, a method for predicting velocity and turbulence structures based on the projected area of the vegetation was proposed. For the emergent canopy, the mean velocity was estimated by relating to a reference canopy of known projected area and

mean velocity. For the submerged canopy, the surface flow layer velocity was determined effectively using the Manning's roughness approach and the depth-averaged canopy velocity was a function of the surface layer velocity and the canopy density. Velocity profile shapes for both canopies were obtained by linking the mean canopy velocity to the projected area profile. Reynolds stresses for the emergent canopy and lower part of the submerged canopy were negligible and a function of depth-averaged canopy velocity. For the upper part of a submerged canopy, Reynolds stresses were a function of the depth-averaged surface layer and canopy velocities. The proportion of the submerged canopy region experiencing higher Reynolds stresses is also a function of the vegetation density.

Declaration

This work has not previously been accepted in substance for any degree and is not concurrently submitted in candidature for any degree.

Signed: 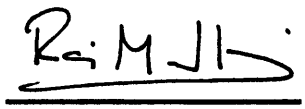

Date: 25 / 10 / 2009

This thesis is being submitted in partial fulfillment of the requirements for the degree of Doctorate of Philosophy (PhD).

Signed: 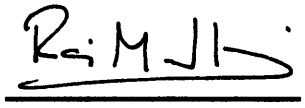

Date: 25 / 10 / 2009

This thesis is the result of my own independent work and investigation, except where otherwise stated. Other sources are acknowledged by explicit references.

Signed: 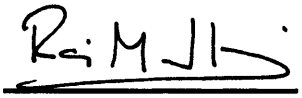

Date: 25 / 10 / 2009

I hereby give consent for my thesis, if accepted, to be available for photocopying and for inter-library loan, and for the title and summary to be made available to outside organizations.

Signed: 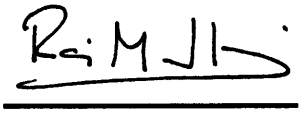

Date: 25 / 10 / 2009

[*This page has been intentionally left blank*]

Acknowledgements

Firstly, completion of this thesis would not have been possible without my first supervisor, Dr. Catherine A.M.E. Wilson. I will be eternally grateful for the patience she has shown me, for backing me up every time I landed myself into trouble and for always making the time for me, even during her maternity leave. I would also like to thank my second supervisor, Dr. Ann Edington, for all her moral support during the most stressful times, and for her useful ideas and advice, particularly with aspects related to the fieldwork and to the biological aspects of the study.

I owe a lot of gratitude to the majority of the technicians at the engineering laboratories who I have troubled at one point or another for various tasks. I would particularly like to thank Mr. Paul Leach and Mr. Lenny Czekaj who have been a great help and were very creative in proposing solutions around difficult practical problems. My thanks also go out to Mr. Brian L. Hooper, Mr. Harry Lane, Mr. Mal Lyall and Mr. Des Sanford. Thanks to Mr. Brian Hargreaves and Mr. Syd Swarbrick for their efficient IT support, to Mr. Owen John from Stores, and to Ms. Kate Osbaldeston, Ms. Julie Cleaver, Mrs. Sheila Stockman, Ms. Rachel Parrot and Ms. Lindsay Ash from the Research Office, and also to Mrs. Chris Lee who has looked after me for most of the eight years I spent at the Cardiff School of Engineering.

I also thank Mr. Phil Hourahine for his patience, particularly for allowing me use of the school vehicle to conduct my field work, especially after getting it stuck on a saltmarsh on the day of the largest high tide of the year. On that note, I would also like to thank Ronin the local farmer for rescuing me by towing the car off the Llanrhidian saltmarsh with his tractor so late in the afternoon.

I am very grateful to all the undergraduate and MSc students who helped with various aspects of the lab work, field work and data analysis as part of their project work. By doing so, they made my life so much easier. Thanks to Wei Chung, Andrew Moverley, Iolo G. Ellis, Poorav Chheda, Toby Bedford and Richard J. Philips, and to my colleagues Timothy Sparks, Patricia Xavier and Laura Trodden.

I also thank Prof. Roger Falconer for his cooperation with the laboratory arrangements, and for his guidance with respect to setting up a numerical model for my study sites, even though this was this was not used in the current thesis.

My thanks also go to Dr Alison Matthews from the Environment Agency for provision of LiDAR data for my study sites, Mr. David Painter from the Countryside Council for Wales for provision of the "West Glamorgan and Llanelli Salt Marsh Survey of Great Britain", and Mr. Nigel Williams from the Wildfowl and Wetlands Trust National Wetland Centre Wales for his cooperation and advice for conducting the field work, and for allowing vehicle access to transport field equipment.

Last but not least, I would like to thank my brother, Refaat Malki, for proof reading this thesis, mum and dad, who mean the world to me, for their continuing patience, love and support over the years, and for always being there for me.

[*This page has been intentionally left blank*]

In memory of Margaret, Sharif & Ayman

[*This page has been intentionally left blank*]

Contents

3 Field Monitoring Programme

4 Vegetation Quantification

5 Laboratory Investigations: Setup and Methodology

6 Laboratory Investigation I: Simulating Vegetation

7 Laboratory Investigation II: *Spartina anglica* Canopies

8 Velocity and Turbulence Prediction Methods

Nomenclature

The following symbols are used in this thesis:

a	=	projected area of obstruction per unit volume (m^{-1})
$\overline{a}$	=	depth-averaged projected area of obstruction per unit volume of a canopy (m^{-1})
$\overline{a}_1, \overline{a}_2$	=	depth-averaged projected area of obstruction per unit volume of 'Canopy 1' and 'Canopy 2' (m^{-1})
a'	=	projected area of obstruction per unit volume based on projected area visible in a photograph of a canopy cross-section (m^2)
$\hat{a}$	=	projected area of obstruction per unit volume at a reference elevation (m^{-1})
a_F	=	projected area of obstruction per unit volume of the leaf portion of the canopy (m^{-1})
a_S	=	projected area of obstruction per unit volume of the stem portion of the canopy (m^{-1})
A	=	flow area (streamwise cross-section) (m^2)
A_C	=	projected area per unit width of canopy (m)
A_i	=	total area of horizontal layer i (m^2)
A_p	=	projected area of obstruction (m^2)
A_{pi}	=	projected area of obstruction in horizontal layer i (m^2)
A_p'	=	visible projected area of obstruction (m^2)
$\hat{A}_p$	=	hidden projected area of obstruction (m^2)
B	=	flume width (m)
C	=	Chezy resistance factor (-)
C_D	=	drag coefficient (-)
$\overline{C_D}$	=	bulk one dimensional drag coefficient for a vegetation canopy or array of cylinders (-)
$\overline{C_{D1}}, \overline{C_{D2}}$	=	bulk one dimensional drag coefficient for 'Canopy 1' and 'Canopy 2' (-)
$\overline{C_D}'$	=	bulk one dimensional roughness coefficient for a vegetation canopy of an array of cylinders (m^{-1})

$\hat{C}_D$	=	bulk two dimensional drag coefficient for a vegetation canopy or an array of cylinders at a reference elevation (-)
$\overline{C_{D\,2D}}$	=	bulk two dimensional drag coefficient for a vegetation canopy or an array of cylinders (-)
d	=	stem or cylinder diameter (mm)
d_0	=	basal stem diameter (mm)
d_{100}	=	the stem diameter at a distance of 100 mm of the base of a plant stem (mm)
D	=	flow depth (m)
D_1	=	flow depth for 'Canopy 1' (m)
D_{ACD}	=	tidal flow depth Above Chart Datum (m)
D_{AOD}	=	tidal flow depth Above Ordinance Datum (m)
D_{max}	=	the flow depth at the time of a high tide event Above Ordinance Datum (m)
D_{MU}	=	the flow depth at the time of a high tide event at Mumbles Above Ordinance Datum (m)
D_{max}	=	the flow depth at the time of a high tide event at Swansea Above Ordinance Datum (m)
E	=	Young's Modulus of Elasticity (MPa)
f	=	Darcy-Weisbach friction factor (-)
f	=	frequency (Hz)
F	=	load (N)
$F_{5\,mm}$	=	load required to cause a 5.0 mm deformation (kg m s^{-2})
F_D	=	drag force (kg m s^{-2})
F_D'	=	drag force per unit volume (kg m^{-2} s^{-2})
F_{fail}	=	force required to cause material failure (kg m s^{-2})
F_G	=	fluid body weight component acting along the longitudinal plane (N)
F_S	=	shear force (N)
Fr	=	Froude number (-)
g	=	gravitational acceleration (ms^{-2})
G	=	Lateral gradient in longitudinal velocity (s^{-1})
G_S	=	surface-flow layer fluid body weight component acting along the longitudinal plane (N)

h_1, h_2	=	The depth of flow during the two high tides during a single tidal cycle Above Chart Datum [ACD] (m)
h_S	=	depth of the surface-flow layer (m)
h_{pen}	=	turbulent shear stress penetration depth (m)
H	=	submergence level, the ratio of water depth to vegetation canopy height (-)
H_{90}	=	90th percentile canopy height based on the projected area of the vegetation (m)
H_{99}	=	99th percentile canopy height based on the projected area of the vegetation (m)
H_i	=	submergence level of a class (-)
H_T	=	submergence hours, (submergence × time) (hrs)
i	=	index (-)
k	=	canopy height Reynolds number exponent (-)
k_s	=	equivalent sand roughness (m)
K	=	dimensionless shear parameter indicative of the magnitude of shear in the flow (-)
l	=	length of stem segment (m)
l	=	turbulent length scale (m)
L	=	length of channel reach (m)
m	=	gradient of a line or curve e.g. $y = mx + c$ (-)
m	=	moisture content (%)
M	=	stem density (m^{-2})
M_{DRY}	=	dry mass of vegetation per unit bed area (kg m^{-2})
$M_{DRY(BASE)}$	=	dry mass of vegetation per unit bed area at the base (kg m^{-2})
M_{WET}	=	mass of vegetation per unit bed area (kg m^{-2})
$M_{WET(BASE)}$	=	mass of vegetation per unit bed area at the base (kg m^{-2})
MKE	=	mean kinetic energy per unit mass (m^{2}s^{-2})
n	=	number of horizontal sections in a canopy cross section (-)
n	=	Manning's coefficient for bed roughness (m$^{-1/3}$s)
n_S	=	Manning's coefficient specific to the surface flow (m$^{-1/3}$s)
O_p	=	relative vegetation obstruction (-)
p	=	porosity (-)

P	=	pressure (kg $m^{-1}s^{-2}$)
P_b	=	buoyant production (kg m^2s^{-3})
P_s	=	shear production (kg m^2s^{-3})
P_w	=	wake production (kg m^2s^{-3})
Q	=	flow rate (m^3s^{-1} *unless specified otherwise*)
$Q_{measured}$	=	measured flow rate (ls^{-1})
$Q_{flow\ meter}$	=	flow rate according to the flow meter reading (ls^{-1})
r	=	stem radius (m)
R	=	hydraulic radius (m)
R^2	=	goodness of fit (-)
Re	=	Reynolds number (-)
Re_d	=	stem Reynolds number (-)
Re_T	=	canopy height Reynolds number (-)
s	=	stem spacing (mm)
S_0	=	bed gradient (-)
S_1, S_2	=	bed gradient for 'Canopy 1' and 'Canopy 2' (-)
Str	=	Strouhal number (-)
t	=	time (s *unless specified otherwise*)
t_i	=	time for a class identified by i (hrs)
t'	=	the duration between first inundation and maximum flow depth during high tide (s)
t_{HT}	=	time of high tide (s)
T	=	canopy height (m)
TKE	=	turbulent kinetic energy per unit mass (m^2s^{-2})
U	=	depth-averaged longitudinal velocity (m s^{-1})
U_1	=	longitudinal velocity through the constricted area of a staggered array (ms^{-1})
U_2	=	longitudinal velocity through the non-constricted area of a staggered array (ms^{-1})
U_C	=	maximum velocity through a cylinder array (ms^{-1})
U_S	=	average velocity through the surface-flow layer (ms^{-1})
u, v, w	=	longitudinal, lateral and vertical instantaneous velocity components (ms^{-1})

$\overline{u}$, $\overline{v}$, $\overline{w}$	=	time-averaged longitudinal, lateral and vertical velocity components (ms^{-1})
u', v', w'	=	turbulent fluctuations in the time-averaged longitudinal, lateral and vertical velocity components (ms^{-1})
$\langle\overline{u}\rangle$, $\langle\overline{v}\rangle$, $\langle\overline{w}\rangle$	=	double-averaged (in space and time) longitudinal, lateral and vertical velocity components (ms^{-1})
$\widetilde{u}$, $\widetilde{v}$, $\widetilde{w}$	=	spatial fluctuations in the double-averaged longitudinal, lateral and vertical velocity components ($m\ s^{-1}$)
$-\rho u'w'_C$	=	depth-averaged Reynolds stress in the canopy ($kg\ m^{-1}s^{-2}$)
$-u'w'_{max}$	=	peak Reynolds stress for a submerged canopy (m^2s^{-2})
$\hat{u}$	=	longitudinal velocity at a reference elevation (ms^{-1})
u_*	=	shear velocity (ms^{-1})
V	=	volume of vegetation (m^3)
x, y, z	=	distances along the longitudinal, lateral and vertical axes (m)
z_0	=	bed elevation (m)
$z_{0.1}$	=	distance from the bed to the elevation where the Reynolds stress is 10% of τ_{max} (m)
z''	=	deflected vegetation height (m)
$z_{m.p.}$	=	distance from the base of a stem to the midpoint of a given segment of the stem (m)
α	=	slope exponent (-)
β	=	flow depth exponent (-)
β_C	=	canopy depth correction factor (-)
ε	=	error (-)
ε	=	strain (-)
η_1, η_2	=	the water surface level above a datum for locations 1 and 2 (m)
$\partial\eta$	=	water surface height difference (m)
κ	=	von Karman constant (-)
λ	=	proportion of projected area of vegetation to total flow area per unit length (m^{-1})
λ_x	=	wavelength (m)
μ	=	dynamic viscosity ($N\ sm^{-2}$)
ν	=	kinematic viscosity ($m^2\ s^{-1}$)
ξ	=	uniformity of projected area coefficient (-)

ρ = fluid density (kg m^{-3})

σ = stress (N m^{-2})

σ_L = local variability in O_p (-)

$\bar{\sigma}_L$ = 12 month average local deviation in O_p (-)

$\tilde{\sigma}_L$ = transect average local deviation in O_p (-)

σ_S = spatial deviation in O_p (-)

σ_T = temporal deviation in O_p (-)

τ = total shear stress (kg $m^{-1}s^{-2}$)

$\bar{\tau}$ = depth-averaged total shear stress (kg $m^{-1}s^{-2}$)

τ_0 = bed shear stress (kg $m^{-1}s^{-2}$)

τ_{max} = maximum shear stress (kg $m^{-1}s^{-2}$)

τ_v = viscous shear stress (kg $m^{-1}s^{-2}$)

θ = angle formed between the bed and the horizontal (°)

ϕ = Reynolds stress profile shape coefficient (-)

[*This page has been intentionally left blank*]

1 Introduction to the Research

1.1 Context of the Current Research

Sea levels are rising due to global warming (UK Climate Impacts Programme, 2002), and the associated flooding of coastal communities is an issue of major concern. Only relatively recently has the importance of saltmarshes as a natural means of coastal defence been fully appreciated. Saltmarsh vegetation is capable of modifying water currents, dampening waves, promoting the deposition of suspended sediments in the flow, stabilising settled sediments, as well as providing an environment for numerous organisms (Shi *et al.* 1995). A recent report by the UK Environment Agency (EA, 1996) claimed that an 80m width of saltmarsh fronting a sea wall could reduce the costs of flood defences from £5000 to £400 per metre.

Vegetated flows are encountered in many environmental problems, yet the dominant processes characterising them are not fully understood. Studies conducted using natural vegetation are not as common as those that use simulated vegetation based on arrays of uniform rigid cylinders. The latter model may lead to an over simplification of the canopy morphology and hence, the complex flow structure associated with real vegetation cannot be fully reproduced. A better understanding of the velocity and turbulence structures through vegetation is fundamental for a better appreciation of the influence of riverine and marine plants on aquatic ecosystems.

Spartina anglica is one of the saltmarsh plant species investigated in this thesis. The species is found along parts of the British coastline and has been the subject of a number of studies. The effects of this particular species on the velocity of the flow through and over the canopy have been investigated by a number of researchers (Pethick *et al.*, 1990; Shi *et al.*, 1995; Shi *et al.*, 1996). The aforementioned studies were conducted using real vegetation rather than simulated vegetation (e.g. Kouwen and Unny, 1973; Nepf, 1999; Wu *et al.*, 1999 and others) and show reductions in flow velocities within the canopy. Pethick *et al.* (1990), Shi *et al.* (1995) and Shi *et al.* (1996) have identified that a better understanding of flow dynamics through saltmarsh canopies is required to formulate a cohesive sediment transport model applicable to saltmarsh environments. Although the consideration of sediment transport is beyond the scope of this study, the processes are dependent on the critical velocities or bed tractive forces required to keep sediment particles in

suspension (Yalin, 1972). Uncertainties arise when attempting to predict the effects of vegetation on flow dynamics. A drag force term was widely used for this purpose by various authors (e.g. Dunn *et al.*, 1996 and Nepf, 1999).

Saltmarshes display a complex interaction between chemical, biological, hydrological and geological processes. An in-depth study of the ecosystem requires some level of consideration to be paid to each of these areas. However, due to the nature of research relevant to the aforementioned mechanisms, each of these areas is considered as a specialist subject, and there is a tendency to differentiate rather than unite these processes (Frey and Basan, 1978).

The purpose of the research presented in this thesis is to investigate the influence of saltmarsh vegetation on velocity and turbulence structures to improve the understanding of how saltmarshes can act as a form of natural sea defence. The objectives of this thesis can be listed as follows:

1. To identify what constitutes 'typical saltmarsh conditions', including the types of species that can be encountered and the common range of bed gradients.
2. To identify what constitutes 'typical flow conditions' for typical saltmarshes, including the common ranges of flow velocities and flow depths.
3. To identify and characterise the vegetation properties that are most likely to affect velocity structure, turbulence structure and the hydraulic resistance of a saltmarsh.
4. To identify factors that may influence the vegetation properties, either spatially across a site, or seasonally over the duration of the year and to determine the extent of any such influence.
5. To investigate the influence of typical saltmarsh vegetation covers on velocity and turbulence structure.
6. To characterise the hydraulic resistance of saltmarsh canopies by linking properties of the vegetation to the resulting velocity and turbulence structures.
7. To evaluate the suitability of uniform cylinder models that are widely used to simulate natural canopies in physical laboratory and hydrodynamic numerical modelling studies.
8. To propose methods for the prediction of velocity and turbulence properties of the flow for typical saltmarsh canopies.

1.2 The Use of Saltmarshes in Coastal Management

1.2.1 Climate Change and Rising Sea Levels

Climate change can be a controversial topic of debate with experts divided over the contribution of human activities to changes in climate. For instance, it is uncertain whether a more pronounced elevation in global temperatures in recent years is attributed to short-term variability, or to longer-term trends (e.g. Intergovernmental Panel on Climate Change, 2008). Nevertheless, Hulme *et al.* (2002) reported a rise in global temperature of 0.6 °C over the course of the twentieth century, 0.4 °C of which occurred since the 1970s, and the 1990s was the warmest decade globally. As a result of rising temperatures, sea levels are also rising. This arises from two main processes; first, the rising temperatures result in the expansion of the water volume contained in the globe's oceans. Secondly, the elevated temperatures result in the melting of glaciers and icecaps as well as the Greenland and the Arctic ice sheets.

The Intergovernmental Panel on Climate Change (IPCC) reported global sea level rise estimates of 1.7 ± 0.5 mm yr^{-1} over the 20^{th} century, 1.8 ± 0.5 mm yr^{-1} between 1961 and 2003, and 3.1 ± 0.7 mm yr^{-1} between 1993 and 2003 (IPCC, 2008). This may potentially affect coastal systems in a number of ways. For example, coastal erosion is likely to occur as higher-elevation stretches of land previously not prone to tidal inundation becomes inundated regularly; it may result in more extensive coastal inundation and higher storm-surge flooding and changes to surface and groundwater quality are likely to be observed. The impacts of such changes and their severity will inevitably vary spatially and temporally due to the wide variability of coastlines. These environmental impacts will result in related socioeconomic consequences, including: the loss of property and coastal habitats; an increase in flood risk and the potential loss of life; damage to coastal protection works and other infrastructure; and an increase in disease risk, such as diarrhea and cholera (IPCC, 2001).

1.2.2 Approaches to Coastal Management

The Department for Environment, Food and Rural Affairs (DEFRA) proposes four approaches for local authorities to manage the coastlines under their jurisdiction: No active interventions, advance the line, hold the line or managed realignment (DEFRA, 2006).

"No active interventions" involve doing nothing to combat the effects of coastal erosion and allowing the profile of the coast to be modified naturally in response to wave action and rising sea levels. This is not practical where there are developments (e.g. housing or industrial) near the coast. However, from an environmental point of view, this may be the most sensible course of action as coastal evolution is very difficult and expensive to prevent or reverse.

"Advance the line" involves significant land reclamation. However, the reclaimed land will usually lie on areas that have been previously eroded and as such, will require significant protection, or at least, can be expected to follow a similar course over time. This approach is very site specific and not widely used.

"Hold the line" involves sustaining the coast at its current level by maintaining the current level of sea defence or introducing a new one. This process is very costly and requires careful assessment to determine if the benefits are significant enough to justify the ongoing maintenance of existing defences.

"Managed realignment" (or managed retreat) involves the removal of an existing sea defence and allowing the sea to flood the area behind it, and rebuild natural saltmarshes, often on areas of previously reclaimed saltmarsh. There are a number of ways to achieve this; either by removing all or part of a sea wall, or by incorporating a pipe or spillway into the existing sea wall (Edmunds and Robertson, 2005).

1.3 A Brief Overview of Saltmarshes

1.3.1 Saltmarsh Topography

Coastal saltmarshes are defined as vegetated flats colonised by halophytes (salt-tolerant plants) and occurring in the intertidal zone, and as such, experience regular tidal inundation (Allen, 2000). The vegetation cover usually varies between the lower, middle and upper saltmarshes. The upper saltmarsh is the most inland and highest in elevation. The lower saltmarsh experiences longer periods of inundation rendering the conditions more suitable to different species than would be found in the middle and upper saltmarshes, as the frequency of tidal inundation will determine the salinity and the moisture of the substrate. Thus, conditions will be more suited to different species at different elevations (Gray, 1992). Morris *et al.* (2002) showed that

there is an increase in the production of organic material in *Spartina alterniflora* production with increasing depth below mean high tide, until an optimal depth is reached below which, no vegetation can sustain life.

The greatest level of sediment deposition can be observed along the lower marsh as this region is flooded for longer periods and hence, sediment settling takes place over a longer period. Since the middle and upper marshes are submerged for shorter periods, a wider range of plant species grow in competition, and so, these regions can be more diverse in flora (e.g. Gray 1992; Boorman, 1999). The lower saltmarsh is predominantly, if not entirely, populated with halophytes (species that thrive in saline soils, widely accepted as saltmarsh vegetation types). At higher elevations, glycophytes (plants intolerant of salt), associated with inland, non-saline environments are common (Rodwell, 2000). Due to the high level of variability in tide magnitudes, durations of tidal inundation, and site topography, it is difficult to assign clear boundaries between the different levels of marshes as quite often they tend to blend into each other (Frey and Basan, 1978). Saltmarshes are often encroached with channel networks known as creeks. These can vary in size and density for different saltmarshes and tend to diminish in size with distance in the landward direction.

Below the lower saltmarsh, there often lie expansive stretches of mudflats. These provide ideal feeding sites for wildfowl and wading birds due to the mud being rich with invertebrates. These mudflats are also rich in sediment, some of which is suspended during tidal cycles and carried onto the saltmarshes. Once settled, the sediments are stablised by the vegetation and less likely to be resuspended. Through this process, saltmarshes have demonstrated an ability to gain elevation, and in the face of rising sea levels, they may be able to maintain their position within the intertidal zone (e.g. Beeftink, 1977).

1.3.2 Saltmarshes in Context

Until the 1980s, saltmarshes have been considered areas of coastal wasteland, and the land was often reclaimed for various purposes including agriculture, industrial developments, caravan sites and coastal marinas (e.g. King and Lester, 1995; Boorman, 1999). For many reasons, saltmarshes today are considered to be extremely valuable assets. Moreover, King and Lester (1995) discussed the difficulties in putting a value to coastal wetlands, since some of their functions are difficult to quantify in

terms of economic gain. Aside from their function as a sea defence, and their conservational value due to the provision of habitats for many plant and animal species, and the provision of sites for many wildfowl and wading birds each winter, saltmarshes are valuable for a number of other purposes. These include recreational use and locations for educational or research activities. Saltmarsh vegetation can also improve water quality by acting as a filter for pollutants and excess nutrients (e.g. Vernberg, 1993; Boorman, 1999 and others).

Of particular interest to the current study is the ability of coastal wetlands to function as sea defences. Their effectiveness is highlighted by the figures presented by the Environment Agency (1996) demonstrating that an 80m width of saltmarsh fronting a sea wall can reduce the cost of the wall from £ 5000 m^{-1} to £ 400 m^{-1} (Table 1-1), although the figures vary depending on the local conditions (King and Lester, 1995). The width of saltmarsh needed will depend on the level of exposure of the site, which will be influenced by the topography, and on the nature of the vegetation cover. These complex ecosystems vary in terms of species composition, creek morphology and saltmarsh edge morphology, all of which will affect the 'defensive' wave energy dissipation capabilities of a saltmarsh.

Due to the expense associated with traditional sea defences, particularly with the continuing rise in sea levels, alternative methods for coastal management, such as managed realignment, or the recreation of intertidal wetlands are becoming more economically attractive, particularly as many sea walls are near the end of their design lives (Möller *et al.*, 1996).

Table 1-1 Effectiveness of saltings in coastal defence (taken from Environment Agency, 1996)

Width of saltings (m)	Height of crest wall (m)	Cost per metre of seawall (£)
0	12	5000
6	6	1500
30	5	800
60	4	500
80	3	400

1.3.3 The Variability of Saltmarsh Vegetation

Numerous studies have been conducted on the influence of uniform cylinders on the hydrodynamics of canopy flow for a uniform array (e.g. Li and Shen, 1973; Nepf *et al.*, 1997a; Nepf *et al.*, 1997b; Nepf, 1999; Stone and Shen, 2002 and others).

Whilst their dimensions, volumes, distribution and structure can be more accurately and easily determined, they are not representative of the complex morphology associated with natural vegetation, such as saltmarsh vegetation. It is useful to characterise the structure and distribution of vegetation material in a way that can be related to the hydraulic processes taking place. Numerous species are usually encountered on a natural wetland. These need to be considered separately, as they will vary in material properties (e.g. stiffness) and physical properties (e.g. stem diameter, leaf shape and size) and will consequently have different effects on the flow.

Saltmarsh vegetation varies both spatially and temporally. Spatial variation can occur either due to the nature of the location (e.g. with proximity to creek networks or with ground elevation), or the natural variation in the species. Temporal variation occurs due to the seasonal variations associated with the growth and dieback cycle of the species (Collinson, 1988). Such variations may be reflected in the height of the canopy, the diameter of the stem, or the density of the vegetation, where density may be quantified by determining the stem density or mass per unit bed area.

Traditionally, ecologists whose primary aim is the identification of the different species and investigating their adaptation and competition within the environment, have conducted classification of vegetation. Ecologists may also be interested in characteristics of a saltmarsh that reflect its history (Boorman, 1999). Saltmarsh vegetation classification reviews were presented by Shimwell (1971) and Whittaker (1973). Since then, a system of classification of natural habitats according to the vegetation they accommodate has been developed for all vegetation types and species. This is known as the National Vegetation Classification (NVC) and was published as the fifth volume of the British Plant Communities (Rodwell, 2000).

In the context of coastal management, a study is likely to focus on either the velocity and turbulence structure through the saltmarsh canopy, or the associated sedimentary processes (e.g. sediment transport, suspension and deposition). Classification of the vegetation solely based on the species type is not sufficient for the purposes of the study. Instead, a more physical means of quantification is necessary to relate the vegetation structure and quantity to the resulting hydrodynamics (Neumeier, 2005). The quantification approach will depend on the vegetation structure and the nature of the study. Gacia *et al.* (1999) found a good correlation between the ratio of projected leaf area to ground area of sea grass to the amount of sediment retention, whilst Leonard and Luther (1995) found a good

correlation between the stem density of emergent *Juncus roemerianus* and *Spartina alterniflora* canopies and the turbulence intensity within the vegetation (see Figure 2.26b in Section 2.4.2). The physical quantification of vegetation used in this study through consideration of various parameters such as the projected area of obstruction, stem density and canopy height is discussed in Chapter 4.

Seasonal variation patterns were shown by Morris and Haskin (1990) for *Sp. alterniflora* in South Carolina (Figure 1-1). The study shows that the vegetation has a maximum density towards the late summer months and a minimum early in the year. The density was parameterised in terms of biomass density. Although these observations may be linked to longer hours of sunlight exposure, vegetation growth is affected by many factors such as the salinity of the soil, its redox potential (readiness to gain electrons and hence, become reduced) and the depth of the water table (Sanchez *et al.*, 1996). It is also affected by the nutrient and sediment loading, oxygen availability, and competition between plant species (Pennings and Callaway, 1992). Rainfall and mean sea level will affect plant growth, as these will influence the salinity of the sediment, and for every species, there is an optimal salinity range within which production is most intense, whilst a particularly high salinity level can be fatal even for halophytes (Morris and Haskin, 1990). High salinity levels can arise where evapotranspiration is high in the absence of regular flooding (Phleger, 1971).

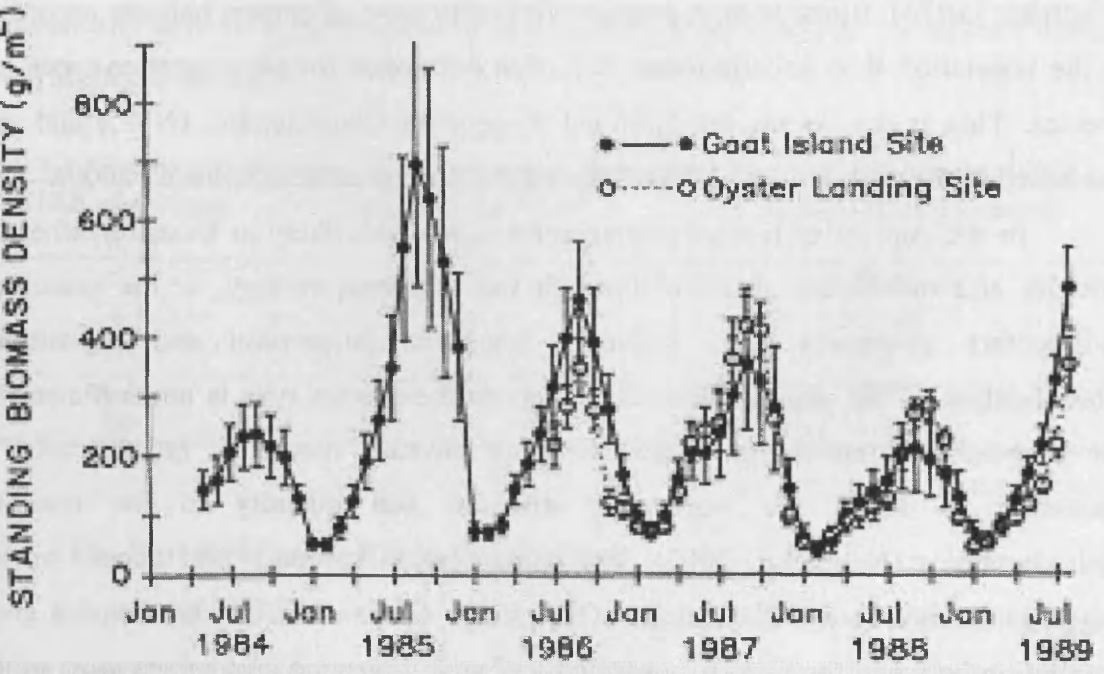

Figure 1-1 Monthly vegetation density and stem density measurements for *Sp. alterniflora* (taken from Morris and Haskin, 1990)

1.3.4 The Loss of Saltmarshes due to Coastal Squeeze

Coastal saltmarshes can adapt to rising sea levels through two mechanisms. The first mechanism, mentioned in 1.3.1, involves the long-term sediment deposition across the saltmarsh surface resulting in an increase in ground elevation over time (e.g. Beeftink, 1977). Secondly, as the mean sea level rises, the saltmarsh is forced to move inland onto higher ground. Although the land originally occupied by the saltmarsh may be eroded, the saltmarsh itself survives the increase in water level and continues to provide coastal protection and to promote biodiversity. Most saltmarshes in the UK are backed by seawalls that prevent them from migrating inland. Hence, with rising sea levels, a considerable area of saltmarsh may be lost (Boorman *et al.*, 1989). This is known as the concept of 'coastal squeeze', and a considerable proportion of the saltmarshes along the coasts of the UK are at risk of disappearing.

1.3.5 The Implications of Saltmarshes on Coastal Hydrodynamics

Saltmarshes can modify the local hydrodynamics in a number of ways to provide protection to the coastline. Saltmarsh vegetation is capable of both reducing flow velocities within the vegetation region so that the settlement of sediment particles is more readily achieved (e.g. Pethick *et al.*, 1990; Christiansen *et al.*, 2000), and stabilising settled sediments by binding the substrate together through their roots (e.g. Boorman, 1999). During more extreme storm events, the front of a saltmarsh is eroded; however the eroded material remains along the adjoining mudflats and is available for subsequent deposition during calmer periods. This may extend the length of mudflats fronting the saltmarshes (Pethick, 1992).

Ultimately, the most effective mechanism through which saltmarshes provide protection to adjoining seawalls is through the absorption of wave energy. An 80m length of saltmarsh can result in a 40% reduction in wave heights through the reduction of flow depth, wave breaking and frictional losses (Brampton, 1992). Möller *et al.* (1996) compared wave energy dissipation over 200 metres of mudflat and 200 metres of the adjoining saltmarsh along Stiffkey saltmarshes along the North Norfolk coast in eastern England. The measurement transect was positioned normal to the coastline and experienced a decrease in energy of between 1.9% and 55.3% for the mudflat compared to 47.4% and 100% for the saltmarsh. In a similar study along the same saltmarsh, where the transect was positioned normal to the direction of the

dominant wave approach, Möller *et al.* (1999) observed a 29% reduction in energy over the mudflats compared to 82% over the saltmarsh.

Photographs of typical saltmarshes taken during this study are presented in Figure 1-2 and Figure 1-3 as an example for the reader of the field situation.

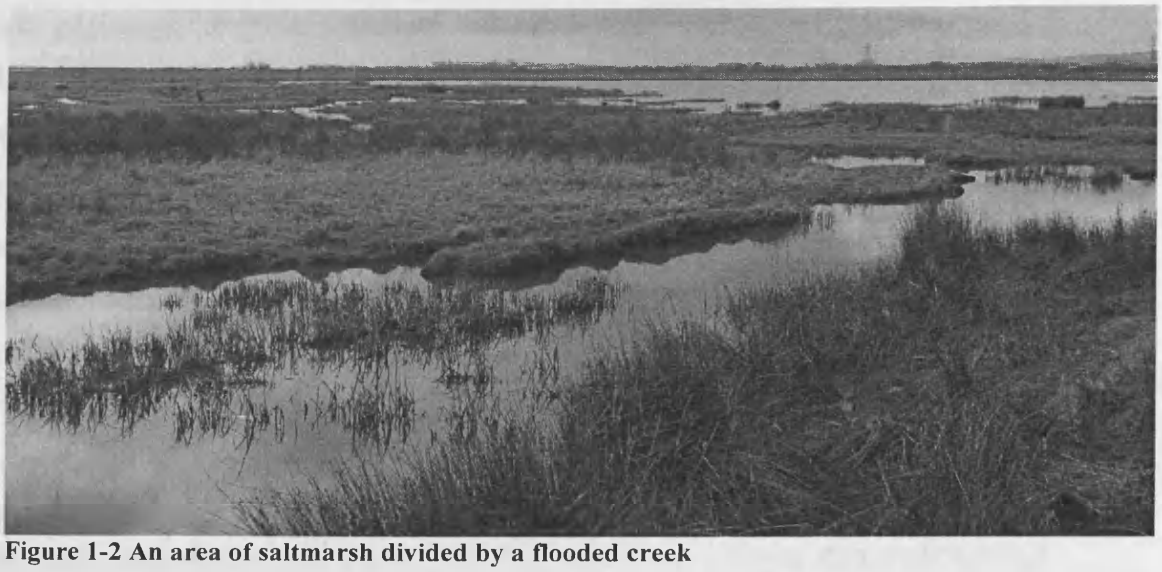

Figure 1-2 An area of saltmarsh divided by a flooded creek

Figure 1-3 A saltmarsh becoming submerged with an incoming tide

1.4 Basic Definitions

Some commonly used terms are defined at this point to avoid confusion.

1.4.1 Saltings

The term is synonymous with 'saltmarshes', sometimes also referred to by some authors as 'salt marshes', and refers to coastal wetlands located in the intertidal zone and hence, experience both dry and inundated periods frequently due to tidal patterns. The vegetation located on these wetlands is halophytic, meaning that they require a saline environment to survive.

1.4.2 'Submergence'

A number of different variations of the terms 'submerged' and 'emergent' have been used by different authors to describe situations where the flow depth is greater or less than the vegetation height respectively. Throughout this thesis, the term 'emergent' is used to describe the former scenario, where the flow depth is less than the vegetation height, see Figure 1-4a, whilst 'submerged' is used to describe the latter, where the flow depth is greater than the vegetation height, see Figure 1-4b. Furthermore, the term 'submergence', denoted as H, is defined as the ratio of flow depth, D, to vegetation height, T, to characterise this property. The parameter is more meaningfully used to characterise submerged canopies as the exact canopy height under emergent conditions may be unknown and in rigid vegetation does not affect the hydraulic resistance and hence, the flow characteristics.

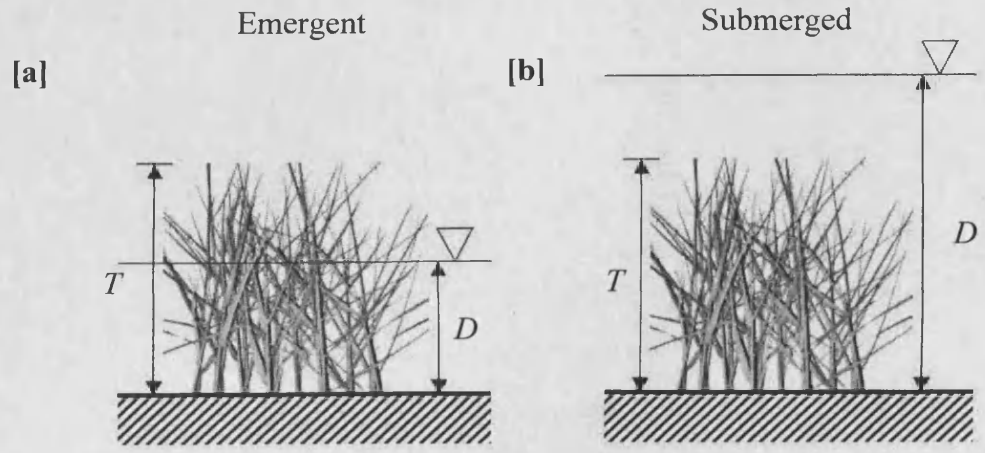

Figure 1-4 The notations used to describe the canopy height, *T*, and flow depth, *D*, under [a]: emergent and [b]: submerged conditions.

1.4.3 The 'Canopy'

Biologists use the term 'canopy' in reference to the leaves of the vegetation. However, as confirmed by various sources within the literature, engineers commonly use the same term in reference to the entire vegetation layer above soil level (e.g. Wilson and Shaw, 1977; Shi *et al.*, 1996; Ackerman and Okubo, 1993 and others). This latter approach is adopted in this thesis, and the leaf part of the canopy is referred to as the 'foliage'. For submerged conditions, the region above the canopy (where the water elevation is greater than the canopy height in Figure 1-4b) is referred to as the 'surface flow layer', and the top of the canopy is referred to as the 'canopy-surface flow layer interface'. The region close to the bed where foliage is usually absent or scarce is referred to as the 'stem' region. This is illustrated in Figure 1-5.

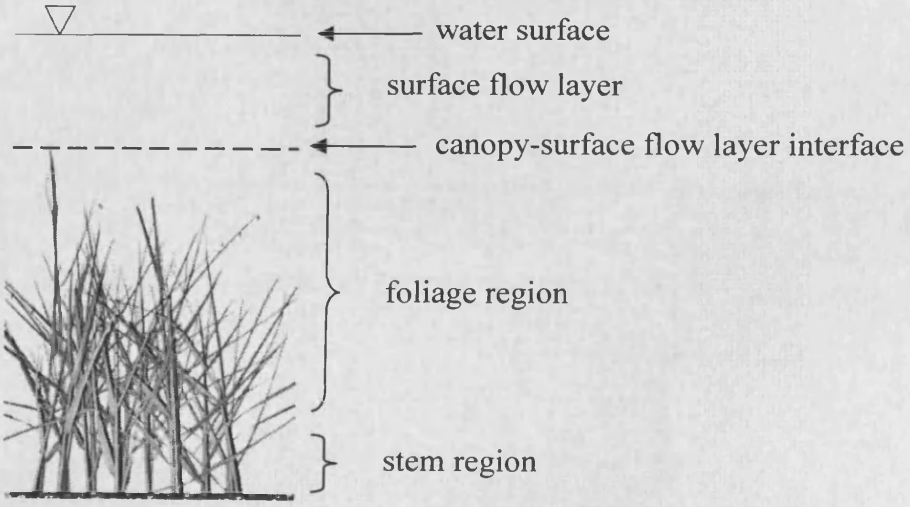

Figure 1-5 The terminologies used to describe the canopy and surface flow layers.

1.5 Concluding Remarks

1.5.1 Research Objectives and Methodology

The aim of the research presented in this thesis is to investigate the effects of saltmarsh vegetation canopies on flow dynamics, and particularly how the obstruction due to the vegetation gives rise to drag forces and affects the turbulence structure of the flow, which in turn affects the velocity profile shapes. First, some consideration was given to quantifying the vegetation, which can be complicated due to the heterogeneous structure of vegetation canopies, however, this is important to relate the canopies to the resulting flow dynamics. A fieldwork programme was then designed and executed to quantify vegetation and other parameters, such as bed gradients and water depth profiles. The findings were used to design laboratory experiments that are representative of typical saltmarsh environments to facilitate the investigation of the flow dynamics. Experiments were conducted using vegetation samples collected during the summer and winter periods to investigate the significance of the variation in vegetation properties on flow dynamics. Some of the experiments were also repeated using arrays of plastic straws to evaluate the suitability of uniform cylinder arrays for simulating vegetation canopies. By considering drag forces and the turbulence structures in relation to the velocity profiles for various stem densities, bed gradients and submergence levels, a series of empirical relationships are suggested for predicting the velocity profile through vegetation canopies.

1.5.2 Thesis Layout

In Chapter 2, a detailed account is presented of research conducted that is relevant to vegetated flows, particularly in the context of saltmarsh vegetation. The results from an extensive fieldwork programme are presented in Chapter 3. Practical methods for the quantification of vegetation are discussed in Chapter 4. The methodology for the laboratory programme is described in Chapter 5, the results from a comparison between the impacts of uniform cylinder arrays and *Spartina anglica* canopies on hydrodynamics is presented in Chapter 6, and a more in-depth study of the hydrodynamics through *Spartina anglica* canopies is presented in Chapter 7. In Chapter 8, a prediction method applicable to the velocity and turbulence profiles

through vegetation canopies is proposed. The final conclusions to the thesis are presented in Chapter 9 along with recommendations for further work.

2 A Review of Flows through Vegetation in Open Channels

2.1 Flow Resistance due to Bed Roughness

2.1.1 Flow Over a Rough Bed

A number of empirical resistance coefficients are used to characterise the surface roughness of open channels, pipes and floodplains. Such coefficients combine all sources of resistance, such as bed friction and drag due to the presence of physical obstructions producing a single parameter e.g. Chezy's resistance factor, C, Darcy-Weisbach friction factor, f, and Manning's n. Flow resistance arises due to bed friction when the flow passes over a rough surface, although depending on the context, other factors may also contribute to this, such as the bed geometry, bed forms and meandering of a channel in the case of open channel flow. Where roughness elements protrude into the flow domain, (e.g. reed beds), some of the resistance is due to the drag force arising from the plant stems obstructing the flow. The magnitude of the flow resistance may also depend on the vegetation type and height in relation to the flow depth. Although the aforementioned coefficients represent all sources of resistance, by definition, these formulae are only applicable where the roughness elements do not protrude significantly into the flow and resistance is mainly due to bed roughness. The formulae were developed on the assumption that the flow is uniform such that the longitudinal weight component of the flow is equal to the force of the resistance. The roughness parameters are commonly functions of the area-mean velocity, U, the bed gradient, S_0, and the hydraulic radius, R (the ratio of flow area to the wetted perimeter):

$$n = \frac{R^{2/3} S_0^{1/2}}{U} \qquad \text{[Equation. 2.01]}$$

$$f = \frac{8gRS_0}{U^2} \qquad \text{[Equation. 2.02]}$$

$$C = \frac{U}{\sqrt{RS_0}} \qquad \text{[Equation. 2.03]}$$

Manning's n and the Chezy coefficient are only applicable where the flow is fully turbulent (e.g. Chadwick and Morfett, 1986). Of these coefficients, Manning's n is the most widely used, and values are available for a number of different surfaces e.g. wood, clay, gravel and grass beds (e.g. Chow, 1959). Application of these formulae is common for flow over rough beds, which is characterised by a logarithmic velocity profile (Section 2.1.2) above the laminar boundary layer, within which the effects of the bed roughness take effect. For flow over a rough surface, the thickness of this boundary layer is usually very small compared to a vegetated flow where the logarithmic profile is displaced starting above the vegetation canopy (Stephan and Gutknecht, 2002). Within the vegetation layer, the velocity profile will be affected by the vegetation quantity, structure and morphology. These characteristics are difficult to represent through an empirical resistance coefficient.

2.1.2 Logarithmic Velocity Profiles

Above a rough bed, or in the surface flow layer above the canopy in the case of vegetated flows, the velocity profile shape can be described using a logarithmic relationship for a fully developed flow. This can be described mathematically through Prandtl's logarithmic law as modified by Nikuradse (e.g. Chow, 1959; French, 1985 and others) as follows:

$$\frac{u}{u_*} = \frac{1}{\kappa} \ln \frac{z}{k_S} + \phi \qquad \text{[Equation. 2.04]}$$

where u is the longitudinal velocity at a given elevation, z, κ is the von Karman constant (typically 0.4), k_S is the equivalent sand-grain roughness, ϕ is an integration constant and u_* is the shear velocity. The shear velocity is defined as:

$$u_* = \sqrt{\frac{\tau_0}{\rho}} \qquad \text{[Equation. 2.05]}$$

where τ_0 is the shear stress at the boundary, which can be either the bed in the case of a rough bed, or the deflected vegetation height in the case of a submerged canopy

(Stephan and Gutknecht, 2002), and ρ is the fluid density. The parameter is referred to as a velocity due to its units, but is actually a measure of shear stress.

Further work has been conducted on Prandtl's logarithmic law to apply it to the surface flow layer above a vegetation canopy, and different authors have proposed a number of modified versions. In addition to the parameters included in the original law in Equation 2.04, some of the modifications may also include the deflected height of the vegetation, z'', the difference between the deflected vegetation height and the zero-plane displacement, z' (Figure 2-1), a parameter referred to as k_P which is similar to the equivalent sand grain roughness, k_S in concept but applicable to plant canopies, the hydraulic radius and a modified von Karman constant. Stephan and Gutknecht (2002) provide a comprehensive summary of the different modifications applied to Prandtl's logarithmic law.

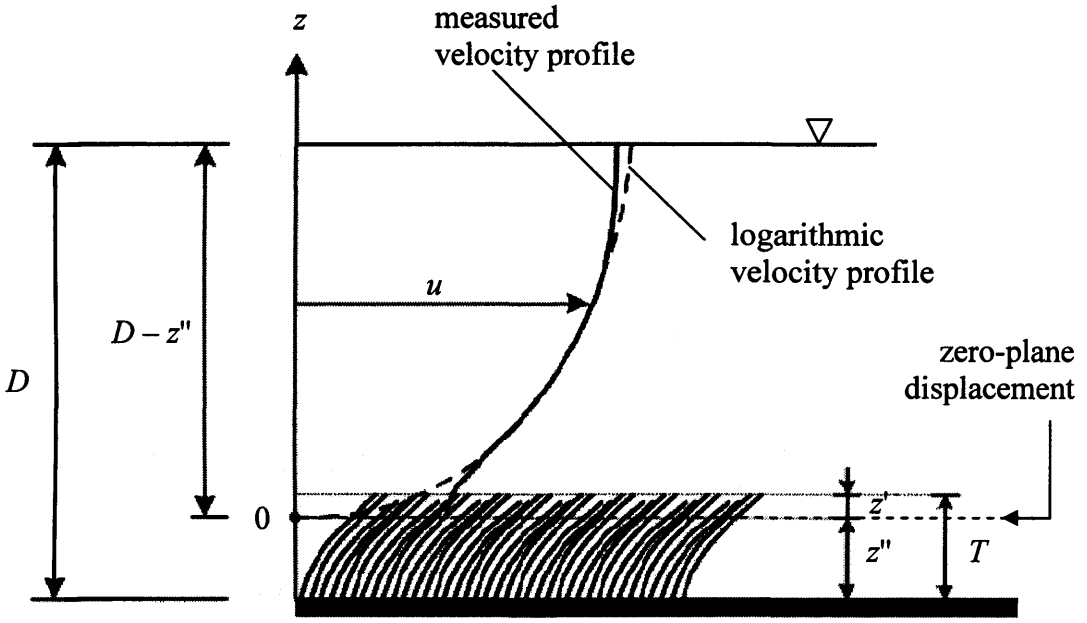

Figure 2-1 Longitudinal velocity profile above submerged vegetation, where T is the deflected height of the vegetation, z'' is the zero-plane displacement, z' is the difference between the deflected height of the vegetation and the zero-plane displacement, D is the flow depth and u is the longitudinal velocity (taken from Stephan and Gutknecht, 2002).

The variations proposed on the original logarithmic law operate on the basis that Equation 2.04 can be modified with a zero-plane displacement i.e. the distance from the bed above which the velocity profile shape can be described as being logarithmic (see Figure 2-1). This approach assumes that a state of equilibrium is achieved, where the rate of turbulence production and dissipation are balanced along

the point where the log law profile commences (López and García, 1997). This has been demonstrated by a number of authors (e.g. López and García, 1997; Nepf, 1999 and others), who have considered the dissipation rate and wake production terms within the turbulent kinetic energy budget (Section 2.5.6). The authors have shown the production and dissipation to be of similar magnitudes and they suggest that this indicates that the balance between the two terms controls turbulence levels within the canopy.

2.1.3 Uniform Flow Conditions

The experiments conducted in this study (Chapters 6 and 7) have all been conducted under uniform flow conditions whereby the total energy line, which is an imaginary line consisting of the depth of flow and the velocity head, is parallel to the bed slope. For uniform flow over a rough bed, the weight component of the water body acting along the plane of the bed and the opposing shear force must balance each other (Figure 2-2) such that:

$$\tau_0 BL = \rho g AL \sin\theta \qquad \text{[Equation. 2.06]}$$

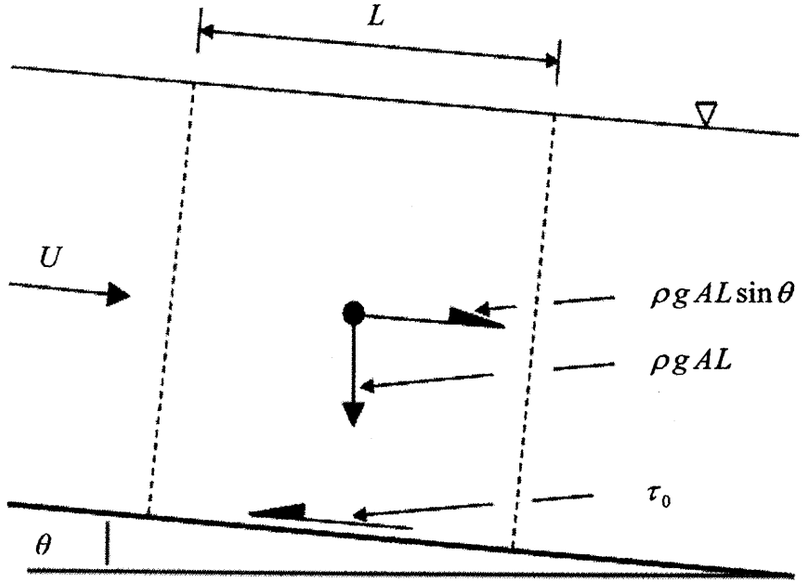

Figure 2-2 Body force diagram for uniform flow over a rough surface, where L is the reach length of a unit volume, U is the depth-averaged longitudinal velocity, A is the flow area, θ is the angle of the bed slope, and τ_0 is the bed shear stress (taken from Chadwick and Morfett, 1998)

where τ_0 is the bed shear stress, ρ is the fluid density, g is the gravitational acceleration, A is the cross-sectional area of the flow domain in the longitudinal direction, B is the flume width, L is a unit length of flow domain, and $\sin\theta$ (often denoted as S_0 throughout this thesis) is the bed slope.

2.1.4 Three-Dimensional Shallow Flows

Momentum conservation for fluid flow is described by the Navier-Stokes equations. These can be simplified for flow in the longitudinal direction by the x-direction momentum equation as follows:

$$\frac{\partial u}{\partial t}+\frac{\partial u^2}{\partial x}+\frac{\partial uv}{\partial y}+\frac{\partial uw}{\partial z}=gS_0-\frac{1}{\rho}\frac{\partial P}{\partial x}+\frac{\mu}{\rho}\left(\frac{\partial^2 u}{\partial x^2}+\frac{\partial^2 u}{\partial y^2}+\frac{\partial^2 u}{\partial z^2}\right) \qquad \text{[Equation 2.07]}$$

where u, v and w are the velocity components in the longitudinal (x), lateral (y) and vertical (z) directions respectively, g is the gravitational acceleration, S_0 is the bed gradient, ρ is the fluid density, P is the hydrostatic pressure of the fluid (due to the height of the water column) and μ is the dynamic viscosity. For shallow flows, particularly in natural vegetated environments such as saltmarshes and wetlands, where pressure difference is the main driving force of the flow, advective accelerations (in the x, y or z directions) are often negligible, and Equation 2.07 can be simplified in terms of the local acceleration:

$$\frac{\partial u}{\partial t}=gS_0-\frac{1}{\rho}\frac{\partial P}{\partial x}-\frac{F_D'}{\rho} \qquad \text{[Equation 2.08]}$$

$$\frac{\partial u}{\partial t}=gS_0-\frac{1}{\rho}\frac{\rho g(\eta_1-\eta_2)}{\partial x}-\frac{F_D'}{\rho} \qquad \text{[Equation 2.09]}$$

$$\frac{\partial u}{\partial t}=gS_0-g\frac{\partial \eta}{\partial x}-\frac{F_D'}{\rho} \qquad \text{[Equation 2.10]}$$

where η is the water depth (Figure 2-3) and F_D' is the drag force per unit volume due to the vegetation or other obstacles obstructing the flow (Section 2.2.6).

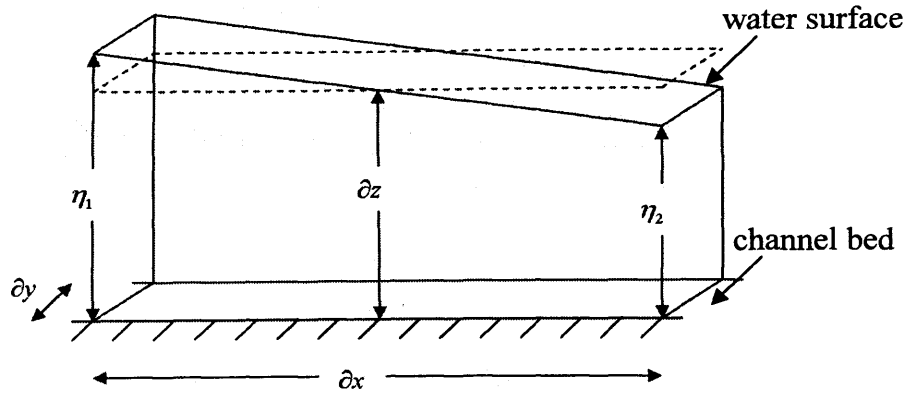

Figure 2-3 Schematic diagram illustrating pressure driven shallow flows (taken from Chow, 1959)

2.2 Physical Obstruction of the Flow

2.2.1 Characterising the Flow Regime

The experiments conducted by Reynolds in the late 19th century investigating the transition of a flow from the laminar to the turbulent state (e.g. Chadwick and Morfett, 1986) showed that the onset of turbulence was dependant on the fluid velocity and viscosity, and a length scale. Thus, the Reynolds number, Re, was introduced as a dimensionless parameter (with no units) to characterise this property as follows:

$$\mathrm{Re} = \frac{\rho u l}{\mu} \qquad \text{[Equation 2.11]}$$

where ρ is the fluid density (approximately 1000 kgm^{-3} for water between 0°C and 30°C), μ is the dynamic viscosity (approximately 0.001 $kgm^{-1}s^{-1}$ for water at 20°C), u is the velocity, and l is the turbulence length scale. The size of the turbulence length scale depends on the flow conditions. For instance, in open channel flows, the length scale is often the channel width or depth, or the hydraulic radius, whilst for pipe flows, the diameter of the pipe is often used.

The Reynolds number is a measure of the ratio of inertial to viscous forces within the fluid. Viscous forces arise due to the friction between fluid particles as they move past each other, whereas inertial forces are the result of the acceleration of the fluid in accordance with Newton's second law. For a laminar flow, the Reynolds

number is relatively low, and viscous forces predominate, whereas for a turbulent flow, the Reynolds number is higher, and inertial forces predominate (Prandtl, 1935).

For flow through a rough channel, two different types of turbulence length scales can be defined to charaterise the flow : a minimum and a maximum turbulence length scale. The minimum length scale for a rough bed is the equivalent sand grain roughness which characterises the size of the roughness elements responsible for turbulence generation. The maximum length scale is the hydraulic radius, which for a wide channel is equivalent to the flow depth. This characterises the maximum theoretical size of turbulent structures that may form within the flow.

When considering flow past a cylinder, and particularly in the context of a cylinder array, it is common to use the stem Reynolds number (Re_d) whereby the stem diameter is the length scale since any large scale eddies are disrupted by the stems and replaced by eddies formed within the stem wake at the scale of the stem (Nepf *et al.*, 1997b). This is given by:

$$Re_d = \frac{\rho u d}{\mu} \qquad \text{[Equation 2.12]}$$

where d is the average stem diameter. In fact, Zavistoski (1994) showed that the width and length of a wake forming downstream of a single cylinder is a function of the cylinder diameter. The diameter is therefore equivalent to the minimum turbulence length scale. For dense arrays of cylinders, the size of the wake may be limited by downstream cylinders, and for the turbulent structures forming within the wakes, the maximum length scale is the spacing between the cylinders.

2.2.2 General Concept of Flow around an Obstruction

When a flow field is physically obstructed by an object, two different types of drag force arise: frictional (or viscous) and form (or pressure) drag. Frictional drag arises in the region immediately adjacent to the surface of the body (the boundary layer, see Figure 2-4) resulting in a reduction in velocity due to the boundary's skin friction and is therefore a function of the total surface area of the object. As the flow becomes more laminar (below a stem Reynolds number of 200 for a single cylinder, see Section 2.2.4), frictional drag, which is responsible for the dissipation of flow

energy without the generation of turbulence, becomes more important (e.g. Douglas *et al.*, 1979). The second type, form drag, arises due to the pressure difference created across the obstructing body in the longitudinal direction and is dependant on the form of the object. It is therefore a function of the projected area of the object.

It is common to consider the cumulative effects of frictional and form drag simultaneously, the sum of which is referred to as the profile drag. The drag force created by a body in a flow stream, F_D, is given by the formula:

$$F_D = \frac{1}{2}\rho C_D A U^2 \qquad \text{[Equation. 2.13]}$$

where C_D is a drag coefficient, ρ is the fluid density, U is the area mean velocity in the free stream (where the flow is not affected by the bed, walls, or the cylinder wake), and A is the projected area of the body. The drag coefficient is expressive of the drag force and hence, is dependant on the body shape, stiffness, size, surface roughness and the flow regime (turbulent, laminar or transitional) as indicated by the stem Reynolds number (Section 2.2.1). It is a measure of the reduction in velocity caused by the obstruction making it a useful parameter for evaluating the drag associated with a given obstacle.

As the flow accelerates to move around an obstacle, and moves with higher velocities near its perimeter, there is a drop in dynamic pressure along the surface of the object compared to the pressure at the upstream face, termed the stagnation point due to minimal fluid movement at this location (Figure 2-4). At the downstream end, the magnitude of the pressure is less than the upstream value due to energy dissipation in the turbulent wake region (Figure 2-4), except for situations of laminar flow (below a stem Reynolds number of 0.5). The pressure difference results in a drag force opposing to the flow direction, and along with frictional forces on the boundary, also results in flow reversal giving rise to vortices, and a separation point in the flow is established downstream of the body (Figure 2-4). Consequently, the wake structure is closely associated with the turbulence level of the flow and hence, is dependant on the Reynolds number. A larger wake results in a greater form drag.

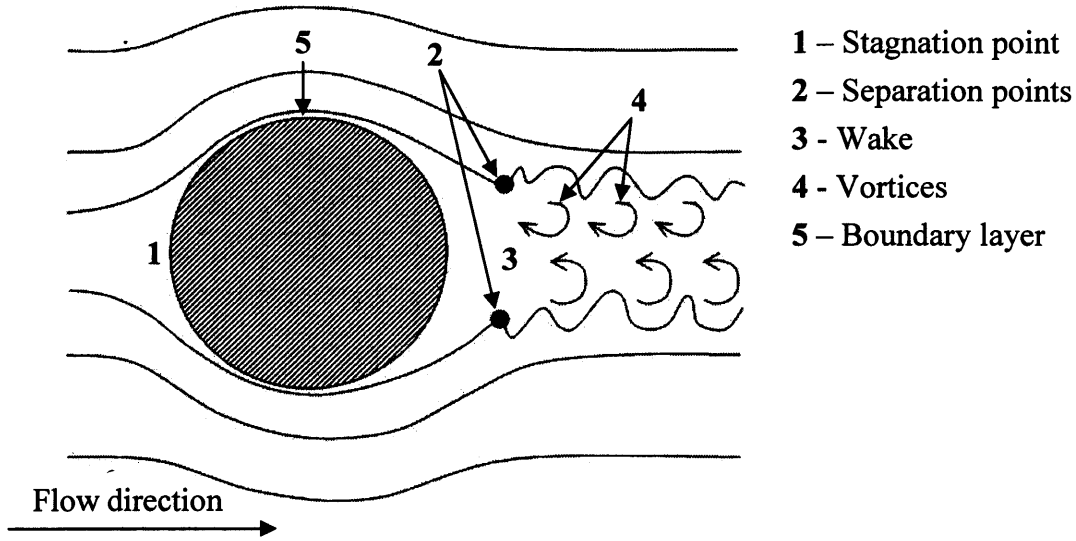

Figure 2-4 Flow structure around an immersed body (taken from Douglas *et al.*, 1979)

2.2.3 Flow Structure past a Single Emergent Cylinder

Flow past a single cylinder has been widely researched and is presented in many fluid mechanics text books (e.g. Schlichting, 1955; Douglas *et al.*, 1979 and others). The relationship between the drag coefficient, C_D, and the Reynolds number, Re, referred to here as the $C_D - \mathrm{Re}_d$ curve, where Re_d is the Reynolds number where the cylinder diameter is used as the characteristic length scale (Section 2.2.1), is presented in Figure 2-5. Changes in wake structure with increasing Reynolds number, which have been identified through flow visualisation using tracers, are presented in Figure 2-6. Velocity measurements through *Spartina* canopies indicate that velocities were generally between 0.01 ms^{-1} and 0.01 ms^{-1} in the vegetation layer (e.g. Shi *et al.*, 1995; Christiansen *et al.*, 2000; Neumeier and Ciavola, 2004 and others). Stem diameters for *Spartina anglica* were determined in this study and generally ranged between 4 mm and 6 mm depending on the time of year. For these values, it is predicted that stem Reynolds numbers in *Spartina* saltmarsh vegetation would range between values of 40 and 600.

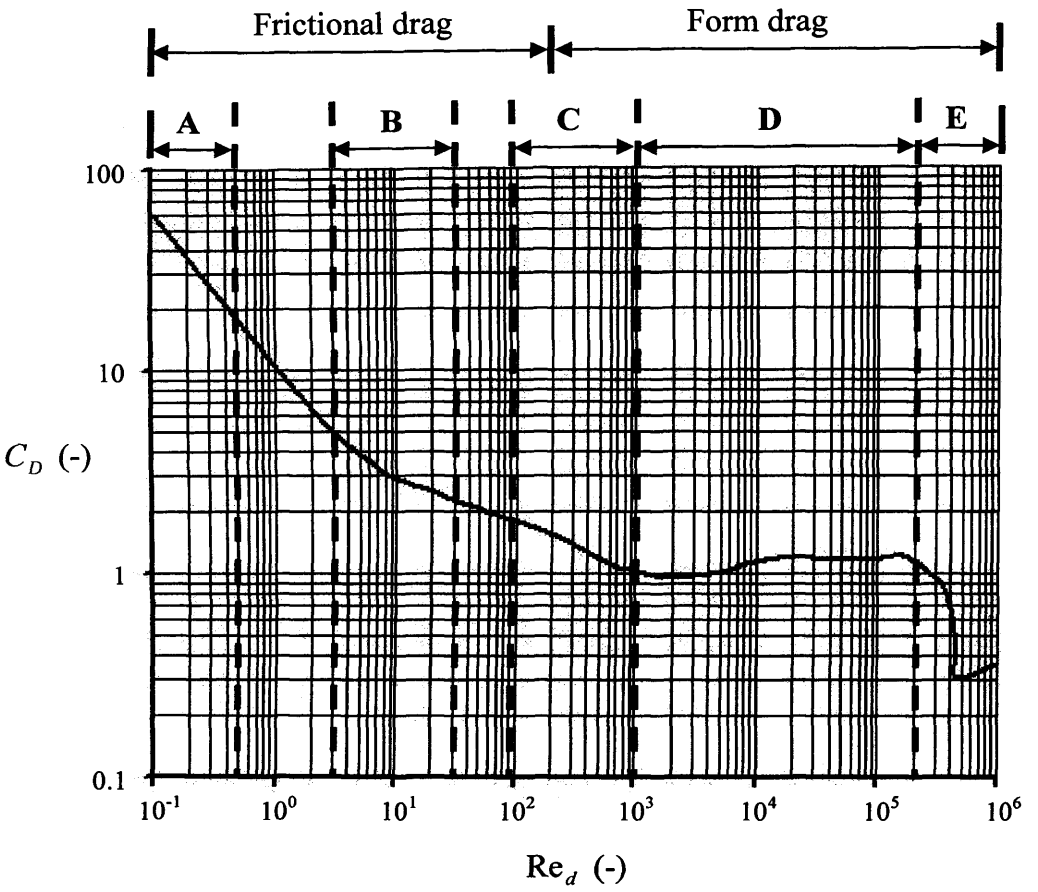

Figure 2-5 Variations in the drag coefficient, C_D, with the stem Reynolds number, Re_d for a single cylinder (reproduced from Schlichting, 1955)

At very low Reynolds numbers ($Re_d < 0.5$), the flow remains laminar and no energy dissipation takes place, hence the pressure is equal on both upstream and downstream faces of the cylinder. Pressure drag is therefore negligible, and the total drag is nearly entirely due to skin friction drag. Due to the low velocities of the flow in this Reynolds number range, there is significant contact between the fluid and the cylinder resulting in a high level of resistance due to friction corresponding to relatively high C_D values. This corresponds to region 'A' in Figure 2-5 and Figure 2-6.

At slightly higher Reynolds numbers ($2 < Re_d < 30$), the boundary layer separates at the separation point resulting in a curvature in the $C_D - Re_d$ curve (region 'B' in Figure 2-5 and Figure 2-6), and vortices begin to form within the wake which are initially symmetrical, circulating in opposing directions, and remain stationary downstream of the cylinder. The symmetrical eddies are elongated with

increasing Reynolds number and begin to oscillate at values of around 90 (Douglas et al., 1979).

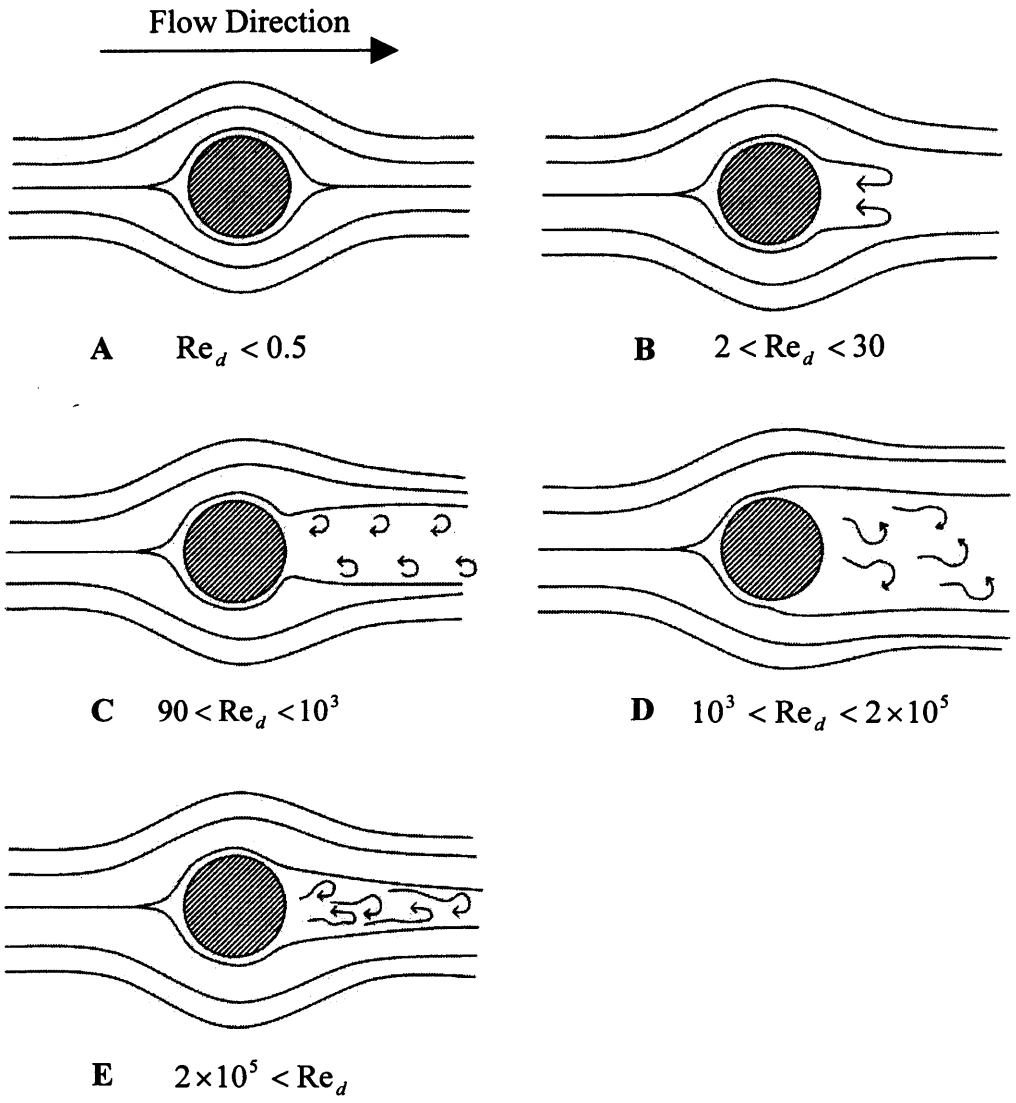

Figure 2-6 The different sages of the development of a fully turbulent wake with increasing stem Reynolds number for flow past a cylinder (taken from Douglas *et al.*, 1979)

For low Reynolds numbers ($2 < Re_d < 30$), bed shear is small, and the pressure, which diminishes in value as the fluid accelerates around the object, returns to a relatively similar value at the downstream surface with a small negative pressure gradient across the cylinder in the direction of the flow. Secondary currents arise due to a positive pressure gradient in the vertical plane on the downstream face of the cylinder due to a large near-bed velocity gradient as the flow passes over the rough bed (Vogel, 1994). Nepf *et al.* (1997b) observed this through visualisation by releasing a dye stream near the base of a single cylinder.

With further increasing values of the Reynolds number (Re_d), up to 10^3, the vortices break away from the cylinder and are washed downstream (region 'C' in Figure 2-5 and Figure 2-6). Williamson (1992) suggested that vortex shedding for a single cylinder commences around a stem Reynolds number of 50, whilst Gerrard (1977) suggested a range between 55 and 70 and Douglas *et al.* (1979) suggested a stem Reynolds number of 90 as shown in Figure 2-6. For a higher Reynolds number, vortices are released with greater intensity from both sides of the cylinder forming a 'vortex street'.

The production of turbulence in the wakes of cylinders is a process through which the mean kinetic energy (*MKE*) of the flow is converted to turbulent kinetic energy (*TKE*) as large turbulent motions are broken down into smaller structures (Wilson and Shaw, 1977). These are defined as:

$$MKE = \frac{\rho\left(u^2 + v^2 + w^2\right)}{2} \qquad \text{[Equation. 2.14]}$$

$$TKE = \frac{\rho\left(u'^2 + v'^2 + w'^2\right)}{2} \qquad \text{[Equation. 2.15]}$$

where u, v and w are the instantaneous longitudinal, lateral and vertical velocity components respectively, u', v' and w' are the average root mean squares of the instantaneous fluctuations in the respective velocity components and ρ is the fluid density.

'Dissipation' (ε) is the process through which *TKE* is converted to other forms of energy, e.g. heat and sound, and through this process, energy is effectively removed from the flow. Up to a Reynolds number (Re_d) of 10^3, an increase in the Reynolds number corresponds to an increase in the turbulence level within both the free stream and the cylinder wake. As the turbulence levels in the free stream increase, the contribution of the cylinder wake to the total turbulence level of the flow (the total turbulence level of both the free stream and the cylinder wake) decreases. Thus, the contribution of the cylinder wake towards reducing the energy of the flow through dissipation becomes less significant. The cylinder becomes less effective as a source of resistance to the flow, and this corresponds to a reduction in C_D (Figure 2-5).

For a Reynolds number (Re_d) up to a value of 2×10^5, the vortices become less organised until they eventually disappear and the wake becomes fully turbulent (region 'D' in Figure 2-5 and Figure 2-6). At this stage, the total drag on the cylinder is nearly entirely due to form drag. Above this value, the boundary layer becomes turbulent prior to separation, the separation point moves further along the downstream end of the cylinder resulting in a considerable drop in C_D (region 'E' in Figure 2-5 and Figure 2-6). Thus, since the drag coefficient for a single cylinder is affected by the wake structure, its magnitude is a function of the stem Reynolds number (Nepf, 1999).

Li and Shen (1973) characterise the separation of the boundary layer around the cylinder into three regimes: sub-critical, critical, and supercritical, and hence, the regimes are dependent on the Froude number defined as:

$$\mathrm{Fr} = \frac{U}{\sqrt{gd}} \qquad \text{[Equation 2.16]}$$

where U is the mean velocity, g is the gravitational acceleration, and d is the cylinder diameter, which can be substituted for an alternative length scale depending on the context. The dimensionless parameter is a function of the ratio of inertial to gravitational forces (e.g. Chow, 1959; French, 1985; Chadwick and Morfett, 1986 and others). The three regimes correspond to values less than unity for sub-critical flow, equal to unity for critical flow, and greater than unity for supercritical flow. Li and Shen (1973) observed that the angle of separation of the boundary layer downstream of the cylinder varies according to the regime as follows: between 72° and 90° for sub-critical flow, approximately 135° for critical flow, and 110° for supercritical flow.

Another mechanism contributing to plant canopy turbulence occurs on the upstream face of cylinders of plant stems near the base. A rigid obstruction in a flow field results in an adverse pressure gradient. This creates a separation point near the bed in the flow upstream of the object with an upward rotation resulting in a 'horseshoe' shaped vortex wrapped around the bottom of the obstruction accompanied by a bulge in the longitudinal velocity profile downstream of the cylinder (Figure 2-7 from Sumer *et al.*, 1997). Baker (1979), Niederoda and Dalton (1982) and Dargahi, (1989) conducted reviews of work on the formation of horseshoe vortices.

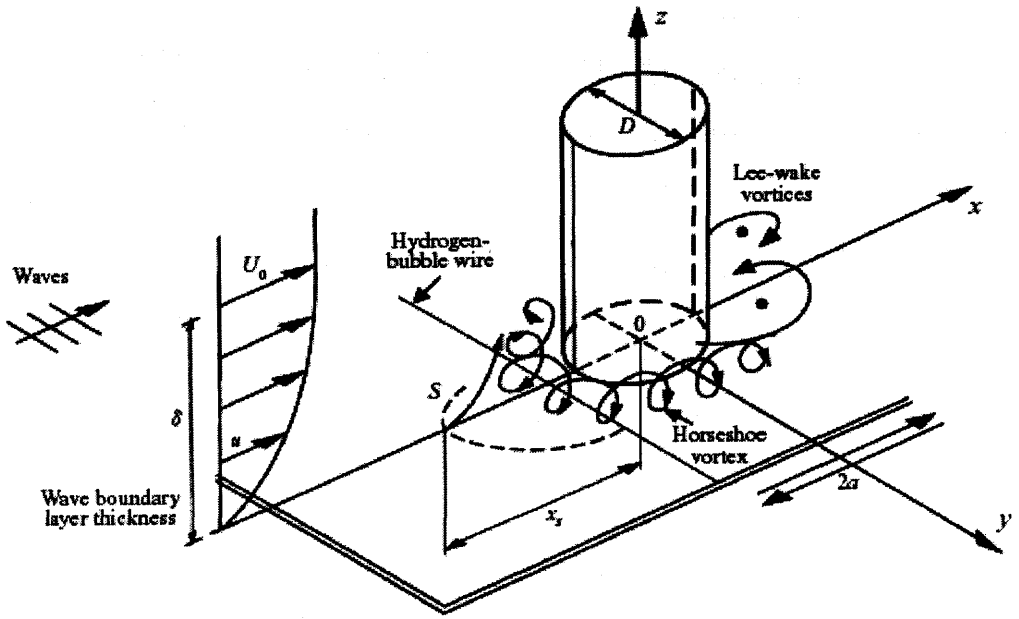

Figure 2-7 Formation of a 'Horseshoe' vortex (taken from Sumer *et al.*, 1997)

2.2.4 The Laminar – Turbulent Transition

After examination of the velocity irregularities associated with 'vortex shedding' within the wake, Williamson (1992) proposed that for an isolated cylinder, the transition from a laminar to a fully turbulent wake occurs at a Reynolds number (Re_d) of 180 while others suggest a value of 200 (e.g. Nepf, 1999). The flow around a cylinder is 'laminar' at very low Reynolds numbers (below a value of approximately two). Above this value, and up to the transition value, the turbulence structure within the wake develops with increasing Reynolds number as outlined in Section 2.2.3. However, the wake is not considered to be fully turbulent within this range, and is therefore the transition range. Within the transition range, vortices are two-dimensional and act in the longitudinal and lateral planes. Above the transition value, the wake becomes 'turbulent' whereby the vortices develop into three-dimensional structures spanning the longitudinal, lateral and vertical planes.

The flow structure around a cylindrical element obstructing the flow, such as a plant stem, is characterised, as mentioned previously, by the stem Reynolds number (Section 2.2.1), and also by the Strouhal number (Str). The Strouhal number is important when analysing unsteady flow problems and is the ratio of inertial forces to the unsteadiness of the flow due to the obstruction created by the cylinder or stem. This is defined as (e.g. Douglas *et al.*, 1979):

$$\mathrm{Str} = \frac{fd}{u} \qquad \text{[Equation. 2.17]}$$

where f is the frequency of the vortex shedding, d is the cylinder diameter and u is the velocity of flow. The parameter describes oscillating flow mechanisms, and is a measure of the frequency of vortex shedding in the wake of the cylinder.

Besides changes to the flow structure in the free stream, the flow within the wake of a cylinder will also vary through the different stages of transition. When the free stream flow is laminar, and the Reynolds number is sufficiently large ($\mathrm{Re}_d > 30$), two organised rows of vortices are formed downstream of the cylinder (Section 2.2.3). In the laminar range ($\mathrm{Re}_d < 180$), two forms of shedding can occur, namely 'parallel' and 'oblique' (Williamson, 1992). Parallel shedding (Figure 2-8a) occurs at much lower stem Reynolds numbers ($\mathrm{Re}_d < 65$). For a given Reynolds number, oblique shedding occurs at a lower frequency compared to parallel shedding as indicated by a lower Strouhal number for the former type (see Figure 2-9 where the solid curve is presented for reference). There is a sudden shift from parallel to oblique shedding corresponding to a discontinuity in the Strouhal-Reynolds relationship around a stem Reynolds number of 65.

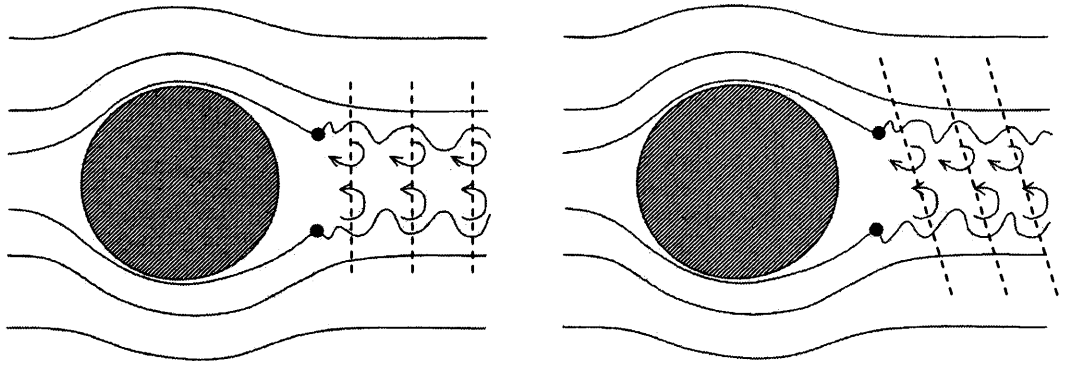

[a] $50 < \mathrm{Re}_d < 65$ [b] $65 < \mathrm{Re}_d < 180$

Figure 2-8 [a]: Parallel and [b]: oblique shedding of vortices in the wake of a cylinder in the laminar range below a stem Reynolds number, Re_d, of 180. The dotted lines have been added to better illustrate the alignment of the vortices (produced based on information presented in Williamson, 1992)

Williamson (1992) illustrated how changes in the modes of three-dimensional shedding within the wake with increasing Reynolds number correspond to irregularities in the Strouhal-Reynolds number relationship as demonstrated in Figure

2-9. For an isolated cylinder, vortex shedding, illustrated previously in Figure 2-6 by regions 'C', 'D' and 'E', commences between regions 'B' and 'C', corresponding to a Reynolds number range between values of 30 and 90. In the same context, Williamson (1992) reported that above a Reynolds number of 180, the flow becomes turbulent. At a value up to 260, finer-scale longitudinal vortex structures begin to form. Between Reynolds numbers of 230 and 360, there is a transition between the aforementioned modes of vortex shedding corresponding to a second discontinuity in the Strouhal-Reynolds relationship. This is not as abrupt as the first discontinuity (Figure 2-9), as the vortex shedding alternates between the two forms within the transition range. Beyond the second discontinuity, the wake becomes fully turbulent consisting of fine scale turbulence.

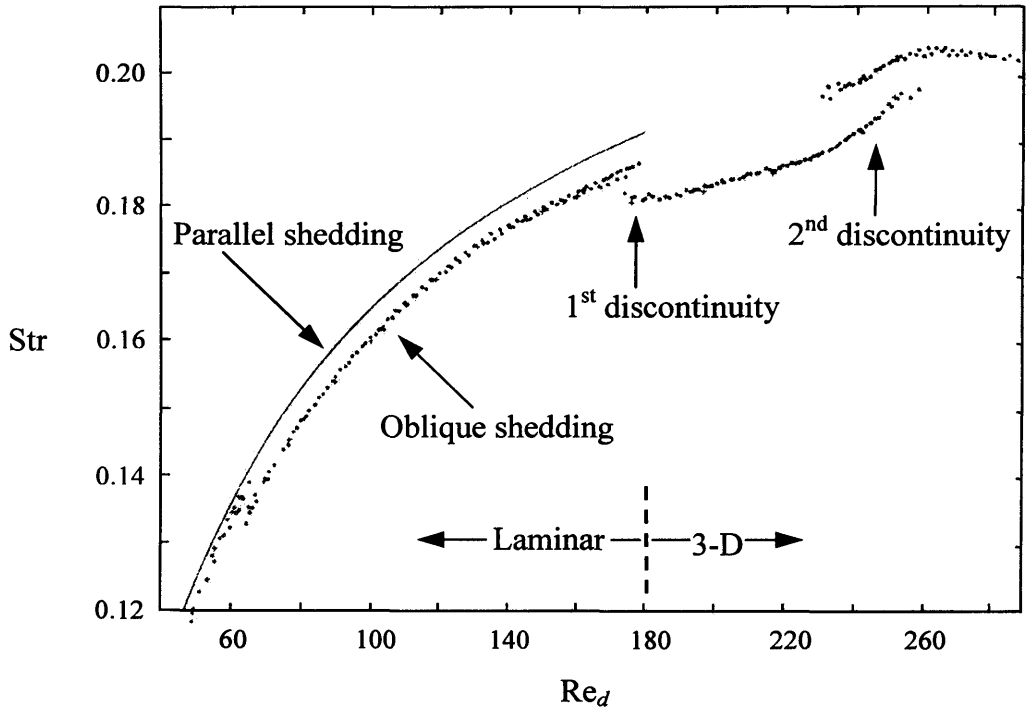

Figure 2-9 The relationship between the Strouhal number, Str, and the stem Reynolds number, Re_d, over the laminar and transitional range (taken from Williamson, 1992). The solid curve is presented for reference to show the Strouhal values for parallel shedding above the transition stem Reynolds number value of 65.

2.2.5 Flow Structure for Emergent Cylinder Pairs

When two cylinders are considered, the problem becomes more complicated as the wake from the upstream cylinder may have an impact on the downstream cylinder depending on the proximity of the two cylinders. The effect of the wake on

the velocity and turbulence around the downstream cylinder is referred to as 'wake interference'. Due to the turbulent nature of the wake, a significant proportion of the mean kinetic energy of the flow is converted to turbulent kinetic energy (as mentioned in Section 2.2.3), and the downstream cylinder experiences a lower impact velocity on its upstream face. Furthermore, the wake of the upstream cylinder may cause the separation point (Figure 2-4) on the downstream cylinder to be shifted further downstream. Both these mechanisms contribute to a reduction in the pressure gradient across the cylinder, and hence, a reduction in drag corresponding to a lower drag coefficient (Zukauskas, 1987; Luo *et al.*, 1996; Nepf, 1999). This is the concept of the 'sheltering' effect described by Raupach (1992).

Nepf (1999) proposed that this applies to cases where the Reynolds number is above a value of 200 and hence, turbulent wake production is significant. Below this value, wake turbulence is negligible, and Nepf (1999) believes that further work is required to understand the implications on wake interference and the effects on bulk drag coefficients representative of groups of cylinders or plants (to be discussed in the next section).

Zdravkovich (1977) presented a review of previous work conducted on pairs of cylinders in various arrangements. The researcher reported that data available is limited and is usually collected to investigate a specific engineering problem and is therefore rather fragmented. Wake interference is dependent on numerous parameters e.g. cylinder diameter and spacing, surface roughness, angle of stagger and Reynolds number. Nevertheless, Zdravkovich (1977) observed that the effects are very evident, particularly where the cylinders are only a few diameter spacings apart.

A further mechanism can occur in staggered arrays, or in situations where the stem spacings are relatively small (less than three diameters) and the downstream cylinder is slightly offset such that it does not fall within the wake of the upstream cylinder (Zdravkovich, 1977). This forces the flow into the wake of the upstream cylinder, as illustrated in Figure 2-10b (Figure 2-10a shows a greater lateral distance between the cylinders whereby the wake is unaffected by the downstream cylinder). Due to the acceleration of the flow, there is a reduction in pressure on the inner sides of the cylinders resulting in an overall positive pressure difference giving rise to 'lift', causing the cylinders to be pulled towards each other. Depending on the flexibility of the cylinders, resonance may occur.

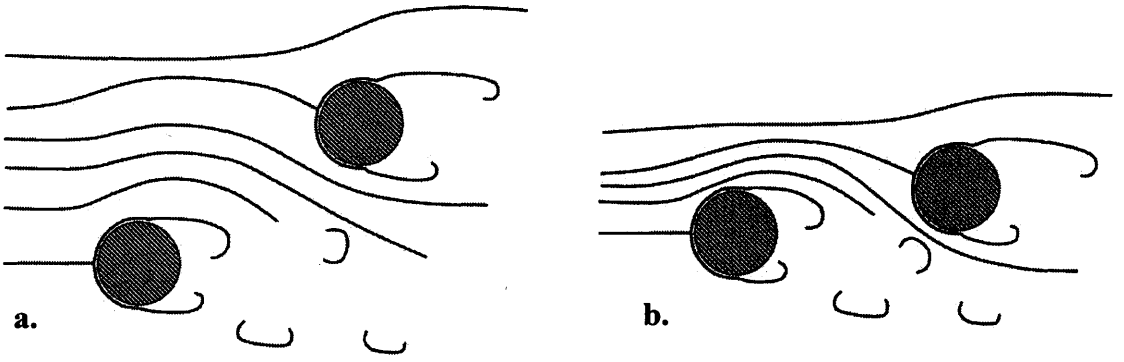

Figure 2-10 Two staggered cylinder arrangements where [a] the lateral distance is large enough such that the downstream cylinder does not affect the wake from the upstream cylinder, and [b]: the lateral distance is relatively smaller causing the free flow to be entrained into the path of the upstream cylinder's wake (taken from Zdravkovich, 1977)

2.2.6 Flow Structure through Groups of Emergent Cylinders

In Section 2.2.2, the drag equation (Equation 2.14), for an object obstructing a flow field was introduced. Researchers working on uniform cylinder arrays simulating vegetation canopies (e.g. Dunn *et al.*, 1996; Nepf, 1999 and others) have proposed that the equation is modified to quantify the total drag force per unit volume, F_D', as follows:

$$F_D' = \frac{1}{2}\rho \overline{C_D} \bar{a} U^2 \qquad \text{[Equation. 2.18]}$$

where $\overline{C_D}$ is a bulk drag coefficient that is characteristic of the array properties (e.g. cylinder diameter, spacing and arrangement), $\bar{a}$ is the projected area of obstruction per unit volume, ρ is the fluid density, and U is the mean free stream velocity. In the context of a single object obstructing the flow, $\bar{a}$ refers to the frontal projected area visible in a cross-section of the flow area, and not the total surface area of the object, since the drag is dominated by form-drag. While the total drag force per unit volume, F_D', includes the form and friction drag components, friction drag is negligible within the transitional and turbulent flow regimes ($200 < \mathrm{Re}_d$).

In situations where the stem density is unknown, or the projected area cannot be determined, it is common to group the projected area per unit volume, $\bar{a}$, and use

the bulk drag coefficient, $\overline{C_D}$, (e.g. Kadlec, 1990; Wu *et al.*, 1999 and others) to define a bulk roughness coefficient as follows:

$$\overline{C_D}' = \bar{a}\overline{C_D} \qquad \text{[Equation. 2.19]}$$

Raupach (1992) suggests that for sparse arrays, where the projected area of obstruction per unit volume approaches zero, the interaction of cylinder wakes with downstream cylinders (Section 2.2.5) can be ignored. However, for higher stem densities, up to a ratio of basal stem area to total ground area of 0.1, it is reasonable to assume that any given cylinder is only affected by the wake of the closest upstream cylinder. Above this value, wake interference becomes even more complex as the drag on a particular cylinder will be affected by the wakes of numerous cylinders positioned upstream, or even lateral to the cylinder. For a given flow rate, the number of stem wakes within the flow volume per unit bed area is directly proportional to the stem density, which in turn, can influence the turbulence level of the flow since turbulence in vegetated flows is generated at the stem scale (Nepf *et al.*, 1997b). However, there will be a greater drag force with increasing stem density, and hence, a decrease in the mean velocity (accompanied by an increase in flow depth) corresponding to a lower Reynolds number which is associated with less turbulence. Nepf *et al.* (1997b) demonstrated that the relationship between stem density and the fraction of the bed area occupied by turbulent wakes is non-linear (Figure 2-11).

Nepf *et al.* (1997b) conducted a statistical analysis based on the random positioning of cylindrical stems with a prescribed projected area of obstruction and wake size associated with each stem. The researcher's model demonstrated that the proportion of the plan-view area of the flow domain occupied by stem wakes increased linearly with stem density for low stem densities, and the range for which this is applicable is dependant on the ratio of turbulent wake area to stem area (the wake ratio), and hence, the Reynolds number (Figure 2-11). For higher stem densities, where exact values will also depend on the Reynolds number, the wakes overlap, and the increase becomes non-linear. This is also evident at low stem densities where the wake size is large, as indicated by higher 'wake ratios', which are defined as the ratio of turbulent wake area to stem area (Figure 2-11).

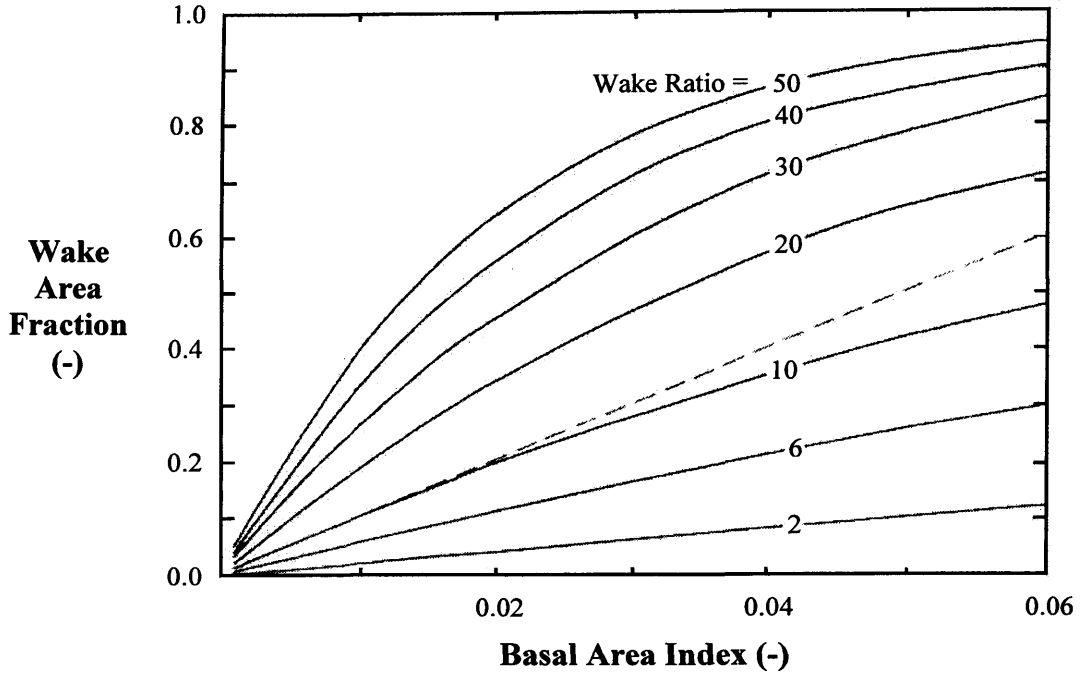

Figure 2-11 The relationship between the 'wake area fraction', defined as the fraction of the plan area occupied by turbulent wakes, and the 'basal area index', defined as the fraction of the plan area occupied by stems, for a range of 'wake ratios', defined as the ratios of turbulent wake area to stem area, which is dependant on the stem Reynolds number. The dotted line shows a linear relationship for a wake ratio of 10 for illustrative purposes (taken from Nepf *et al.*, 1997b)

The non-linear relationship between stem density and flow structure was shown by Nepf (1999), who considered the variation in normalised longitudinal velocity, *U*, (Figure 2-12a), and turbulent kinetic energy, *tke*, (Figure 2-12b), with the array density, *ad*. Values were normalised using the non-vegetated mean velocity, U_0, and turbulent kinetic energy, tke_0. The results presented by the author are averages of five measurements distributed laterally across the flume at the longitudinal midpoint of the array to correct for heterogeneity of the flow field at the scale of the cylinders. The array density parameter, *ad*, is a dimensionless parameter that accounts for the total quantity of vegetation, which is the product of the projected area per unit volume, *a*, and the stem diameter, *d*.

An increase in *ad* caused an increase in hydraulic resistance, and hence, a reduction in flow velocity (Figure 2-12a). For relatively low array densities, the turbulent kinetic energy increases with *ad*, but then decreases at higher values (Figure 2-12b). This is due to the contrasting effects of a reduction in turbulent kinetic energy associated with the lower velocities, and an increase in turbulent kinetic energy

associated with the presence of the obstruction. The latter effect dominates for sparse vegetation ($10^{-6} < ad < 10^{-4}$).

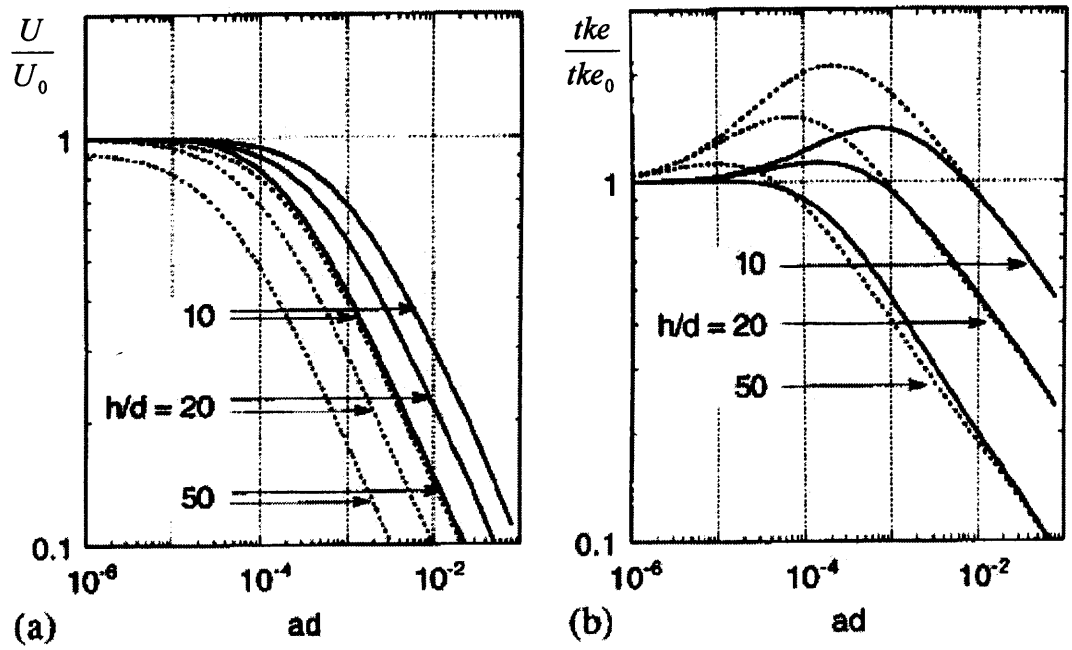

Figure 2-12 Comparison of [a]: flow velocity and [b]: turbulent kinetic energy under vegetated and non-vegetated flow conditions for three ratios of depth to stem diameter (h/d). A subscript of (O) denotes the non-vegetated cases (taken from Nepf, 1999)

Li and Shen (1973) considered the effects of various parallel and staggered cylinder setups on velocity and drag by the linear superposition of the velocity defect due to each cylinder and applying the drag equation (Equation 2.19) with a constant drag coefficient value of 1.2. The authors proposed a mathematical model incorporating a "wake superposition approach", whereby the decay of each cylinder wake was determined independently of any effects due to nearby cylinder wakes. The approach velocity on each cylinder was calculated, from which the associated drag forces were determined from the drag equation (Equation 2.19) using the drag coefficient for a single cylinder (Figure 2-5). The analysis was conducted for stem densities ranging between 0.16 and 0.43 stems m^{-2}, and for stem Reynolds numbers between 100000 and 160000 (the analysis was conducted for large cylinders with 152 mm diameters hence the low stem densities and high stem Reynolds numbers). The results demonstrated the significance of cylinder positions on the overall resistance to the flow, and that staggered arrangements created the largest flow resistance due to less wake sheltering. Based on observations for cylinder pairs, whereby drag coefficients decrease as the stem spacings decrease, Nepf (1999) used a numerical

model to extrapolate these observations to estimate cumulative sheltering effects and bulk drag coefficients for groups of cylinders. The author predicted that the bulk drag coefficients were equal for both random and staggered arrays at very low stem densities (lower than 245 stems m^{-2} for 6.4 mm diameter dowels equating to an *ad* value of up to 0.1 approximately). However, as the stem density increased above this density, there was a more rapid decrease in the bulk drag coefficient for the staggered arrays, where cylinders were aligned and wake sheltering was more significant compared to the random array (see Figure 2-13).

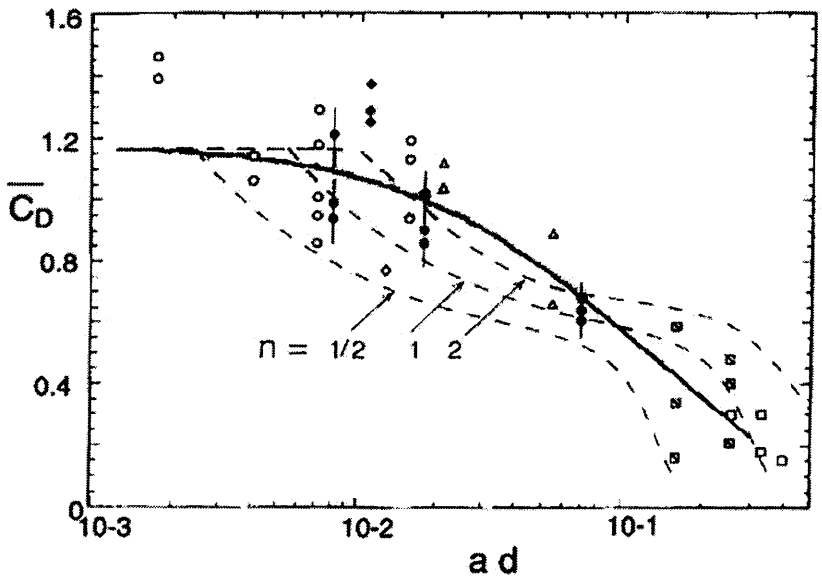

Figure 2-13 The bulk drag coefficient, $\overline{C_D}$, as predicted based on a wake interference model for random (solid line) and staggered (dashed lines) arrays. n is the staggered arrays pitch (ratio of longitudinal to lateral row spacing). (taken from Nepf, 1999)

Kiya *et al.* (1980) demonstrated that an increase in the vorticity (a measure of the rotation or circulation of the flow) of a shear flow, synonymous with the shear arising due to the presence of upstream cylinders, delays the onset of vortex shedding (the shedding of vortices downstream of a cylinder). The magnitude of the vorticity of a shear flow increases with stem density. The critical stem Reynolds number when vortex shedding commences increases nearly linearly with the magnitude of shear in the flow (Figure 2-14a). The shear parameter, K, was defined as:

$$K = \frac{Gd}{U} \qquad \text{[Equation. 2.20]}$$

where U is the mean longitudinal velocity, d is the cylinder diameter and G is the lateral gradient of the longitudinal velocities (see Figure 2-14b). Nepf *et al.* (1997a) also demonstrated this in a study on cylinder arrays at stem densities of 280, 430 and 1700 stems m^{-2} (corresponding to basal area indices of 0.008, 0.012 and 0.048 respectively), where vortex shedding commenced at stem Reynolds numbers of 300, 330 and 360 respectively. Meanwhile, Nepf *et al.* (1997b) reported initial vortex shedding between stem Reynolds numbers of 150 and 200 for stem densities between 200 and 2000 stems m^{-2} (corresponding to basal area indices of 1.2 and 24 respectively).

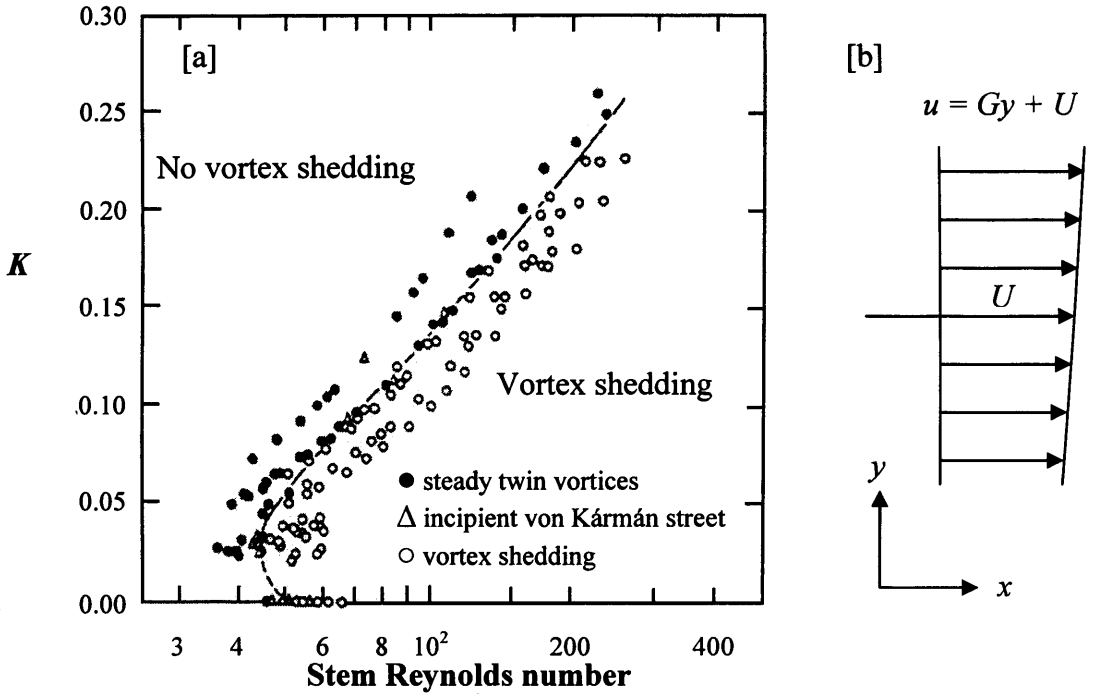

Figure 2-14 [a]: Boundary between vortex shedding and no vortex shedding in shear flow where K is the shear parameter (non-dimensional vorticity of the shear flow) Experiments were conducted on a horizontal bed (taken from Kiya *et al.*, 1980) [b]: A birds-eye view of a flow section characterising the shear parameter, *K*, which is calculated using the lateral gradient in longitudinal velocity, *G*.

In Section 2.2.4, the transition from a laminar to turbulent wake was discussed and related to a decrease in drag coefficient with increasing stem Reynolds number. For a single cylinder, the transition was stated to occur around a stem Reynolds number of 200. However, as shown by the work of Kiya *et al.* (1980), the different stages of the development of the turbulence structure can be delayed within a group of cylinders, whereby the critical Reynolds number value above which vortices are produced in the wakes of stems resulting in a turbulent flow is dependant on the stem

diameters and the stem spacings. Furthermore, in the context of a natural vegetation canopy, Nepf (1999) suggests that the transition may not be as abrupt as an array of uniform cylinders due to the variability in stem diameters, and may span over a range of Reynolds numbers.

2.3 Natural Vegetated Flows

2.3.1 Longitudinal Variability of Vegetation Canopies

Plant properties (e.g. stem density, stem diameter and canopy height) can vary significantly spatially due to natural variability. In vegetated flows, this will directly affect the velocity and turbulence structure within, and in the case of submerged canopies, above the vegetation. Therefore, there is a possibility that a limited number of velocity measurements will be unrepresentative of the 'typical' flow structure through the vegetation. This uncertainty may be remedied through the concept of 'double-averaging'.

In double-averaging, flow parameters such as flow velocities and velocity fluctuations, are averaged both in time and space. The concept of spatially-averaging was introduced by Wilson and Shaw (1977) to attempt to account for the suppression of turbulence by vegetation, as well as the extraction of momentum from the flow. For best results, averaging should be conducted over a large section to minimise the influence of the heterogeneity of the vegetation and background turbulence in the flow. The double-averaging approach was later formalised by Raupach and Shaw (1982). The concept is thought to be fundamental to the study of wake production, which is defined as the process of converting mean kinetic energy (*MKE*) and large scale turbulent kinetic energy already in the flow into turbulent kinetic energy (*TKE*) at the stem scale (Wilson and Shaw, 1977) (Section 2.2.3).

Instantaneous and time-averaged velocities can be defined as follows:

$$(u,v,w)=(\overline{u},\overline{v},\overline{w})+(u',v',w') \qquad \text{[Equation 2.21]}$$

$$(\overline{u},\overline{v},\overline{w})=(<\overline{u}>,<\overline{v}>,<\overline{w}>)+(\widetilde{u},\widetilde{v},\widetilde{w}) \qquad \text{[Equation 2.22]}$$

where u, v and w refer to the instantaneous longitudinal (x-direction), lateral (y-direction) and vertical (z-direction) velocity components respectively, $\overline{u}$, $\overline{v}$ and $\overline{w}$

are the time-averaged velocities, u', v' and w' are the fluctuating components of the time-averaged velocities, $<\overline{u}>$, $<\overline{v}>$ and $<\overline{w}>$ are the double-averaged velocities in time and space, $\widetilde{u}$, $\widetilde{v}$ and $\widetilde{w}$ are the spatial fluctuations of the respective time-averaged velocities.

Products of the fluctuating components give rise to terms that describe the shear stresses in the flow. These include the Reynolds stress, $-\rho<\overline{u'w'}>$, and the term, $-\rho<\overline{\widetilde{u}\,\widetilde{w}}>$, which has been coined the 'form-induced' stress (Gimenez-Curto and Corniero Lera, 1996), although it was originally referred to as the 'dispersive stress' by Wilson and Shaw (1977). The form-induced stress components $<\overline{\widetilde{u}}>$ and $<\overline{\widetilde{w}}>$ are a measure of spatial variation in time-averaged velocities and may serve as a measure of the spatial variation of the time-avaerged streamwise and vertical velocity components. For unidirectional flow, shear stress components acting along the *x-z* plane are the most significant. These will be discussed in Section 2.5.2.

2.3.2 Vertical Variability of Vegetation Canopies

The hydraulic resistance due to vegetation is dependant on plant morphology (the form and structure of a plant). In Figure 2-15, flow conditions that occur for different types of vegetation are illustrated in the form of schematic diagrams. For each situation, typical velocity profiles that may occur are shown. The shapes of the profiles reflect the level of physical obstruction at different depths within the flow field. For atmospheric flows, a reversal in the wind velocity gradient such as that illustrated in Figure 2-15 c and d has been observed in forest canopies (Shaw, 1977) resulting in a bulge in the velocity profile lower down in the canopy.

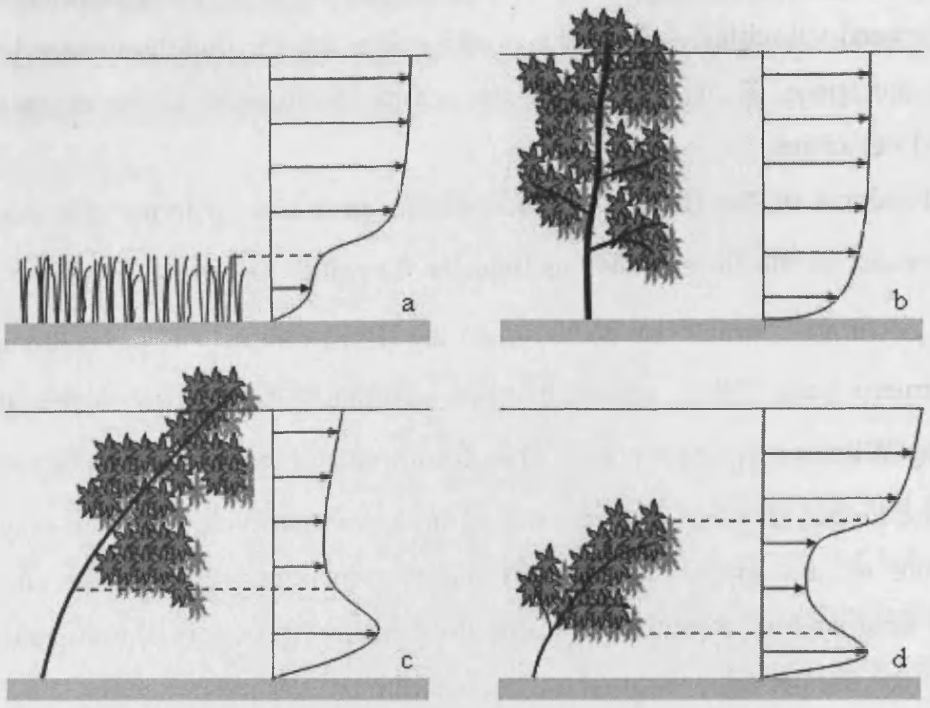

Figure 2-15. Flow conditions for different types of vegetation: a) submerged conditions, b) emergent conditions, c) emergent conditions with canopy and bottom flow, d) submerged conditions with canopy and bottom flow (taken from Bolscher *et al.*, 2005)

The vertical variation of vegetation also influences the turbulence structure. In a laboratory investigation, Anderson and Charters (1982) introduced both laminar and turbulent flows to a canopy of *Gelidium nudifrons*; a bushy aquatic vegetation species that grows on coastal rocks. For an initially laminar flow, turbulent vortices were generated downstream of vegetation fronds for flow velocities above a critical value (0.13 m s^{-1} for *Gelidium*) forming a vortex street, which was observed by releasing a tracer upstream of the canopy. The vortices formed at every frond, collectively leaving the canopy. Anderson and Charters (1982) proposed that this was the means for canopy-induced turbulence. For an initially turbulent flow, drag forces from the interaction with the fronds of the plants resulted in the absorption of energy from the flow, and hence, turbulence from the incoming flow was removed.

Neumeier (2005) investigated methods for the quantification of plant material and its vertical distribution within the canopy. Figure 2-16 shows some of his results. The lateral obstruction plots quantify the vegetation density and how it varies with elevation within the canopy. When compared to the measured velocities, the effects of the vertical distribution of plant material on the flow are evident, whereby with increasing elevation, as the vegetation obstruction decreases, the velocities increase.

There is also a significant increase in velocity above the canopy where there is no vegetation obstruction.

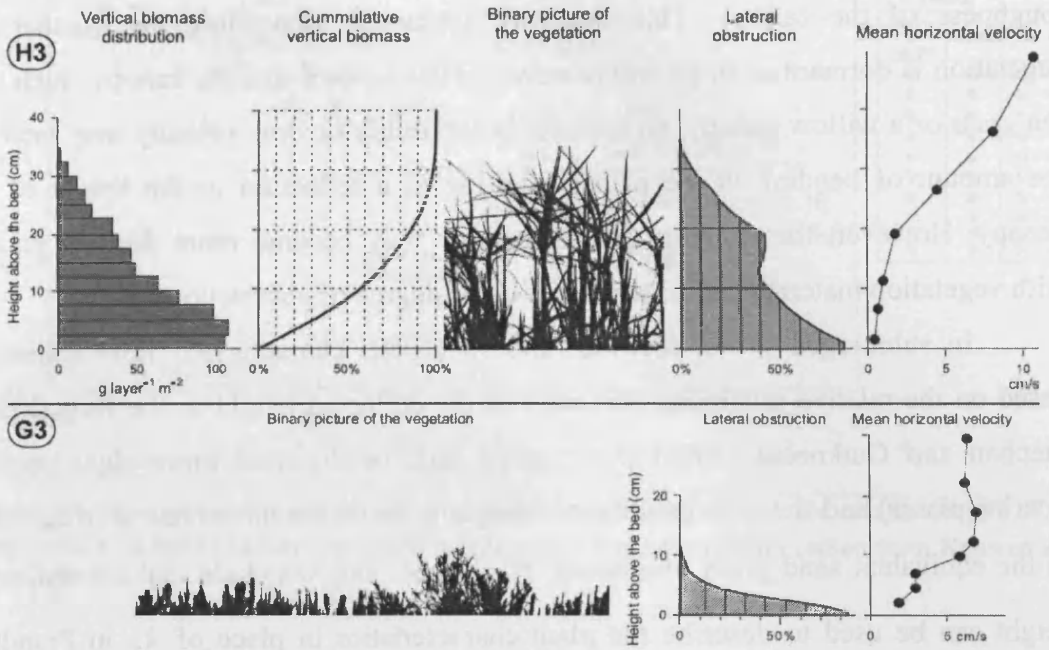

Figure 2-16. Examples of the vertical variation of vegetation obstruction for two different locations (H3: *Sp. anglica* marsh, G3: *Salicornia/ Suaeda marsh*). On the right hand side of the figure are examples of the velocity profiles measured at each location. (taken from Neumeier, 2005)

2.3.3 Effects of Vegetation Flexibility

Finnigan (1979) proposed that where a vegetation element displays some tendency to bend, oscillation will occur when turbulent eddies are released by upstream stems at a similar frequency to the relaxation period of the stem causing it to resonate. Oscillation may be magnified when a stem vibrates rapidly due to the vortex street of an upstream wake (Blevins, 1977). This may contribute to a further augmentation of turbulence levels as the oscillating stems effectively absorb kinetic energy from the flow, and release it as turbulent kinetic energy half an oscillation cycle later (Ackerman and Okubo, 1993). This was observed by Ackerman and Okubo (1993) in a *Zostera marina* canopy (a type of sea grass), whereby large turbulent eddies entering the canopy were broken down and their energy was absorbed by the vegetation resulting in an oscillation of the vegetation stems and smaller scale eddies formed due to 'mechanical' turbulence from the vibrating vegetation. The production of turbulence is accompanied by energy dissipation,

whereby turbulent kinetic energy is converted to other energy forms, such as heat (Raupach and Thom, 1981).

The flexibility of natural vegetation may also influence the hydraulic roughness of the canopy. This can vary seasonally depending on whether the vegetation is dormant or in growth (Kouwen, 1988). For a flexible canopy, such as a sea grass or a willow canopy, an increase in flexibility or flow velocity may increase the amount of bending in the plants resulting in a reduction in the height of the canopy. However, the resulting shorter canopy may become more densely packed with vegetation material and in turn increase the degree of obstruction.

In submerged flows, Kouwen and Li (1980) characterised flow resistance based on the relative roughness (the ratio of the deflected height to the flow depth). Stephan and Gutknecht (2002) investigated this for different macrophyte species (marine plants) and showed the deflected height to be of the same order of magnitude as the equivalent sand grain roughness, k_S. Hence, they conclude that the deflected height can be used to describe the plant characteristics in place of k_S in Prandtl's logarithmic law (Section 2.1.2) to predict the velocity profile above the canopy.

Kouwen and Unny (1973) linked the stiffness of a vegetation canopy to the hydraulic roughness by introducing the *MEI* parameter to characterise the vegetation's resistance to deformation under different flow conditions, where M is the stem density, and the product of E, the Young's modulus of elasticity, and I, the second moment of area is equivalent to the vegetation's flexural rigidity. The researchers created simulated vegetation covers using flexible plastic strips of different thicknesses and material to vary the average stiffness of the canopies, which ranged for the flow conditions implemented between 'erect', 'waving' and 'prone' states. In Figure 2-17, the Manning's roughness coefficient, n, is plotted against the product of the flow velocity, U, and the hydraulic radius, R. The plot effectively shows the relationship between the Manning's roughness coefficient and the Reynolds number. The magnitudes of n were similar where the ratio of the apparent vegetation height, z'', to the flow depth, D, was similar. The findings highlight the importance of the deflected height of the vegetation in characterising the bed roughness.

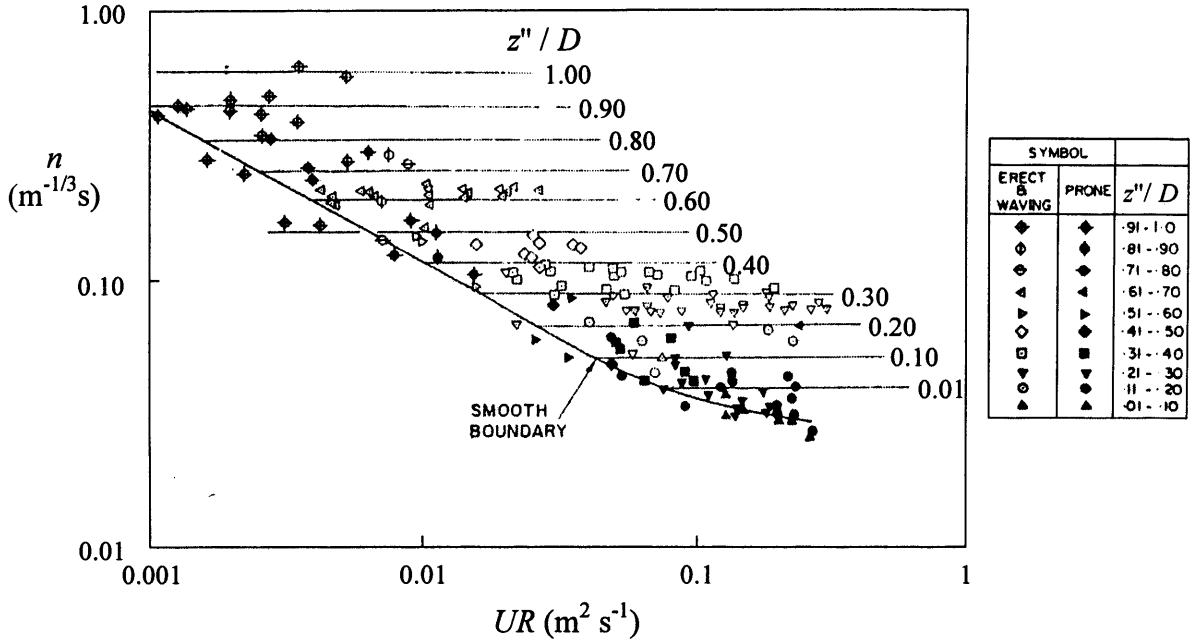

Figure 2-17 Variation of the Manning's roughness coefficient, *n*, with the relative height of the roughness. *z*'' is the apparent vegetation height, and *h* is the flow depth (taken from Kouwen and Unny, 1973)

Kouwen (1988) suggests collective consideration of the components of *MEI* as a single parameter as they are often difficult to determine individually due to the high variability in natural vegetation. The researcher determined *MEI* estimates in field conditions through a 'drop board' method, whereby a board of known weight and dimensions was allowed to fall onto the vegetation and the amount of compression within the vegetation was used to characterise its physical properties. This was achieved by comparison with the compressions resulting from dropping the board on a number of grass linings of known *MEI* values, which were determined by the author from flow resistance data. The researcher showed there is a strong correlation between *MEI* and the non-compressed vegetation height.

Vegetation canopies are often simulated in laboratory studies using rigid uniform cylinders (e.g. Dunn *et al.*, 1996; Nepf *et al.*, 1997a; Nepf *et al.*, 1997b; Fairbanks, 1998; Nepf, 1999 and others). Such models usually aim to depict stiff vegetation, which simplifies the complex morphological structure of plant canopies by avoiding the influence of vegetation flexibility on hydraulic resistance. Flexible canopies were simulated using flexible elements in a number of studies (e.g. Kouwen *et al.*, 1969; Kouwen and Unny, 1973; Dunn *et al.*, 1996; Nepf and Vivioni, 2000; Ghisalberti and Nepf, 2002 and others). The vertical variability of vegetation flexibility was also considered in some studies. Nepf and Vivioni (2000) fitted

flexible strips above a rigid cylinder base to simulate the more flexible upper region of the canopy, whilst Wilson *et al.* (2003) used flexible rods with and without frond attachments to simulate the larger momentum absorbing surface area associated with the increase in leaf content at higher elevations. The increase in projected area resulted in a greater reduction in flow velocities. The fronds also altered the transfer of momentum between flow within the canopy and the surface-flow layer, and thus, the flow structure varied significantly over the flow depth between the two scenarios.

2.3.4 Effects of Submergence

The hydraulic roughness of a vegetation cover is strongly dependent on the level of submergence of the vegetation as the velocity and turbulence structure through the canopy vary significantly between the emergent and the submerged states, and continue to vary with increasing submergence. This was shown by Wu *et al.* (1999) in a study whereby they proposed that the bushes and shrubs found on wetlands could be simulated using a horsehair mattress. Although the horsehair mattress created a porous medium for the investigation, there is no structural relationship between the mattress and the vegetation. In Figure 2-18a, flow velocities and roughness coefficients for various flow depths are presented for four canopy heights: 15, 30, 45 and 60 mm, and a bed gradient of 0.01025 under both emergent and submerged conditions. The researchers derived an expression for Manning's roughness coefficient, n, by equating the standard drag equation (Equation 2.19) to the Manning's equation (Equation 2.01) for uniform flow conditions:

$$n = \left(\frac{D^{2/3}}{\sqrt{2g}}\right)\sqrt{\overline{C_D}'} = \left(\frac{D^{2/3}}{\sqrt{2g}}\right)\sqrt{\overline{a}\overline{C_D}} \qquad \text{[Equation 2.23]}$$

$$n = \left(\frac{D^{1/6}T^{1/2}}{\sqrt{2g}}\right)\sqrt{\overline{C_D}'} = \left(\frac{D^{1/6}T^{1/2}}{\sqrt{2g}}\right)\sqrt{\overline{a}\overline{C_D}} \qquad \text{[Equation 2.24]}$$

for emergent and submerged conditions respectively where D is the flow depth, $\overline{C_D}'$ is the bulk roughness coefficient (Section 2.2.6), $\overline{a}$ is the projected area per unit volume of the canopy, $\overline{C_D}$ is the bulk drag coefficient, g is the gravitational

acceleration, S_0 is the bed gradient and for submerged conditions, T is the vegetation height which is characteristic of the canopy roughness..

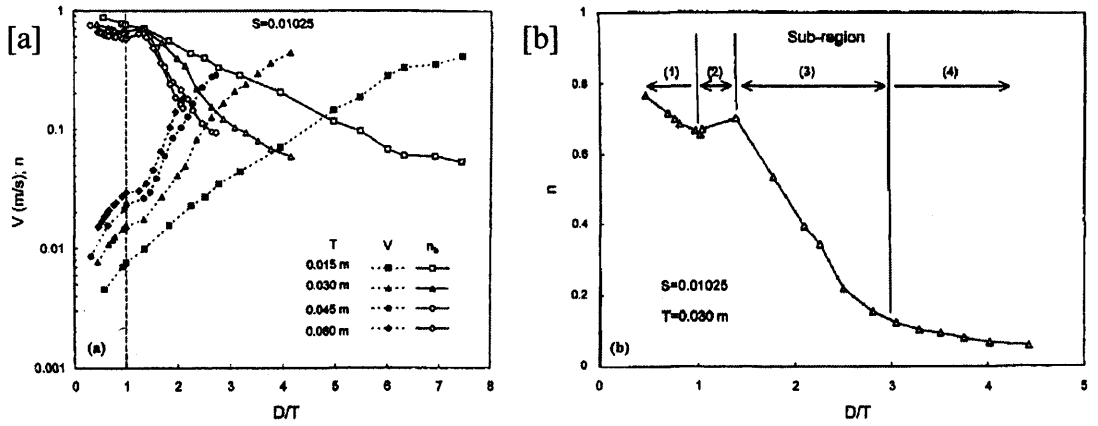

Figure 2-18 - (a) Variations of flow velocity and Manning's roughness coefficient, *n*, with Flow Depth, *D*, for various vegetation heights, *T*, and a bed slope of 0.01025; (b) Four sub regions of the *n* curve (taken from Wu *et al.*, 1999)

Wu *et al.* (1999) proposed that the shape of the Manning's roughness coefficient curve can be characterised into four regions according to the extent of submergence as shown in Figure 2-18b. For emergent conditions (Region '1'), the submerged part of the canopy, and hence, the hydraulic resistance increases with flow depth causing a reduction in flow velocity. The relative increase in flow depth compared to flow velocity results in an apparent decrease in the Manning's roughness coefficient, *n*.

For submerged conditions, a shear layer arises around the canopy-surface flow layer interface (Section 2.5.1). For low submergence levels (below 1.4 and corresponding to Region '2'), an increase in flow depth results in a relatively low increase in velocity. In Region '3', the longitudinal weight component of flow exceeds the shear force along the interface, flow velocity increases, and the roughness coefficient decreases. As the submergence level increases further (Region '4'), the roughness coefficient converges towards an asymptotic value specific to each canopy (Wu *et al.*, 1999). Kadlec (1990) presented similar trends based on the roughness coefficient, $\overline{C_D}'$ (Section 2.2.6) for different canopies (Figure 2-19).

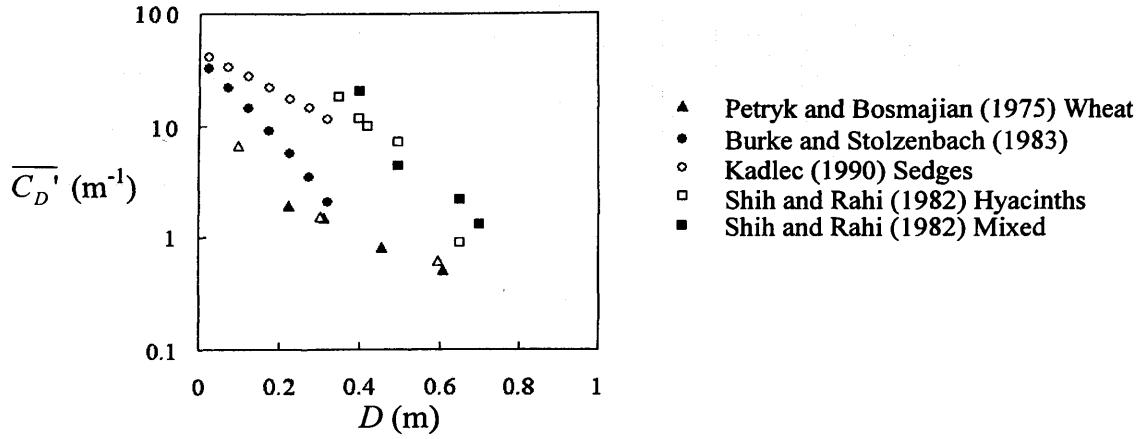

Figure 2-19 The exponential decrease in the vegetation resistance coefficient, $\overline{C_D'}$, with flow depth, D, for a range of vegetation types from various studies (taken from Kadlec, 1990)

2.3.5 A One-Dimensional Drag Coefficient

For vegetated conditions, friction along the bed and the walls of the flume are considered negligible in comparison to the drag force due to the vegetation. Therefore, for emergent vegetation, and under uniform flow conditions (Section 2.1.3), the weight component of the water body acting along the bed slope, F_G, must equate to the drag force due to the vegetation, F_D (Figure 2-20):

$$F_D = F_G \qquad \text{[Equation 2.25]}$$

$$\frac{1}{2}\rho A_p \overline{C_D} U_C^2 = \rho TBLg \sin\theta \qquad \text{[Equation 2.26]}$$

$$\frac{1}{2}\rho\, \bar{a}\overline{C_D} U_C^2 = \rho g \sin\theta \qquad \text{[Equation 2.27]}$$

$$\overline{C_D} = \frac{2g\sin\theta}{\bar{a}U_C^2} \qquad \text{[Equation 2.28]}$$

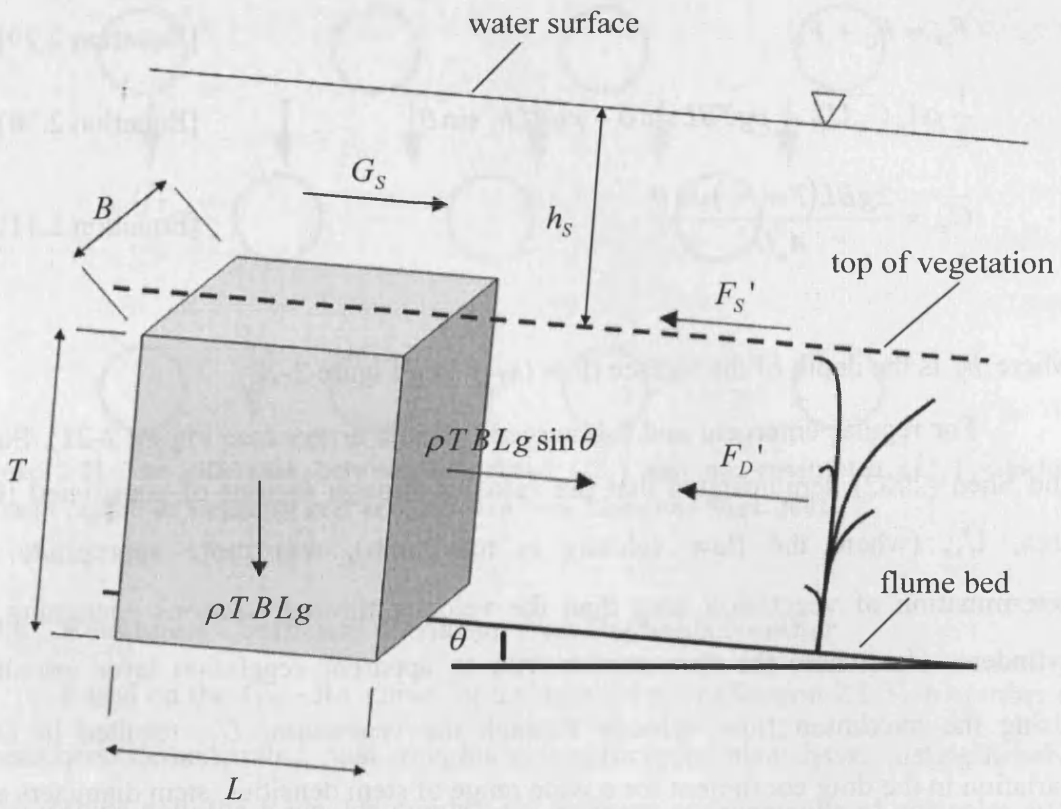

Figure 2-20 Body force diagram for uniform flow through a vegetation canopy, where F_D' is the drag force balancing the weight component of the flow through the vegetation layer, G_S is the gravitational force component due to the surface flow layer along the flow plane and F_S' is the shear force along the top of the canopy balancing the weight component of the surface flow layer.

where $\overline{C_D}$ is the bulk drag coefficient, ρ is the fluid density, T is the height of the emergent vegetation canopy, B and L are the lateral and longitudinal dimensions of the flow volume (see Figure 2-20), U_C is the depth-averaged velocity, θ is the angle formed between the bed and the horizontal, A_p is the total projected area of obstruction, and $\overline{a}$ is the projected area of obstruction per unit volume. It is important to note that when applying this formula to groups of cylinders or natural vegetation, the projected area of the vegetation refers to the total plant material area and includes the 'hidden' cylinders or 'hidden' plant material behind the cylinder or plant material directly in contact with the flow. Fathi-Maghadam and Kouwen (1997) commented on the significance of 'hidden' vegetation, the area of which plays a significant role in momentum absorption. For submerged conditions, a shear force, F_S, arises along the canopy-surface flow layer interface to balance the gravitational force, G_S, due to the surface layer (Wu *et al.*, 1999) (Figure 2-20). The force balance becomes:

$$F_D = F_G + F_S \qquad \text{[Equation 2.29]}$$

$$\frac{1}{2}\rho A_p \overline{C_D} U_C^2 = \rho g T B L \sin\theta + \rho g B L h_S \sin\theta \qquad \text{[Equation 2.30]}$$

$$\overline{C_D} = \frac{2gBL(T + h_S)\sin\theta}{A_p U_C^2} \qquad \text{[Equation 2.31]}$$

where h_S is the depth of the surface flow layer (see Figure 2-20).

For regular emergent and submerged cylinder arrays (see Figure 2-21), Stone and Shen (2002) demonstrated that the velocity through regions of constricted flow area, U_1, (where the flow velocity is maximum), was more appropriate for determination of vegetation drag than the velocity through sections containing no cylinders, U_2 (where the flow moves with an apparent vegetation layer velocity). Using the maximum flow velocity through the vegetation, U_1, resulted in little variation in the drag coefficient for a wide range of stem densities, stem diameters and Reynolds numbers. Substitution for the average vegetation layer velocity, U_2, yielded a wide range of drag coefficient values for the same range of flow and canopy conditions. Under such circumstances, the depth-averaged velocity, U, in Equations 2.24 and 2.27 must be defined carefully. However, for high stem densities implemented in vegetation studies (e.g. 200 to 2000 stems m^{-2} in Nepf (1999) and 800 to 1610 stems m^{-2} in current study), it is difficult to distinguish between constricted and non-constricted regions as a number of stems had to be removed to accommodate an Acoustic Doppler Velocimeter (ADV) head. An ADV is an instrument that measures flow velocity and turbulence data through the Doppler principle. This is discussed in more detail in Section 5.2.7.

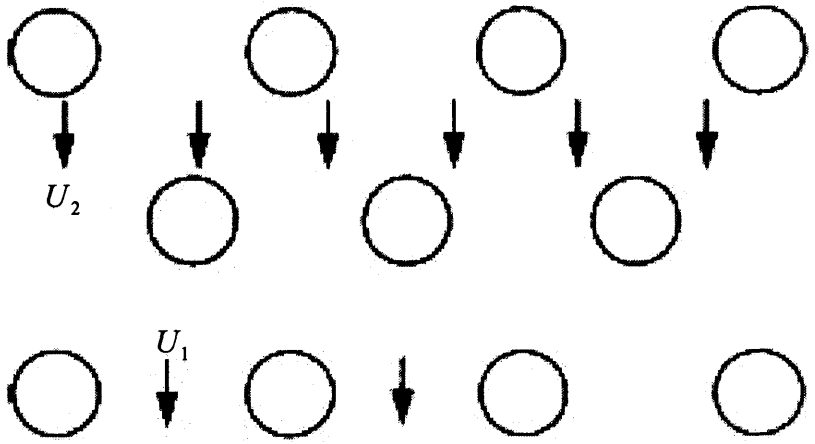

Figure 2-21 The difference between constricted (U_1) and non-constricted (U_2) velocities through regular or staggered grid arrays (taken from Stone and Shen, 2002)

2.3.6 Roughness Coefficient Variation with Reynolds Number

Based on the $C_D - \mathrm{Re}$ curve for a single cylinder (Section 2.2.3), a number of researchers demonstrated that roughness coefficients also have distinguishable relationships with the Reynolds number for different arrangements of obstacles such as arrays of cylinders, plastic strips (e.g. Kouwen *et al.*, 1969), grass beds (e.g. Ree and Palmer, 1949), or horsehair mattresses as used by Wu *et al.* (1999). Ree and Palmer (1949) introduced the *n-UR* design curves whereby the Manning's roughness coefficient was plotted against the product of the flow velocity, *U*, and the hydraulic radius, *R*. The product parameter (*UR*) is equivalent to the Reynolds number and the plots show the variation in Manning's roughness coefficient depending on the level of turbulence in the flow. The shape and position of each plot was unique to the bed roughness, and as such, provided that the bed roughness can be characterised and matched to one of the curves, the resistance properties can be predicted for different flow conditions. As with the *n-UR* curves, the $C_D - \mathrm{Re}$ curves may reach asymptotic values at higher Reynolds numbers (Wu *et al.*, 1999). This can be seen in the standard $C_D - \mathrm{Re}$ curve for a single cylinder above a stem Reynolds number of 10^3 where the curve converges towards a drag coefficient value of unity (Section 2.2.3).

Wu *et al.* (1999) produced plots of $\overline{C_D}' - \mathrm{Re}_T$, where $\overline{C_D}'$ is the roughness coefficient (Section 2.2.6), and Re_T is the canopy height Reynolds number for different types of vegetation cover. When using the vegetation height as the turbulence length scale, the flow structure can be characterised as laminar for a

Reynolds number below 500, transitional up to a value of 12,500, above which the flow becomes fully turbulent (Kadlec, 1990). Figure 2-22 shows the plot produced by the researchers for emergent canopies of different types of grasses and a horsehair mattress used by Wu *et al.* (1999) to simulate a dense vegetation cover. The plots, which are presented along logarithmic axes, suggest that similar vegetation types result in log-plots with similar gradients (or exponents if non-logarithmic axes are used), and a decrease in bed gradient results in a vertical shift in the positions of the plots towards the *x*-axis. Tsihrintzis *et al.* (2001) produced a similar plot incorporating a wider range of conditions, such as bed gradients, vegetation types and a greater Reynolds number range up to 240000, and this is reproduced here in Figure 2-23. Both plots are based on the data reported in the studies listed in Table 2-1.

For the range of Reynolds numbers examined in the studies presented in Figure 2-22 and Figure 2-23, the decrease in $\overline{C_D}'$ with increasing Re_T was exponential. The relationship between the two parameters, as proposed by Wu *et al.* (1999), can be represented as follows:

$$\overline{C_D}' \propto \mathrm{Re}_T^{-k} \qquad \text{[Equation 2.32]}$$

where Wu *et al.* (1999) suggested the exponent, k, is specific to the vegetation type. k is a useful parameter because it enables the calculation of the bulk roughness coefficient for a given Reynolds number.

For the dense wheat crops studied by Turner and Chanmeesri (1984), the values of k ranged between 0.33 and 0.52 for bed gradients between 0.002 and 0.003. These were lower in magnitude than the k values for the canopies examined by Chen (1975) and Kadlec (1990) at similar Reynolds number ranges (see Table 2-1). For the natural turf surface examined by Chen (1975), k was around 1.5 for bed gradients between 0.001 and 0.316. For the sedge cover studied by Kadlec (1990), k ranged between 1.15 and 1.26 for bed gradients between 0.000001 and 0.001. For the horsehair mattress used by Wu *et al.* (1999), k was around unity for bed gradients between 0.00383 and 0.041.

Table 2-1 Details of studies considered in Figure 2-22 & Figure 2-23.

Study	Study Type	Reynolds Numbers Re_T (-)	Flow Regime as defined by Kadlec (1990)	Roughness Surface	k (-)
Chen (1976)	Lab	$100 < Re_T < 30000$	Laminar, Transitional & Turbulent	Natural turf surfaces	1.33
Chiew & Tan (1992)	Field	$400 < Re_T < 2000$	Laminar & Transitional	2 densities of Cow grass (*Axonopus Compressus*). To achieve dense cover, vegetation was allowed to grow for one month	0.98 – 1.04
Fathi-Maghadam & Kouwen (1997)	Lab	$5000 < Re_T < 240000$	Transitional & Turbulent	Pine & cedar tree saplings	0.20 – 0.77
Hall & Freeman (1994)	Lab	$5000 < Re_T < 30000$	Transitional & Turbulent	Reeds (400 & 800 stems m^{-2})	1.03 – 1.16
Kadlec (1990)	Field	$1 < Re_T < 10000$	Laminar & Transitional	Sedge cover. Bed slopes = 0.001, 0.0001, 0.00001, 0.000001	1.15 – 1.26
Ree & Palmer (1949)	Lab	$3000 < Re_T < 10000$	Transitional	Natural turf surfaces	1.4
Turner & Chanmeesri (1984)	Lab	$200 < Re_T < 10000$	Laminar & Transitional	Wheat crops. Densities (stems m^{-2}): A = 2190, B = 1650, D = 1650, E = 1630, G = 1020, H = 1020. Bed slopes: A = 0.002, B = 0.002, D = 0.0025, E = 0.0028, G = 0.003, H = 0.0027	0.33 – 0.52
Wu *et al.* (1999)	Lab	$20 < Re_T < 3000$	Laminar & Transitional	Horsehair mattress	1.00

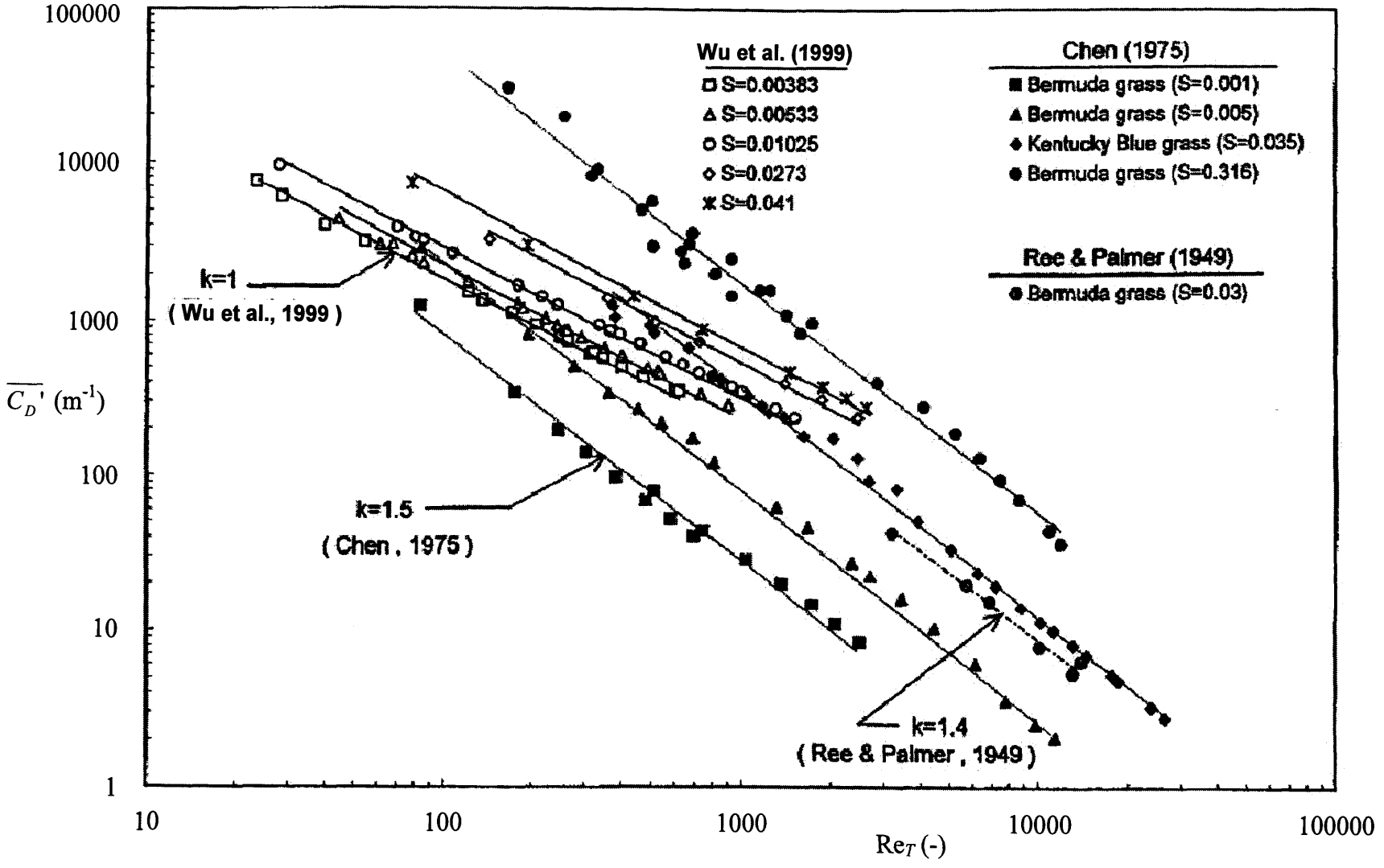

Figure 2-22 Relationship between the bulk roughness coefficient and the canopy Reynolds number for emergent conditions (taken from Wu *et al*, 1999). Data from current study included.

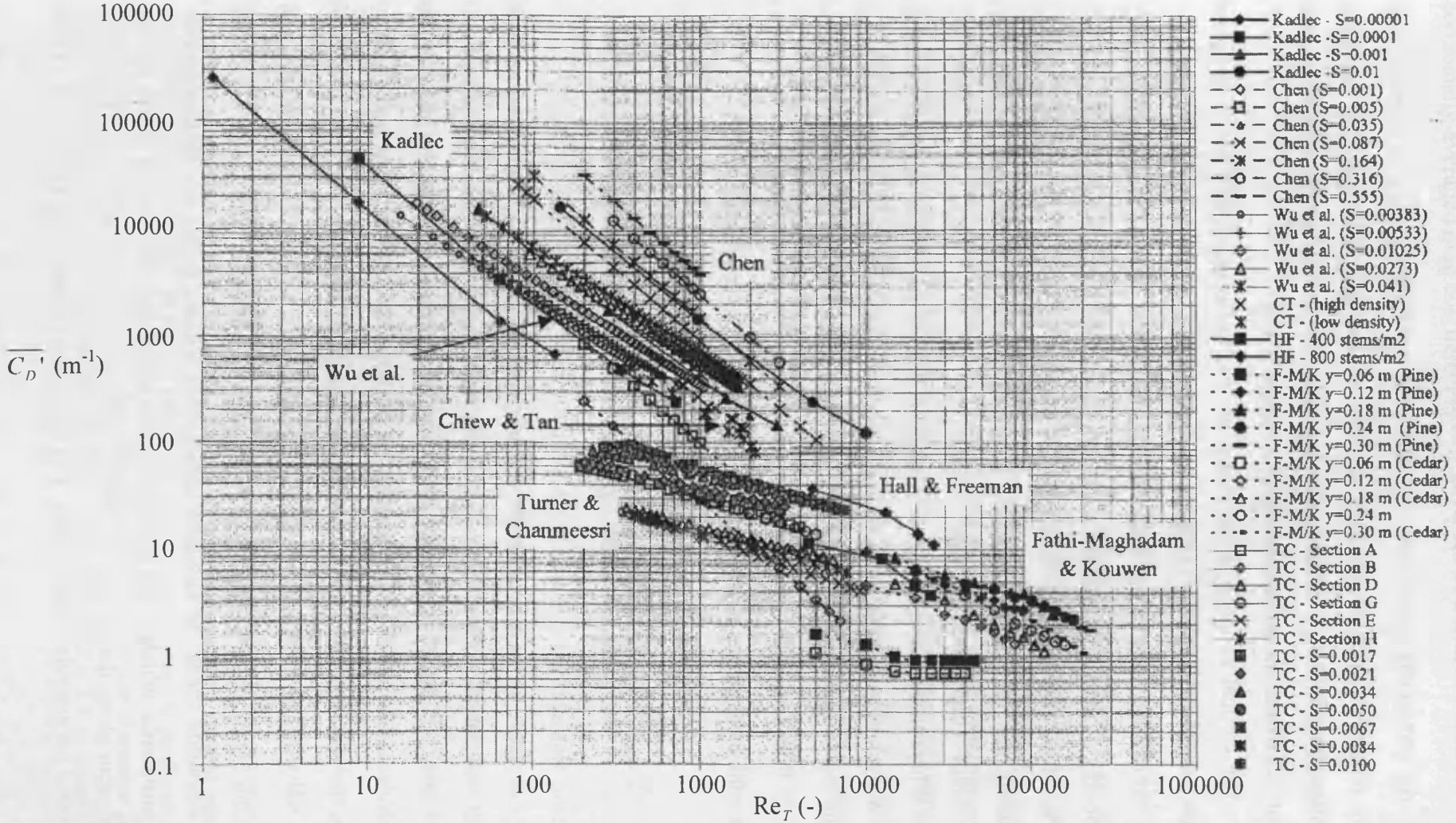

Figure 2-23 Relationship between the roughness coefficient and the canopy Reynolds number for Emergent Conditions (taken from Tsihrintzis *et al.*, 2001). Data from current study included.

2.3.7 Vertical Variation of the Drag Coefficient

As previously discussed, the bulk drag coefficient, $\overline{C_D}$, is dependant on canopy properties such as the level of wake sheltering (Section 2.2.5), vegetation flexibility (Section 2.3.3), submergence level (Section 2.3.4), the quantity of material (Section 2.2.6) and its vertical variability (Section 2.3.2).

The vertical variation in the drag force due to the vegetation was investigated in more detail by Dunn *et al.* (1996), who defined a two-dimensional drag coefficient, $C_{D\,2D}$, which can vary in the longitudinal and vertical directions depending on the morphology of the vegetation and the canopy structure. For emergent vegetation, it is often assumed that the drag coefficient is constant over the height of the canopy presuming the vertical variation in projected area of obstruction is "relatively insignificant" (Lightbody and Nepf, 2006a).

Where there is considerable variation in vertical vegetation structure, or where the flow dynamics become more complex for submerged conditions due to the shear near the top of the canopy (Section 2.3.4), Dunn *et al.* (1996) derived an expression for $C_{D\,2D}$ from the x-direction momentum equation. This is rewritten to include terms for the total shear stress, τ, and the drag force due to the vegetation:

$$\frac{\partial u}{\partial t}+u\frac{\partial u}{\partial x}+w\frac{\partial u}{\partial z}=-\frac{1}{\rho}\frac{\partial P}{\partial x}+\frac{1}{\rho}\frac{\partial \tau}{\partial z}+gS_0-\frac{1}{2}C_{D\,2D}au^2 \qquad \text{[Equation. 2.33]}$$

where t is time, u, v and w are the instantaneous longitudinal, lateral and vertical velocity components respectively, x and z are distances along the longitudinal and vertical axis, P is pressure, τ is the total shear stress, which includes the bed, viscous and turbulent shear stresses, g is the gravitational acceleration, S_0 is the bed gradient, and a is the projected area per unit volume occupied by the plants.

Substituting the velocity terms in Equation 2.32 to include time-averaged and fluctuating components (Section 2.3.1) gives rise to a product term ($-\rho\overline{u'w'}$) known as the Reynolds stress (or turbulent stress). This equates to the momentum transfer due to turbulence which is the Reynolds stress associated with the x-z plane. Similar stresses occur along the x-y and y-z planes, although for steady uniform unidirectional flows, these are considered negligible. The derivation presented by Dunn *et al.* (1996)

is summarised in Appendix I, and the expression for the two-dimensional horizontally-averaged drag coefficient is:

$$C_{D\,2D} = \frac{gS_0 - \frac{d}{dz}\left(\overline{u'w'}\right)}{\frac{a}{2}\overline{u}^2} \qquad \text{[Equation 2.34]}$$

In the formulation developed by Dunn *et al.* (1996), the drag force was added independently to the conservation of momentum equation as a body force. Wilson and Shaw (1977) argue that whilst this will achieve a representative momentum balance, the equation cannot be used to examine the complex turbulent structures of the flow. They argue that to achieve this, the general stress equation, which is derived from the conservation of momentum equation, must be examined. The stress equation contains higher-order terms that have been associated with various processes including wake production, turbulent kinetic energy production and transport by a number of researchers (e.g. Wilson and Shaw, 1977; Raupach and Shaw, 1982; López and García, 1997; Finnigan, 2000 and others).

2.4 Velocity Profiles through Real Vegetation Canopies

2.4.1 Laboratory Studies of Flow through *Spartina* Canopies

Due to the difficulties of working in field conditions, a considerable number of studies on natural vegetation have been carried out in the laboratory, under controlled conditions. This is useful for investigating the complex flow dynamics that are influenced by many factors, such as the vegetation height, density, structure, flow depth, bed slope and the Reynolds number of the flow. Some of the difficulties associated with working under field conditions are discussed briefly in Section 2.4.2.

Pethick *et al.* (1990) attempted to investigate the flow processes that occur within saltmarsh canopies that may be linked to the failure of the vegetation to colonise the mudflats adjacent to the marsh. *Sp. anglica* was planted in vast quantities across the Humber estuary between 1940 and 1962. At the time of publication, the authors reported that the vegetation was concentrated in two-metre diameter patches located in 'hollows' in the surrounding mudflat. They installed a 5.5 m length of *Sp.*

anglica in a laboratory flume (0.3 m wide and 7.5 m long). The vegetation was collected during late summer with an average height of 0.45 m and installed at a stem density of 400 stems m^{-2} in a regular grid formation. Estuarine water containing sediment of known concentration and particle sizes (150 ppm and 10-100 μm respectively) was allowed to flow through the vegetation at a depth of 0.4m and a velocity of 0.05 ms^{-1}. The researchers measured a series of velocity profiles within the vegetation.

The flow was characterised by a two-stage velocity profile consisting of a lower, and an upper profile, separated by a discontinuity. In the upper profile, shear stresses were greater than the critical values required to maintain suspension for sediment transport. Critical shear velocity values are dependant on the particle size and density because heavier particles require a greater shear stress for them to remain suspended. In the lower profile, much lower shear stresses were achieved, and hence, settling of sediments occurred more readily. Pethick *et al.* (1990) suggest that the total amount of suspended sediments can be related to the height of the water column (the total flow depth), although they argue that the height of the sub-layer (the lower region of the water column where shear stresses are sub-critical) is more important.

Shi *et al.* (1995) investigated the effects of *Sp. anglica* on flow dynamics whereby vegetation samples collected were chopped down to 0.3m, equal to the average height of the canopies measured in the Humber estuary. These were used to cover a 2.0m length of a flume at a stem density of 350 stems m^{-2}. The experiments were conducted with the vegetation at 20%, 40%, 60%, 80% and 100% of its original height by cutting part of the canopy to investigate the velocity profiles for different levels of submergence. The experiments were conducted at area mean flow velocities not exceeding 0.051 ms^{-1} corresponding to the mean value measured by the researchers in the field and within a range of stem Reynolds numbers between 110 and 200. Velocity profiles from the experiments, which were measured at a distance of 1.3m from the leading edge of the canopy, are presented in Figure 2-24.

At the lower submergence levels (1.160 and 1.442), Shi and his fellow workers compared the profile shapes to an 'S' shape due to a maxima arising around the mid-canopy depth, and minima near the top of the canopy. This feature was not observed at submergence levels of 1.88 or greater highlighting the problems associated with the scaling method implemented to achieve higher submergence levels. For a submergence level of 1.16, the vegetation was in its natural form, and for

1.44, only 20% of the vegetation had been cut from the top of the plants. The 'S' shaped profiles were attributed to higher levels of obstruction associated with greater foliage content in the upper part of the canopy, although they may be associated with the non-uniform flow conditions under which the study was conducted. The authors concluded that the velocity gradient-reversal is a feature of flow within a saltmarsh canopy. This feature was not visible in flow through submerged uniform cylinder arrays (e.g. Dunn *et al.*, 1996; López and García, 1997; Fairbanks, 1998; Finnigan, 2000 and others). A semi-logarithmic profile was also observed above the canopy.

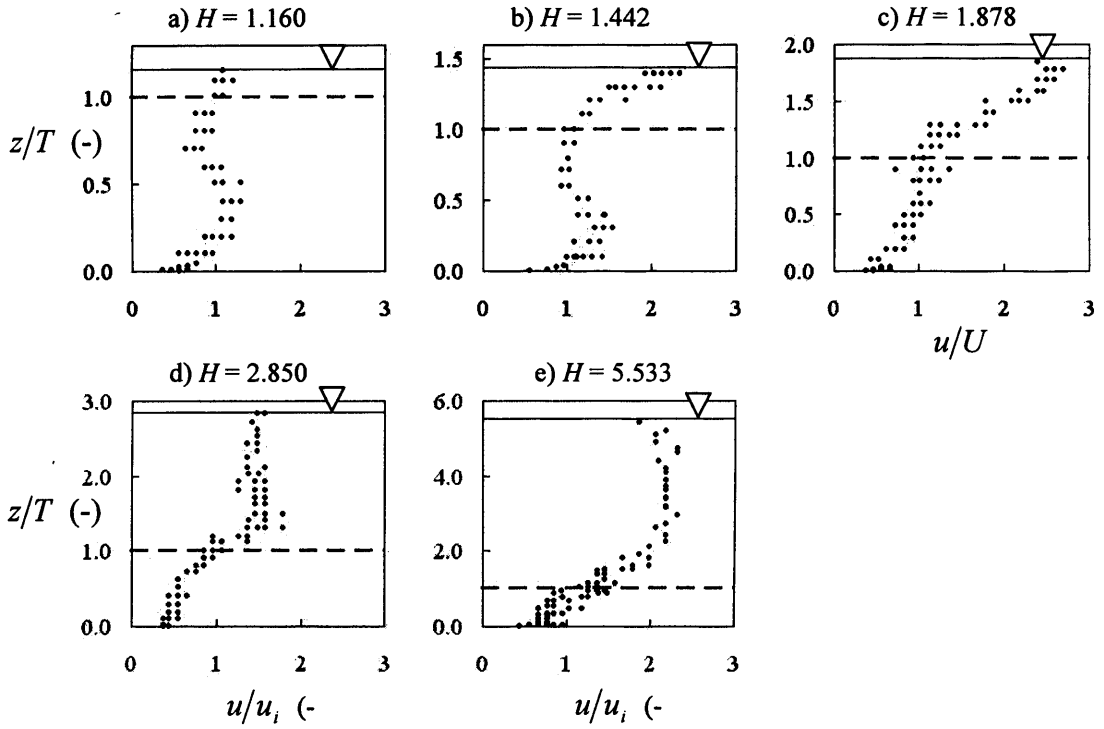

Figure 2-24 Longitudinal velocity profiles for experiments of flow through submerged *Spartina anglica* conducted by Shi *et al.* (1995) for submergence levels of 1.16, 1.44, 1.89, 2.85 and 5.53. The dashed lines indicate the top of the vegetation. Five velocity profiles over five different heights of canopy were measured. H is the submergence level, z is the elevation, T is the canopy height, u is the longitudinal velocity and u_i is the mean longitudinal velocity at the canopy-surface flow layer interface. Plots reproduced from Shi *et al.* (1995).

In an extension to their previous study, Shi *et al.* (1996) considered a greater range of stem densities (133, 200 and 350 stems m^{-2}) based on measurements along the Humber estuary, and linked the vertical velocity profile and associated shear velocity in and above *Sp. anglica* to the deposition of cohesive suspended sediments. Velocity profiles were measured at three different distances from the leading edge of

the canopy (0.7m, 1.2m and 1.7m) to monitor the development of the profile shape with distance into the vegetated region.

A higher stem density resulted in a greater velocity reduction and a smaller bed shear stress, which the authors suggest, may enhance the deposition of cohesive suspended sediments. They proposed that the distribution of suspended sediments was also affected by the morphology of the plants as their stems and leaves can trap or retain suspended particles.

The laboratory studies discussed above were conducted under non-uniform flow conditions (Section 2.1.3). Although this is more representative of field conditions, the influence of the vegetation on flow dynamics is more difficult to evaluate due to the significance of the hydrostatic pressure term in the conservation of momentum equation (Section 2.1.4). Furthermore, variation in velocity profiles with distance from the leading edge of the canopy is usually assumed to be solely due to the development of the boundary layer and hence the separate effects of the heterogeneity of the vegetation are difficult to assess.

2.4.2 Field Measurements of Flow through Saltmarsh Canopies

Although laboratory studies are useful for evaluating flow through vegetation under controlled conditions, it is difficult to recreate the complexity of a vegetation canopy in the natural environment. For reconstructed laboratory models, plants are often cleaned, trimmed and arranged evenly along a flume section. Furthermore, it is difficult to examine the vegetation under fully submerged conditions, a condition that commonly occurs along coastal wetlands, since laboratory flumes are often too shallow to achieve this without cutting down the vegetation and altering its structure. Most of the studies presented in this section focus on the collection of field data to improve the understanding of flow characteristics and mechanisms through saltmarsh vegetation.

Field studies on flow through saltmarsh canopies have been very limited due to the difficulties associated with working on coastal wetlands. The velocities encountered are extremely low, usually between 0.5 and 5.0 cm s^{-1} such that a high spatial resolution of readings is necessary (Neumeier and Ciavola, 2004) to detect the influence of the vegetation cover on velocity and turbulence characteristics. Also, tidal currents are extremely variable, and measurements need to be collected in a short

space of time, whilst the surrounding vegetation and cohesive substrate must not be disturbed during the installation and usage of the measuring equipment. Furthermore, most of the data collected relates to sites similar in characteristics in terms of low tidal ranges and dominating vegetation species, usually *Spartina alterniflora* or *Juncus roemerianus* (Leonard and Reed, 2002). UK based studies have focused on a species similar to *Spartina alterniflora*, namely *Spartina anglica* which is common along British coastal saltmarshes (e.g. Neumeier, 2005; Neumeier and Amos, 2004).

Leonard and Luther (1995) measured flow velocities in and above canopies of *Spartina alterniflora*, *Juncus roemerianus* and *Distichlis spicata*. The researchers used hot-film anemometry probe arrays to monitor velocity characteristics, and recorded the highest flow velocities during the flooding and the ebbing of the tide, although values were generally below 0.1 ms^{-1}, and the flow was usually within the transitional range. The velocity profile shapes were non-uniform over the height of the vegetation, and were closely linked to the morphology of the vegetation (Figure 2-25). *Distichlis spicata* was more consistent in structure over the height of the canopy, whereas *Juncus roemerianus* consists of a denser foliage region that commences around 50mm above the bed, which the authors attributed to a minimum velocity occurring around 100 mm above the bed.

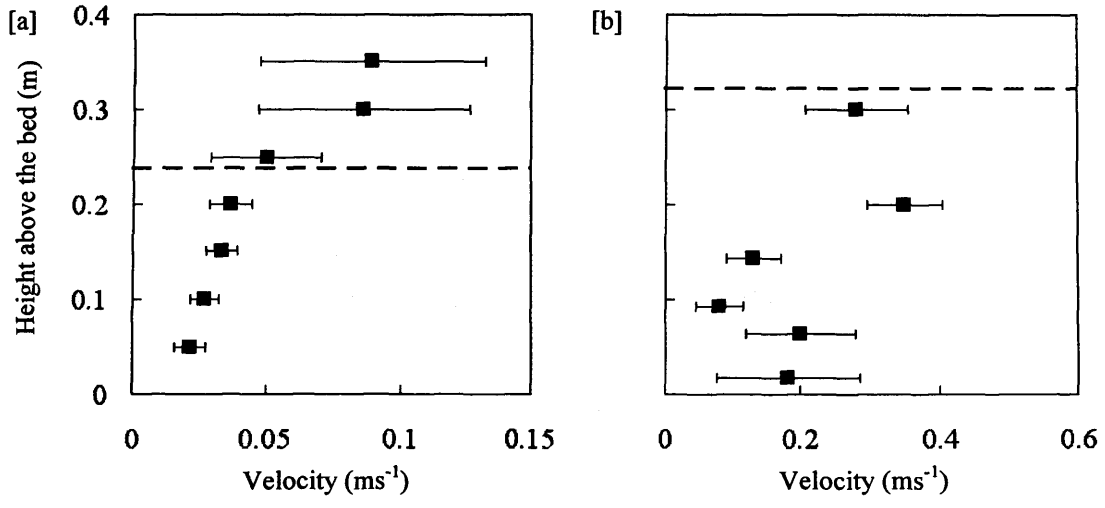

Figure 2-25 Velocity Profiles through (a) a submerged *Distichlis spicata* canopy, and (b) and emergent *Juncus roemerianus* canopy (reproduced from Leonard & Luther, 1995)

During the slack water (the period between the flood and the ebb), flow velocities were considerably lower. Saltmarshes prone to two types of tidal conditions

were investigated by the authors: semidiurnal, where high tides (as well as low tides) occur twice during a tidal day and slack water was defines as periods when velocities were below 0.005 ms^{-1}; and diurnal, where only one high tide occurs during a tidal day and the minimum recorded velocities were around 0.0075 ms^{-1}. Furthermore, flow velocities decreased with distance into the canopy from the edge as the boundary layer develops, and the lowest velocities were recorded in the regions with the highest stem densities. This was also observed for turbulence intensity, which is indicative of the turbulent kinetic energy of the flow (Figure 2-26).

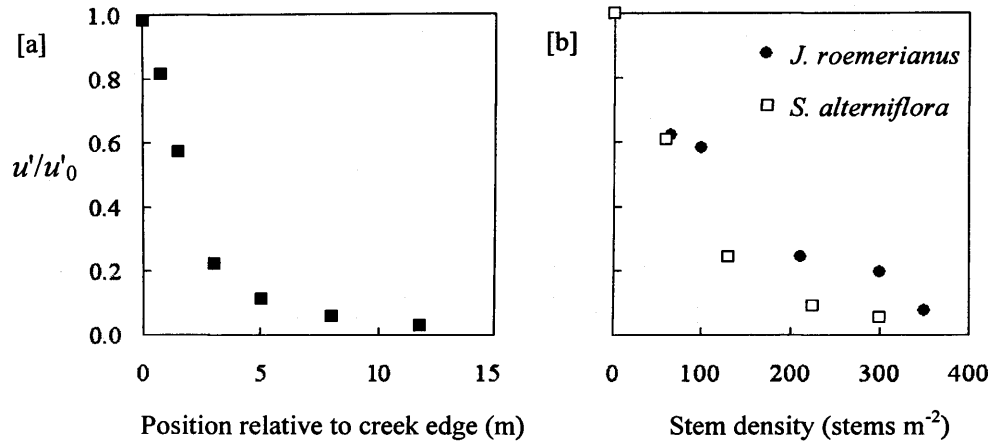

Figure 2-26 Reduction of turbulence intensity, u', normalised by the turbulence intensity at the edge of the canopy u'_0 (a) with increasing distance into a marsh canopy and (b) as a function of plant type and density (reproduced from Leonard & Luther, 1995)

Christiansen *et al.* (2000) considered the relationship between velocity and turbulence structure and sediment transport over a *Sp. alterniflora* saltmarsh. Sediment deposition occurred during the rising of a tide, regardless of magnitude, and once settled, no remobilisation of sediments took place due to low bed shear stresses. Fine sediments were subject to flocculation due to hydrogen bonding and thus, settled at higher rates than if they had settled individually. This was thought to be facilitated by low turbulence levels and flow velocities, which were below 0.1 ms^{-1} (Figure 2-27). Numerous other studies have been conducted on sediment deposition across saltmarshes investigating the vegetation's ability to stabilise sediments and protect against bed erosion as well as the relevance of site topography, particularly the locations of creek networks near which, sediment deposition is greater, and sediment

resuspension is more common (e.g. French *et al.*, 1995; Leonard and Luther, 1995; Boorman *et al.*, 1989; Brown, 1998).

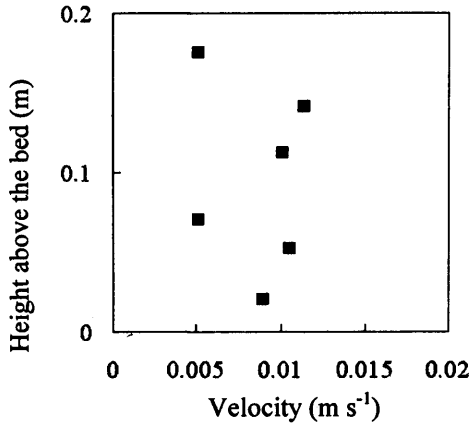

Figure 2-27 Velocity profile through a *Spartina alterniflora* canopy during a rising tide with an amplitude of 85 cm (reproduced from Christiansen *et al.*, 2000)

Leonard and Reed (2002) argued that the velocity and turbulence structures over saltmarshes could vary considerably for different sites, even when the sites experience similar tidal ranges and host similar vegetation species. The researchers examined a number of data sets from different saltmarsh sites from the United Kingdom and across the United States with various tidal ranges and dominant vegetation species, including *Spartina alterniflora* and *Atriplex portuloides* canopies (Figure 2-28). Velocity profile shapes were non-uniform within the canopy, and varied due to differences in vegetation properties and structure. For example, the velocity profiles through the *Atriplex portuloides* canopy were less 'predictable' and it was suggested that this was due to the vegetation being more vine-like in nature and buoyant, thus moving with increasing water depth during each flooding event. However, the researchers did not consider quantification of the plant canopies in each study to relate the morphology of the canopies to the velocity profiles and the canopies were simply characterised by identifying the dominant species.

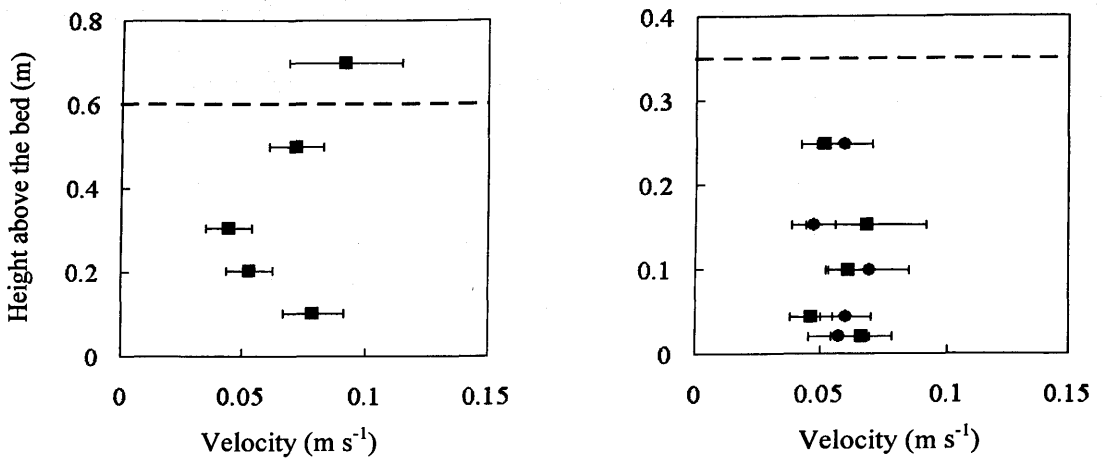

Figure 2-28 Longitudinal velocity profiles through (a) a submerged *Spartina alterniflora* canopy and (b) an emergent *Atriplex portuloides* canopy in (b), ■ and • represent profiles that were collected during separate and consecutive inundation events respectively (Leonard & Reed, 2002)

Neumeier and Ciavola (2004) measured flow velocity profiles at two locations over a *Spartina maritime* saltmarsh in Portugal. The researchers quantified the vegetation based on the mass of material per unit ground area to relate the profile shapes to the quantity of the vegetation. Velocity profiles were recorded at various stages during a tidal cycle covering the vegetation in both its emergent and submerged states (Figure 2-29).

The researchers identified that for emergent conditions (e.g. B1, B2, B3 and B4), the velocity profiles were often linear, occasionally increasing in magnitude towards the top of the profiles (e.g. B4 and C4). The increase occurs for greater flow depths, where the upper part of the canopy, which contains less vegetation material, becomes submerged. The velocity profiles for submerged conditions (e.g. B7, B8, B9, B10, B11 and B12) had similar shapes to the emergent cases within the canopy region, and increased logarithmically above the vegetation. During the early stages of a flooding tide, or near the end of an ebbing tide (e.g. B10), flow velocities in the surface flow layer were relatively low, and a logarithmic profile was less obvious. By monitoring two locations along the same saltmarsh, the authors identified that there was a significant difference in the tidal currents due to the topography of the site.

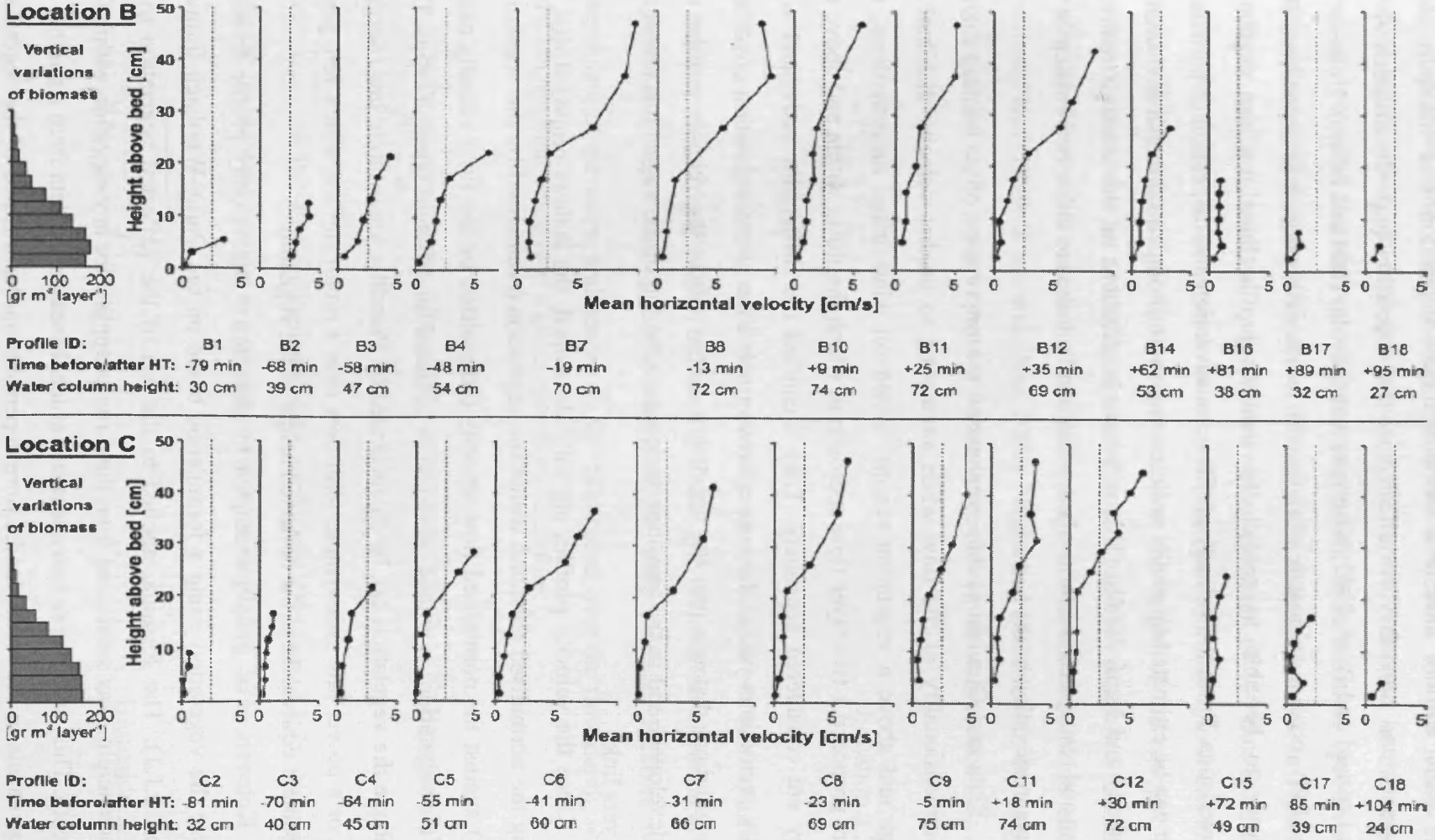

Figure 2-29 Velocity profiles through a *Spartina maritima* canopy at various stages during a tidal cycle. The vertical dashed lines mark the 2.5 cm s^{-1} position (taken from Neumeier & Ciavola, 2004)

2.4.3 Prediction of Velocity Profiles in Vegetated Flows

Some authors have considered sediment deposition and transport along saltmarshes and how they are affected by the vegetation (e.g. Christiansen *et al.*, 2000; Leonard and Reed, 2002; Neumeier and Ciavola, 2004 and others). However, to successfully predict saltmarsh evolution in terms of erosion and deposition, it is necessary to be able to predict the velocity profile based on the vegetation characteristics. From the velocity profiles, the advection and dispersion of particulate matter can be estimated to predict sediment transport through a saltmarsh environment (Lightbody and Nepf, 2006b). This will have implications on the levels of sediment settling and resuspension near the bed which can be linked to either bed erosion or the increase in elevation of the bed level.

Plate and Quraishi (1965) emphasised the importance of accounting for the three-dimensionality of the flow when attempting to predict velocity distributions through and above a vegetation canopy. Based on wind-tunnel measurements, the authors proposed a two-layer flow approach in which the flows within and above the canopy are considered separately. They identified the difficulties associated with velocity predictions within the region between the edge of the vegetation cover and the longitudinal distance into the vegetation canopy where the velocity profiles are fully developed, and in the transition region near the top of the vegetation where the two layers link.

Once the velocity profiles are fully developed, the authors proposed that by plotting the normalised elevation within the vegetation (normalised by the vegetation height) against the normalised flow velocity (normalised by the flow velocity at the top of the vegetation), a unique curve can be obtained for different types of crops. The flow above the vegetation can be characterised by Prandtl's logarithmic law (Section 2.1.2), or a power law synonymous with flow over a rough surface with a zero plane displacement equivalent to the deflected height of the vegetation.

Kouwen *et al.* (1969) attempted to characterise the velocity profile through and over the vegetation using a formulation based on the Darcy-Weisbach formula (Section 2.1.1). The formula, applied to the top of the deflected vegetation as a reference height, was subtracted from the formula applied for any elevation within the flow depth. This gave rise to two constants which, based on the data from a number of drainage canals in the Netherlands, were dependent on the stiffness of the vegetation

and its density respectively. This indicated the significance of vegetation properties on influencing velocity structure.

Lightbody and Nepf (2006a) introduced a method for predicting velocity profiles within emergent canopies based on the vertical variation in the vegetation structure, provided that the velocity and vegetation characteristics, specifically the projected area and drag coefficient at a reference elevation are known. In Figure 2-30, a velocity profile normalised by the velocity at an elevation of 150 mm from the bed is presented alongside the vertical variation for the *Spartina alterniflora* canopy. The drag coefficient was assumed to be constant over the height of the canopy. This is considered reasonable for natural canopies because it has been suggested that the drag coefficient shows little variation for a wide range of Reynolds numbers and stem densities (Nepf, 1999; Stone and Shen, 2002). Neglecting bed friction, the vegetation drag is equated to the pressure head and the momentum equation is reduced to:

$$\frac{1}{2}\overline{C_D}\bar{a}U^2 = g\frac{\partial \eta}{\partial x} \qquad \text{[Equation 2.35]}$$

where $\overline{C_D}$ is the bulk drag coefficient, $\bar{a}$ is the projected area per unit volume, U is the depth-averaged longitudinal velocity, g is the gravitational acceleration, x is the longitudinal distance and η is the height of the water surface. Pressure head is independent of elevation, and hence, $\overline{C_D}\bar{a}u^2$ is constant over the flow depth, where u is the longitudinal velocity at a given elevation. Therefore:

$$u \propto \frac{1}{\sqrt{\overline{C_{D2D}}a}} \qquad \text{[Equation 2.36]}$$

where $\overline{C_{D2D}}$ is the two-dimensional drag coefficient (Section 2.3.7). Normalising using the momentum balance at a reference elevation (Equation 2.36) gives:

$$\frac{u}{\hat{u}} = \sqrt{\frac{\hat{C}_D\hat{a}}{\overline{C_{D2D}}a}} = \sqrt{\frac{\hat{a}}{a}} \qquad \text{[Equation 2.37]}$$

where $\hat{C}_D$ is the drag coefficient at the reference elevation, and $\hat{a}$ is the projected area per unit volume at the reference elevation. Since the drag coefficient is assumed constant over the canopy height, $\hat{C}_D$ and $\overline{C_{D2D}}$ cancel out. The procedure can yield good results for emergent canopies, but for submerged conditions, where the Reynolds stress becomes significant within the vegetation layer (Section 2.5.3), velocity predictions are likely to be less representative of actual velocities.

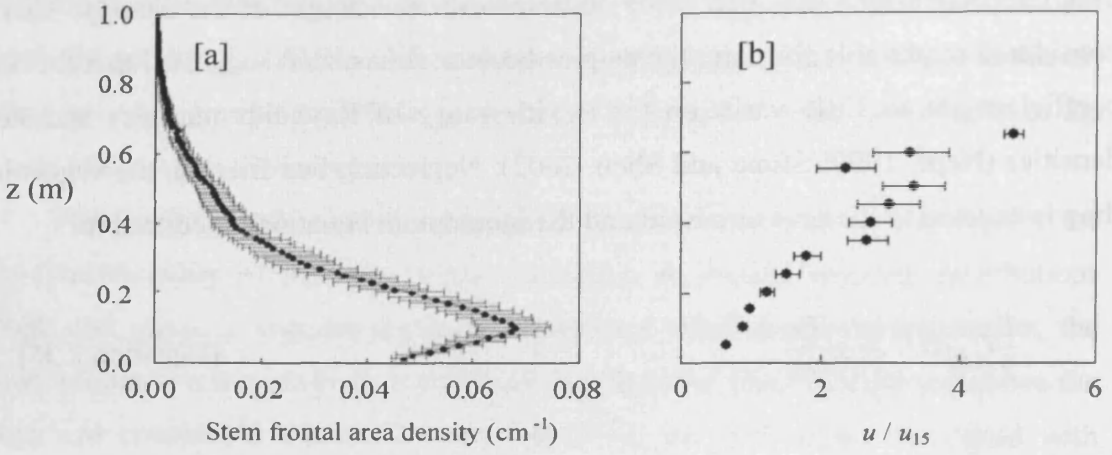

Figure 2-30 (a) the average stem frontal area density and (b) a longitudinal velocity profile for flow through a *Spartina alterniflora* canopy. (taken from Lightbody & Nepf, 2006a)

For submerged conditions, the logarithmic law has been used extensively to describe the velocity profile shapes in the surface-flow region above the vegetation canopy (Section 2.1.2).

2.5 Mixing Layers in Submerged Canopies

2.5.1 The Complexity of Flows through Submerged Vegetation

For submerged vegetation, the effects of the roughness sub-layer created due to the presence of the canopy extend beyond the top of the canopy and into the free surface (Raupach and Thom, 1981). The turbulence structure is complex and requires the consideration of various factors, such as the hydrodynamic drag, vortex production (magnitude and frequency), viscous dissipation and turbulent kinetic energy (Finnigan, 2000). Flow through the vegetation is dominated by large-scale coherent turbulent structures forming in the wake region of plant stems and

decreasing in intensity with distance in the downstream direction (Raupach and Thom, 1981). These structures are complex patterns of pressure, velocities and water particle movements. The mechanisms of their creation, dissipation and interaction with the foliage of a plant canopy are fundamental to the understanding of flow through vegetation (Raupach and Thom, 1981; Finnigan, 2000).

A second characteristic of the turbulence structure of a submerged canopy is associated with the existence of a 'skimming' flow above the canopy. The flow in the surface flow layer, which is not obstructed by vegetation, flows at considerably higher velocities than the flow in the obstructed vegetation layer. This can give rise to a large velocity gradient across the canopy-surface flow layer interface, and high levels of Reynolds stress (Section 2.5.2). This is the basis on which a 'mixing layer', initially introduced by Raupach *et al.* (1989), forms (Section 2.5.4). The effects of the 'skimming' flow on the turbulence structure are not restricted to the region around the canopy-surface flow layer interface, and can protrude into the canopy.

2.5.2 General Concept of Shear Stresses

The total shear stress of a fluid, τ, can be defined as follows:

$$\tau = \tau_v - \rho < \overline{u'w'} > -\rho < \widetilde{\widetilde{u}\widetilde{w}} > \qquad \text{[Equation 2.38]}$$

whereby τ_v is the viscous stress, and the terms '$-\rho < \overline{u'w'} >$' and '$-\rho < \widetilde{\widetilde{u}\widetilde{w}} >$', which arise from the procedure of double-averaging in space and time (Section 2.3.1), correspond to the Reynolds stress and the form-induced stress respectively.

Viscous shear stresses occur when the flow is laminar and the fluid moves along individual planes. For flow over a rough surface, a boundary layer forms near the bed. Within this layer, flow is strongly affected by the resistance of the surface, flow velocities are very low, and the flow is laminar in the sub-layer (Schlichting, 1955). According to boundary-layer theory, the fluid particles immediately adjacent to the surface are assumed stationary, and velocity increases with elevation in the boundary layer until the flow is no longer laminar at the outer edge of the layer. The edge of the boundary layer may also be characterised as the elevation at which the fluid adopts a longitudinal velocity equal to that of the flow. Within the laminar boundary layer, as two layers of fluid move parallel to each other, the velocity of the

upper layer is reduced due to friction between the two layers, and a shear stress arises as a result of this loss of velocity. The viscous shear stress is defined as:

$$\tau_v = \mu \frac{\partial u}{\partial z} \qquad \text{[Equation 2.39]}$$

where μ is the dynamic fluid viscosity, the value of which is 1.00×10^{-3} Nsm^{-2} at a temperature of 20°C, and $\partial u/\partial z$ is the longitudinal velocity gradient in the vertical plane.

The "form-induced" stress (Section 2.3.1) is associated with a flow passing through a heterogeneous medium such as a vegetation canopy. The magnitude of the form-induced stress can therefore be indicative of the spatial variability, or the heterogeneity of the canopy.

At higher Reynolds numbers, when the flow is turbulent, Reynolds stresses occur due to the random turbulent fluctuations in fluid momentum. According to Nepf (1999), these are significant at stem Reynolds numbers above 200, although according to Kadlec (1990), the flow is not fully turbulent until the stem Reynolds number exceeds 1000. However, Nepf (1999) acknowledges that in a vegetation canopy, shear in the flow due to the presence of upstream obstructions can delay the onset of vortex shedding (Sections 2.2.3 and 2.2.6).

The Reynolds stress peaks in magnitude near the top of the canopy, where there is a strong discontinuity between the high resistance vegetation layer and the unobstructed surface flow layer causing a steep velocity gradient across the interface (Tsujimoto *et al.*, 1992). Nepf and Vivioni (2000) showed that the flow had a tendency to seep upwards from the canopy and into the surface flow layer causing a decrease in the drag coefficient near the top of the canopy. The researchers claim that the upward transfer of momentum results in further amplification of turbulence levels, and a peak in Reynolds stress is observed near the top of the canopy.

2.5.3 Reynolds Stress Penetration

A number of studies on submerged vegetated flows have identified a peak in Reynolds stress accompanied by an inflection point within the velocity profile at the

top of the submerged canopy (e.g. Tsujimoto *et al.*, 1992; Ikeda and Kanazawa, 1996; Finnigan, 2000; Järvelä, 2005 and others). Furthermore, Finnigan (2000) identified a peak in wake production just below this level. Nepf (1999) defined the wake production as the work done against the drag force resulting in the conversion of mean kinetic energy into turbulent kinetic energy.

The influence of a large longitudinal velocity gradient across the canopy-surface flow layer interface is not usually limited to the region around the interface, and elevated Reynolds stress values can often be detected at lower elevations within the canopy (e.g. Tsujimoto *et al.*, 1992; Ikeda and Kanazawa, 1996; Finnigan, 2000; Järvelä, 2005 and others). The depth of the aforementioned 'influence' can depend on the magnitude of the peak Reynolds stress near the interface and the density of the vegetation. The elevated Reynolds stress is absorbed with increasing distance into the vegetation, often reaching negligible levels near the bed. Nepf and Vivioni (2000) attempted to parameterise the distance required to absorb the Reynolds stress and reduce it to such a negligible level, and defined the 'penetration depth' as the distance from the top of the vegetation layer to the depth within the canopy where the Reynolds stress equals 10% of the peak value (Figure 2-31). The authors found the penetration depth to increase with submergence depth. Below the 'penetration depth', vertical momentum exchange was negligible, and the flow can be determined by the consideration of the pressure and bed gradients, and the vegetative drag. Above the 'penetration depth', vertical momentum exchange was more significant and the flow structure was more difficult to predict.

In studies where uniform cylinders were used to simulate vegetation canopies (e.g. Dunn *et al.*, 1996; Fairbanks, 1998), Reynolds stress penetration was very significant, often reaching the bed. This is illustrated in Figure 2-32 where some of the data from Fairbanks (1998) is presented. This shows the significance of plant foliage which is absent in uniform cylinder models towards the Reynolds stress penetration characteristics.

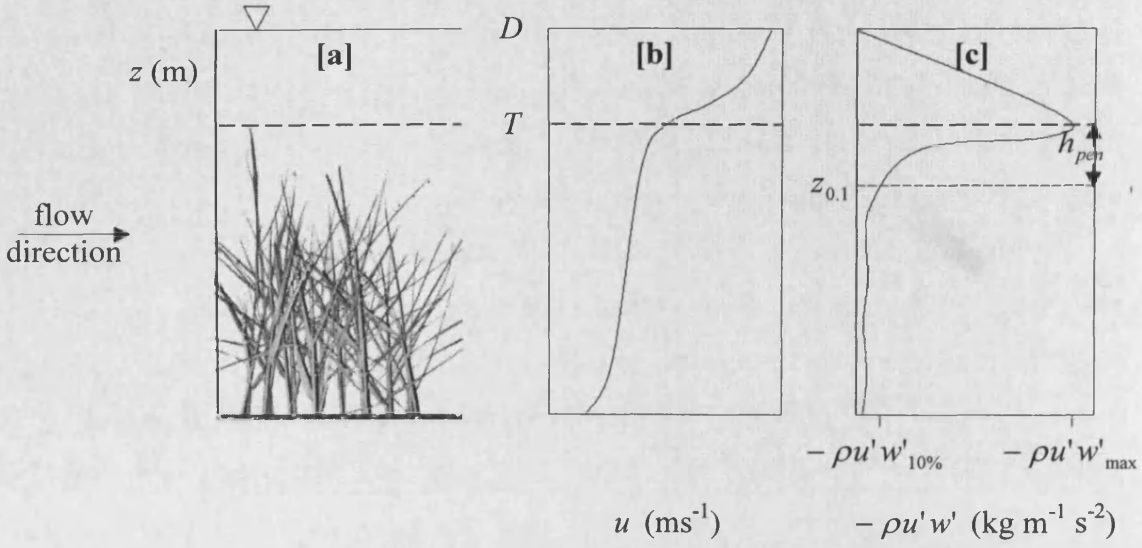

Figure 2-31 A schematic diagram illustrating [a]: flow through a submerged vegetation canopy and the associated [b]: velocity and [c]: Reynolds stress profiles. z is the distance from the bed, *D* is the flow depth, *T* is the vegetation height, *u* is the longitudinal velocity $z_{0.1}$ is the distance from the bed to the elevation where the Reynolds stress, $-\rho u'w'$, is 10%, $-\rho u'w'_{10\%}$, of the maximum value, $-\rho u'w'_{max}$ and h_{pen} is the Reynolds stress penetration depth. The penetration depth is marked on the Reynolds stress plot by means of a faint dotted line.

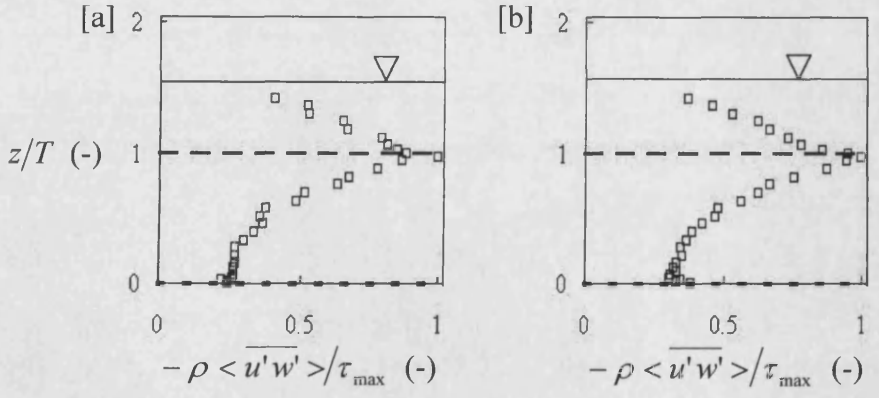

Figure 2-32 Normalised Reynolds stress profiles for experiments conducted by Fairbanks (1998) on rigid dowels coated with [a] fine and [b] coarse sand paper. The bold dotted line denotes the top of the vegetation, whilst the faint dotted line indicates the depth of shear penetration.

2.5.4 The Mixing Layer Analogy

Instability arises due to a strong inflection point in the longitudinal velocity profile along the canopy-surface flow layer interface. This characteristic of canopy

flows is thought to render the 'mixing layer' analogy, initially introduced by Raupach *et al.* (1989), more applicable than treating the canopy region as an extension of the boundary layer from the rough bed (Finnigan, 2000). Furthermore, Raupach *et al.* (1996) investigated the turbulence structure within and above a range of natural and artificial vegetation canopies. The authors observed mean velocity, Reynolds stress and velocity standard deviations to decay towards the bed, and identified the inflexion in mean velocity at the top of the canopy. Comparing the top of the canopy to the region above the vegetation, there was a decrease in velocity standard deviations and an increase in the correlation coefficient (defined as the ratio of the Reynolds stress per unit mass, $\overline{u'w'}$, to the product of the time-averaged RMS velocity fluctuating components $[\overline{u'}]$ and $[\overline{w'}]$). This suggests that the turbulence structure was more organized above the canopy. Skewness of the velocity fluctuating components within the canopy indicated that the main turbulent movements were those of 'sweeps' (see Section 2.5.5 for definition). The aforementioned characteristics identified by Raupach *et al.* (1996) render the 'mixing layer' analogy more appropriate for characterising the flow through a submerged canopy. The concept of momentum transport by means of 'ejections' and 'sweeps' in rough boundary flows was originally introduced by Townsend (1961).

Raupach *et al.* (1989) defined the 'mixing layer' as a shear layer that forms along an interface between two adjacent fluid bodies moving with different velocities. The layer is dominated by large-scale coherent turbulent structures (Brown and Roshko, 1974), and its thickness can be defined as the depth of flow over which the longitudinal velocity profile gradient is a maximum. Although this analogy was initially introduced for terrestrial vegetation, it is thought to be valid for submerged vegetated flows across the canopy-surface flow layer interface (Ghisalberti and Nepf, 2002).

Finnigan (2000) summarised the stages of the development of the coherent structures dominating the mixing layer. First, as the shear due to the inflexion in the longitudinal velocity exceeds a threshold, an instability known as the primary Kelvin-Helmholtz instability arises from the background turbulence (Figure 2-33a). In the second stage, transverse vortices form at a similar wavelength to the initial instability, denoted by λ_x (Figure 2-33b). In the third stage, 'kinking' results in the vortex

structures, longitudinal instabilities are amplified and coherent structures form in both the lateral and longitudinal directions (Figure 2-33c).

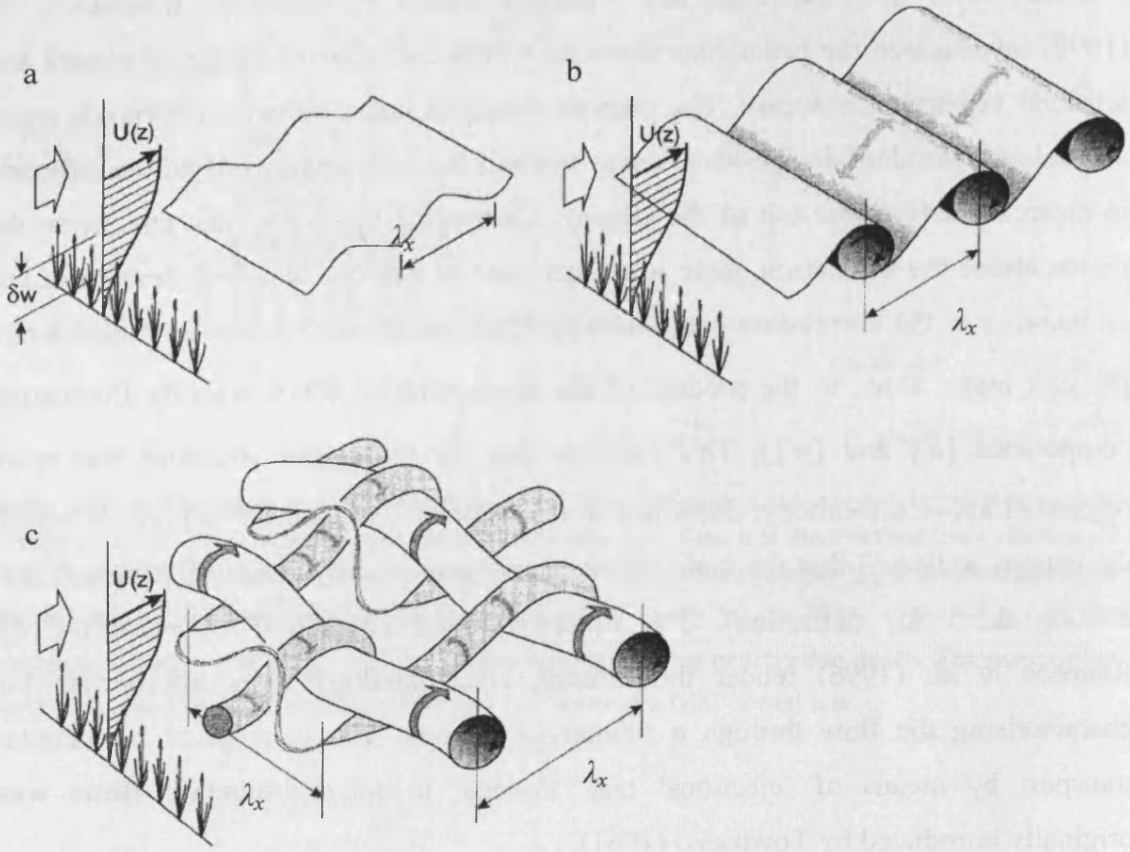

Figure 2-33 Stages of the development of the mixing layer (taken from Finnigan, 2000)

2.5.5 The Quadrant Analysis

Lu and Willmarth (1973) introduced the 'quadrant-hole technique' to identify coherent structures in the flow by associating them with certain patterns in velocity data. To identify and assess rotations in the vertical plane, the turbulent fluctuations in the vertical and longitudinal components of the velocity profile are plotted as illustrated in the schematic diagram presented in Figure 2-34. Points falling in the second quadrant (when the turbulent fluctuations of the longitudinal and vertical velocity components are $u' < 0$ and $0 < w'$ respectively) correspond to ejections whereby parcels of water are transported upwards and out of the canopy. Points falling in the fourth quadrant ($0 < u'$ and $w' < 0$) correspond to sweeps whereby the water parcels are swept downwards and into the vegetation layer.

This approach has been used by a number of researchers (e.g. Raupach and Thom, 1981; Finnigan, 2000) to characterise the rotating vortices by the direction of

the longitudinal and vertical turbulent fluctuations. If the vegetation is flexible, a travelling wave, which has been termed 'monami', has been observed along the top of the plants and it has been suggested that this is a reaction to these motions (Fonseca and Kenworthy, 1987; Ackerman and Okubo, 1993; Grizzle *et al.*, 1996; Ghisalberti and Nepf, 2002).

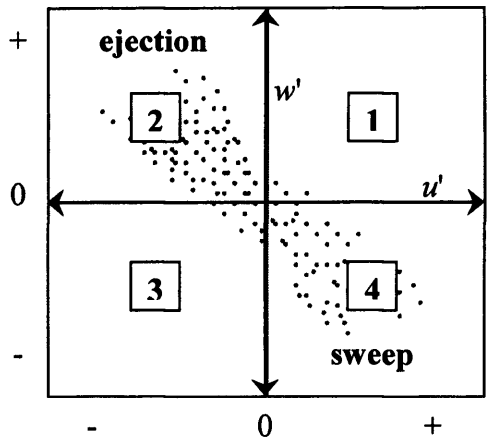

Figure 2-34 Schematic diagram illustrating the 'quadrant-hole technique'

2.5.6 The Turbulent Kinetic Energy Budget

An in-depth consideration of the turbulence characteristics of the flow through vegetation canopies is beyond the scope of this study. Turbulence modelling is a complicated research area in its own right whereby numerous researchers have developed various numerical models to understand and predict such complex processes (e.g. Rodi, 1980).

A number of authors considered the mechanisms affecting the conversion of mean kinetic energy per unit mass, *MKE*, and turbulent kinetic energy per unit mass, *TKE* (e.g. Raupach, 1992; López and García, 1997; Finnigan, 2000 and others). Raupach *et al.* (1996) suggest the turbulent kinetic energy budget can be summarised as consisting of the following mechanisms:

$$\frac{\partial}{\partial t}\frac{\left(\overline{u'}^2+\overline{v'}^2+\overline{w'}^2\right)}{2} = P_s + P_w + P_b + T_t + T_P - \varepsilon \qquad \text{[Equation 2.40]}$$

Where P_s is the shear production, P_w is the wake production, P_b is the buoyant production (the vertical movement of the fluid due to differences in temperature which affects the fluid density), T_t is the turbulent transport, T_P is the pressure transport, and ε is the dissipation. Buoyancy effects are negligible where the fluid density is consistent i.e. where salinity and temperature are relatively constant. The actual terms are derived by applying time and volume averaging (Equation 2.21 and Equation 2.22) to the parameters in the conservation of momentum equation (Equation 2.07). The resulting equation for adiabatic flow (where the effects of heat transfer are ignored) is adapted from Finnigan (2000) and presented using the notation from Section 2.3.1:

$$\left(\frac{\partial}{\partial t}+<\overline{w}>\frac{\partial}{\partial z}\right)<\overline{u'u'}>=-<\overline{u'w'}>\frac{\partial<\overline{u}>}{\partial z}-\left\langle\overline{\widetilde{u}\widetilde{w}}\frac{\partial\widetilde{u}}{\partial z}\right\rangle+\frac{g}{T_0}<\overline{w'\theta'}>$$

$$P_s \qquad\qquad P_w \qquad P_b$$

$$-\frac{\partial<\overline{\widetilde{w}\widetilde{u}\widetilde{u}}/2>}{\partial z}-\frac{\partial<u'u'w'>}{\partial z}-\frac{\partial<\overline{p'w'}>}{\partial z}+\nu\frac{\partial^2<\overline{u'u'}>/2}{\partial z\partial z}-\nu\left\langle\frac{\partial u'}{\partial z}\frac{\partial u'}{\partial z}\right\rangle$$

$$T_d \qquad T_t \qquad T_p \qquad T_v \qquad \varepsilon$$

\+ waving terms [Equation 2.41]

The schematic diagram in Figure 2-35 illustrates how each component varies with elevation within and above the canopy for submerged conditions (Finnigan, 2000).

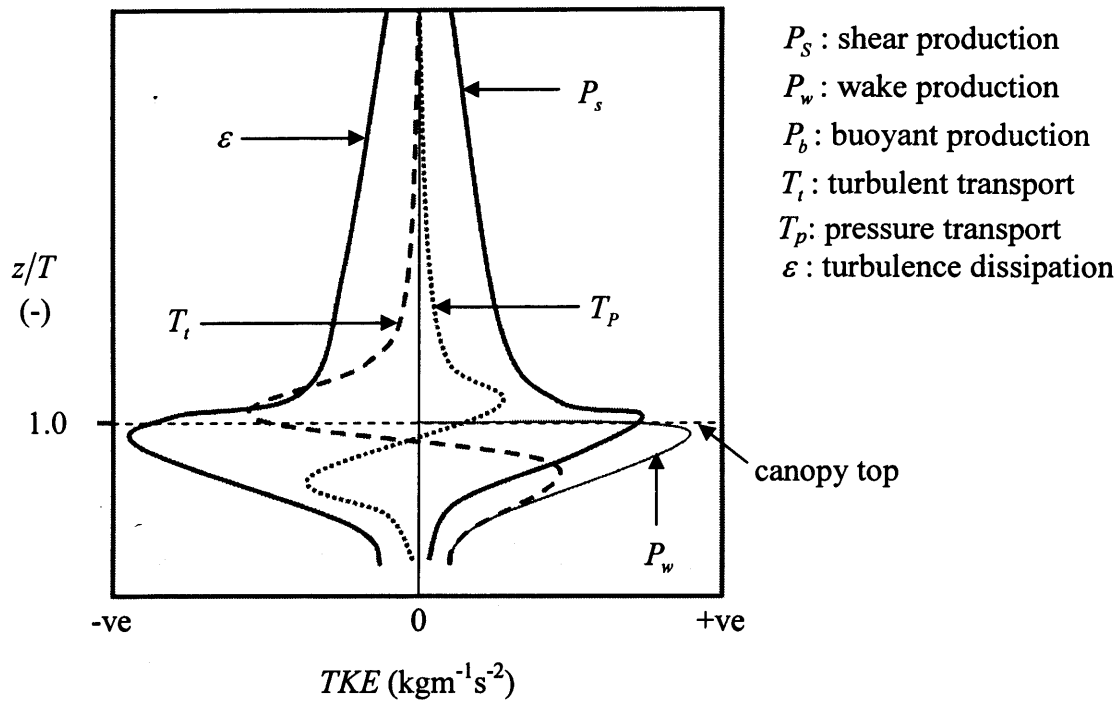

Figure 2-35 Schematic diagram of the turbulent kinetic energy (*TKE*) budget for submerged vegetated flow. The horizontal dotted line denotes the top of the vegetation layer. *T* is the canopy height and *z* is the elevation above the bed (reproduced from Finnigan, 2000)

Turbulent transport (T_P) is significant within the canopy layer, and in the region immediately above the vegetation, whereby the negative values near the top of the canopy indicate a loss, and the positive values over most of the canopy height indicate a gain. This suggests that turbulence within the canopy is not locally generated (Raupach *et al.*, 1996). Shear production (P_s) peaks near the top of the canopy due to the peak in shear stress associated with the inflexion point in the velocity profile near the interface. Below the interface, wake production (P_w) is the dominant production term and accounts for the conversion of mean kinetic energy (*MKE*) to turbulent kinetic energy (*TKE*) (Finnigan, 2000). Turbulence generated within the canopy is rapidly converted to other energy forms, such as heat and sound energy, corresponding to a large dissipation (ε) (Raupach *et al.*, 1996). At elevations considerably above the canopy (Raupach *et al.* (1996) propose $z > 2T$), there is a balance between shear production (P_s) and dissipation (ε), and the budget reduces to:

$$P_s = \varepsilon \qquad \text{[Equation 2.42]}$$

For emergent conditions, turbulence production within the stem wakes, (P_w), far exceeds that due to bed shear over most of the flow depth (Nepf *et al.*, 1997a) and the budget reduces to:

$$P_w = \varepsilon \qquad \text{[Equation 2.43]}$$

2.6 Concluding Remarks

Research conducted on vegetated flows is very broad in nature due to the large variation in morphology of aquatic vegetation and the flow conditions they are exposed to. For instance, studies in the literature were conducted on a wide range of vegetation covers including bushes (e.g. Righetti and Armanini, 2002), macrophytes (e.g. Stephan and Gutknecht, 2002) and flexible grasses. However, in this thesis, the theory and studies most relevant to vegetated flows in the context of coastal saltmarshes, and particularly *Spartina anglica* saltmarshes were presented.

One of the greatest challenges in evaluating the hydraulic resistance of vegetated flows is the characterisation of the level of obstruction of a canopy and relating it to the morphology of the vegetation and its physical properties to link it to the resulting velocity and turbulence structures. This can be most conveniently achieved by considering the bulk drag coefficient which can be either one or two-dimensional depending on whether drag forces and mean velocities are evaluated for the canopy layer or for individual point elevations within it respectively. This varies from the drag coefficient for a single cylinder in that it accounts for the effects of adjacent plants. Such effects are significant within a canopy particularly where the 'sheltering effect' takes place. The impact velocity on the upstream face of a plant is reduced due to the wake of an upstream plant causing a reduction in the drag force. The probability of 'wake sheltering' taking place increases with stem density since the stem spacings become smaller. The bulk drag coefficient, and hence, the drag force, are strongly affected by the turbulence structure and as such, are a strong function of the Reynolds number.

A key focus of this review was on the influence of simulated canopies on velocity and turbulence structures, although it is suggested that uniform cylinder models often lead to oversimplifications of the complex morphology associated with

vegetation. For instance, within a natural canopy, the velocity and turbulence structure usually vary both longitudinally (in the direction of the flow) due to the natural variability of the vegetation, and vertically due to the variation in canopy structure between the stem and the foliage regions. The material stiffness of the vegetation and the submergence level also influence the hydraulic resistance of the canopy.

For submerged canopies, the turbulence structure is considerably more complex than for emergent conditions. The turbulence structure for a submerged canopy is largely influenced by the formation of a 'mixing layer' along the canopy-surface flow layer interface due to the mean velocity of the surface flow layer being considerably higher than the adjacent canopy layer. Thus, rotational vortices form in the vertical plane, an inflexion in the longitudinal velocity profile can be seen, and a peak in the Reynolds stress takes place near the canopy-surface flow layer interface which results in an elevation of the Reynolds stress within the upper part of the canopy.

The theory and literature presented in this review attempt to provide an account of the relevant fluid dynamics principles required to understand a study investigating the influence of coastal saltmarsh vegetation canopies on velocity and turbulence structure, and the drag forces that arise due to the obstruction that they create in tidal flows.

[*This page has been intentionally left blank*]

3 Field Monitoring Programme

3.1 Introduction

A field study was conducted at two saltmarsh sites: the Llanelli saltmarsh, located along the northern coast of the Loughor estuary, and the Gower saltmarsh, located along its southern coastline. The vegetation cover along the first site is relatively dense compared to the latter saltmarsh, where grazing occurs by sheep and horses. The key vegetation species dominating the saltmarsh was identified as *Spartina anglica*. The majority of the field work was conducted between July 2005 and June 2006. For each month, the sampling collection conducted across the field sites is referred to as a 'sampling event'.

Due to the importance of the vegetation cover to the nature of this thesis, a separate chapter was devoted to the characterising vegetation properties (Chapter 4). In this chapter, firstly bed levels and bed gradients were determined from LiDAR data. Bed gradients are useful for calculating one-dimensional roughness coefficients such as the Manning's roughness coefficient.

Secondly, water elevations were measured using floating buoys and pressure transducers and used to characterise the inundation profile across the saltmarshes during high tide events. The information was used to determine submergence levels, which are known to influence the hydraulic resistance properties of vegetation. A submergence predictor is developed in this chapter that can be used to predict the submergence levels for a large area of saltmarsh simultaneously.

The findings presented in this chapter were used later in Chapter 7 to design a series of laboratory studies within a range of conditions that is representative of the natural saltmarshes monitored.

3.2 Site Description

3.2.1 The Loughor Estuary

Two sites along the Loughor Estuary were monitored; the Llanelli site (N51° 40', W4° 8'), and the Gower site (N51° 38', W4° 11') (Figure 3-1). The Llanelli site is

relatively small (approximately 2 km by 0.5 km), compared to the Gower site (approximately 6 km by 1.5 km). It is covered by the Wildfowl and Wetlands Trust (WWT) National Wetland Centre Wales, and is home to numerous wildfowl and migrating bird populations. Consequently, the site is strictly managed and experiences little human presence, thus providing a convenient environment for monitoring local vegetation species in an undisturbed environment. The key vegetation species identified along the Llanelli saltmarsh was *Spartina anglica*. Along the Gower site, sheep and horses heavily grazed the vegetation. The vegetation cover was considerably shorter than the non-grazed vegetation along the Llanelli site throughout the year.

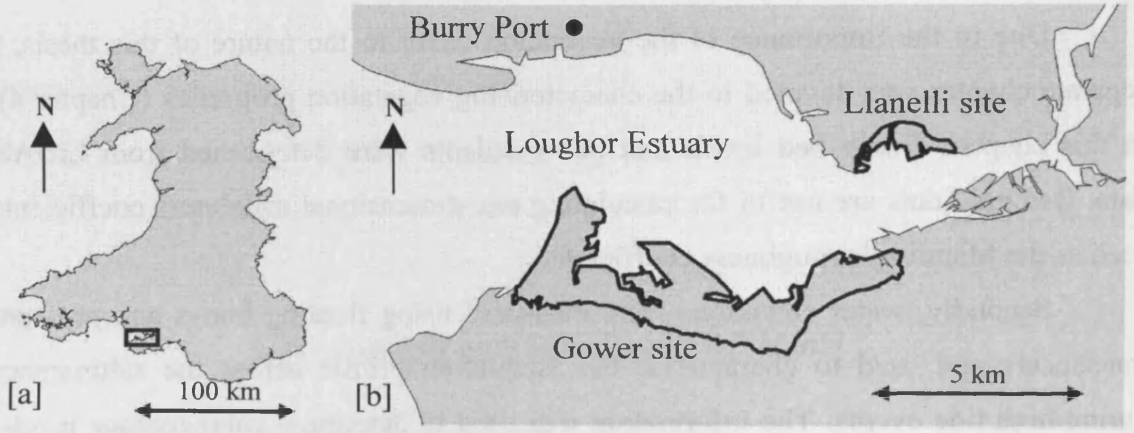

Figure 3-1 [a]: Location of the study area on the map of Wales. [b]: The study sites highlighted along the Loughor Estuary. Plot produced from data collected by Ordinance Survey.

3.2.2 Remote Sensing Data for the Loughor Estuary

3.2.2.1 Aerial Photographs

A number of black and white aerial photographs taken of the Llanelli and Gower saltmarsh sites over different periods are available from the Air Photograph Unit of the National Assembly for Wales. Photographs are available from 1946, 1947, 1978 and 1994, and Landsat images acquired by satellite were available for 1990 and 2000. These were analysed by Williams (2004) visually to determine changes in the land occupied by saltmarsh vegetation, and the ground coverage was determined through a Geographical Information System package (GIS). Considering the

photographs were in black and white, the accuracy of this approach is uncertain. The areas of saltmarsh at the Llanelli site between 1946 and 2000 as determined by Williams (2004) are presented in Table 3-1. The aerial photographs from 1947, 1978 and 1994 are presented in Figure 3-2, along with the outlines of the *Spartina anglica* coverage according to Williams (2004). The most significant increase in land occupied by vegetation was observed between 1947 and 1978 compared to other consecutive photographs. The area of saltmarsh land also increased on the North Gower site despite an average sea level rise of 1.7 mm yr^{-1} $\pm$ 0.3 according to tide gauge data between 1950 and 2000 (Church and White, 2006). However, by considering the period between each photograph, there is clearly a decrease in the level of increase in area up to 1978 (see Table 3-1). This is followed by a continuous decrease in saltmarsh area beyond 1978. This may be due to 'coastal squeeze' (see Section 1.3.4).

Table 3-1 Surface area of saltmarsh at the Llanelli site between 1946 and 2000 (taken from Williams, 2004)

Year	Area of saltmarsh (km^2)	Increase in Area per year
1946	2.21	
1947	2.31	10.0%
1978	3.29	3.2%
1990	3.17	-1.0%
1994	3.16	-0.2%
2000	3.10	-1.0%

Williams (2004) also considered a section of saltmarsh along the southern bank of the Loughor estuary; however, this did not coincide with the Gower site monitored here. However, for the site considered by Williams (2004), following a dramatic increase in saltmarsh ground area between 1947 and 1978, there was a slight decrease in the ground area covered by saltmarsh in the images recorded during the following years. The author attributed the changes in saltmarsh areas along the two sites to deposition and erosion. The field survey conducted here revealed high levels of grazing along the Gower site, whereby a gradual decrease in saltmarsh area was observed from 1978 onwards which was greater than the decrease in area observed for the Llanelli site where grazing was negligible. Saltmarshes are known to have the ability to maintain their position within the intertidal zone through promoting sediment deposition and stabilising settled sediments (e.g. Shi *et al.*, 1995; Shi *et al.*, 1996 and others).

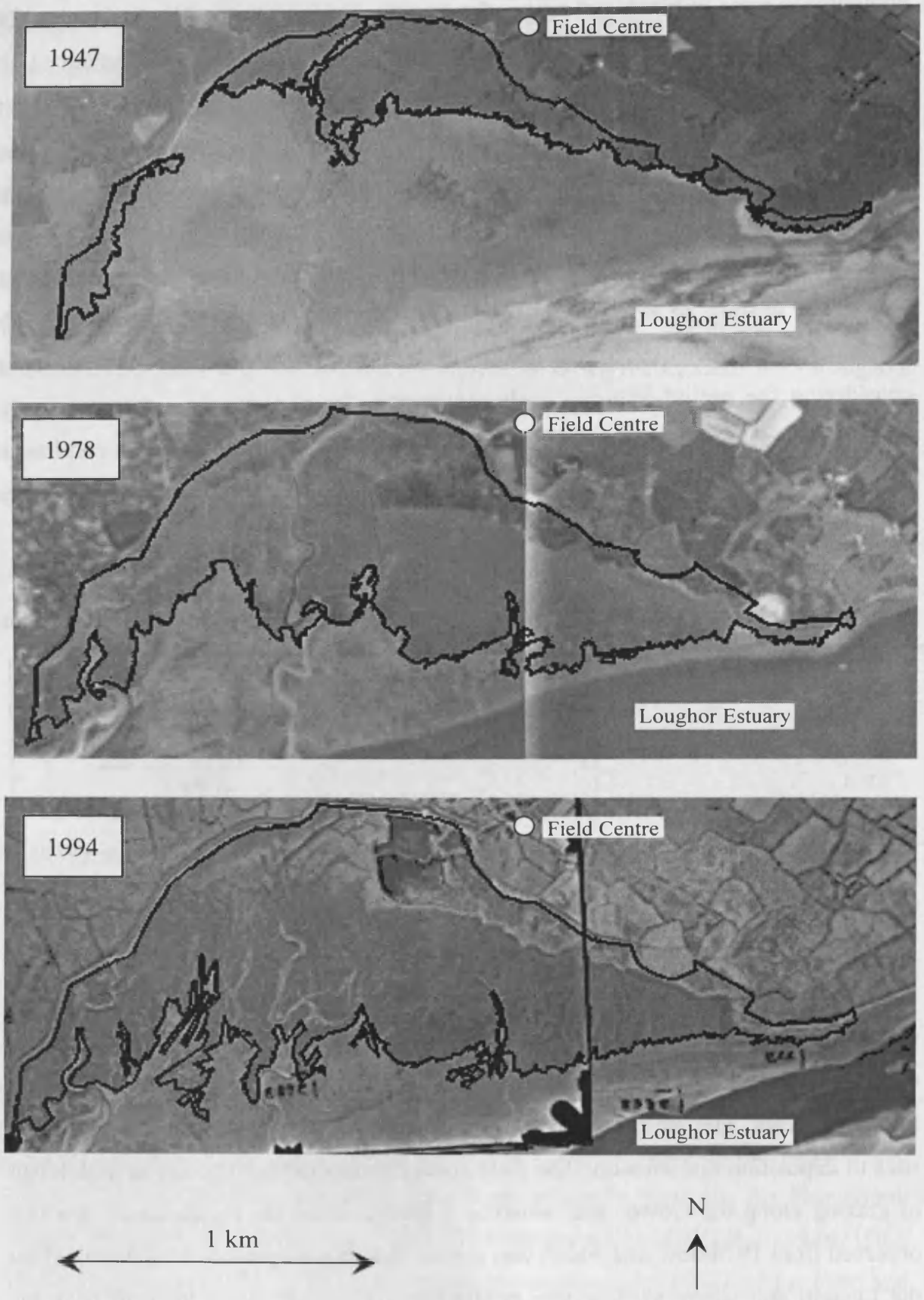

Figure 3-2 Aerial photographs of the Llanelli saltmarsh from 1947, 1978 and 1994. The land covered by saltmarsh vegetation is highlighted by the black outline (from Williams, 2004)

3.2.2.2 LiDAR Data Set

Light Detection and Ranging (LiDAR) data was obtained for the Loughor Estuary from the Environment Agency (Figure 3-3). LiDAR is an airborne optical remote sensing technology in which the scatter in reflected laser signals is analysed to determine the distance from an aircraft to the ground. The technology involves the determination of the distances to objects based on the delay between transmission of laser pulses, and the detection of the reflected signals. For the Llanelli and Gower sites, LiDAR data was collected on the 30th January 2003, at a 2-metre grid resolution. The Environment Agency quotes all data collected using this procedure before September 2004 at an accuracy of +/- 0.25m in the vertical direction. The results of the ground-truthing survey conducted by the agency shows that the data met this accuracy (Figure 3-4).

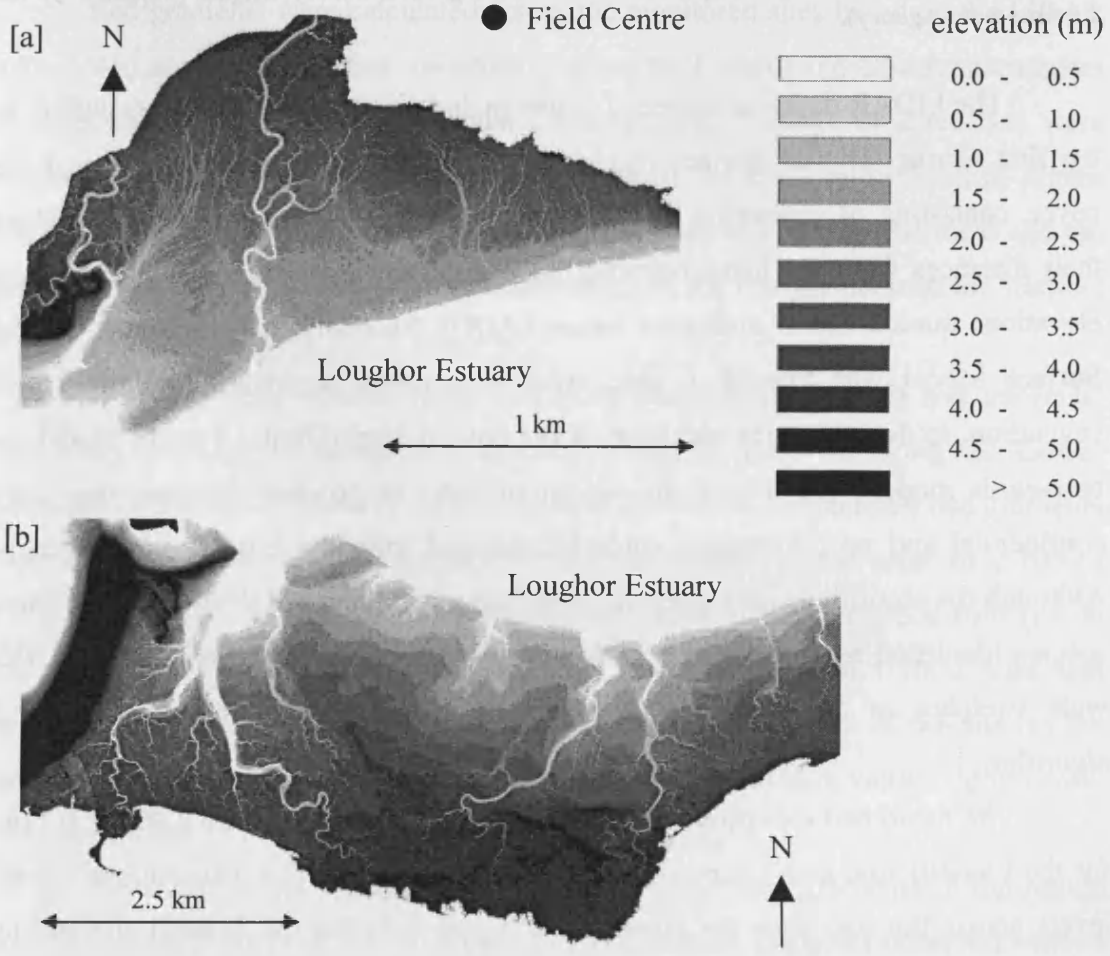

Figure 3-3 LiDAR data presented according to elevation above ordinance datum (AOD) through a GIS package (ArcGIS) for [a]: Llanelli site; [b]: Gower site. Plots produced from LIDAR data collected by the Environment Agency.

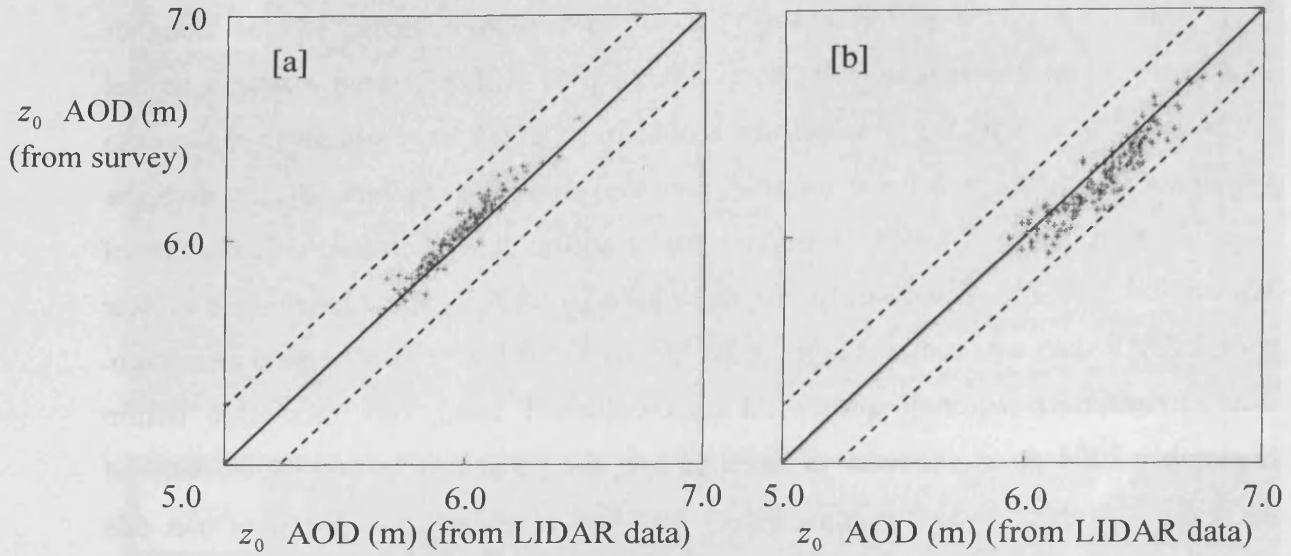

Figure 3-4 Ground truthing verification of LiDAR data for [a]: Llanelli site; [b]: Gower site. The graph is reproduced from a plot provided by the Environment Agency to accompany the filtered data. The solid line denoted LIDAR surface heights equal to GPS ground survey heights, and the dotted lines denote a range of ± 0.25m of the GPS ground survey height. (Supplied by the Environment Agency).

The LiDAR data was provided in two main formats at a 2 m grid resolution. In the first format (Digital Surface Model, or elevation model), the elevations of the cover, consisting of vegetation, buildings or bare ground, were calculated based on their distances from the plane carrying the remote sensing instrumentation, and the elevations quoted above ordinance datum (AOD). Secondly, data from the Digital Surface Model was filtered to strip away all objects, particularly buildings and vegetation, to determine the elevation of the ground level (Digital Terrain Model, or bare-earth model). Details of the algorithm used to process the data was kept confidential and no information could be obtained from the Environment Agency. Although the algorithm was successful in isolating buildings and the dense vegetation species identified as *Halimione portulacoides* which bordered saltmarsh creeks, the wide stretches of *Spartina anglica* covers were not captured by the processing algorithm.

The mean bed elevations above ordinance datum (AOD) were 2.46m ± 0.11m for the Llanelli site, and 1.72m ± 0.11m for the Gower site. The distributions of bed levels across the two sites are presented in Figure 3-5a for the Llanelli site and in Figure 3-5b for the Gower site.

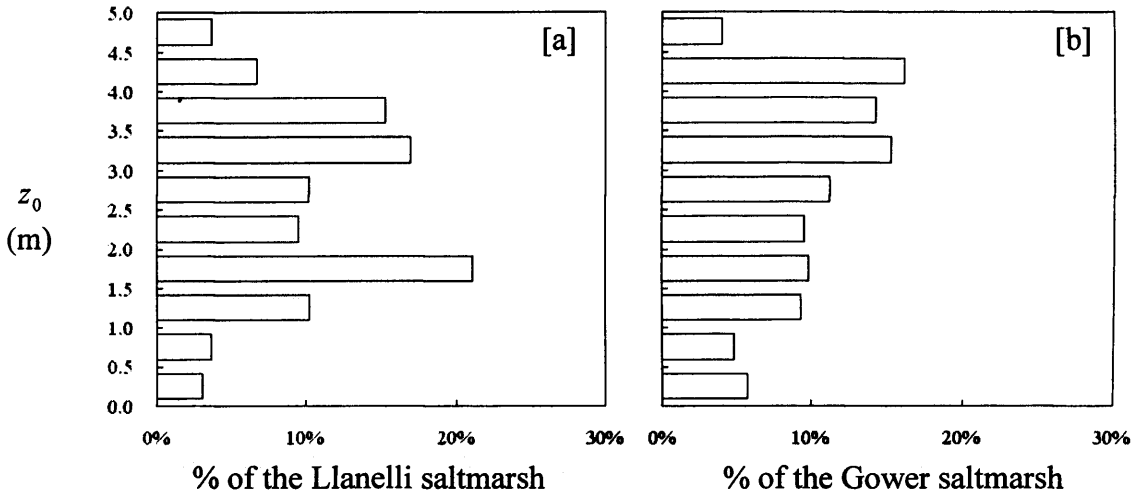

Figure 3-5 Bed elevation distributions for the [a]: Llanelli site; [b]: Gower site, based on the LiDAR data

3.2.2.3 Bed Gradients Calculated from LiDAR Data

Bed gradients were calculated across the monitored sites based on the LiDAR data. A series of transects were investigated along the Llanelli and Gower saltmarshes to determine the range of bed gradients encountered. A range of directions were evaluated, e.g. North-South and across the width of the site as illustrated in Figure 3-6. Also, a range of transect lengths were investigated to compare the local and the global bed gradients, indicating little dependency of the bed gradient on the transect size.

The field work monitoring for this study was conducted along five transects: two along the Llanelli saltmarsh (transects A and B), and two along the Gower saltmarsh (transects D, E and F). In the region of transect A, the steepest bed gradients were observed in the north to south direction. These were in the order of 1:100 to 1:300 (Figure 3-6). Similar values were observed perpendicular to the coastline (i.e. in the northeast to southwest direction), although gradients down to 1:1000 were also common. The shallowest gradients were observed along the width of the site (in the east to west direction), particularly in locations further inland with values significantly less than 1:1000.

The analysis was repeated along the Gower site. Bed gradients in the region around transect D are presented in Figure 3-7. The steepest gradients observed were in the southwest to northeast direction, and these ranged between 1:300 and 1:600. Shallower gradients were observed in the south to north, and in the east to west

directions, with values ranging between 1:500 and 1:1300, whilst in the northwest to southeast direction, gradients were significantly shallower with values less than 1:2500.

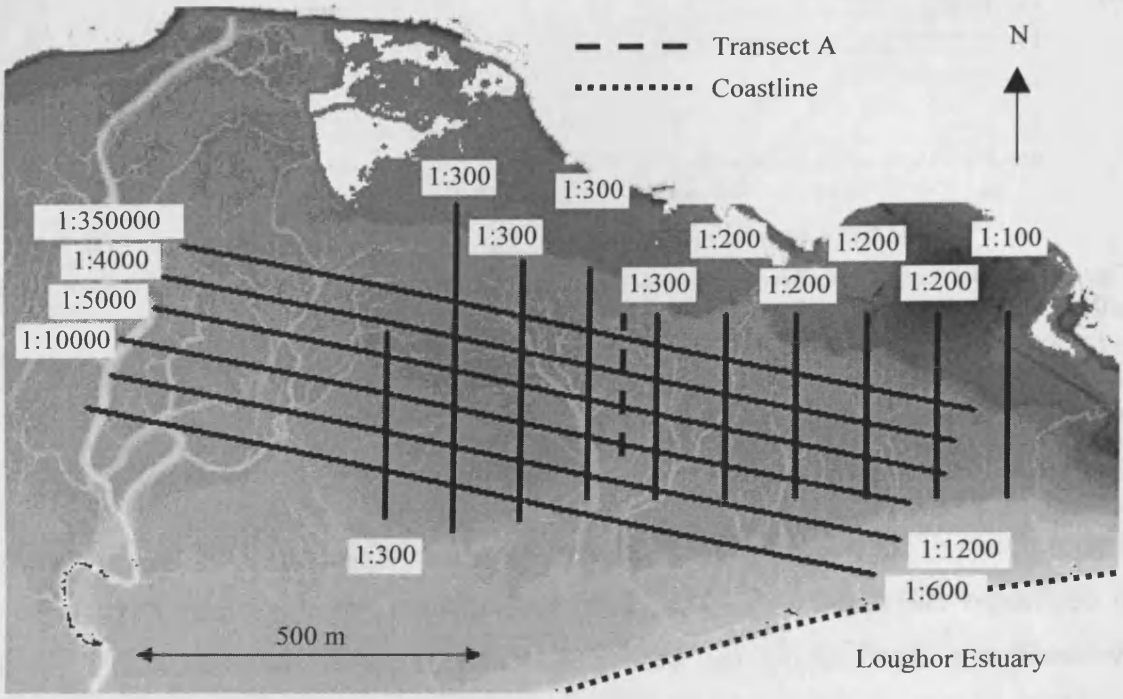

Figure 3-6 Bed gradients around transect A as calculated from LiDAR data

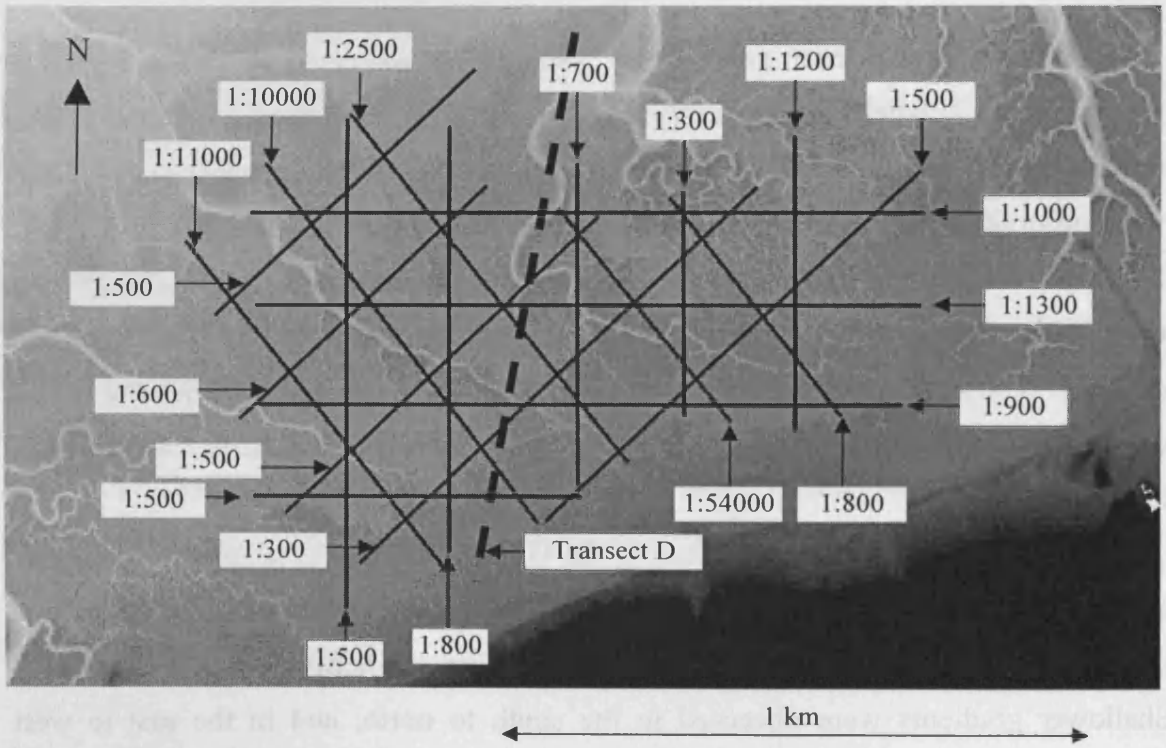

Figure 3-7 Bed gradients around transect D as calculated from LiDAR data

3.2.3 Monitoring Locations

Five transects were monitored during the field study: two along the Llanelli saltmarsh (transects A and B), and two along the Gower saltmarsh (transects D, E and F). Each transect consisted of a number of sampling locations, and each location consisted of four or five sampling points within close proximity to each other. The sampling locations were selected along a North-South direction which was usually equivalent to the maximum gradient as shown by the LiDAR data presented in Section 3.2.2.3. Where data was collected to characterise the vegetation, four sampling points; 'a', 'b', 'c', and 'd', were arranged in a square formation with 5.0m edges at each location, and each point distinguished by a coloured marker. This is illustrated in the schematic diagram of Transect B presented in Figure 3-8. In some cases, additional sampling was conducted at a fifth sampling point; 'e', although this was not marked, and varied in position with each sampling event as discussed later. Results from the characterisation of the vegetation are presented in Chapter 4. Despite the smaller size of the Llanelli site, two transects were monitored to determine the consistency of the vegetation cover across the site, namely, transects A and B (Figure 3-9). Transects D, E and F were monitored along the Gower site (Figure 3-10). The first point along each transect (A1, B1, D1, E1, F1) were the most inland whilst points A6, B7, D4, E4 and F6 were the closest to the estuary.

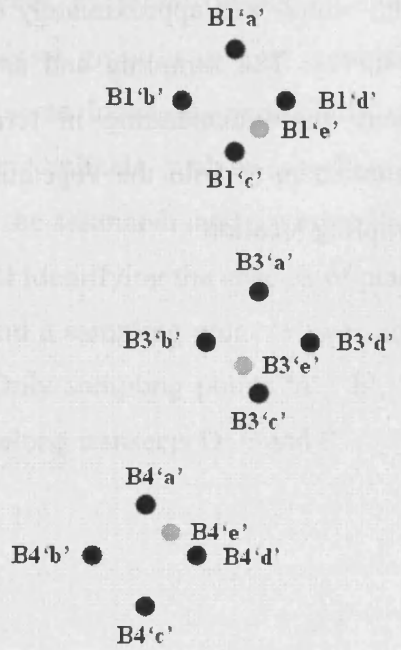

Figure 3-8 A schematic diagram illustrating Transect B, and the four sampling locations where *Sp. anglica* was monitored: B1, B3 and B4. Each sampling location consisted of four main points labelled 'a', 'b', 'c' and 'd' as well as a fifth sampling point, 'e' which was chosen at random during each sampling event and at each sampling location.

The dominant species of vegetation identified at the Llanelli site was *Spartina anglica* (common cordgrass). This is consistent with the findings of the Salt Marsh Survey of Great Britain County Report for West Glamorgan and Llanelli (Burd, 1989), although according to the report, a number of other species were identified along the Eastern, Western and Northern peripherals of the site. These locations fell outside the region where the fieldwork was conducted, the focus of which was to characterise the most significant species encountered on the sites. A second species, namely *Salicornia*, was identified during the spring in areas dominated by *Spartina anglica*, although in relation to the high concentration of *Sp. anglica* in these regions, *Salicornia* was relatively insignificant. A third species was identified as *Halimione* (sea purslane), however, this was restricted to the banks of creeks.

Even at the local scale, variability in vegetation, to some extent, was likely. Hence, *Sp. anglica* sampling was repeated at sampling points 'a', 'b', 'c' and 'd' for each monitoring location to attempt to capture the level of heterogeneity in the vegetation. Following sampling at a fifth position, namely 'e', the vegetation sampled was harvested and the sample quantified in the laboratory according to the weight of plant material (Section 3.3). The exact location of point 'e' at each sampling location varied slightly during each sampling event, but was chosen within the vicinity of points 'a', 'b', 'c' and 'd'. Samples were measured at the four points, and sample 'e' harvested during each sampling event, which was approximately every month over the duration of the 12-month field survey. The sampling and analysis procedures applied for examining point 'e' were more demanding in terms of laboratory resources, namely oven space and containers to hold the vegetation, and only one sample could be analysed for each sampling location.

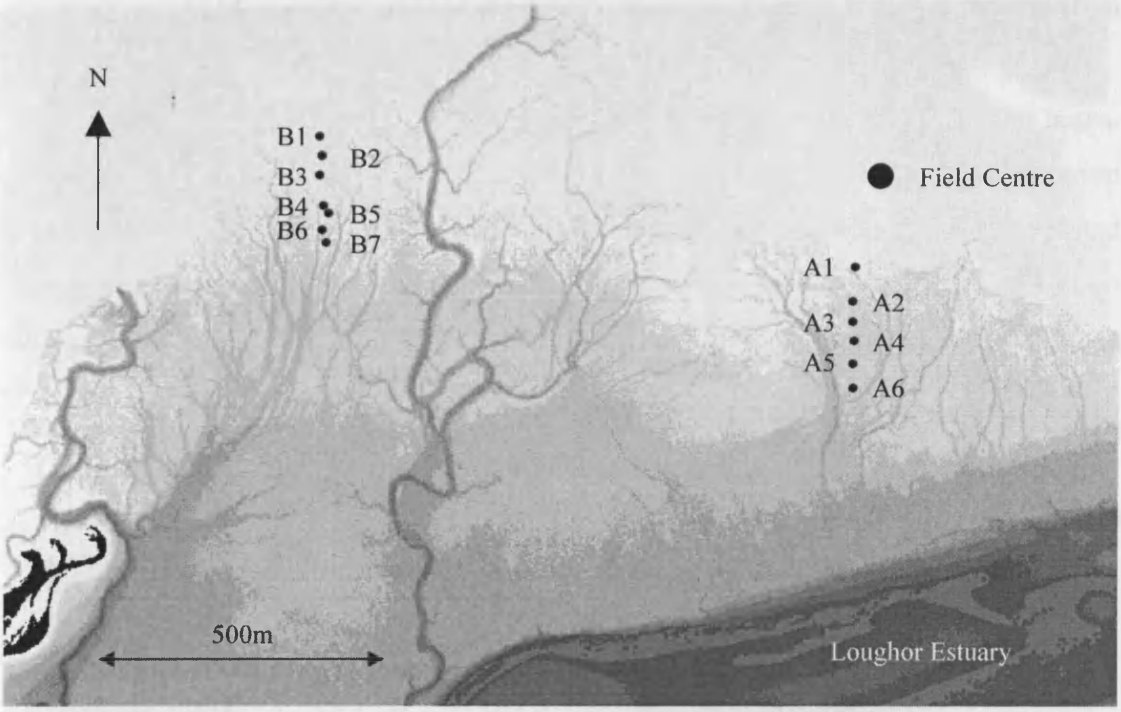

Figure 3-9 Transects A and B on the Llanelli site. Plot produced from LIDAR data collected by the Environment Agency.

Numerous species were identified along transects D, E and F on the Gower site. According to the Salt Marsh Survey of Great Britain County Report for West Glamorgan and Llanelli (Burd, 1989), the most dominant of these include *Puccinellia* (common saltmarsh grass), *Salicornia* (glasswort), *Sp. anglica* (common cordgrass), *Festuca* (blue fescue), *Plantago* (plantains) and *Limonium Armenia* (sea lavender). The vegetation species grow in various combinations and quantities across the site (Burd, 1989). At some locations, particularly where the vegetation was not easily accessible to grazing animals, such as sampling point F7, *Sp. Anglica* was identified. However, most of the saltmarsh land covering the North coast of the Gower was very heavily grazed, and identifying the species of plants was difficult. Vegetation was too short to harvest, and a sampling point 'e' was not designated as described earlier for the Llanelli site. Only sampling points 'a', 'b', 'c' and 'd' were designated to each sampling location along transects D, E and F.

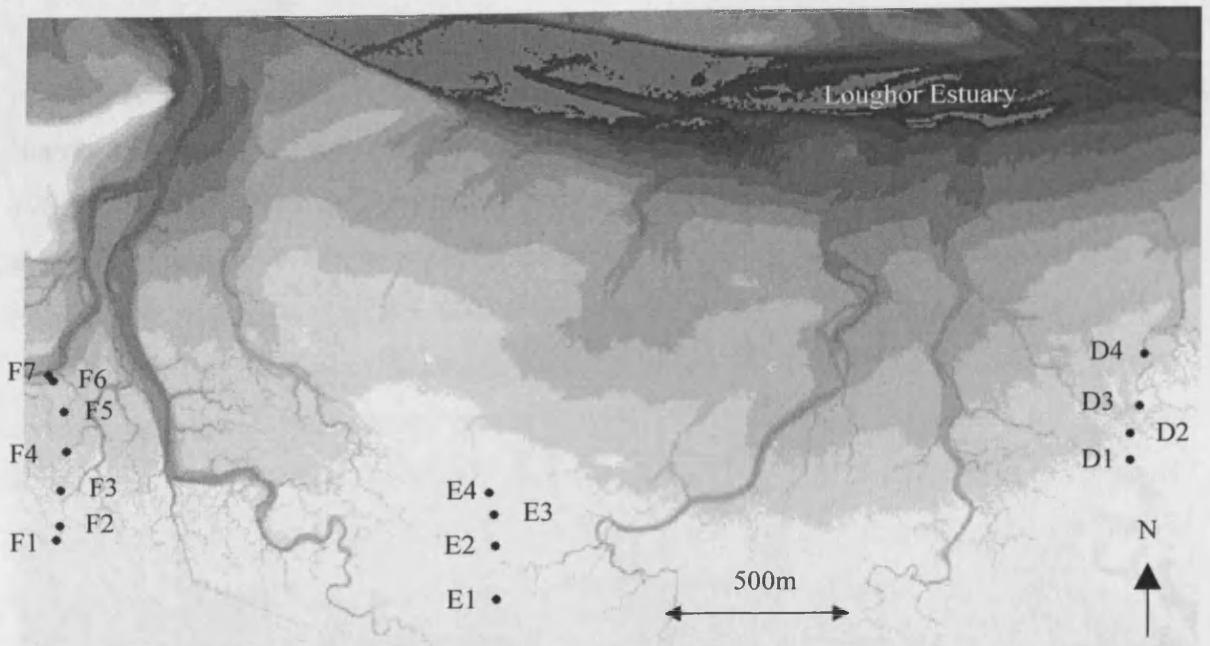

Figure 3-10 Transects D, E and F on the Gower site. Plot produced from LIDAR data collected by the Environment Agency.

3.3 Tidal Inundation of *Spartina anglica* Saltmarshes

3.3.1 The Significance of Vegetation Submergence

Submergence is defined as the ratio of flow depth to vegetation height. The hydraulic resistance of a vegetation cover is strongly dependant on the level of submergence (see Section 2.3.4). The aim of the work presented in this section is to determine the range of submergence levels that may be encountered along a natural saltmarsh. Based on these findings, the submergence levels implemented in a laboratory investigation designed to investigate the effects of *Sp. anglica* canopies on hydrodynamics (see Chapter 7) will be selected to fall within this range.

3.3.2 Chart Datum and Ordinance Datum

Two different datum levels are used for referencing water depths during a tidal cycle and ground elevations known as Chart Datum and Ordinance Datum respectively (Figure 3-11). Tidal levels are quoted relative to chart datum (CD); approximately the lowest water level due to astronomical effects, particularly the positions of the sun and the moon relative to the earth, but excluding meteorological effects, such as wind and rain. Chart datum varies for different locations, and is

assigned to avoid negative values, and tide levels are quoted above chart datum (ACD).

Ordinance datum, OD, is a vertical datum used to derive altitudes on maps, and is commonly equivalent to the mean sea level. In Great Britain, ordinance datum is defined as the mean sea level at Newlyn in Cornwall, and elevations are quoted above ordinance datum (AOD). The difference between ordinance datum and chart datum varies for different locations, and is equal to 5.00m at Mumbles, near Swansea (Figure 3-12).

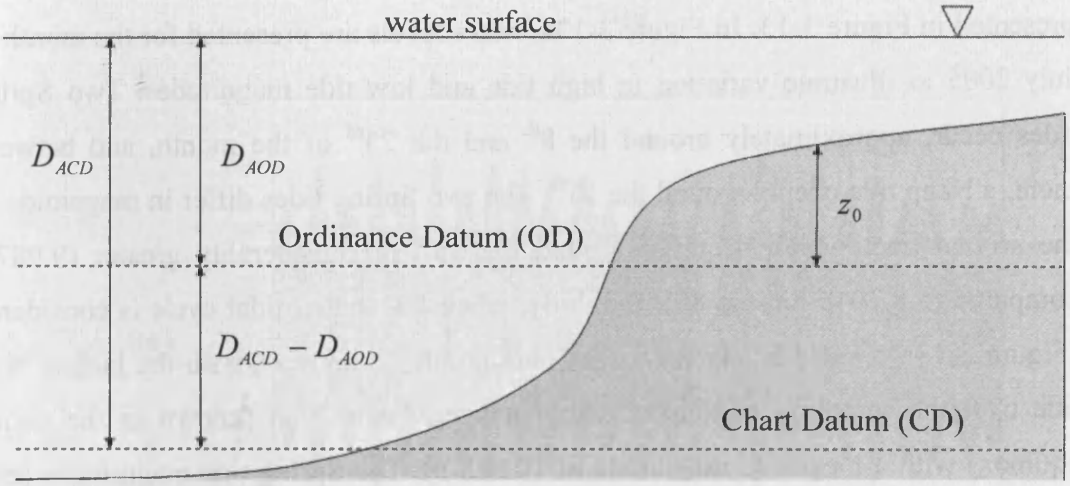

Figure 3-11 Schematic diagram of water depth for a typical tidal event, quoted above ordinance datum, D_{AOD}, and above chart datum, D_{ACD}

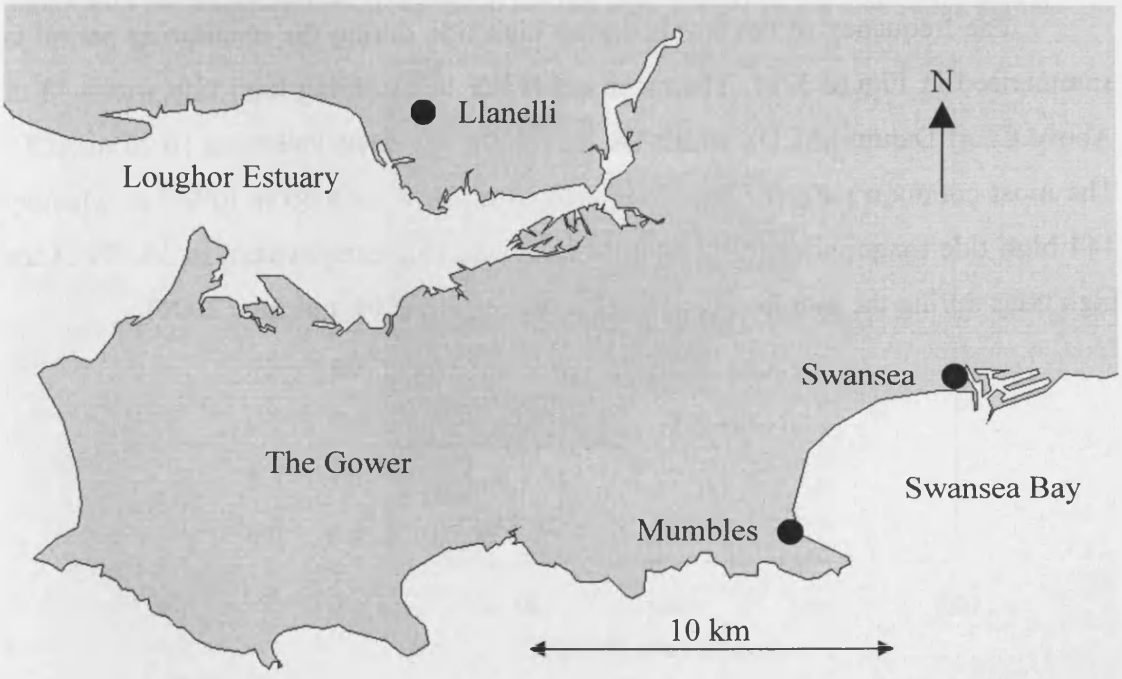

Figure 3-12 Map showing the locations of the Loughor Estuary in relation to Swansea and Mumbles. Map produced from Ordinance Survey data.

3.3.3 Tides and Tidal Cycles

Predictions of high tide magnitudes are presented for numerous towns and cities located along the British coastline in the Admiralty tide tables. The closest location to the study sites where predictions are available is the city of Swansea (see Figure 3-12). Historic sea level data is also available from the British Oceanographic Data Centre and are logged at most major ports around the country. The nearest port to the monitored sites where data is available is Mumbles, which is approximately 5.7 km from the city of Swansea (see Figure 3-12). The data for the monitoring period is presented in Figure 3-13. In Figure 3-13a, water levels are presented for the month of July 2005 to illustrate variation in high tide and low tide magnitudes. Two Spring tides occur, approximately around the 8th and the 23rd of the month, and between them, a Neap tide occurs around the 15th. The two Spring tides differ in magnitude as the second one, which occurred around the 23rd is considerably greater (9.987m compared to 8.704m on the 8th). Similarly, when the annual tidal cycle is considered (Figure 3-13b), water levels vary from one month to the next, with the largest high tide over the sampling period occurring in late March 2006 (known as the vernal equinox) with a measured magnitude of 10.628 m. The Spring tide magnitudes peak again in late summer around September (known as the autumnal equinox), where in 2005, water levels reached 10.261m above sea level.

The frequency of sea levels during high tide during the monitoring period is summarised in Figure 3-14. The mean sea water level during high tide was 8.48 m Above Chart Datum (ACD), whilst the maximum sea water level was 10.26 m ACD. The most common range of sea water levels was between 8.50 m to 9.0 m whereby 144 high tide magnitudes fell within this bracket. This is equivalent to 19.7% of the high tides during the monitoring period (between July 2005 and June 2006).

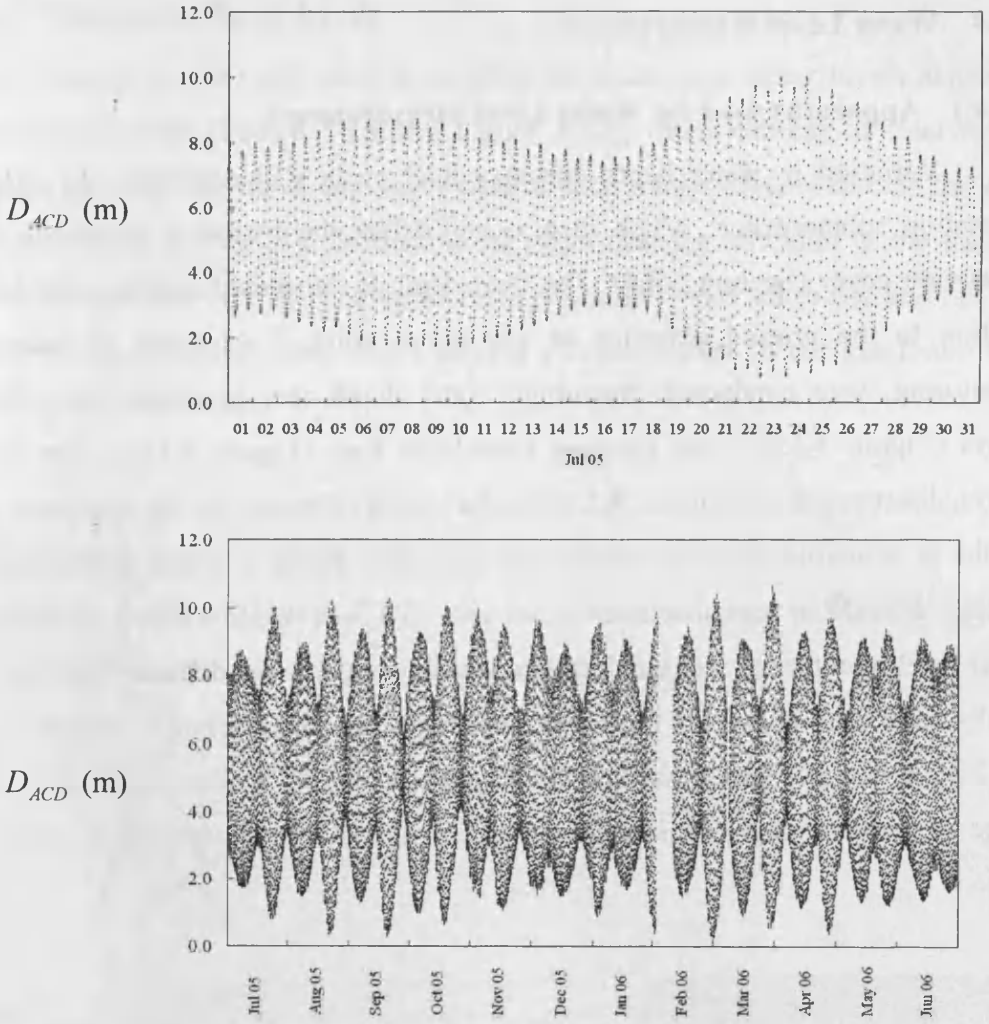

Figure 3-13 Sea water levels at Mumbles (a) for July 2005 and (b) for the monitoring period

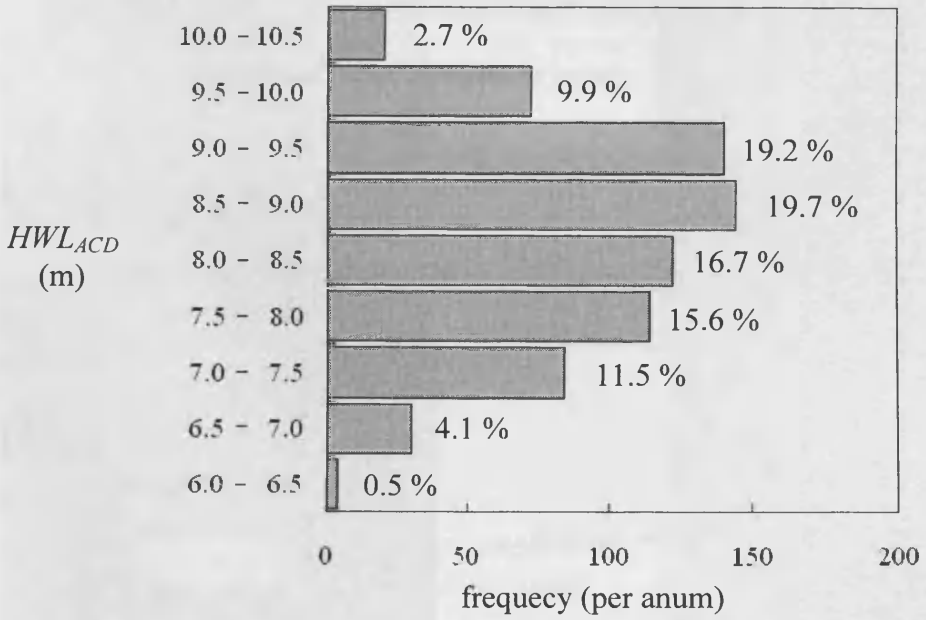

Figure 3-14 High Water Levels (*HWL*) during high tide at Mumbles (Above Chart Datum). Levels are divided into classes with a range of 0.5 m and the frequency per annum of each class is shown.

3.3.4 Water Level Measurements

3.3.4.1 Apparatus used for Water Level Measurements

Variation in water depth during a tidal cycle will determine the extent of vegetation submergence, which in turn will affect the hydraulic resistance of the vegetation cover (Section 2.3.4). The flow depth is dependent on the water level in relation to the ground elevation at any given point. Two types of water level monitoring were conducted: maximum water depth measurements using floating buoys (Figure 3-15b), and pressure transducer logs (Figure 3-15a). The floating buoys, discussed in Section 3.3.4.2, offered a means of measuring the maximum water depths at numerous locations across the field sites during a single tidal event. The pressure transducer logs, discussed in Section 3.3.4.3, provided a means of continuous water level monitoring over the duration of tidal events at two different locations. The results were used to predict the submergence profile for an area of saltmarsh which can have a range of bed elevations and vegetation canopy heights resulting in a wide range of water depths and inundation periods across the site during a single tidal cycle.

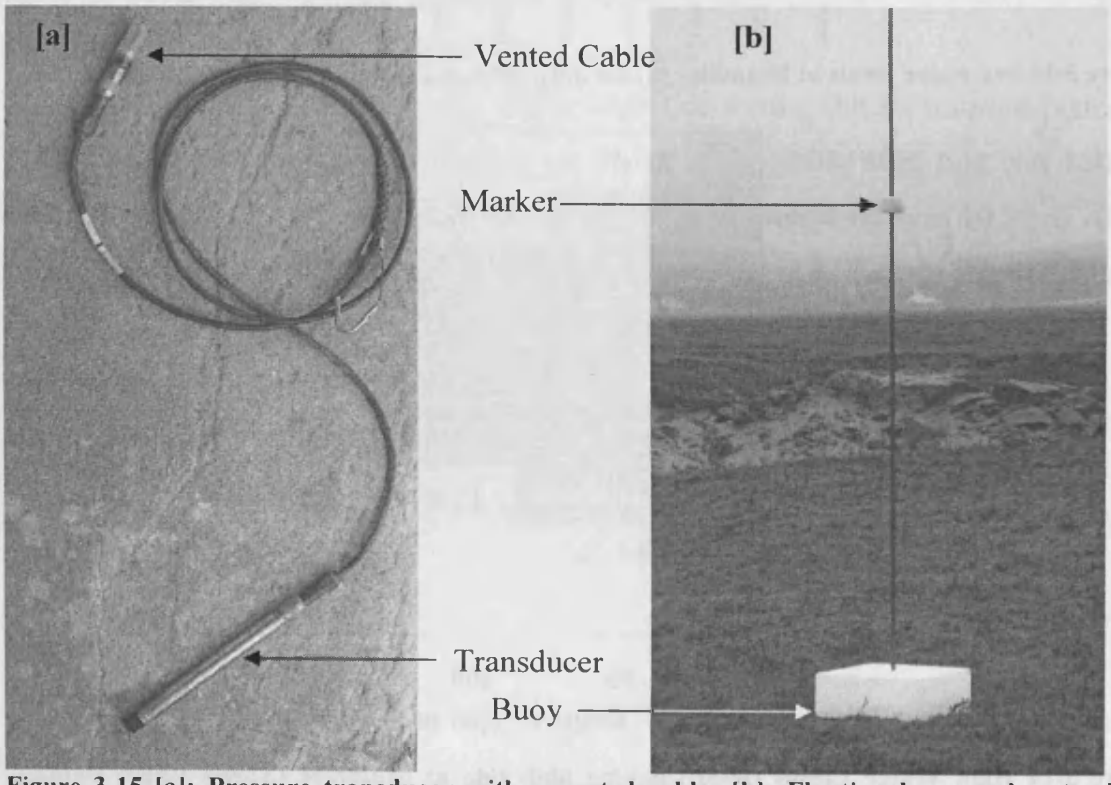

Figure 3-15 [a]: Pressure transducer with a vented cable; [b]: Floating buoy and water level marker.

3.3.4.2 Maximum Water Levels

Floating buoys were used to measure the maximum water levels across the monitored transects (Figure 3-16 and Figure 3-17), for a number of tidal events. Sampling points at the north and south ends of each transect were selected for water level monitoring as well as a third sampling point near the midpoint of the transect. The buoys were deployed at the measurement points and were left to rise and fall with the tide along a guiding pole, whilst forcing a foam marker to the maximum level attained (Figure 3-15b).

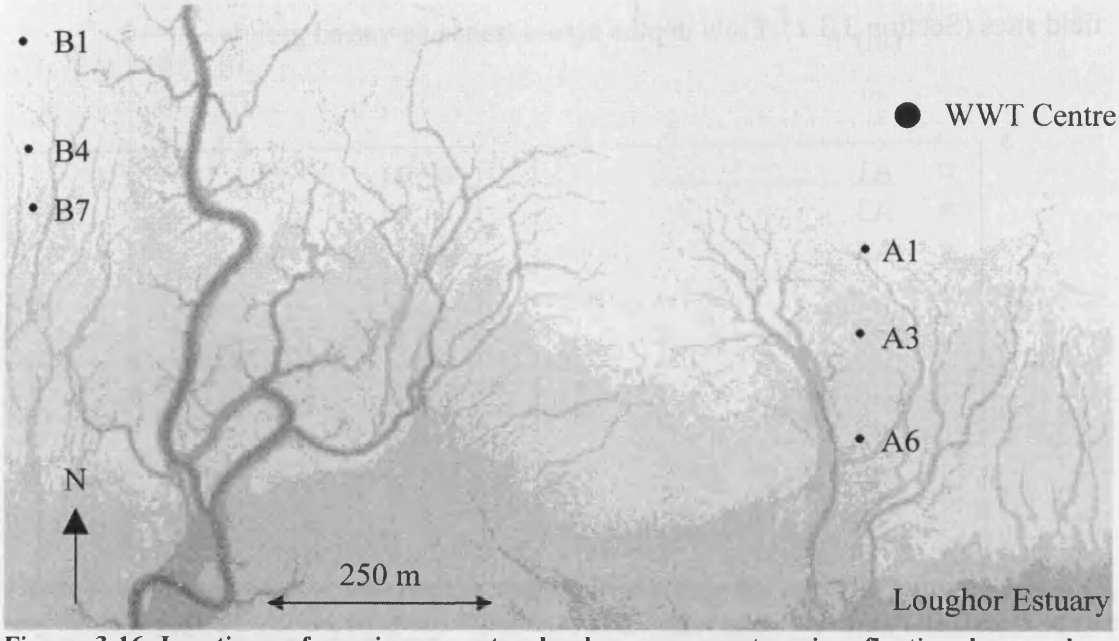

Figure 3-16 Locations of maximum water level measurements using floating buoys along transects A and B. Plot produced from Environment Agency LiDAR data.

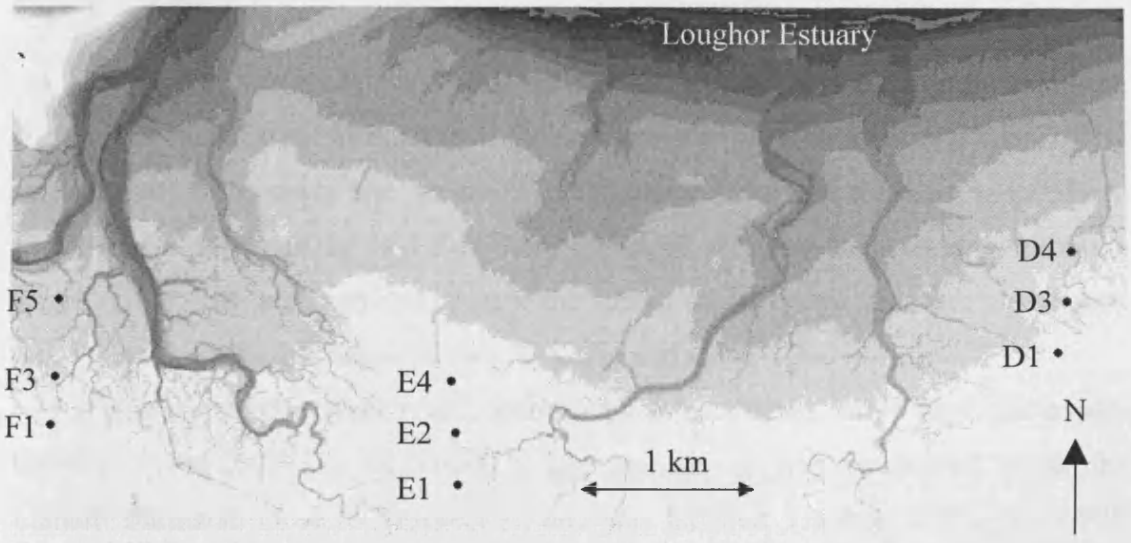

Figure 3-17 Locations of maximum water level measurements using floating buoys along transects D, E and F. Plot produced from Environment Agency LiDAR data.

The maximum height was measured and recorded during the following visit, and the marker was reset to the starting position. Measurements are presented for transects 'A' and 'B' in Figure 3-18 and for transects 'D', 'E' and 'F' in Figure 3-19. For transects 'A' and 'B' where the measurements were more abundant, the relationships between the flow depths and high tide magnitudes predicted at Swansea in the Admiralty tide tables for each sampling point were linear. For transects 'D', 'E' and 'F', the data was more limited, and relationships were less apparent due to scatter in the data. This is likely due to meteorological factors which may affect the water depth along the transects compared to the high tide magnitudes at Swansea near the field sites (Section 3.3.1). Flow depths across transects varied greatly.

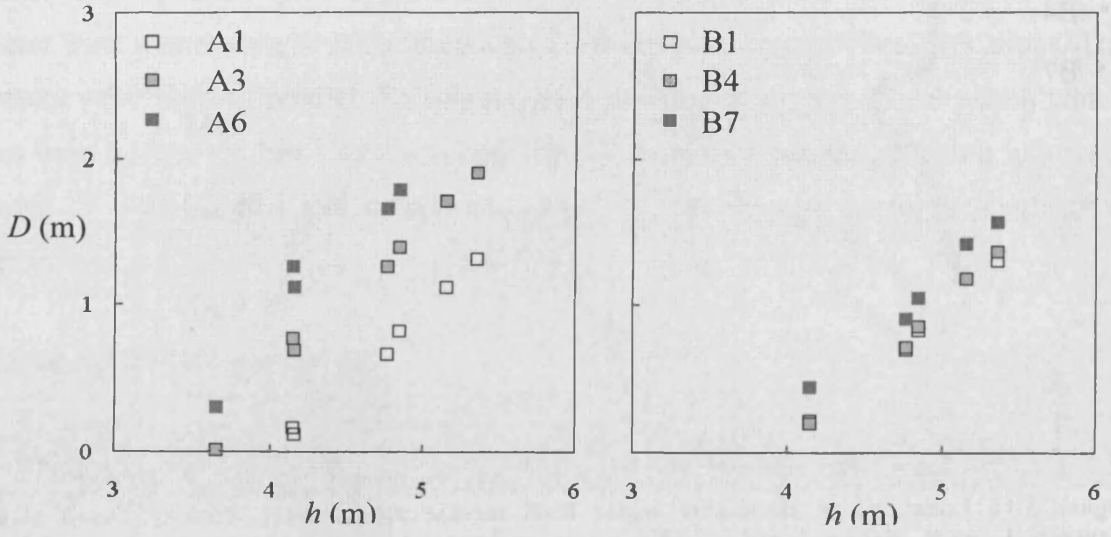

Figure 3-18 The relationship between the predicted magnitude of a high tide AOD, *h* (from easytide.com), and the flow depth, *D*, at the locations of water level monitoring points along transects A and B

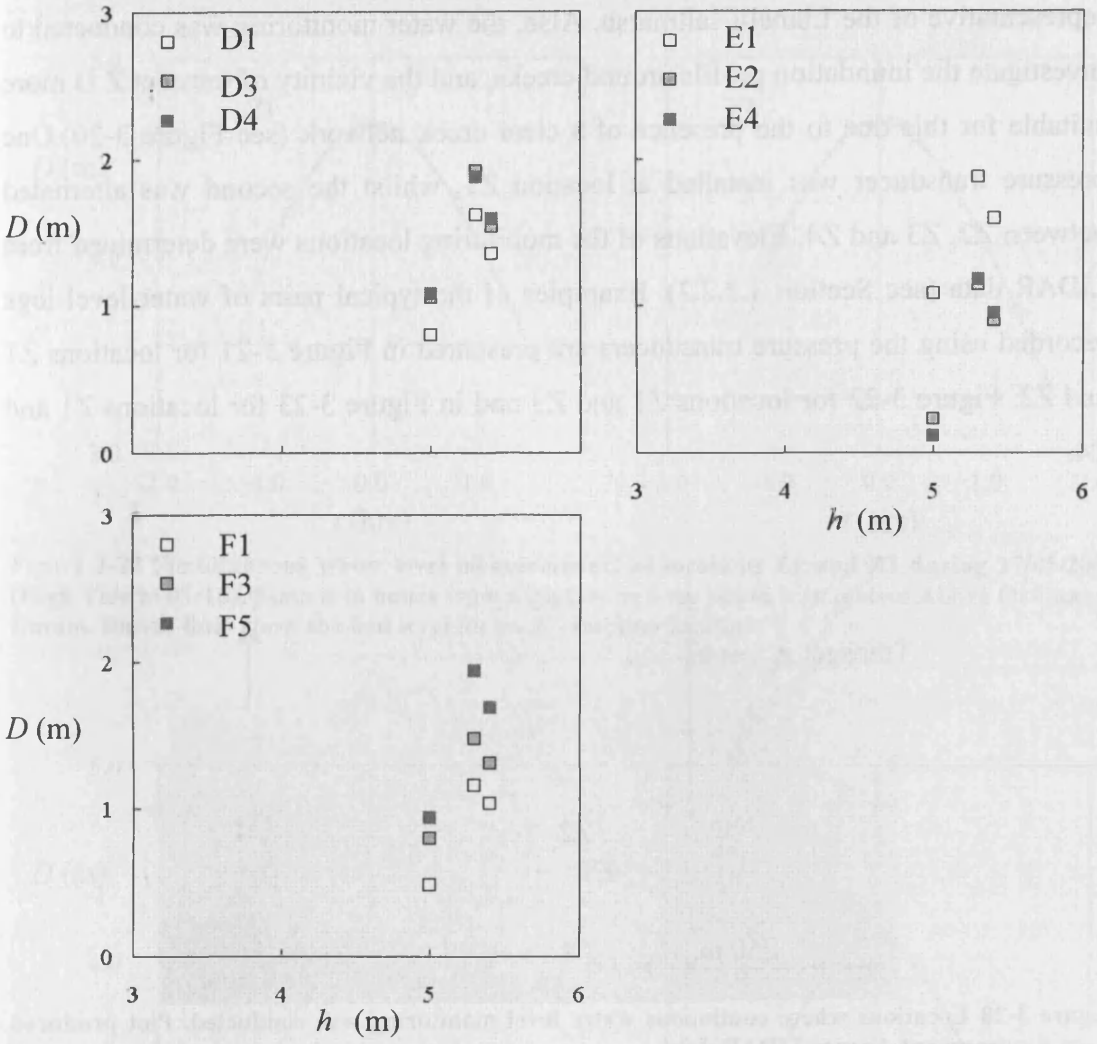

Figure 3-19 The relationship between the magnitude of a high tide AOD, h (from easytide.com), and the flow depth, D, at the locations of water level monitoring points along transects D, E and F

3.3.4.3 Continuous Water Level Monitoring

Two pressure transducers were used to log water depths at different sampling points simultaneously. Level TROLL 500 instruments (manufactured and supplied by In Situ Inc.) were used. The accuracy of the instruments is quoted as +/-0.05% at 15°C. Water depths of up to 1.5 m were measured for some tidal events, although larger tidal events were avoided because the vented cables on the pressure transducers (see Figure 3-15a) must remain above the water surface.

The continuous water level monitoring was conducted for 36 high tide events between 01/04/2007 and 20/05/2007. The monitoring was conducted along the Llanelli saltmarsh close to Transect A, and was labelled Transect Z (Figure 3-20). Although transect Z is at a different locality to transects A and B, the location is

representative of the Llanelli saltmarsh. Also, the water monitoring was conducted to investigate the inundation profile around creeks, and the vicinity of transect Z is more suitable for this due to the presence of a clear creek network (see Figure 3-20).One pressure transducer was installed at location Z1, whilst the second was alternated between Z2, Z3 and Z4. Elevations of the monitoring locations were determined from LiDAR data (see Section 3.2.2.2). Examples of the typical pairs of water level logs recorded using the pressure transducers are presented in Figure 3-21 for locations Z1 and Z2, Figure 3-22 for locations Z1 and Z3 and in Figure 3-23 for locations Z1 and Z4.

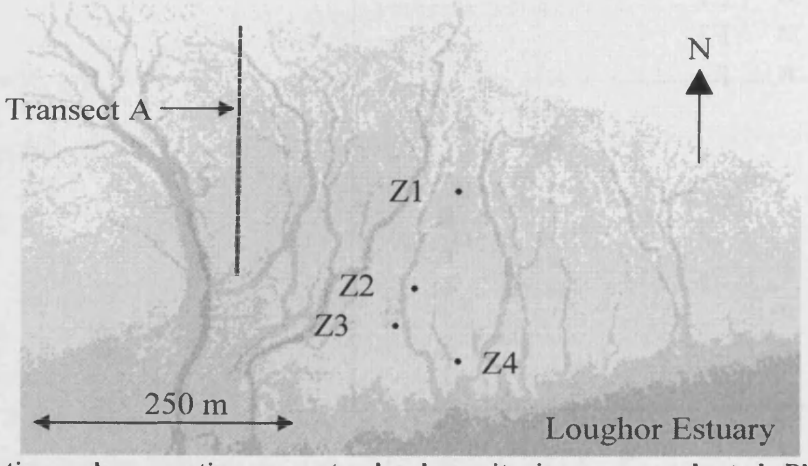

Figure 3-20 Locations where continuous water level monitoring was conducted. Plot produced from Environment Agency LiDAR data.

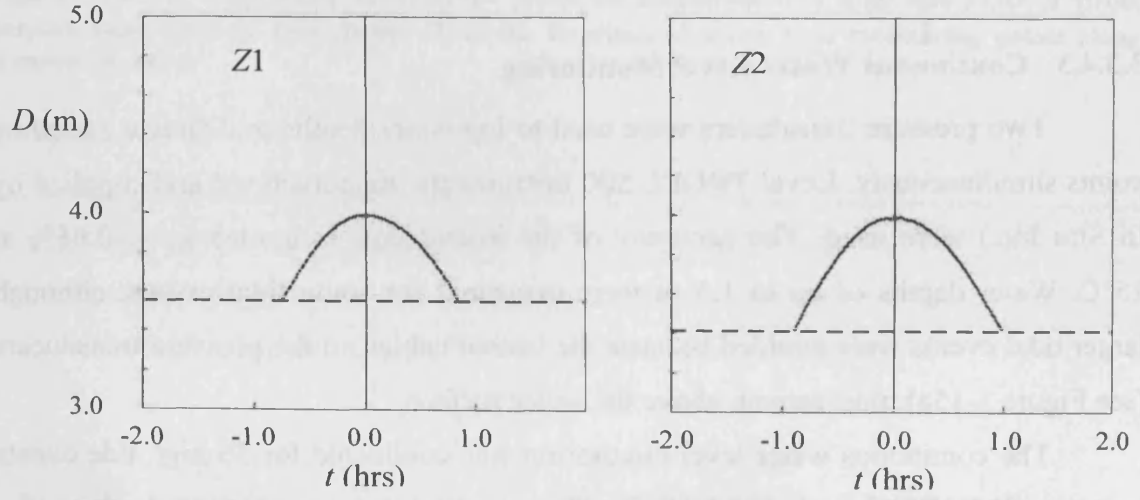

Figure 3-21 Simultaneous water level measurements at locations Z1 and Z2 during 03/05/2007 (High Tide at 19:59). Time is in hours from high tide and the depth is in metres Above Ordinance Datum. Dotted lines show the bed level for each sampling location.

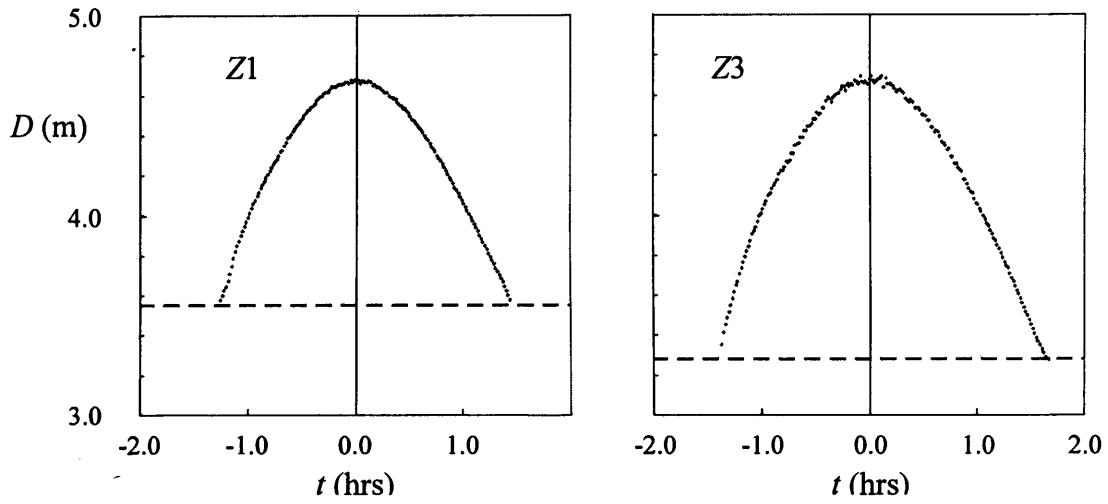

Figure 3-22 Simultaneous water level measurements at locations Z1 and Z3 during 17/05/2007 (High Tide at 07:16). Time is in hours from high tide and the depth is in metres Above Ordinance Datum. Dotted lines show the bed level for each sampling location.

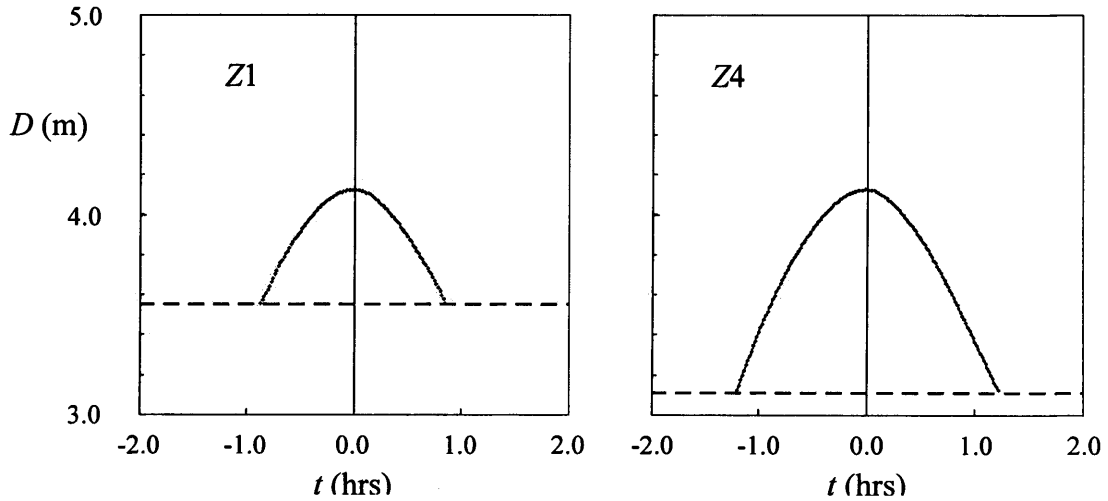

Figure 3-23 Simultaneous water level measurements at locations Z1 and Z2 during 04/04/2007 (High Tide at 08:15). Time is in hours from high tide and the depth is in metres Above Ordinance Datum. Dotted lines show the bed level for each sampling location.

3.3.4.4 Characterising the Inundation Profile

Each inundation cycle taking place over a high tide event conformed to a parabolic profile which was described by means of a symmetrical second-order polynomial trend line centred about the y axis, and intersecting it at a value of unity. The equation of the trend line can be described as follows:

$$\frac{D}{D_{\max}} = A\left(\frac{t - t_{HT}}{2t'}\right)^2 + 1 \qquad \text{[Equation 4.01]}$$

where D is the water depth at time t, and the maximum water depth, $D_{\max}$, occurs at a time of t_{HT}, $2t'$ is the duration of tidal inundation, and A is the trend line coefficient.

To derive general equations applicable to different tide magnitudes, the water depth was normalised by the maximum value, and the time parameter by the tidal event duration i.e. the duration over which the water level was greater than the ground level for a given location. In Figure 3-24, an inundation profile from sampling point Z1 is presented as an example.

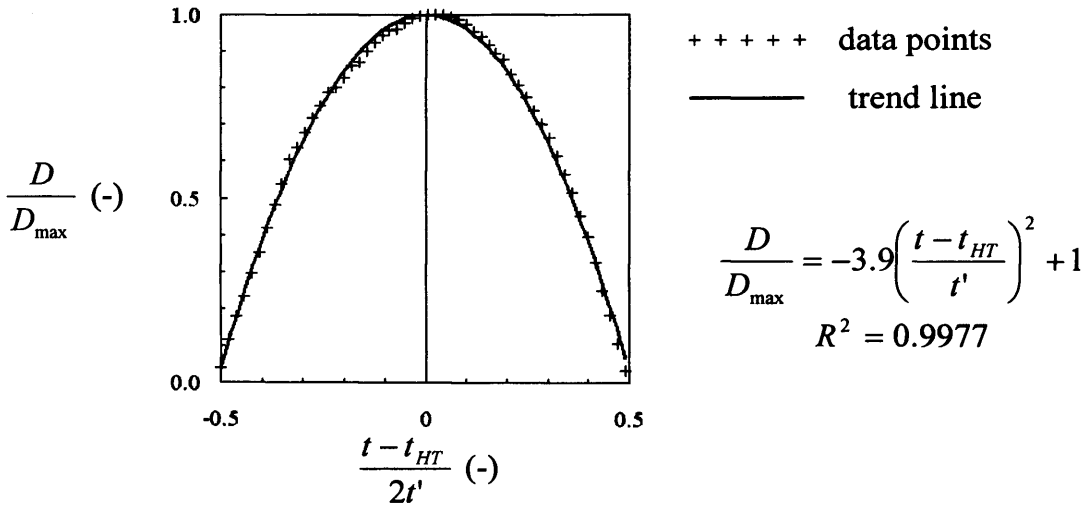

Figure 3-24 Temporal variation of flow depth elevation at monitoring point Z1 on 01/04/2007 where high tide occurred at 19:08. D is the flow depth, $D_{\max}$ is the maximum flow depth which occurs at t_{HT}, the time of high tide. t is the time during a tidal event, t' is the total duration of the tidal event, and R^2 is the coefficient of determination.

The procedure for describing the profile shapes was repeated for each sampling point individually by investigating the trend lines for all events during which pressure logs were collected. There was little variation in the value of the constant, A, between the different sampling points, as presented in Table 3-2.

Table 3-2 Summary of Inundation Profile Shape trend line statistics

	A		
Z1	-3.9	±	4.4%
Z2	-4.1	±	1.7%
Z3	-4.5	±	5.0%
Z4	-4.2	±	4.4%

It was mentioned earlier that one pressure transducer was maintained at location Z1 whilst a second transducer was rotated between the remaining locations and inundation profiles were therefore available for location Z1 for all high tide events monitored. Hence, the flow depth at locations Z2, Z3 and Z4 could be equated in terms of the flow depth at Z1 as shown in Figure 3-25. Meanwhile, the maximum flow depth at location Z1 could be determined based on the available High Water Level measurements recorded by the British Oceanographic and Demographic Centre at Mumbles (Figure 3-26).

The high tide flow depths, D_{HT}, were determined for different tidal events, as presented in Figure 3-26, and related to the inundation period, t', for each sampling point (Figure 3-27). The flow depth increased at any given location increased according to the following relationship:

$$t' = 2.5 D_{HT}^{0.5} \qquad \text{[Equation 4.02]}$$

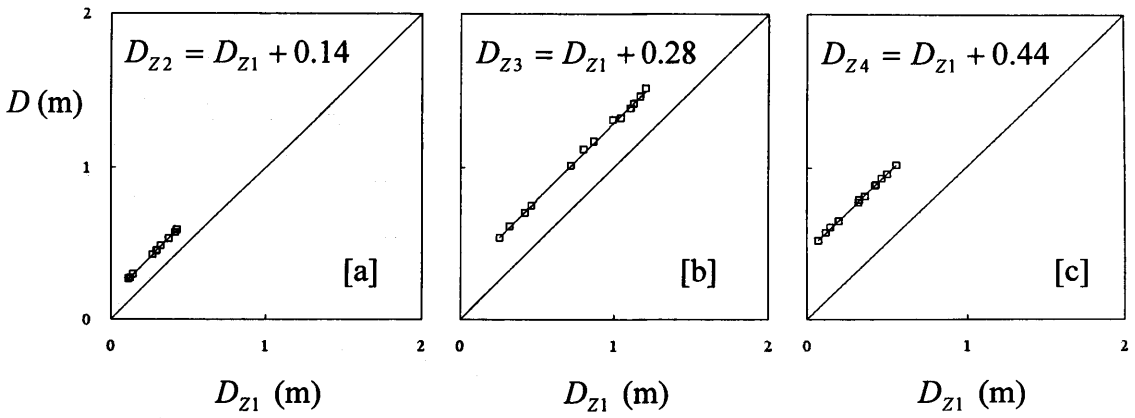

Figure 3-25 Water elevations (D) calculated from pressure logs for pairs of sampling points along transect Z. The relationships presented are for predicting the water elevation at locations Z2, Z3 and Z4 from the water elevation at location Z1.

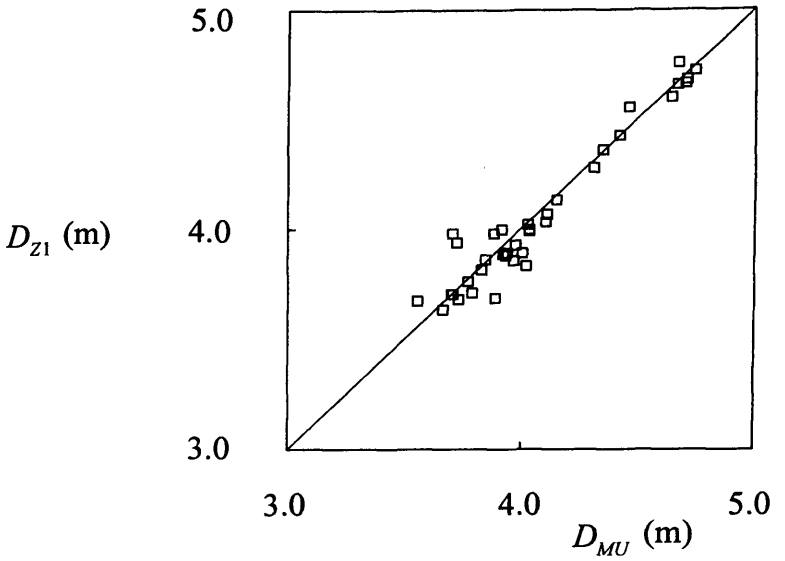

Figure 3-26 Flow depth for High Water Levels at Z1 (D_{Z1}) in relation to the levels recorded at Mumbles as obtained from the British Oceanographic and Demographic Centre (D_{MU}).

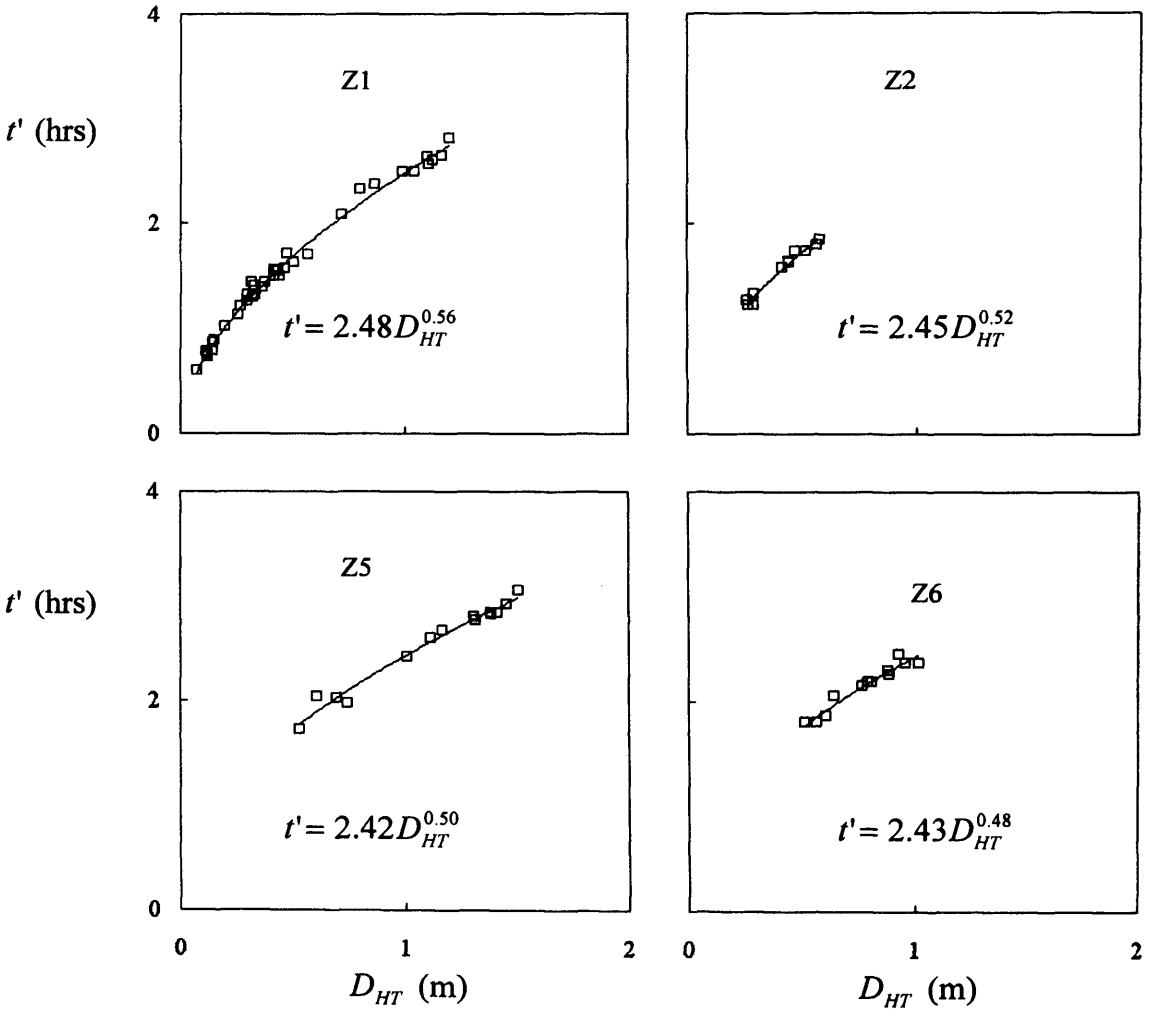

Figure 3-27 the relationship between the duration of inundation (t') and the maximum depth attained (D_{HT}) during the cycle for each sampling point

In Figure 3-28, the flow depths across transect Z for a high tide of 9.5m magnitude at Swansea are illustrated as an example.

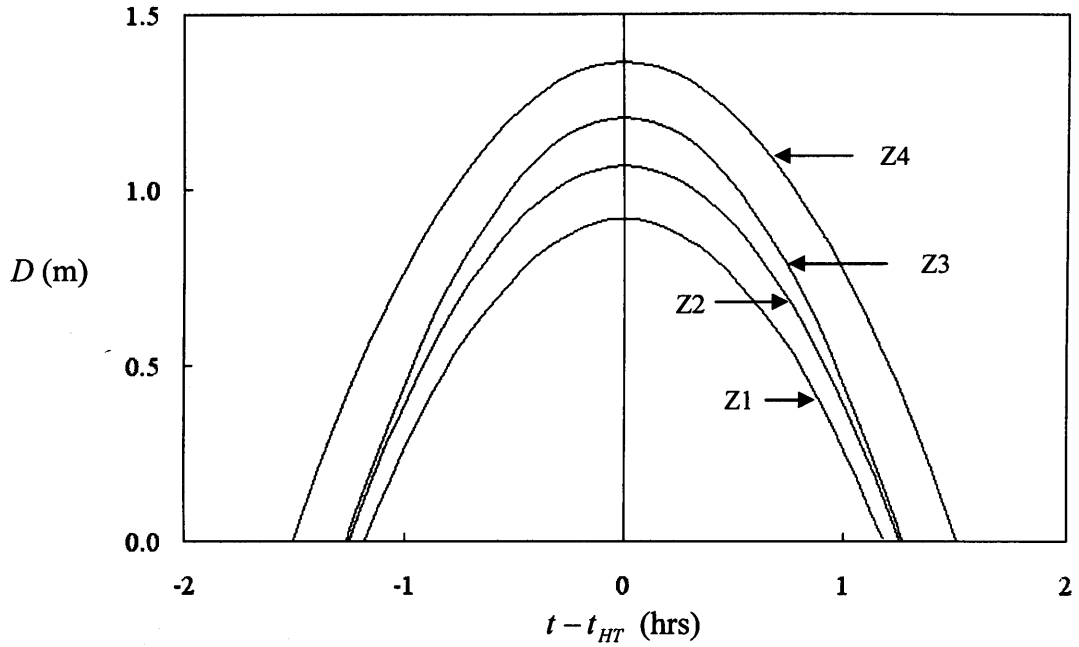

Figure 3-28 Inundation model for a tidal event with a high tide of magnitude 4.5m AOD

3.3.4.5 Predicted Vegetation Submergence Profiles

The variation in vegetation submergence level over the duration of a high tide event could be predicted from the bed elevation, inundation profile and canopy height. Vegetation canopy heights were quantified and the results are presented in the following chapter in Section 4.3.3. For demonstrating the relationship, an average *Spartina anglica* canopy height of 308 mm is assumed based on the mean 90th percentile canopy height from the data. A bed elevation of 2.455m was imposed based on the mean bed elevation for the Llanelli saltmarsh as determined from the LiDAR data in Section 3.2.2.2. Based on the 12-month tide data presented in Section 3.3.3, the model was applied for the mean high tide level of 8.48 m Above Chart Datum (equivalent to 3.48 m Above Ordinance Datum) and the maximum high tide level of 10.26 m ACD (equivalent to 5.26 m AOD). The mean high tide and maximum high tide result in the profiles presented in Figure 3-29a and Figure 3-29b respectively. For a mean high tide event, where the sea level is 3.48 m AOD during high tide, tidal inundation of the ground at the mean bed elevation level is estimated to last 1.8 hours during the tidal event and the maximum submergence level during high tide is

estimated to be 1.9. For the maximum tide magnitude of 5.26 m AOD, tidal inundation is estimated to last 3.9 hours and the maximum submergence level is estimated to be 5.4.

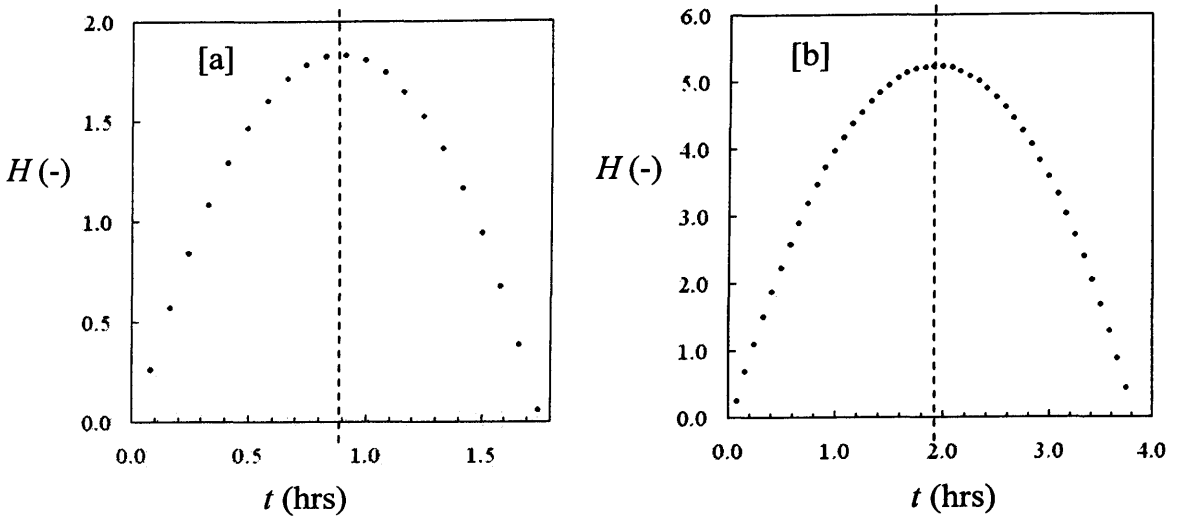

Figure 3-29 Submergence model results for a bed elevation of 2.455 m, a canopy height of 0.308 m and [a]: a mean high tide of 3.48 m AOD; [b]: a maximum high tide of 5.26 m AOD.

3.3.4.6 Estimated Annual Vegetation Submergence Levels

The relationship presented in the previous section was applied to two of the sampling points monitored along transect A (A3 and A6) for the monitoring period (July 2005 to June 2006). For the model, monthly canopy heights were selected based on the 90th percentile canopy heights for *Spartina* (see Section 4.3.3). Water levels for the monitoring period were obtained from the British Oceanographic and Demographic Centre and are presented in Section 3.3.3, and bed elevations were determined from the LiDAR data presented in 3.2.2.2. For A3 and A6, the bed elevations were 3.483m and 3.075m AOD respectively. Results are presented in Figure 3-30 where submergence levels were divided into classes with a range of 0.25, and the duration of the submergence level falling within each class during the monitoring period is shown. As expected, A3, which is higher in elevation, experienced considerably lower submergence during the monitoring period. To quantify this property, the parameter 'submergence hours' is introduced. This is defined as follows:

$$H_T := \sum_{i=1}^{i=n} H_i t_i \qquad \text{[Equation 4.03]}$$

where i is the class number, n is the total number of classes, H_i is the submergence level of a class and t_i is the duration in hours during a twelve-month period that the aforementioned submergence is observed at a sampling points. Values calculated for A3 and A6 were 1400 and 2910 hours respectively indicating that submergence at A6 was considerably more significant.

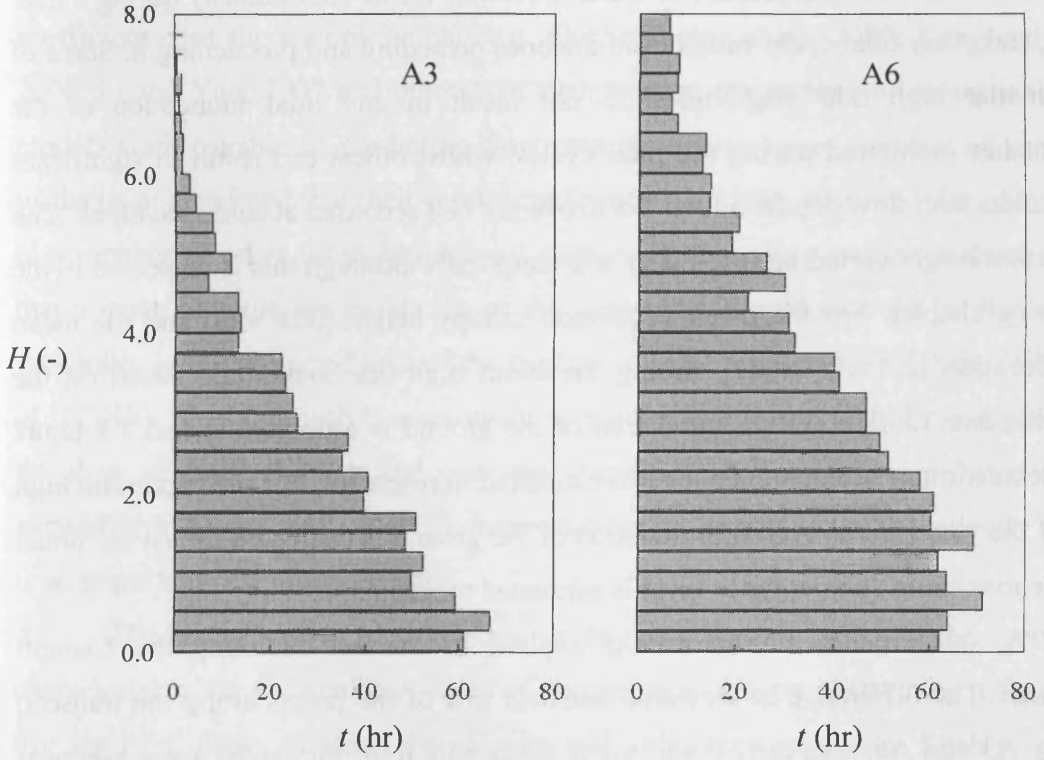

Figure 3-30 Results from the submergence model applied to A3 and A6 along transect A.

3.4 Concluding Remarks

Bed gradients and elevations and water levels were monitored enabling the characterisation of the bed conditions and the flow patterns that are characteristic of the saltmarshes monitored. The information collected was used in the design of the

laboratory experiments to recreate conditions which are relevant to the field sites. The results from the laboratory investigation are reported in Chapter 7.

The results reported from the field survey highlight the complexity of field conditions. Examination of the local geography of the sites indicated a wide range of bed gradients, ranging from negligible gradients to gradients of up to 0.01, and the saltmarshes were overridden by a complex network of creeks that varied in size and density across the sites. These affected the abundance and location of certain vegetation species.

Submergence is determined by the bed elevation, water elevation and the height of the vegetation. The bed elevation varies across a saltmarsh and generally increases away from the coast. The water elevation varies continuously during a tidal cycle, and every tidal cycle varies from the ones preceding and proceeding it. Some of the smaller high tide magnitudes do not result in any tidal inundation of the saltmarshes monitored during the tidal cycles, whilst others can result in significant inundation with flow depths over 2.5m above the bed recorded at some locations. The vegetation height varied both spatially and temporally although this is presented in the following chapter. For the mean vegetation canopy height (308 mm) and the mean bed elevation (2.455m AOD), during the mean high tide magnitude based on the available data (3.48m AOD) inundation of the ground is estimated to last 1.8 hours and the maximum submergence level is estimated to reach 1.9. For the maximum high tide of the year (5.26m AOD), inundation of the ground is estimated to last 2.9 hours and the maximum submergence level is estimated to reach 5.4.

A submergence predictor was applied to transect A along the Llanelli saltmarsh. The difference in elevation between tow of the points along the transect, namely A3 and A6, was only 0.4m, yet if the results from the model were averaged for the inundated periods (i.e. 'dry' periods are ignored), then the estimated average submergence level at the two points are 1.93 and 2.59 respectively. The predicted maximum submergence levels at A3 and A6 are approximately 7.5 and 9.0 respectively, and the total periods of inundation are 725 and 1125 hours respectively. This illustrates the wide range of flow conditions that can be observed on a single saltmarsh.

4 Vegetation Quantification

4.1 Introduction

In two dimensional depth-averaged numerical modelling studies, vegetation resistance is often simplified and characterised through bulk parameters, such as a bulk drag coefficient (e.g. $\overline{C_D}$ in this study, Hammer and Kadlec, 1986; Jenkins and Greenway, 2005 and others), a Manning's roughness coefficient (Somes *et al.*, 1999), or a Darcy-Weisbach friction factor (Fiedler and Ramirez, 2000). In three-dimensional numerical models, vegetation is often assumed to be homogeneous and modelled as an array of uniform cylinders with a constant projected area and drag coefficient over the canopy height (e.g. Fischer-Antze *et al.*, 2000; Kang and Choi, 2006; Li and Yan, 2007 and others). In such studies, the authors often argue that the models were capable of predicting flow patterns across large stretches of vegetated wetlands and claimed that their results conformed well with measured data. However, in a number of other three-dimensional numerical modelling studies, authors agreed that a more accurate representation of the vegetation should account for the vertical variability in the projected area of the vegetation (e.g. Wilson *et al.*, 2006a; Wilson *et al.*, 2006b). This approach is more useful in studies concerned with the complexity of the flow structure through and over the vegetation, and how it is affected by the variability in plant morphology. In these studies, the prediction of the velocity profile is an important part of the research.

The quantification of vegetation in the current study refers to the concept of characterising the physical properties of a vegetation canopy obstructing a flow field that are most likely to affect the velocity and turbulence structures. Such properties include the projected area of obstruction, porosity, material stiffness, stem density per unit bed area and stem diameter. Such properties are likely to vary considerably with elevation over the height of a canopy, and may affect the flow structure in different ways. For instance, a greater level of 'wake sheltering' (Section 2.2.5) is likely for larger stem diameters which can be attributed to larger stem wakes, and for higher stem densities where the stems are more closely spaced together. Quantification of vegetation properties is often neglected in hydrodynamic studies due to the difficulty in measuring the parameters and the high level of variability associated with natural

materials. However, vegetation quantification is necessary to evaluate the obstruction of the flow created by the canopy.

In this chapter, the quantification of vegetation canopies encountered during the field study presented in Chapter 3 is considered. Variation in the density of *Sp. anglica* was quantified over the height of the canopy using two methods employed by Neumeier and Amos (2004). In one method, vegetation obstruction was quantified using digital photographs of canopy cross-sections, and for the second approach, the mass of material in consecutive 20 mm sections along the canopy height was determined. The photographic method offered a more rapid approach for the collection of large amounts of data. The method was non-destructive; hence, monthly repetition of the sampling procedure at the same locations was possible. From the photographs, the relative obstruction, total projected area and percentile canopy heights were determined. Local, spatial and temporal variation in the vegetation was also studied.

4.2 The Photographic Method

4.2.1 The Structure of a *Spartina anglica* canopy

The morphology of the vegetation was classified into three regions. In the lower 50 mm of the canopy closest to the bed, the projected area of obstruction was largely composed of the plant stalks and this was referred to as the stem region (Figure 4-1). In contrast, the higher part of the canopy, above an elevation of 100 mm, was composed mainly of foliage and hence is referred to as the foliage region. In the section of canopy between the stem and foliage regions, there is a gradual increase in projected area of obstruction as the quantity of leaf volume increases steadily with elevation and in this thesis, this is referred to as the transition region.

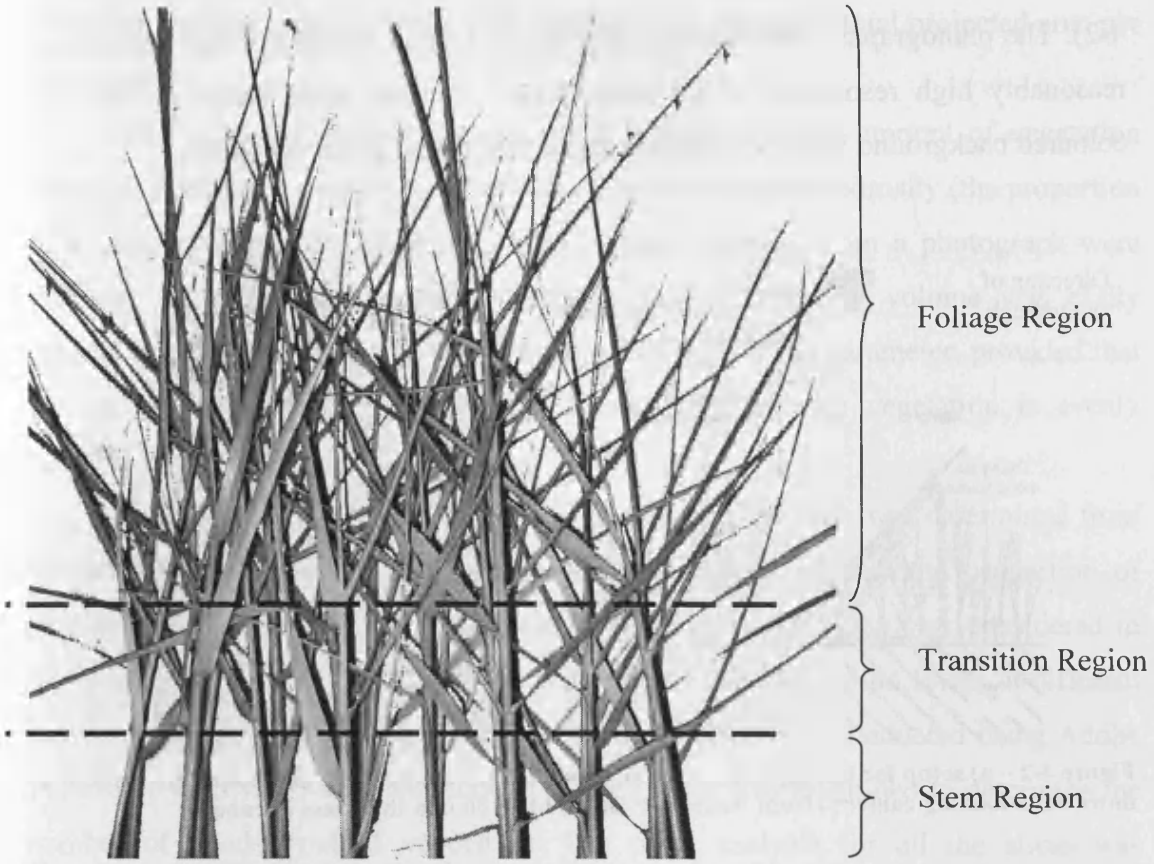

Figure 4-1 The morphology of a *Spartina anglica* canopy. The divisions are provided as a guideline and may vary from canopy to canopy and with the time of year.

4.2.2 Concept and Methodology

The distribution of vegetation material was difficult to quantify due to the complexity of its natural structure. It was achieved in the field and laboratory investigations by using a photographic method similar to that used by Neumeier (2005). To ensure results were representative of the vegetation's natural form and structure, analysis was conducted *in situ* to ensure the canopy was not disturbed. The vegetation was photographed and the images were analysed to determine the amount of plant material present. The method was non-destructive so that the monitoring could be repeated at the same locations monthly to determine any temporal variations in the quantity of plant material.

For a given unit volume, the projected area of obstruction was assumed to be a function of the vegetation density, where vegetation density is defined as the vegetation mass per unit volume. On this basis, the vegetation density was assessed by analysing photographs of canopy cross-sections that were 100mm in thickness (Figure

4-2). The photographs were taken using a digital Canon Powershot A80 camera at a reasonably high resolution of 4.0 mega pixels. A 0.6m wide and 0.8m tall red-coloured background was used for easy distinction of the green vegetation.

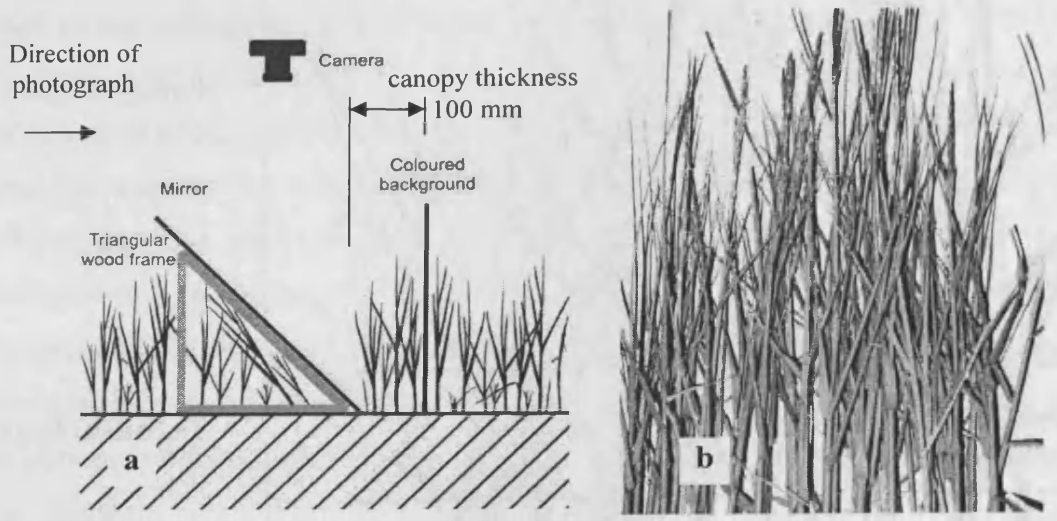

Figure 4-2 – a) setup for taking lateral photographs of the canopy using an oblique mirror and a downward-looking camera (from Neumeier, 2005) b) a 100 mm thickness of canopy.

4.2.3 Projected Area of Obstruction

Given that the cross-sectional photographs were taken for a 100mm thickness of canopy, and the width of the background was 600mm, the sampling volume of each photograph, V, is given by:

$$V = 0.6 \times 0.1 \times \Delta z \qquad \text{[Equation 4.01]}$$

where Δz is the height of the sample volume. Vegetation occupies a proportion of this volume, and from a two-dimensional photograph, the visible projected area of the vegetation can be determined. Furthermore, a proportion of the total projected area of the canopy remains hidden behind the visible part of the canopy. Where the stem densities are known, the total projected areas can be estimated to account for hidden plant material (see Section 5.3.2). However, where the photographic method was used to quantify vegetation canopies in the natural environment in the fieldwork programme presented, the stem densities were unknown, and demonstrated considerable variation (Section 4.4.4), thus, only the visible projected areas are presented. To distinguish between the two parameters here, a' denotes the visible

projected area per unit volume, whilst *a* denotes the estimated total projected area per unit volume.

The projected area of obstruction is indicative of the amount of vegetation material. Whilst determination of the volume and the absolute porosity (the proportion of a sample volume occupied by voids) of plant material from a photograph were difficult, the projected area of obstructing material per unit volume was easily determined. The porosity of the material is a function of this parameter, provided that the sampling section is of a small thickness, and that the vegetation is evenly distributed over the sampling volume.

The amount of vegetation material obstructing the flow was determined from the photographs by considering the pixel content to determine the proportion of vegetation to the total area of the photograph. The cross-section was considered in horizontal layers of 20 mm thickness to determine the obstruction levels at different elevations within the canopy (Figure 4-3). The analysis was conducted using Adobe Photoshop 6.0, where the pixel content of each layer was examined to determine the number of pixels void of vegetation. The pixel analysis for all the slices was combined to determine the distribution of plant material over the height of the canopy (e.g. Figure 4-3).

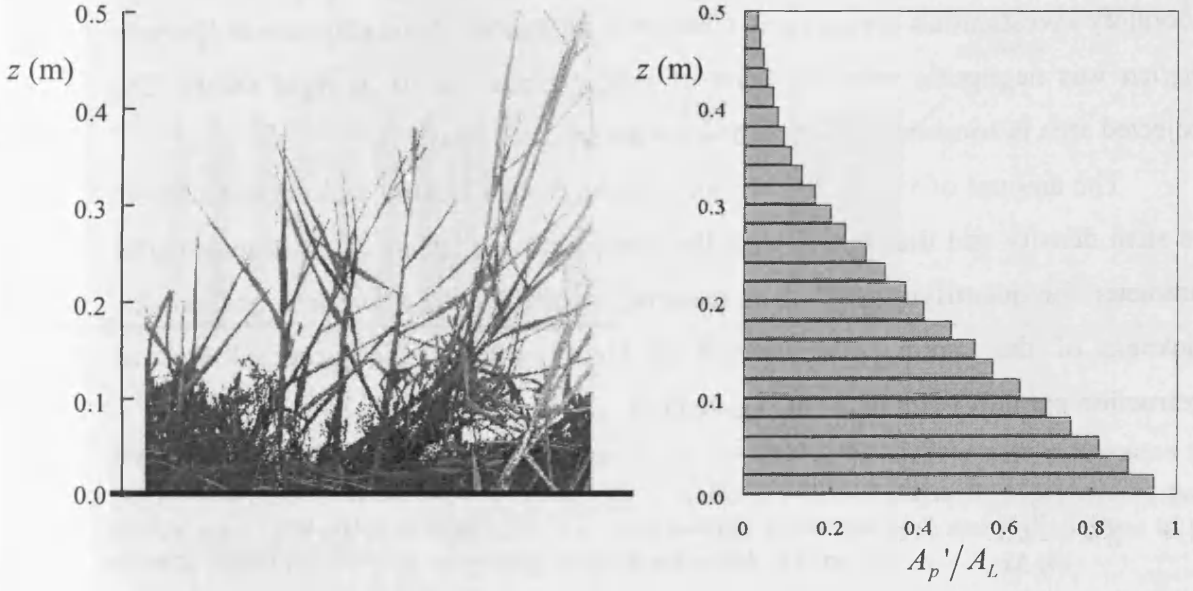

Figure 4-3 Proportion of area occupied by vegetation for horizontal sections of a canopy cross-section based on a photograph taken *in-situ* where z is the elevation of a layer above the bed, A_p' is the visible projected area of vegetation for a given layer, and A_L is the total sample area of the layer

Presented in Figure 4-3 is a cross-section photograph of a natural saltmarsh canopy. In Figure 4-4, profiles of total projected area per unit volume are presented for artificially constructed canopies of *Spartina anglica*, and plastic drinking straws. The profiles of projected area vary because in the laboratory, stems were installed in an orderly, upright fashion and the more developed plants were selected because they were easier to install (Section 5.2.4.2). Selection of the more developed plants also helps to achieve some consistency between the plants used to construct the three vegetation canopies with stem densities of 810, 1160 and 1850 stems m^{-2}. In a natural environment, plants exist in a wider range of sizes accompanied by decomposing material and other loose plant parts that often fall and are retained near the bottom of the canopy. Furthermore, the vegetation experiences periods of regular tidal inundation during which the canopy may be affected by the impact of the flow, and the plants are not always fully vertical. All these factors contribute to differences between the shapes of the projected area profiles for the natural and constructed canopies (Figure 4-4a). In a natural canopy, there is a steady increase in obstructing material towards the bed, whereas in the constructed canopy, there is a clear decrease in the lower part of the canopy where there is an absence of smaller plants, leaves, or other loose debris. For more flexible species, the morphology of the vegetation may vary with the level of inundation however, based on observations during the laboratory investigation presented in Chapter 7, alterations to the structure of *Spartina anglica* was negligible with the level of submergence due to its rigid nature. The projected area is constant with elevation for the uniform array.

The amount of vegetation within a photographed canopy will depend on both the stem density and the thickness of the canopy photographed. A more meaningful parameter for quantifying the plant material density, which takes into account the thickness of the canopy, Δx (defined in Figure 4-2), is the projected area of obstruction per unit volume, a (m^{-1}) given by:

$$a = \frac{A_p}{A_L \Delta x} \qquad \text{[Equation 4.02]}$$

where A_p is the total projected area of the canopy. A_L is the total flow area occupied by the canopy, and Δx is the thickness of the canopy photographed, which

in this case was maintained at 100 mm. This thickness allowed for a reasonable section of the canopy to be analysed such that the results were more representative of the vegetation, yet not too thick so that the background was visible to enable the distinction between the projected areas occupied by vegetation compared to those void of vegetation.

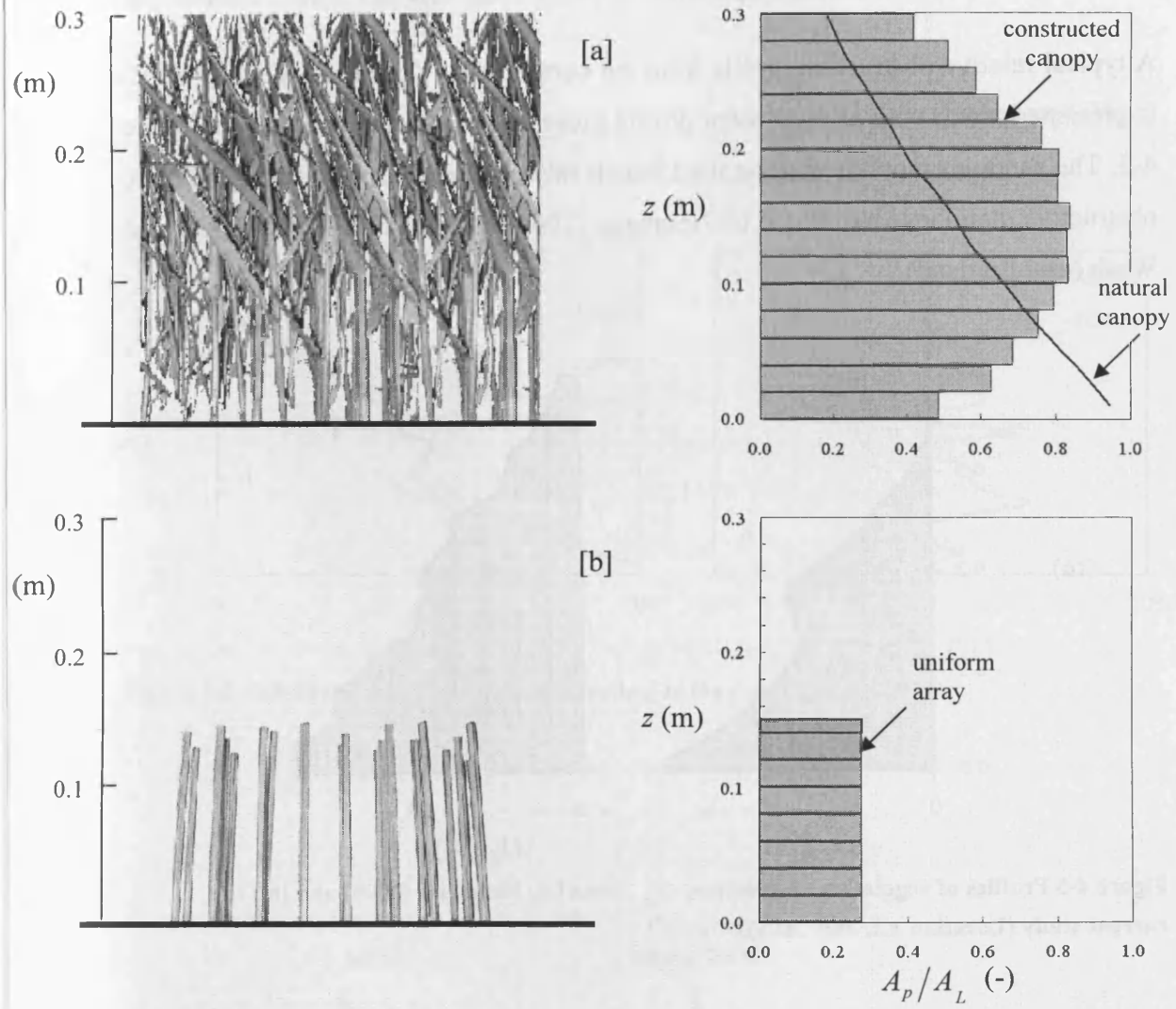

Figure 4-4 The ratio of total projected area, A_p, to the flow area, A_L, for a given elevation for [a]: a constructed *Spartina anglica* canopy; [b]: a uniform array of plastic drinking straws. Both plots are for 1850 stems m^{-2} canopies, z is the elevation above the bed, and the solid line in [a] shows a typical profile for a natural *Sp. anglica* saltmarsh canopy

The relative vegetation obstruction at a given elevation, O_p, was defined as the percentage of the flow area A_i, at elevation z, occupied by the projected area of the canopy, A_{pi}. This can be equated as follows:

$$O_p = \frac{A_{pi}}{A_i} \times 100 \qquad \text{[Equation 4.03]}$$

A typical relative obstruction profile from the current study (Location A2, July 2005) is presented along with an equivalent profile presented by Neumeier (2005) in Figure 4-5. The canopies monitored along the Llanelli saltmarsh appear to be taller and more obstructive than those monitored by Neumeier (2005) on the North-West shore of the Wash (east England).

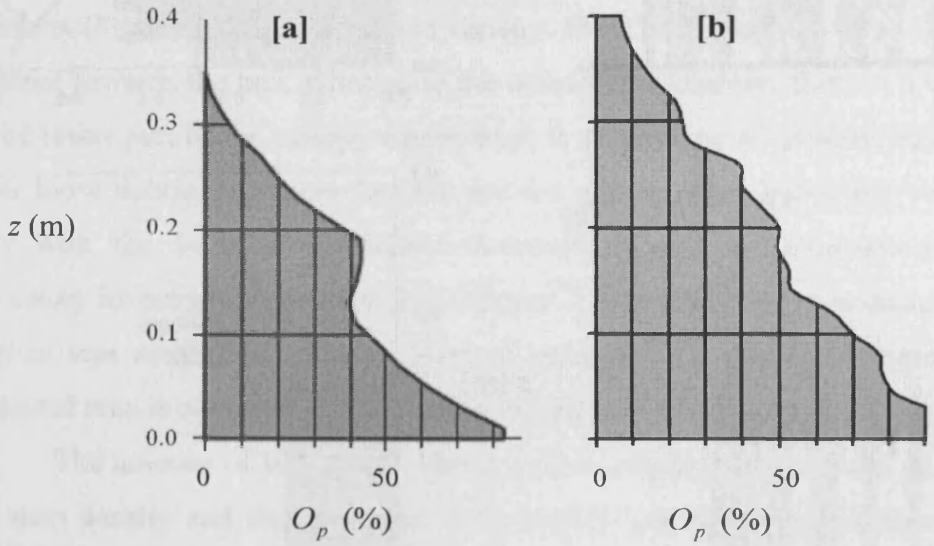

Figure 4-5 Profiles of vegetation obstruction, O_p, from [a]: Neumeier (2005) and [b]: the current study (Location A2, July 2005).

4.2.4 Sensitivity Testing of the Photographic Method

During field-application of the photographic method, a number of factors can give rise to variations in the analysed results. These include the canopy depth, the brightness of daylight (this may vary between cloudy and clear days), and the angle the mirror forms with the ground. Sensitivity of the calculated vegetation obstruction,

O_p (percentage flow area occupied by vegetation), to slight variations in each of the three variables was investigated. Figure 4-6 shows the different results obtained from the photographic method for a 0.08m, 0.10m and 0.11m canopy thickness, ∂x, (Figure 4-7) for the same sample of vegetation during one of the sampling events. The error, ε, was normalised using a canopy depth correction factor, β_C, which corrects for the magnitude of deviation from the recommended canopy thickness of 0.10m (Neumeier, 2005). The correction factor is defined as follows:

$$\beta_C = \frac{\partial x}{0.10} \qquad \text{[Equation 4.04]}$$

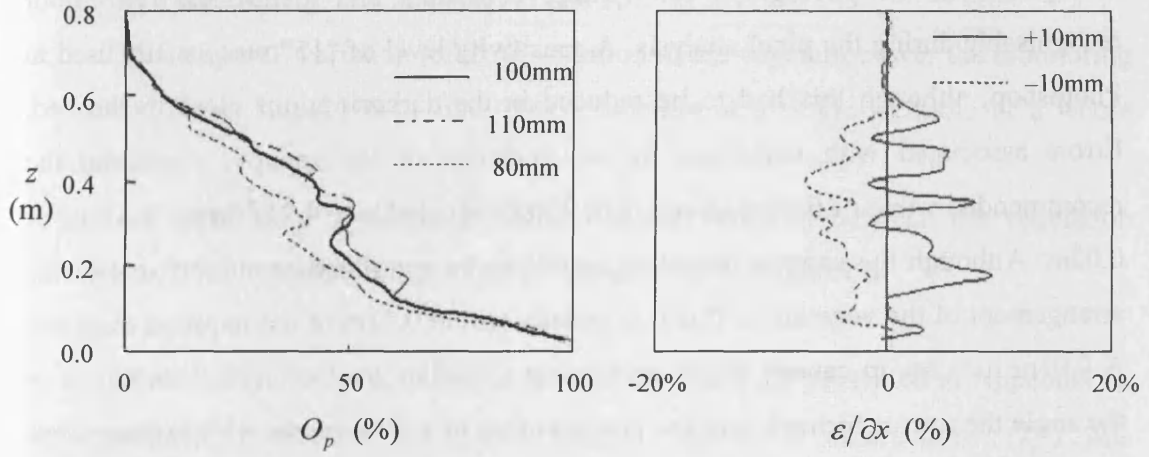

Figure 4-6 Sensitivity of the photographic method to the canopy thickness

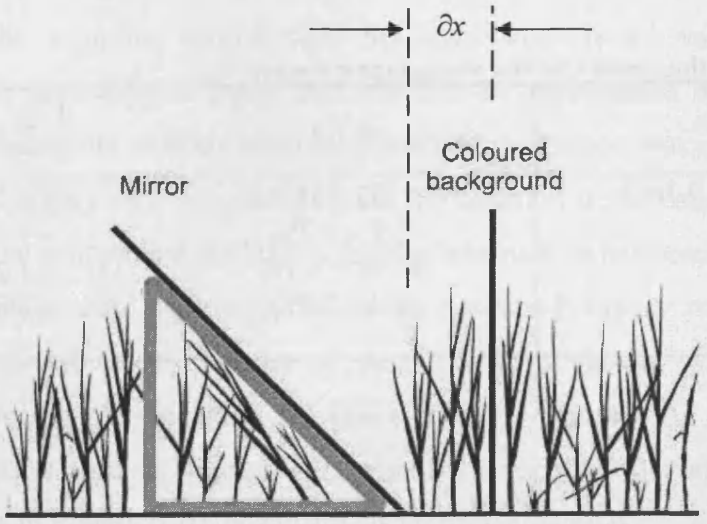

Figure 4-7 Instrument set-up used in the photographic method for quantification of vegetation, and the definition of the canopy thickness, ∂x. The image is taken from Neumeier (2005)

Results from the sensitivity testing for different factors are summarised in Table 4-1. Brightness levels were dependent on weather conditions and daylight hours. This was likely to be the most significant cause for errors, especially as it cannot be controlled. The mean 'brightness error', calculated based on the projected area of obstruction, determined from a number of photographs taken of the same canopy cross-section for a range of daylight conditions was $\pm$ 3%. The user error, which was $\pm$ 1.8%, refers to the difference in results obtained when the analysis was repeated for the same photograph three times and the difference in results compared. Differences were incurred because before analysis of the photographs can be conducted, considerable photograph editing is required to substitute the red background in the photograph for a more consistent and identifiable red colour recognisable during the pixel analysis. A sensitivity level of "15" was usually used in Photoshop, although this had to be reduced in the darker regions close to the bed. Errors associated with variations in the thickness of the canopy, ∂x, from the recommended value of 0.10m (Neumeier, 2005), equated to $\pm$ 4.2% for a ∂x value of 0.02m. Although the canopy thickness could not be controlled accurately due to the arrangement of the vegetation, this was usually within 0.01m of the required distance. A 0.01m increase in canopy depth resulted in a smaller error of 1.7%. Variations in the angle the mirror formed with the ground of up to $\pm$ 5° from the 45° position were explored, although this resulted in a relatively small mean error of up to $\pm$ 1.2%.

Table 4-1 - Sensitivity testing results for the photographic method

	ε (-)	$\frac{1}{n}\sum_{i=1}^{i=n}\varepsilon$ (-)
Canopy thickness (+/- 0.1m)	-14.1% – 18.4%	$\pm$ 4.2%
Brightness	-5.1 – 9.7%	$\pm$ 3.0%
Mirror angle (+/- 5°)	-8.7% – 5.4%	$\pm$ 1.2%
User error	-8.2 – 3.5%	$\pm$ 1.8%

4.2.5 Local, Spatial and Seasonal Variations in Obstruction Profiles

The photographic method was used to quantify *Spartina anglica* canopies along transects A and B on the Llanelli site, and the grazed saltmarshes at the Gower site covered by transects D, E and F (Section 3.2.3). The data revealed three types of variation in the vegetation: local, spatial and temporal.

1. The 'local' component refers to the variation in the vegetation canopy around each sampling location according to the data collected at the four sampling points; 'a', 'b', 'c' and 'd' e.g. A2a, A2b, A2c and A2d.
2. The 'spatial' component refers to the variation between the sampling locations along a transect e.g. A2, A3, A4, A5 and A6.
3. The 'temporal' variation refers to variation in the vegetation over the monitoring period (from July 2005 to June 2006), whether at a single location, or a whole transect.
4. The 'large-scale' variation is defined as the variation between the vegetation along different transects e.g. transect A compared to transect B.

Details of how the variation terms are calculated are presented in Appendix II. As explained in Section 4.2.3, the relative vegetation obstruction (O_p) was determined for 20 mm layers over the canopy height. In Figure 4-8, the relative vegetation obstruction of the canopy is presented for location A2 for each month during the sampling period with the associated 'local' variations, which were calculated according to Equation 10.03 and are represented by the horizontal bars. The twelve-month average relative vegetation obstruction was included as a reference on each monthly plot to better illustrate the variation in the canopy over the sampling period. The canopy had the highest level of obstruction between the months of August and November, and the lowest obstruction between February and May. Similar trends were observed across the rest of the transect as shown by the average relative vegetation obstruction along the entire transect (transect A) for the twelve-month monitoring period in Figure 4-9, where the 'spatial' deviations were calculated according to Equation 10.09 and are also represented by horizontal bars.

In Figure 4-10, the mean vegetation obstruction at each location is presented, where temporal variations were calculated according to Equation 10.07. The relative vegetation obstruction approached a value of 100% near the bed for all canopies examined, and diminished in value with elevation. The reduction was approximately linear over the lower 300 mm of canopy height, and above this level, there was a significant decrease in relative vegetation obstruction with elevation. The physical quantification of the canopy is considered in more detail in Section 4.2.6.

Sp. anglica was monitored at five sampling locations (A2, A3, A4, A5 and A6) along transect A. The 'local' variation of the relative vegetation obstruction along the transect and with time is summarised in Figure 4-11. The standard deviations of the relative vegetation obstruction levels determined for the four sampling points at each sampling location ('a', 'b', 'c' and 'd') over the twelve-month sampling period are presented in Figure 4-11a to represent the spatial difference in 'local' variation across the transect (refer to Equation 10.04). In Figure 4-11b, the monthly standard deviations of the four sampling points at each sampling location, averaged over the five locations monitored along transect A are presented to represent the temporal difference in 'local' variation (refer to Equation 10.05). According to the analysis, of the five locations that were monitored, and over the twelve-month period of monitoring, 'local' variation was greatest at locations A3 and A4, and during the month of October 2005.

The 'temporal' and 'spatial' variations in the relative vegetation obstructions across transect 'A' and over the course of the monitoring period are summarised in Figure 4-12. These were calculated according to Equations 10.07 and 10.09 respectively. The most amount of 'temporal' variation was observed at the most inland locations, namely, 'A2' and 'A3', whilst the highest amount of 'local' variability was observed during October and November 2005 for most of the canopy height.

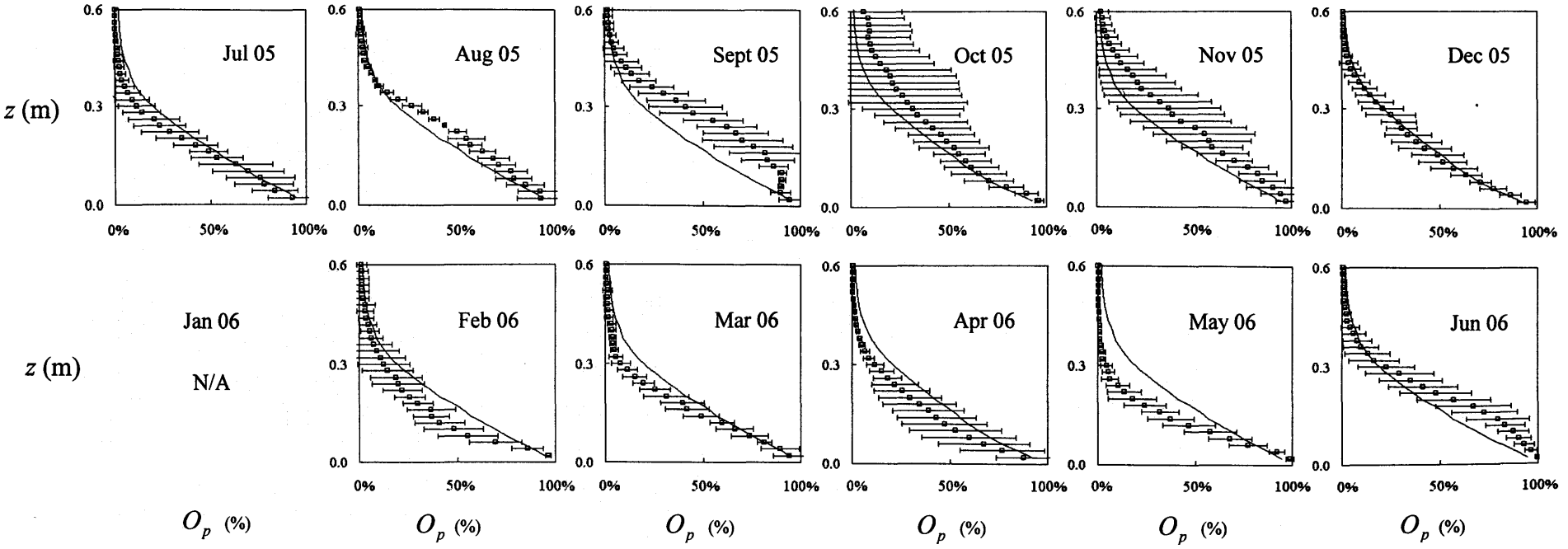

Figure 4-8 Vertical profiles of the monthly relative vegetation obstruction, O_p, at location A2. The solid line denotes the twelve-month average, and horizontal bars denote the 'local' variation. z is the elevation above the bed.

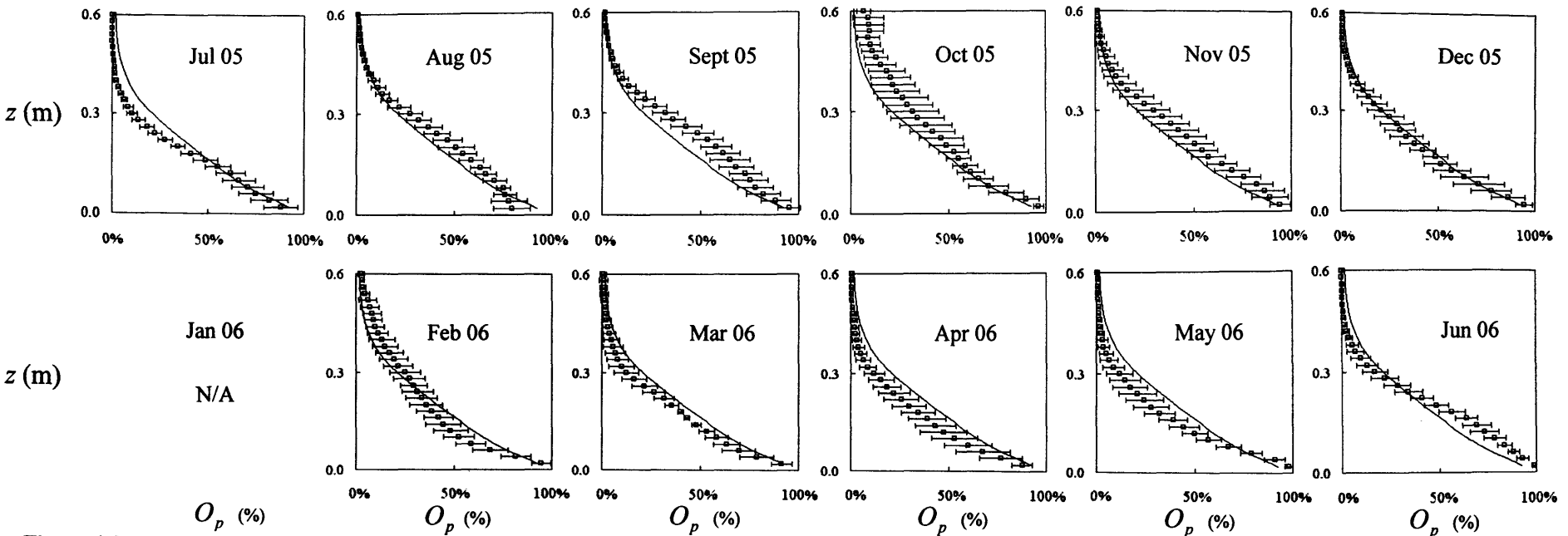

Figure 4-9 Vertical profiles of the monthly relative vegetation obstruction, O_p, for Transect A. The solid line denotes the twelve-month average, and horizontal bars denote the 'local' and 'spatial' variation. z is the elevation above the bed.

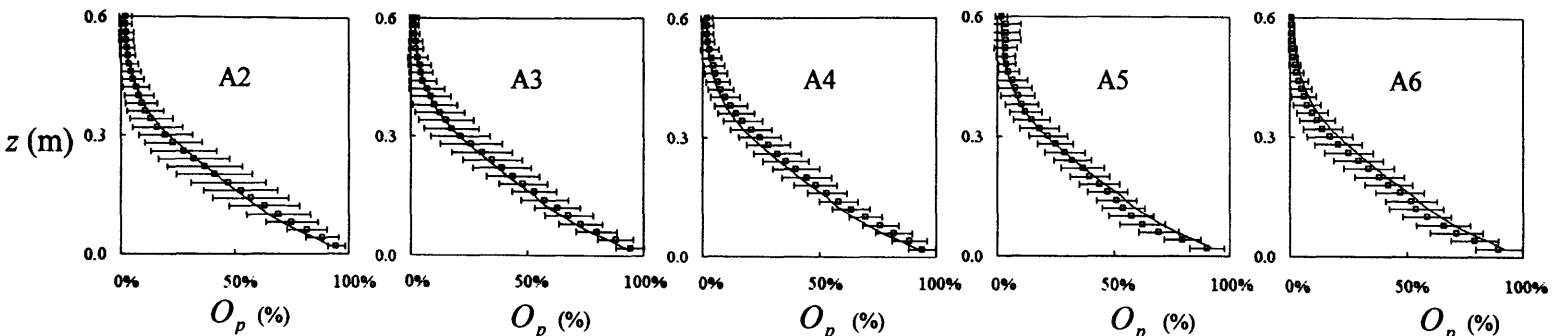

Figure 4-10 Twelve-month average relative vegetation obstruction, O_p, of the vegetation at five different locations along Transect A. z is the elevation above the bed.

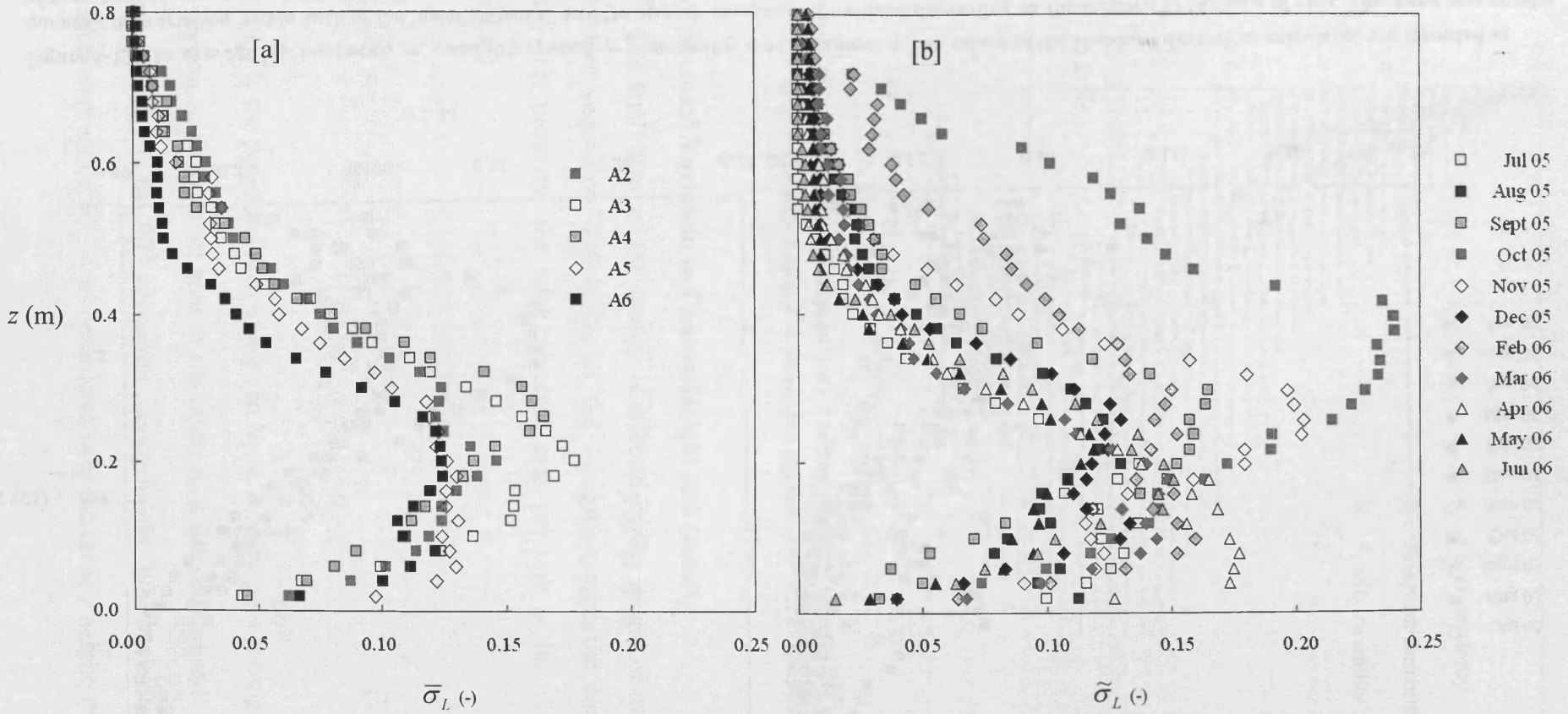

Figure 4-11 The Average Standard Deviations in the vegetation obstruction, O_p, along Transect A for [a]: each location along transect A over the duration of the sampling period; [b]: all locations along Transect A during each month of the sampling period. $\overline{\sigma}_L$ denotes the standard deviation of the annual average vegetation obstruction for each sampling location, and $\widetilde{\sigma}_L$ denotes the standard deviation of transect A for each month.

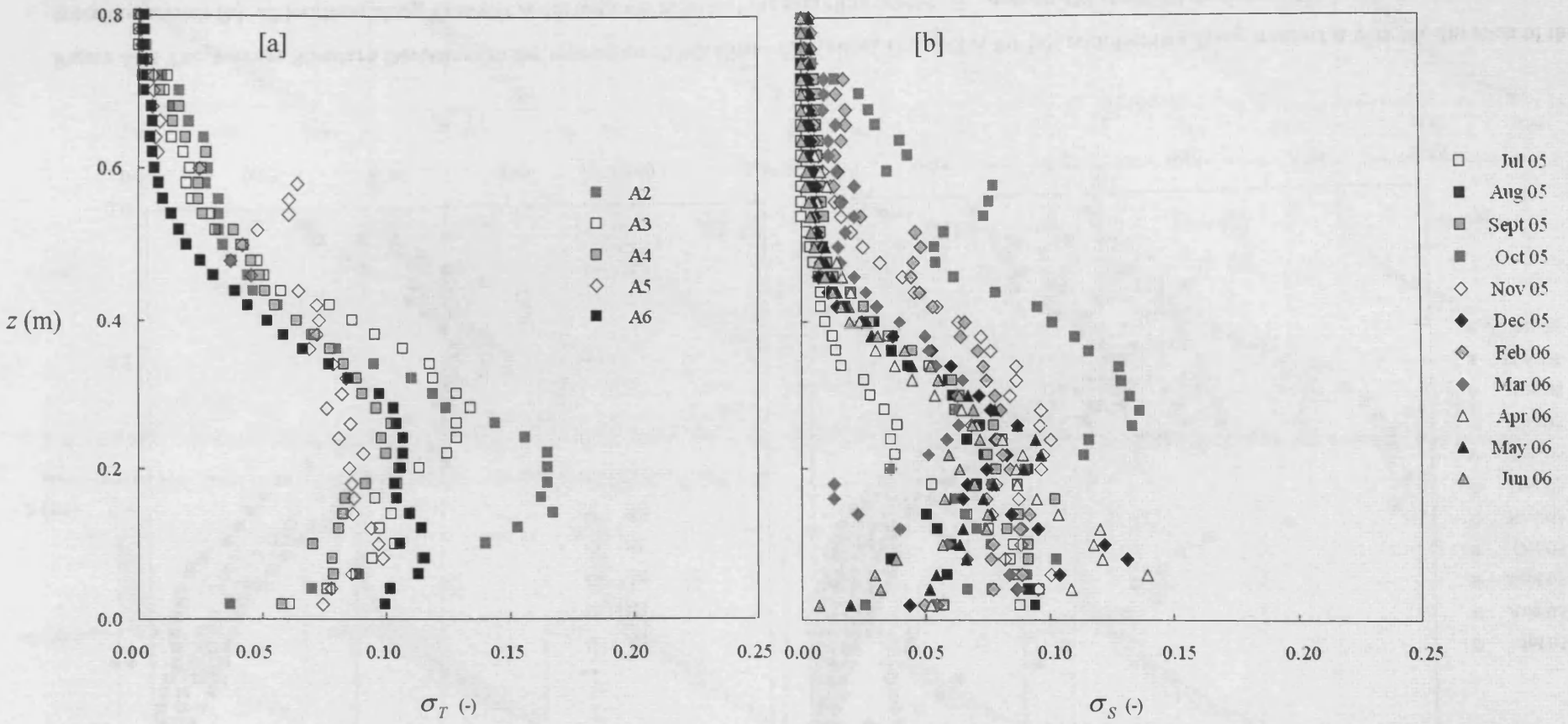

Figure 4-12 The average [a]: temporal, σ_T , and [b]: spatial, σ_S variability along transect A.The values of the standard deviations calculated are intended to quantify the variation within each of the 'local', 'spatial' and 'temporal' components outlined depending on the location or the time of year. The mean magnitudes of these variations are summarised for Transects 'A' and 'B' in Figure 4-13 indicating that the 'local' variation was the most significant, followed by the 'temporal' and finally, the 'spatial' variations.

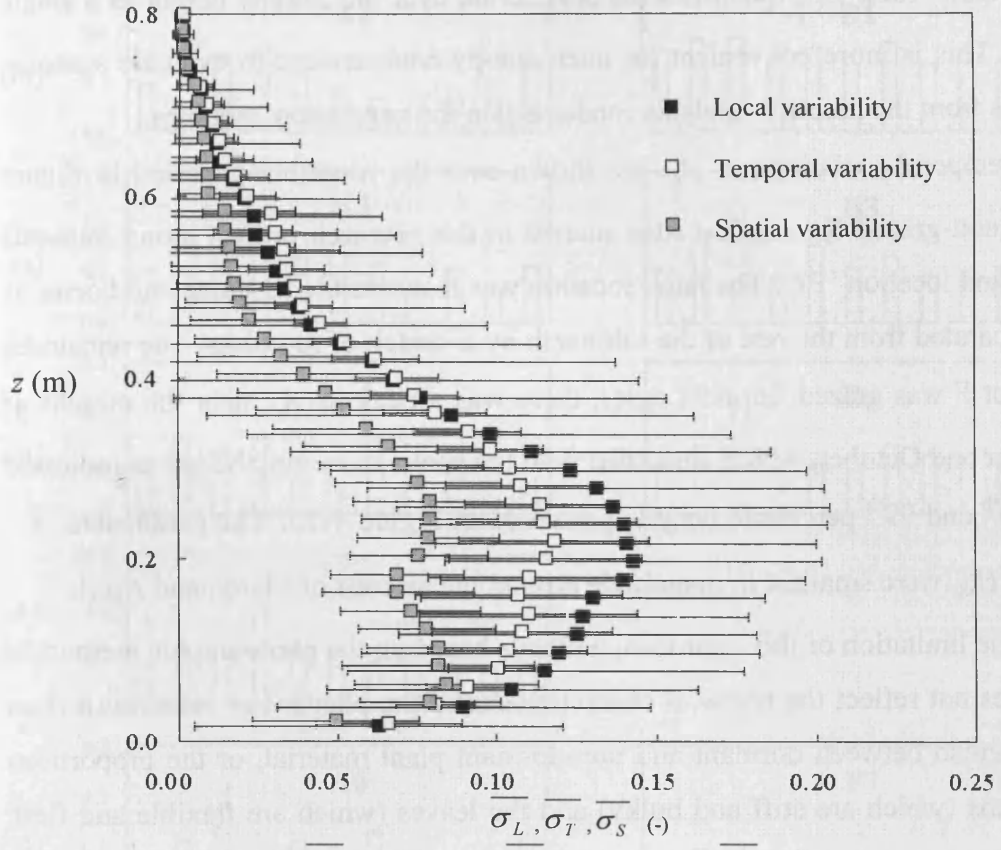

Figure 4-13 Mean Local ($\overline{\sigma_L}$), Temporal ($\overline{\sigma_T}$) and Spatial ($\overline{\sigma_S}$) variability with standard deviations in *Spartina anglica* vegetation across the Llanelli site

4.2.6 Seasonal Variation in Canopy Height and Density

The total 'size' of the canopy is affected by the height of the vegetation and the relative vegetation obstruction of the vegetation over the canopy height. To quantify this property, the total projected area per unit width of canopy, A_C, is defined as:

$$A_C = \frac{1}{n} H_{90} \sum_{i=1}^{i=n} \frac{A_{p\,i}}{A_i} \qquad \text{[Equation 4.05]}$$

where $A_{p\,i}$ is the projected area of a given layer, *i*, based on a photograph of a canopy cross-section, A_i is the total area of the layer, *n*, is the number of layers forming the canopy, and H_{90} is the 90th percentile canopy height. Whilst profiles of the relative vegetation obstruction, O_p, was considered over the canopy height, the total projected

area per unit width, A_C, quantifies the obstruction over the canopy height as a single quantity. This is more convenient for inter-canopy comparisons to evaluate seasonal variations from the monthly analysis conducted on the vegetation canopies.

Temporal variations in A_C are shown over the monitoring period in Figure 4-14 for non-grazed *Sp. anglica* sites studied in this research project along transects 'A', 'B' and location 'F7'. The latter location was inaccessible to sheep and horses as it was separated from the rest of the saltmarsh by a stretch of mudflats. The remainder of transect F was grazed. In most cases, there was a peak in A_C near the months of September and October, which coincided with the peaks in canopy height as indicated by the 90^{th} and 99^{th} percentile heights presented in Figure 4-15. The parameters A_C, H_{90} and H_{99} were smallest in magnitude around the months of March and April.

One limitation of this approach, which is based on the photographic method, is that it does not reflect the physical characteristics of the plants. For instance, it does not distinguish between dormant and non-dormant plant material, or the proportions of the stems (which are stiff and bulky) and the leaves (which are flexible and flat). Also, it attempts to predict the amount of obstruction, which is in fact a volume of plant material within a unit sampling volume, based on the projected area of the obstruction. However, this method enabled sampling to be repeated at the exact same location since it is a non-destructive method, which is critical in assessing seasonal trends in vegetation growth.

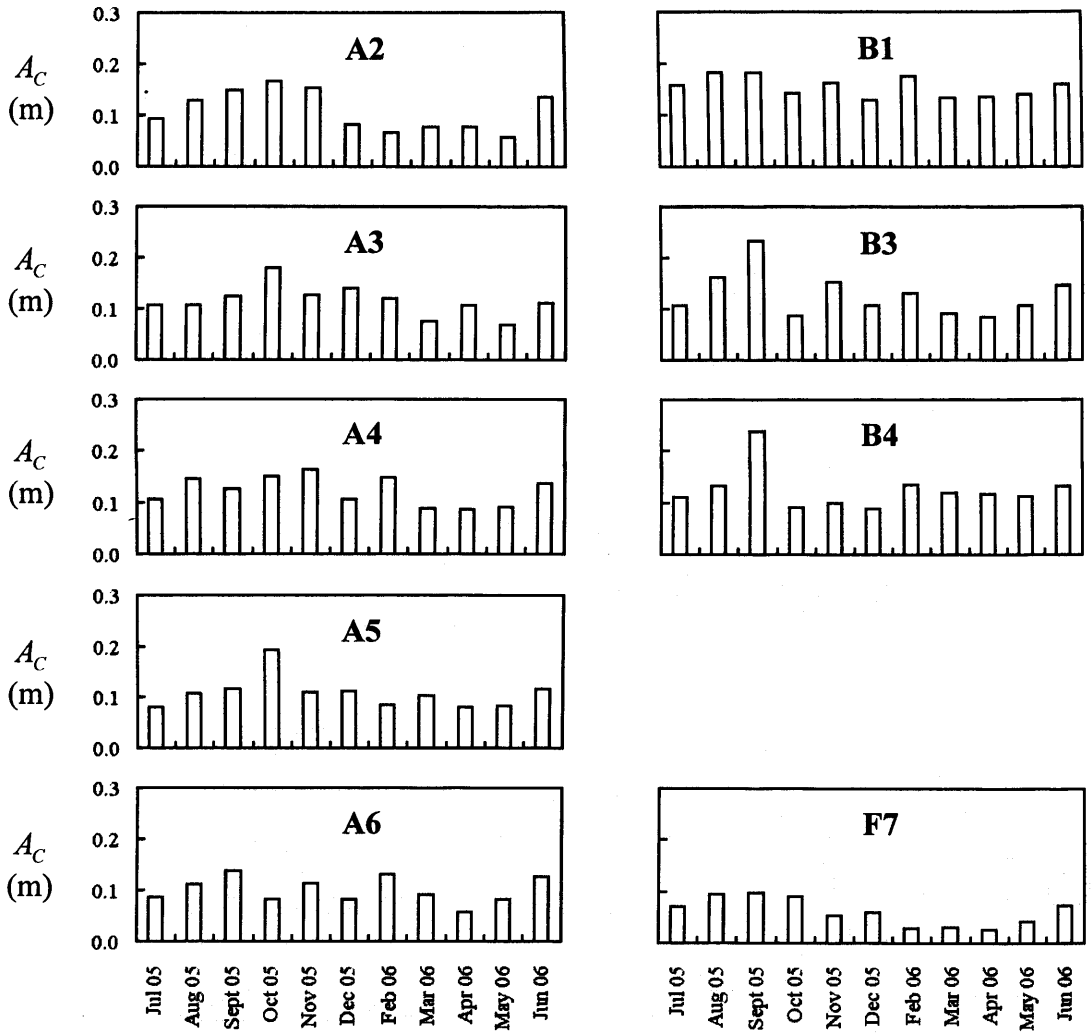

Figure 4-14 The total projected area per unit width of canopy, A_C, for non-grazed *Sp. anglica* monitored along transects A, B and F using the photographic method.

Variations in the appearance of the canopy are illustrated in Figure 4-16 where canopy photographs at sampling point 'A2' are presented for three different sampling events during the months of December 2005, March 2006 and June 2006. There was a large contrast in the canopies between the months of March and June. In June, fresh green plant shoots were observed. Based on the results presented, and the canopy cross-section photographs taken, the shoots appeared to grow through the summer months peaking in height and density around September. This was indicated by H_{90}, H_{99} and A_C (Figure 4-14 and Figure 4-15). Although not visible in the photographs, in December, the vegetation lost its green colouration and became yellow and more brittle. Around March, the canopy height and canopy density reached minimum values. Being a perennial plant, the vegetation was dormant around this time of the year.

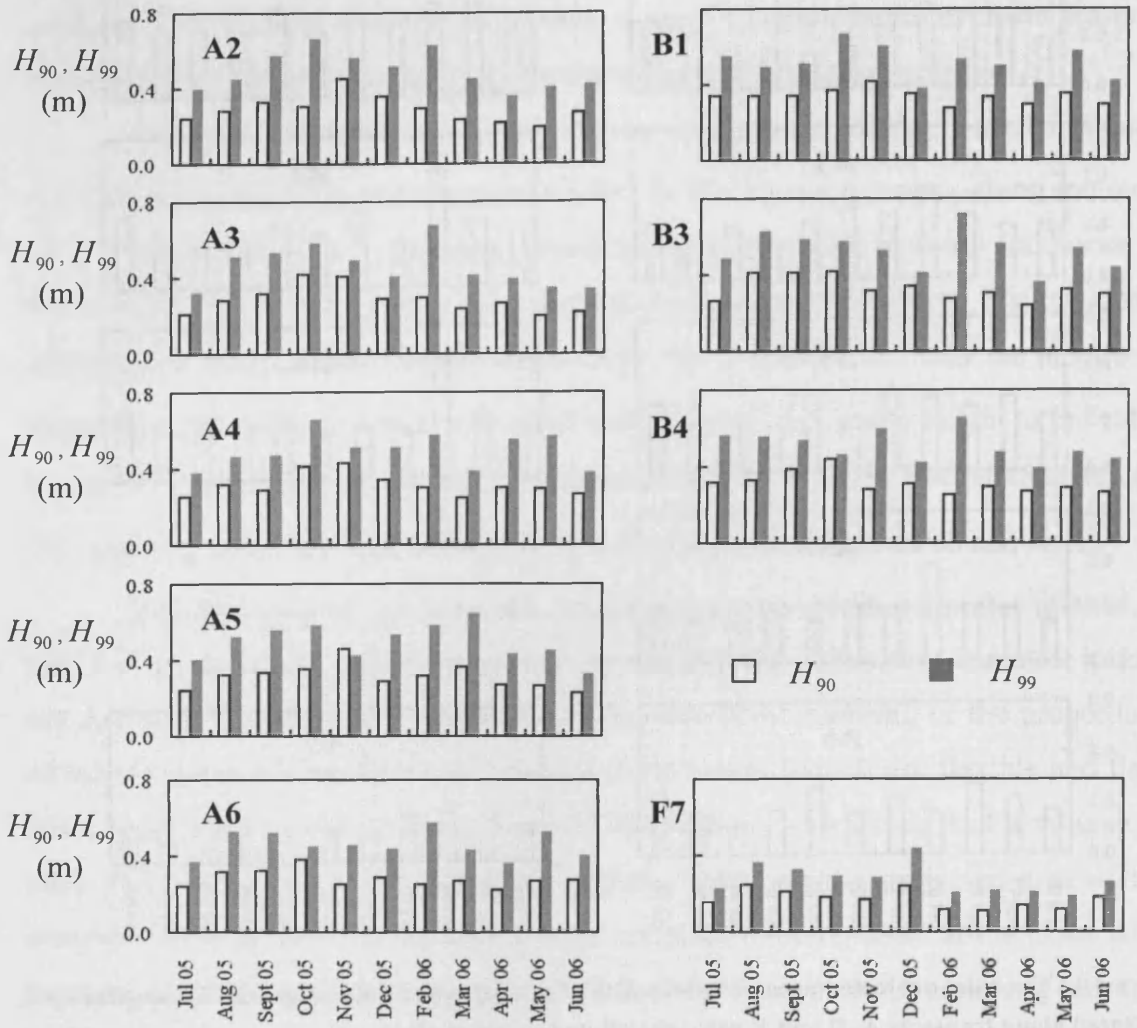

Figure 4-15 H_{90} **and** H_{99} **values for non-grazed *Sp. anglica* along transects A, B and F**

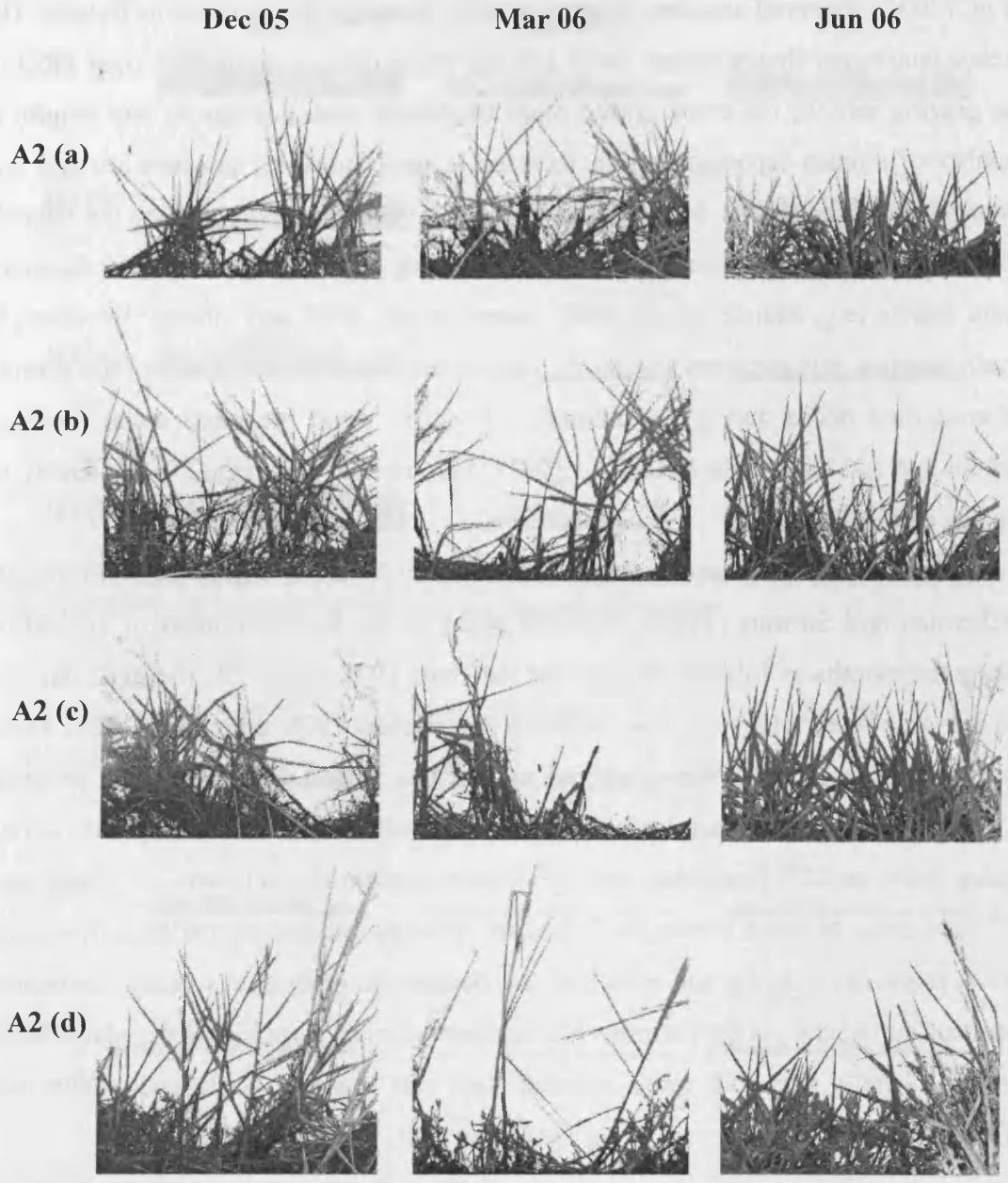

Figure 4-16 Photographs of a typical sampling point on the Llanelli site illustrating local and temporal variations in the vegetation structure

The vegetation on the Gower site displayed less temporal variation in the projected area of obstruction throughout the year. Examples of vegetation photographs from transect D and transect E are shown in Figure 4-17 and Figure 4-18 respectively. The vegetation was shorter during the winter months, which was also reflected in the H_{90} and H_{99} values (Figure 4-19) and in A_C values (Figure 4-20). This may be associated with increased sunlight exposure in the summer, and may have also been associated with increased sheep grazing in the winter period. Linnane

et al. (2001) observed seasonal grazing patterns amongst Kerry cows in Ireland. The author concluded that although daily grazing times remained constant over most of the grazing season, the cows grazed more frequently with decreasing day length. A number of studies reported that an increase in environmental temperature and day length were accompanied by a decline in grazing time amongst sheep as the animals adapted to poor forage during the winter by grazing for longer periods and dispersed more widely (e.g. Shinde *et al.*, 1997; Ashuto *et al.*, 2002 and others). However, in sheep farming, it is common to provide supplements in the form of other food sources to meet their needs during the autumn and winter when the grass cover becomes mature and less digestible (DEFRA, 2007). This is likely to reduce the intensity of grazing on the marshes.

In a study on annual above-ground growth on a *Typha latifolia* marsh, Dickerman and Stewart (1986) observed peaks in the total dry mass of vegetation during the months of July and August for the years 1978 and 1979. The mass per unit ground area was relatively low between November 1978 and May 1979. Fresh *Spartina anglica* shoots were observed around this period during the field program (e.g. see Figure 4-16). Thus, lower vegetation densities across the Gower site during winter; between 22nd December and 21st March, and spring; between 21st March and 21st June, may, to some extent, be linked to variations in grazing patterns. However, this is more likely to be the effect of the decline in vegetation quality commonly observed during the cooler periods. The natural seasonal variation of the plant height for the Llanelli site was more marked than the seasonal variation, which was influenced by grazing patterns, along the Gower site.

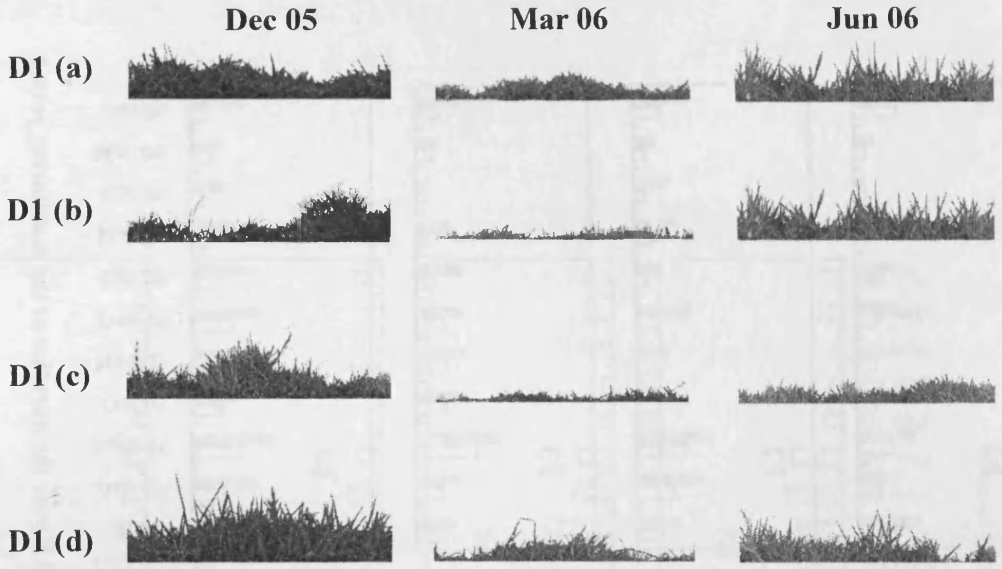

Figure 4-17 Photographs of a typical sampling point along transect D on the Llanrhidian site illustrating local and temporal variations in the vegetation structure

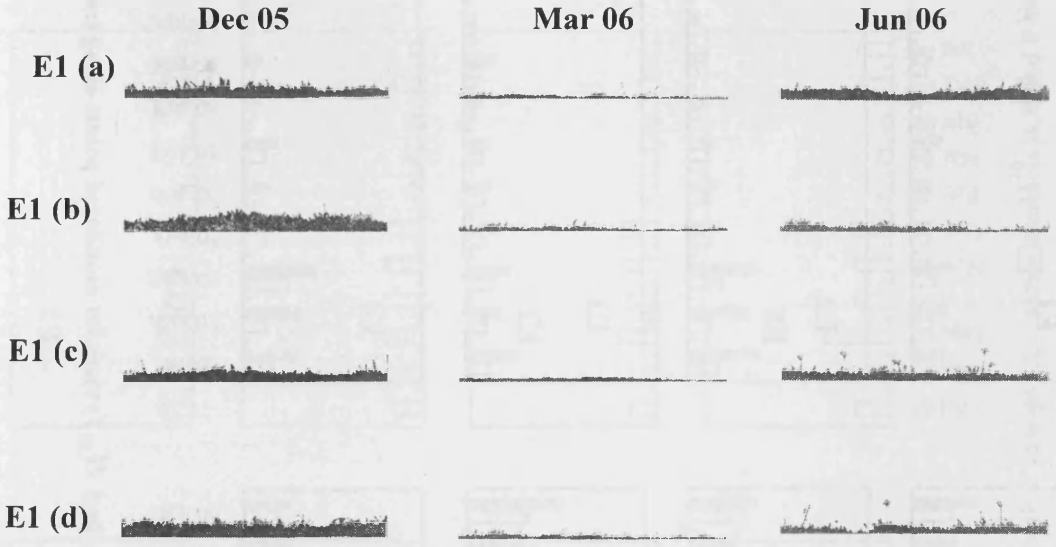

Figure 4-18 Photographs of a typical sampling point along transect E on the Llanrhidian site illustrating local and temporal variations in the vegetation structure

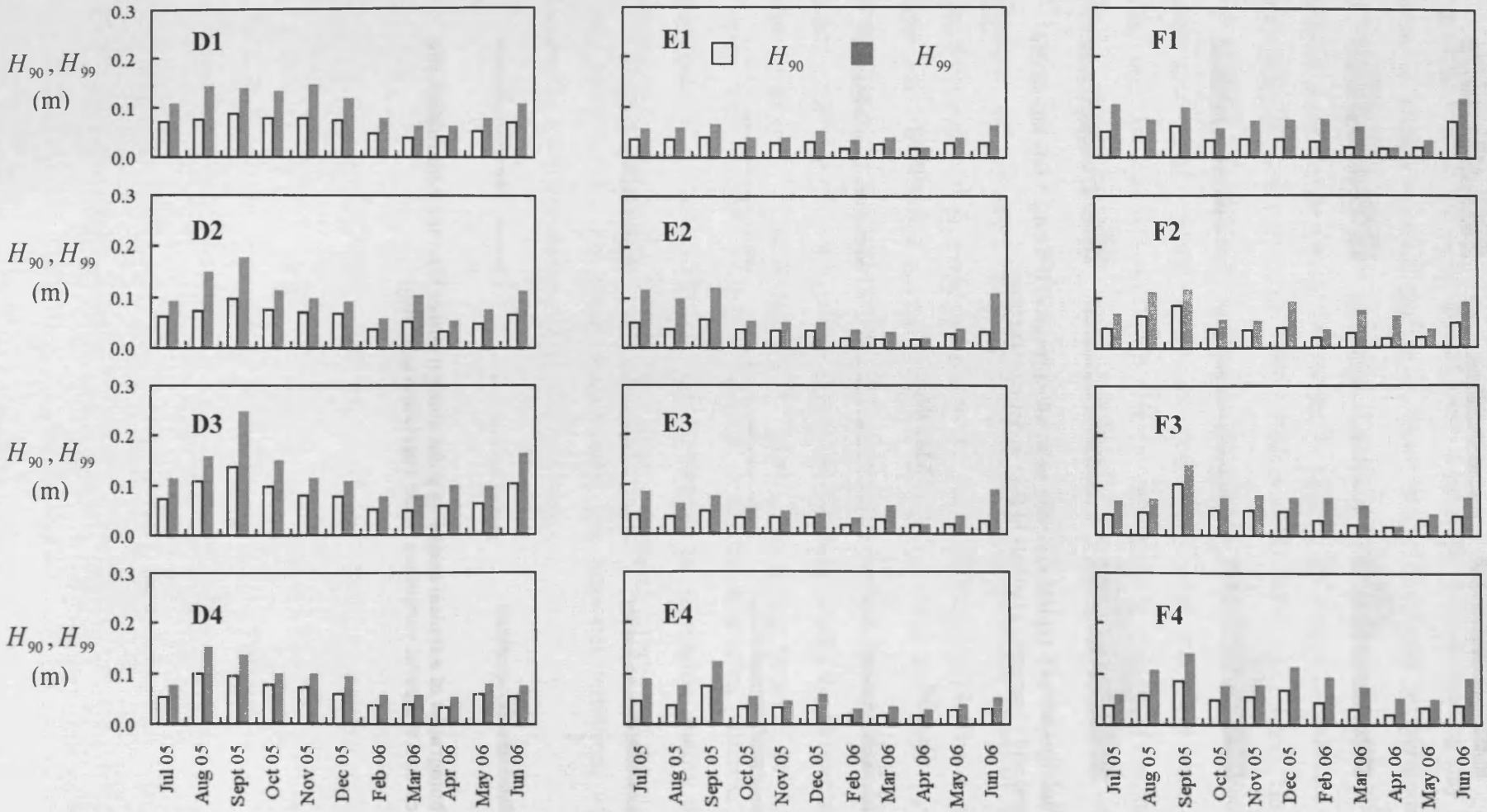

Figure 4-19 90th and 99th percentile heights (H_{90} and H_{99}) values for monitored points along transects D, E and F over the duration of the monitoring period

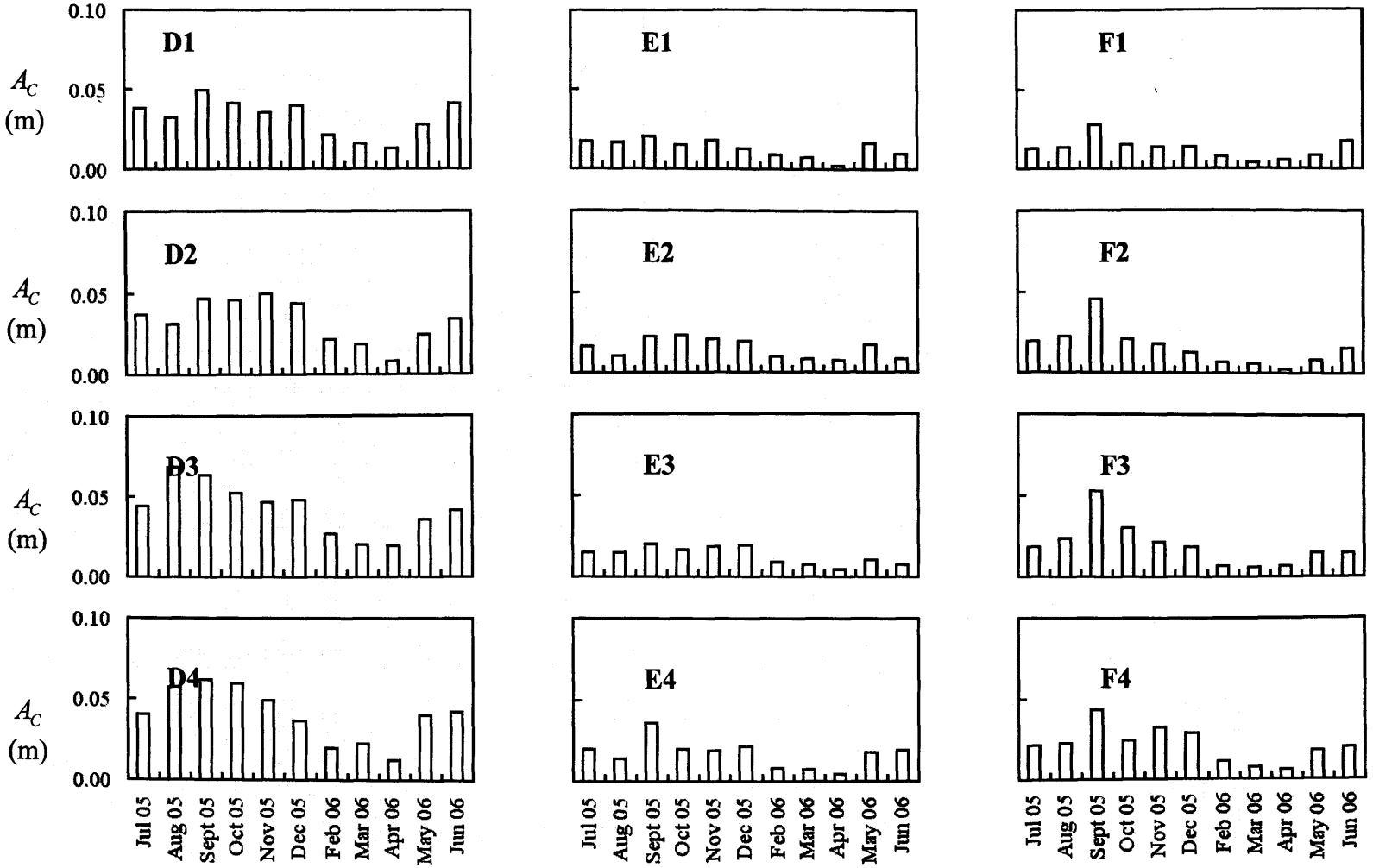

Figure 4-20 The total projected area per unit width of canopy, A_C, along transects D,E and F over the monitoring period.

The differences in vegetation properties such as vegetation height, relative vegetation obstruction, and seasonal patterns, offer possibilities for comparisons between the effectiveness of grazed versus non-grazed marshes in protecting the coast. Average values of the ninetieth percentile height (H_{90}) and the total projected area per unit width (A_c) are summarised in Figure 4-21 and Figure 4-22 respectively for both the Llanelli saltmarsh, and for the heavily grazed vegetation cover along the Gower saltmarsh. The heavy use of the Gower saltmarsh for grazing was reflected in the shortness of the vegetation (smaller H_{90} values), which in turn resulted in a much lower relative vegetation obstruction, O_P. Average 90th percentile heights for the vegetation across the Gower site varied between 0.028m $\pm$ 49.8% and 0.083m $\pm$ 38.6%.

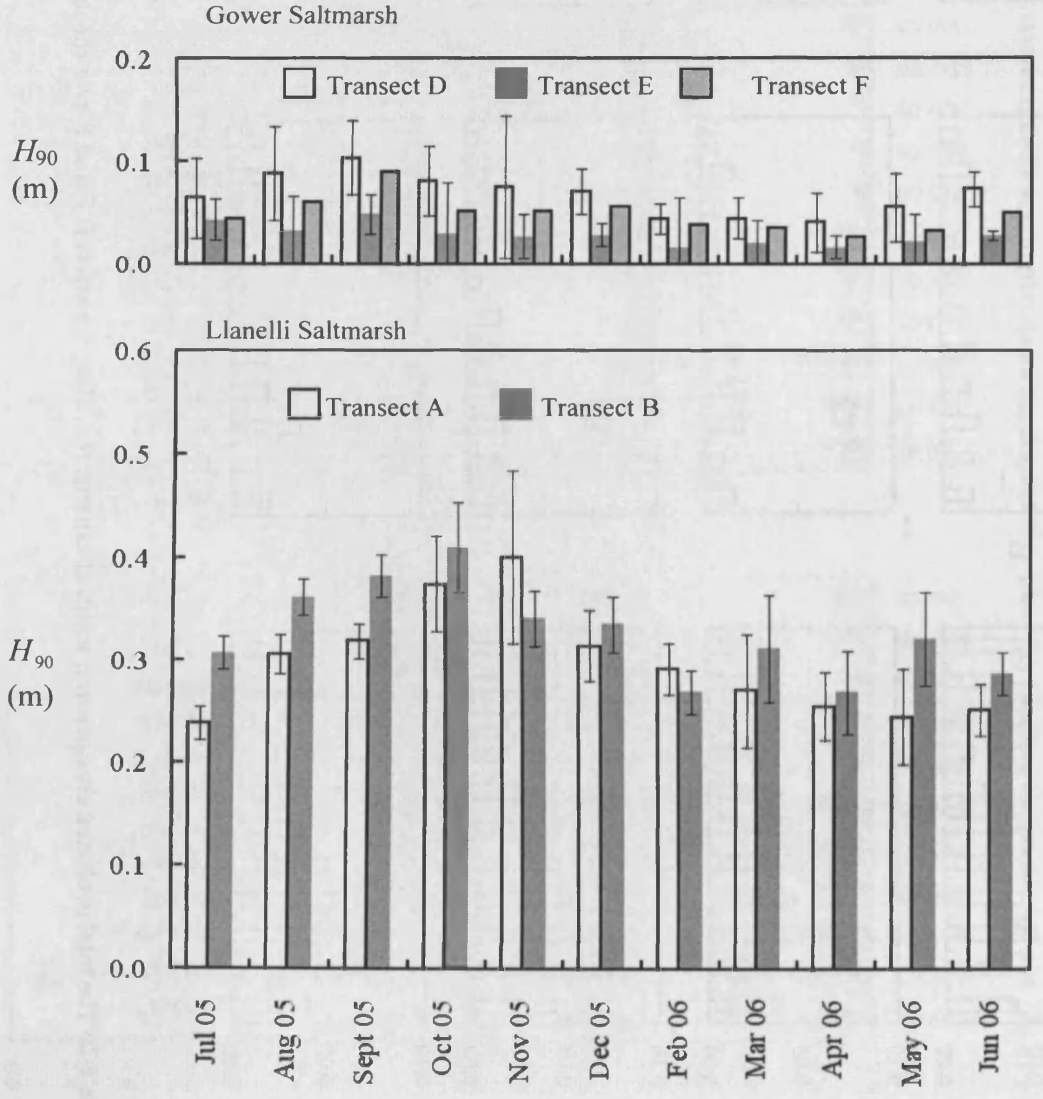

Figure 4-21 Average monthly 90th percentile canopy height, H_{90}, for the Llanelli and Gower sites.

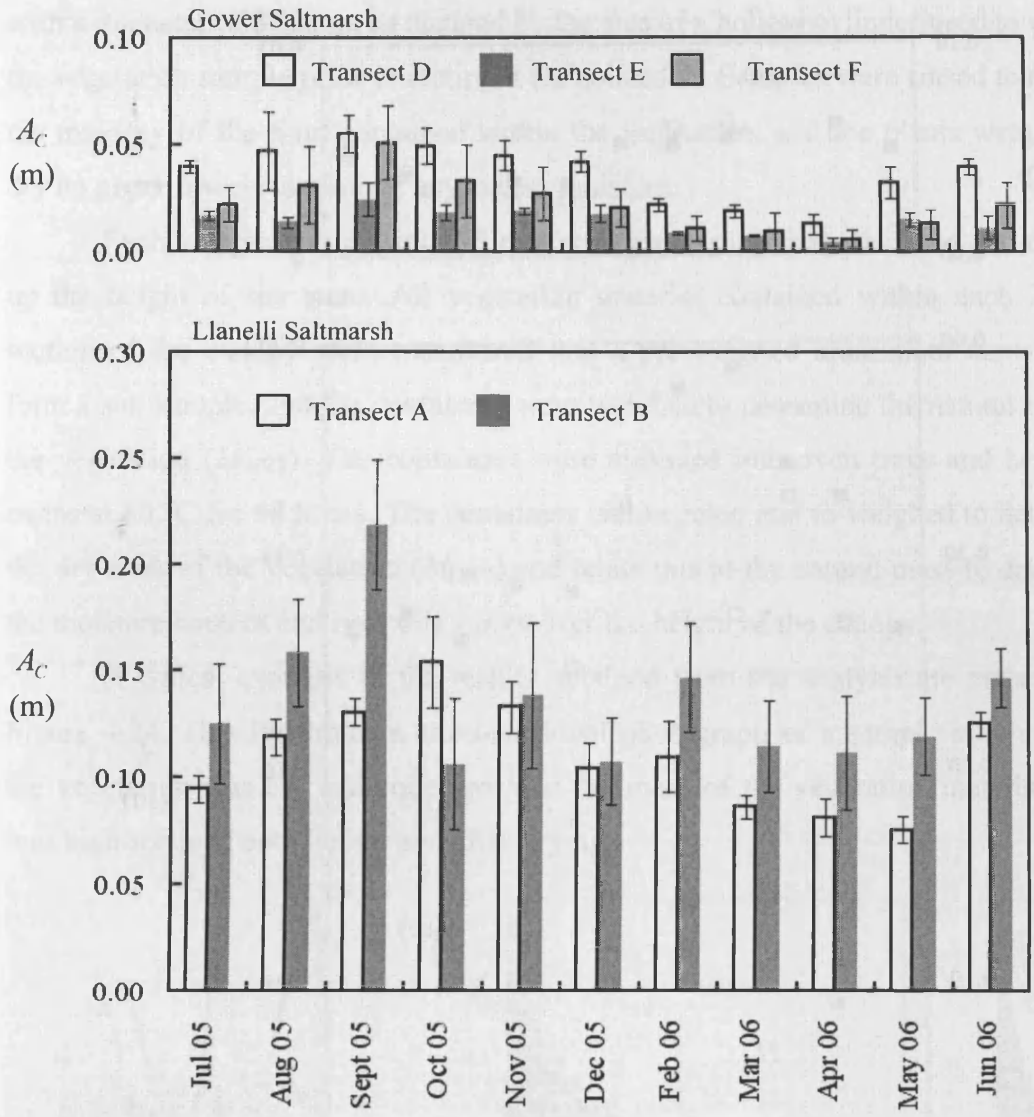

Figure 4-22 Average projected area per unit width of canopy, A_C, for the Llanelli and Gower sites.

The 90th percentile canopy height, H_{90}, and the projected area per unit width, A_C, indicated similar trends of vegetation growth over the monitoring period (Figure 4-23). H_{90} values indicated a thicker vegetation cover than A_C for the non-grazed vegetation (Figure 4-23b). However whereas for grazed vegetation, where there was less variability in the morphology of the vegetation, both parameters indicated a similar vegetation cover (Figure 4-23a).

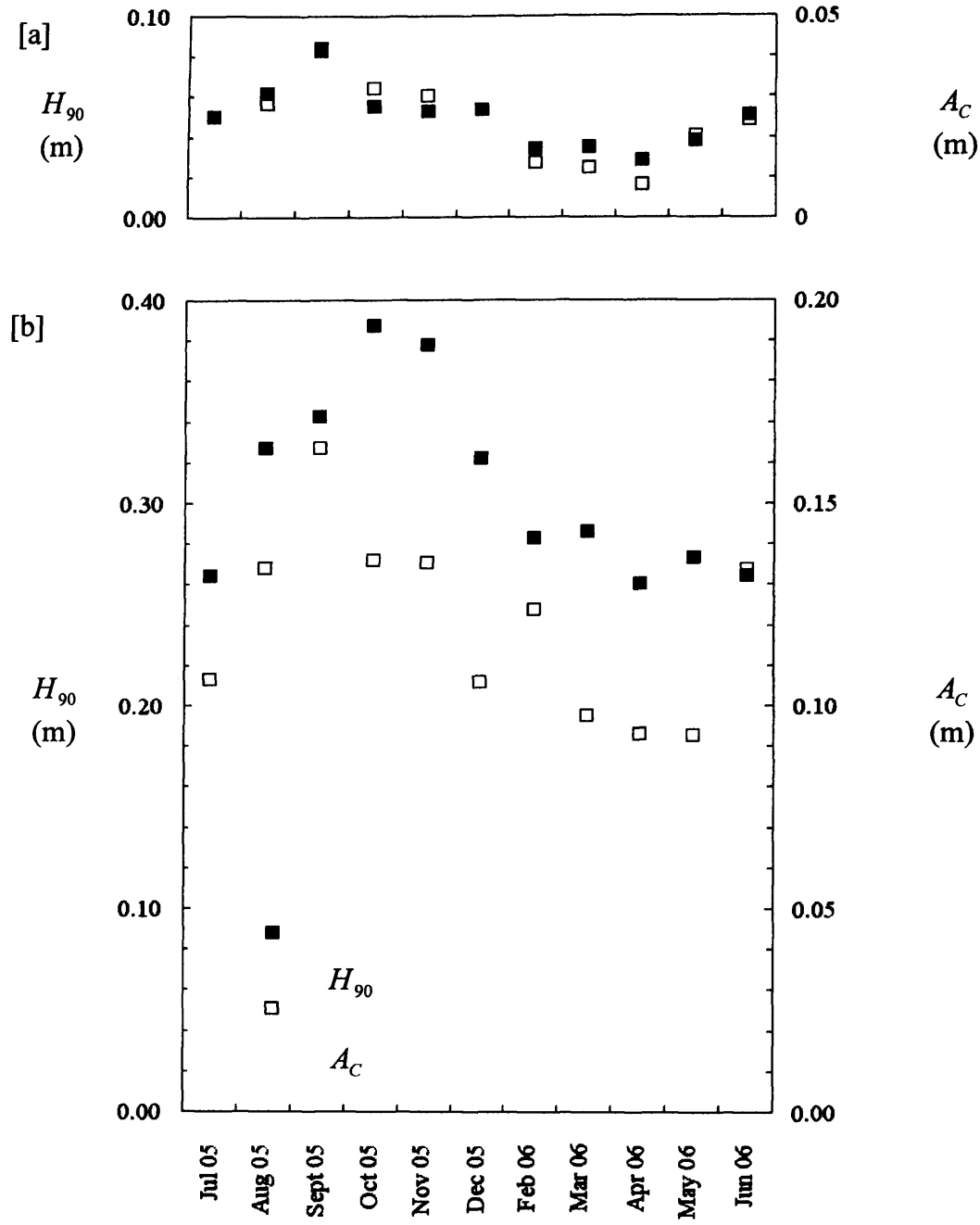

Figure 4-23 Seasonal variation over the monitoring period in the 90th percentile canopy height, H_{90}, and the projected area per unit width, A_C, for [a]: the Gower saltmarshes, and [b]: the Llanelli saltmarsh.

4.3 Quantification of Vegetation based on the Mass of Material

4.3.1 Concept and Methodology

Vegetation samples were quantified based on the mass of material within a unit volume. To conduct this analysis, samples of *Spartina anglica* were collected by cutting the stems at the base of the plants. Each sample covered a circular ground area

with a diameter of 375 mm as dictated by the size of a hollow cylinder used to contain the vegetation sample prior to cutting it for collection. Samples were rinsed to remove the majority of the mud contained within the vegetation, and the plants were left to dry on paper towels to remove any excess moisture.

Each sample was cut into 25 mm sections starting from the base and moving up the height of the stem. All vegetation material contained within each 25 mm section of the canopy were transferred into a pre-weighed aluminium container to form a sub-sample, and the containers were weighed to determine the natural mass of the vegetation (M_{WET}). The containers were arranged into oven trays and heated in ovens at 80 °C for 48 hours. The containers were cooled and re-weighed to determine the dry mass of the vegetation (M_{DRY}) and relate this to the natural mass to determine the moisture content and how this varies over the height of the canopy.

A typical example of the results obtained from the analysis are presented in Figure 4-24. This illustrates a cross-sectional photograph of a sample *in situ* before the vegetation was cut and collected, and the mass of the vegetation material in 25 mm high sections both before and after drying.

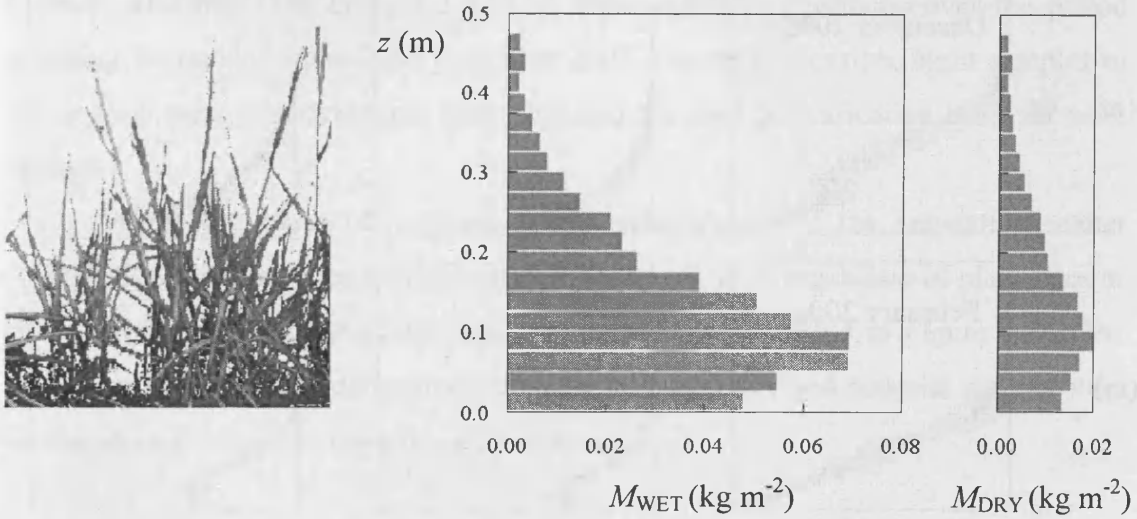

Figure 4-24 Mass of vegetation matter before and after drying and a photograph of the sample

4.3.2 The Relationship between Mass of Material and Projected Area

The projected area of obstruction as determined from the photographic method was compared to the vegetation density determined from the mass of vegetation material, both before and after drying. The two quantification methods were discussed in the previous sections. A number of *Sp. anglica* samples were quantified according to these methods and the results are summarised in Figure 4-25.

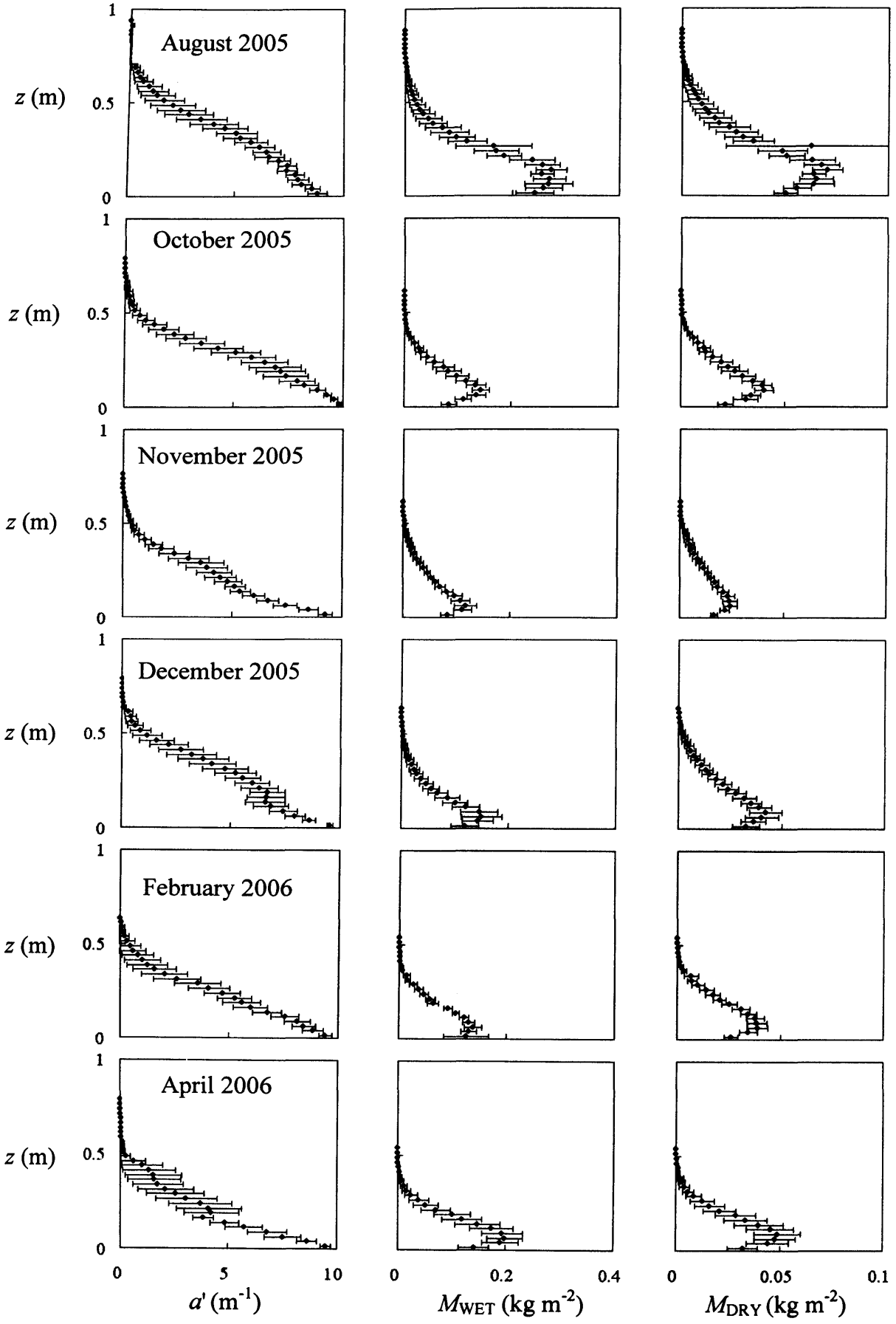
August 2005
October 2005
November 2005
December 2005
February 2006
April 2006
z (m)
1
0.5
0
0
5
10
a' (m-1)
0
0.2
0.4
MWET (kg m-2)
0
0.05
0.1
MDRY (kg m-2)

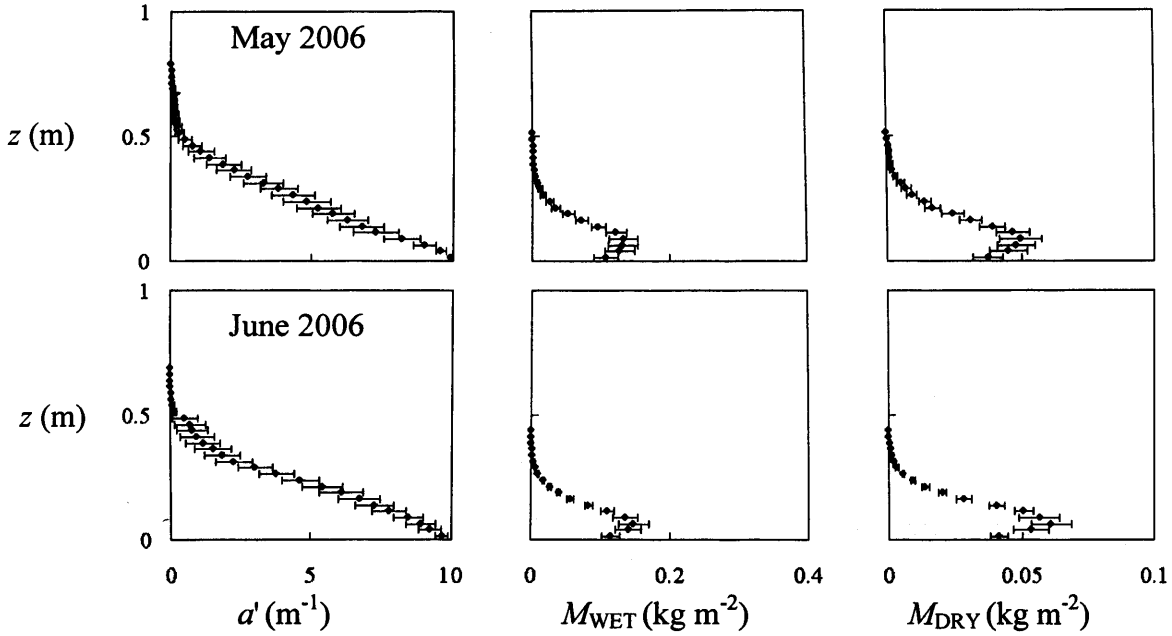

Figure 4-25 Comparison between the visible projected area of obstruction per unit volume, a', and the mass of material in the natural (M_{WET}) and the dry (M_{DRY}) states between August 2005 and June 2006.

The samples were collected from locations along transects A and B along the Llanelli saltmarsh (see Section 3.2.3) on eight different occasions over the period spanning between August 2005 and June 2006. On each occasion, eight samples of *Sp. anglica* were photographed, harvested and the two quantification methods were applied.

Where the mass of vegetation was determined, all the vegetation matter covering the sampling area was collected for quantification regardless of plant sizes or condition. Mean values over the sampling period are presented in Figure 4-26. The vegetation mass profiles determined from the natural and dried material showed very similar shapes. Moisture content, m, is defined as:

$$m = \frac{M_{WET} - M_{DRY}}{M_{DRY}} \qquad \text{[Equation 4.06]}$$

where M_{WET} is the natural mass and M_{DRY} is the dry mass of a sample volume. Moisture content was higher near the base of the plants and there was less difference between the natural and dried weights of the vegetation for the upper parts of the

plants. The moisture content of the vegetation ranged between 0.75 near the base and 0.45 at the top of the canopy at an elevation of 0.65 m from the bed.

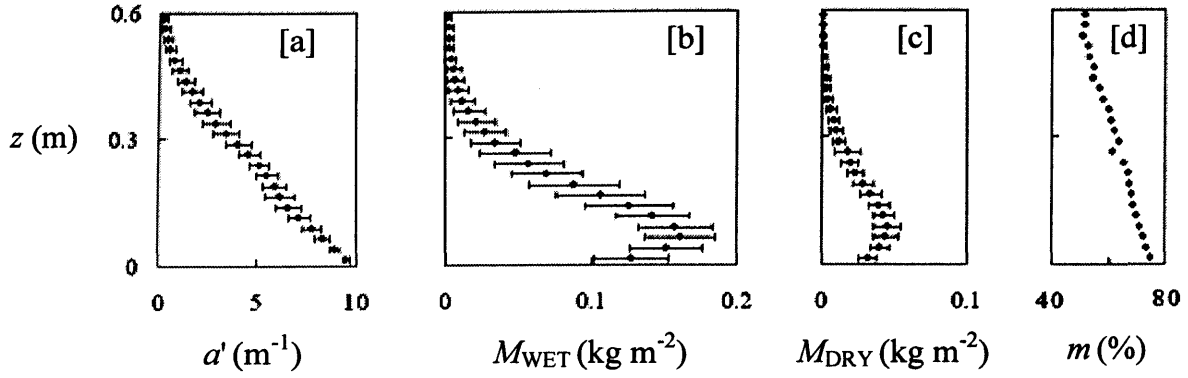

Figure 4-26 One-year average profiles of the distribution of vegetation material with elevation according to [a]: the visible projected area of obstruction per unit volume; [b]: the natural mass of material; [c]: the dry mass of material; and [d]: the percentage distribution of moisture content during the sampling period between August 2005 and June 2006

The profile of mean projected area per unit volume for the monitoring period according to the photographic method is presented in Figure 4-26a. The proportion of the total vegetation as a function of elevation is presented according to the natural and dried weights in Figure 4-26b and Figure 4-26c respectively. The projected area profile indicates that a greater surface area of vegetation is located in the upper part of the canopy (between an elevation of 0.3m and 0.6m above the bed) which is negligible in mass as shown by the profiles of vegetation mass. This can be attributed to the heterogeneous nature of the vegetation morphology whereby the relationship between the projected area and the mass of plant material varies considerably between the foliage region in the upper canopy and the stem region near the bed.

The lower part of the canopy comprised mainly stems and was greater in mass, but due to its compact and more organised arrangement, appears to occupy less of the flow domain when quantified using the technique to determine the projected area (the photographic method). At an elevation of 76 mm above the bed, a 25 mm horizontal section contains 8.2% of the vegetation according to the photographic method compared to 11.4% and 10.3% according to the natural and dry mass quantification methods. The mass quantification of the vegetation in its natural state suggests a slightly larger proportion of the vegetation is located lower down in the canopy compared to the dry mass. This is because a greater amount of moisture is retained in the upper part of the canopy giving the impression that there is a greater mass of vegetation material.

As a comparison between the two quantification methods, profiles of projected area of obstruction and vegetation mass (natural and dry) were normalised by the basal values at the lowest point in the canopy. The normalised vegetation mass values are presented as a ratio of the normalised projected area values over the height of the canopy in Figure 4-27. The normalised profiles show that the vegetation mass quantification leads to an under-prediction of the quantity of vegetation in the lower region of the canopy compared to the photographic method, and an over prediction higher up in the canopy. For the most extreme cases, the vegetation mass quantification method produces an estimate of the proportion of material in its natural state (M_{WET}) at an elevation of 88 mm above the bed 50.6% greater than the photographic method. After drying, the peak vegetation mass occurs at an elevation of 113mm, and the proportion from the vegetation mass quantification is 77.5% greater. Higher up in the canopy, at an elevation of 438 mm, the proportion of the vegetation material according to the mass quantification was 61.0% less than the photographic method, compared to 31.5% less at an elevation of 413 mm after drying.

Although the photographic method (Section 4.2.2) was capable of quantifying the surface area of obstruction, it does not distinguish between the cylindrical stems in the region near the bed and the flat foliage higher up in the canopy. The quantification of plant material based on its mass was therefore employed as an attempt to make this distinction in quantitative terms.

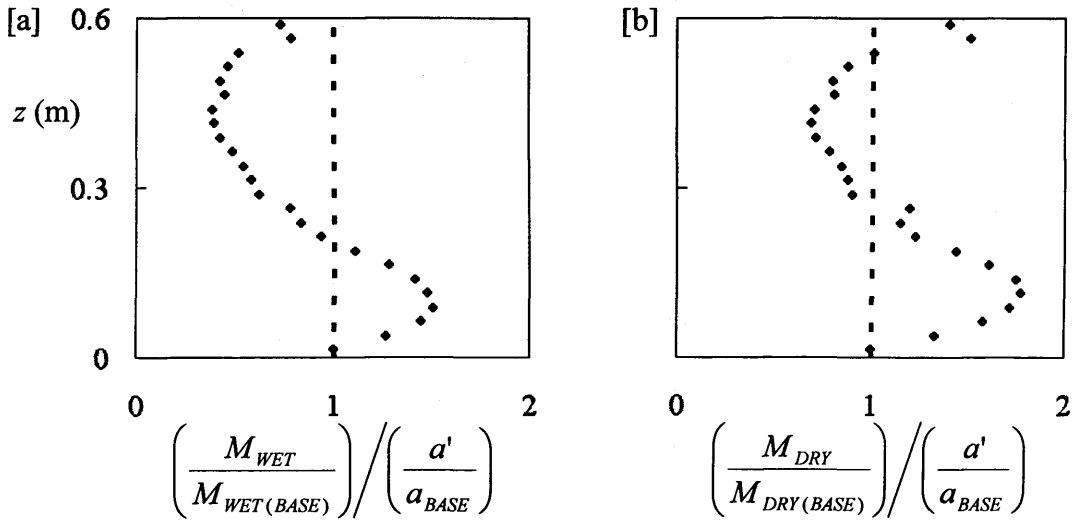

Figure 4-27 Comparison between the quantification of a canopy according to the projected area per unit volume profile and the distribution of the [a]: natural mass of material; and [b]: the dry mass of material using the one-year averages.

For field data collection, the mass of a sample is much more convenient to determine than the stem density, which can be time consuming. Yet the stem density of a canopy has a strong influence on the hydrodynamics of canopy flows (see Section 2.2.6). Thus, based on the data collected, the trend presented in Figure 4-28 relate the vegetation mass covering a unit bed area to the stem density.

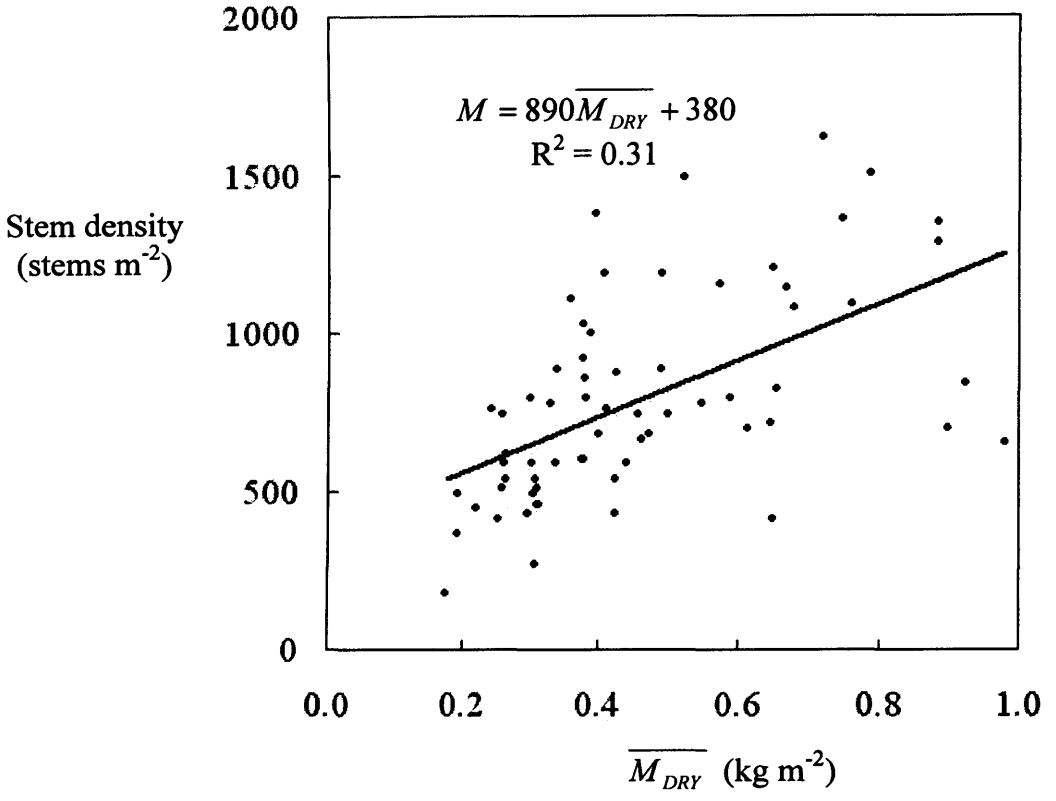

Figure 4-28 The relationship between dried mass per unit bed area, $\overline{M_{DRY}}$ and the stem density of natural *Spartina anglica* canopies. M is the stem density.

4.3.3 Determination of Canopy Height

Due to the variability in the heights of individual stems, there is some degree of uncertainty when defining the canopy height. Instead, the 90 and 99 percentiles were used to compare the canopy height at different locations across the monitored sites as well as for different times of the year. These equate to the heights below which 90 and 99 percent of the total vegetation obstruction were contained in the sample. The 90 and 99 percentiles were calculated for total cross-sectional areas of obstruction (H_{90} and H_{99}) and the vegetation mass (D_{90} and D_{99}) (Figure 4-29).

Percentile heights were calculated for the data from the sample analysis presented earlier in Section 4.3.2. The 90th and 99th percentile heights based on projected area, natural and dried masses of vegetation are presented for the samples analysed in Figure 4-30. The average 90th percentile height calculated from the projected area of obstruction was 0.347 m $\pm$ 2.3%. The values calculated based on the vegetation samples in their natural and dried states were 0.249 m $\pm$ 2.7% and 0.280 $\pm$ 3.3% respectively. The 99th percentile height determined from the projected area of obstruction was 0.529 m $\pm$ 3.4%, whilst based on the mass of the vegetation, the values were 0.297 $\pm$ 4.4% and 0.430 $\pm$ 4.7% for the vegetation samples in their natural and dried states respectively.

Canopy heights determined for the samples summarised in Figure 4-30 based on the photographic method and the mass of vegetation in the wet and dry states were compared. Heights determined based on the mass of plant material were consistently smaller than those calculated from the projected areas of obstruction (the photographic method). The top part of the canopy is largely composed of leaf tips with a large surface area for a relatively small amount of material. This is why the canopy height based on the projected area of obstruction is greater than the height based on the mass of material.

As the values presented above show, there was a considerable difference in the 90th and 99th percentile values for both the projected area and mass quantification methods. As shown by the plots presented in Figure 4-29, there is relatively little increase in projected area and mass of plant material above the 90th percentile level and up to the 100 percent level due to the sparseness of vegetation material in this region (between 90% and 100%). Hence, it is proposed that the 90th percentile height is used as an index height to characterise canopy height.

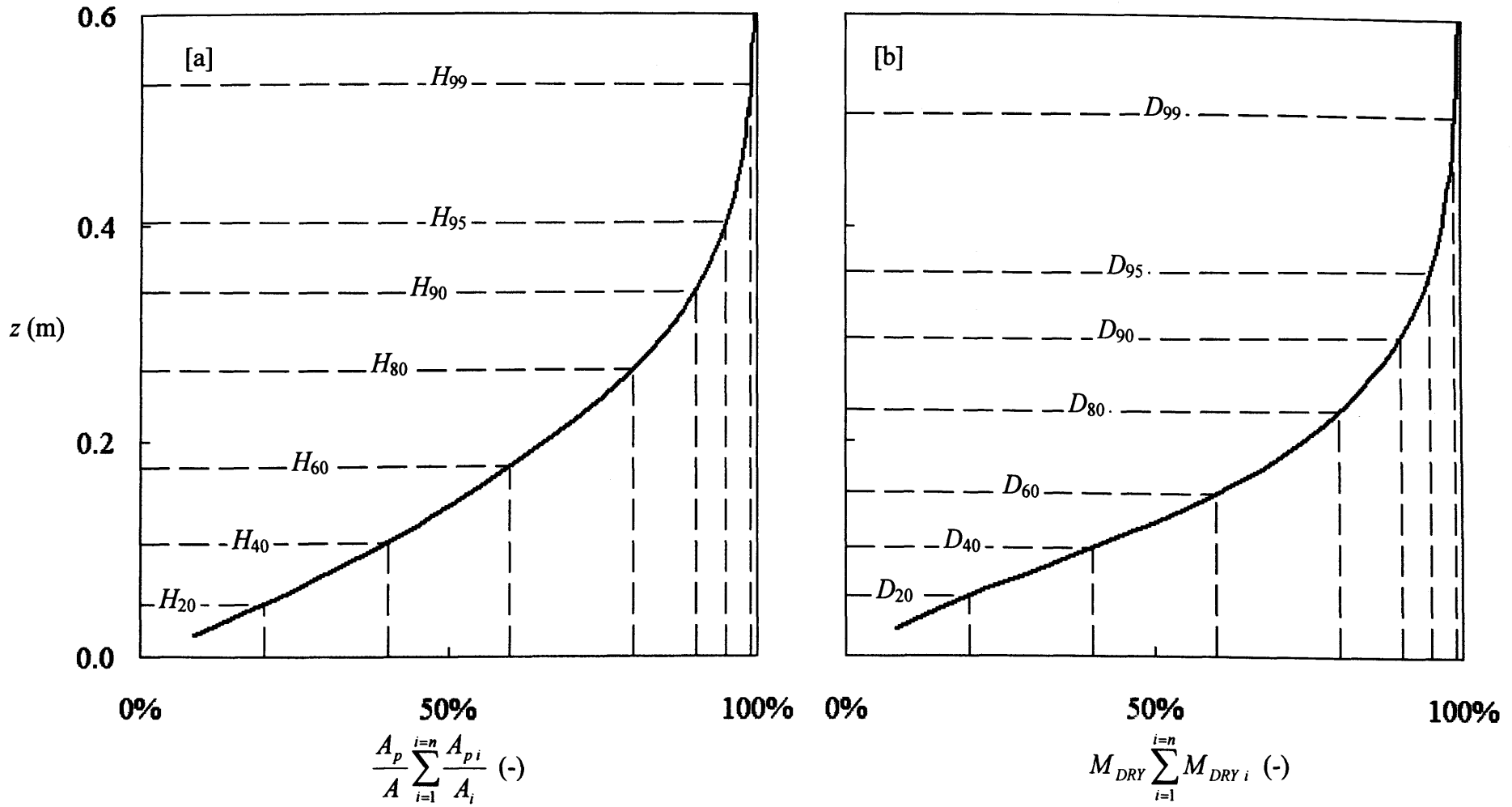

Figure 4-29 Percentile heights of *Spartina anglica* based on 12 months of measurements across two transects based on [a]: projected area and [b]: mass of material. *n* refers to the nth layer, which is the layer of the canopy at any given elevation, A_p is the projected area of the canopy, A is the flow area occupied by the canopy, $A_{p\,i}$ is the projected area of layer i of the canopy, A_i is the flow area of layer i, M_{DRY} is the dry mass of the canopy, $M_{DRY\,i}$ is the dry mass of layer i of the canopy.

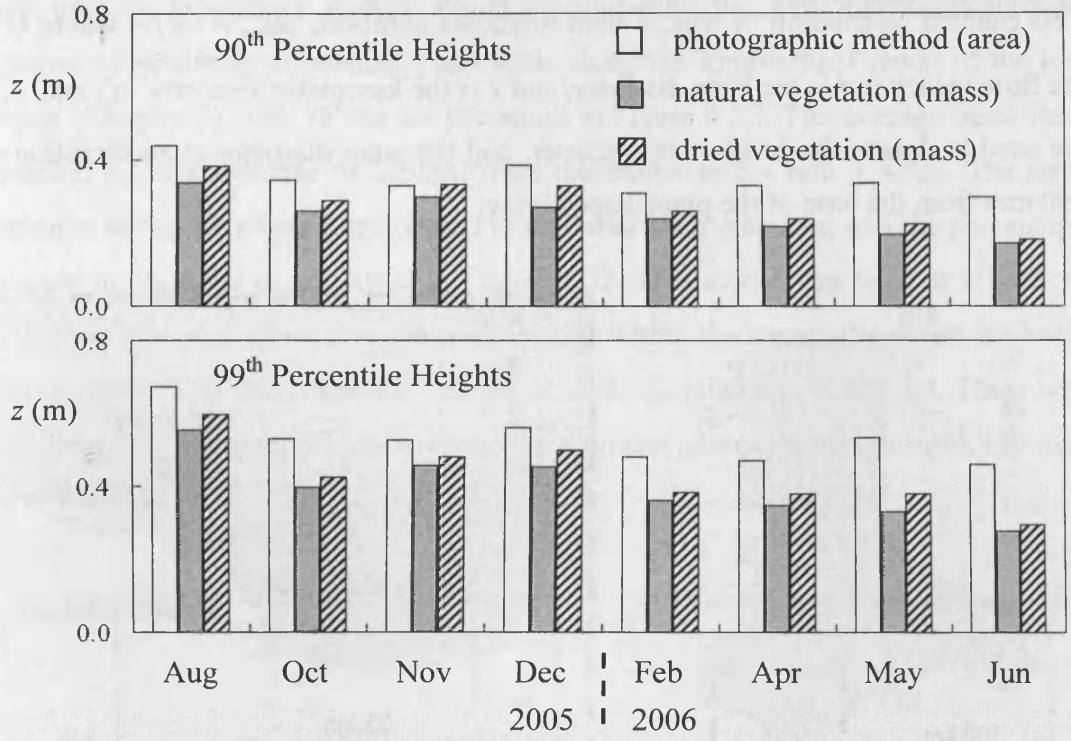

Figure 4-30 90 and 99 percentile heights of *Sp. anglica* vegetation along Llanelli saltmarsh according to the photograph and vegetation mass quantification methods

4.4 Quantification of the Physical Properties of the Vegetation

4.4.1 Stem Diameter and its Variation with Elevation

Stem diameters were measured at the base and at an elevation of 100 mm from the base along individual plant stems using an electronic vernier calliper. This was conducted for two samples of 160 stems each collected during May and June 2006 respectively from the Llanelli saltmarsh during the fieldwork programme, and for three samples collected during August 2006 at the Peterstone Wentlooge saltmarsh for the laboratory study (Figure 4-31). Average values for all samples analysed are presented in Table 4-2. The three samples collected during August 2006 were used to construct vegetation canopies in the laboratory with stem densities of 800, 1160 and 1850 stems m^{-2} respectively. These are referred to in Table 4-2 as samples 1, 2 and 3 respectively and the stem diameters were measured for 200 stems from each sample. Unfortunately, the range of values collected was not sufficient to identify seasonal variations in stem diameters. Although stem diameters were not collected for the full

monitoring period, they provide an indication of typical stem diameters encountered. This enabled calculation of typical stem Reynolds numbers, $\mathrm{Re}_d = Ud/\nu$ where U is the flow velocity, d is the stem diameter, and ν is the kinematic viscosity. d_0 and d_{100} are used to denote the basal stem diameter, and the stem diameter at an elevation of 100 mm from the base of the plant respectively.

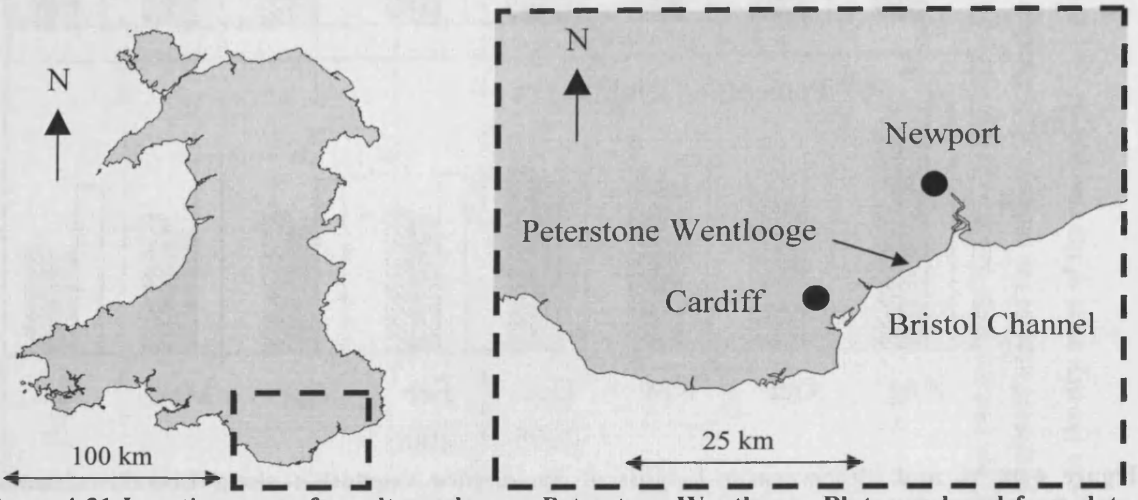

Figure 4-31 Location maps for saltmarsh near Peterstone Wentlooge. Plots produced from data collected by Ordinance Survey.

Table 4-2 - Average stem diameters at the base of the plants, d_0, and 100mm from the base of the stems, d_{100}, during May, June and December 2006, and September 2007

	d_0 (mm)	d_{100} (mm)
May 2006	4.01 ± 1.50	4.39 ± 0.69
Jun 2006	4.61 ± 0.45	2.76 ± 0.89
Aug 2006 (Sample 1)	4.26 ± 0.48	4.43 ± 1.05
Aug 2006 (Sample 2)	5.72 ± 0.42	5.03 ± 0.97
Aug 2006 (Sample 3)	5.51 ± 0.47	4.58 ± 1.10

To assess the variation in stem diameters with elevation along the stem, the stem diameters of 70 stems collected in August 2006 were measured at 20 mm intervals from the base of each stem. Diameters were measured using a Vernier caliper and measurements were recorded for the orientations resulting in the widest and narrowest diameters and the values were averaged. The stems were selected from a number of larger samples that were harvested as part of the field-work (Section 4.3.1) so that they were representative of the range of stem diameters observed across the Llanelli saltmarsh (Section 4.2.1). Stems shorter than 0.2m were excluded; including them is likely to result in greater stem diameter variations. However, the

main purpose of this analysis was to determine the dimensions of larger plants. These were used in laboratory studies aimed at evaluating the hydrodynamics through canopies of relatively consistent plant sizes along the longitudinal reach of the test section (Chapter 7). The values are presented in Figure 4-32. The average basal stem diameter, d_0, at a distance of 20 mm from the base was 5.4 mm $\pm$ 4.4%. The stem diameters along the stems were related to the basal stem diameter, and the percentage decrease in diameter is presented in Figure 4-32. This model was used as a basis to predict the stem diameters at various elevations within the canopy based on the basal stem diameter. The stem diameter decreased with elevation above the bed. There was a considerably more significant decrease in diameter above an elevation of 140 mm above the bed.

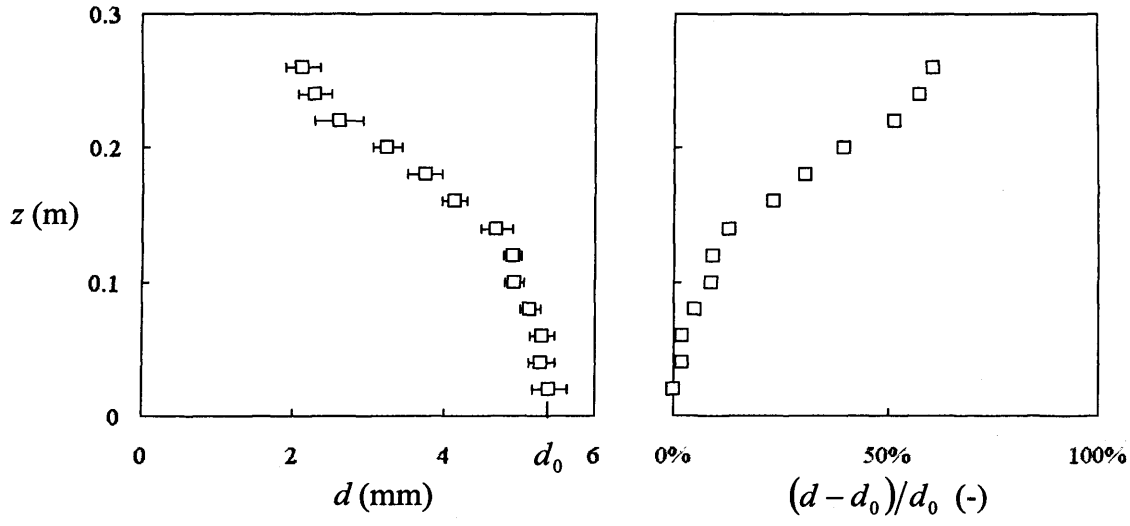

Figure 4-32 Variation in stem diameter at different elevations within a canopy. d is the stem diameter and d_0 is the basal stem diameter.

4.4.2 Porosity of the Vegetation

The porosity of a material is defined as the ratio of the volume of voids to that of the sample volume. The volumes of *Sp. anglica* samples were determined by a British Standards method in (BS 1377-2 (1990)). This is a standard procedure for determining the bulk and dry densities of a soil sample by measuring the mass of a sample and its water displacement. The volume was determined by immersion in a tank of water and the water displacement of water was measured. An apparatus similar to that described in BS 1377-2 (1990) (Figure 4-33) was assembled for this procedure.

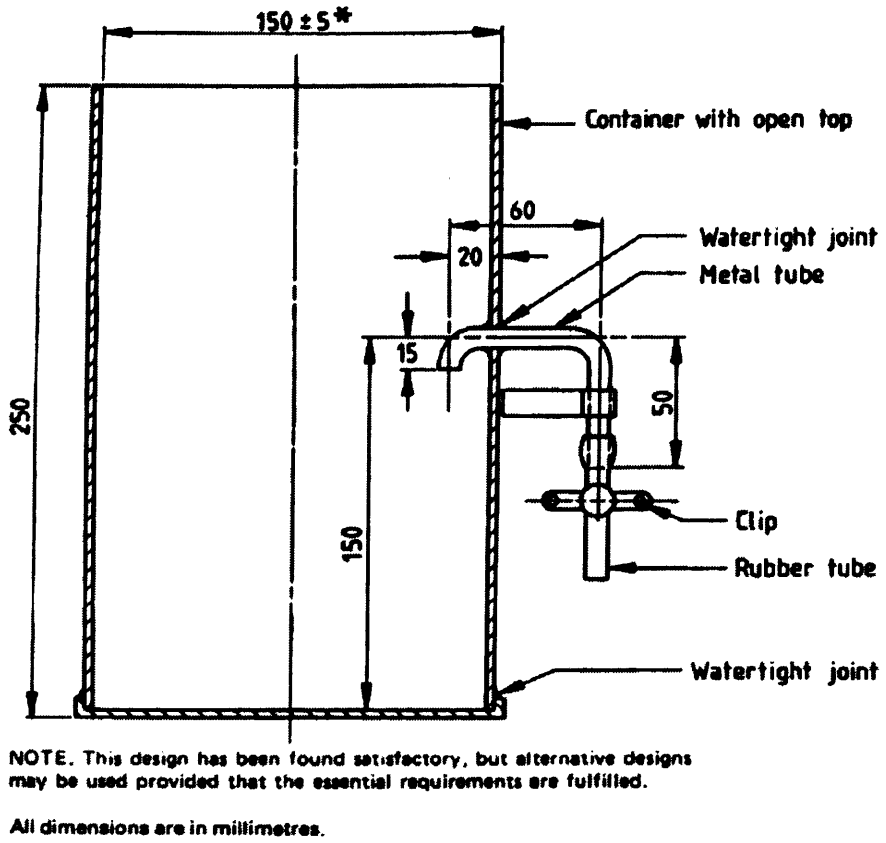

Figure 4-33 Apparatus used to determine water displacement of a sample (from BS1377-2, 1990)

To determine the volume occupied by each sample, the 99th percentile height, H_{99}, was used (Section 4.3.3). The samples were collected from a circular bed area of 375 mm diameter. From this value, along with the volume of vegetation, V_{veg}, as calculated from the volume of water displaced by the sample, the porosity of the vegetation, p, was calculated. Values for the months of May and June 2006 are summarised in Table 4-3. Despite the vegetation appearing to be densely packed, porosity values were very high (99.6 $\pm$ 0.1% for May 2006 and 99.4 $\pm$ 0.1% for June 2006). This indicates that it is reasonable to ignore the volume occupied by the vegetation when calculating the force due to the body weight of the fluid when performing a force balance (see Section 2.3.5).

Average porosities for *Sp. anglica* canopies can be related to results obtained from the photographic method. The method assumes that variations in the projected area of obstruction over the canopy height are proportional to the quantity of material creating the obstruction. Predicted variations in porosity with elevation through the canopy are presented for sampling points A4 and A5 for the months of May and June 2006 in Figure 4-34.

Table 4-3 Porosity values for *Sp. anglica* samples collected in May and June 2006, where H_{99} is the 99th %ile canopy height, V is the volume of vegetation, and p is the porosity of the vegetation

	May 2006			June 2006		
	H_{99} (m)	V (m^3)	p (-)	H_{99} (m)	V_{veg} (m^3)	p (-)
A2	0.505	2.899×10^{-04}	0.9948	0.510	2.638×10^{-04}	0.9953
A3	0.470	1.448×10^{-04}	0.9972	0.425	2.614×10^{-04}	0.9944
A4	0.485	2.251×10^{-04}	0.9958	0.440	2.358×10^{-04}	0.9951
A5	0.474	1.770×10^{-04}	0.9966	0.425	2.360×10^{-04}	0.9950
A6	0.425	1.014×10^{-04}	0.9978	0.488	2.581×10^{-04}	0.9952
B1	0.603	2.045×10^{-04}	0.9969	0.343	2.976×10^{-04}	0.9921
B5	0.351	2.368×10^{-04}	0.9939	0.470	2.797×10^{-04}	0.9946
B7	0.681	2.765×10^{-04}	0.9963	0.363	2.899×10^{-04}	0.9928

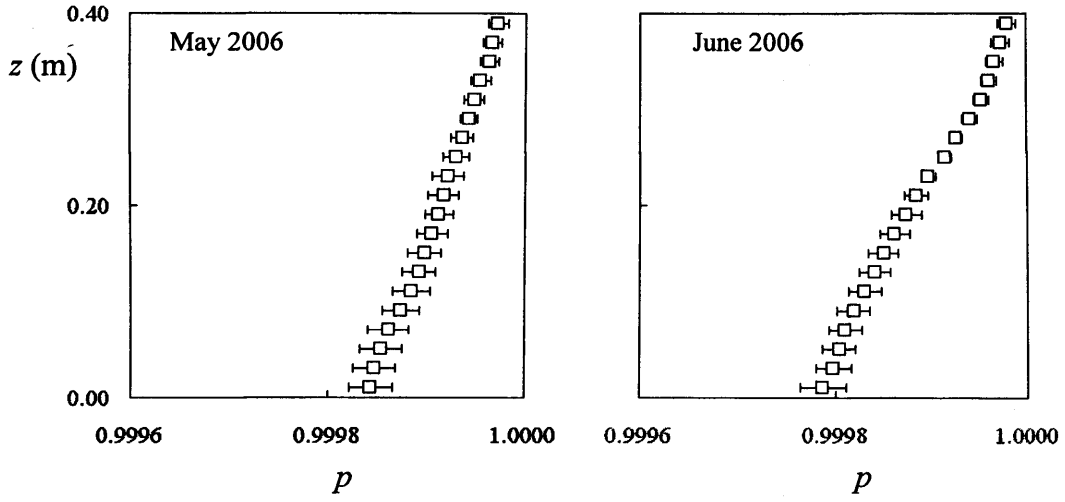

Figure 4-34 The porosity of *Sp. anglica* based on eight samples collected from Llanelli saltmarsh in each of the months of May and June 2005

4.4.3 Stiffness of the Vegetation

The three-point bending test (BS 2782-10, 1977) can be used to determine the Modulus of Elasticity, E, its flexural stress, σ, flexural strain, ε, and the stress-strain response curve of a material. The preparation and testing of the material is relatively simple. This was conducted on vegetation segments to determine the stiffness of the material. For each test, a 50 mm length of stem was installed into the apparatus illustrated by the schematic diagram presented in Figure 4-35. The instrument was connected to a computer and operated automatically, gradually increasing the load, F, to the centre of the segment and recording the maximum deflection within the segment, Δx for each increment. A typical load-displacement diagram is presented in Figure 4-36a showing the increase in displacement in the direction of the load up to

five millimetres. Under sufficient loading, a brittle material will eventually fail corresponding to a sharp drop in the load-displacement curve, although the tests were terminated before reaching this value. Segments were only tested up to a load large enough to cause a five millimetre deflection. Within the context of coastal saltmarshes, failure of the material is not of primary concern since the vegetation will not experience loads of large enough magnitude for failure to take place. Also, fresh vegetation is not very brittle and it is difficult to identify the point of failure as the material is strongly bound together and gradually breaks under a large loading.

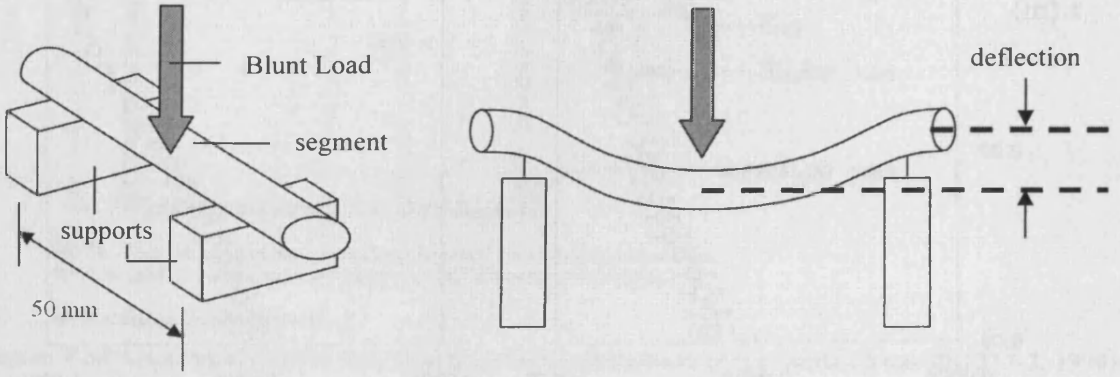

Figure 4-35 Schematic diagram illustrating the three-point bending test

The stress-strain curve is also presented in Figure 4-36b. At lower loads, deformation in the segment is elastic and removing the load would return the segment to its original shape. At this stage, the stress-strain relationship is linear. With increasing load, the deformation becomes plastic and the stress-strain relationship becomes curved. The stress, σ, and strain, ε, for a cylindrical span are given by:

$$\sigma = \frac{Fl}{\pi r^3} \qquad \text{[Equation 4.07]}$$

$$\varepsilon = \frac{6\Delta x d}{l^2} \qquad \text{[Equation 4.08]}$$

where l is the span of the segment, the value of which was 50 mm for these tests, r is the radius and d is the diameter.

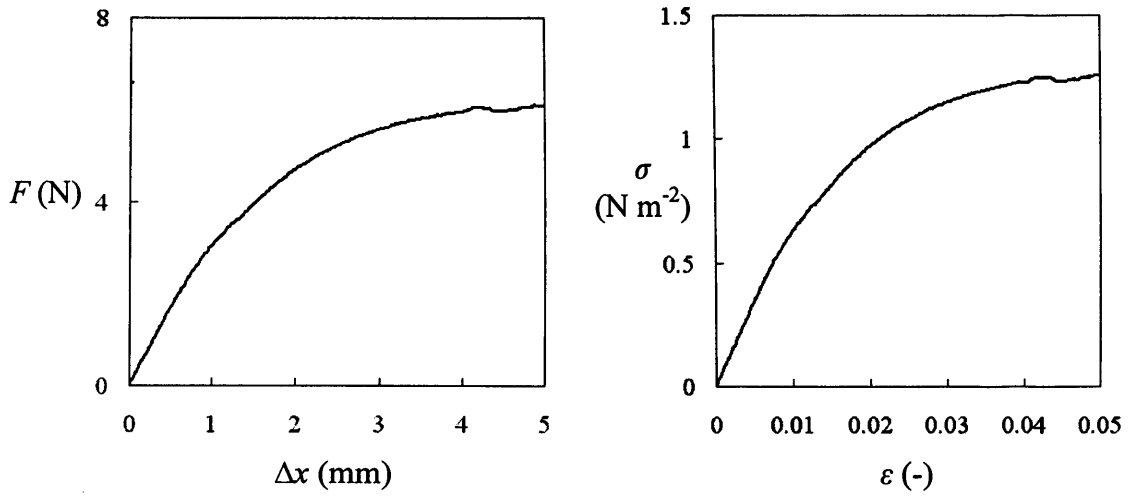

Figure 4-36 [a]: A typical force-displacement curve; [b]: the associated stress-strain curve based on a three-point bending test conducted on a 50 mm span of a *Sp. anglica* stem

The three point bending test was conducted on a sample of 50 stems of *Sp anglica* collected in October 2007. For each stem, five segments, each 60 mm in length were tested (the span length for the testing was 50 mm). The 60 mm segments were measured starting from the base, such that the edges of the segments were at distances of 0 mm, 60 mm, 120 mm, 180 mm, 240 mm and 300 mm from the base. The mean diameter and the force of failure values for each section of the plants are summarised in Table 4-4. The maximum force required to cause a five millimetre deflection in each segment tested decreased with distance from the base due to a decrease in the diameter of the segment.

Table 4-4 Summary of statistics from the three-point bending test analysis

section from base (mm)	diameter (mm)	F_{fail} (N)	E (MPa)	EI (Pa m^4)
0 - 60	4.81 ± 5.6 %	7.32 ± 15.4 %	395 ± 22.5 %	9.559×10^{-3} ± 16.0 %
60 - 120	4.65 ± 5.3 %	6.01 ± 21.5 %	411 ± 19.3 %	9.304×10^{-3} ± 19.6 %
120 - 180	4.30 ± 5.8 %	4.53 ± 20.4 %	508 ± 19.3 %	8.210×10^{-3} ± 18.8 %
180 -240	3.78 ± 6.7 %	4.28 ± 24.2 %	710 ± 22.6 %	6.854×10^{-3} ± 22.0 %
240 - 300	3.43 ± 7.4 %	3.88 ± 19.3 %	882 ± 23.4 %	5.769×10^{-3} ± 22.2 %

The Young's Modulus of Elasticity, E, is a measure of the stiffness of a material and is defined as the slope of the stress-strain curve within the elastic region. It can be determined from the slope of the force deformation curve where the

relationship is linear (i.e. elastic). Plant stems are assumed to be circular in cross-section, and the Young's Modulus of Elasticity for a circular section is given by:

$$E = \frac{\sigma}{\varepsilon} = \frac{Fl^3}{12\Delta x \pi r^4} = \frac{l^3 m}{12\pi r^4} \qquad \text{[Equation 4.09]}$$

where r is the radius of the circular section and m is the slope of the force-deformation curve within the elastic part of the curve which follows Hooke's law. Modulus of Elasticity values for the segments tested are summarised in Table 4-4.

With increasing distance from the base of the plants, the total 'flexural stiffness', as characterised by EI decreased indicating that the plants were stiffer near the base and hence, less prone to deflexion. EI is the product of the Modulus of Elasticity, E, and the second moment of area, I (defined as $\pi r^4/4$ for a cylinder, where r is the cylinder diameter). The plant stems consist of a stiffer outer shell, and a more flexible inner membrane. For the smaller segments typically found higher up in the plants, more of the stem is made up of the stiffer membrane hence a higher Modulus of Elasticity, E, is observed. Near the bed, the stems contain more of the flexible membrane and the Modulus of Elasticity values are lower although the stems are considerably larger in diameter, thus although the material is more flexible in this region, the overall stiffness of the stems is greater compared to the foliage at the top of the canopy. Hence, the parameter EI gives a more realistic representation of the apparent stiffness of the material regardless of the size of the sample. A plot of the EI values for all the stem segments investigated is presented in Figure 4-37 showing a general increase with the size of the segment diameter. EI values are also summarised in Table 4-4.

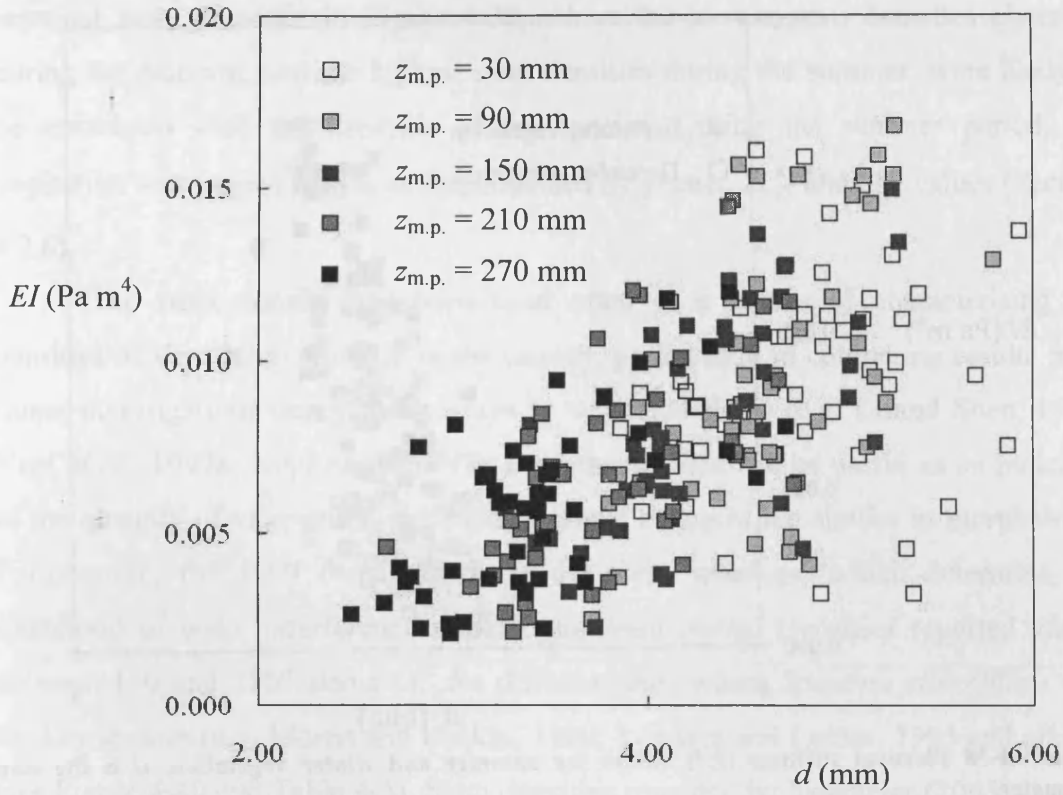

Figure 4-37 The increase of the 'flexural stiffness' of plant stem segments (*EI*) with diameter.

The analysis was repeated to compare samples collected during December 2006 and September 2007. In September 2007, the vegetation was green and the plants were relatively larger in diameter and height, and the plant leaves appeared longer and larger in surface area. During December 2006, the vegetation appeared dormant with a loss of its green colouration, appearing yellow and becoming more brittle. To assess the contrast in material properties between the September and December vegetation, the three-point bending test was applied and the results are presented in Figure 4-38.

The 50 mm segments required for the test were taken from the middle of each stem. The moduli of elasticity (E) calculated for the summer vegetation were significantly higher than those for the winter vegetation. For the September 2007 vegetation, segments had a mean diameter of 4.5 mm $\pm$ 16.9%, had a mean modulus of elasticity of 460 MPa $\pm$ 19.3%, and a mean EI of 8.757×10^{-3} Pa m^4 $\pm$ 19.2%. Contrastingly, the December 2005 vegetation segments averaged 4.0 mm $\pm$ 30.4% in diameter, had a mean modulus of elasticity of 242 MPa $\pm$ 32.6%, and a mean EI of 3.120×10^{-3} Pa m^4 $\pm$ 32.3%.

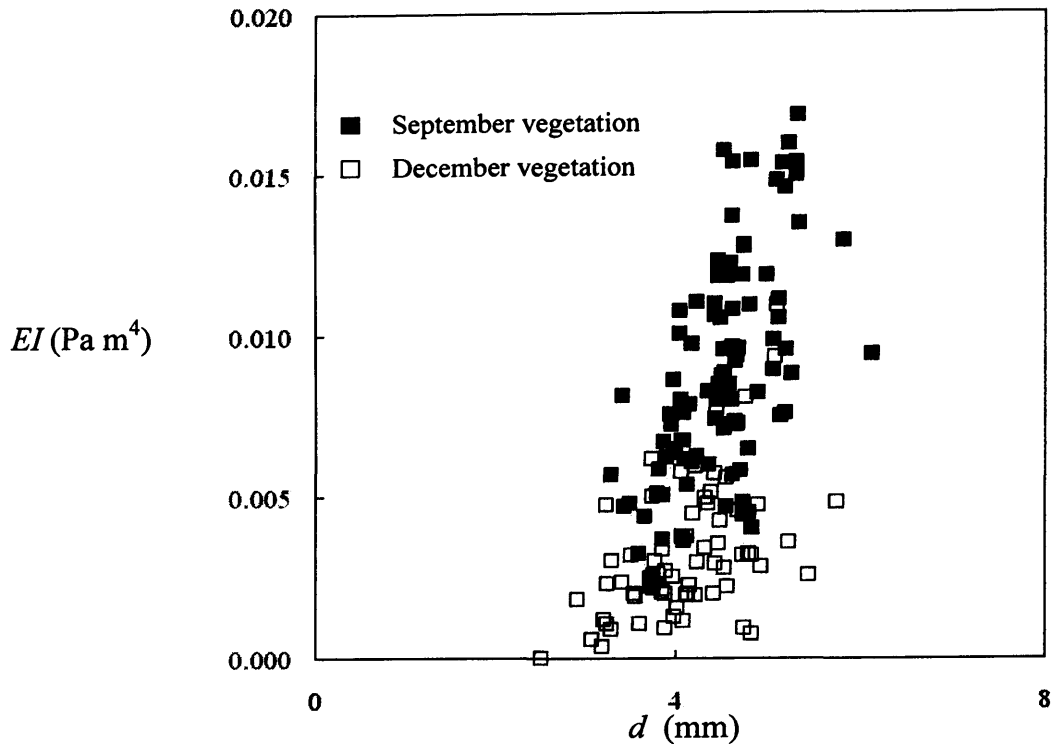

Figure 4-38 Flexural stiffness (*EI*) values for summer and winter vegetation. *d* is the stem diameter.

4.4.4 Stem Density

Vegetation samples were collected from sampling locations along transects A and B throughout the monitoring period (see Section 3.2.3). A tube was used to isolate the vegetation covering a circular ground area with a diameter of 375 mm, the plants were trimmed at the ground level, and the number of stems was counted. Stem densities calculated from the samples are presented in Figure 4-39. Sampling was conducted monthly, and the monitoring period commenced in the summer of 2005 and ended in the spring of 2006. For the entire monitoring period, the average stem densities observed were 835 stems m^{-2} $\pm$ 6.8% for transect 'A', and 947 stems m^{-2} $\pm$ 16.4% for transect 'B'. Stem densities demonstrated large fluctuations both spatially and temporally over the monitoring period. In the seaward direction, and with decreasing elevation, there was an increase in stem density along transect A, and a decrease along transect B. The spatial variations are more likely reflective of the large degree of heterogeneity of vegetation. The densities recorded are similar to those observed by Morris and Haskin (1990) in *Spartina alterniflora* saltmarshes, and by Neumeier (2005) in a *Spartina anglica* saltmarsh (Figure 4-40). Trends observed in

seasonal stem densities in Figure 4-39, where the lowest stem densities observed during the Autumn, and the highest stem densities during the summer, were likely to be associated with the lifecycle of the species. During the summer period, the vegetation was largest in size as demonstrated by greater H_{90} and A_C values (Section 4.2.6).

The stem density has been used often as a means of characterising the densities of vegetation material in the canopy, particularly in comparing results from flume investigations on cylinder arrays to vegetated flows (e.g. Li and Shen, 1973; Nepf *et al.*, 1997a; Nepf *et al.*, 1997b and others). This can be useful as an indicator of the quantity of vegetation, particularly where canopies are similar in morphology. Furthermore, the stem density dictates the stem spacings, which determine the likelihood of wake interference with downstream stems. Densities reported varied between 130 and 2500 stems m^{-2} for different sites where *Spartina alterniflora* was the key species (e.g. Morris and Haskin, 1990; Leonard and Luther, 1995 and others) (see Figure 4-40 and Table 4-5). Stem densities recorded by Neumeier (2005) along a *Spartina anglica* saltmarsh were similar to the stem densities observed along the Llanelli saltmarsh in the current study.

Table 4-5 Details of the studies presented in Figure 4-40

Author	Site	Location	Key Species
Darke & Megonigal (2003)	Gleason Marsh	Virginia, US	*Pontedaria cordata* *Leersia orizoides* *Zizania aquatica*
	Walkerton Marsh	Virginia, US	*Pontedaria cordata* *Leersia orizoides* *Zizania aquatica* *Spartina cynosuroides*
Gambi *et al.* (1990)	San Juan Island	Washington, US	*Zostera marina*
Leonard & Luther (1995)	Bayou Chitigue	SE Louisiana, US	*Spartina alterniflora*
	Old Oyster Chitigue	SE Louisiana, US	*Spartina alterniflora*
	Cedar Creek	WC Florida, US	*Juncus roemerianus*
Morris & Haskin (1990)	Goat Island Site	S Carolina, US	*Spartina alterniflora*
	Oyster Landing Site	S Carolina, US	*Spartina alterniflora*
Neumeier (2005)	Freiston Shore	The Wash, UK	*Spartina anglica*
Current Study	Llanelli Marsh	S Wales, UK	*Spartina anglica*

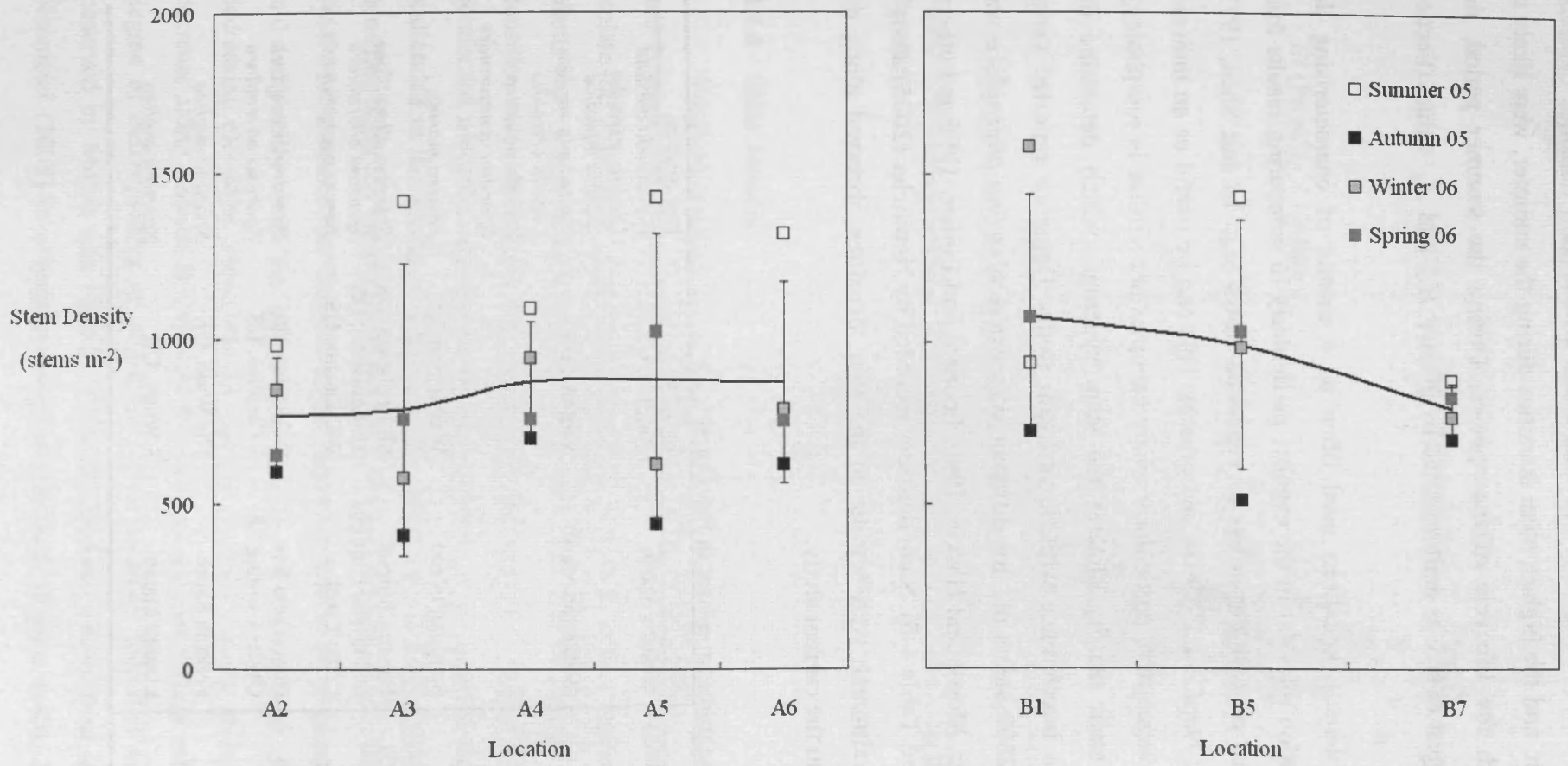

Figure 4-39 *Spartina anglica* stem densities counted at sampling locations on transects A and B and categorised by the four seasons. The bold line denotes the year-average for a given location with standard deviations shown, and the dotted lines show the stem densities implemented in the laboratory study presented in Chapter 7. The seasons are defined as follows: Summer is between 21st June and 22nd September; Autumn is between 22nd September and 22nd December; Winter is between 22nd September and 21st March; Spring is between 21st March and 21st June.

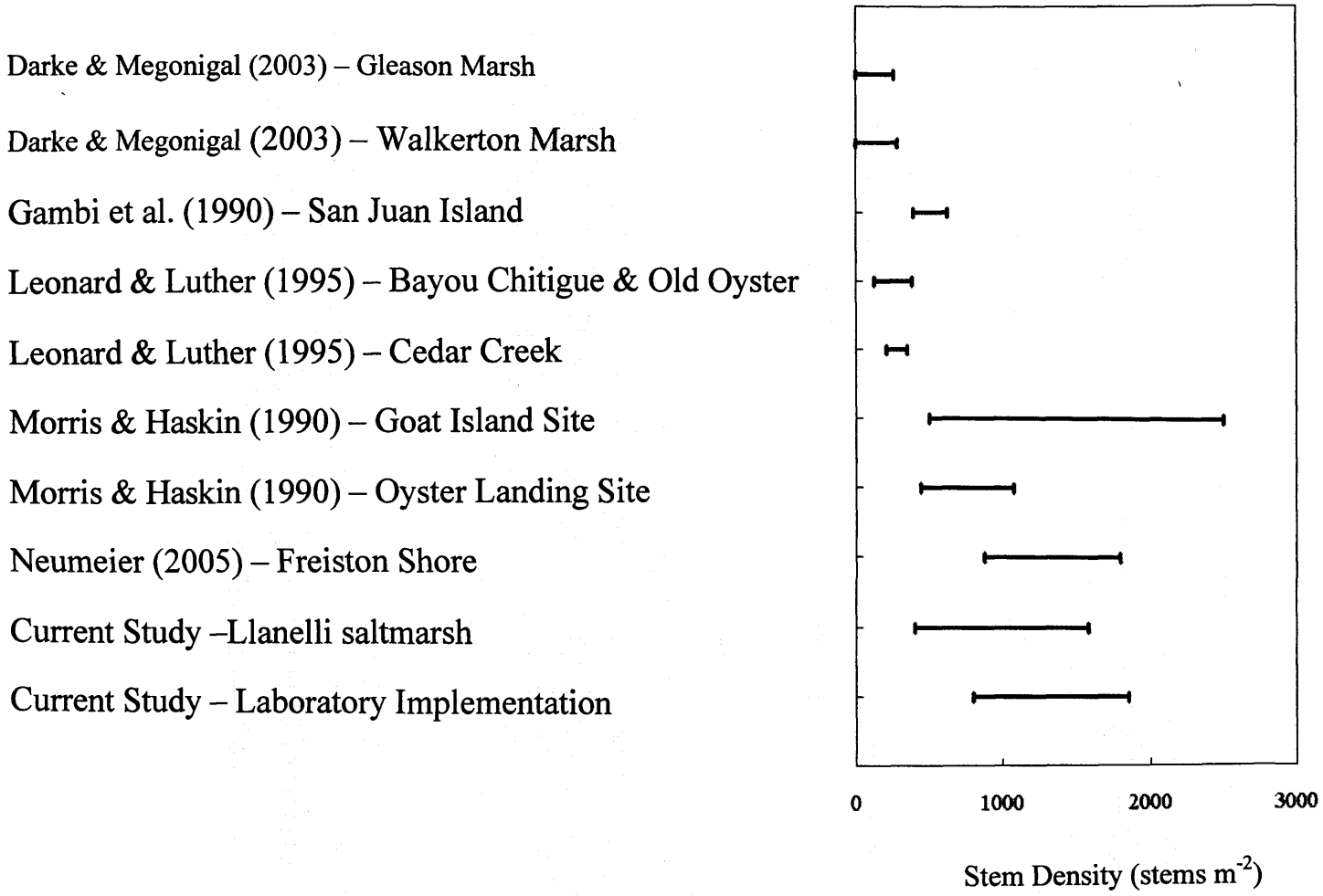

Figure 4-40 Ranges of stem density observed in natural aquatic environments from a number studies, and the range of densities implemented in the laboratory experiments herein

4.5 Concluding Remarks

The vertical variation in *Spartina anglica* was quantified using two different methods. First, it was quantified according to its projected area of obstruction, and secondly, according to the mass of plant material. Both parameters were quantified for sections of small increment along the height of the canopy to determine the distribution of plant material. Both methods identified that there was a large volume of plant material lower down in the canopy, and this gradually decreased with elevation up to the top of the vegetation.

The top of the canopy was difficult to identify as each stem of vegetation varied randomly in height. Choosing the tallest stem would have been unrepresentative of the total canopy. Instead, the 90^{th} and 99^{th} percentiles were determined for each parameter to facilitate the comparison of different samples. Taking the 90^{th} percentile as an index height, *Sp. anglica* canopy heights varied between 0.27m ($\pm$ 8.2 %) and 0.34m ($\pm$ 5.9 %) at different times of the year. Values were based on an average value across the Llanelli saltmarsh. For the 99^{th} percentiles, the range of values determined was between 0.42m ($\pm$ 15.0 %) and 0.54m ($\pm$ 15.1 %). The higher standard deviations reflected the higher level of uncertainty associated with using the 99^{th} percentile. It is proposed that the 90^{th} percentile height is a good guide to the canopy height.

The photographic method did not distinguish between variations in plant parts. A stem of *Sp. anglica* typically had a lower projected area of obstruction near the base due to the exclusive presence of the plant stem, whereas higher up in the canopy, where a large proportion of the canopy was composed of leaves, the projected area was much higher, but the plant material was much more flexible.

Results from the photographic method can be used to distinguish between the morphologies of natural canopies, constructed canopies in the laboratory environment and uniform cylinder arrays. The amount of vegetation material in a natural canopy steadily increased towards the bed due to the presence of fallen or decomposing plant parts, smaller shoots, or even other vegetation species growing near the bed. Constructed canopies would usually consist of neatly arranged larger plants resulting in an organised

canopy with a clear stem region near the bed, and a higher projected area of obstruction at the mid-height due to a higher concentration of plant foliage.

The quantification of the canopies based on the mass of vegetation material produced slightly different profiles compared to the projected area profiles. The mass quantification showed a decrease in the amount of material near the bed, and a peak approximately 100 mm above the bed. The projected area method suggested the amount of material continued to increase towards the bed. Furthermore, the mass quantification method results suggest that the canopies were slightly shorter than the heights determined from the photographic method. The thinner plant parts near the top of the canopy were low in mass but high in projected area.

Stem densities were counted for *Sp. anglica* samples collected across the Llanelli saltmarsh over the monitoring period. Average densities observed varied between 589 stems m^{-2} during the Autumn and 1174 stems m^{-2} during the Summer. Stem diameter measurements were only taken for the months of May, June, September and December. The smallest average diameter was observed in June (2.76 mm) reflecting the new offspring of fresh vegetation. In September, the diameters were largest with an average value of 4.65 mm following a period of intensive growth. The average diameter decreases to 4.12 mm during December when the vegetation begins to decay.

The vegetation appeared greener and healthier during the summer months compared to the period between January and April when the vegetation became yellow in colour and more brittle. This was reflected in values of Young's Modulus of Elasticity, which were determined for samples of *Sp. anglica* collected during September and December. Average values of 460 MPa and 242 MPa were observed respectively highlighting the decrease in stiffness of the plant stem as the vegetation ages.

The *Sp. anglica* canopies were considerably taller during the summer months. The vegetation grew in size from June, reaching a maximum spatially averaged height of 0.34 m $\pm$ 5.9% (90^{th} percentile height), and decreasing steadily in height between September and November. A minimum 90^{th} percentile canopy height of 0.27 m $\pm$ 8.2 % was observed during March, although the canopy height was fairly consistent at this level for the remainder of the year (between November and May). Trends observed in canopy

heights reflect the change in the quantity of vegetation, which also increased in density during the summer months.

Ultimately, it is difficult to simulate a natural plant stem with an artificial material that varies significantly in morphology and uniform cylinder arrays are often implemented on the assumption that the plants resemble the cylinders. In the case of *Spartina anglica*, that can only be justified for the stem region near the bed. Hence, due to the large contrast in morphology between vegetation and simulated canopies, the hydraulic resistance characteristics determined from experimental studies on uniform cylinder models and the associated velocity and turbulence structures cannot be easily adapted to the natural environment.

5 Laboratory Investigations: Setup and Methodology

5.1 Introduction

A range of laboratory experiments were conducted to investigate the influence of different canopies on velocity and turbulence structures. Details of the experiments and the apparatus used are presented in this chapter. Different procedures for recording measurements that are applied in the experiments are also described.

A range of bed gradients, stem densities, emergence and submergence levels were imposed. Values for these variables were selected based on the findings of the field monitoring programme presented in Chapter 4, so that the experiments were conducted for a range of conditions that were representative of typical saltmarshes. The submergence level, H, was defined as the ratio of flow depth, D, to vegetation height, T. Values of H less than unity indicate an emergent condition meaning that the vegetation canopy projects through the water surface, whilst values of H greater than unity indicate a submerged condition with the flow depth being greater than the canopy height.

The experiments were conducted using three different types of canopy: uniform cylinder arrays, constructed vegetation canopies using vegetation collected during August 2006 (non-dormant or summer vegetation), and constructed vegetation canopies using vegetation collected during February 2007 (dormant or winter vegetation). The characterisation of the vegetation canopies is also considered in this chapter. Details of the experiments conducted for each type of canopy are summarised in Table 5-1, Table 5-2 and Table 5-3 respectively.

Table 5-1 Details of experiments conducted using uniform cylinder arrays

Test No.	Stem Density [stems m^{-2}]	Bed Gradient S_0	Vegetation Height T [m]	Reynolds Number Re_d	Flow Depth D [m]	Submergence Level $H = D / T$
S-1000	800	1/1000	0.15	430	0.20	1.33
M-1000	1160	1/1000	0.15	330	0.20	1.33
D-1000	1850	1/1000	0.15	230	0.20	1.33
S-0300	800	1/300	0.15	840	0.20	1.33
M-0300	1160	1/300	0.15	560	0.20	1.33
D-0300	1850	1/300	0.15	420	0.20	1.33

Table 5-2 Details of the experiments conducted using *Sp. anglica* plants during Aug 2006

Test No.	Stem Density [Stems m^{-2}]	Bed Gradient S_0 [-]	Vegetation Height T [m]	Flow Depth D [m]	Reynolds Number Re_d	Submergence $H = D / T$	Flow Rate Q [ls^{-1}]
S-T12	800	1/300	0.53	0.25	420	0.47	7.0
S-T11	800	1/300	0.53	0.20	430	0.38	5.3
S-M11	800	1/300	0.15	0.20	450	1.33	6.8
S-S11	800	1/300	0.10	0.20	600	2.00	12.9
S-V10	800	1/300	0.05	0.15	890	3.00	13.9
S-T22	800	1/1000	0.53	0.25	200	0.47	3.4
S-T21	800	1/1000	0.53	0.20	230	0.38	2.7
S-M21	800	1/1000	0.15	0.20	250	1.33	3.9
S-S21	800	1/1000	0.10	0.20	350	2.00	7.4
S-V20	800	1/1000	0.05	0.15	360	3.00	8.0
M-T12	1160	1/300	0.53	0.25	340	0.47	5.5
M-T11	1160	1/300	0.53	0.20	360	0.38	4.2
M-M11	1160	1/300	0.15	0.20	340	1.33	5.3
M-S11	1160	1/300	0.10	0.20	480	2.00	10.6
M-V10	1160	1/300	0.05	0.15	770	3.00	12.4
M-T22	1160	1/1000	0.53	0.25	160	0.47	2.6
M-T21	1160	1/1000	0.53	0.20	160	0.38	1.9
M-M21	1160	1/1000	0.15	0.20	210	1.33	3.1
M-S21	1160	1/1000	0.10	0.20	260	2.00	5.8
M-V20	1160	1/1000	0.05	0.15	440	3.00	6.8
D-T12	1850	1/300	0.53	0.25	250	0.47	4.4
D-T11	1850	1/300	0.53	0.20	270	0.38	3.5
D-M11	1850	1/300	0.15	0.20	240	1.33	4.6
D-S11	1850	1/300	0.10	0.20	370	2.00	10.7
D-V10	1850	1/300	0.05	0.15	480	3.00	10.9
~~*D-T22~~	~~1850~~	~~1/1000~~	~~0.53~~	~~0.25~~	~~160~~	~~0.47~~	~~2.9~~
~~*D-T21~~	~~1850~~	~~1/1000~~	~~0.53~~	~~0.20~~	~~170~~	~~0.38~~	~~2.2~~
D-M21	1850	1/1000	0.15	0.20	110	1.33	2.2
D-S21	1850	1/1000	0.10	0.20	180	2.00	5.5

*Tests D-T22 and D-T21 were excluded from this report due to an error incurred in the adjustment of the flume bed gradient.

Table 5-3 Details of the experiments conducted using *Sp. anglica* plants during Feb 2007

Test No.	Stem Density [Stems m^{-2}]	Bed Gradient S_0	Vegetation Height T [m]	Flow Depth D [m]	Reynolds Number Re_d	Submergence $H = D / T$	Flow Rate Q [ls^{-1}]
S-T21m	800	1/1000	0.53	0.20	410	0.38	6.8
S-M21m	800	1/1000	0.15	0.20	600	1.33	10.7
S-S21m	800	1/1000	0.10	0.20	760	2.00	17.8
S-V20m	800	1/1000	0.05	0.15	1000	3.00	19.2

5.2 Laboratory Setup

5.2.1 Flume Description

The flume studies were conducted in a 0.3m wide, 0.3m deep and 10m long slope-adjustable flume with glass sidewalls (see Figure 5-1). At the upstream end, a head tank provided a consistent flow at the upstream boundary over the flow depth. A 50 mm length of honeycomb flow-straightener was used to minimise turbulence in the inflow. Flow depth through the flume was controlled at the downstream end by a lever-adjustable weir, downstream of which, the flow funneled into a large storage tank.

A manual lever controlled the bed gradient. The flume bed was repeatedly levelled following minor bed slope adjustments until the two bed gradients of 0.001 and $0.00\dot{3}$, which were imposed in this study were achieved. The lever setting was marked for future reference.

The glass walls of the flume in which the experiments were conducted are smooth and would create negligible resistance to the flow. Furthermore, flow parameters were measured along the centreline of the flume to reduce the impact of wall effects on measurements. A width to depth ratio greater than 6.0 is normally required for wall effects do to be negligible. Values for the experiments were much lower than this value, ranging between 1.2 and 2.0 for flow depths of 0.15m, 0.20m and 0.25m. However, for flow through dense vegetation, boundary effects due to the roughness of the bed and the walls can usually be neglected.

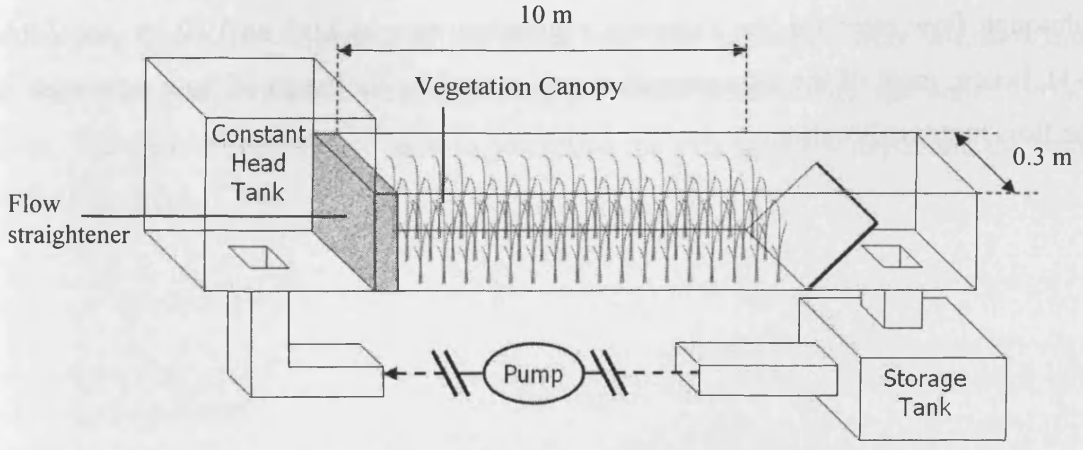

Figure 5-1 Schematic diagram outlining the flume setup used for the experiments.

5.2.2 Discharge Measurement

A pump controlled by a digital flow meter facilitates discharge through the flume. The flow meter was calibrated by testing the pump for a number of flow settings, and compared against the measured volumetric flow rate, which was calculated based on the duration required to fill a 100.8 litre container. The procedure was repeated three times to obtain an average value from which the measured flow rate, $Q_{measured}$, was calculated. In Figure 5-2a, the flow meter readings, $Q_{flow\ meter}$, are compared to the measured flow rates. At lower flows, the two conformed well, whilst at higher values, there was an increase in the underestimation of the flow rate by the flow meter. However, at the highest flow rate of 13.5 l/s ($Q_{flow\ meter}$), the time required to fill the bin was 5.8 $\pm$ 0.1s compared to 53.6 $\pm$ 0.5s for the lowest flow rate of 1.7 l/s. At higher flow rates, the sampling periods were considerably shorter, and the likelihood of error was significant. For instance, a difference of 1.5s in the recorded time for the highest flow rate would have rendered a value equal to that displayed by the flow meter.

Errors in the flow meter readings based on the calculated measurements are shown to increase with flow rate in Figure 5-2b. It is therefore uncertain whether the errors are due to an increase in human error at higher flow rates, or due to the flow meter. However, the flow meter readings were only used to determine the setting required for uniform flow, and the values were not used in any calculations. Thus, instead of calculating an area-mean velocity based on flow rate, a depth-averaged velocity was calculated based on measured velocities. Flow rates for the experiments on the August vegetation (see Table 5-2) ranged between 1.9 l/s and 13.9 l/s, (although flow rates for the February vegetation were as high as 19.2 l/s, see Table 5-1), hence, most of the experiments were covered by the range of flow rates used in the flow meter calibration.

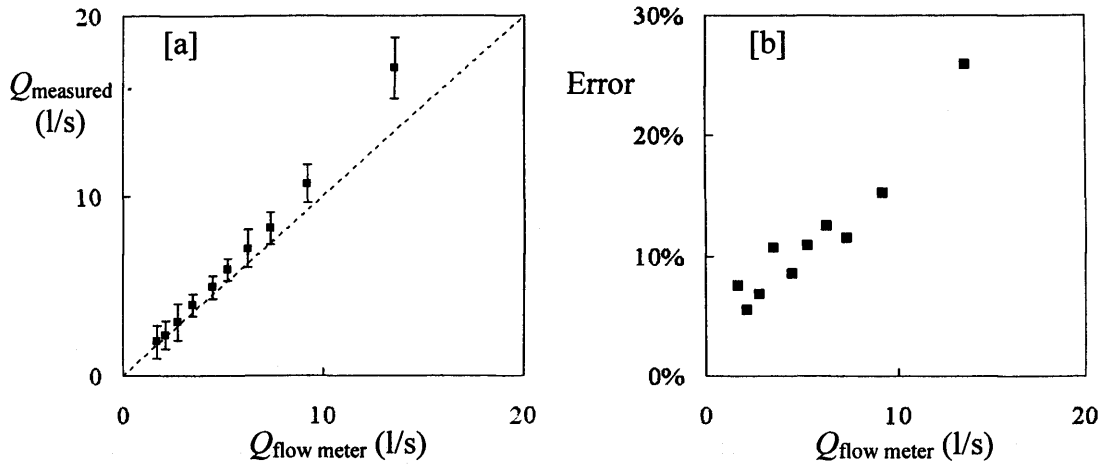

Figure 5-2 [a]: Comparison between flow meter readings and measured volumetric flow rates for the flume pump; [b]: Errors in the flow meter readings for different flow rates

5.2.3 Flow Depth Measurement

A water level gauge was installed onto a platform mounted onto the railings of the flume. The vernier scale on the gauge enabled precise readings to the nearest 0.1 mm. The gauge was used to measure the water surface level relative to a datum at five locations: 3.5m, 4.5m, 5.5m, 6.5m and 7.5m along the length of the flume. These distances were measured from the upstream end of the flume. The datum was set to the flume bed elevation for convenience. The measurement locations were selected so as to cover a representative length of the flume, whilst avoiding the upstream and downstream regions where the flow is likely to be more significantly affected by the inlet and outlet boundaries.

Elevations of the flume bed were also recorded at the measurement locations. These varied slightly due to either the positioning of the railings with respect to the underlying flume, or the profile of the flume bed. The variations were within 0.3mm of the mean bed level and were corrected for when determining the water surface level. The measurements were used to determine the average flow depth and the water surface gradient.

5.2.4 Installation of the Cylinders and Vegetation

5.2.4.1 Uniform Cylinder Arrays

Uniform cylinder arrays were created by installing 170 mm long plastic drinking straws into 20 mm deep plastic honeycomb sheets. The plastic straws were 6.0 mm and the honeycombe pores were 6.2 mm according to the design specifications of the material.

To minimise turbulence generation due to the perforated bed surface, aluminium foil was glued onto the honeycomb sheets using Solvitol heavy-duty spray adhesive. The foiled honeycomb sheets were screwed onto plastic bases for support, and the surface marked and pierced at the desired stem density for each experiment (800, 1160 and 1850 stems m^{-2}). The stem densities were selected within the range of values observed at the Llanelli and Lanrhidian field sites (Section 3.2.3). The specific values were determined by the pore spacings. For the stem densities investigated, the stems were spaced four, five and six pores apart in the diagonal direction along the honeycomb sheets (Figure 5-3). These equated to diagonal stem spacings of 32.0mm, 38.4mm and 44.8mm respectively (Table 5-4). The plastic bases supporting the prepared *Sp. anglica* canopies were also attached to the base of the flume using silicon sealant.

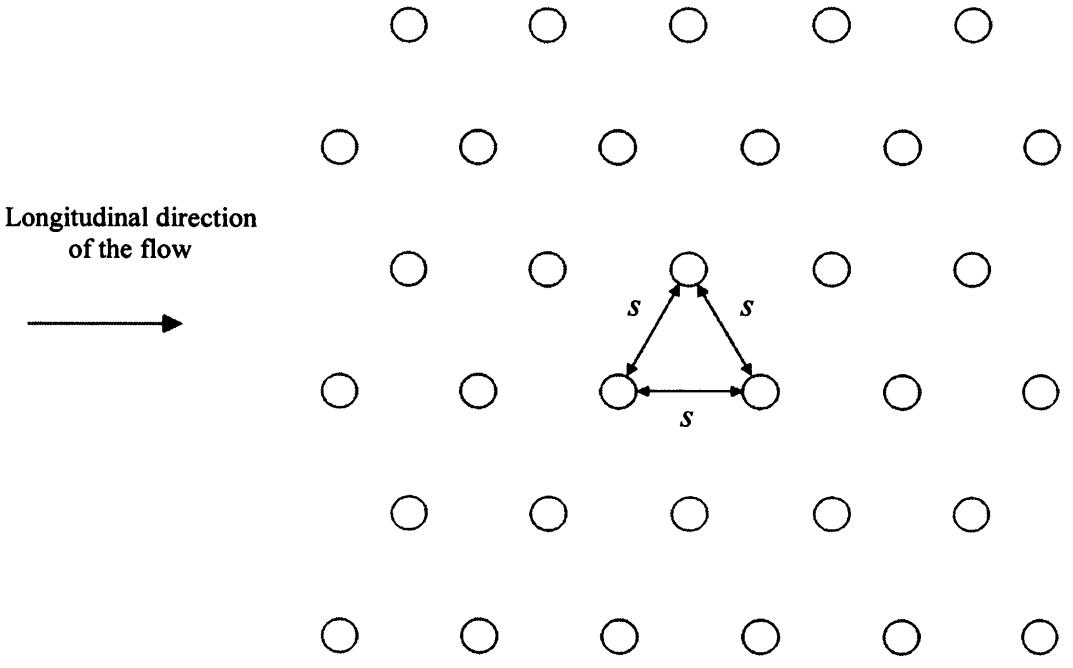

Figure 5-3 The longitudinally staggered array arrangement implemented in the flume experiments. The plastic honeycomb sheets used to hold the Spartina anglica stems influenced the pattern. *s* is the distance between the stems.

Table 5-4 Stem spacings for each stem density implemented in this study.

Canopy density (stems m^{-2})	s (mm)
800	38.0
1160	31.5
1850	25.0

The aluminium lining created a smooth bed surface in regions void of vegetation to reduce bed generated turbulence over the hollow honeycomb pores. In emergent vegetated flows, turbulence production within the stem wakes far exceeds that due to bed shear over most of the flow depth. It is thought that the influence of the bed is limited to within a distance of one stem diameter (Nepf *et al.*, 1997a).

5.2.4.2 Constructed Vegetation Canopies

Vegetation samples used in this laboratory study were collected near Peterstone Wentlooge along the Severn Estuary between Cardiff and Newport (Figure 5-4). The site was chosen for convenience due to its proximity, and the abundance of *Spartina anglica*, the species of interest. During collection, the vegetation was cut at the base of each stem. Plants were installed in a similar method to the one described in Section 5.2.4.1 for the uniform cylinder arrays and silicon sealant was used to hold the stems in place.

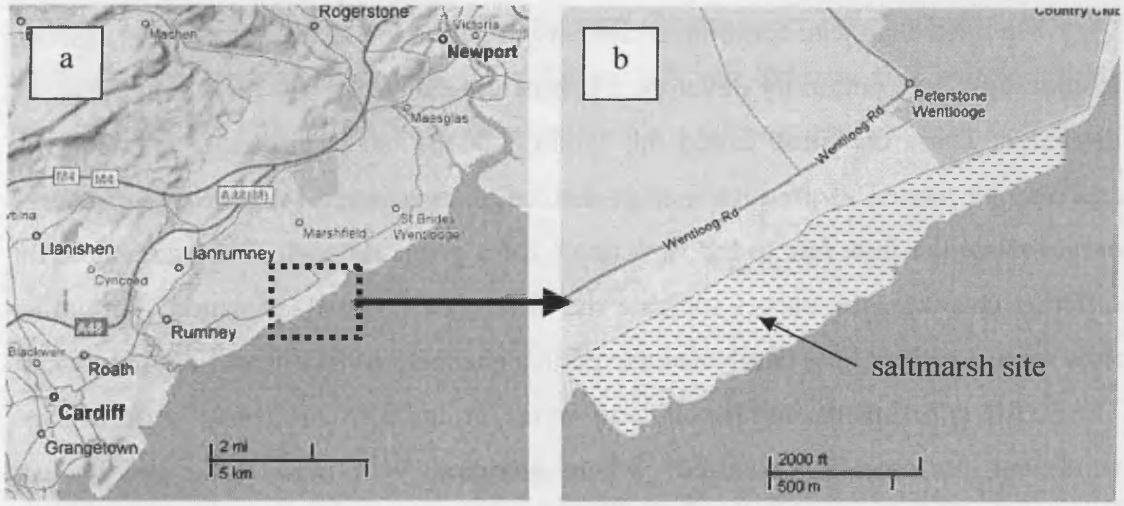

Figure 5-4 [a]: location map of Peterstone Wentlooge with respect to the nearby cities of Newport and Cardiff; [b]: location of the saltmarsh near Peterstone Wentlooge. Maps were taken from www.maps.google.co.uk

The effects of fresh summer and mature winter vegetation on flow structure were compared. In the northern hemisphere, by convention, summer is accepted as the

period between the summer solstice (~21st June), and the autumn equinox (~22nd September). Winter is the period between the winter solstice (~22nd December), and the vernal equinox (~21st March) (Her Majesty's Almanac Office, 2000). The majority of the experiments were conducted during August 2006, and some were repeated during February 2007. Therefore, by convention, plants collected during these periods were representative of summer and winter vegetation.

To achieve a range of submergence levels throughout the experimental programme (Table 5-2), the vegetation was trimmed from its full height to 150 mm, 100 mm and 50 mm. Therefore, for all experiments conducted for submerged canopies, the vegetation was 'cropped' in nature and does not truly represent the natural morphology, however, this was necessary to achieve submerged conditions in the flume available for this investigation (see Section 5.2.1). A steel tube was suspended from a platform using string, and the platform was mounted onto the flume railings. The elevation of the steel tube was adjusted to the required canopy height. This was used as a guide along the flume to trim the top of the vegetation using a pair of large scissors. The trimmed segments were removed during the process to avoid the accumulation of loose material within the canopy.

5.2.5 Rating Curves and Establishment of Uniform Flow Conditions

In open channels, continuous discharge measurements are impractical. Instead, relationships are commonly developed between the stage, or the flow depth, and the discharge. These are often called the 'rating', or the 'stage-discharge relationship', and may be plotted to produce a stage-discharge, or a rating curve. Stage-discharge curves relate the flow rate to the flow depth for a given channel. When compared for different channels, the curves indicate the difference in flow resistance. For similar flow rates, a greater flow depth is achieved in a channel with a higher flow resistance.

All experiments conducted here were for uniform or nearly uniform flow conditions. For each flow condition, where alterations were made to the bed gradient or the vegetation canopy (stem density or vegetation height), a stage-discharge curve was produced. Flow conditions are listed in Table 5-2. A number of flow rates were implemented, the magnitudes of which varied for different canopies. Stage-discharge curves were produced covering the required flow depths to achieve the desired submergence level for each experiment (Table 5-2). For each flow rate, the water

surface gradient relative to the cannel bed was determined as described in Section 5.2.3. Six weir height settings were implemented resulting in three positive and three negative water surface gradients. For a positive gradient, the flow depth is greater at the downstream end of the flume. The six gradients were used to determine the required weir setting to achieve a zero-gradient surface water profile.

5.2.6 Changes in Vegetation Hydraulic Properties during the Experiments

For each stem density of the constructed vegetation canopies (see Section 5.2.4.2), a range of bed gradients and vegetation heights were examined, and the experiments were conducted over a period of up to nine days. This was in addition to a day for collection and a day for installation of the vegetation. There was concern that the vegetation properties may be modified significantly as plant matter decomposed over the duration of the study of each stem density. Decomposition was likely affected by a number of factors, particularly the room temperature, water temperature, water quality and the duration and extent to which the vegetation was immersed in water. An appropriate period over which the hydraulic resistance of the vegetation remained relatively constant is therefore difficult to define, as this will depend on the laboratory conditions at the time the experiments were conducted. To assess change in the hydraulic resistance of the vegetation, a canopy was created at a density of 800 stems m^{-2} and stage-discharge curves were determined at two-day intervals. The curves are presented in Figure 5-5 and indicate that over a 13-day period, there was little variation in the vegetation's resistance properties.

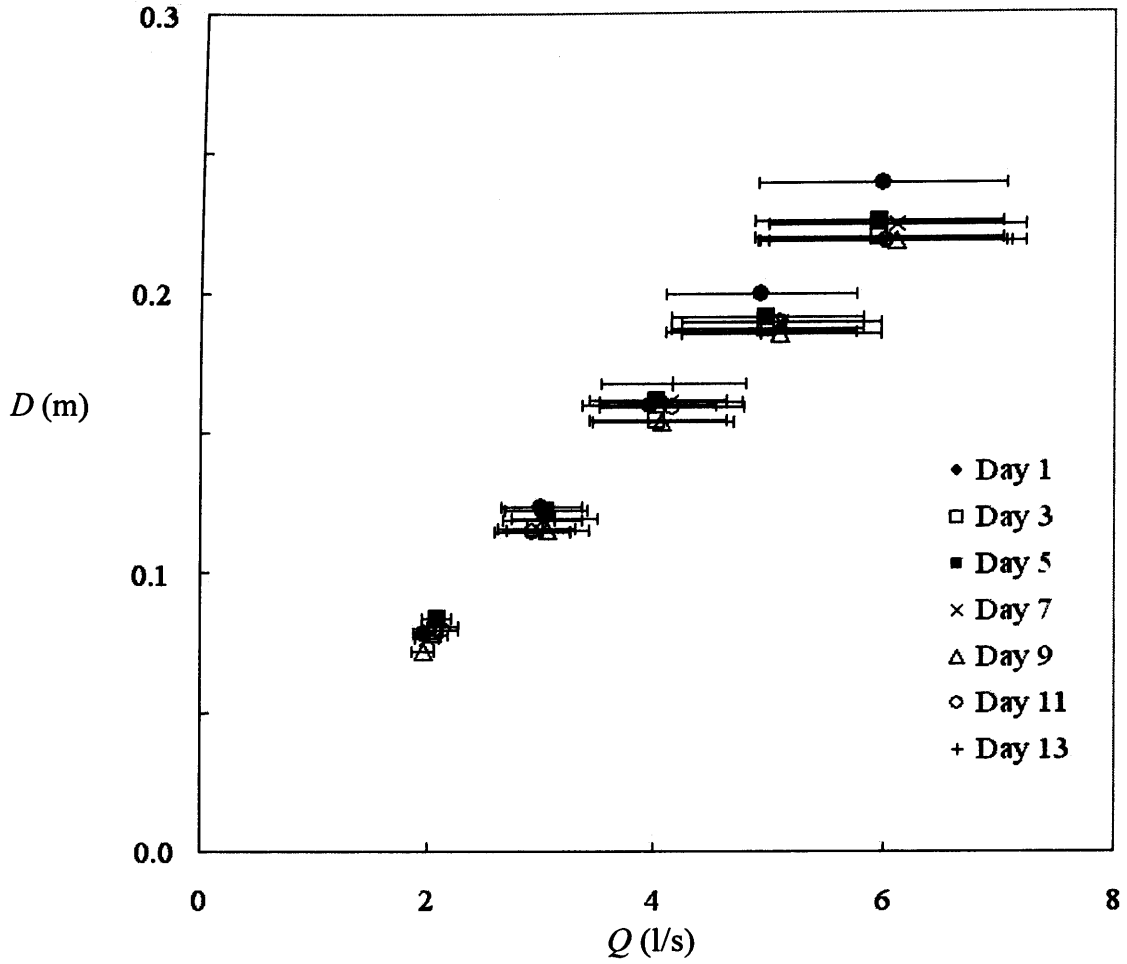

Figure 5-5 Variations in the stage-discharge relationship for an emergent, sparse *Spartina anglica* canopy with a stem density of 800 stems m^{-2} over a two-week period. *D* is the flow depth and *Q* is the flow rate. Error bars indicate the errors in flow rates based on the pump reliability evaluation conducted in Section 5.2.2. The error in flow depth measurements is estimated at ± 0.1 mm.

5.2.7 Measurement of Velocity and Turbulence Statistics

Three dimensional velocity components (u, v and w) corresponding to the x, y and z-axes were measured using two 25 Hz Nortek Acoustic Doppler Velocimeters (ADVs). The instruments operate on the Doppler principle, whereby the echo of short acoustic pulses of known frequencies is detected, and the shift in frequency between the transmitted and received pulses is used to determine the water velocity (Nortek AS, 1997). The instruments were used to measure velocity statistics over a three-minute period. The duration was selected following a number of trial runs where measurements were conducted over longer periods of up to 20 minutes. This determined the size of the sample required to minimise the error in the cumulative time-averaged velocity sufficiently e.g. Figure 5-6. The longitudinal velocity

calculated based on a three-minute period resulted in an error of less than 1.2% from the cumulative time-averaged value after 10 minutes. At 25Hz, over a three-minute period, 4500 measurements were recorded for each parameter. The measured data was saved and then processed through the WinADV software to extract time-series data and calculate time-averaged values of the velocity (u, v, w) and turbulence (e.g. u', w', $u'w'$ etc.) parameters.

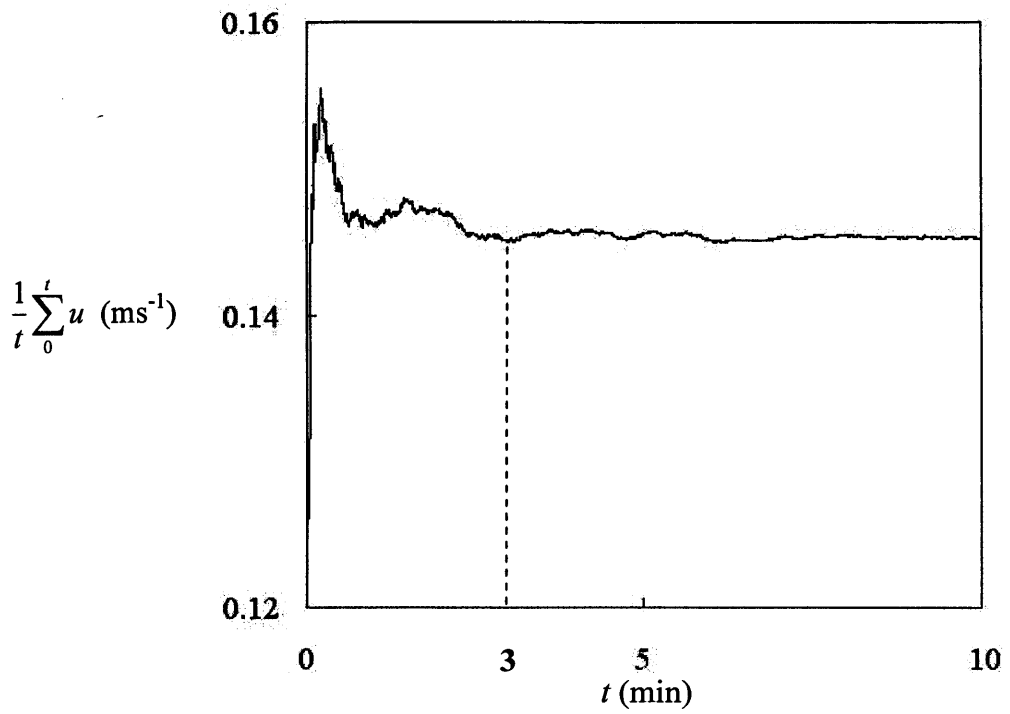

Figure 5-6 Cumulative time-averaged longitudinal velocities over periods of up to 10 minutes highlighting the larger errors associated with a sampling period of one minute. The velocities were recorded at an elevation of 30mm above the bed for vegetation collected in February 2007, a stem density of 800 stems m^{-2}, a canopy height of 100 mm and a bed gradient of 1/1000. t is time, u is the instantaneous velocity at time, t'.

Each ADV comprises a transmitter and three acoustic receivers (Nortek AS, 1997). The receivers are mounted on three short arms at equal spacings surrounding the transmitter (see Figure 5-7). The cylindrical sampling volume, 9 mm in height and 15 mm in diameter, is located approximately 50 mm from the transmitter. The path between the sampling volume and the transmitters must remain unobstructed. Due to the high density of the vegetation canopies, it was necessary to clear some of the vegetation to accommodate the ADVs.

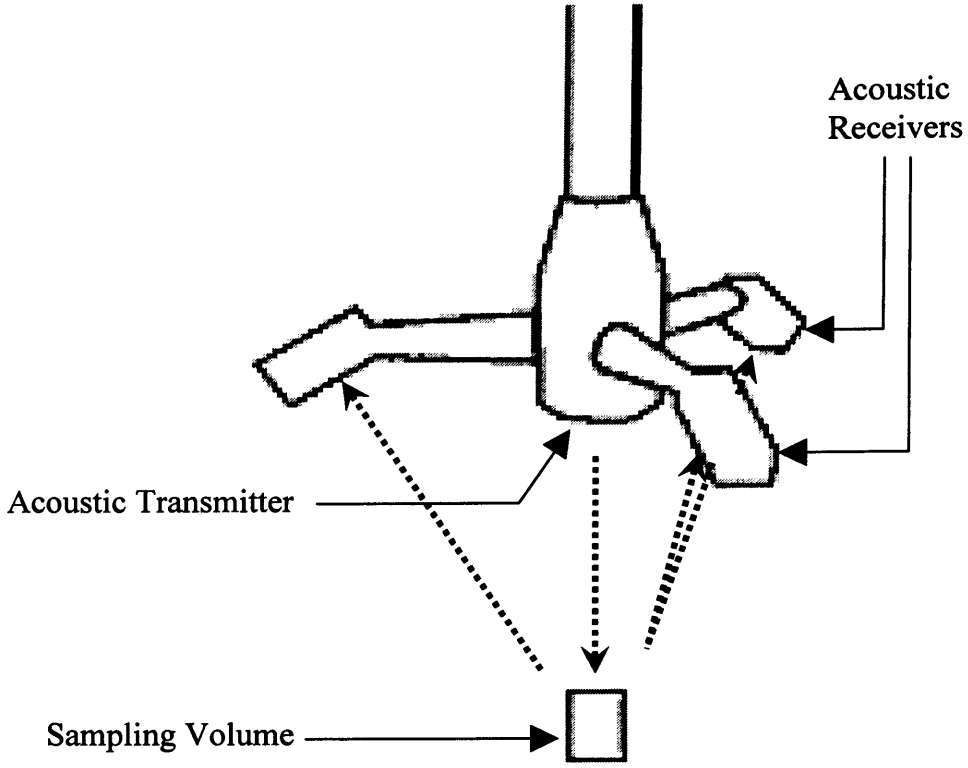

Figure 5-7 Schematic Diagram showing the components of an Acoustic Doppler Velocimeter (ADV) head (taken from Nortek AS, 1997).

The strength of the signal echo is quantified in terms of the signal-to-noise ratio (SNR) (Nortek AS, 1997). According to Nortek AS (1997), to ensure the data is of good quality, this must be equal to or greater than 15 dB. The SNR may fall below this value if there are not enough suspended particles in the water to scatter the acoustic signals, in which case it is necessary to add more seeding material. Seeding material was added to the water supply to maintain the SNR above this level, and compressed air was used to aerate the water storage tank to minimise settling of the seeding material.

Two different ADVs were used: one with an upward-facing sensor, and one with a downward-facing sensor, to measure a vertical profile at 5mm increments over the full flow depth. For flow depths of 0.20m and 0.25m, the overlap between the two instruments was located at the mid-flow depth. For a depth of 0.15m, the lowest elevation at which the upward facing sensor was capable of recording measurements was 85mm above the bed. Hence, the overlap was located 95mm above the bed. An overlap of 10 mm was measured by both upward and downward facing ADV to ensure the measurements were consistent.

5.2.8 Time-averaged and Spatially-averaged Parameters

To account for the effects due to the heterogeneity of the vegetation on the flow, velocity and turbulence parameters were measured at a number of different locations along the flume. Whilst four velocity profiles were measured for each constructed vegetation canopy, only two profiles were measured for the uniform cylinder arrays. This was thought to be appropriate since the arrays were uniform in structure.

At each measurement location along the length of the flume, a full profile was measured extending from approximately 5.0 mm above the bed, up to 5.0 mm below the water surface. For the constructed vegetation canopies, the four profiles were spaced 0.65m apart at distances of 3.50m, 4.15m, 4.80m and 5.45m from the upstream end of the flume. For the uniform cylinder arrays, profiles were measured at distances of 4.15m and 5.45m from the upstream end. Velocity and turbulence statistics were spatially averaged over the four profiles to minimise features of the flow profiles that may be associated with the local flow structure (Section 2.3.1). Nevertheless, it should be stressed that considering the high level of variability in vegetation, four profiles cannot ensure the elimination of bias from the data, and ideally a much greater number of profiles should be used. The focus of this study was to investigate the flow structure, rather than the level of bias in the measurements hence, a compromise was made to investigate a wider range of variables as outlined in Section 5.1.

In Figure 5-8, the time-averaged longitudinal velocities at the four profiles and their spatially-averaged values are presented as an example to illustrate the spatial variability. In Figure 5-9, the temporal-average RMS (root mean square) of the turbulent fluctuations in the longitudinal velocity for the same experiment at the four individual profiles, and the spatially-averaged profile are presented. Fluctuations in both parameters within the canopy and the surface flow layers highlight the importance for recording measurements at multiple locations. Variation between the longitudinal velocities at the four profile locations were small and this can be attributed to the uniform flow conditions implemented. Variation was more significant between the fluctuating components of the longitudinal velocities because these are associated with turbulent structures within the flow which are random in nature.

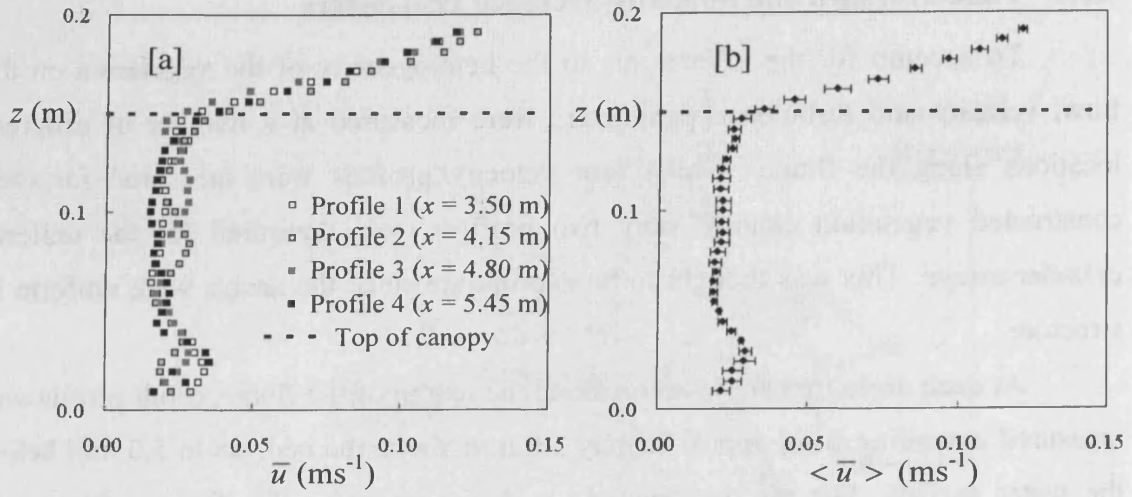

Figure 5-8 a: Single-point time-averaged and; b: double-averaged longitudinal velocities for a 1850 stems m^{-2} canopy, 0.001 bed gradient, and vegetation height of 150 mm where x is the longitudinal distance along the flume. "Bars" indicate the standard deviation of the spatial variation.

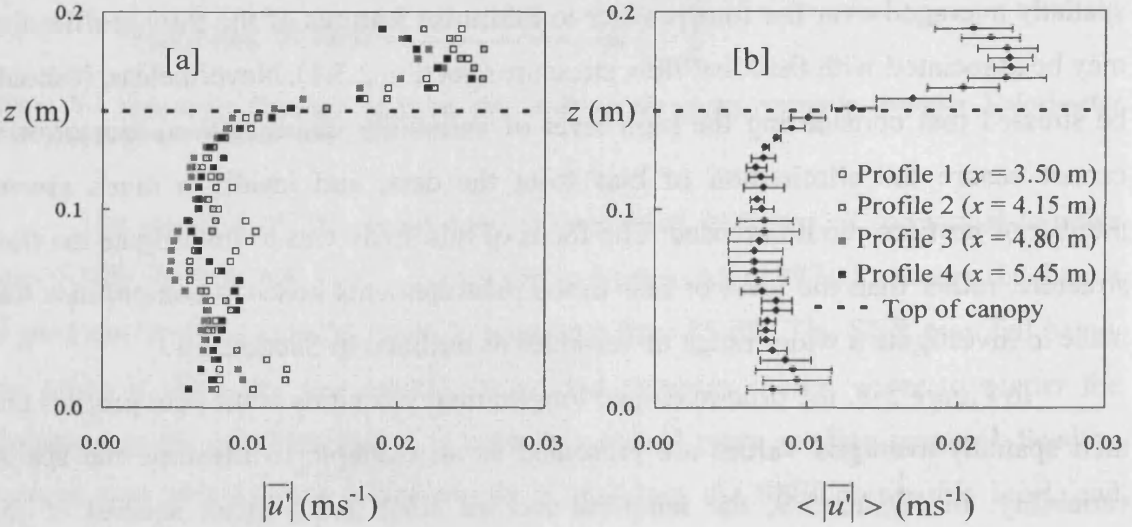

Figure 5-9 a: Single-point time-averaged and; b: double-averaged RMS values of instantaneous fluctuations in longitudinal velocities for a 1850 stems m^{-2} canopy, 0.001 bed gradient, and vegetation height of 150 mm where x is the longitudinal distance along the flume. "Bars" indicate the standard deviation of the spatial variation.

For comparison of the results from experiments conducted for different bed gradients, for different stem densities, and at different submergence levels, velocity and turbulence parameters were normalised by the depth-averaged longitudinal velocity, U, unless specified otherwise. This is defined as follows:

$$U = \frac{1}{D}\int_{z=0}^{z=D} <\overline{u}> \mathrm{d}z \qquad \text{[Equation 5.01]}$$

where z is the elevation and D is the flow depth. An alternative parameter for normalising is the area-mean velocity calculated from the flow rate and the cross-sectional flow areas (see Section 5.2.2). Although both parameters were very similar in value, the depth-averaged velocity based on measurements recorded along the centreline of the flume is less likely to be affected by the flume walls (Section 5.2.1) and is more accurate than the discharge measured by the flow meter (see Section 5.2.2). Despite difference in flow regime between the cropped canopy and surface flow layers, the depth-averaged velocity was used for normalising the entire flow depth to facilitate comparison between flow structures within the two layers.

5.3 Quantification of the Vegetation Canopies

5.3.1 The *Spartina anglica* Species

The most abundant species identified along the saltmarshes monitored during the field study (see Chapter 3), was *Spartina anglica*. This species was in the laboratory investigations conducted to study the effects of saltmarsh vegetation on the velocity and turbulence structures. *Sp. anglica* is described by Fitter *et al.* (1984) as an often abundant, loosely clustered creeping perennial (having a lifecycle lasting longer than two years), commonly planted to stabilise coastal mud. Its stems stout to 130 cm. Its leaves are yellow-green in colour and can be either flat or channelled, and up to 15 mm in width. Its inflorescence (the arrangement of flowers on the axis) is in a cluster up to 35 cm in length and consisting of 3 to 6 spikes with the axis ending in a 50 mm bristle well above the top spike. Spikelets are one-flowered and unawned (non-bristled). The anthers are 8-12 mm and flower between July and November. It commonly occurs along wet coastal mud and according to the optimum range of growth conditions for the species, it is most likely to be found along most English and Welsh coastlines. The plant is illustrated in Figure 5-10.

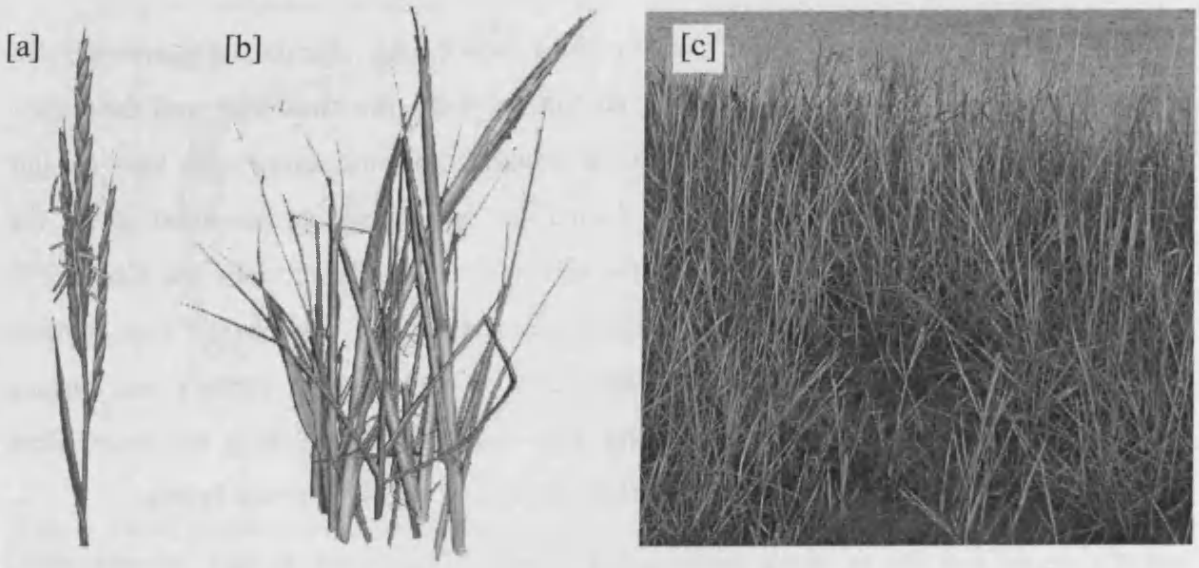

Figure 5-10 *Spartina anglica* [a]: a schematic diagram taken from Keeble Martin (1965) [b]: a sample of stems collected from one of the study sites [c]: a *Spartina anglica* canopy on the Llanelli saltmarsh

5.3.2 Sheltering Effect of the Vegetation

Cross-sectional photographs of vegetation canopies can be used to determine the projected area of a canopy (see Section 4.2). However, the visible projected area of obstruction does not truly represent the amount of vegetation material within the section. Due to the overlapping of the vegetation, part of the canopy remains hidden behind other plant parts. For laboratory constructed canopies, where stem densities are known, the total projected area of obstruction of the canopy can be determined by quantifying the projected area of each stem individually, and calculating the sum of the projected areas of all stems within a section of canopy. A sample of 56 stems of *Spartina anglica* was selected and the stems were quantified individually according to the photographic method (Section 4.2) to determine a vertical profile of projected area for each stem. The stems were then installed into a sheet of plastic honeycombe to create three 100 mm thick canopies with stem densities of 800, 1160 and 1850 stems m^{-2} (56 stems was the number of stems required to create a 100 mm thick section at the highest stem density). The canopy thickness was selected based on the thickness implemented in the photographic method and the stem densities were selected based on the canopies implemented in the laboratory experiments. After the canopies were constructed, the photographic analysis was conducted again to determine the visible projected area for each canopy. The actual projected area of each canopy was

calculated by addition of the projected areas of the stems within each canopy. The average projected area of obstruction per stem is presented in Figure 5-11a.

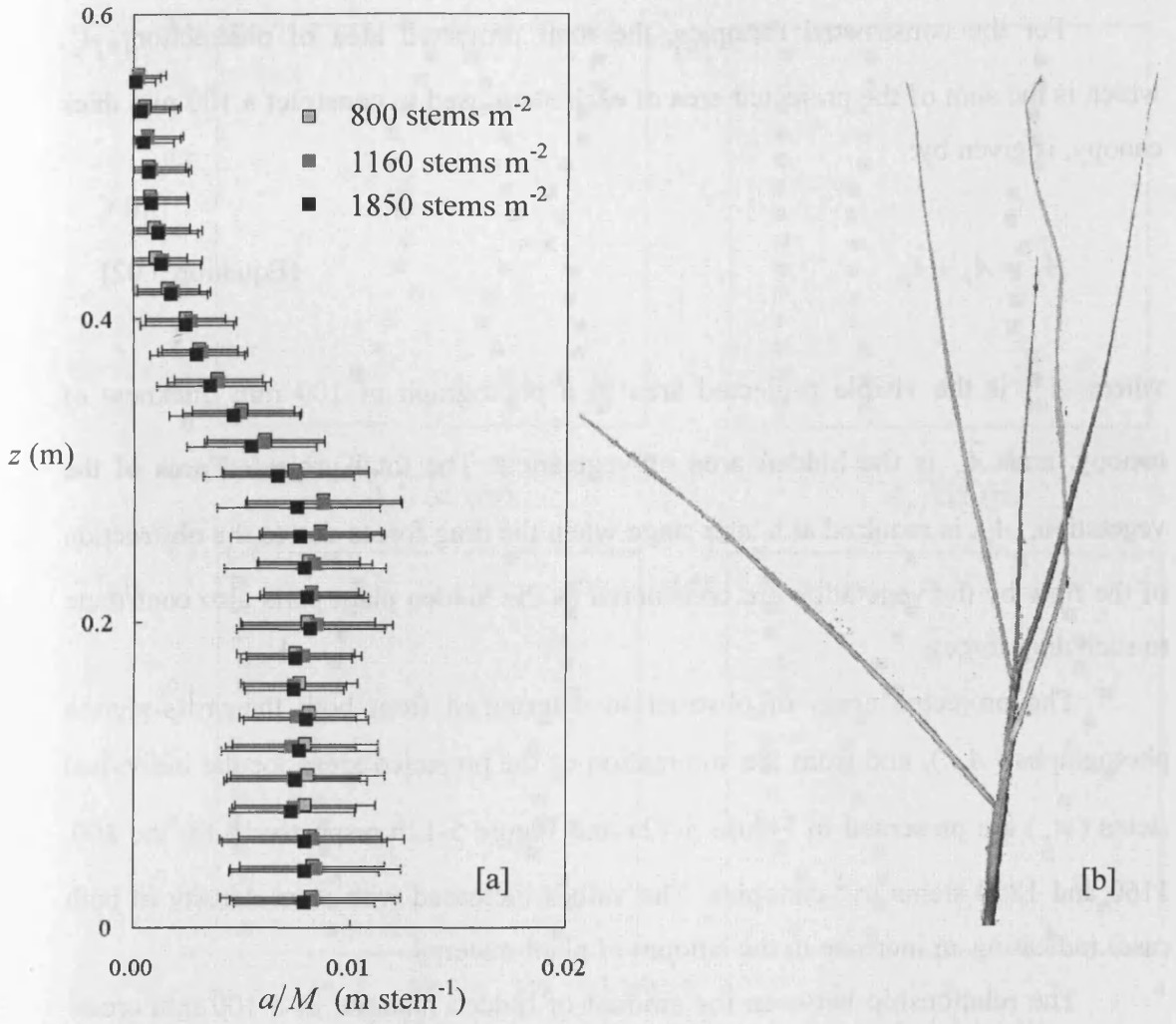

Figure 5-11 [a]: Average projected area of obstruction per stem used to construct three canopies with stem densities of 800, 1160 and 1850 stems m^{-2} to investigate variations in the degree of vegetation overlap. a is the projected area per unit volume, M is the number of stems per unit bed area, and z is the elevation above the bed. [b]: a typical *Spartina anglica* stem.

Experiments were conducted at flow depths of up to 250 mm (Section 5.1). The projected area of obstruction was fairly uniform in magnitude from the bed level up to an elevation of 280 mm above the bed. Values of projected area per stem averaged over this section of the canopy (0 – 280 mm) were for 800 stems m^{-2}: 1.605 m^{-1} $\pm$ 2.0 %, for 1160 stems m^{-2}: 1.597 m^{-1} $\pm$ 3.2 %, and for 1850 stems m^{-2}: 1.546 m^{-1} $\pm$ 1.7 %. Above the 280 mm level, the projected area rapidly decreases with elevation up to 560 mm, which was the height of the tallest plants used in this analysis. A typical *Spartina anglica* stem is shown in Figure 5-11b. Due to the heterogeneity of

the vegetation, there was a large variation in the heights of individual plants. Furthermore, towards the top of the plants, leaves become thinner towards the tip, giving rise to the decrease in projected area observed.

For the constructed canopies, the total projected area of obstruction, A_p, which is the sum of the projected area of each stem used to construct a 100 mm thick canopy, is given by:

$$A_p = A_p' + \hat{A}_p \qquad \text{[Equation 5.02]}$$

where A_p' is the visible projected area in a photograph of 100 mm thickness of canopy, and $\hat{A}_p$ is the hidden area of vegetation. The total projected area of the vegetation, A_p, is required at a later stage when the drag forces due to the obstruction of the flow by the vegetation are considered as the hidden plant parts also contribute to such drag forces.

The projected areas of obstruction determined from both the cross-section photographs (A_p'), and from the summation of the projected areas for the individual stems (A_p) are presented in Figure 5-12a and Figure 5-12b respectively for the 800, 1160 and 1850 stems m^{-2} canopies. The values increased with stem density in both cases indicating an increase in the amount of plant material.

The relationship between the amount of hidden material in a 100 mm cross-section photograph and the amount of visible material was investigated as presented in Figure 5-12d. The amount of hidden material increased with stem density, as shown in Figure 5-12c. For the lower 300 mm of canopy above the bed, the average amount of hidden material as a proportion of the total projected area of plant material was 30.8%, 58.0% and 76.1% for sections with stem densities of 800, 1160 and 1850 stems m^{-2} respectively. Due to the increase in the amount of hidden material with stem density, the total projected areas per unit volume presented in Figure 5-12b, indicated a significantly greater increase in projected area compared to the visible projected area per unit volume profiles presented in Figure 5-12a. The increase from 800 stems m^{-2} to 1160 stems m^{-2}, corresponding to an increase of 45.0% in stem density, and from 800 stems m^{-2} to 1850 stems m^{-2}, corresponding to an increase of 131.3% in

stem density, result in depth-averaged increases of 150.8% and 466.0% respectively in the total projected area per unit volume.

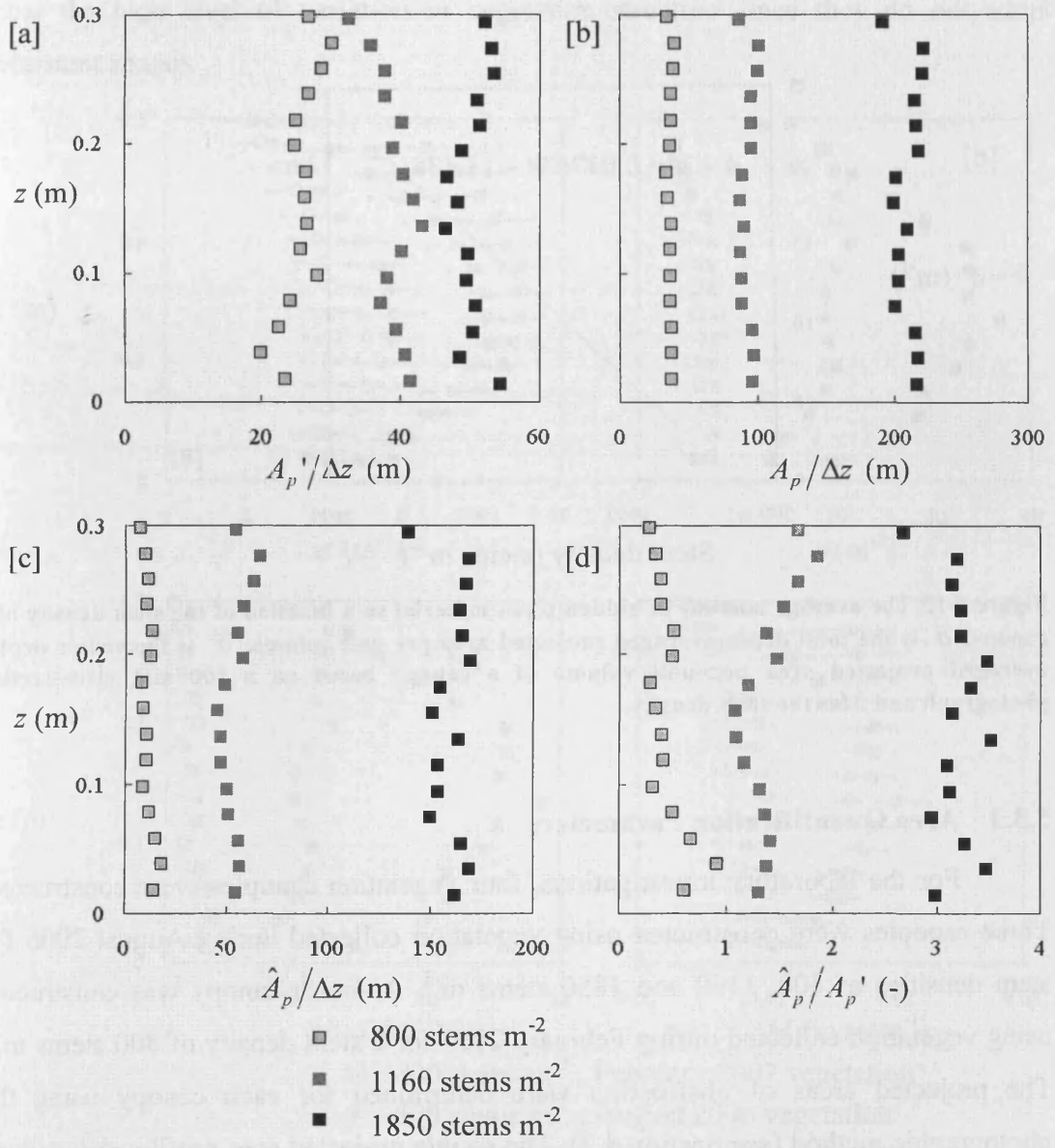

Figure 5-12 [a]: Visible projected area of obstruction, A_p', [b]: total projected area, A_p, and [c]: hidden projected area, $\hat{A}_p$, per unit height of canopy, Δz, for a 100mm thickness of canopy and [d]: the ratio of hidden to visible projected area for 800, 1160 and 1850 stems m^{-2}.

The amount of hidden plant material per unit volume within a canopy section can be estimated from the depth-averaged values of the visible projected area per unit volume, $\bar{a}'$ for a given stem density. This is determined from 100 mm cross-section photographs of *Spartina anglica* canopies depending on the stem density through the linear trend-line presented in Figure 5-13. The method is used throughout the thesis to

evaluate the total projected area of obstruction, A_p, and to calculate the projected area per unit volume, $\overline{a}$, except in the case of the field work where the stem densities were unknown.

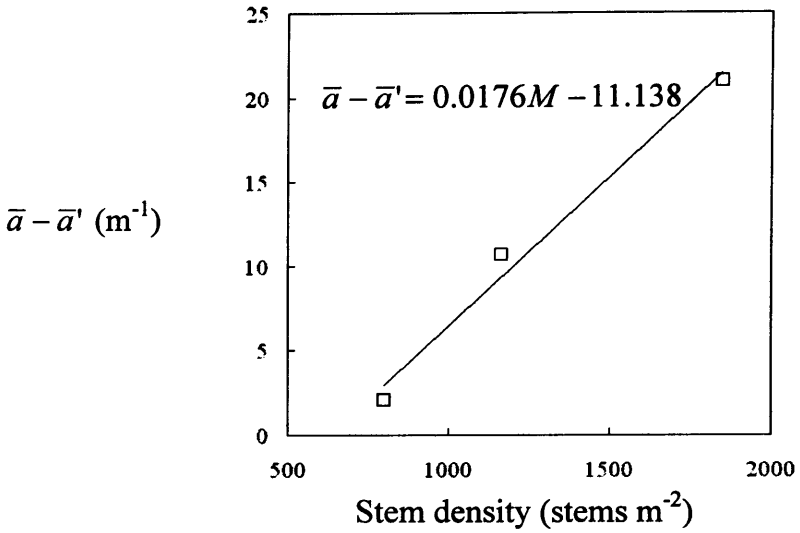

Figure 5-13 The average amount of hidden plant material as a function of the stem density of a canopy. $\overline{a}$ is the total depth-averaged projected area per unit volume, $\overline{a}'$ is the visible depth-averaged projected area per unit volume of a canopy based on a 100 mm cross-section photograph and M is the stem density.

5.3.3 Area Quantification Parameters

For the laboratory investigations, four vegetation canopies were constructed. Three canopies were constructed using vegetation collected during August 2006 for stem densities of 800, 1160 and 1850 stems m^{-2}. A fourth canopy was constructed using vegetation collected during February 2007 for a stem density of 800 stems m^{-2}. The projected areas of obstruction were determined for each canopy using the photographic method (see Section 4.2). The visible projected area profiles determined from the photographs are presented in Figure 5-14a. These were corrected for hidden material according to the methodology discussed in Section 5.3.2. For each stem density, the photographic method was applied to four cross-sections of canopy taken at each of four locations where velocity and turbulence profiles were measured totalling 16 cross-sections for each canopy. The amount of hidden or sheltered material for each stem density is presented in Figure 5-14c, and the projected area of obstruction per unit volume for each canopy following correction is presented in Figure 5-14b. For the region up to 250 mm above the bed, average values were 7.2 m^{-}

^{1}, 11.4 m^{-1} and 16.7 m^{-1} for the 800, 1160 and 1850 stems m^{-2} canopies of August vegetation respectively. The proportion of the total projected area hidden for the three stem densities was equivalent to 30.8%, 58.0% and 76.1% respectively. The profiles show the high level of variation in vegetation structure since they do not adopt consistent shapes.

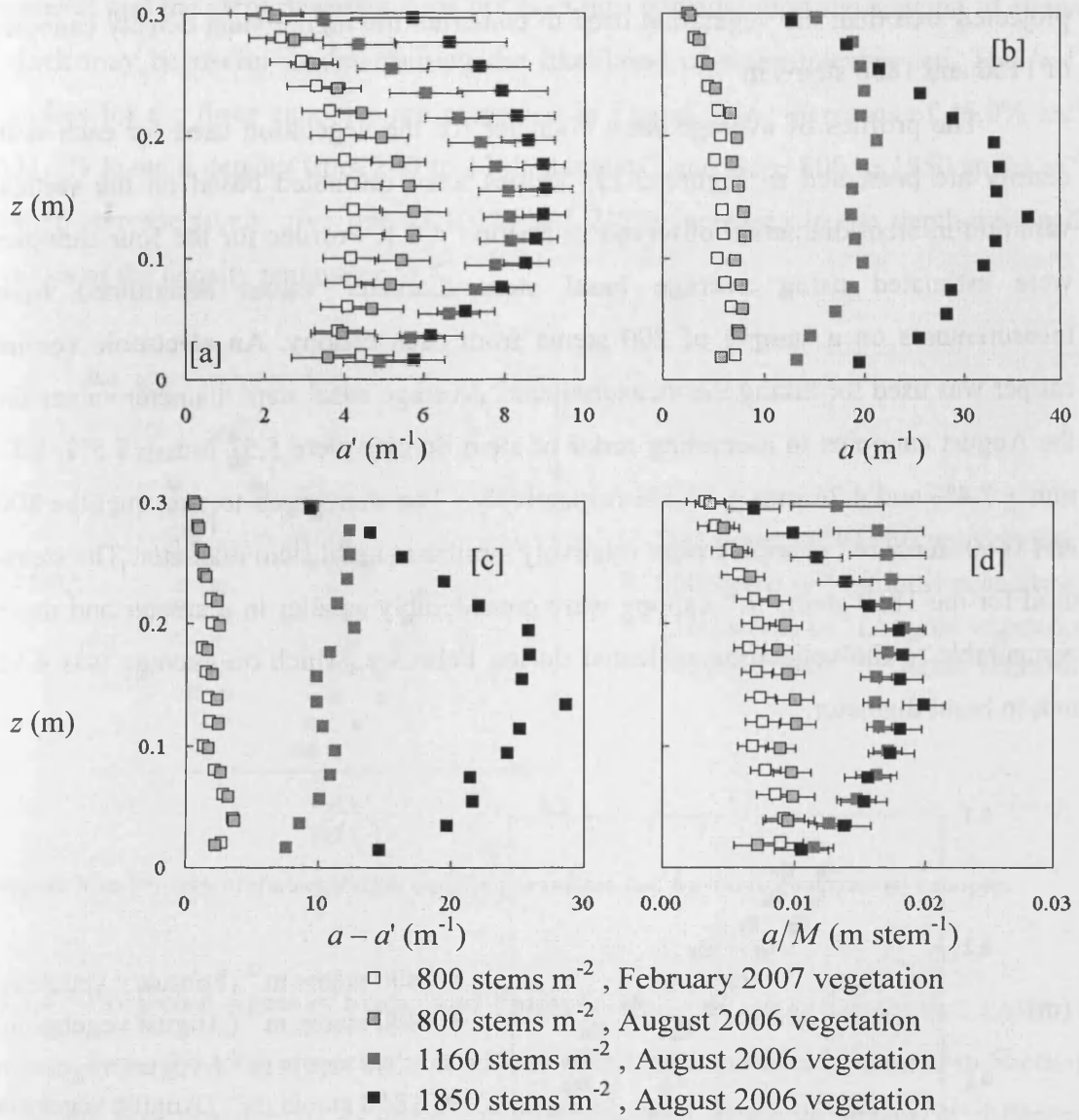

Figure 5-14 [a]: Visible projected area of obstruction per unit volume, *a'*; [b]: total projected area of obstruction per unit volume, *a*; [c]: hidden projected area of obstruction per unit volume; and [d]: projected area of obstruction per stem for 800, 1160 and 1850 stems m^{-2} *Spartina anglica* canopies

Based on the projected area per unit volume profiles and the associated stem density for each profile, the average projected area per stem is presented in Figure 5-14d. For the three August vegetation stem densities examined, in increasing order of magnitude, the average projected areas per unit height per stem were 0.008 m $stem^{-1}$ ±

25.8%, 0.016 m stem^{-1} ± 12.3% and 0.015 m stem^{-1} ± 25.0% respectively (the value for the February vegetation used was 0.007 m stem^{-1} ± 24.8%). The 1160 and 1850 stems m^{-2} canopies have very similar projected area per stem values. The stems used to construct the lowest stem density were comparable in size to the vegetation collected during February 2007. These resulted in a considerably smaller canopy projected area than the vegetation used to construct the higher stem density canopies of 1160 and 1850 stems m^{-2}.

The profiles of average stem diameter for the vegetation used for each stem density are presented in Figure 5-15. Values were estimated based on the vertical variation in stem diameters observed in Section 4.4.1. Profiles for the four canopies were estimated using average basal stem diameter values determined from measurements on a sample of 200 stems from each canopy. An electronic vernier caliper was used for taking the measurements. Average basal stem diameter values for the August canopies in ascending order of stem density were 5.51 mm ± 8.5%, 5.72 mm ± 7.4% and 4.26 mm ± 11.3% respectively. The stems used to construct the 800 and 1160 stems m^{-2} canopies were relatively similar in basal stem diameter. The stems used for the 1850 stems m^{-2} canopy were considerably smaller in diameter and more comparable to the vegetation collected during February, which on average was 4.12 mm in basal diameter.

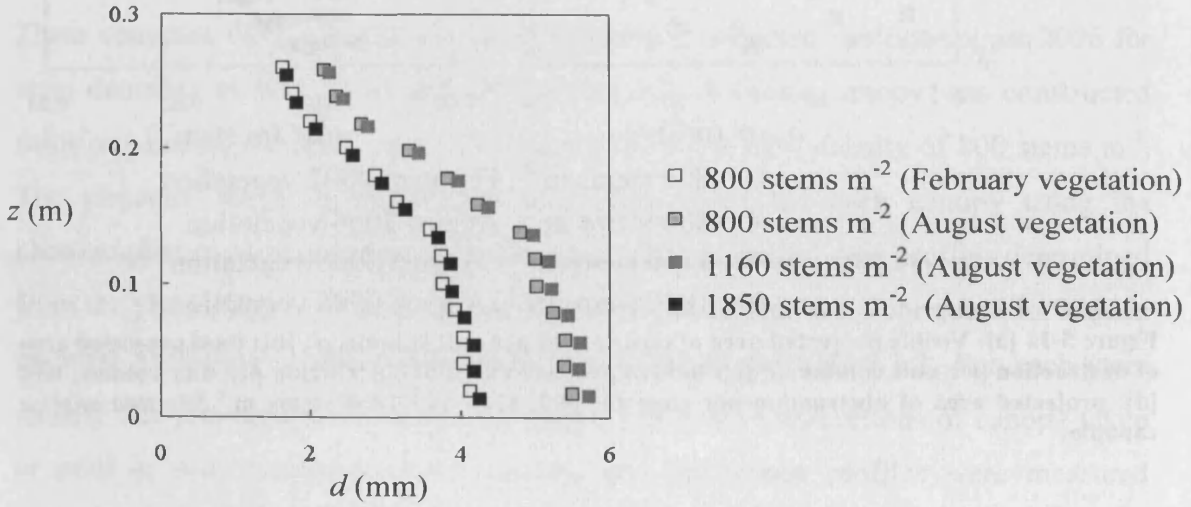

Figure 5-15 Stem diameter profiles for four constructed canopies

Nepf (1999) defines vegetation density '*ad*' as the product of the projected area of obstruction per unit volume and the average stem diameter. One feature of this

parameter is that it is dimensionless. Furthermore, it accounts for both the amount of material causing an obstruction to the flow, and the stem diameter. In the context of vegetated flows, the stem diameter is the turbulent length scale since large-scale turbulent structures are broken down and smaller vortex structures form within the wake of cylinders or stems. Parameterising the density in terms of the volume of material and the stem diameter does not take into consideration the spacing of stems which may be useful in determining the likelihood of wake-interference. The '*ad*' profiles for the three canopies are presented in Figure 5-16. Increases of 45.0% and 131.3% in stem density from 800 to 1160 stems m^{-2} and from 800 to 1850 stems m^{-2} canopies respectively give rise to 161% and 217% increases in the depth-averaged values of the density parameter '*ad*'.

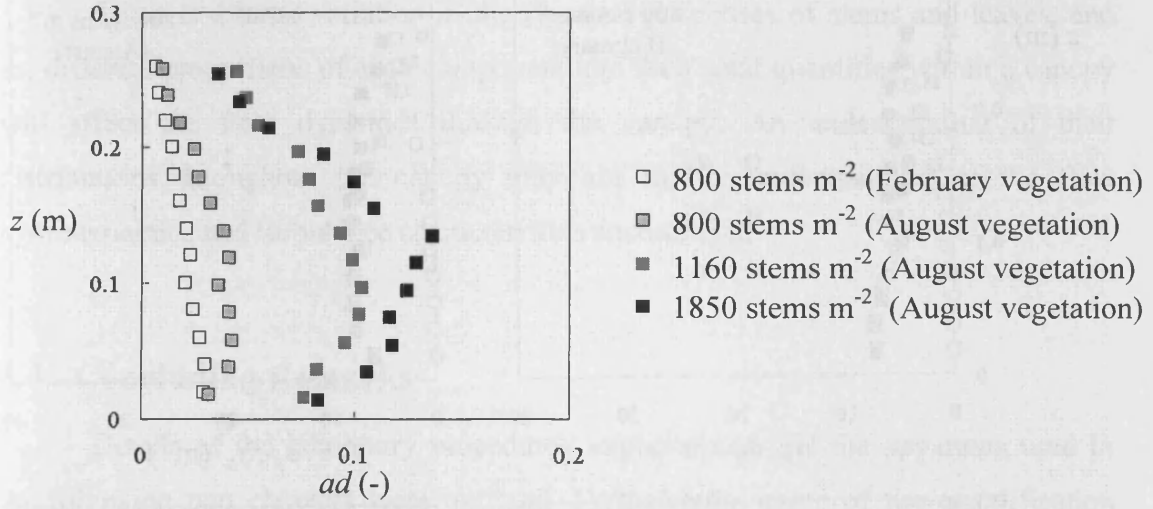

Figure 5-16 Profiles of the vegetation density parameter, *ad*, for three constructed canopies

5.3.4 Projected Areas of Stems and Foliage

From the total projected area and stem diameter profiles presented in Section 5.3.3, it was possible to estimate the proportion of stems to leaves at different elevations. It was assumed that the projected area near the bed was comprised entirely of vegetation stems. The projected area due to stems was assumed to decrease with elevation in accordance with the trends observed for the stem diameters in Figure 5-15. If the projected area of obstruction due to the plant stems is subtracted from the total projected area of obstruction for each canopy, then the projected area of obstruction due to the leaves in the canopy can be determined. The projected area of

obstruction due to the stems and the leaves for the four constructed canopies are presented in Figure 5-17.

For the three August vegetation canopies, there was some variation in the amount of foliage as a proportion of the total projected area as presented in Figure 5-18, which is due to the natural variability of the vegetation. For the February vegetation, the foliage forms a considerably greater proportion of the canopy, particularly at higher elevations, and this is in part due to the significantly smaller diameters of the stems (Section 5.3.3). In the upper part of the canopy with the example of the February vegetation, 50% or more of the canopy is composed of foliage.

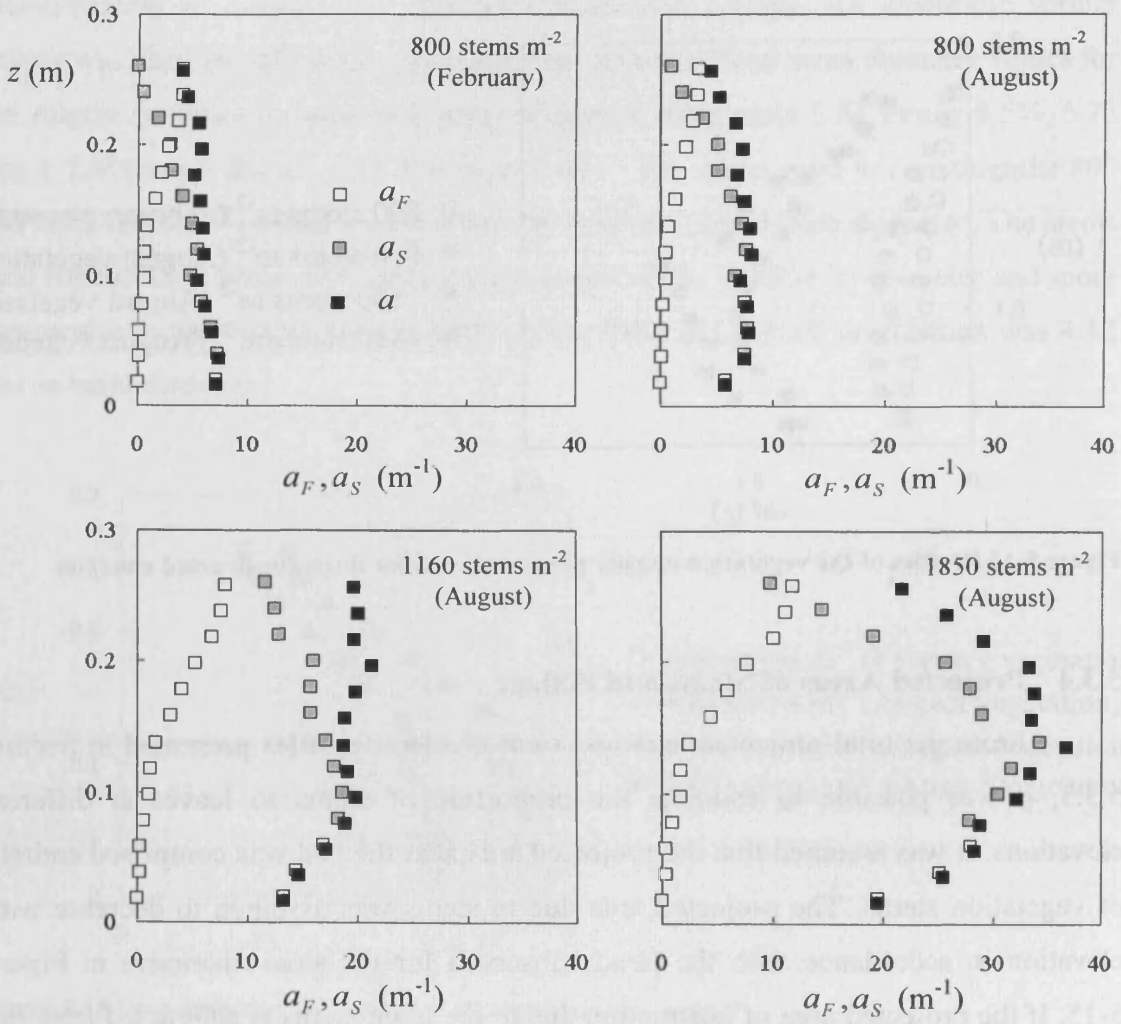

Figure 5-17 Projected area of obstruction per unit volume due to stems (a_S) and leaves (a_F) for three constructed canopies. a is the total area per unit volume.

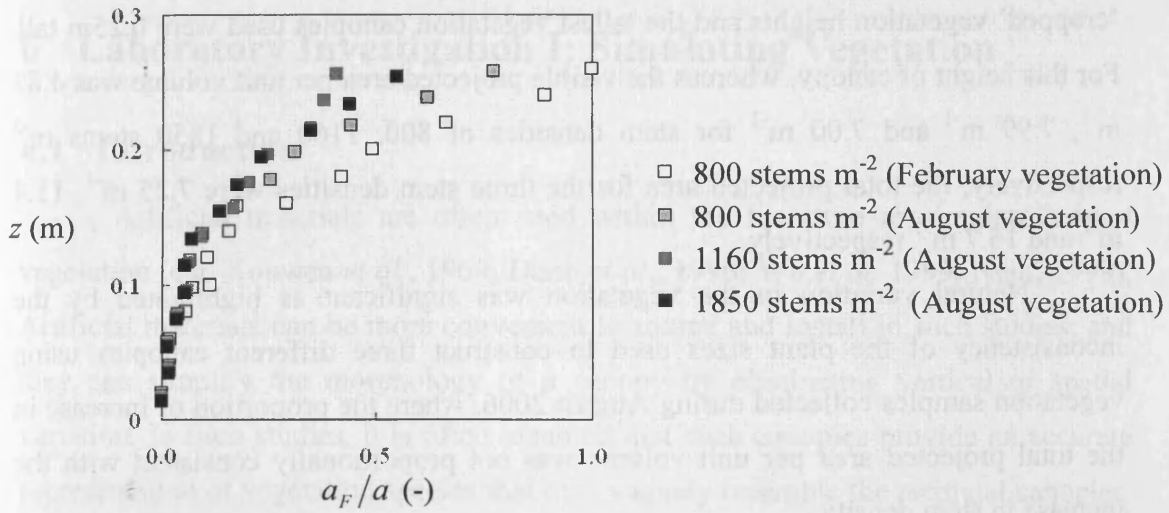

Figure 5-18 The projected area of the foliage, a_F, as a proportion of the total projected area, a, for 800, 1160 and 1850 stems m^{-2} canopies

There is a large variation in the physical properties of stems and leaves, and so, different proportions of each component and their total quantities within a canopy will affect the flow dynamics through the canopy. An understanding of their distributions throughout the canopy may aid in the understanding of the flow hydrodynamics and turbulence characteristics encountered.

5.4 Concluding Remarks

Details of the laboratory procedures implemented and the apparatus used in the following two chapters were outlined. Furthermore, some of the quantification methods presented in Chapter 4 for field canopies were applied to the constructed vegetation canopies used in the laboratory experiments.

One of the advantages of working in a laboratory environment is that the worker has control over numerous factors which in a natural environment would be difficult, if not impossible to control. For constructed vegetation canopies in the environment, stem densities can be counted easily, and the total projected area of the canopy can also be determined by quantifying each stem within a sample section of the canopy individually. It is therefore possible to correct profiles of 'visible' projected area for any 'hidden' material not visible in the photographs, and thus produce profiles of the 'total' projected area of obstruction. This procedure was applied to the *Spartina anglica* canopies constructed for the purpose of the laboratory investigation. The experiments were conducted for a range of flow depths and

'cropped' vegetation heights and the tallest vegetation canopies used were 0.25m tall. For this height of canopy, whereas the visible projected area per unit volume was 4.83 m^{-1}, 7.99 m^{-1} and 7.00 m^{-1} for stem densities of 800, 1160 and 1850 stems m^{-2} respectively, the total projected area for the three stem densities were 7.25 m^{-1}, 11.4 m^{-1} and 16.7 m^{-1} respectively.

Natural variation in the vegetation was significant as highlighted by the inconsistency of the plant sizes used to construct three different canopies using vegetation samples collected during August 2006, where the proportion of increase in the total projected area per unit volume was not proportionally consistent with the increase in stem density.

6 Laboratory Investigation I: Simulating Vegetation

6.1 Introduction

Artificial materials are often used within the literature to simulate natural vegetation (e.g. Kouwen *et al.*, 1969; Dunn *et al.*, 1996; Wu *et al.* 1999; Nepf, 1999). Artificial materials can be more convenient to source and install in such studies, and they can simplify the morphology of a canopy by eliminating vertical or spatial variation. In such studies, it is often assumed that such canopies provide an accurate representation of vegetation species that may vaguely resemble the artificial canopies. For instance, one might assume that a rigid grass-type vegetation, such as *Spartina anglica*, which is the subject of this study, may be simulated using arrays of uniform cylinders due to its cylindrical and upright stemmed nature.

The velocity and turbulence structures through submerged *Spartina anglica* canopies are compared to uniform cylinder arrays to evaluate the suitability of the cylinder model as a means of simulating the natural plants. Contrary to the assumptions mentioned above, *Spartina anglica* shows considerable vertical and spatial variation in projected area as identified during the field study (see Section 4.2.3). The comparison is conducted using non-dormant vegetation collected during August 2006.

One of the key differences in morphology between vegetation canopies and uniform cylinder arrays is the presence of plant 'foliage' in the vegetation canopies. The influence of foliage on velocity and turbulence structures is to be investigated. Furthermore, real vegetation displays a significant level of variation of vegetation material due to its heterogeneous nature. The amount of vegetation material within the canopy is usually higher in the foliage region compared to the stem region. Such a distribution of material will likely affect the velocity structure throughout the canopy. For submerged conditions, the higher velocities within the surface flow layer are likely to affect the flow in the canopy region differently for the vegetation and the uniform cylinders. Distinguishing between the influence of the mixing layer (Section 2.5.4), and the influence of the variability of the vegetation on the resulting velocity profiles may be difficult. For a uniform cylinder array, variability in the vegetation is absent enabling a more focused examination of the shear layer flow. Details of the

experiments conducted for this comparison using uniform cylinder arrays and constructed vegetation canopies are presented in Table 6-1 and Table 6-2 respectively.

Table 6-1 Details of experiments conducted using uniform cylinder arrays

Test No.	Stem Density [stems m^{-2}]	Bed Gradient S_0	Vegetation Height T [m]	Reynolds Number Re_d	Flow Depth D [m]	Submergence Level $H = D / T$
S-1000	800	1/1000	0.15	430	0.20	1.33
M-1000	1160	1/1000	0.15	330	0.20	1.33
D-1000	1850	1/1000	0.15	230	0.20	1.33
S-0300	800	1/300	0.15	840	0.20	1.33
M-0300	1160	1/300	0.15	560	0.20	1.33

Table 6-2 Details of experiments conducted using *Sp. anglica* plants during Aug 2006

Test No.	Stem Density [Stems m^{-2}]	Bed Gradient S_0 [-]	Vegetation Height T [m]	Flow Depth D [m]	Reynolds Number Re_d	Submergence $H = D / T$	Flow Rate Q [ls^{-1}]
S-M11	800	1/300	0.15	0.20	450	1.33	6.8
S-M21	800	1/1000	0.15	0.20	250	1.33	3.9
M-M11	1160	1/300	0.15	0.20	340	1.33	5.3
M-M21	1160	1/1000	0.15	0.20	210	1.33	3.1
D-M11	1850	1/300	0.15	0.20	240	1.33	4.6
D-M21	1850	1/1000	0.15	0.20	110	1.33	2.2

6.2 A Comparison between Vegetation and Cylinder Morphology

The structure of the constructed vegetation canopies was highly variable over the height of the canopy (Figure 6-1a) compared to the cylinder arrays which had a very uniform structure over the height of the cylinders (Figure 6-1b).

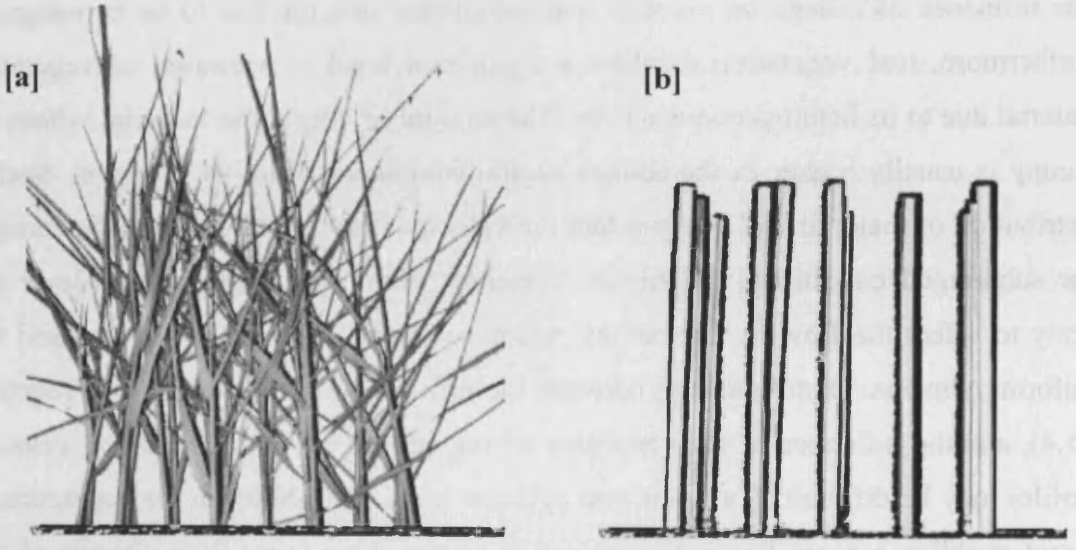

Figure 6-1 Typical examples of constructed canopies consisting of [a]: *Spartina anglica* and [b]: uniform cylinders.

Many of the uniform cylinder model experiments documented (e.g. Nepf *et al.*, 1997a; Nepf *et al.*, 1997b; Fairbanks, 1998; Nepf, 1999 etc.) were conducted for emergent conditions. In these studies, the time-averaged velocity structure was relatively constant over most of the flow depth, although longitudinal velocities tend to decrease towards the bed due to the boundary.

Figure 6-2 and Figure 6-3 present the depth-averaged projected area characteristics for the canopies and show the contrasting nature of the constructed vegetation canopies and the uniform cylinder arrays. The canopies constructed of real plant material displayed an increase in projected area in the foliage region in the upper canopy for the August samples. This was not observed for the February sample where the foliage was considerably smaller in surface area. Despite the similarity in stem densities and basal diameters, the uniform cylinder arrays were considerably lower in projected area. This was due to the absence of plant foliage despite the mean stem diameters being slightly smaller (5.51 mm, 5.72 mm and 4.26 mm for stem densities of 800, 1160 and 1850 stems m^{-2}) compared to the 6.00 mm diameter cylinders.

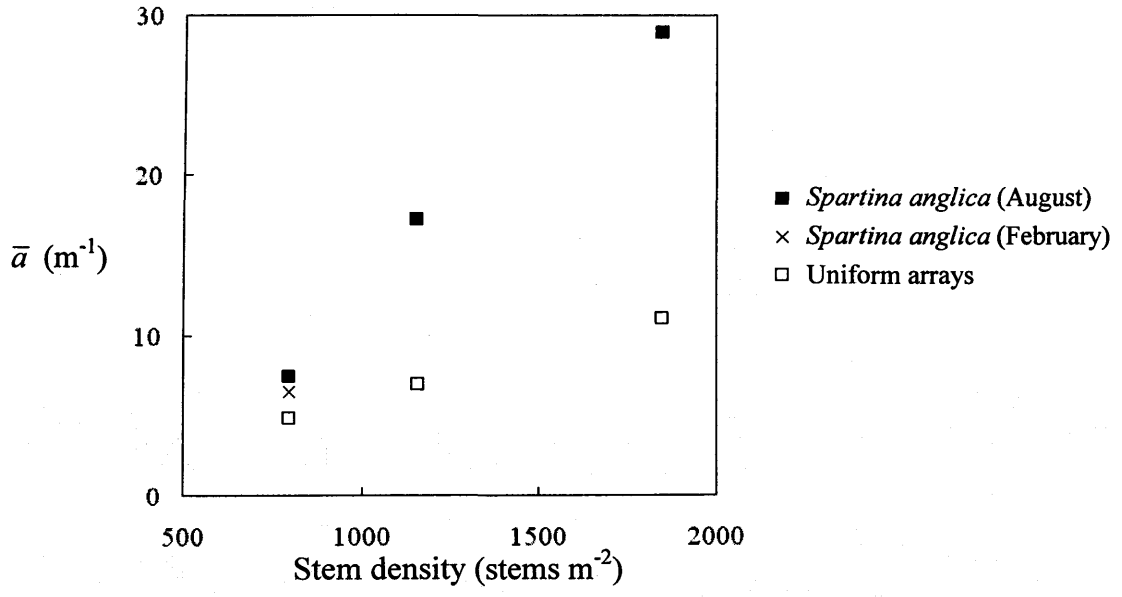

Figure 6-2 Variation of the depth-averaged projected area per unit volume, $\bar{a}$, with stem density for *Spartina anglica* canopies, and uniform cylinder arrays.

For the higher stem densities (1160 and 1850 stems m^{-2}), the constructed vegetation canopy had at least twice the projected area per unit volume over most of the canopy height. Even compared to the February constructed vegetation canopy and the lowest stem density of 800 stems m^{-2}, the projected area of the uniform cylinder

array was also significantly lower. The difference between the projected areas of the uniform cylinders and the August vegetation canopies was even more pronounced with increasing stem density. This can be attributed to the increase in the amount of foliage in the vegetation canopies. This highlights the difference in canopy structure, and suggests that the uniform cylinder model may not always represent vegetation canopies accurately as assumed by numerous authors (e.g. Dunn *et al.*, 1996; Nepf *et al.*, 1997a; Nepf *et al.*, 1997b; Fairbanks, 1998; Nepf, 1999 etc.).

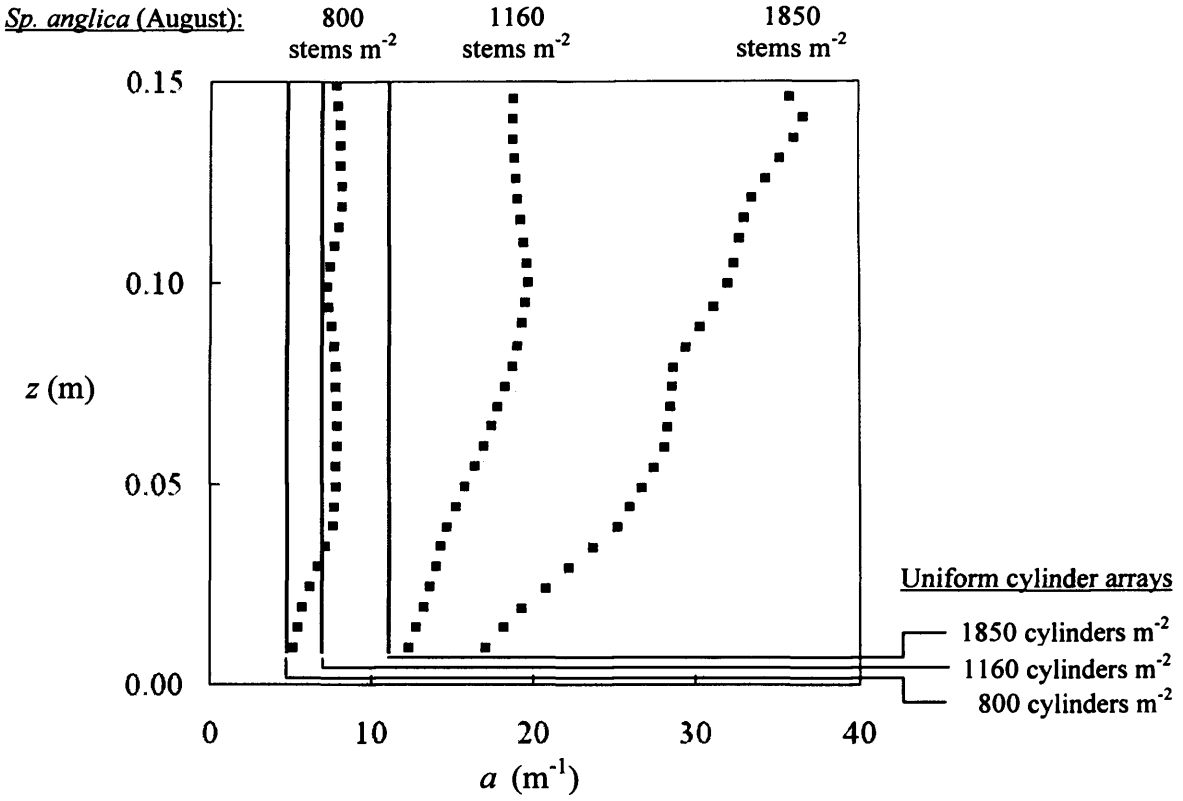

Figure 6-3 Projected area per unit volume profiles for the constructed vegetation canopies (■) and uniform cylinder arrays (solid lines). In increasing order of magnitude, the August canopies and the uniform cylinder arrays correspond to stem densities of 800, 1160 and 1850 stems m^{-2}.

6.3 One-Dimensional Measurements

6.3.1 Stage-Discharge Relationships

The experiments were conducted for uniform flow conditions (see Section 5.2.5). Stage-discharge curves for the uniform cylinder arrays and constructed canopies listed in Section 6.1 are presented in Figure 6-4. The plots show the relatively lower hydraulic resistance of a uniform cylinder array compared to a

constructed vegetation canopy for an equal stem density and bed gradient. The lower hydraulic resistance of the cylinder arrays can be attributed to a lesser degree of obstruction (Figure 6-2). For a flow depth of 0.20 m (equivalent to a submergence level, H, of 1.33), the discharge for the uniform cylinder arrays was between 27% and 42% higher than for the constructed vegetation canopies for an equal stem density and bed gradient. The percentage increase in discharge increased with increasing stem density and with bed gradient.

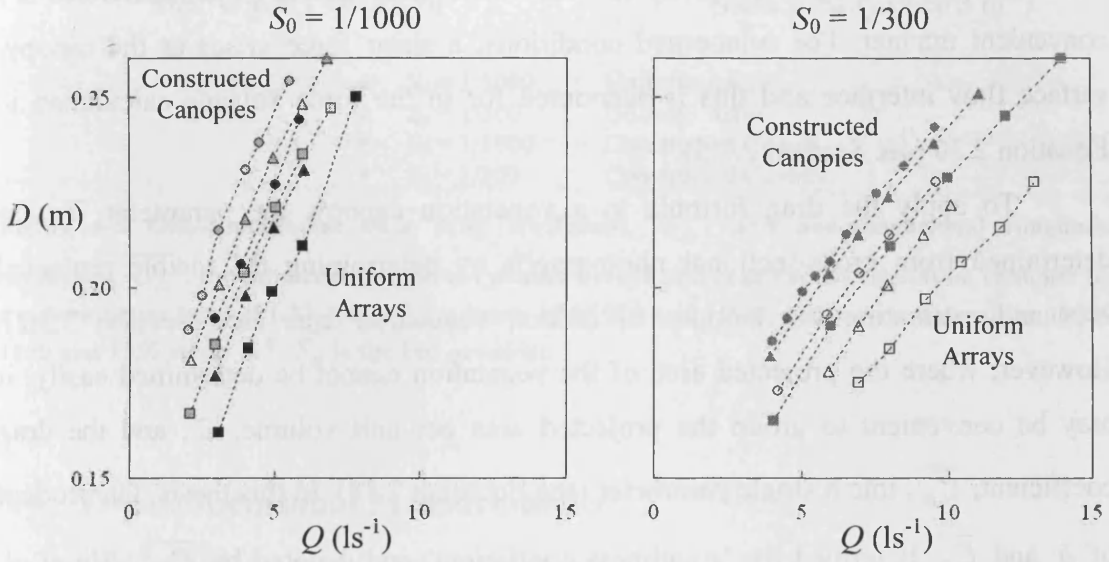

	Stem Density (stems m^{-2})	S_0	Hydraulic Radius Reynolds number	Stem Diameter Reynolds number	Canopy
■	800	1/1000	$5600 < Re_R < 6200$	$400 < Re_d < 440$	Uniform Array
▲	1160	1/1000	$3300 < Re_R < 4400$	$230 < Re_d < 310$	Uniform Array
●	1850	1/1000	$2900 < Re_R < 3300$	$200 < Re_d < 230$	Uniform Array
□	800	1/300	$11000 < Re_R < 12300$	$770 < Re_d < 860$	Uniform Array
△	1160	1/300	$7000 < Re_R < 7900$	$490 < Re_d < 550$	Uniform Array
○	1850	1/300	$5700 < Re_R < 6200$	$400 < Re_d < 440$	Uniform Array
⊡	800	1/1000	$3700 < Re_R < 6100$	$210 < Re_d < 320$	Constructed Canopy
⊿	1160	1/1000	$2400 < Re_R < 4100$	$140 < Re_d < 280$	Constructed Canopy
⊙	1850	1/1000	$1600 < Re_R < 4000$	$100 < Re_d < 150$	Constructed Canopy
■	800	1/300	$6700 < Re_R < 11300$	$380 < Re_d < 580$	Constructed Canopy
▲	1160	1/300	$4200 < Re_R < 7200$	$240 < Re_d < 480$	Constructed Canopy
●	1850	1/300	$3400 < Re_R < 6600$	$200 < Re_d < 320$	Constructed Canopy

Figure 6-4 Stage-Discharge relationships for the submerged 150 mm uniform cylinder arrays and constructed vegetation canopies for stem densities of 800, 1160 and 1850 stems m^{-2} and bed gradients of 1/300 and 1/1000. D is the flow depth, Q is the flow rate according to the flowmeter, and S_0 is the bed gradient. Re_R is the hydraulic radius Reynolds number, Re_d is the stem diameter Reynolds number, and Reynolds number ranges are given for the canopy region.

6.3.2 One-Dimensional Bulk Drag Coefficient

Previously in Section 2.2.6, the average drag force per unit volume produced by vegetation over the depth of the canopy, F_D', was characterised by Equation 2.18. In studies where drag coefficients were calculated for uniform cylinder arrays, the parameter $\overline{a}$ was used which was equivalent to the projected area per unit volume occupied by the cylinders, a measure of the array density (e.g. staggered arrays by Dunn *et al*, 1996; or randomly arranged arrays by Nepf, 1999 etc.). The definition allows the projected area of a group of 'uniform' obstructions to be parameterised in a convenient manner. For submerged conditions, a shear force arises at the canopy-surface flow interface and this is accounted for in the force balance calculation in Equation 2.30 (see Section 2.3.5).

To apply the drag formula to a vegetation canopy, the parameter $\overline{a}$ was determined from cross-sectional photographs by determining the visible projected area and estimating the amount of hidden vegetation area (see Section 5.3.2). However, where the projected area of the vegetation cannot be determined easily, it may be convenient to group the projected area per unit volume, $\overline{a}$, and the drag coefficient, $\overline{C_D}$, into a single parameter (see Equation 2.18). In this thesis, the product of $\overline{a}$ and $\overline{C_D}$ is termed the 'roughness coefficient' and denoted by $\overline{C_D}'$. Wu *et al.* (1999) claim that the one-dimensional roughness coefficient varies with vegetation type. Furthermore, for a given vegetation type, $\overline{C_D}'$ also varies with vegetation density.

One-dimensional bulk drag coefficients, presented in Figure 6-5a, showed little variation with values ranging between 0.9 and 1.3 for the uniform arrays, and between 1.0 and 1.7 for the constructed canopies. Values reflect the natural variability in the case of the constructed canopies, as well as variation in turbulence structure. One-dimensional roughness coefficients presented in Figure 6-5b increased consistently with stem density for both the constructed canopies and the uniform arrays reflecting an increase of total obstruction to the flow despite the effects of the turbulence structure at the stem scale.

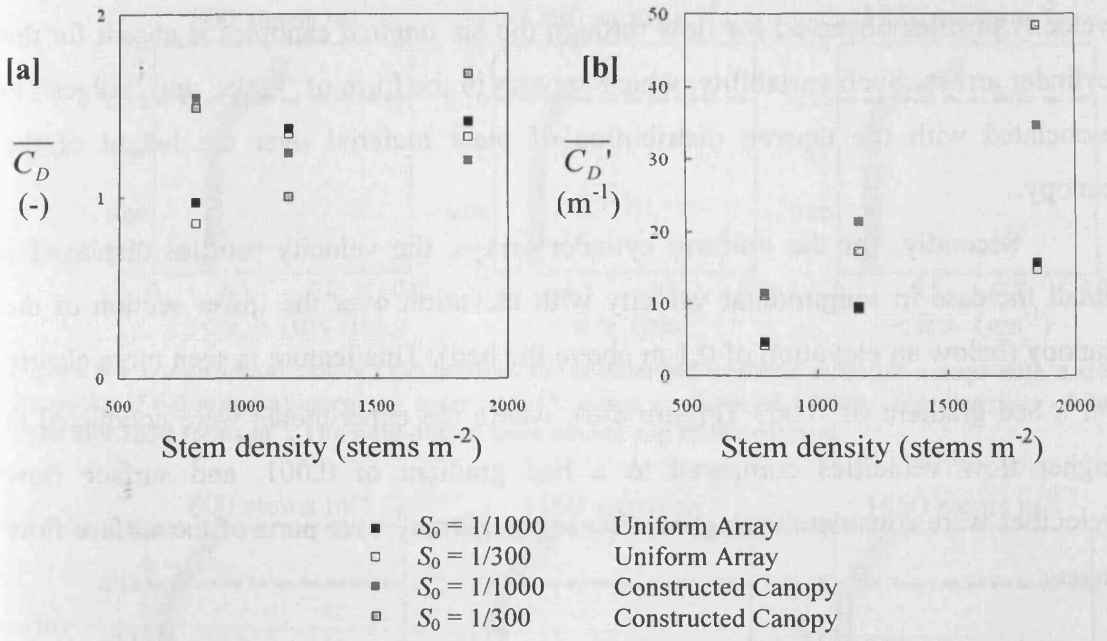

Figure 6-5 One-dimensional bulk drag coefficient, $\overline{C_D}$, and one-dimensional roughness coefficient, $\overline{C_D}'$, for submerged uniform cylinder arrays and constructed vegetation canopies for a submergence level of 1.33, for bed gradients of 1/1000 and 1/300, and for stem densities of 800, 1160 and 1850 stems m^{-2}. S_0 is the bed gradient.

6.4 Two-Dimensional Measurements

6.4.1 Double-Averaged Parameters

Velocity and turbulence parameters are calculated based on measurements averaged spatially along the flume length as well as temporally over the three minute period of ADV operation. Four profiles were monitored for the constructed vegetation canopies and two profiles for the uniform cylinder arrays (see Section 5.2.7 for more detail).

6.4.2 Longitudinal Velocity Profiles

Longitudinal velocity profiles are presented for the uniform cylinder arrays in Figure 6-6 and Figure 6-8 (for bed gradients of 0.003 and 0.001 respectively) and for the constructed vegetation canopies in Figure 6-7 and Figure 6-9. submerged *Spartina anglica* canopies in (Figures 5.24 and 5.25). The profiles appear to have two key features that differentiate the velocity structure through the cylinders from that through the constructed vegetation canopy. Firstly, the vertical variability in the

velocity profiles observed for flow through the *Sp. anglica* canopies is absent for the cylinder arrays. Such variability, which appears in the form of 'kinks' and 'bulges', is associated with the uneven distribution of plant material over the height of the canopy.

Secondly, for the uniform cylinder arrays, the velocity profiles displayed a small increase in longitudinal velocity with elevation over the lower section of the canopy (below an elevation of 0.1 m above the bed). This feature is seen more clearly for a bed gradient of $0.00\dot{3}$ (Figure 6-6), where the experiments were conducted at higher flow velocities compared to a bed gradient of 0.001, and surface flow velocities were considerably higher, exceeding 0.2 ms^{-1} over parts of the surface flow layers.

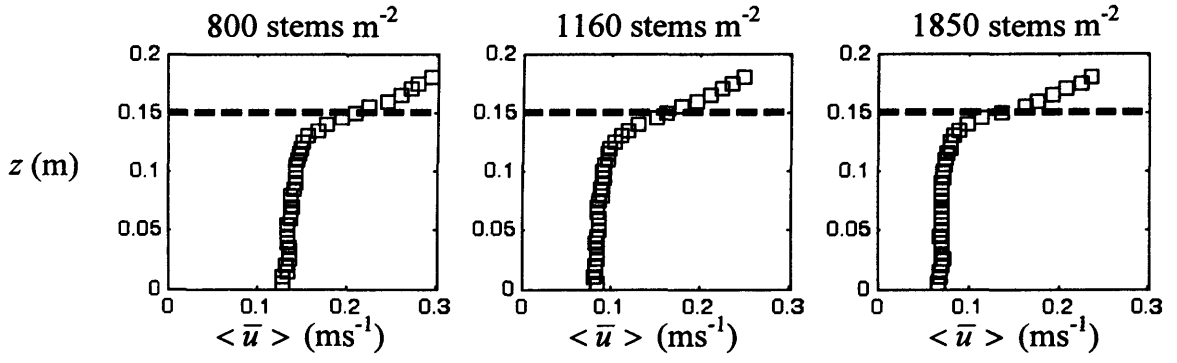

Figure 6-6 Longitudinal velocity (u) profiles for submerged uniform cylinder arrays with a stem diameter of 6.0 mm, submergence level of 1.33, a bed gradient of 1/300, stem densities of 800, 1160 and 1850 stems m^{-2}. The bold dotted lines denote top of the canopy.

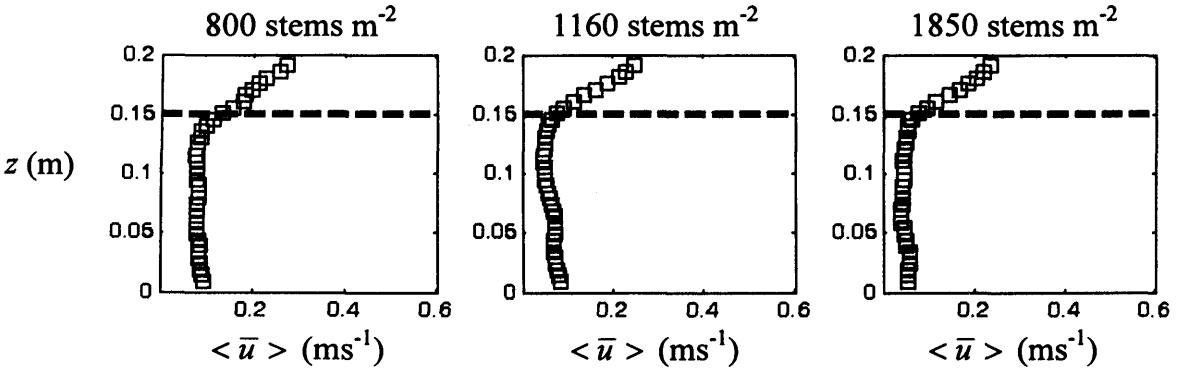

Figure 6-7 Longitudinal velocity (u) profiles for submerged constructed vegetation canopies for a submergence level of 1.33, a bed gradient of 1/300, stem densities of 800, 1160 and 1850 stems m^{-2}. The bold dotted lines denote top of the canopy.

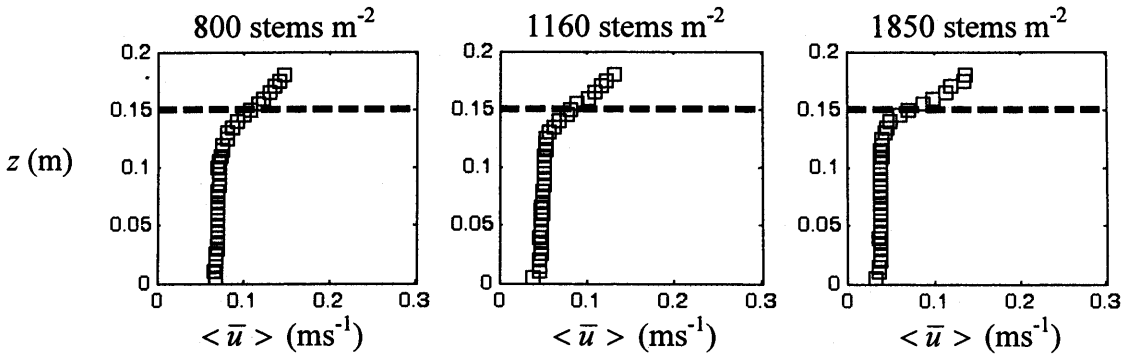

Figure 6-8 Longitudinal velocity (u) profiles for submerged uniform cylinder arrays with a stem diameter of 6.0 mm, submergence level of 1.33, a bed gradient of 1/1000, stem densities of 800, 1160 and 1850 stems m^{-2}. The bold dotted lines denote top of the canopy.

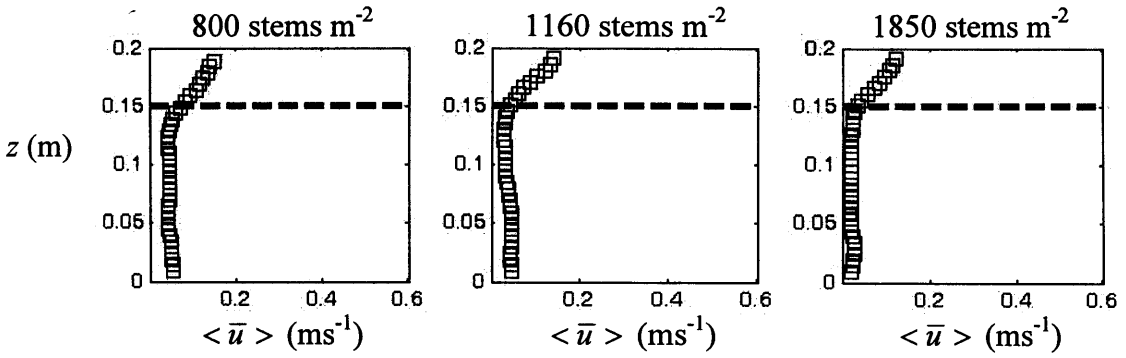

Figure 6-9 Longitudinal velocity (u) profiles for submerged constructed vegetation canopies for a submergence level of 1.33, a bed gradient of 1/1000, stem densities of 800, 1160 and 1850 stems m^{-2}. The bold dotted lines denote top of the canopy.

6.4.3 Normalised Longitudinal Velocity Profiles

The normalised longitudinal velocity profiles, for both uniform cylinder arrays and constructed vegetation canopies, are presented in Figure 6-10 and Figure 6-11 for bed gradients of $0.00\dot{3}$ and 0.001 respectively. The normalised velocity profiles are fairly uniform for the uniform cylinder arrays until the canopy-surface flow layer interface is approached. This is in contrast to the constructed vegetation canopy where the velocity profiles reflect the heterogeneous nature of real vegetation.

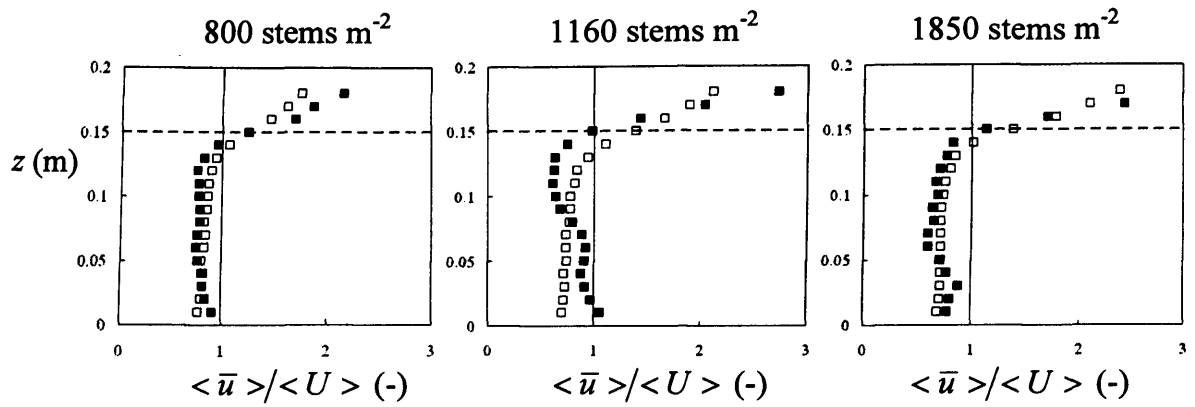

Figure 6-10 Normalised longitudinal velocity (u) profiles for submerged uniform cylinder arrays with a stem diameter of 6.0 mm (□) and constructed vegetation canopies (■), for a submergence level of 1.33, a bed gradient of 1/300, and stem densities of 800, 1160 and 1850 stems m^{-2}. U is the depth-averaged longitudinal velocity for the flow depth. The bold dotted lines denote the top of the canopy, and the faint vertical lines denote a longitudinal velocity equal to the depth-averaged value, U.

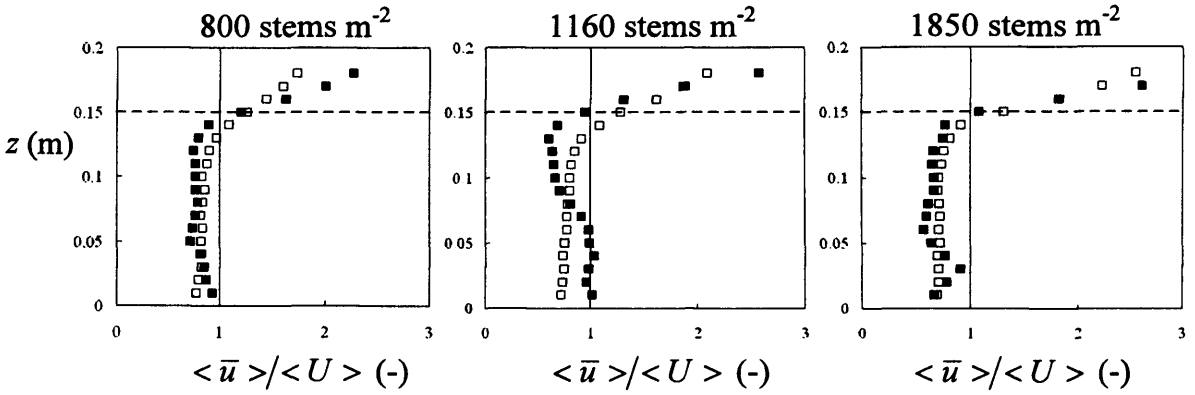

Figure 6-11 Normalised longitudinal velocity (u) profiles for submerged uniform cylinder arrays with a stem diameter of 6.0 mm (□) and constructed vegetation canopies (■), for a submergence level of 1.33, a bed gradient of 1/1000, and stem densities of 800, 1160 and 1850 stems m^{-2}. U is the depth-averaged longitudinal velocity for the flow depth. The bold dotted lines denote the top of the canopy, and the faint vertical lines denote a longitudinal velocity equal to the depth-averaged value, U.

For the uniform cylinder arrays, the normalised depth-averaged longitudinal velocities ranged between 0.8 and 0.9 over most of the canopy layer and decreased in magnitude with increasing stem density. This is shown more clearly in Figure 6-12a, whilst the increase in the normalised depth-averaged longitudinal velocity of the surface flow layer with stem density is shown in Figure 6-12b. The trends in both figures were linear for a bed gradient of 0.001 where canopy and surface flow layer velocities were considerably lower (Section 6.4.1). However, for a bed gradient of $0.00\dot{3}$, where velocities were higher compared to the shallower gradient, the trends between normalised depth-averaged velocities in the surface or canopy layers and the

stem density were non-linear. The constructed vegetation canopies followed similar trends in both figures.

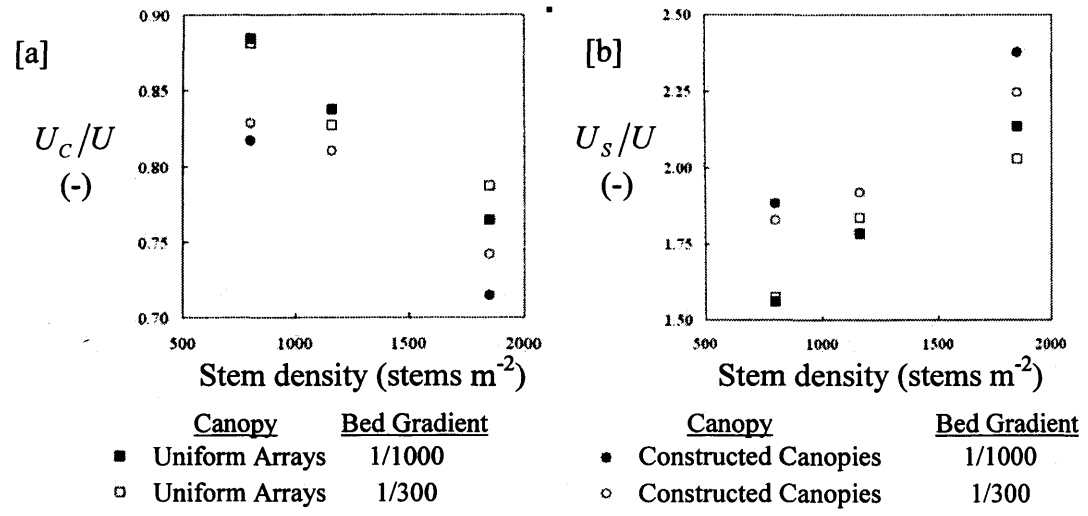

Figure 6-12 Variation in normalised depth-averaged longitudinal [a]: canopy layer (U_C), and [b]: surface flow layer (U_S) velocities with the stem density for uniform cylinder arrays and constructed vegetation canopies for a submergence level of 1.33. U is the depth-averaged longitudinal velocity for the flow depth.

Nepf *et al.* (1997b) also observed a similar feature for emergent uniform cylinder arrays, whereby longitudinal velocities were relatively constant for most of the flow depth. A selection of velocity profiles measured by the authors is presented in Figure 6-13 for stem densities between 200 and 2000 stems m^{-2}. Experiments were repeated for each stem density by implementing a range of flow rates resulting in depth-averaged velocities ranging between 0.032 and 0.131 ms^{-1} (equivalent to stem Reynolds numbers between 190 and 790). There was little variation in the shapes of the mean velocity profiles for the different stem densities considered.

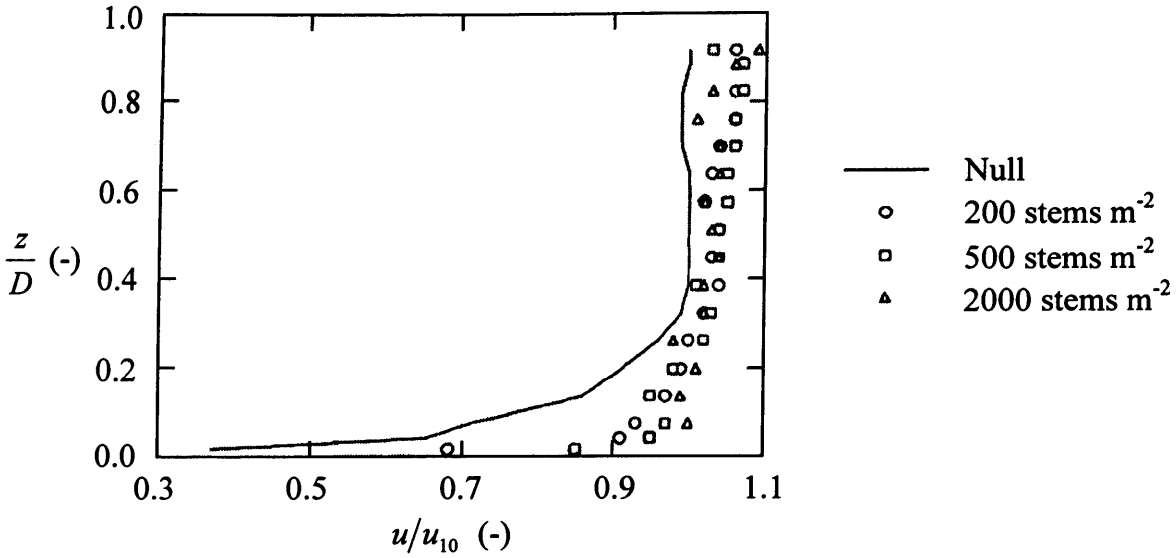

Figure 6-13 Profiles of normalised mean longitudinal velocity for emergent uniform cylinder arrays with densities of 0 (null), 200, 500 and 2000 stems m^{-2}. z is the elevation, D is the flow depth, u is the longitudinal velocity and u_{10} is the longitudinal velocity at an elevation of 100 mm for the null condition. Taken from Nepf *et al.* (1997b).

6.4.4 Reynolds Stress Profiles

The normalised Reynolds stress profiles for the uniform cylinder arrays and constructed vegetation canopies are presented in Figure 6-14 and Figure 6-15 for bed gradients of 0.00$\dot{3}$ and 0.001 respectively. Peak values were detected very close to the canopy-surface flow layer interface.

For the steeper bed gradient of 0.00$\dot{3}$, the experiments were conducted at higher flow rates and the longitudinal velocities, and hence the associated velocity fluctuations, were considerably higher. As would be expected, the Reynolds stress values were considerably higher, particularly near the canopy-surface flow layer interface and in the region immediately above the canopies. For the uniform cylinder arrays, Reynolds stress values within the canopy were considerably higher for the higher stem density of 1850 stems m^{-2} compared to the sparser density of 800 stems m^{-2} where a greater difference in zonal velocities between the canopy and surface flow layers was observed even though longitudinal velocities were marginally lower for a higher stem density (see Section 6.4.2). For the constructed vegetation canopies, Reynolds stresses within the canopy decreased with increasing stem density where it is possible that the increase in projected area due to the foliage may contribute to the reduction of Reynolds stresses.

To evaluate the influence of the peak Reynolds stress above a canopy on the underlying flow within the canopy, the Reynolds stress penetration depth was determined. This is defined as the distance from the top of the vegetation to the elevation within the canopy where the Reynolds stress is 10% of the peak value (see Section 2.5.3). For the constructed vegetation canopies, the Reynolds stress penetration depth decreased with increasing stem density. The increase in projected area due to the plant material may be associated with a reduction in the magnitude of the penetration. However, for the uniform cylinder arrays, Reynolds stress penetration was greater for the higher stem densities (1160 and 1850 stems m^{-2}). For a bed gradient of 0.001 (see Figure 6-15), there was little difference between the penetration depths for the 1160 and 1850 stems m^{-2} canopies, for which the peak Reynolds stress values were also very similar (0.4 kg $m^{-1}s^{-2}$). Although only three stem densities were examined, the results may suggest that the peak Reynolds stress and its penetration depth reach asymptotic values with increasing stem density for similar flow conditions. This may be associated with the flow regime; stem Reynolds numbers ranged between 200 and 650 for the three stem densities compared to between 150 and 520 for the constructed canopies. Nevertheless, the data shows a relatively deeper Reynolds stress penetration in a uniform cylinder array compared to a constructed vegetation canopy.

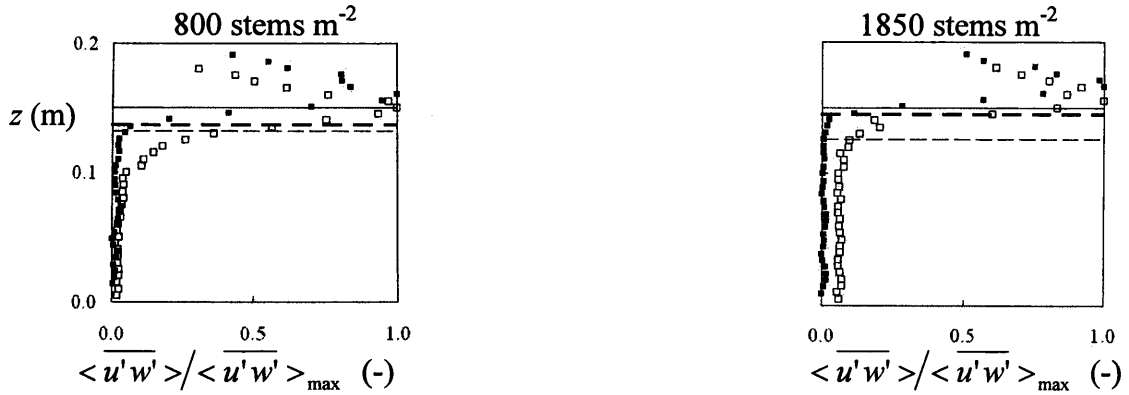

Figure 6-14 Normalised Reynolds stress profiles for submerged uniform cylinder arrays with a stem diameter of 6.0 mm (□), and constructed vegetation canopies (■) for a submergence level of 1.33, bed gradient of 1/300 and stem densities of 800 and 1850 stems m^{-2}. The bold dotted lines denotes Reynolds stress penetration for constructed vegetation canopies and faint dotted line denotes penetration for uniform cylinder arrays. Solid lines denote the top of the canopy.

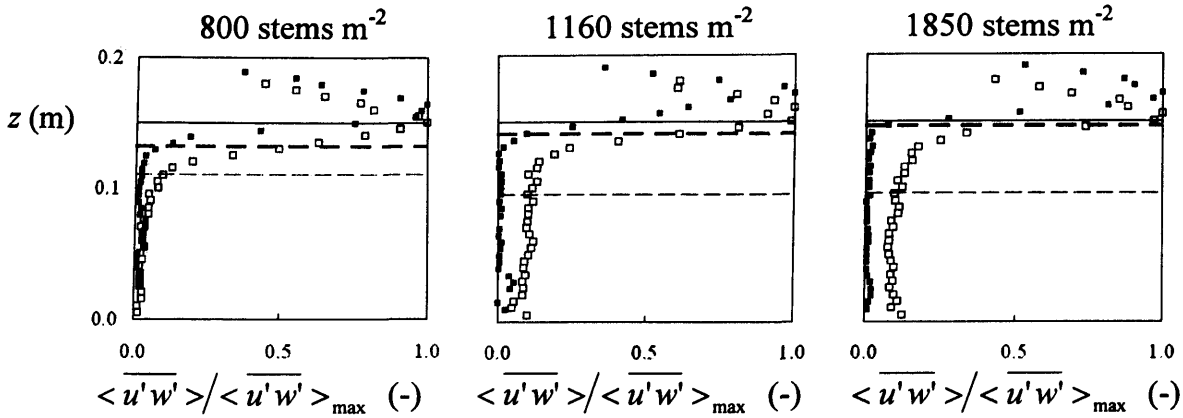

Figure 6-15 Normalised Reynolds stress profiles for submerged uniform cylinder arrays with a stem diameter of 6.0 mm (□), and constructed vegetation canopies (■) for a submergence level of 1.33, bed gradient of 1/1000 and stem densities of 800, 1160 and 1850 stems m^{-2}. The bold dotted lines denotes Reynolds stress penetration for constructed vegetation canopies and faint dotted line denotes penetration for uniform cylinder arrays. Solid lines denote the top of the canopy.

Due to the higher longitudinal velocities implemented for the steeper bed gradient of 0.00$\dot{3}$, the flow was more turbulent (stem Reynolds numbers ranged between 340 and 1200 for the three stem densities) and peak Reynolds stress values were considerably higher compared to the experiments conducted for a bed gradient of 0.001 (values range between 0.9 and 1.5 kg $m^{-1}s^{-2}$). For these relatively higher values, the turbulence structure, and hence the Reynolds stress profiles were inconsistent in shape over the canopy height when compared to other stem densities. Relating the stress penetration depth to the stem density was more difficult.

Dunn *et al.* (1996) conducted similar experiments on uniform cylinder arrays with considerably lower stem densities ranging between 90 and 780 stems m^{-2} and a similar stem diameter to the experiments presented herein (6.35 mm). Stem Reynolds numbers varied between 900 and 4700 within the canopy region for the range of experiments. The Reynolds numbers were considerably higher than the values for the uniform cylinder arrays in the current study, for which ranged between 200 and 860 (see Figure 6-4). The peak Reynolds stress values for submerged conditions were also considerably higher than those observed in the current study ranging between 1.96 and 14.2 kg m^{-1} s^{-2}. As would be expected, for the higher stem densities implemented in this study, Reynolds stress penetration into the uniform cylinder arrays was considerably lower than that observed by Dunn *et al.* (1996).

6.4.5 Two-Dimensional Drag Coefficients

Profiles of the two-dimensional drag coefficient, $C_{D\,2D}$, are presented in Figure 6-16 and Figure 6-18 for the uniform cylinder arrays (for bed gradients of $0.00\dot{3}$ and 0.001 respectively) and in Figure 6-17 and Figure 6-19 for the constructed vegetation arrays. The profiles for the uniform cylinder arrays indicate that values were relatively constant over most of the canopy height. Depth-averaged values of the drag coefficient over the height of the arrays, $\overline{C_{D\,2D}}$, were 0.8 $\pm$ 0.1 (standard deviation), 1.3 $\pm$ 0.2 and 1.2 $\pm$ 0.2 for cylinder densities of 800, 1160 and 1850 cylinders m^{-2} respectively. These values were similar to those for the constructed vegetation canopies, which were 1.3 $\pm$ 0.4, 1.0 $\pm$ 0.5 and 1.2 $\pm$ 0.3 for the equivalent stem densities. There was considerably greater variation in the drag coefficients over the height of the constructed vegetation canopies as highlighted by the greater standard deviations.

For the uniform cylinder arrays, $C_{D\,2D}$ values fluctuated in the upper part of the canopy due to the combined effects of changes in both the longitudinal velocity and Reynolds stress magnitudes. With the exception of the 1160 stems m^{-2} canopy for the steeper bed gradient of $0.00\dot{3}$, there was a peak in $C_{D\,2D}$ a short distance below the top of the canopy. The peaks correspond to a sharp increase in Reynolds stress with elevation as illustrated in Figure 6-20 for a bed gradient of $0.00\dot{3}$. A large gradient in Reynolds stress is indicative of turbulence production. Through turbulence production, the mean kinetic energy is converted into turbulent kinetic energy and this is reflected in higher drag coefficients. Above the peak in Reynolds stress, drag coefficients decreased towards the top of the canopy due to an increase in longitudinal velocity and Reynolds number. Although the profiles for the vegetation were variable over the canopy height, there was no evidence of any recurring patterns in the drag coefficients near the top of the canopy for the canopies considered. This can be attributed to lower Reynolds stresses within the canopies as observed in Section 6.4.4, which was attributed to the dense foliage cover found in natural vegetation.

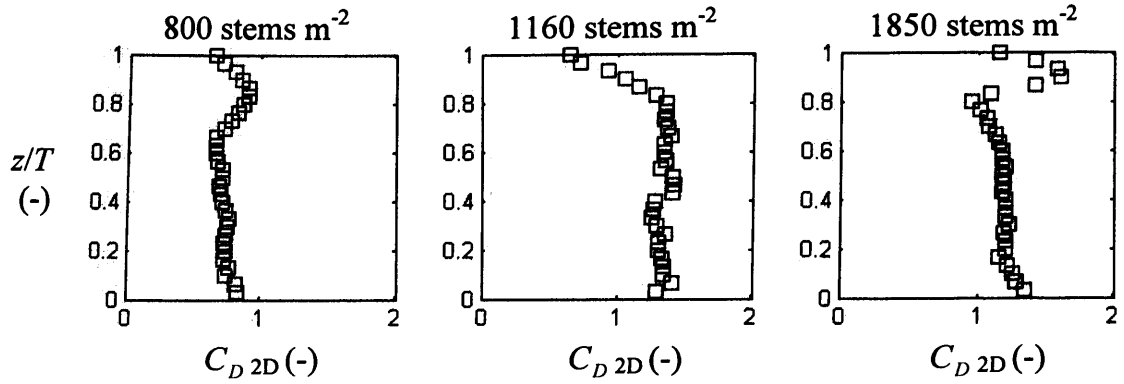

Figure 6-16 Two-dimensional bulk drag coefficient profiles for submerged uniform cylinder arrays with a stem diameter of 6.0 mm, submergence level of 1.33, a bed gradient of 1/300, stem densities of 800, 1160 and 1850 stems m^{-2}.

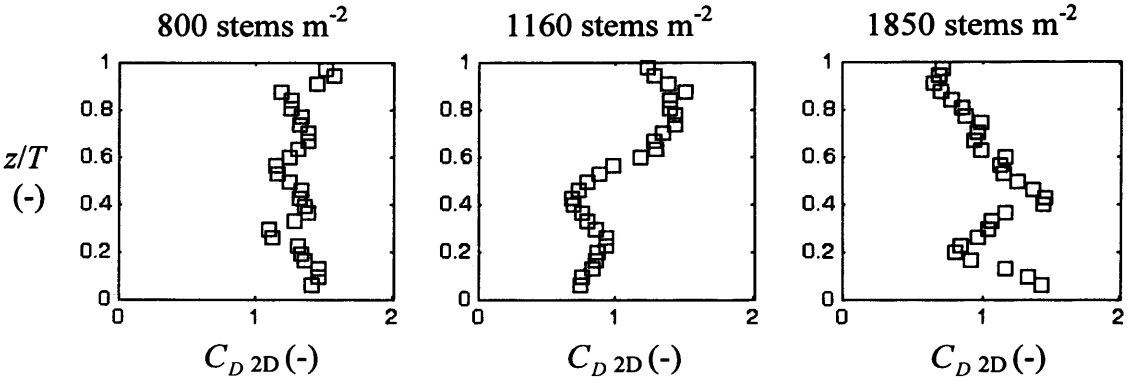

Figure 6-17 Two-dimensional bulk drag coefficient profiles for submerged constructed vegetation canopies for a submergence level of 1.33, a bed gradient of 1/300, stem densities of 800, 1160 and 1850 stems m^{-2}.

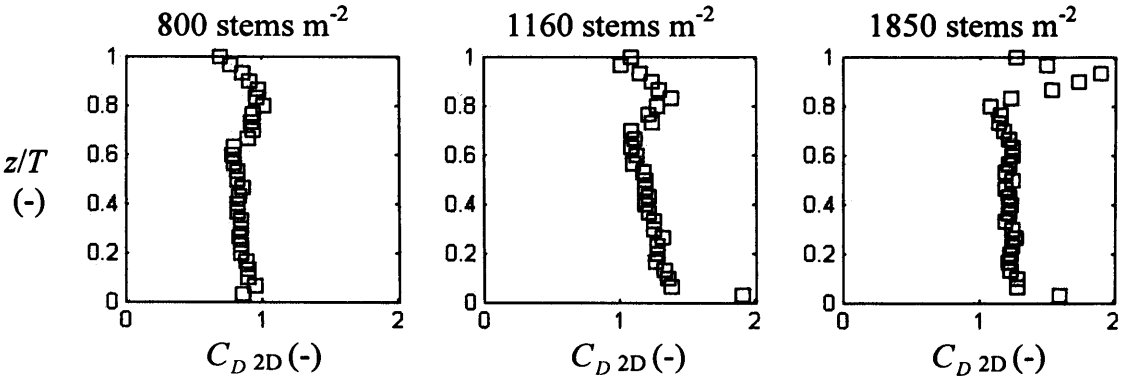

Figure 6-18 Two-dimensional bulk drag coefficient profiles for submerged uniform cylinder arrays with a stem diameter of 6.0 mm, submergence level of 1.33, a bed gradient of 1/1000, stem densities of 800, 1160 and 1850 stems m^{-2}.

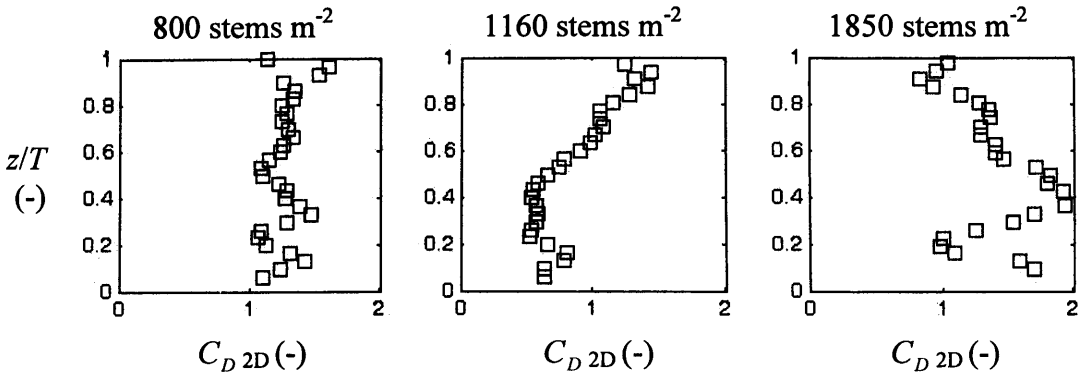

Figure 6-19 Two-dimensional bulk drag coefficient profiles for submerged constructed vegetation canopies for a submergence level of 1.33, a bed gradient of 1/1000, stem densities of 800, 1160 and 1850 stems m^{-2}.

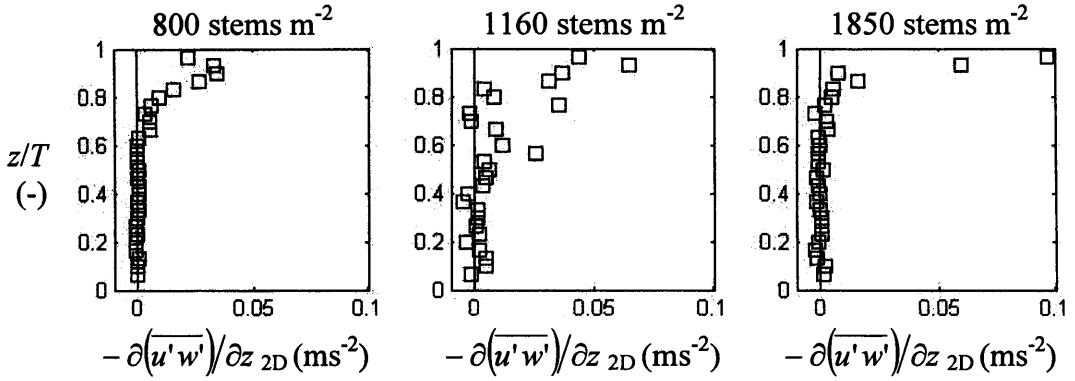

Figure 6-20 The vertical gradients in Reynolds stresses for submerged uniform cylinder arrays with a stem diameter of 6.0 mm, submergence level of 1.33, a bed gradient of 1/300, stem densities of 800, 1160 and 1850 stems m^{-2}.

For the uniform cylinder arrays considered by Dunn *et al.* (1996) (see 6.4.4), $C_{D\,2D}$ values ranged between 0.6 and 1.8 over the canopy height. There was considerably more variation in the two-dimensional drag coefficient over the canopy height for the uniform cylinder arrays implemented by Dunn *et al.* (1996) compared to those implemented here. This can be attributed to a number of factors, namely that the uniform cylinder arrays in this study were considerably higher in stem density, the peak Reynolds stress above the canopy was lower and the Reynolds stress penetration was smaller. Depth-averaged drag coefficients ($\overline{C_{D\,2D}}$) ranged between 1.1 and 1.5. The span of the range was relatively small, particularly when the wide range of peak Reynolds stress values near the canopy-surface flow layer interface (1.96 kg m^{-1}s^{-2} - 14.2 kg m^{-1}s^{-2}) and depth-averaged canopy layer velocities (0.19 ms^{-1} - 0.63 ms^{-1}) are considered. The depth-averaged values were of a similar order of magnitude to the depth-averaged drag coefficients ($\overline{C_{D\,2D}}$) calculated in this study for uniform cylinder arrays with densities of 1160 and 1850 cylinders m^{-2} (1.3 and 1.2 respectively).

6.5 Concluding Remarks

A range of experiments were conducted for both constructed vegetation canopies and uniform cylinder arrays under submerged conditions. The main objective of the experiments was to address the differences between the velocity and turbulence structures between the two types of canopy.

The difference between the hydraulic resistance of the constructed vegetation canopies and the uniform cylinder arrays was reflected in the stage-discharge curves. Comparison of the curves showed that discharge for the uniform cylinder arrays was between 27% and 42% higher for a flow depth of 200 mm depending on the stem density. The experiments were conducted to the three stem densities of 800, 1160 and 1850 stems m^{-2} and the percentage value increased with stem density. The difference in hydraulic resistance was also reflected in the Manning's roughness coefficient values for the 150 mm tall canopies. Values for the uniform cylinder arrays ranged between 0.062 and 0.106 for the three stem densities whilst for the constructed August vegetation canopies, values ranged between 0.087 and 0.151.

The lower projected area of obstruction per unit volume of the uniform cylinder array relative to the constructed vegetation canopy resulted in a lower hydraulic resistance for all the stem densities examined. For the submergence level examined, the discharge was a factor of 1.3 – 1.4 times larger for the uniform cylinder array than the constructed vegetation canopy. This is based on a flow depth of 0.2 m, which was implemented for all experiments. For the stem densities examined, this corresponds to Manning's n values of between 0.07 – 0.12 for the uniform cylinder arrays and 0.09 – 0.15 for the constructed canopies. . The bulk drag coefficient ($\overline{C_D}$), which is characteristic of the drag force per stem within the canopy, ranged between 0.04 and 0.2 for the constructed August vegetation canopies and between 0.9 and 1.4 for the uniform cylinder arrays. The roughness coefficient ($\overline{C_D}'$), which is characteristic of the total drag force of a vegetation canopy, varied between 4.1 m^{-1} and 16 m^{-1} for the uniform cylinder arrays, and between 11 m^{-1} and 48 m^{-1} for the constructed August vegetation canopies for a submergence level (H) of 1.33

For the uniform cylinder arrays, there was little variation in the longitudinal velocity over the depth of the canopy compared to the constructed canopies. The longitudinal velocities increased marginally with elevation. The increase in longitudinal velocity with elevation was not observed in the constructed vegetation

canopies. The foliage may have contributed to reducing the effects of the "skimming" flow associated with a higher velocity surface flow layer on the underlying canopy layer.

There was greater vertical movement within the flow in the canopy layer for the constructed vegetation canopies compared to the uniform cylinder arrays as reflected by the greater magnitude of vertical velocities. Within the canopy layer, vertical movement was generally in the upward direction, particularly close to the canopy-surface flow layer interface due to vortices in the shear layer along the interface.

The depth of Reynolds stress penetration was deeper into the canopy layer for the uniform cylinder arrays than for the constructed vegetation canopies. The depth of Reynolds stress penetration increased with increasing stem density, particularly for a bed gradient of 0.001. For the constructed vegetation canopies, although the velocities did not consistently increase in the canopy layer with elevation, there were fluctuations in the form of 'bulges' due to the uneven distribution of vegetation material over the canopy height. The Reynolds stress penetration decreased with increasing stem density for the constructed vegetation canopies, particularly for relatively low Reynolds numbers (below a stem Reynolds number of 640), but increased for the uniform cylinder arrays. Foliage in the constructed canopies was believed to contribute to the reduction of Reynolds stress penetration into the canopy. This was despite the foliage having a lower mass per unit volume than the stem region.

With increasing stem density, the amount of foliage in the constructed vegetation canopy also increased and hence the reduction of Reynolds stress penetration. This was reflected in a greater percentage increase in total projected area for the constructed vegetation canopies than for the uniform cylinder arrays. For instance, a 131% increase in stem density (from 800 to 1850 stems m^{-2}) resulted in an increase in a 289% increase in the depth-averaged projected area per unit volume for a 150 mm tall canopy (from 7.4 m^{-1} to 28.9 m^{-1}), but only a 131% increase for the uniform cylinder arrays (from 4.8m^{-1} to 11.1m^{-1}).

In the absence of foliage for the uniform cylinder arrays, an increase in stem density resulted in a greater relative difference in hydraulic resistance between the canopy and surface flow layers, and hence, a stronger shear layer along the interface between the two layers. For the lowest stem density (800 stems m^{-2}), the peak

Reynolds stress magnitude was identical for both the constructed vegetation canopy and the uniform cylinder array. For the middle stem density (1160 stems m^{-2}) the peak Reynolds stress was 99% higher for the uniform cylinder array, and for the highest stem density examined (1850 stems m^{-2}), it was 115% higher. For the same submergence level, the depth-averaged longitudinal velocities were consistently between 30% and 40% higher for the uniform cylinder arrays than the constructed canopies. However, the observed peak Reynolds stress was between 100% and 120% greater for the uniform cylinder arrays for the higher stem densities of 1160 and 1850 stems m^{-2} (there was negligible difference in peak Reynolds stress magnitudes for the lowest stem density of 800 stems m^{-2}). For a higher stem density, the magnitude of the peak Reynolds stress above the canopy was greater, and without the dampening effect of foliage, Reynolds stress penetration into the canopy was deeper.

There was less variation in the two-dimensional drag coefficient ($C_{D\,2D}$) over the canopy height for the uniform cylinder arrays with depth-averaged values ranging between 0.8 and 1.3. $C_{D\,2D}$ values were of a similar magnitude to those for the constructed vegetation canopies which ranged between 1.0 and 1.3, however there was considerably more variation over the canopy height. For the uniform cylinder arrays, there was a peak in $C_{D\,2D}$ a short distance below the canopy top. The peak is attributed to the change in magnitude of Reynolds stress below the interface. The location of the peak in $C_{D\,2D}$ is linked to the high level of turbulence production in the shear layer.

Uniform cylinder laboratory models are useful for evaluating the hydrodynamics through a canopy under controlled conditions, and with little variability in the structure of the canopy. However, such models fail to simulate the complex morphology associated with vegetation, which result in more complex velocity profiles and turbulence structures. The vegetation cover along a saltmarsh can be variable in terms of the concentration and size of the plants. Furthermore, the vertical distribution of plant material in vegetation canopies is usually non-uniform and unlike the uniform cylinder models.

7 Laboratory Investigation II: *Spartina anglica* Canopies

7.1 Introduction

In Section 2.4.1, a number of laboratory studies on vegetated flows through saltmarsh canopies were discussed. Canopies in such studies were often short in length, spanning 5.5m or less according to the studies reported in Section 2.4.1. Velocities were usually measured at locations where the flow structure may not have been fully developed (e.g. Pethick *et al.*, 1990; Shi *et al.*, 1995; Shi *et al.*, 1996 and others). This may give rise to uncertainties when determining the impact of the vegetation on the hydrodynamics. Vegetation canopies were used in the studies listed above, however, vegetated flow studies are often performed on uniform cylinder models which are used to simulate vegetation canopies (e.g. Li and Shen; 1973; Nepf *et al.*, 1997a; Nepf *et al.*, 1997b; Nepf, 1999; Stone and Shen, 2002 and others). Consequently, the impact of the non-uniformity in plant material on the velocity profile and turbulence structure has seldom been looked at.

A laboratory programme was designed to investigate the effects of a common saltmarsh species, namely *Spartina anglica*, on the velocity and turbulence structure of fully developed uniform flows. *Sp. anglica* was a key vegetation species identified at the Llanelli and Lanrhidian field sites (Section 3.2.3). Plant morphology will be linked to the velocity structure using the measured velocity and turbulence data presented in the current chapter (Section 7.3) and the results from the vegetation quantification (Section 5.3).

The velocity and turbulence structure through vegetation canopies was examined by evaluating the time-averaged velocities in the longitudinal and vertical directions and the associated fluctuating components for each mean velocity. These were used to determine other parameters that characterise the flow such as the stem Reynolds number, the "form-induced" stress and the Reynolds stress. Linking plant morphology to the resulting hydraulic resistance was achieved by introducing a one-dimensional bulk drag coefficient, $\overline{C_D}$, characterising the hydraulic resistance properties of a canopy over the height of the vegetation. A two-dimensional counterpart, $C_{D\,2D}$, was used to characterise the hydraulic resistance of the vegetation

at a given elevation within the canopy. This is given by Equation 2.34, the derivation of of which is presented in Appendix I.

The one-dimensional drag coefficient, $\overline{C_D}$, offers a less complex approach for evaluating the hydraulic resistance of the entire canopy. This is more convenient for comparisons of the hydraulic resistance due to vegetation under different conditions such as stem densities, bed gradients and submergence levels. However, the two-dimensional coefficient, $C_{D\,2D}$, is more suitable for examining a single canopy in more detail by evaluating the variation in vegetation characteristics and flow structure (velocity and turbulence structure) with elevation. The latter parameter could potentially be used to predict velocity profiles within the canopy, which would be extremely relevant to the study of vegetated flows. Both parameters are dependent on the morphology of the vegetation, although $C_{D\,2D}$ is also dependent on the Reynolds stress in the canopy. The Reynolds stress is not used in the one-dimensional calculation of $\overline{C_D}$.

A range of bed gradients, stem densities, emergence and submergence levels were imposed. Values for these variables were selected based on the findings of the field monitoring programme presented in Chapters 3 and 4, so that the experiments were conducted for a range of conditions that were representative of typical saltmarshes. The submergence level, H, was defined as the ratio of flow depth, D, to vegetation height, T. Values of H less than unity indicate an emergent condition meaning that the vegetation canopy projects through the water surface, whilst values of H greater than unity indicate a submerged condition with the flow depth being greater than the canopy height. Canopies constructed from vegetation samples collected during August 2006 and February 2007 were studied through a series of experiments. The aim was to distinguish between the material properties of younger summer and mature winter plants. Summer vegetation collected during August 2006 was examined for a wide range of flow conditions (Table 7-1). A selection of these tests was repeated using mature winter plants collected during February 2007 (Table 7-2). The contrast in stiffness between the relatively flexible August vegetation, and the relatively brittle February vegetation was discussed in Section 4.4.3 based on samples collected during September 2007 and December 2006. There was considerable variation in the Reynolds number, Re_d, for the experiments, however,

values were consistently within the vortex shedding range of values between 90 and 1000 (see Section 2.2.3).

Table 7-1 Details of the experiments conducted using *Sp. anglica* plants during Aug 2006

Test No.	Stem Density [Stems m^{-2}]	Bed Gradient S_0 [-]	Vegetation Height T [m]	Flow Depth D [m]	Reynolds Number Re_d	Submergence $H = D / T$	Flow Rate Q [ls^{-1}]
S-T12	800	1/300	0.53	0.25	420	0.47	7.0
S-T11	800	1/300	0.53	0.20	430	0.38	5.3
S-M11	800	1/300	0.15	0.20	450	1.33	6.8
S-S11	800	1/300	0.10	0.20	600	2.00	12.9
S-V10	800	1/300	0.05	0.15	890	3.00	13.9
S-T22	800	1/1000	0.53	0.25	200	0.47	3.4
S-T21	800	1/1000	0.53	0.20	230	0.38	2.7
S-M21	800	1/1000	0.15	0.20	250	1.33	3.9
S-S21	800	1/1000	0.10	0.20	350	2.00	7.4
S-V20	800	1/1000	0.05	0.15	360	3.00	8.0
M-T12	1160	1/300	0.53	0.25	340	0.47	5.5
M-T11	1160	1/300	0.53	0.20	360	0.38	4.2
M-M11	1160	1/300	0.15	0.20	340	1.33	5.3
M-S11	1160	1/300	0.10	0.20	480	2.00	10.6
M-V10	1160	1/300	0.05	0.15	770	3.00	12.4
M-T22	1160	1/1000	0.53	0.25	160	0.47	2.6
M-T21	1160	1/1000	0.53	0.20	160	0.38	1.9
M-M21	1160	1/1000	0.15	0.20	210	1.33	3.1
M-S21	1160	1/1000	0.10	0.20	260	2.00	5.8
M-V20	1160	1/1000	0.05	0.15	440	3.00	6.8
D-T12	1850	1/300	0.53	0.25	250	0.47	4.4
D-T11	1850	1/300	0.53	0.20	270	0.38	3.5
D-M11	1850	1/300	0.15	0.20	240	1.33	4.6
D-S11	1850	1/300	0.10	0.20	370	2.00	10.7
D-V10	1850	1/300	0.05	0.15	480	3.00	10.9
~~*D-T22~~	~~1850~~	~~1/1000~~	~~0.53~~	~~0.25~~	~~160~~	~~0.47~~	~~2.9~~
~~*D-T21~~	~~1850~~	~~1/1000~~	~~0.53~~	~~0.20~~	~~170~~	~~0.38~~	~~2.2~~
D-M21	1850	1/1000	0.15	0.20	110	1.33	2.2
D-S21	1850	1/1000	0.10	0.20	180	2.00	5.5
D-V20	1850	1/1000	0.05	0.15	240	3.00	5.9

*Tests D-T22 and D-T21 were excluded from this report due to an error incurred in the adjustment of the flume bed gradient.

Table 7-2 Details of the experiments conducted using *Sp. anglica* plants during Feb 2007

Test No.	Stem Density [Stems m^{-2}]	Bed Gradient S_0	Vegetation Height T [m]	Flow Depth D [m]	Reynolds Number Re_d	Submergence $H = D / T$	Flow Rate Q [ls^{-1}]
S-T21m	800	1/1000	0.53	0.20	410	0.38	6.8
S-M21m	800	1/1000	0.15	0.20	600	1.33	10.7
S-S21m	800	1/1000	0.10	0.20	760	2.00	17.8
S-V20m	800	1/1000	0.05	0.15	1000	3.00	19.2

7.2 One-Dimensional Measurements

7.2.1 Stage-Discharge Relationships

7.2.1.1 Emergent Vegetation

In Figure 7-1, stage-discharge curves (Section 5.2.5) are presented for emergent conditions where the August vegetation was long enough to protrude through the water surface (test numbers S-T21, M-T21, S-T12, M-T12 and D-T12, see Table 7-1 for details). Discharge rates in Figure 7-1 were determined using the flowmeter readings. One curve represents the February vegetation case for which the stem density was 800 stems m^{-2} (test number S-T21m). This stem density is equivalent to the sparsest of the stem densities investigated using vegetation harvested in the summer. A decrease in flow resistance within the canopy due to decreasing stem density is indicated by the downward transposition of the curves. This meant that for a given flow depth, greater discharge could be conveyed with decreasing stem density and hence, flow velocities were greater.

As one would expect, for a steep slope, a greater discharge was conveyed for a given flow depth. The effects of changes in stem density and bed gradient on the flow depth are summarised in Table 7-3 for the canopies examined. Although increasing the bed gradient appeared to have a more significant effect on the flow depth, the relative difference between the two bed gradients investigated was significantly greater than the differences between the three stem densities. The increase from a bed gradient of 0.001 to $0.00\dot{3}$ is equivalent to an increase of 233%, which is considerably greater than the percentage increases from 800 stems m^{-2} to 1160 stems m^{-2} (45%) or from 800 stems m^{-2} to 1850 stems m^{-2} (131%). A winter vegetation canopy was also considered which created significantly less flow resistance than that created by the summer vegetation canopy with the same bed slope of 0.001 and stem density of 800 stems m^{-2}. As mentioned earlier in Section 7.1, the Reynolds number ranges for each canopy, which are presented in Figure 7-1, varied for the different canopies, however, they fell within the range of values that are characteristic of vortex shedding (between 90 and 1000).

Table 7-3 The effects of increasing bed gradient and decreasing stem density on the flow depth.

First canopy		Second canopy		Percentage difference		Effect on flow depth
S_0 (-)	Stem density (Stems m^{-2})	S_0 (-)	Stem density (Stems m^{-2})	S_0 (-)	Stem density (Stems m^{-2})	ΔD (%)
0.001	800	0.00$\dot{3}$	800	233%	-	54.4%
0.001	1160	0.00$\dot{3}$	1160	233%	-	54.4%
0.001	1160	0.001	800	-	-31.0%	-25.8%
0.00$\dot{3}$	1160	0.00$\dot{3}$	800	-	-31.0%	-25.6%
0.00$\dot{3}$	1850	0.00$\dot{3}$	800	-	-56.8%	-36.8%

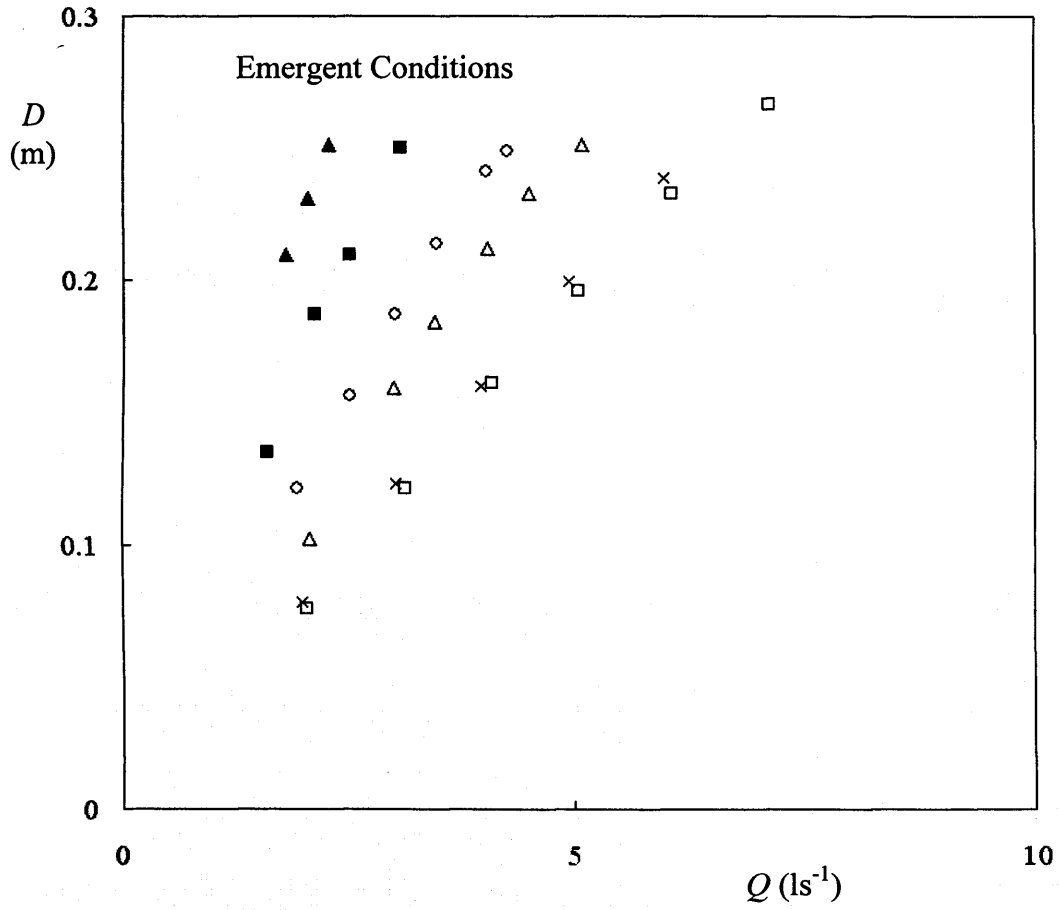

	Stem Density (stems m^{-2})	S_0	Season	Hydraulic Radius Reynolds number	Stem Diameter Reynolds number
×	800	1/1000	Winter	$4300 < Re_R < 7700$	$290 < Re_d < 300$
■	800	1/1000	Summer	$2800 < Re_R < 3800$	$210 < Re_d < 230$
▲	1160	1/1000	Summer	$2500 < Re_R < 2800$	$160 < Re_d < 170$
□	800	1/300	Summer	$4500 < Re_R < 8500$	$470 < Re_d < 490$
△	1160	1/300	Summer	$4100 < Re_R < 6300$	$360 < Re_d < 390$
○	1850	1/300	Summer	$3600 < Re_R < 5300$	$230 < Re_d < 240$

Figure 7-1 Stage-Discharge curves for emergent *Spartina anglica* canopies for stem densities of 800, 1160 and 1850 stems m^{-2} and bed gradients of 1/300 and 1/1000. D is the flow depth, Q is the flow rate, and S_0 is the bed gradient.

7.2.1.2 Submerged Conditions

Stage-discharge curves (Section 5.2.5) are presented in Figure 7-2, Figure 7-3 and Figure 7-4 for 50mm, 100mm and 150mm cropped canopy heights respectively with stem densities of 800, 1160 and 1850 stems m^{-2} and bed gradients of 0.001 and $0.00\dot{3}$. For a given flow rate, the uniform flow depth increased with increasing stem density and decreasing bed slope as observed in section 7.2.1.1 for emergent conditions.

The trends associated with variations in bed gradients and with stem density are summarised in Table 7-4 and Table 7-5 respectively. The statistics in Table 7-4 indicate that the percentage increase in uniform flow depth with bed gradient was similar for both canopy heights of 100 mm and 150 mm. There was also little variation in the percentage increase in uniform flow depth for each of the three stem densities investigated, particularly for the two lower densities. Based on the statistics presented in Table 7-5, a greater decrease in stem density resulted in a greater increase in uniform flow depth, and the increase was greater for the 150 mm canopy, compared to the 100 mm canopy.

Table 7-4 Percentage increase in uniform flow depth associated with an increase in bed gradient from 1/1000 to 1/300 (233%) for canopies with stem densities of 800, 1160 and 1850 stems m^{-2}, and cropped canopy heights of 100mm and 150mm.

	Increase in flow depth (%)		
Stem density (stems m^{-2})	800	1160	1850
150 mm canopy	43.9 %	43.9 %	50.3 %
100 mm canopy	40.2 %	42.4 %	47.2 %

Table 7-5 Percentage increase in uniform flow depth associated with an decrease in stem density from 1160 to 800 stems m^{-2} (31.0%), and from 1850 to 800 stems m^{-2} (56.8%)

	Increase in stem density	Increase in flow depth (%)	
Canopy height	%	$S_0 = 0.001$	$S_0 = 0.00\dot{3}$
150 mm	-31.0 %	16.6 %	16.5 %
	-56.8 %	29.8 %	20.7 %
100 mm	-31.0 %	10.6 %	13.8 %
	-56.8 %	18.0 %	10.6 %

Similar trends were difficult to determine for a canopy height of 50mm (Figure 7-2). Reynolds numbers for flow through the 50 mm cropped canopy ($450 < Re_d < 2190$) were considerably greater than those for the 100 mm ($250 < Re_d < 1480$), 150 mm ($150 < Re_d < 1000$) and emergent ($140 < Re_d < 490$) canopies. Stem

Reynolds numbers were calculated based on the area mean velocity, U_A, and the basal stem diameters.

The Stage-discharge relationships for the 50 mm height canopy presented in Figure 7-2 did not converge with decreasing flow rate towards a flow depth equal to the canopy height as observed for the 100 mm and the 150 mm canopies in Figure 7-3 and Figure 7-4 respectively. This is likely a feature of the considerably higher Reynolds number ranges for flows through the 50 mm canopies, which were therefore excluded from the comparisons discussed in this section.

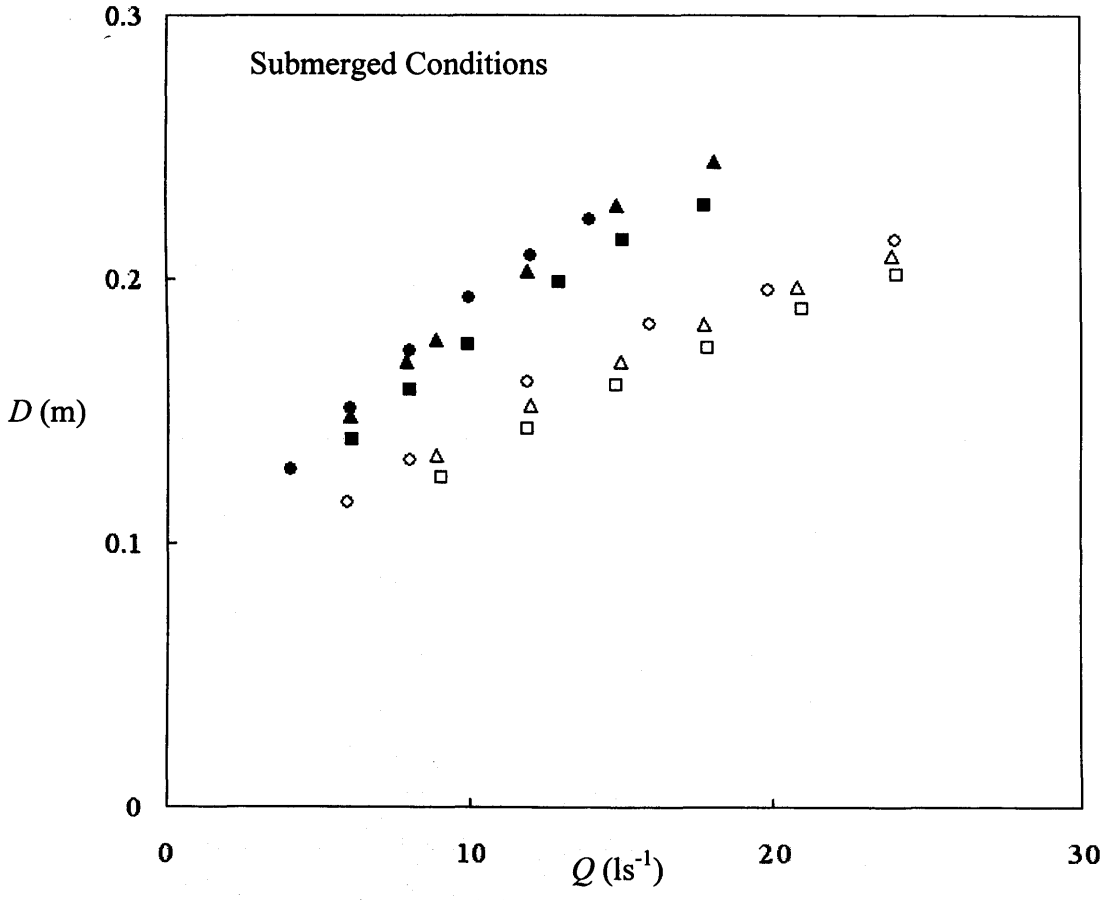

Stem Density (stems m^{-2})	S_0	Season	Hydraulic Radius Reynolds number	Stem Diameter Reynolds number
■ 800	1/1000	Summer	$10500 < Re_R < 23500$	$810 < Re_d < 1430$
▲ 1160	1/1000	Summer	$10100 < Re_R < 23000$	$780 < Re_d < 1410$
● 1850	1/1000	Summer	$7200 < Re_R < 18800$	$450 < Re_d < 890$
□ 800	1/300	Summer	$16500 < Re_R < 34200$	$1340 < Re_d < 2190$
△ 1160	1/300	Summer	$15800 < Re_R < 33300$	$1280 < Re_d < 2180$
○ 1850	1/300	Summer	$11200 < Re_R < 32900$	$740 < Re_d < 1590$

Figure 7-2 Stage-Discharge relationships for a submerged 50 mm cropped canopy for stem densities of 800, 1160 and 1850 stems m^{-2} and bed gradients of 1/300 and 1/1000. *D* is the flow depth, *Q* is the flow rate, and S_0 is the bed gradient.

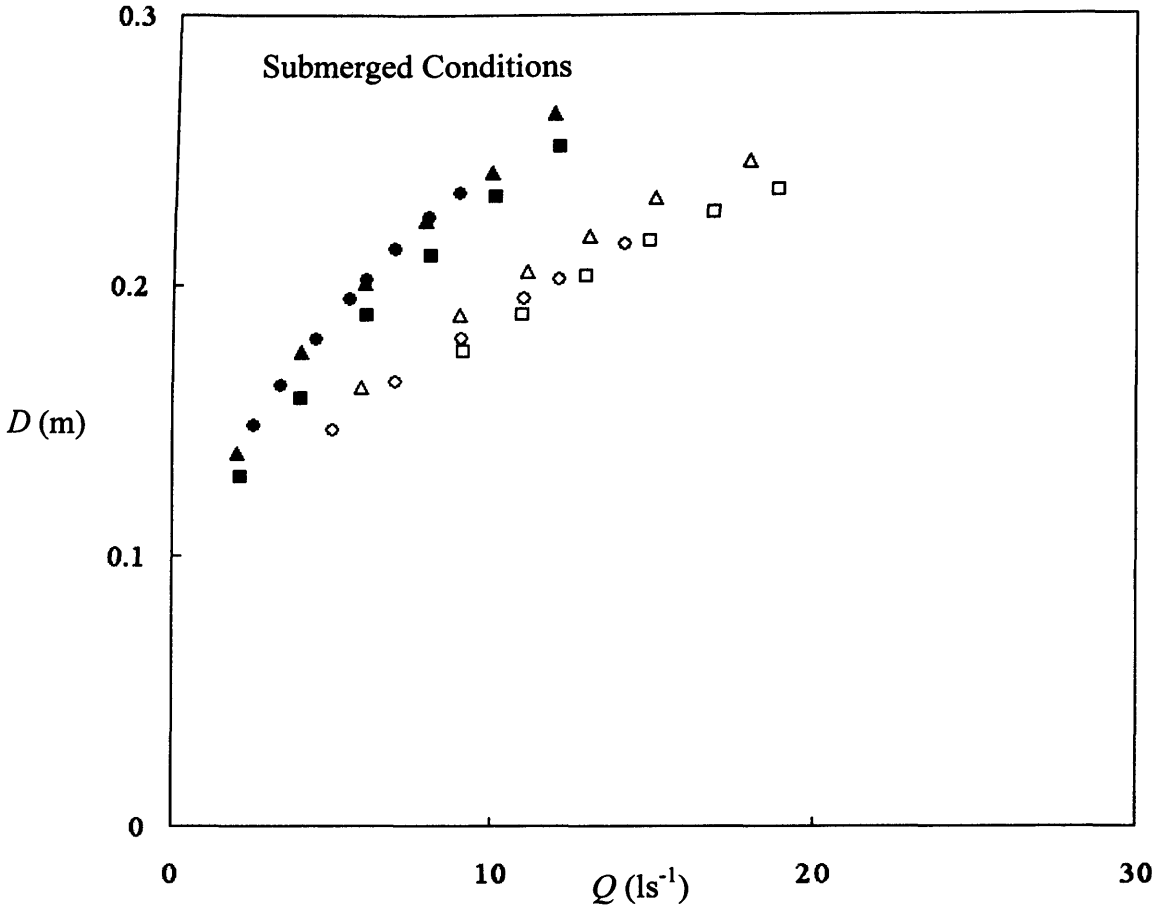

Stem Density (stems m^{-2})	S_0	Season	Hydraulic Radius Reynolds number	Stem Diameter Reynolds number
■ 800	1/1000	Summer	$3900 < Re_R < 15000$	$310 < Re_d < 880$
▲ 1160	1/1000	Summer	$3600 < Re_R < 14400$	$290 < Re_d < 860$
● 1850	1/1000	Summer	$4300 < Re_R < 11700$	$250 < Re_d < 540$
□ 800	1/300	Summer	$14000 < Re_R < 24600$	$960 < Re_d < 1480$
△ 1160	1/300	Summer	$9600 < Re_R < 22800$	$700 < Re_d < 1400$
◇ 1850	1/300	Summer	$8500 < Re_R < 19400$	$490 < Re_d < 930$

Figure 7-3 Stage-Discharge relationships for submerged 100 mm tall *Spartina anglica* canopies for stem densities of 800, 1160 and 1850 stems m^{-2} and bed gradients of 1/300 and 1/1000. D is the flow depth, Q is the flow rate, and S_0 is the bed gradient.

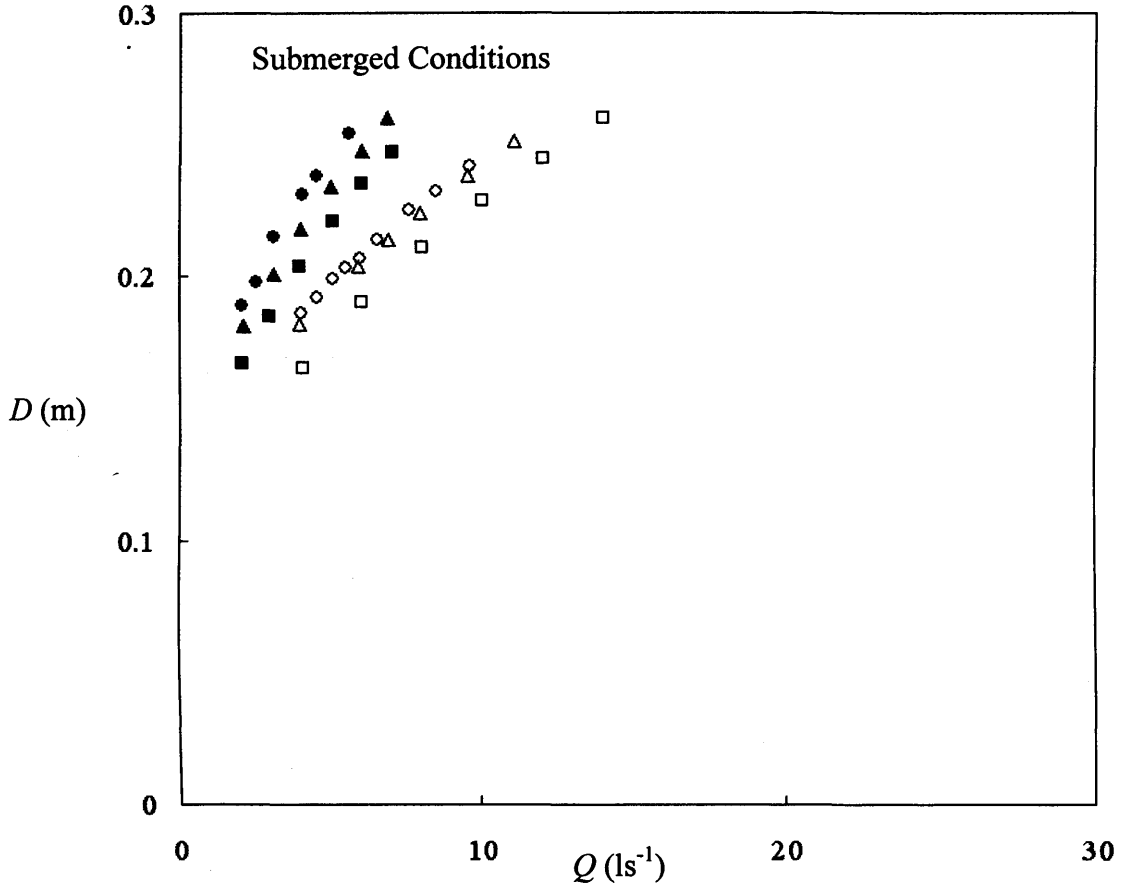

	Stem Density (stems m^{-2})	S_0	Season	Hydraulic Radius Reynolds number	Stem Diameter Reynolds number
■	800	1/1000	Summer	$3200 < Re_R < 8800$	$230 < Re_d < 520$
▲	1160	1/1000	Summer	$3200 < Re_R < 8400$	$220 < Re_d < 500$
●	1850	1/1000	Summer	$3000 < Re_R < 6900$	$150 < Re_d < 300$
□	800	1/300	Summer	$6400 < Re_R < 17000$	$450 < Re_d < 1000$
△	1160	1/300	Summer	$5900 < Re_R < 13800$	$410 < Re_d < 840$
◇	1850	1/300	Summer	$6000 < Re_R < 12200$	$310 < Re_d < 560$

Figure 7-4 Stage-Discharge relationships for submerged 150 mm tall *Spartina anglica* canopies for stem densities of 800, 1160 and 1850 stems m^{-2} and bed gradients of 1/300 and 1/1000. *D* is the flow depth, *Q* is the flow rate, and S_0 is the bed gradient.

7.2.2 One-Dimensional Drag Coefficients

7.2.2.1 Coefficients for Emergent Conditions

Drag and roughness coefficients were described in Section 2.2.6. One-dimensional bulk drag coefficients, $\overline{C_D}$, and one-dimensional roughness coefficients, $\overline{C_D}'$, are presented for emergent canopies in Figure 7-5a and Figure 7-5b respectively for flow depths of 0.20m and 0.25m. For the emergent canopies, there was little

variation in the coefficients with flow depth for any given stem density. Between 0.20m and 0.25m depths, there was little change in the average canopy resistance over these flow depths. Variations in one-dimensional drag coefficients with degree of submergence, although small, were not consistent as demonstrated by the experiments conducted on the August vegetation. For a bed gradient of 0.001 and with increasing submergence, the drag coefficients increased for the 800 stems m^{-2} canopy, but decreased for the 1160 stems m^{-2} canopy. For a bed gradient of $0.00\dot{3}$, the drag coefficients decreased for stem densities of 800 and 1160 stems m^{-2}, but remained relatively constant for the higher stem density of 1850 stems m^{-2}. These trends reflected the high level of variation in the morphology of the vegetation. They also reflected the difference in the distribution of the vegetation material within the canopy as demonstrated by the projected area of obstruction profiles presented in Section 3.4.3.

For a given bed gradient, a reduction in $\overline{C_D}$ with increasing stem density was indicative of two main phenomena. Firstly, for a canopy with a higher stem density, the stem spacings were smaller. Therefore, the likelihood of stem wakes interacting with downstream stems and reducing the momentum of the flow was higher (Section 2.2.6). Secondly, the longitudinal weight component due to the flow was balanced by a drag force created by a larger number of stems. Although the canopy resulted in a greater resistance to the flow, each stem experienced a smaller proportion of the weight of the flow. This is also shown by the increase in the roughness coefficient ($\overline{C_D}'$) profile with stem density for each bed gradient in Figure 7-5b. $\overline{C_D}'$ represents the total resistive effect of the canopy on the flow.

For the steeper bed gradient of $0.00\dot{3}$, the flow velocity through the canopy layer was higher and the drag coefficients were lower when compared to the canopies at a bed gradient of 0.001. This is likely to be because of the higher Reynolds number at which the steeper bed experiments were conducted. Stem Reynolds numbers for emergent summer vegetation canopies ranged between 160 and 230 for a bed gradient of 0.001, and between 230 and 490 for a bed gradient of $0.00\dot{3}$ (see Figure 7-1). Drag coefficients increase in magnitude with the Reynolds number, particularly within the laminar and transitional ranges ($Re_d < 1000$), as frictional drag becomes insignificant, and the turbulence of the flow increases.

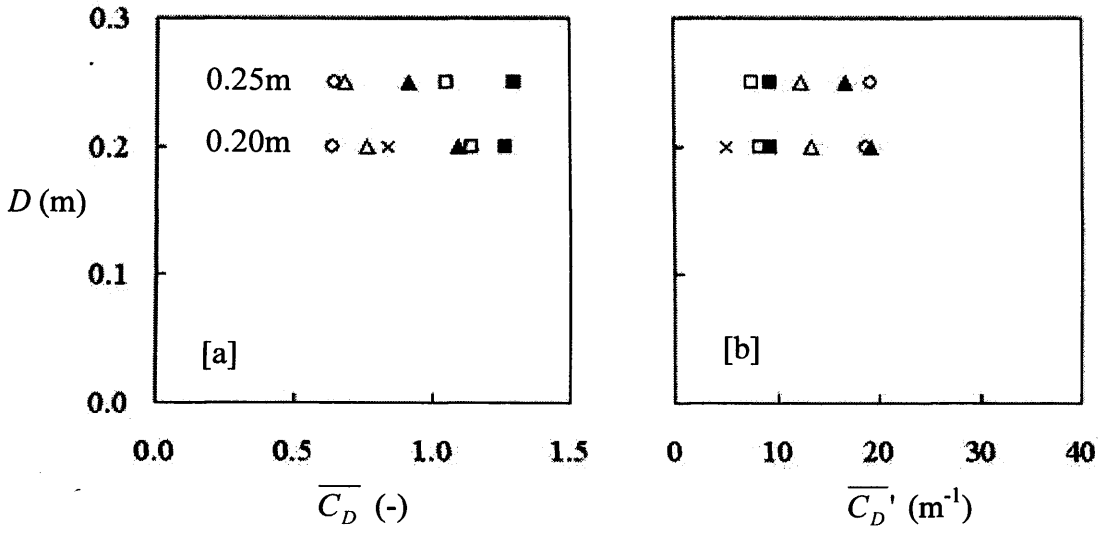

Stem Density (stems m^{-2})	S_0 (-)	Month	Stem Density (stems m^{-2})	S_0 (-)	Month
× 800	1/1000	February	□ 800	1/300	August
■ 800	1/1000	August	△ 1160	1/300	August
▲ 1160	1/1000	August	○ 1850	1/300	August

Figure 7-5 [a]: bulk drag coefficient, $\overline{C_D}$, and [b]: the one-dimensional bulk roughness coefficient, $\overline{C_D}'$, for emergent *Spartina anglica* canopies for flow depths, *D*, of 0.20m and 0.25m, at bed gradients of 1/1000 and 1/300, stem densities of 800, 1160 and 1850 stems m^{-2}, and vegetation collected during the months of August and February. S_0 is the bed gradient.

Values of the Manning's roughness coefficient, *n*, (Section 2.1.1), are presented in Figure 7-6 for the emergent canopies studied. Values were determined for each flow case individually as the flow was unlikely to be fully turbulent. Values ranged between 0.13 and 0.20 for the August canopies. For a given bed slope, Manning's '*n*' increased with stem density. The February canopies resulted in the lowest Manning's *n* value of 0.10.

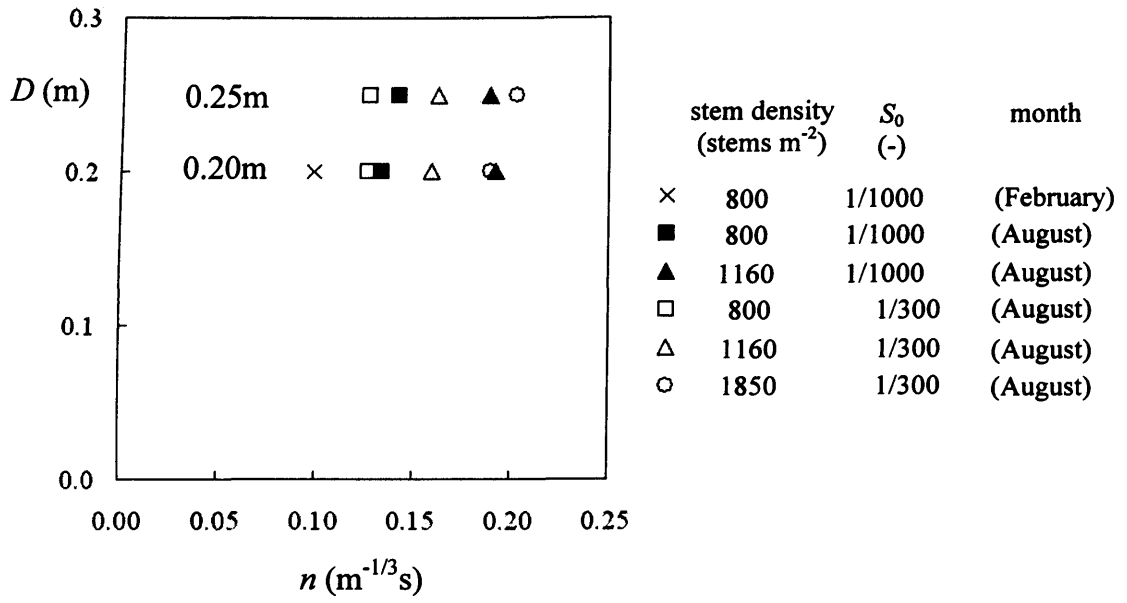

Figure 7-6 Manning's roughness coefficients, *n*, for the emergent *Spartina anglica* canopies studied. *D* is the flow depth, *H* is the submergence level and S_0 is the bed gradient.

7.2.2.2 Coefficients for Submerged Conditions

Drag and roughness coefficients are presented for submerged canopies in Figure 7-7c and Figure 7-7d respectively for submergence levels of 1.33, 2.00 and 3.00. There was a large increase in the projected area component, BLD/A_p with submergence level, H (see Figure 7-7a; B, L, and D are the lateral width, longitudinal length and vertical depth of the flow volume respectively, and A_p is the total projected area of obstruction). The parameter BLD/A_p is effectively the reciprocal of the projected area per unit volume ($1/\overline{a}^2$) of which the bulk drag coefficient is a function (refer to Equation 2.28). Meanwhile, the velocity component, $1/U_C^2$, demonstrated a significant decrease in magnitude with submergence level (see Figure 7-7b; U_C is the depth averaged velocity for the canopy layer). The bulk drag cefficient is also a function of the reciprocal velocity parameter $1/U_C^2$.

Despite the large projected areas of obstruction and high stem densities of the canopies investigated, the volume of the plants were negligible compared to the volume of the flow (Section 3.4.5). Subtraction of the former from the latter had no significant effect of the values of the coefficients $\overline{C_D}$ and $\overline{C_D}'$. The longitudinal weight component of the water volume in the flow direction for a given flow depth

was approximately equal for different stem densities because the porosities of the 800, 1160 and 1850 stems m^{-2} canopies were close to unity (see Section 3.4.5).

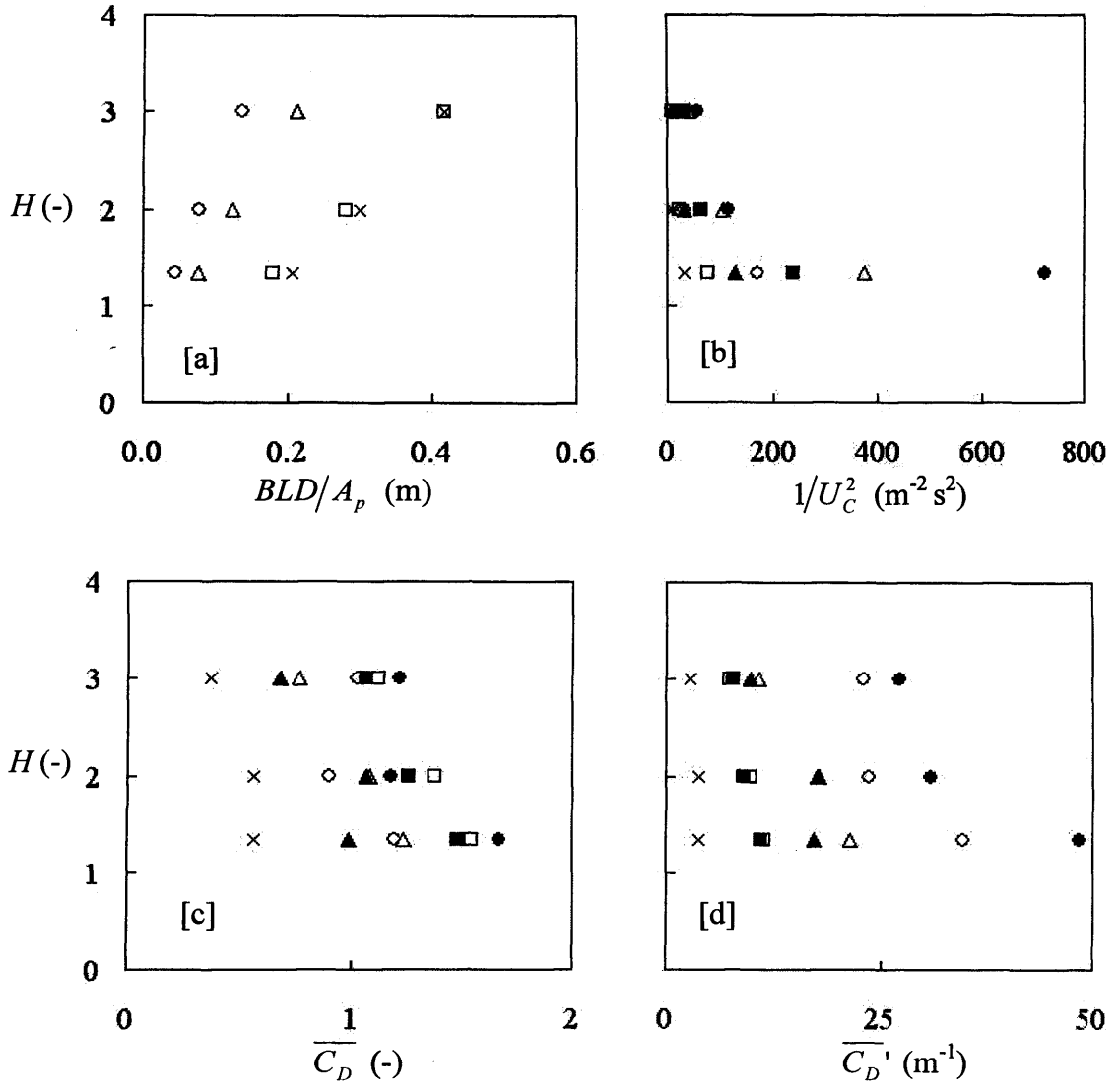

Stem Density (stems m^{-2})	S_0 (-)	Month	Stem Density (stems m^{-2})	S_0 (-)	Month
× 800	1/1000	February			
■ 800	1/1000	August	□ 800	1/300	August
▲ 1160	1/1000	August	△ 1160	1/300	August
● 1850	1/1000	August	◇ 1850	1/300	August

Figure 7-7 Parameters used for the calculations of the one-dimensional bulk drag coefficient, $\overline{C_D}$, and the one-dimensional bulk roughness coefficient, $\overline{C_D}'$, for submerged *Spartina anglica* canopies at submergence levels, *H*, of 1.33, 2.00 and 3.00, at bed gradients of 1/1000 and 1/300, stem densities of 800, 1160 and 1850 stems m^{-2}, and vegetation collected during the months of August and February. A_p is the total projected area of obstruction, BLD is the unit flow volume, where B is the flow width, L is the length longitudinal reach, and D is the flow depth, U_C is the depth-averaged velocity through the canopy layer, and S_0 is the bed gradient.

Values of the Manning's roughness coefficient, n, (Section 2.1.1), are presented in Figure 7-8 for the submerged canopies studied. As observed for the emergent conditions in Section 7.2.2.1, Manning's n increased with increasing stem density for a given bed slope with values ranging between 0.02 and 0.15 for August vegetation canopies, but values decreased with increasing submergence level. This is attributed in part to the cropping of the vegetation and reducing the canopy height to achieve a higher submergence level (see Section 5.2.4.2). The lowest values were observed for the February vegetation canopies ranging between 0.02 and 0.06. The Manning's n values calculated for the constructed vegetation canopies were usually within the range of values documented by Chow (1959) for floodplains covered by brush (bushes and shrubs), which was between 0.035 and 0.160 depending on the density of the brush and the time of year.

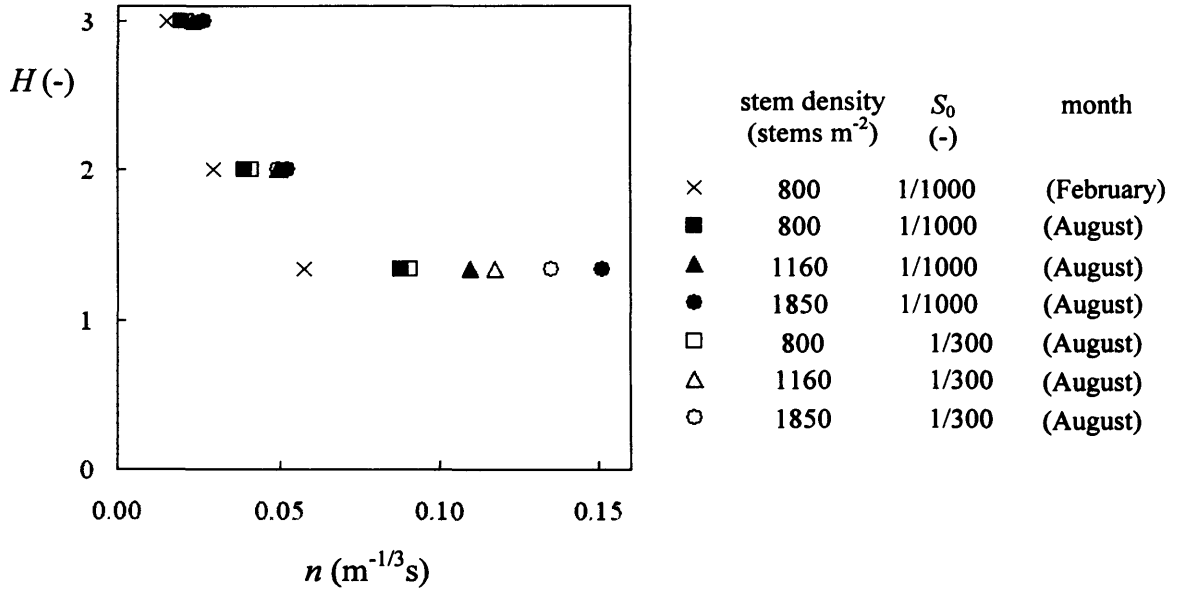

Figure 7-8 Manning's roughness coefficients, n, for the submerged *Spartina anglica* canopies studied. D is the flow depth, H is the submergence level (D/T) and S_0 is the bed gradient.

7.2.3 The $\overline{C_D'}$ - Re_T Relationship

Based on the concept of the drag coefficient – Reynolds number curve for a single cylinder (see Section 2.2.3), Wu *et al.* (1999) produced similar relationship curves for vegetation canopies. The authors replaced the drag coefficient for a single cylinder, C_D, for a roughness coefficient, $\overline{C_D'}$ (Equation 2.19). The roughness

coefficient is more conveniently applied to vegetation canopies, particularly where the projected area is difficult to determine or is unknown. The $\overline{C_D}'$-Re_T curve was discussed in Section 2.3.6, and the concept is applied here to the *Spartina anglica* canopies implemented in the present study.

Based on the flow data collected for the stage-discharge curves (see Section 7.2.1.1), $\overline{C_D}'$-Re_T curves are presented in Figure 7-9 for emergent *Spartina anglica* canopies. An increase in stem density resulted in an upward shift of the $\overline{C_D}'$-Re_T curves indicating a higher drag coefficient for a given Reynolds number. This can be attributed to a greater drag force due to a greater amount of vegetation material. However, for all the emergent canopies considered, there was little variation in the roughness coefficient with changing Reynolds number for the range of Reynolds numbers examined.

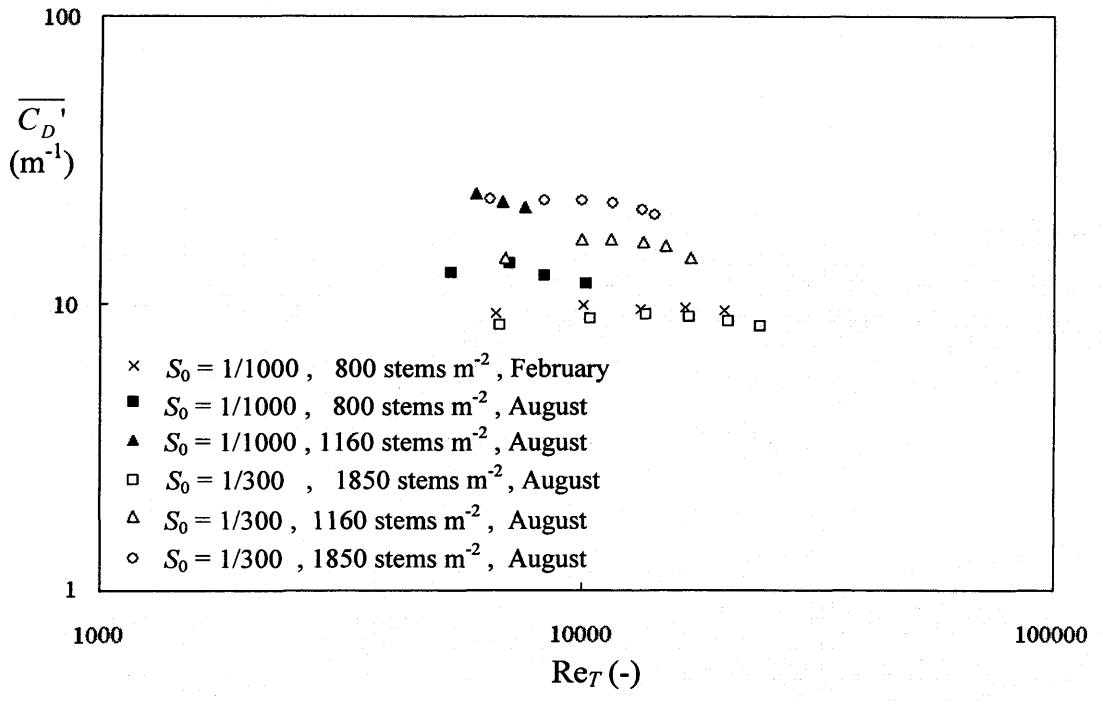

Figure 7-9 The relationship between the bulk roughness coefficient, $\overline{C_D}'$, and the canopy height Reynolds number, Re_T, for the emergent *Spartina anglica* canopies implemented in this study. S_0 is the bed gradient.

To characterise the $\overline{C_D}'$-Re_T relationships for different canopies, Wu *et al.* (1999) proposed comparing values of the exponent of the curves, k, as given in Equation 2.32. Wu *et al.* (1999) suggested the exponent, k, is specific to the vegetation type. k is a useful parameter because it enables the calculation of the bulk roughness coefficient for a given Reynolds number.

Values of k calculated for the emergent *Spartina anglica* canopies examined are presented in Table 7-6. The k values indicate that within the range of Reynolds numbers examined, asymptotic values were reached for a number of experiments where k is equal to or approximately zero. These include the experiments on the February vegetation canopy (bed gradient of 0.001 and stem density of 800 stems m^{-2}), and for some of the August vegetation canopies (bed gradient of 0.003 and stem densities of 1160 and 1850 stems m^{-2}).

Table 7-6 Values of the exponent, *k*, for emergent *Spartina anglica* canopies

	Bed Slope (-)	Stem Density (stems m^{-2})	k (-)
February vegetation	1/1000	800	0.00
August vegetation	1/1000	800	0.46
	1/1000	1160	0.14
	1/300	800	0.15
	1/300	1160	0.00
	1/300	1850	0.00

Wu *et al.* (1999) and later, Tsihrintzis *et al.* (2001), produced $\overline{C_D}'$-Re_T plots for a wide range of natural and artificial canopies from a number of different studies (see Section 2.3.6). The $\overline{C_D}'$-Re_T relationships produced for the wheat canopies investigated by Turner and Chanmeesri (1984) were of closest resemblance to the canopies in this study (see Figure 7-10). The wheat canopies had similar stem densities, ranging between 1020 and 2190 stems m^{-2}, to the stem densities implemented in this study. k values for the wheat canopies ranged between values of 0.33 and 0.52. Pine and cedar tree saplings investigated by Fathi-Maghadam and Kouwen (1997) resulted in similar k values ranging between 0.20 and 0.77. But otherwise, k values determined for the *Spartina anglica* canopies in this study were considerably lower compared to values for most of the emergent canopies presented by Wu *et al.* (1999) and Tsihrintzis *et al.* (2001) (see Section 2.3.6). The lower k values observed in this study correspond to a smaller variation in $\overline{C_D}'$ with Reynolds

number. This may be associated with the dense vegetation arrays implemented, since the stem densities examined were considerably higher than many of the canopies presented by the aforementioned authors, as well as the high Reynolds numbers implemented.

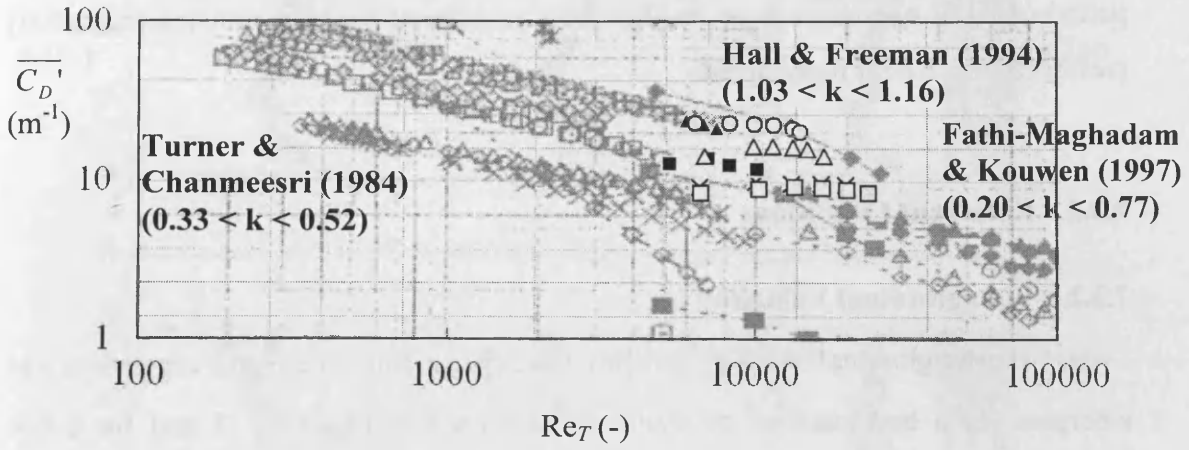

Figure 7-10 The relationship between the bulk roughness coefficient, $\overline{C_D}'$, and the canopy height Reynolds number, Re_T, for the emergent *Spartina anglica* canopies implemented in this study and some of the data presented in Tsihrintzis *et al.* (2001). S_0 is the bed gradient.

In keeping with Tsihrintzis *et al.* (2001), for the data from the present study, an increase in stem density resulted in a vertical upward shift in the $\overline{C_D}'$-Re_T curve (for a given Reynolds number, a higher $\overline{C_D}'$ value was observed). However in disagreement with Tsihrintzis *et al.* (2001), data from this study shows that the parameter k is affected by stem density. The parameter k decreases with increasing stem density (see Table 7-6). This implies that for denser canopies, there would be less variation in the drag coefficient with Reynolds number. This is supported by other data sets, for example the data set for Wheat crops from Turner and Chanmeesri (1984).

7.3 Two-Dimensional Measurements

7.3.1 Double-Averaged Parameters

Velocity and turbulence parameters are calculated based on measurements averaged spatially along the flume length as well as temporally over the three minute period of ADV operation. Four profiles were monitored for each constructed canopy (see Section 5.2.7 for more detail).

7.3.2 Emergent Conditions

7.3.2.1 Longitudinal Velocities

The longitudinal velocity profiles for experiments where the vegetation was emergent for a bed gradient of $0.00\dot{3}$ is presented in Figure 7-11 and for a bed gradient of 0.001 in Figure 7-12. The longitudinal velocities for the emergent condition were relatively constant over the flow depth compared to the submerged cases presented later in Section 7.3.3.1. Fluctuations in velocity magnitudes over the height of the canopy are attributed to the variation in the level of obstruction due to different 'concentrations' of plant material with elevation. The longitudinal velocity profiles for each of the two bed gradients examined contain similar features in the form of maxima and minima for any given stem density, regardless of the flow depth. For the steeper gradient ($0.00\dot{3}$), the experiments were conducted at considerably larger flow rates (see the stage-discharge relationships shown in Figure 7-1), the overall velocities were significantly higher, and such features in the profiles were much more pronounced.

Over the height of the canopy, the vegetation varied in material properties (e.g. modulus of elasticity, see Figure 3.27), in the quantity of plant material per unit volume (e.g. projected area per unit volume and mass of material, see Figure 3.7), and 'type' of plant material. In the upper, 'leafy' part of the canopy, the vegetation was thinner and more flexible, but also much larger in surface area. The smaller frontal area of the stem region near the bed created less physical obstruction, and hence, flow velocities were greater when compared to velocities at the mid-flow depth. Projected area per unit volume profiles are shown in Figure 7-13 for the three stem densities of

800, 1160 and 1850 stems m-2 of *Spartina anglica* canopies which were considered in Figure 7-11 and Figure 7-12.

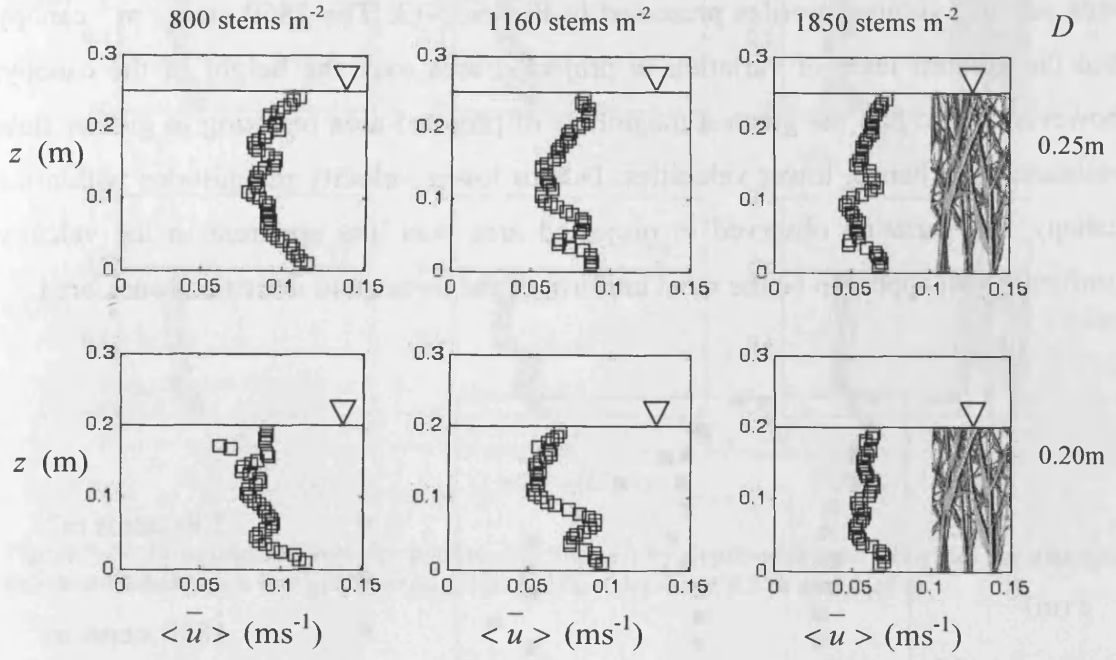

Figure 7-11 Longitudinal velocity profiles for emergent flow and a bed gradient of 1/300 for flow depths of 0.2 m and 0.25 m.

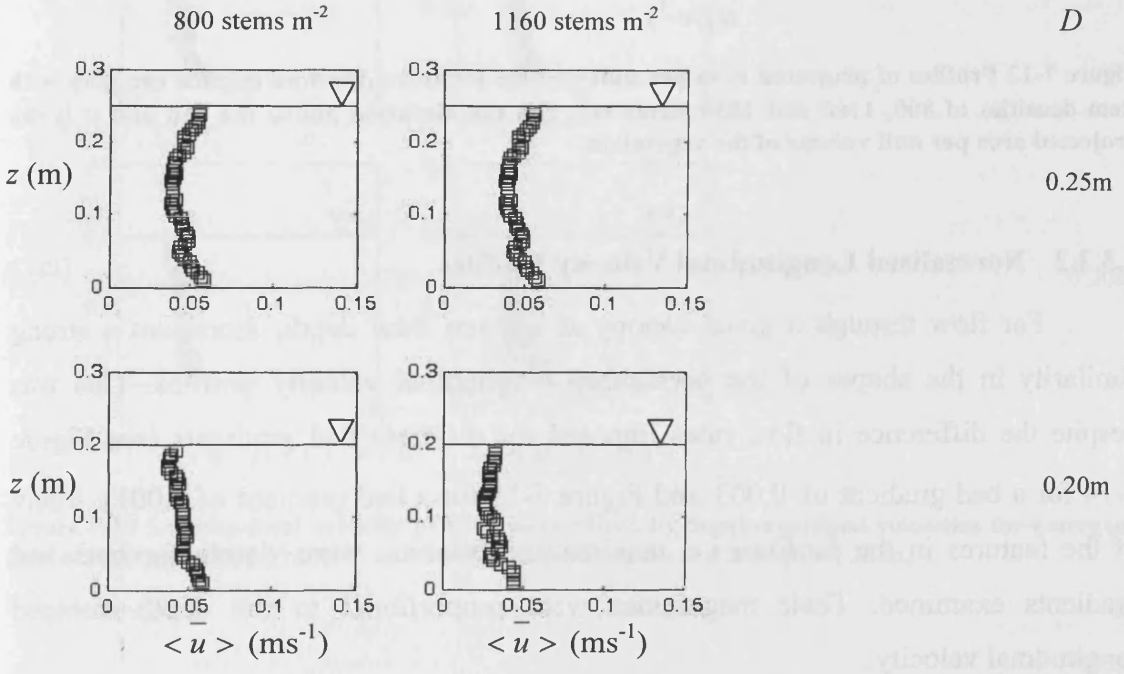

Figure 7-12 Longitudinal velocity profiles for emergent flow and a bed gradient of 1/1000 for flow depths of 0.2 m and 0.25 m.

Differences in the profile shapes between the three stem densities are attributed to the variation in the vegetation samples used to construct each canopy. The vegetation was highly heterogeneous in nature, as demonstrated by the projected area per unit volume profiles presented in Figure 7-13. The 1850 stems m^{-2} canopy had the greatest level of variation in projected area over the height of the canopy, however, it also had the greatest magnitude of projeted area resulting in greater flow resistance and hence, lower velocities. Due to lower velocity magnitudes within the canopy, the variation observed in projected area was less apparent in the velocity profiles which appear to be the most uniform of the three stem densities considered.

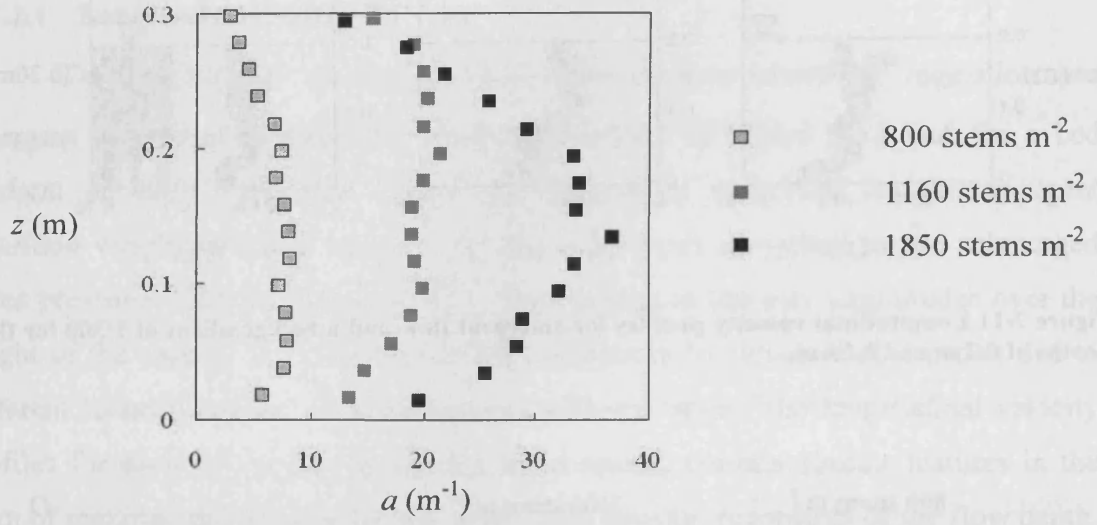

Figure 7-13 Profiles of projected area per unit volume for three *Spartina anglica* canopies with stem densities of 800, 1160 and 1850 stems m^{-2}. z is the elevation above the bed and a is the projected area per unit volume of the vegetation.

7.3.2.2 Normalised Longitudinal Velocity Profiles

For flow through a given canopy at a given flow depth, there was a strong similarity in the shapes of the normalised longitudinal velocity profiles. This was despite the difference in flow rates imposed for different bed gradients (see Figure 7-14 for a bed gradient of $0.00\dot{3}$ and Figure 7-15 for a bed gradient of 0.001). Many of the features in the profiles, i.e. maxima and minima, were visible for both bed gradients examined. Their magnitudes were proportional to the depth-averaged longitudinal velocity.

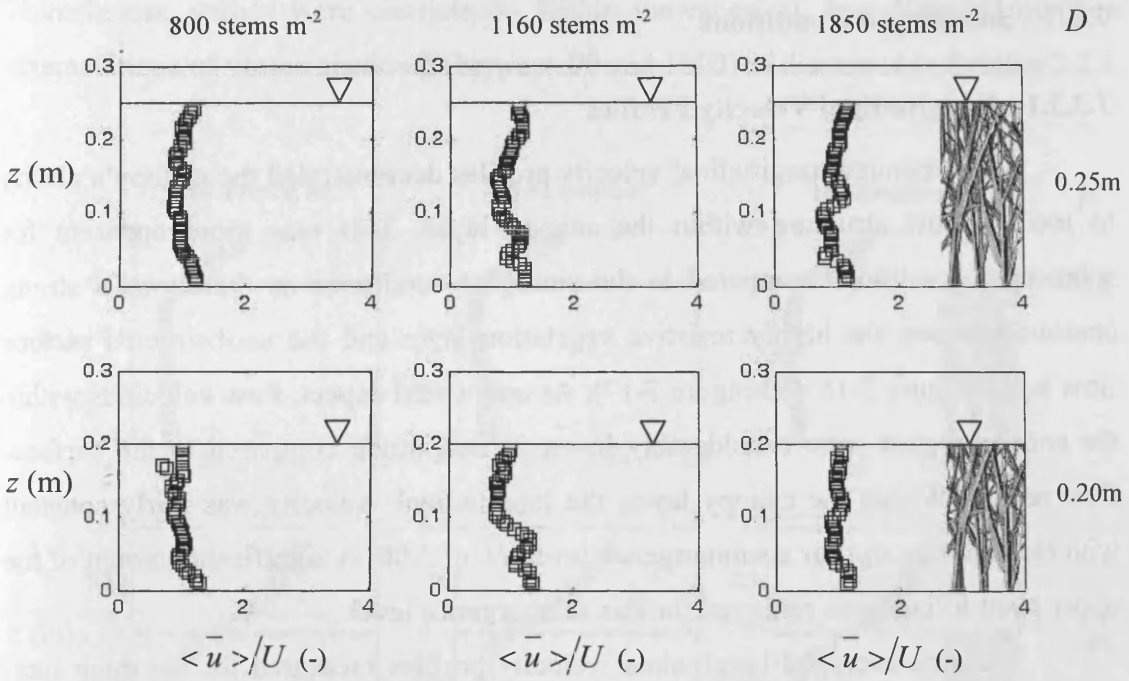

Figure 7-14 Longitudinal velocity profiles normalised by depth-averaged velocities for emergent flow conditions and a bed gradient of 1/300 for flow depths of 0.2 m and 0.25 m.

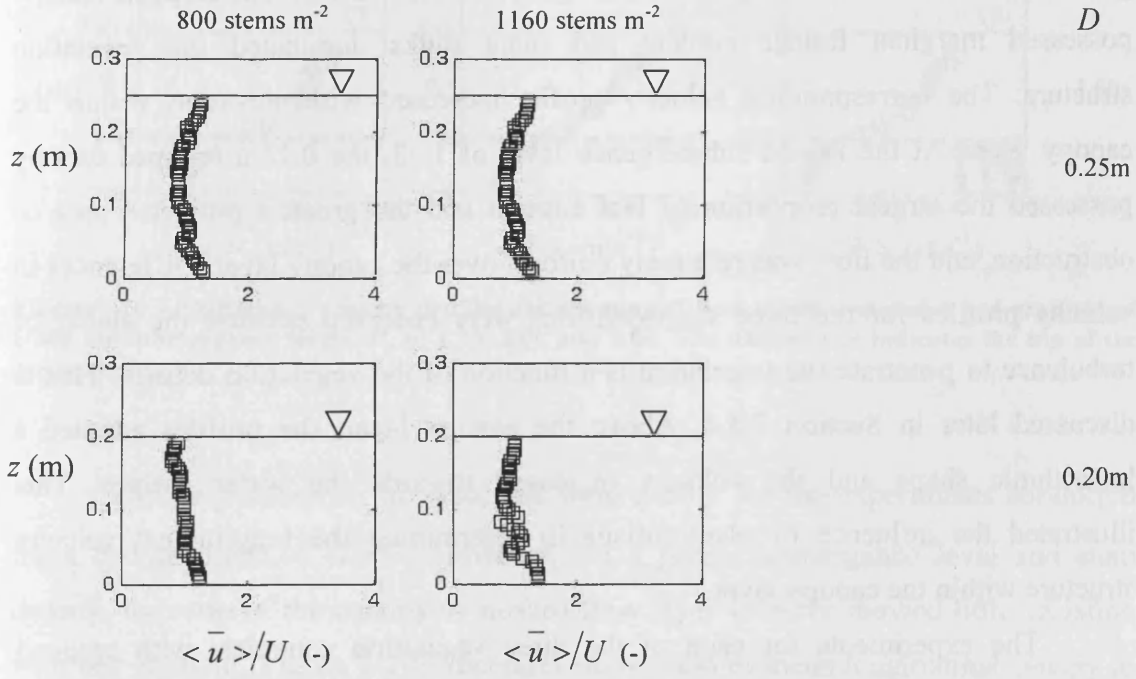

Figure 7-15 Longitudinal velocity profiles normalised by depth-averaged velocities for emergent flow conditions, a bed gradient of 1/1000 and flow depths of 0.2 m and 0.25 m.

7.3.3 Submerged Conditions

7.3.3.1 Longitudinal Velocity Profiles

The measured longitudinal velocity profiles demonstrated the canopy's ability to modify flow structure within the canopy layer. This was more apparent for submerged conditions compared to the emergent conditions as there was a strong contrast between the highly resistive vegetation layer and the unobstructed surface flow layer (Figure 7-16 and Figure 7-17). As one would expect, flow velocities within the canopy region were considerably lower in magnitude compared to the surface-flow region. Within the canopy layer, the longitudinal velocity was fairly constant with elevation except for a submergence level, H, of 3.00. A significant amount of the upper plant foliage was removed for this submergence level.

The time-averaged longitudinal velocity profiles measured for the three stem densities (800, 1160 and 1850 stems m^{-2}) and the three submergence levels are presented in Figure 7-16 for a bed gradient of 0.00$\dot{3}$ and in Figure 7-17 for a bed gradient of 0.001. For the highest submergence of 3.00, the 0.05m cropped canopy possessed marginal foliage content and plant stalks dominated the vegetation structure. The corresponding velocity profile increased with elevation within the canopy layer. At the lowest submergence level of 1.33, the 0.15m cropped canopy possessed the largest proportion of leaf content and the greatest projected area of obstruction, and the flow was relatively uniform over the canopy layer. Differences in velocity profiles for the three stem densities were observed because the ability of turbulence to penetrate the vegetation is a function of the vegetation density. This is discussed later in Section 7.4.4. Above the canopy layer, the profiles adopted a logarithmic shape and the velocity increased towards the water surface. This illustrated the influence of plant foliage in determining the longitudinal velocity structure within the canopy layer.

The experiments for each of the three vegetation canopies, with cropped canopy heights of 0.05 m, 0.10 m and 0.15 m, were performed for two different bed slope conditions (Figure 7-17 and Figure 7-16). This is reflected in the Reynolds number ranges for which the experiments were conducted (Figure 7-18). As would be expected for a given submergence, the stem Reynolds numbers are shown to increase with increasing bed slope. Furthermore the stem Reynolds numbers increase with increasing degree of submergence and decrease with increasing stem density.

Nonetheless, values were consistently within the range of stem Reynold numbers characteristic of vortex shedding (between 90 and 1000) as discussed in Section 2.2.3.

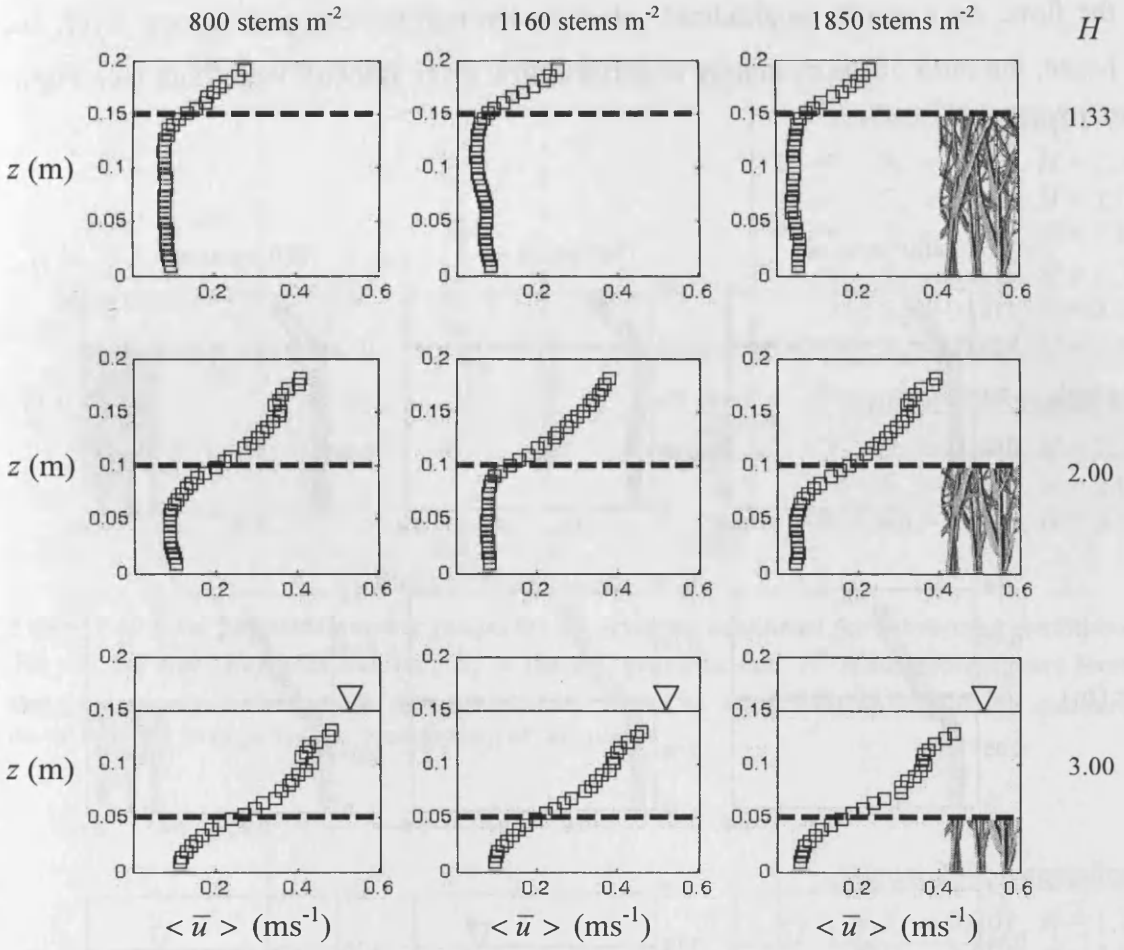

Figure 7-16 Longitudinal velocity profiles for submerged flow conditions and a bed gradient of 1/300 for submergence levels, *H*, of 1.33, 2.00 and 3.00. The dashed line indicates the top of the cropped canopy.

The magnitudes of the velocities were greater for the experiments conducted for a bed gradient of $0.00\dot{3}$. However, for a given submergence level and stem density, the ratio of the canopy to surface flow layer velocity showed little variation with bed gradient (Figure 7-19). Increases in the ratio of mean longitudinal canopy to surface flow layer velocities were inconsistent with the order of submergence levels for each stem density. This was due to a significant modification of the canopy morphologies with increasing submergence level by cropping the vegetation (see Section 5.2.4.2). Due to the vertical variability of the vegetation (see Section 3.4.4), with each reduction of the cropped canopy height, a significant proportion of the

canopy foliage was removed. Consequently, for the highest submergence level of 3.00, the mean projected area of the cropped canopy was significantly lower than the lower submergence levels (1.33 and 2.00) and the canopy created less obstruction to the flow. As a result, longitudinal velocities through the cropped canopy layer, and hence, the ratio of mean canopy to surface flow layer velocity were high (see Figure 7-19).

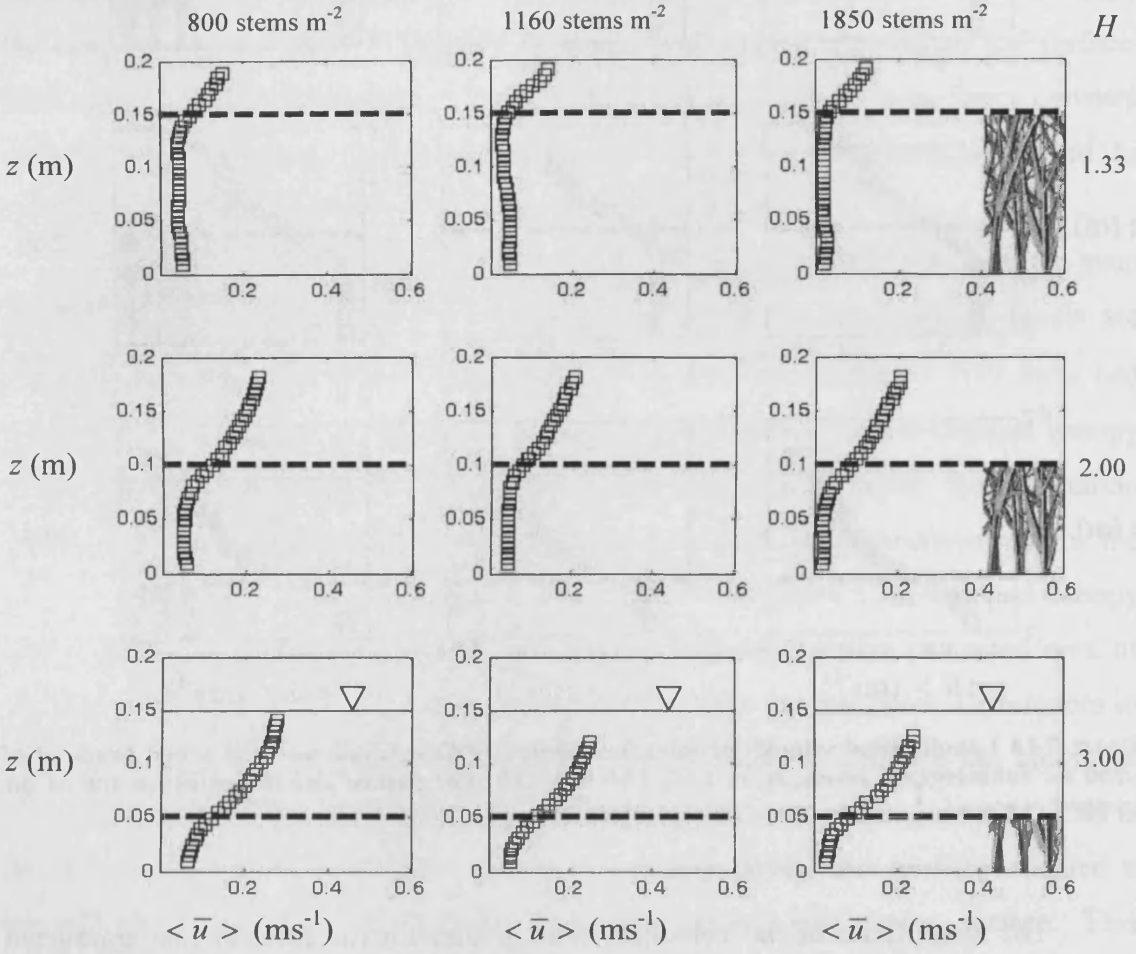

Figure 7-17 Longitudinal velocity profiles for submerged flow conditions and a bed gradient of 1/1000 for submergence levels, *H*, of 1.33, 2.00 and 3.00. The dashed line indicates the top of the cropped canopy.

For some of the experiments shown in Figure 7-16, a 'kink' in the longitudinal velocity profiles was observed near the water surface. This was observed for most of the experiments conducted for the higher submergence levels of 2.00 and 3.00 and for a bed gradient of $0.00\dot{3}$; these experiments being where the longitudinal velocities were highest. Higher surface flow velocities, particularly near the water surface, resulted in higher Reynolds numbers. This can also be seen in higher values of the

fluctuating component of the vertical velocity, *w'*, which is presented later in Section 7.4.5.2. Hence, a turbulent coherent structure may have been the cause for the aforementioned inconsistencies in the longitudinal velocity profiles.

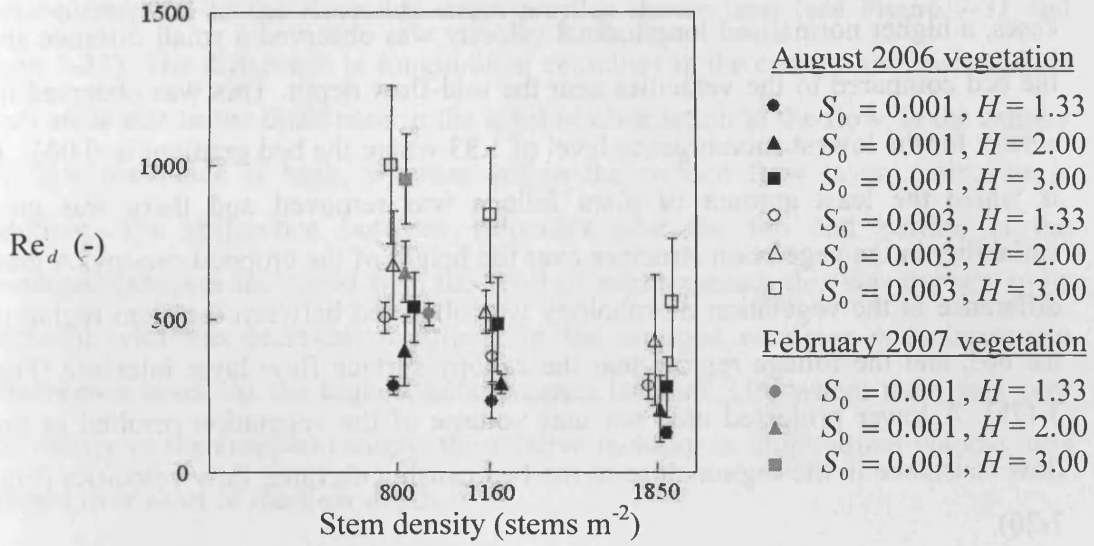

Figure 7-18 Stem Reynolds number ranges for experiments conducted for submerged conditions. Re_d is the stem Reynolds number, S_0 is the bed gradient, and H is the submergence level. Data points were offset about the stem density values to avoid overlapping of the standard deviation bars to improve the presentation of this plot.

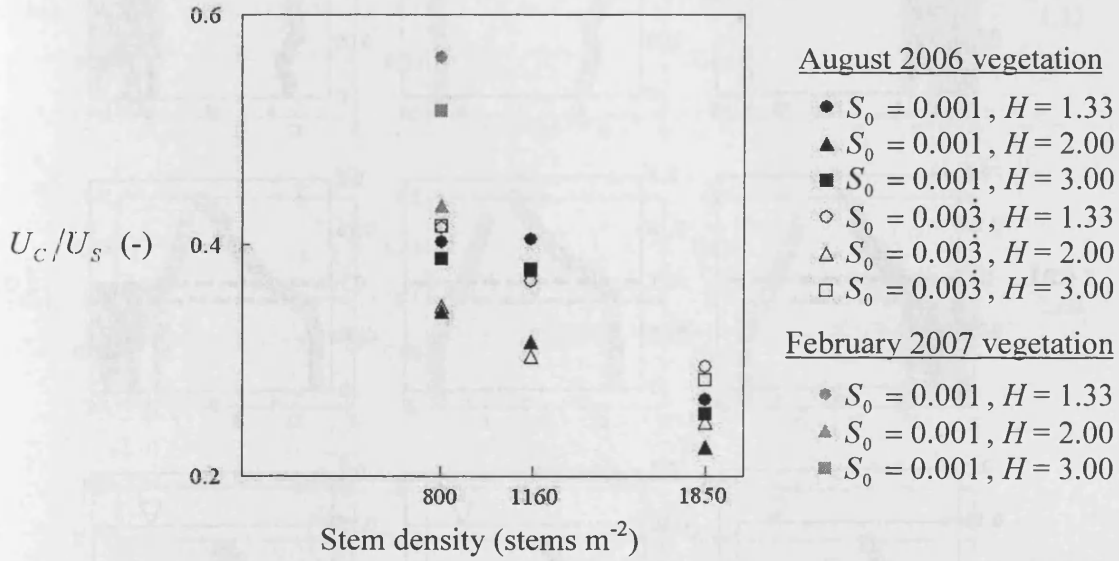

Figure 7-19 The ratio of the depth-averaged velocity within the canopy layer, U_C, to that within the surface flow layer, U_S, for experiments conducted under submerged conditions. S_0 is the bed gradient, and H is the submergence level.

7.3.3.2 Normalised Longitudinal Velocity Profiles

The similarity in shape between the longitudinal velocity profiles for the two bed slopes of $0.00\dot{3}$ and 0.001 for a given submergence level can be seen in the normalised profiles presented in Figure 7-20 and Figure 7-21 respectively. For some cases, a higher normalised longitudinal velocity was observed a small distance above the bed compared to the velocities near the mid-flow depth. This was observed most clearly for the lowest submergence level of 1.33 where the bed gradient is $0.00\dot{3}$. This is where the least amount of plant foliage was removed and there was greater variability in the vegetation structure over the height of the cropped canopy. A greater difference in the vegetation morphology was observed between the stem region near the bed, and the foliage region near the canopy-surface flow layer interface (Figure 3.17b). A lower projected area per unit volume of the vegetation resulted in lower flow resistance in the region close to the bed causing elevated flow velocities (Figure 7-20).

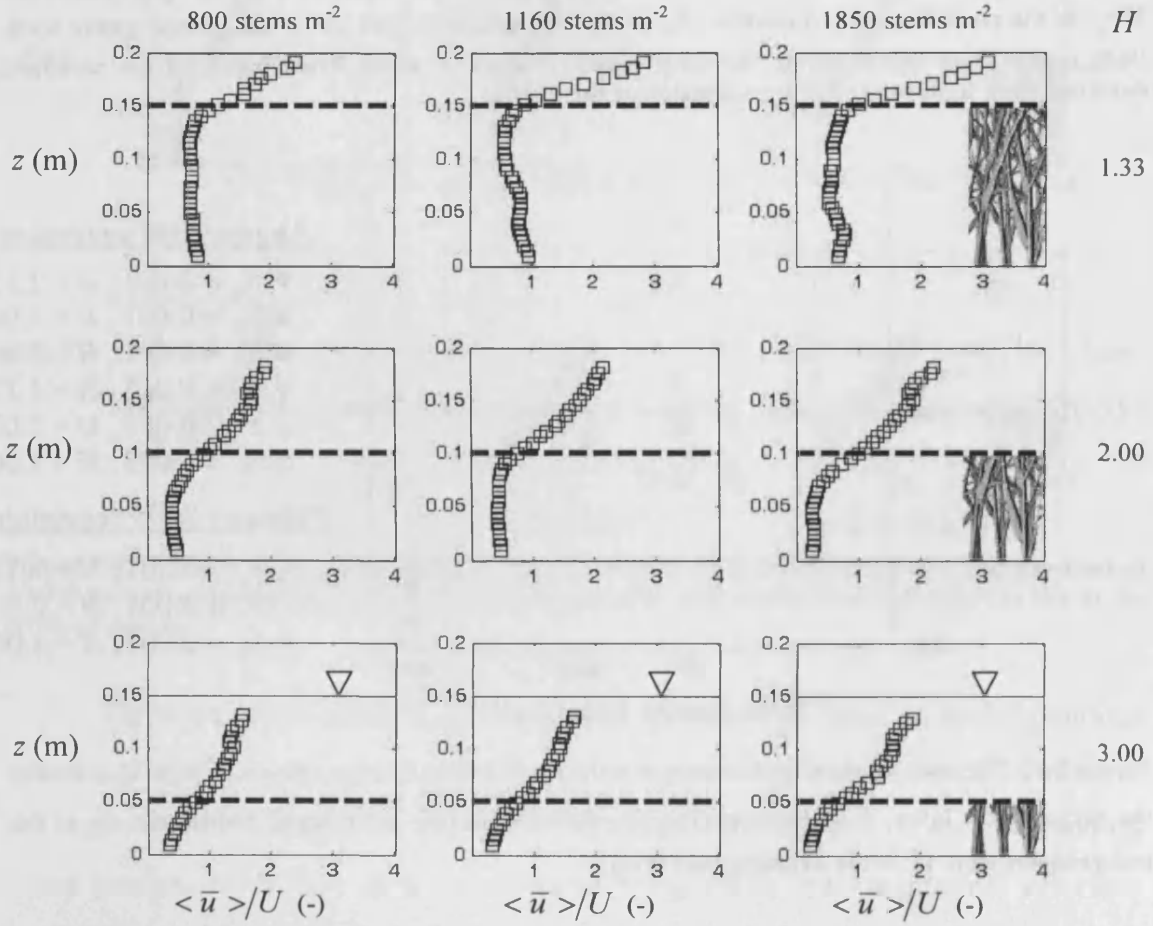

Figure 7-20 Longitudinal velocity profiles normalised by the depth-averaged longitudinal velocities for submerged flow conditions and a bed gradient of 1/300 for submergence levels, *H*, of 1.33, 2.00 and 3.00. The dashed line indicates the top of the vegetation layer.

Near the top of the vegetation, there were considerably large Reynolds stresses in the flow due to a relatively steeper velocity gradient across the canopy-surface flow layer interface for submerged conditions. Gradient profiles for the longitudinal velocity are presented in Figure 7-22 for a bed gradient of 0.001 to illustrate this. These correspond to the Reynolds stress profiles shown later (see Figure 7-31 and Figure 7-32). The difference in longitudinal velocities in the canopy and surface flow layers arose due to the difference in the level of obstruction to the flow; at the canopy top, flow resistance is high, whereas within the surface flow layer, resistance is negligible. The difference between velocities near the top and bottom of the submerged canopies increased with the level of submergence; this was thought to be associated with the decrease of foliage in the cropped canopies with increasing submergence level. At the highest submergence level of 3.00 where there was very little foliage in the cropped canopy, the relative increase in longitudinal velocity was apparent over most of the flow depth.

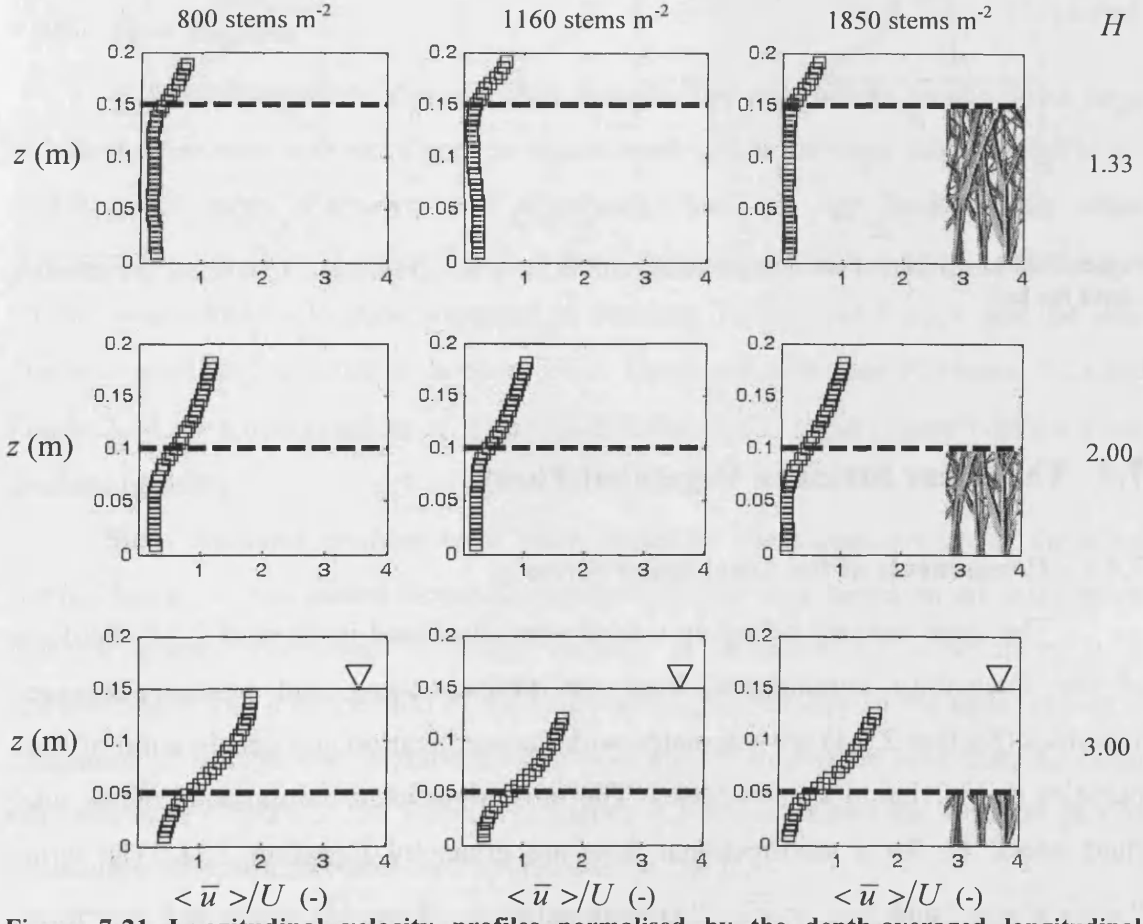

Figure 7-21 Longitudinal velocity profiles normalised by the depth-averaged longitudinal velocities for submerged flow conditions and a bed gradient of 1/1000 for submergence levels, *H*, of 1.33, 2.00 and 3.00. The dashed line indicates the top of the vegetation layer.

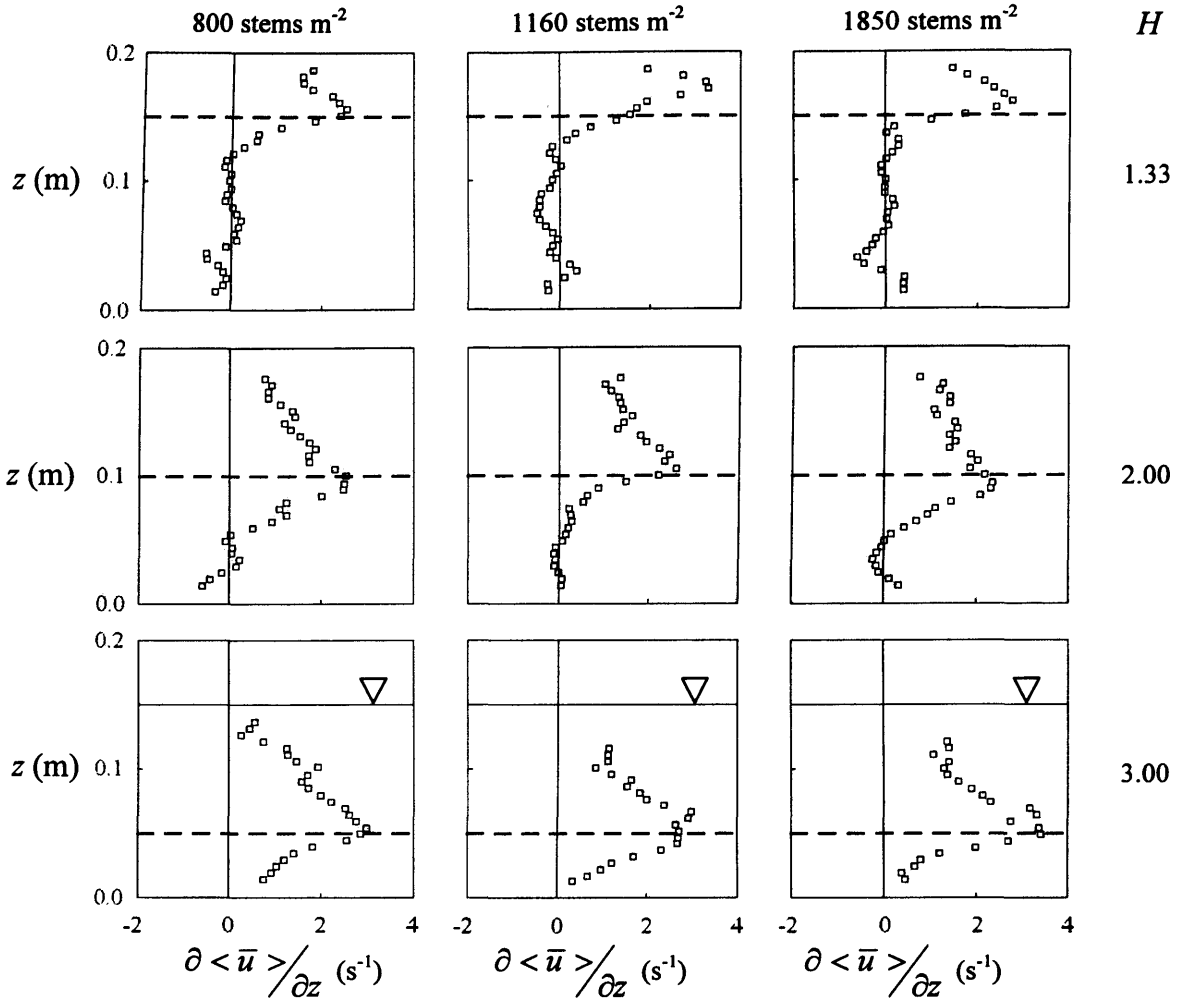

Figure 7-22 Longitudinal velocity gradient profiles for a bed gradient of 1/1000. z is the elevation above the bed.

7.4 The Shear Stress in Vegetated Flows

7.4.1 Components of the Total Shear Stress

The shear stresses acting on a fluid were discussed in Section 2.5.2. Products of the fluctuating components from the time-averaged and spatially-averaged velocities (Section 2.3.1) are associated with the acceleration and deceleration of fluid particles giving rise to shear stresses. The most significant components of the total fluid stress, τ, for a unidirectional flow are given by Equation 2.38. The terms "$-\rho < \overline{u'w'} >$" and "$-\rho < \widetilde{\tilde{u}\tilde{w}} >$" correspond to the Reynolds stress and the "form-induced" stress respectively (refer to Section 2.5.2 for an explanation of the different

types of stresses). Where flow is in the laminar regime, such that the stem Reynolds number is below a value of two (Section 2.2.3), the fluid particles move along organised planes around obstructions. Hence, turbulent perturbations in the flow are thought to be non-existent or scarce and the laminar viscous stresses need to be considered. However, for the experimental study presented in this chapter, these were found to be negligible (see Section 7.4.2).

For submerged conditions, the magnitude of the total shear stress, which is dominated by Reynolds stresses, peaks above the canopy (Section 7.4.4). For a comparison between the stresses through different canopies, where Reynolds or "form-induced" stresses were considered, the profiles were normalised by the maximum total fluid stress value over the flow depth, τ_{max}. However, for emergent conditions, Reynolds stresses were considerably smaller in magnitude as observed by Lightbody and Nepf (2006a). These were normalised by the depth-averaged total fluid stress, $\overline{\tau}$.

7.4.2 Flow Regime

Within a vegetation canopy, it is thought that the canopy breaks down large turbulent structures, and turbulence is regenerated within the stem wakes (Nepf *et al.*, 1997b). The stem diameters are commonly used as the length scale when characterising the flow (Section 2.2.1). Stem Reynolds numbers were calculated based on the longitudinal velocities presented in Sections 7.3.2.1 and 7.3.3.1, and the stem diameter profiles presented in Section 3.4.2. These are presented in Figure 7-23 and Figure 7-24 for a bed gradient of $0.00\dot{3}$, and in Figure 7-25 and Figure 7-26 for a bed gradient of 0.001.

Stem diameter profiles used were based on measurements along the plant stems. Hence, the calculated Reynolds number profiles were based on the assumption that the plants resembled cylinders varying in diameter with elevation. It is acknowledged that a proportion of the *Spartina anglica* canopy in the upper region is composed of foliage that is flat and relatively greater in surface area than the basal stem diameter (Figure 3.20). However, diameters were measured for the stem part of the canopy for simplicity and used to characterise the flow.

For the dense vegetated conditions encountered in saltmarsh canopies, where flow velocities are commonly below 0.01 ms^{-1} (Section 2.4.2), flow through the

vegetation is likely to be laminar. However, as explained in Section 2.2.3, based on the range of flow velocities and stem diameters observed along saltmarshes, stem Reynolds numbers are estimated to range between 40 and 600 within the vegetation. Hence, the experiments conducted for this study usually fall within this range. Transition from laminar to turbulent flow occurs over a Reynolds number range that varies depending on the canopy characteristics. Higher values are associated with higher stem densities due to the effects of wake-interference (Section 2.2.6). For a number of cylinder arrays ranging in density between 200 and 2000 stems m^{-2}, Nepf *et al.* (1997b) observed vortex shedding from stem Reynolds numbers between 150 and 200. Based on the upper limit, the flow within the canopy layers in this study was either transitional or turbulent. The transition between laminar and turbulent flow, assumed at a stem Reynolds number of 200 for the stem densities of 800, 1160 and 1850 stems m^{-2} studied, is marked on the plots.

Vortex shedding within the vegetation canopy is assumed to commence around a stem Reynolds value of 200 as observed by Nepf *et al.* (1997b) (Section 2.2.4). Hence, based on the calculated stem Reynolds numbers from the current study, the flow is thought to be turbulent for the experiments conducted for the emergent condition and for a bed gradient of $0.00\dot{3}$ (Figure 7-23). In Figure 7-25, where the experiments were repeated for a bed gradient of 0.001, stem Reynolds numbers were close to the 200 value for most of the flow depths indicating the flow was likely to be in the transitional range.

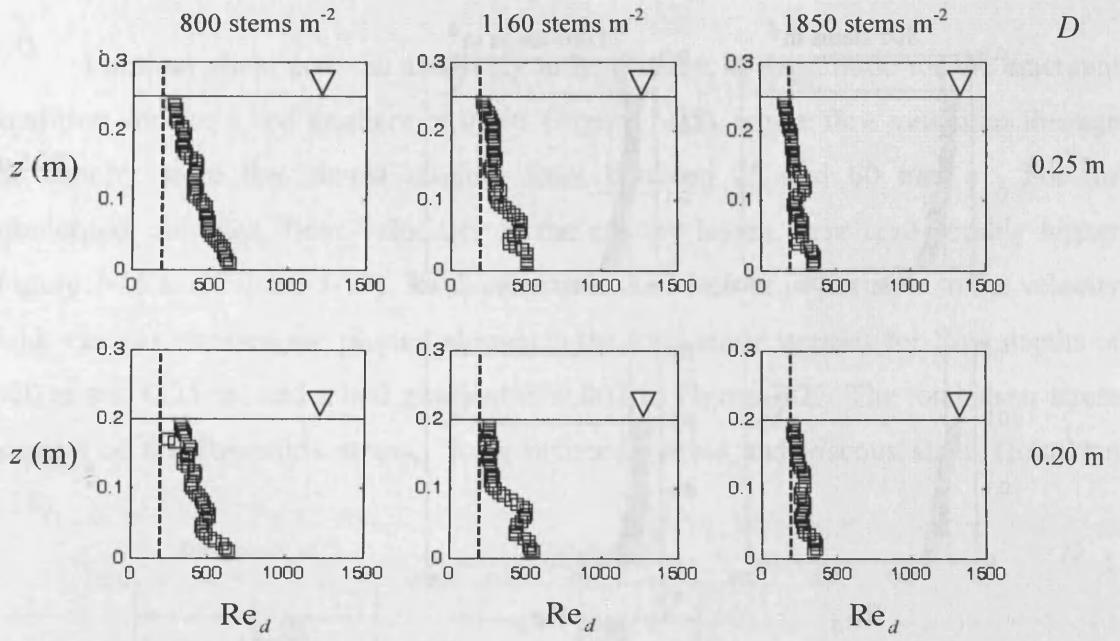

Figure 7-23 Stem Reynolds number profiles for flow through emergent vegetation for three stem densities, flow depths of 0.20 m and 0.25 m and a bed gradient of 1/300. The dashed line marks a stem Reynolds number of 200; the value around which laminar to turbulent transition occurs for dense vegetation.

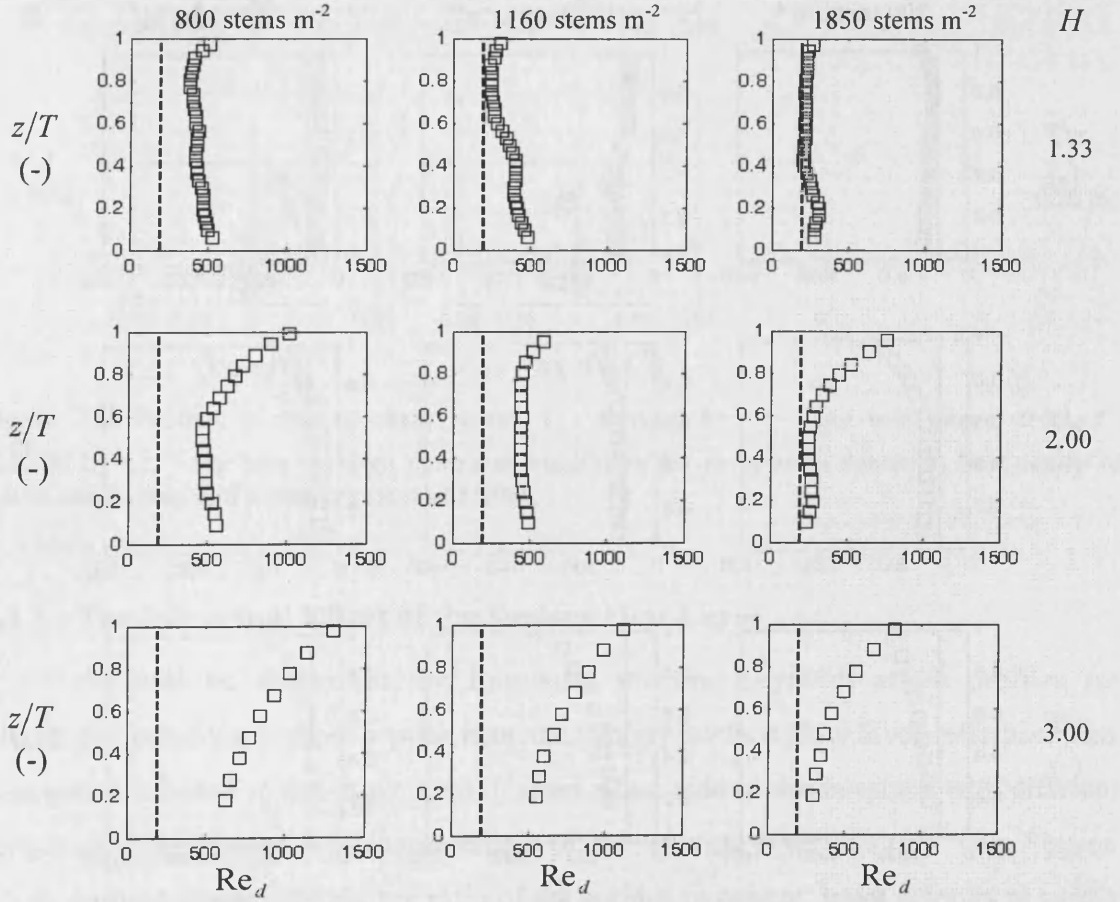

Figure 7-24 Stem Reynolds number profiles for flow through submerged vegetation for three stem densities, submergence levels of 1.33, 2.00 and 3.00, and a bed gradient of 1/300. The dashed line marks a stem Reynolds number of 200; the value around which laminar to turbulent transition occurs for dense vegetation.

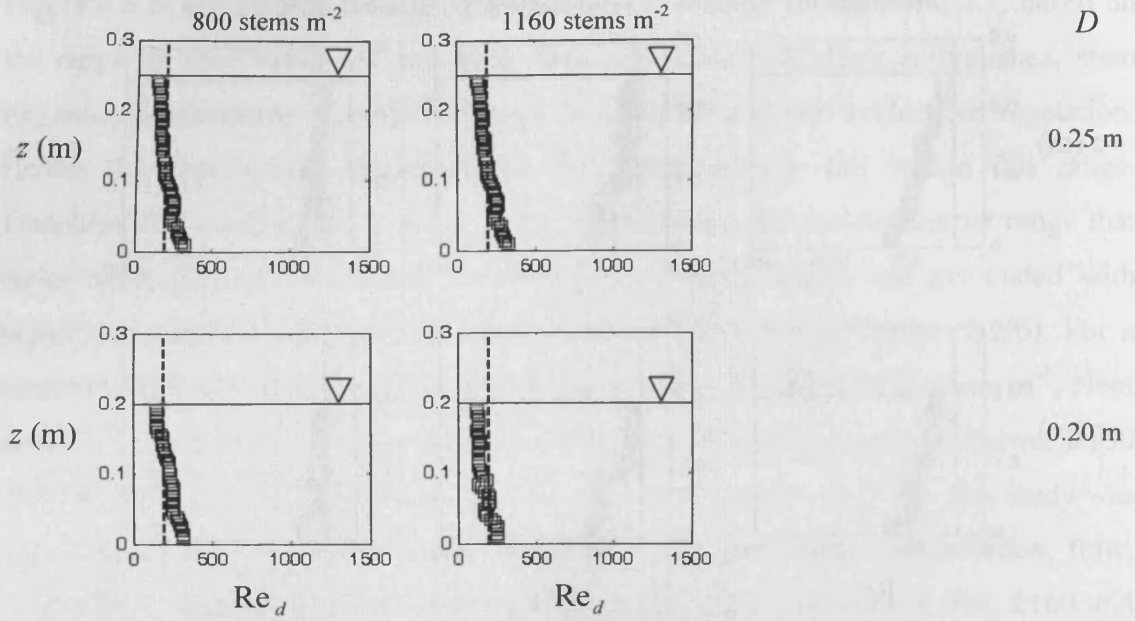

Figure 7-25 Stem Reynolds number profiles for flow through emergent vegetation for three stem densities, flow depths of 0.20 m and 0.25 m and a bed gradient of 1/1000. The dashed line marks a stem Reynolds number of 200; the value around which laminar to turbulent transition occurs for dense vegetation.

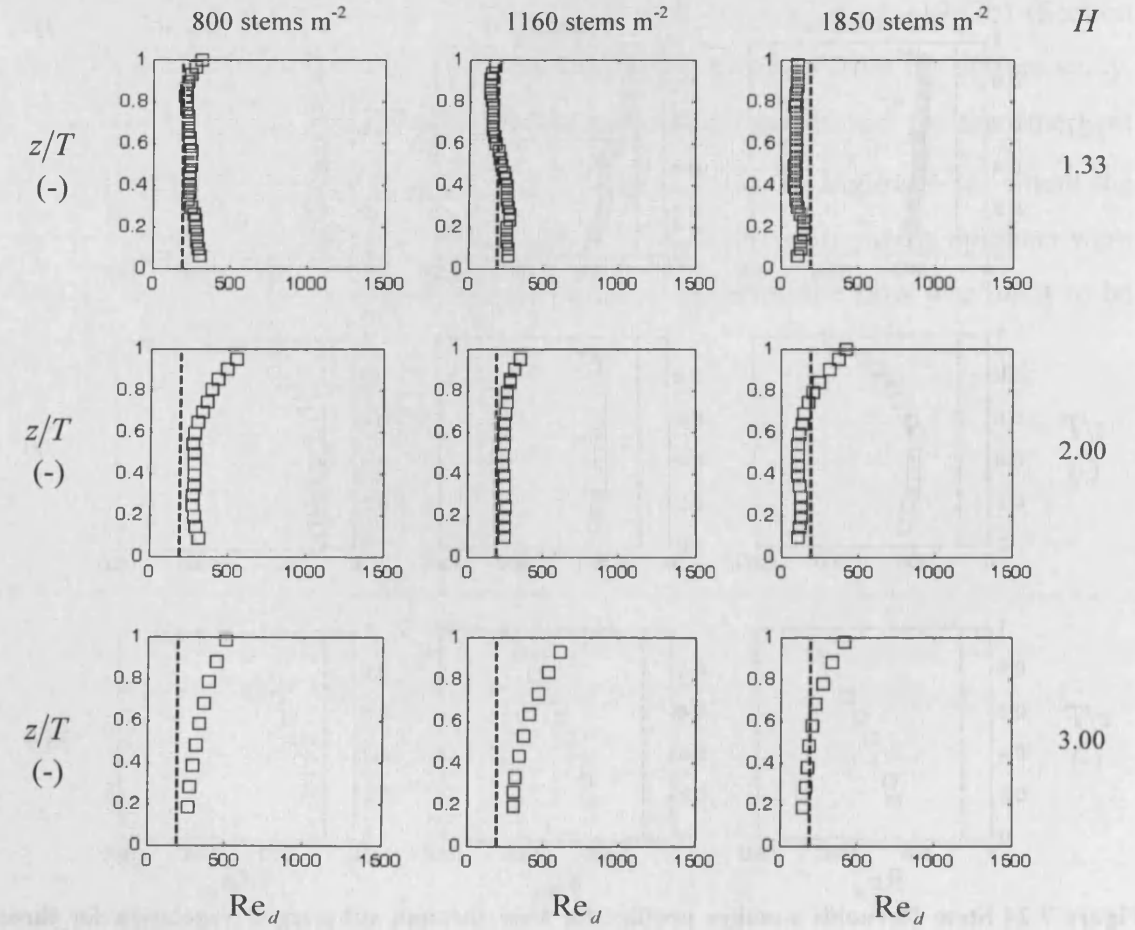

Figure 7-26 Stem Reynolds number profiles for flow through submerged vegetation for three stem densities, submergence levels of 1.33, 2.00 and 3.00, and a bed gradient of 1/1000. The dashed line marks a stem Reynolds number of 200; the value around which laminar to turbulent transition occurs for dense vegetation.

Laminar shear stresses are likely to be greatest in magnitude for the emergent condition and for a bed gradient of 0.001 (Figure 7-25), where flow velocities through the canopy were the lowest ranging from between 25 and 60 mm s^{-1}. For the submerged canopies, flow velocities in the canopy layers were considerably higher (Figure 7-16 and Figure 7-17). To demonstrate their lack of importance to the velocity field, viscous stresses are plotted alongside the total shear stresses for flow depths of 0.20 m and 0.25 m, and a bed gradient of 0.001 in Figure 7-27. The total shear stress consists of the Reynolds stress, "form-induced" stress and viscous stress (Equation 2.38).

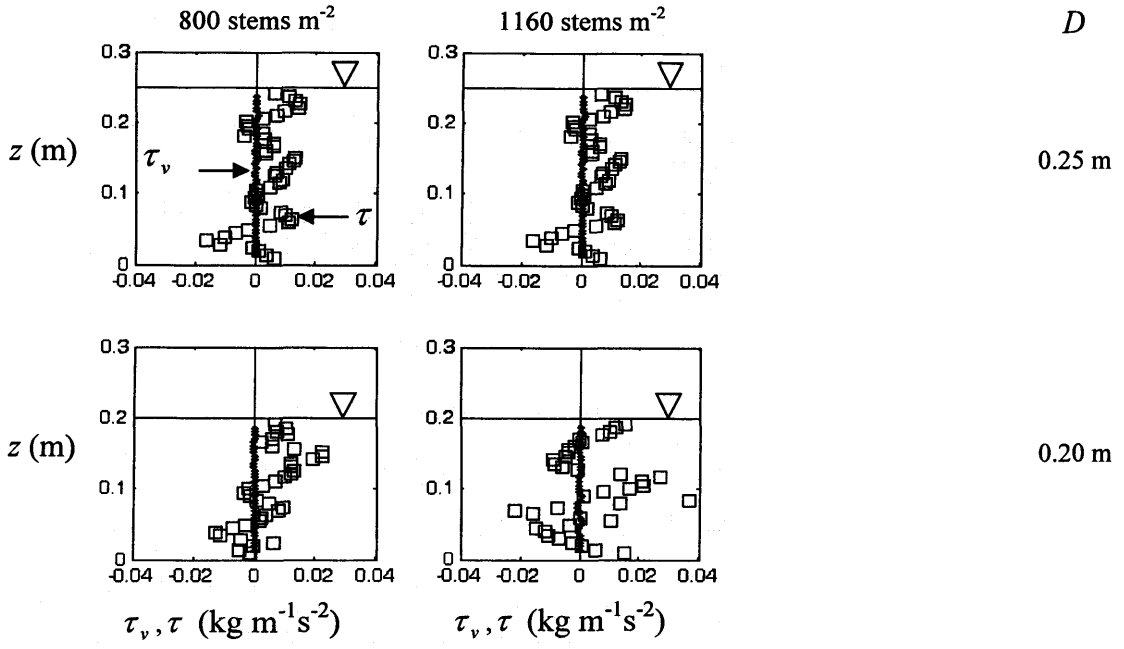

Figure 7-27 Profiles of viscous shear stress, τ_v, denoted by ' • ' and total shear stress, τ, denoted by ' □ ' for flow through emergent vegetation for three stem densities, flow depths of 0.20m and 0.25m, and a bed gradient of 1/1000.

7.4.3 The 'Shearing' Effect of the Surface Flow Layer

As will be shown in the following section, Reynolds stress profiles for submerged conditions show a peak near the canopy-surface flow layer interface. This is largely attributed to the movement of fluid either side of the interface with different velocities. This feature is a characteristic of the 'mixing layer analogy' (see Section 2.5.4). Instead of considering the ratio of the surface to canopy layer velocity to assess the strength of the 'mixing layer', the ratio of the surface layer velocity, U_S, to total

depth averaged velocity, U, presented as functions of the submergence level, H, in Figure 7-28 yielded better results.

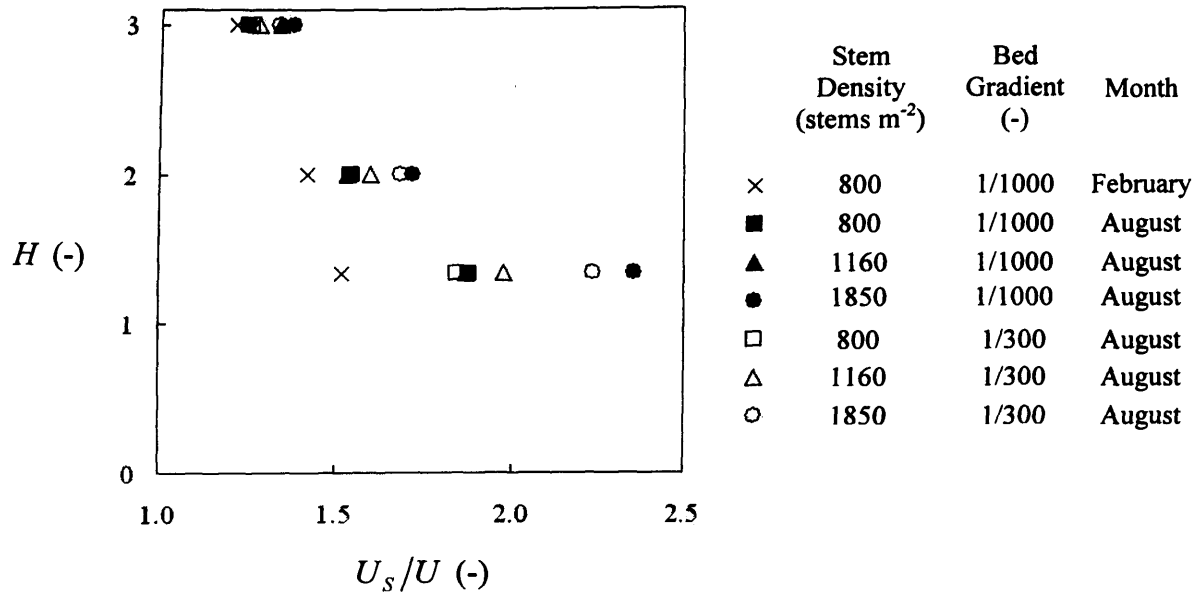

Figure 7-28 Variation in the ratio of the mean surface-flow layer longitudinal velocity, U_S, to the mean longitudinal velocity for the total flow depth, U, with submergence level, H, for experiments conducted for bed gradients of 0.001 and 0.003̇, and for stem densities of 800, 1160 and 1850 stems m^{-2}

Data from experiments on winter vegetation harvested during February 2007, which had a lower projected area per unit volume, are also included. The data from these experiments is discussed in more detail in Section 7.5. The plots indicate a decrease in U_S/U with increasing submergence level, H, due to an increase in longitudinal velocities through the canopy layer. This is due to the scaling method which resulted in modification of the canopy morphology by cropping a significant proportions of the canopy foliage and hence reducing its hydraulic resistance. For each submergence level, U_S/U increased with increasing stem density due to a reduction of longitudinal velocities within the canopy due to a higher level of obstruction. The February canopy, which was even lower in projected area compared to August canopy with equal stem densities (see Section 7.5.2), had the lowest U_S/U values due to higher longitudinal velocities in the canopy layer. There was little variation in U_S/U for different bed gradients except for the higher stem densities of 1160 and 1850 stems m^{-2}. However, U_S/U increased with bed gradient for the first case, and decreased for the latter, thus showing no consistent relationship.

7.4.4 Reynolds Stress Profiles

For emergent conditions, the Reynolds stress profiles are presented in Figure 7-29 for a bed gradient of $0.00\dot{3}$, and in Figure 7-30 for a bed gradient of 0.001. Reynolds stresses were small in magnitude for emergent vegetation, with less variation over the flow depth compared to the submerged canopies presented later in Figure 7-31 for a bed gradient of $0.00\dot{3}$, and in Figure 7-32 for a bed gradient of 0.001. For the emergent cases, the magnitude of peak Reynolds stress ranged between 0.01 and 0.15 kg m^{-1} s^{-2}, compared to 0.17 and 2.46 kg m^{-1} s^{-2} for the submerged canopies. The variability observed in the Reynolds stress profiles in Figure 7-29 and Figure 7-30 may be attributed to the variation in wake generation at different elevations.

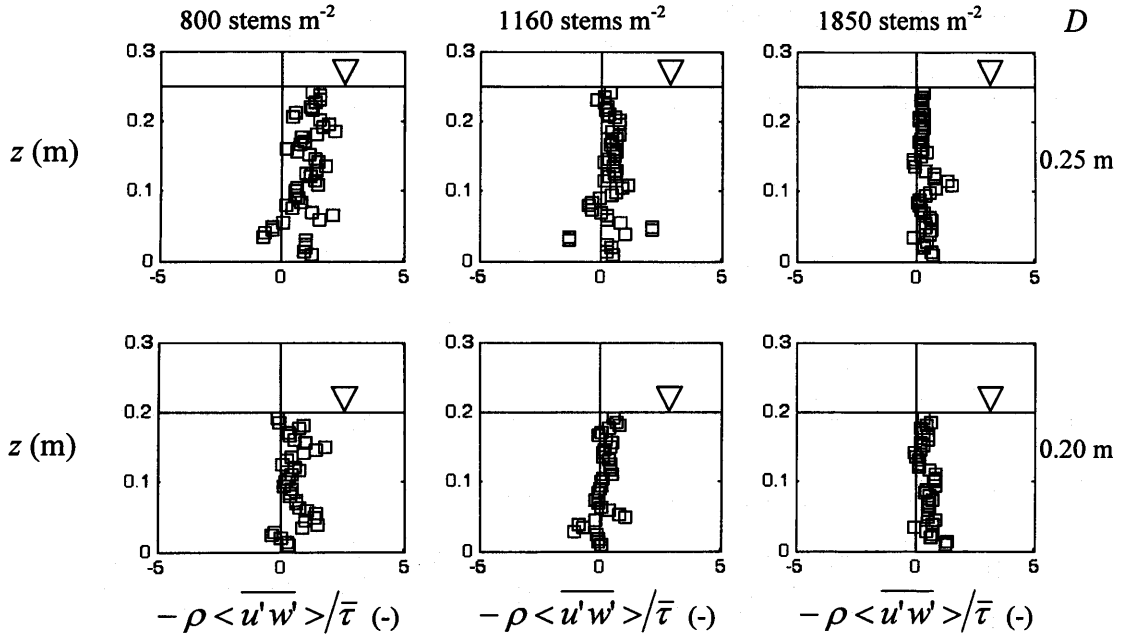

Figure 7-29 Reynolds stress profiles, normalised by the depth-averaged total fluid stress, $\bar{\tau}$, for flow through emergent vegetation for three stem densities, flow depths of 0.20 m and 0.25 m and a bed gradient of 1/300.

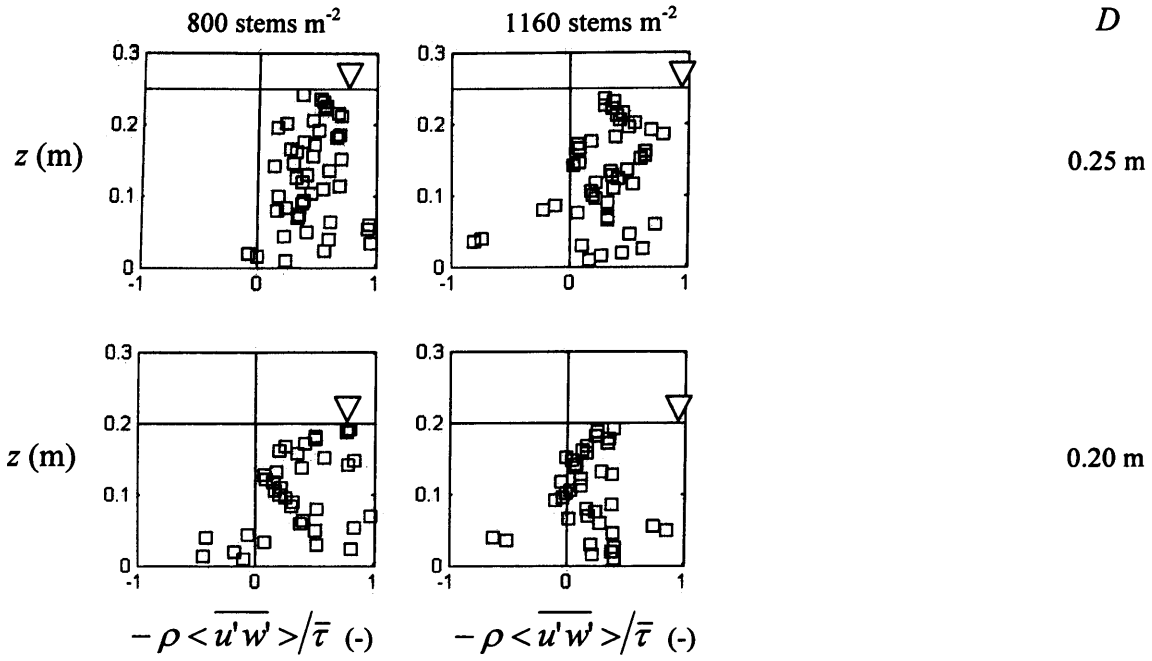

Figure 7-30 Reynolds stress profiles, normalised by the depth-averaged total fluid stress, $\bar{\tau}$, for flow through emergent vegetation for three stem densities, flow depths of 0.20 m and 0.25 m and a bed gradient of 1/1000.

The Reynolds stress profiles through submerged vegetation reach a maximum value a small distance above the top of the canopy in the surface flow layer. This is shown in Figure 7-31 for a bed gradient of $0.00\dot{3}$, and in Figure 7-32 for a bed gradient of 0.001. This was also observed by other researchers (e.g. Gambi *et al.*, 1990; López and García, 1997; Nepf and Vivioni, 2000). The shear layer resulted in elevated Reynolds stresses in the upper parts of the canopies, decreasing into the canopy and reaching negligible and relatively constant values. This was seen most clearly for the lower submergence levels of 1.33 and 2.00 in Figure 7-31a and Figure 7-31b respectively for a bed gradient of $0.00\dot{3}$, and in Figure 7-32a and Figure 7-32b for a bed gradient of 0.001.

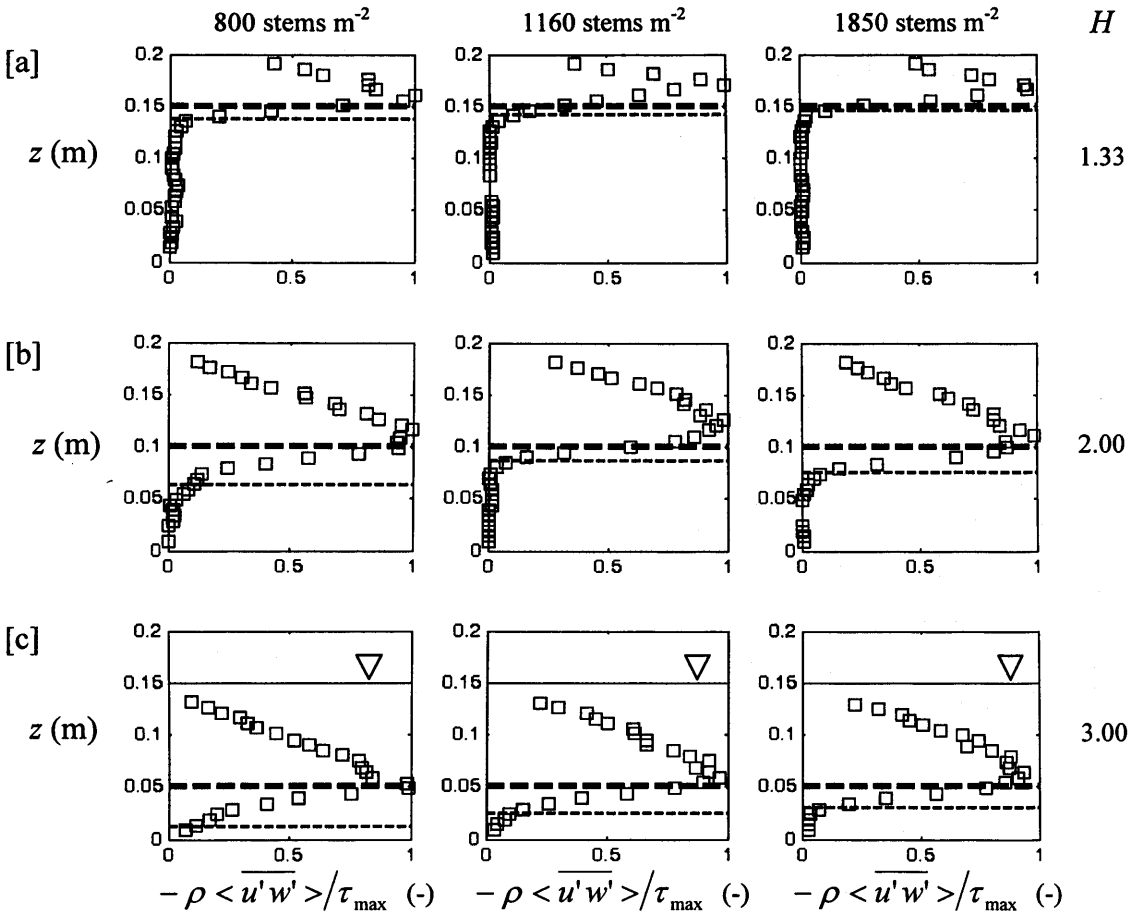

Figure 7-31 Reynolds stress profiles, normalised by the maximum total fluid stress over the flow depth, τ_{max} for flow through submerged vegetation for three stem densities, submergence levels of 1.33, 2.00 and 3.00, and a bed gradient of 1/300. The fainter dotted line corresponds to the turbulent stress penetration depth, and the bold dotted line corresponds to the top of the canopy.

Negligible Reynolds stresses were not only observed near the bed, but within the lower flow depth. To investigate the extent of shear penetration, the penetration depth as defined by Nepf and Vivioni (2000), (Section 2.5.3), was evaluated and shown in Figure 7-31 and Figure 7-32 by faint dotted lines. This was defined as the distance from the top of the cropped canopy to the elevation within the canopy layer where the Reynolds stress is 10% of the peak Reynolds stress value.

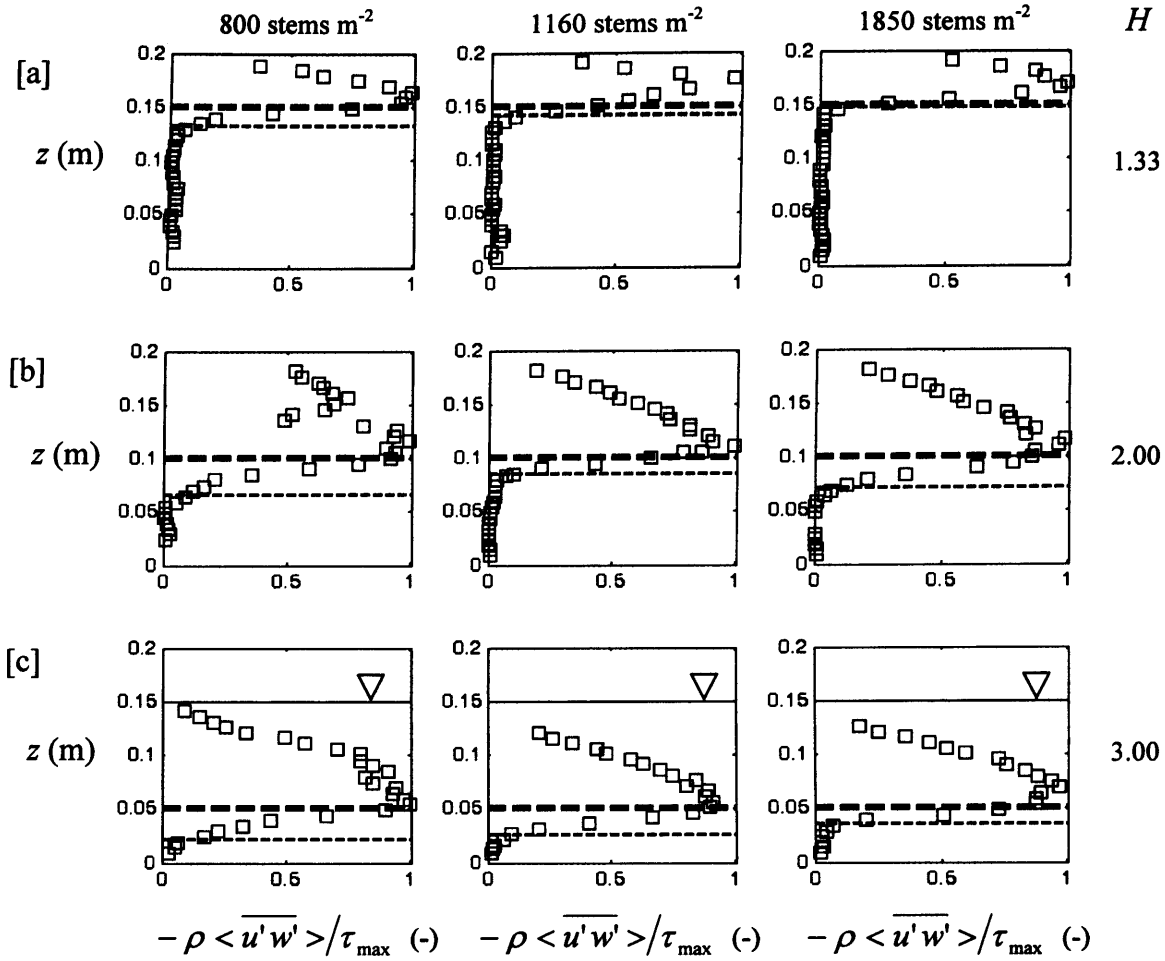

Figure 7-32 Reynolds stress profiles, normalised by the maximum total fluid stress over the flow depth, τ_{max}, for flow through submerged vegetation for three stem densities, submergence levels of 1.33, 2.00 and 3.00, and a bed gradient of 1/1000. The fainter dotted line corresponds to the turbulent stress penetration depth, and the bold dotted line corresponds to the top of the canopy.

For higher submergence conditions, the vegetation was cut down and significant amounts of the foliage cover were removed (see Section 5.2.4.2). For the lowest submergence level (H = 1.33), where the cropped canopy contained a considerable amount of foliage, Reynolds stress penetration was negligible. However, for deeper submergence levels of (H = 3.00), where most of the foliage was removed, and the stems were more comparable to an array of cylinders, penetration was much deeper. For any given 'cropped' vegetation height, there was a tendency for the penetration depth to decrease with increasing stem density. This is believed to be attributed to the increase in projected area of foliage in the upper part of the canopy which significantly reduces Reynolds stresses within the canopy layer.

The results from a number of studies on uniform cylinder arrays indicated that Reynolds stress penetration extended deeply into the canopy, often to the bed (e.g.

Dunn *et al.*, 1996; Fairbanks, 1998). Further results are also presented in Chapter 6 where uniform cylinders were compared to vegetation canopies and showed similar results. This highlights the significance of plant foliage in reducing Reynolds stress penetration. The arrays studied by Fairbanks (1998) had a closer resemblance to the canopies created for the current study if both the projected area per unit volume, $\overline{a}$, and the product parameter, $\overline{a}d_0$, are considered (Table 7-7). d_0 is the basal stem diameter. As discussed in Section 3.5.4, different quantification parameters may be misleading when two different canopies are compared. This is particularly the case when the difference in morphology is significant, for instance, when comparing uniform cylinder arrays to vegetation canopies. However, for the cylinder arrays employed by Fairbanks (1998), $\overline{a}$ and $\overline{a}d_0$ were 3.15 m^{-1} and 0.02 respectively. These were more comparable to the values calculated for the *Spartina anglica* canopies used in this study, particularly for the vegetation canopies constructed using plants collected during the month of February (Table 7-7).

For the uniform cylinder models considered by Fairbanks (1998), Reynolds stress penetration extended to the bed level (see Section 2.5.3). Experiments conducted by Dunn *et al.* (1996) also indicated that penetration often extended close to the bed (Figure 7-33). The plots presented are for a sample of the arrays examined by Dunn *et al.* (1996), for which the bed gradient and submergence levels resembled the conditions employed in the current study most closely. Densities of the arrays for which results have been presented are given in Table 7-7, in terms of $\overline{a}$ and $\overline{a}d_0$. The values indicate that the arrays used by Dunn *et al.* (1996), were considerably lower in "plant material density" than the arrays investigated by Fairbanks (1998) and the *Sp. anglica* canopies considered in the current study.

Lower plant material densities, as parameterised by $\overline{a}$ or $\overline{a}d_0$, may allow a deeper shear stress penetration. Yet, even for the arrays used by Fairbanks (1998), which were higher in density than the arrays studied by Dunn *et al.*, 1996, the penetration depth was much greater compared to the *Sp. anglica* canopies examined here. The *Sp. anglica* canopies had greater $\overline{a}$ and $\overline{a}d_0$ values than both studies. Shear penetration into the arrays examined by Dunn *et al.* (1996) extended close to the bed, except for the array with the largest projected area, $\overline{a}$, and for the lower submergence

level of 1.82. At a higher submergence level of 3.33, where flow velocities and the Reynolds stress magnitudes were greater, penetration was close to the bed.

The higher projected area in the upper part of the *Sp. anglica* canopies may be fundamental in absorbing the turbulent kinetic energy generated from the shear layer. For the lowest submergence of 1.33 in Figure 7-31a and Figure 7-32a, where the vegetation was 150 mm tall, the foliage demonstrated an ability to shelter the canopy layer to the extent where penetration of turbulent shear into the canopy layer was negligible. For a submergence level of 3.00, where the vegetation was cropped to a height of 50 mm most closely resembling arrays of uniform cylinders, the penetration extended deeper into the canopy as seen in Figure 7-31c and Figure 7-32c.

Table 7-7 Canopy and submergence characteristics for the current study and a selection of plastic straws experiments conducted by Dunn *et al.* (1996), and dowel experiments conducted by Fairbanks (1998)

	Test Ref.	stem density (stems m^{-2})	H (-)	s (mm)	$\bar{a}$ (m^{-1})	$\bar{a}d_0$ (-)
Current study	m-SM21	800 (Feb)	1.33	39.6	6.484	0.025
	m-SS21	800 (Feb)	2.00	39.6	6.729	0.027
	m-SV20	800 (Feb)	3.00	39.6	7.260	0.030
	SM21 , SM11	800 (Aug)	1.33	39.6	7.444	0.038
	SS21, SS11	800 (Aug)	2.00	39.6	7.179	0.039
	SV20 , SV10	800 (Aug)	3.00	39.6	6.616	0.036
	MM21 , MM11	1160 (Aug)	1.33	33.0	17.263	0.092
	MS21 , MS11	1160 (Aug)	2.00	33.0	16.313	0.091
	MV20 , MV10	1160 (Aug)	3.00	33.0	14.007	0.080
	DM21 , DM11	1850 (Aug)	1.33	26.4	28.931	0.139
	DS21 , DS11	1850 (Aug)	2.00	26.4	25.990	0.131
	DV20 , DV10	1850 (Aug)	3.00	26.4	22.220	0.115
Dunn *et al.* (1996)	Exp. 01	340	2.85	76.2	1.090	0.007
	Exp. 02	340	1.95	76.2	1.090	0.007
	Exp. 06	90	2.27	152.4	0.273	0.002
	Exp. 08	780	3.33	50.8	2.46	0.016
	Exp. 09	340	1.82	50.8	2.46	0.016
	Exp. 11	190	2.65	101.6	0.615	0.004
Fairbanks (1998)	FS#3 , FS#4	500	1.57	44.9	3.15	0.02

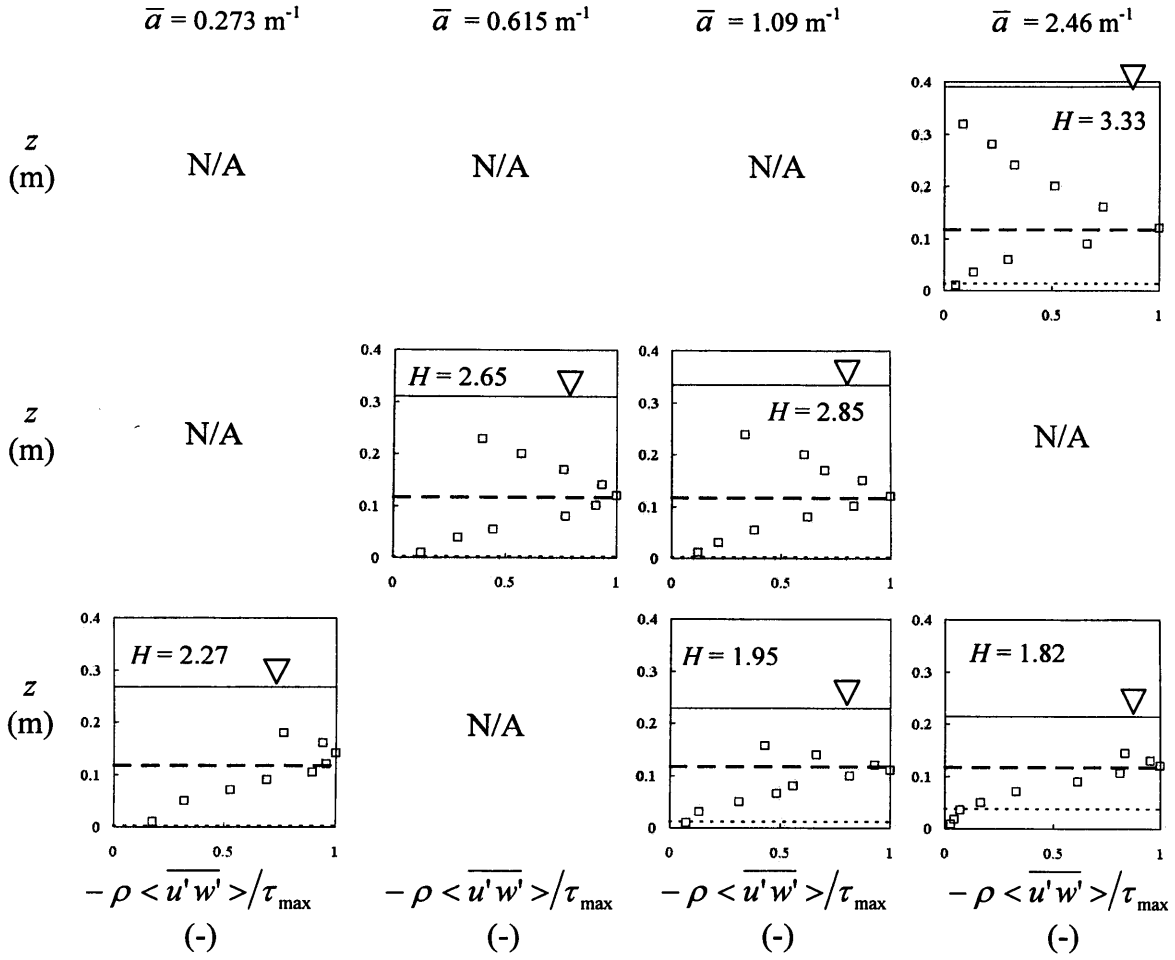

Figure 7-33 Normalised Reynolds stress profiles for arrays of plastic straws (from Dunn *et al.*, 1996) over a bed gradient of 0.0036 and at submergence levels similar to the values of 1.33, 2.00 and 3.00 implemented in this study. $\overline{a}$ refers to the projected area per unit volume, the bold dotted line refers to the top of the array, and the faint dotted line refers to the depth of shear penetration.

The extent of shear penetration into the cropped canopy was related to the amount of plant material in the canopy. In Figure 7-34, the relative penetration, based on all the data considered above, is shown to decrease with increasing plant material within the volume occupied by the canopy. This was characterised by the parameter $\overline{a}\,T$, where T is the height of the canopy. The penetration depth is influenced by the magnitude of Reynolds stress along the canopy-surface flow layer interface which in turn is a function of the longitudinal velocity gradient across the interface. This is shown in Figure 7-35, where penetration depth is shown to decrease with an increase in the depth-averaged longitudinal velocity of the surface flow layer, U_S.

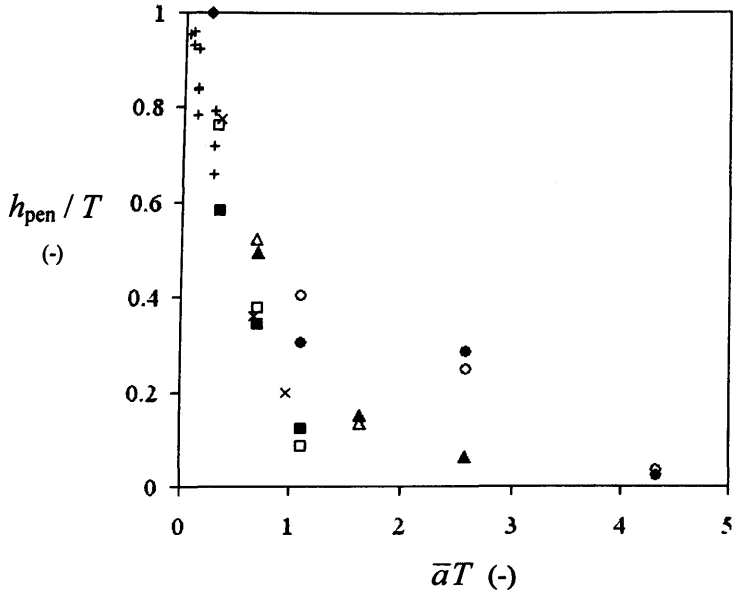

	Stem Density (stems m^{-2})	Bed Gradient (-)
Current Study (August)		
■	800	1/1000
▲	1160	1/1000
●	1850	1/1000
□	800	1/300
△	1160	1/300
○	1850	1/300
Current Study (February)		
×	800	1/1000
Other Studies (Uniform Cylinders)		
+ Dunn et al. (1996)		
	40-400	0.0036-0.0161
◆ Fairbanks (1998)		
	500	0.003

Figure 7-34 Variation in Reynolds stress penetration as a proportion of canopy height with the product of the projected area per unit volume and the canopy height for three *Spartina anglica* canopy densities at submergence levels of 1.33, 2.00 and 3.00, two bed gradients, and for uniform cylinders based on the results from Dunn *et al.* (1996) and Fairbanks (1998) using 6.35 mm diameter cylinder arrays.

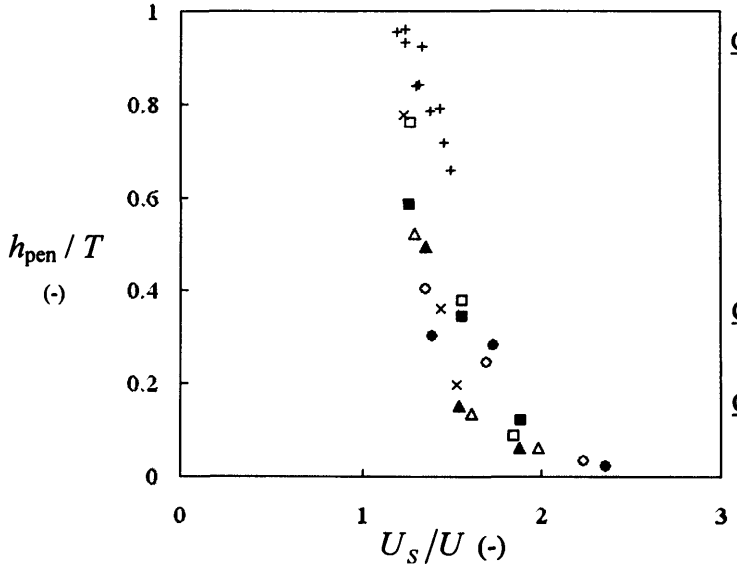

	Stem Density (stems m^{-2})	Bed Gradient (-)
Current Study (August)		
■	800	1/1000
▲	1160	1/1000
●	1850	1/1000
□	800	1/300
△	1160	1/300
○	1850	1/300
Current Study (February)		
×	800	1/1000
Other Studies (Uniform Cylinders)		
+ Dunn et al. (1996)		
	40-400	0.0036-0.0161

Figure 7-35 Variation in Reynolds stress penetration as a proportion of canopy height with the normalised surface flow layer, U_S / U, depth averaged velocities, where U is the total depth-averaged velocity. Results are presented for three *Spartina anglica* canopy densities at submergence levels of 1.33, 2.00 and 3.00, two bed gradients, and for uniform cylinders based on the results from Dunn *et al.* (1996) using 6.35 mm diameter cylinder arrays.

7.4.5 Instantaneous Parameters and Coherent Structures

7.4.5.1 Formation of a Shear Layer

For submerged conditions, a large longitudinal velocity gradient was observed across the canopy-surface flow layer interface (shown in Section 7.3.3.1). Within the canopy, the vegetation reduced the longitudinal velocities. This gave rise to the generation of a horizontal shear layer (see Section 2.5.4), along the canopy-surface flow layer interface in which coherent turbulent structures were produced as illustrated in Figure 7-36. Researchers have suggested that these are Kelvin-Helmholtz waves (Poggi *et al.*, 2004; Ghisalberti and Nepf, 2002; Finnigan, 2000; Nepf and Ghisalberti, 2008). These instabilities occur when velocity shear is present within a fluid and take the form of travelling waves such as those seen travelling on the surface of a liquid (see Section 2.5.4). They can develop into more turbulent structures hence it is common for vortices to occur within the shear layer near the canopy – surface flow layer interface. Furthermore, it has been observed in cylinder arrays that wake production is usually higher in the upper part of the canopy and accounts for the conversion of mean kinetic energy into turbulent kinetic energy resulting in a high level of energy dissipation (e.g. López and García, 1997; Finnigan, 2000 and others).

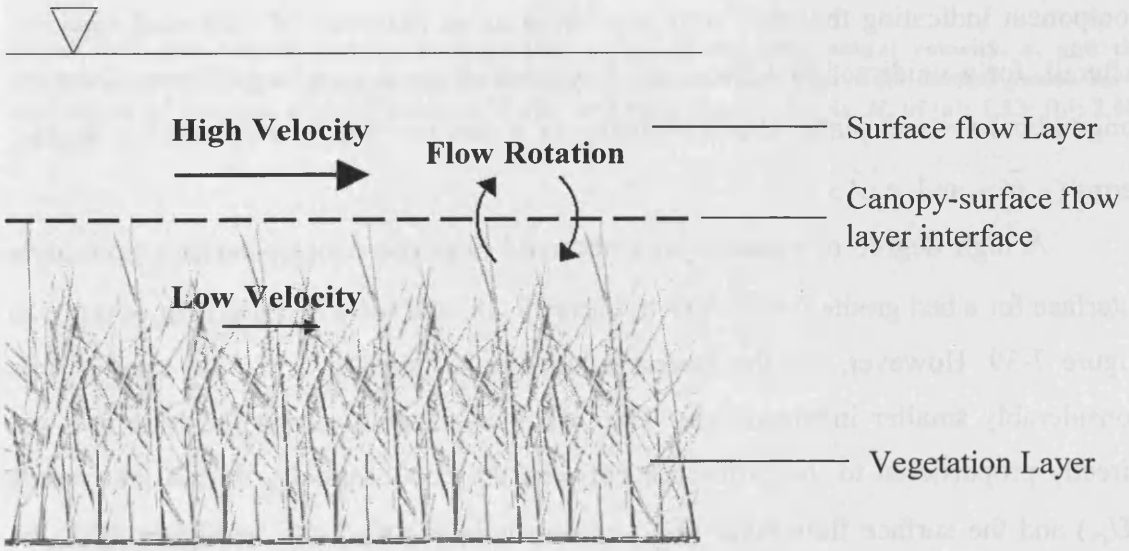

Figure 7-36 Schematic diagram illustrating the rotation that occurs in the flow along the canopy-surface flow layer interface.

7.4.5.2 Rotational Capacity of the Vortices

The rotational capacity of the Kelvin-Helmholtz vortices (as shown in Figure 7-36) is defined as the magnitude of the circular motions of the vortices in the vertical plane at the canopy-surface flow layer interface. More specifically, this refers to their magnitude about the elevation where the maximum turbulent stress occurs, which is marginally above the top of the vegetation (this will be further discussed in Section 7.4.4). Several researchers have defined the rotational capacity of the vortices by the presence of relatively high instantaneous longitudinal velocity fluctuations (e.g. Lu and Wilmarth, 1973; Raupach and Thom, 1981; Finnigan, 2000 and others), particularly where these correspond to peaks in the Reynolds stress (Ghisalberti and Nepf, 2002). Vortices were very small and scarce for a submergence level of 1.33 (Figure 7-37a). Vortices were more pronounced and frequent for the higher submergences of 2.00 and 3.00. For these submergence levels, the longitudinal velocities and Reynolds stress magnitudes were higher such as the example presented in Figure 7-37b and c. In this study, the normalised root mean square of the double-averaged fluctuations in the vertical velocity component, $<\overline{w'}>$, were implimented as a measure of the rotational capacity of the flow to assess vertical movement of the flow about the canopy-surface flow layer interface. Fluctuations in the longitudinal velocity component, $<\overline{u'}>$, produced profiles with similar shapes to the vertical component indicating that they may also serve as an indicator of rotational capacity. Afterall, for a unidirectional flow, the Reynolds stress is most significant along the longitudinal-vertical plane, thus consisting of a product function containing the two terms ($<\overline{u'}>$ and $<\overline{w'}>$).

A high degree of rotation was observed near the canopy-surface flow layer interface for a bed gradient of $0.00\dot{3}$ in Figure 7-38, and for a bed gradient of 0.001 in Figure 7-39. However, for the lowest submergence level of 1.33, the rotation was considerably smaller in magnitude. The rotational capacity about the interface was directly proportional to the difference between the zonal velocity within the canopy (U_C) and the surface flow layer (U_S) as shown in Figure 7-40. In Figure 7-38, the peaks observed in $<\overline{w'}>$ near the water surface for higher submergence levels for the steeper bed gradient of $0.00\dot{3}$, correspond to the peaks observed in the longitudinal velocity within the same region in Figure 7-20. These were associated with higher

Reynolds numbers and hence, a higher level of turbulence as discussed in Section 7.3.3.1.

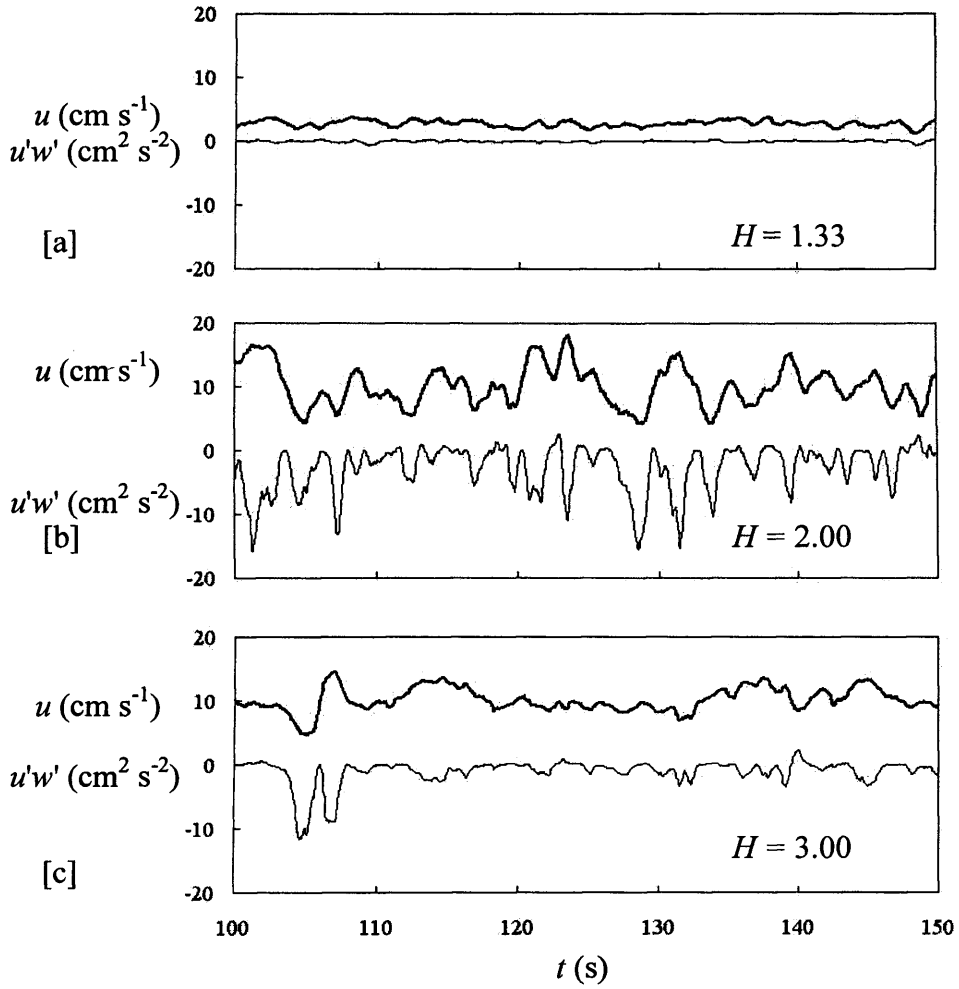

Figure 7-37 One-second moving average time series of the longitudinal velocity, u, and the Reynolds stress, $u'w'$, at the canopy-surface flow layer interface over a 20 second period for a 1850 stems m^{-2} canopy, a bed gradient of 0.001, and submergence levels, H, of [a]: 1.33; [b]: 2.00; [c]: 3.00

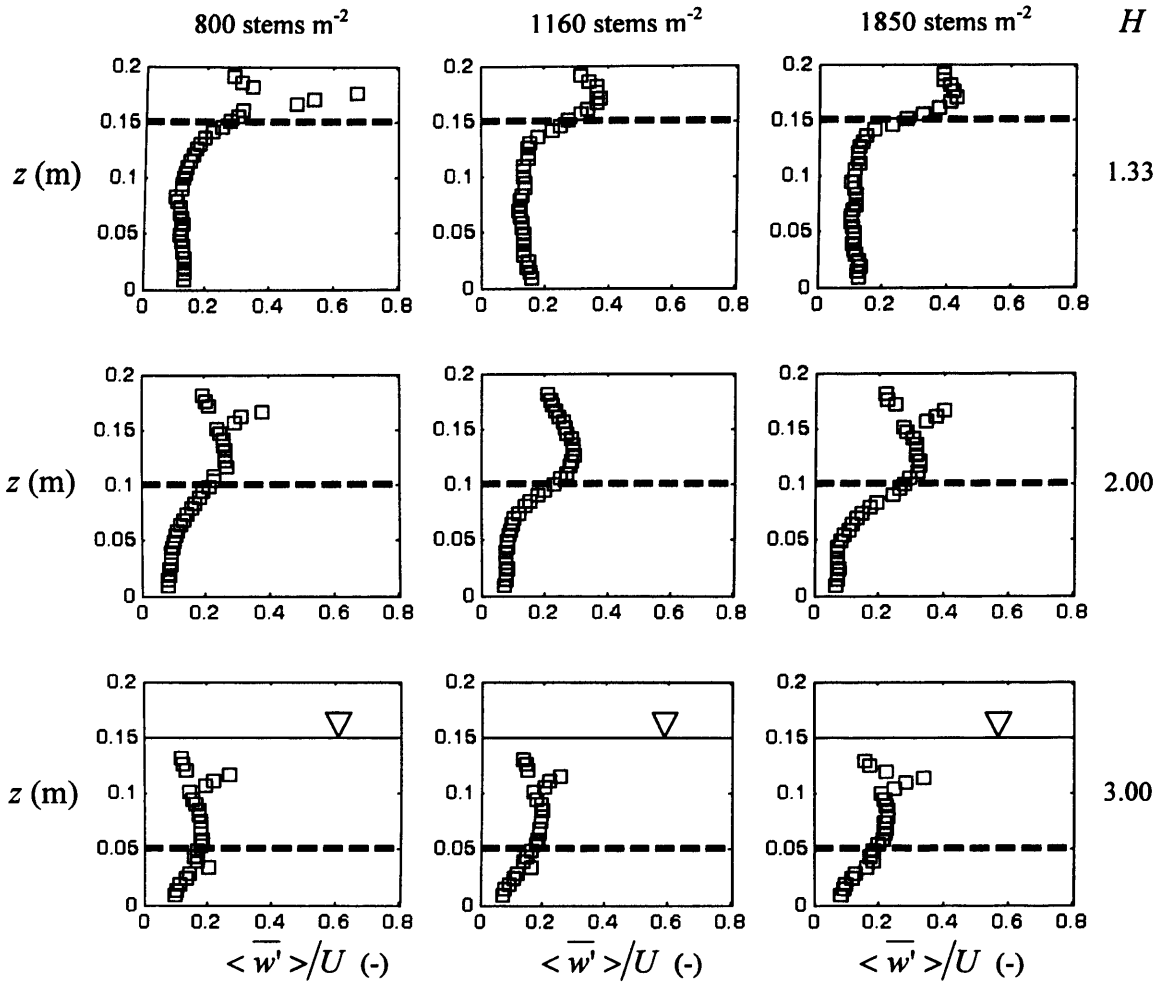

Figure 7-38 Profiles of the vertical velocity fluctuating component, w', normalised by the depth-averaged velocity, U, for a bed gradient of 1/300, and submergence levels of 1.33, 2.00 and 3.00. The dashed line denotes the top of the canopy.

For some of the experiments, such as when the bed gradient was $0.00\dot{3}$ and the submergence 3.00, a peak was observed in the fluctuating component of the vertical velocity, w', a short distance below the water surface. These correspond to the 'kinks' in the longitudinal velocity profiles discussed earlier in Section 7.3.3.1 which may be associated with turbulence in the flow. The effects of these structures did not appear to affect a significant amount of the flow depth, whereas the peaks observed along the canopy-surface flow layer interface were accompanied by elevated $< \overline{w'} >$ values above and below the interface.

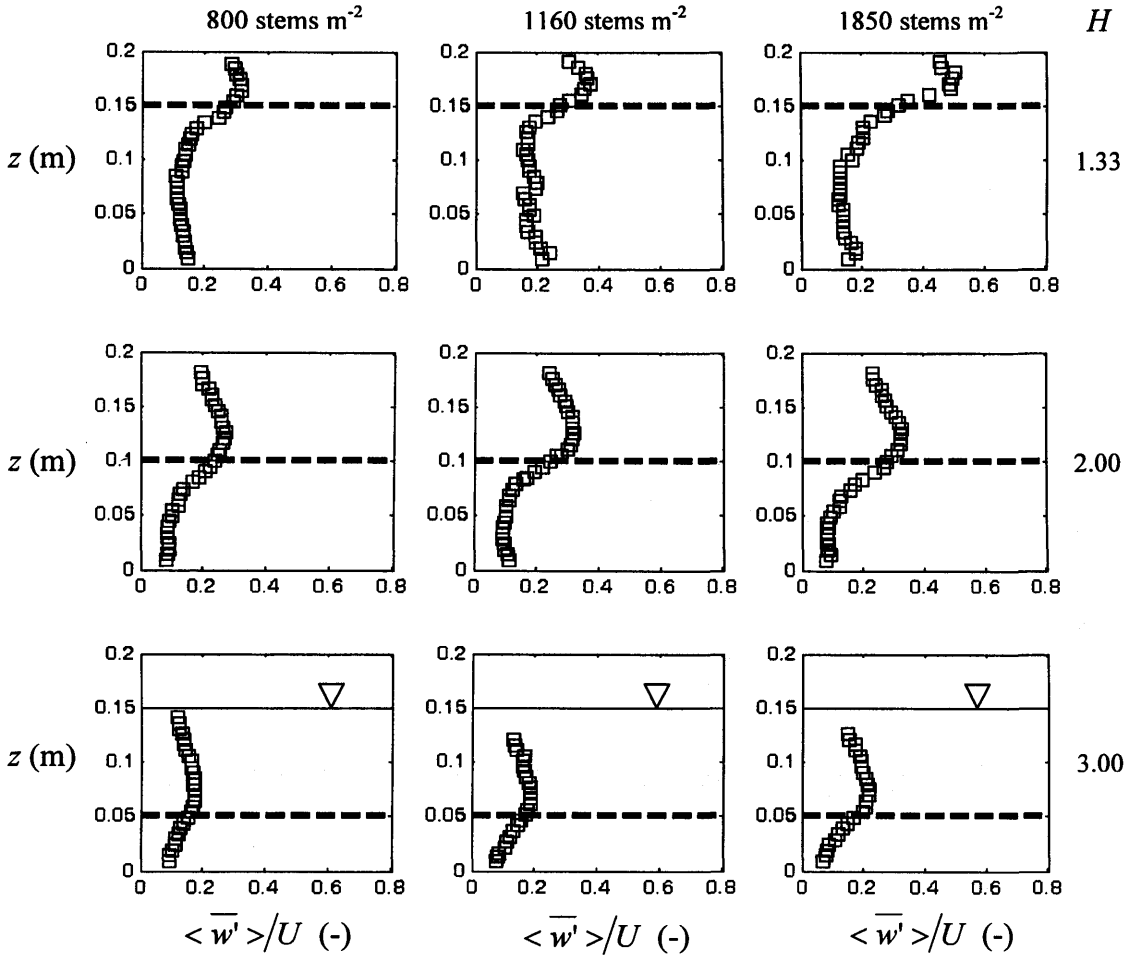

Figure 7-39 Profiles of the vertical velocity fluctuating component, *w'*, normalised by the depth-averaged velocity, *U*, for a bed gradient of 1/1000, and submergence levels of 1.33, 2.00 and 3.00. The dashed line denotes the top of the canopy.

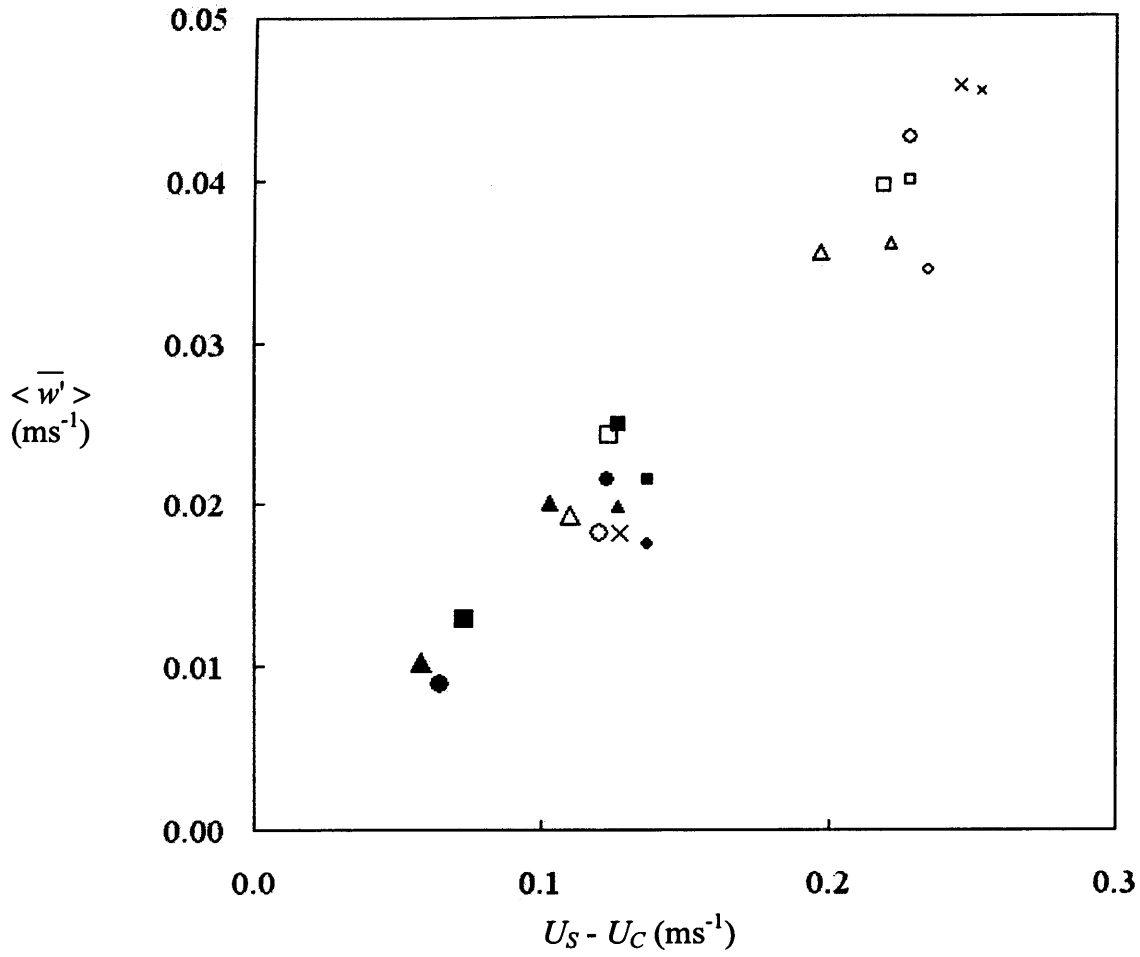

	Stem Density (stems m^{-2})	Bed Gradient (-)	H (-)	Month
×	800	1/1000	1.33	February
×	800	1/1000	2.00	February
×	800	1/1000	3.00	February
■	800	1/1000	1.33	August
■	800	1/1000	2.00	August
■	800	1/1000	3.00	August
▲	1160	1/1000	1.33	August
▲	1160	1/1000	2.00	August
▲	1160	1/1000	3.00	August
●	1850	1/1000	1.33	August
●	1850	1/1000	2.00	August
●	1850	1/1000	3.00	August

Stem Density (stems m^{-2})	Bed Gradient (-)	H (-)	Month
□ 800	1/300	1.33	August
□ 800	1/300	2.00	August
□ 800	1/300	3.00	August
△ 1160	1/300	1.33	August
△ 1160	1/300	2.00	August
△ 1160	1/300	3.00	August
○ 1850	1/300	1.33	August
○ 1850	1/300	2.00	August
○ 1850	1/300	3.00	August

Figure 7-40 The relationship between the vertical velocity fluctuating component at the canopy-surface flow layer interface, w', and the difference between the zonal velocity of the surface flow layer, U_S, and that of the canopy layer, U_C, for 800, 1160 and 1850 stems m^{-2} canopies at bed gradients of 1/300 and 1/1000. The results presented are for submergence levels of 1.33, 2.00 and 3.00.

For the highest submergence of 3.00, where most of the foliage had been removed from the cropped vegetation (see Section 5.2.4.2), the time-averaged fluctuating component of the vertical velocity increased with elevation for most of the canopy height. Comparison of the profiles for different stem densities indicated that for the 800 and 1850 stems m^{-2} canopies, an increase in the time-averaged fluctuating component of the vertical velocity near the canopy top from the mid-flow depth values was apparent over a greater section of the canopy. The 800 stems m^{-2} canopy had the lowest stem density, whilst the 1850 stems m^{-2} canopy was constructed using the plants with the smallest basal stem diameter (Section 4.3.2.5 - 'Sample 1' refers to the vegetation sample used to construct the 1850 stems m^{-2} density canopy). The increase in the time-averaged fluctuating component of the vertical velocity was most apparent for a submergence level of 2.00, where the velocity gradient across the canopy-surface flow layer was considerably higher, giving rise to a relatively higher magnitude of Reynolds stress. Furthermore, the cropped canopy height and foliage content were large, thus facilitating low $< \overline{w'} >$ values over the lower section of the canopy.

7.4.5.3 Quadrant Analysis

In this section, turbulent fluctuations in the longitudinal and vertical directions are presented based on the quadrant analysis method developed by Lu and Willmarth (1973) (Section 2.5.5). The plots are presented for experiments conducted for a bed gradient of $0.00\dot{3}$ where the Reynolds stress, particularly within the upper part of the canopy was greatest (Section 7.4.4). Plots of the fluctuations in the vertical and longitudinal velocity components are presented for elevations equal to 10%, 50% and 100% of the vegetation height above the bed for vegetation heights of 50mm, 100mm and 150mm in Figure 7-41, Figure 7-42 and Figure 7-43 respectively. Flow parameters were measured at four different cross-sections along the flume length (see Section 5.2.8). However, the measurements were not recorded simultaneously, and therefore, the results in this case are presented for the most upstream profile at a distance of 3.5m from the upstream end of the flume.

To assess the turbulence structure in the region close to the bed where the influence of the vortices from the canopy-surface flow layer interface may be negligible, a ratio of elevation to canopy height equal to 10% was considered. Data

points along the w' versus u' plot were centred closer to the origin with some spread along the u' axis as indicated in Figure 7-41c, Figure 7-42c and Figure 7-43c. Near the mid-height of the canopy, where there is more influence from the high Reynolds stress at the top of canopy, the plots were more rounded in shape. This indicated that the longitudinal and vertical fluctuations were more equal in magnitude as shown in Figure 7-41b, Figure 7-42b and Figure 7-43b.

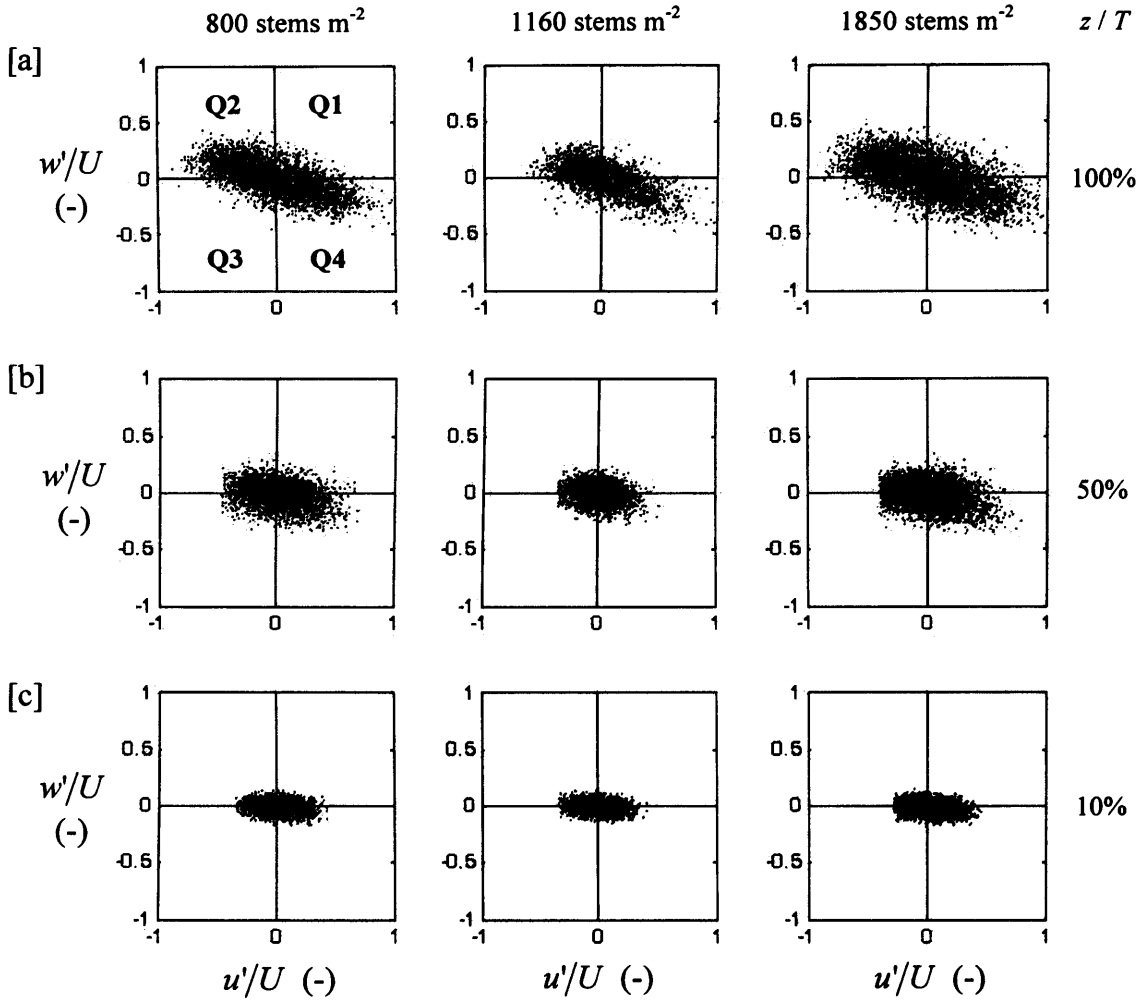

Figure 7-41 Quadrant plots at 10%, 50% and 100% of the vegetation height for three stem densities, a vegetation height of 50mm and a bed gradient of 1/300. Fluctuating velocity components, u' and w' are normalised using the depth-averaged longitudinal velocity, U. The submergence level for these experiments was 3.00 (i.e. the flow depth was 150mm and the canopy height was 50mm).

Along the canopy-surface flow layer interface (100% elevation of the vegetation height), where the vortices were relatively greater in size compared to other elevations within the canopy, scatter in the quadrant plots was greater. The points were distributed around the '$y = -x$' diagonal passing through the second and fourth quadrants. Points in the second quadrant correspond to upward and backward motions, also known as 'ejections' (u' = -ve, w' = +ve). Points falling in the fourth

quadrant correspond to downward and forward moving 'sweeps' (u' = +ve, w' = -ve). Together, these particle movements are indicative of a shear layer (e.g. Raupach and Thom, 1981; Finnigan, 2000 and others). This was observed most clearly for submergence levels of 2.00 and 3.00 in Figure 7-41a, Figure 7-42a, where the longitudinal velocity gradient was large across the canopy-surface flow layer interface (Section 7.3.3.1). For the lowest submergence of 1.33, this effect was only visible for the highest stem density of 1850 stems m^{-2} in Figure 7-43c. For the aforementioned canopy, there was the greatest amount of flow resistance in the upper part of the canopy. This created a higher velocity gradient across the interface. However, the concentration of data points along the 'y = -x' diagonal was less pronounced compared to the higher submergence levels of 2.00 and 3.00 in Figure 7-42a and Figure 7-41a respectively.

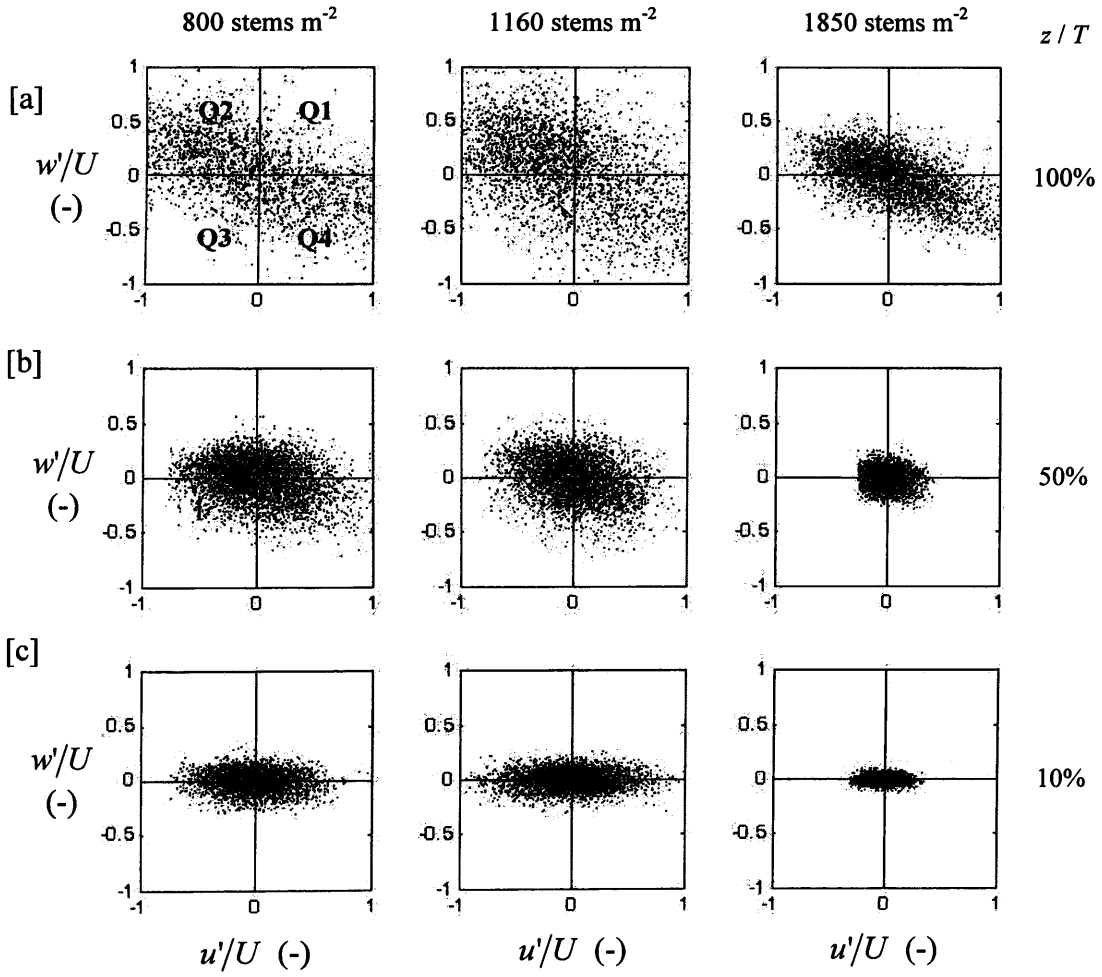

Figure 7-42 Quadrant plots at 10%, 50% and 100% of the vegetation height for three stem densities, a vegetation height of 100mm and a bed gradient of 1/300. Fluctuating velocity components, u' and w' are normalised using the depth-averaged longitudinal velocity, U. The submergence level for these experiments was 2.00 (i.e. the flow depth was 200mm and the canopy height was 100mm).

For a submergence level of 1.33, the plots appeared more rounded in shape near the interface (100% elevation of the vegetation height). There were fewer congregations between the second and fourth quadrants for the lower stem densities of 800 and 1160 stems m^{-2} as shown in Figure 7-43a. For the lowest submergence of 1.33, the thickness of the surface flow layer was shallower forming only 33% of the cropped canopy height, compared to 50% and 75% of the flow depth for submergence levels of 2.00 and 3.00 respectively. Longitudinal velocities throughout the depth were lower (Section 7.3.3.1) and the surface flow layer conveyed less momentum. Furthermore, the longitudinal velocity gradients were lower across the interface, and hence, shear between the two layers was relatively smaller in magnitude. Ejections and sweeps for such conditions were more difficult to distinguish based on the quadrant analysis due to their smaller sizes. They were less visible amongst other turbulent fluctuations in the longitudinal and vertical velocity components u' and w'.

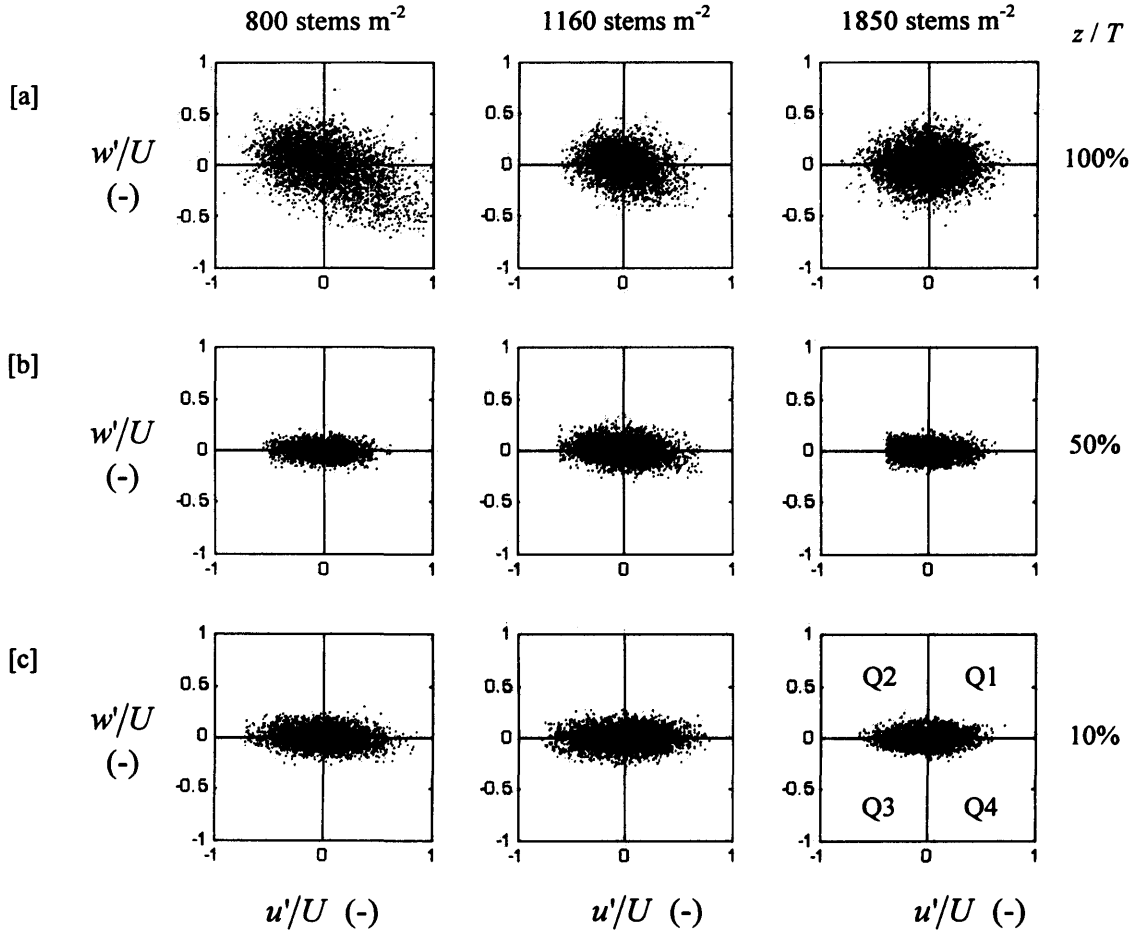

Figure 7-43 Quadrant plots at 10%, 50% and 100% of the vegetation height for three stem densities, a vegetation height of 150mm and a bed gradient of 1/300. Fluctuating velocity components, *u'* and *w'* are normalised using the depth-averaged longitudinal velocity, *U*. The submergence level for these experiments was 1.33 (i.e. the flow depth was 200mm and the canopy height was 150mm).

The ratio of the root mean squares of the vertical fluctuating velocity component, $<\overline{w'}>$, to the longitudinal component, $<\overline{u'}>$, are presented in Figure 7-44 for a bed gradient of $0.00\dot{3}$, and in Figure 7-45 for a bed gradient of 0.001. The profiles indicate the extent of deviation of the scatter along the quadrant plots from a distribution centred along the x or y-axis. Values closer to unity indicate an equal distribution of points along both axes, most likely to form a circular distribution around the origin. Lower values indicate a greater spread of the distribution along the x-axis, and that the fluctuations in the longitudinal component, u' were considerably greater than those in the vertical component, w'.

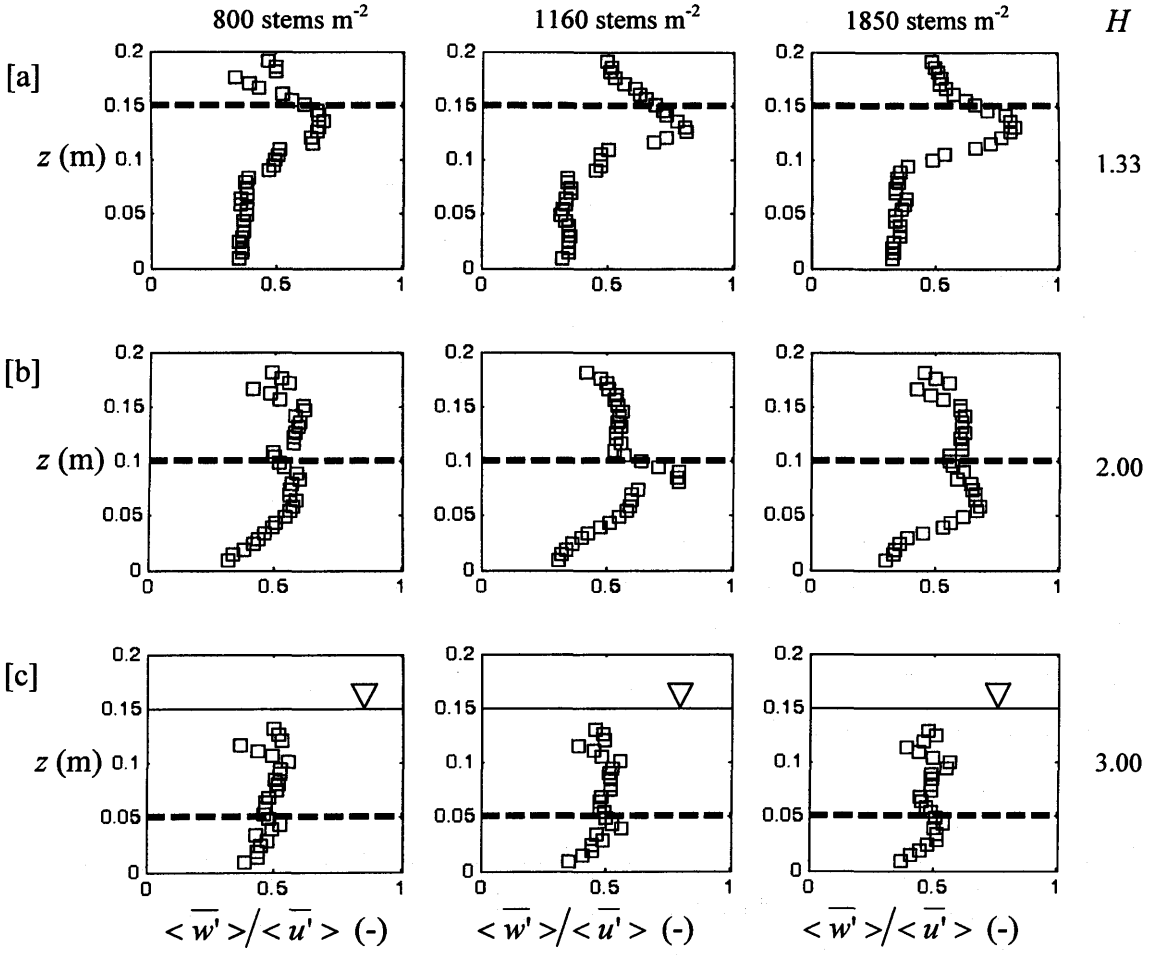

Figure 7-44 Profiles of the ratio of the vertical velocity component fluctuations, w', to the horizontal component, u', over a bed gradient of 1/300, three stem densities, and submergence levels of 1.33, 2.00 and 3.00. The dashed lines denote the top of the vegetation.

Values were consistently lower than unity since the longitudinal velocities, u, and their fluctuating components, u', were considerably greater in magnitude than the vertical components, w and w'. However, there was an increase in the $<\overline{w'}>/<\overline{u'}>$

ratio with elevation within the canopy region due to a relative increase in $<\overline{w'}>$ compared to $<\overline{u'}>$. This is illustrated by the more rounded quadrant plot distributions at the mid-canopy heights in Figure 7-41b for the 50 mm tall cropped canopy, and in Figure 7-42b for the 100 mm tall cropped canopy. The peaks in $<\overline{w'}>/<\overline{u'}>$ occurred a short distance below the top of the vegetation, which was identified by Finnigan (2000) as the region of the canopy where wake production is largest in magnitude for atmospheric flows through plant canopies.

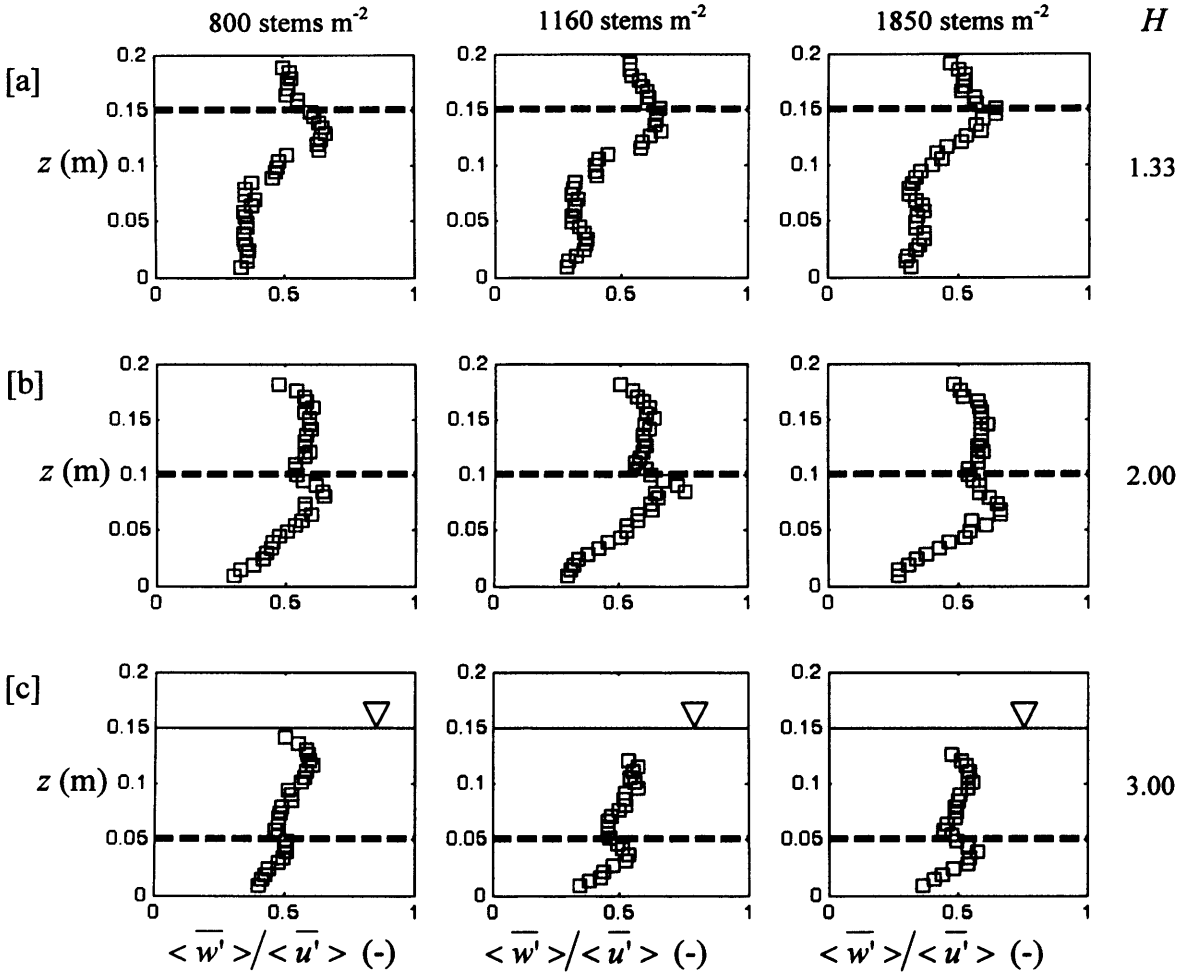

Figure 7-45 Profiles of the ratio of the vertical velocity component fluctuations, *w'*, to the horizontal component, *u'*, over a bed gradient of 1/1000, three stem densities, and submergence levels of 1.33, 2.00 and 3.00. The dashed lines denote the top of the vegetation.

The profile shapes were similar for any given submergence regardless of stem density or bed gradient based on the range of parameters examined. For the 150 mm cropped canopy height (submergence level of 1.33), the magnitude of $<\overline{w'}>/<\overline{u'}>$ decreased into the canopy from the peak value towards an approximately constant minimum value over the lower part of the canopy up to an elevation of about 100 mm

above the bed. This is presented in Figure 7-44a for a bed gradient of $0.00\dot{3}$, and in Figure 7-45a for a bed gradient of 0.001. For the shorter cropped canopy heights of 100 mm which corresponds to a submergence level of 2.00 (Figure 7-44b and Figure 7-45b) and 50 mm (Figure 7-44c and Figure 7-45c), a constant minimum value over a section of the lower canopy was not achieved. This may be attributed to the lack of foliage in the cropped 50mm and 100mm canopies (see Section 5.2.4.2). Furthermore, the full extent of the mixing layer and its effect on the turbulence structure within the canopy layer could not be determined for the 50 mm cropped vegetation (submergence level of 3.00) because the flow structure is not fully developed vertically (the longitudinal velocity has not reached a minimum value as observed for the 1.33 submergence level).

7.4.6 "Form-induced" Stresses

"Form-induced" stresses are a measure of the spatial fluctuations in time-averaged parameters as a result of the variability of the vegetation obstruction (see Section 2.5.2). Profiles of "form-induced" stresses are useful because they can be used as an indicator of level of heterogeneity of a vegetation canopy. Values were calculated based on measurements at four locations. Considering the heterogeneity of vegetation, care must be taken when evaluating the data. More measurements were required to reliably characterise the flow in terms of time-averaged velocity and turbulence parameters.

"Form-induced" stress profiles for selected experiments on emergent canopies are presented in Figure 7-46 corresponding to a bed gradient of 0.001. For emergent conditions, the "form-induced" stresses were more significant throughout the canopy compared to the submerged condition. Selected results are shown in Figure 7-46. Comparison with the Reynolds stress profiles discussed in Section 7.4.4 indicated that for emergent conditions, the "form-induced" stresses offered a slightly greater contribution towards the total stress budget than the Reynolds stresses (Section 7.4.1). For submerged conditions, the Reynolds stresses predominated and "form-induced" stresses were relatively insignificant. The normalised "form-induced" stresses are considerably greater within the emergent canopies compared to the submerged canopies as seen in Figure 7-47 due to the insignificance of the Reynolds stresses in the absence of a 'shearing' layer along the top of the canopy layer.

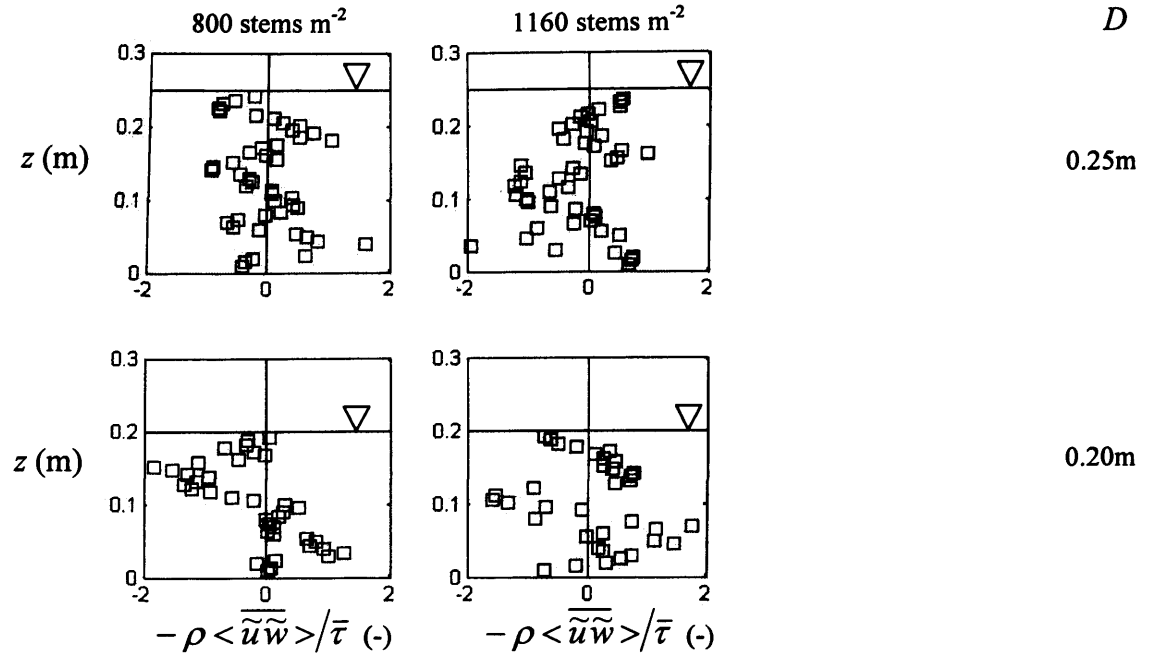

Figure 7-46 "Form-induced" stress profiles, normalised by the depth-averaged shear stress, $\bar{\tau}$, for flow through emergent vegetation for three stem densities, flow depths of 0.20 m and 0.25 m and a bed gradient of 1/1000.

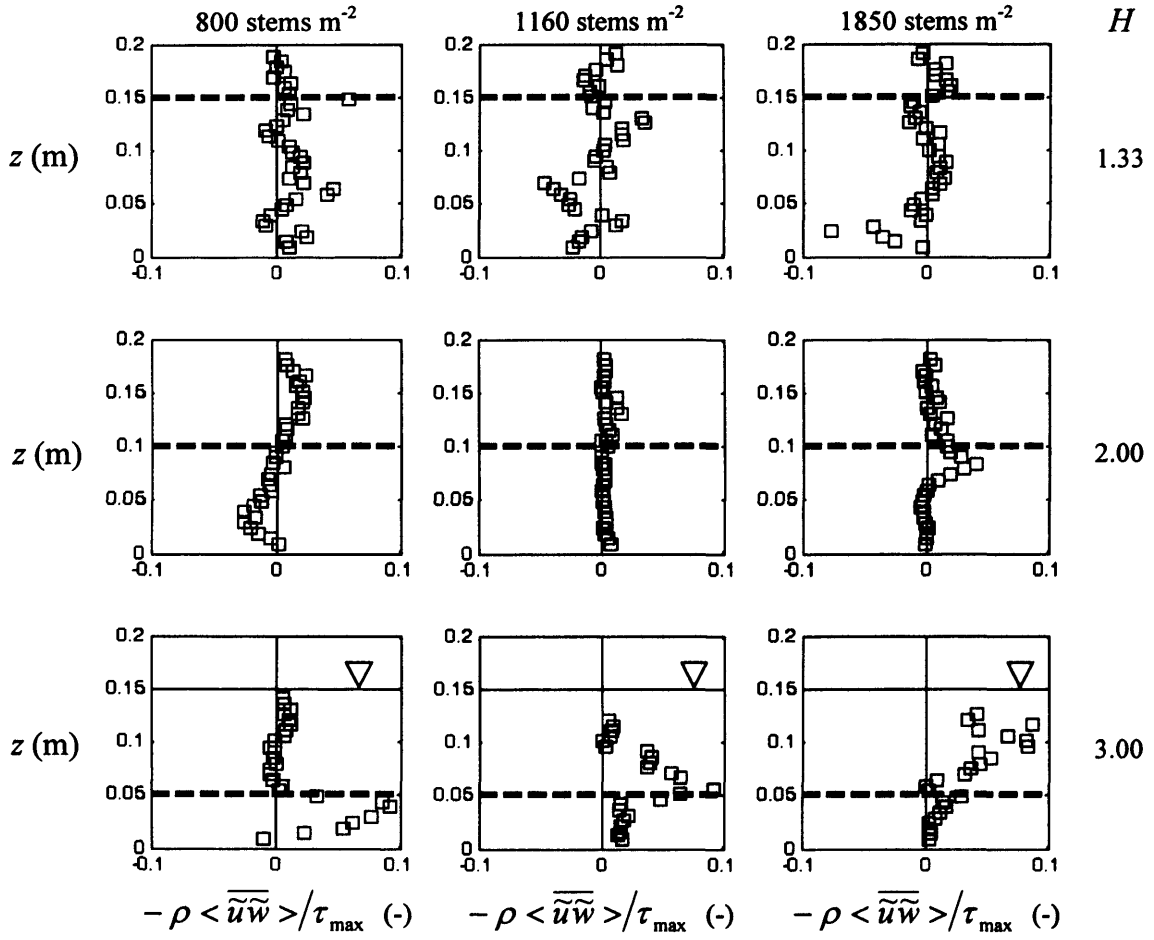

Figure 7-47 "Form-induced" stress profiles, normalised by the maximum shear stress over the flow depth, τ_{max}, for flow through submerged vegetation for three stem densities, submergence levels of 1.33, 2.00 and 3.00, and a bed gradient of 1/1000.

7.5 The Impact of Seasonality on Flow Parameters

7.5.1 The Summer-Winter Comparison

A sample of the experiments conducted using vegetation collected during the month of August 2006 (Section 7.3), were repeated using vegetation collected during February 2007. Seasonal variations in vegetation morphology were linked to the velocity and turbulence structures. Plant properties, such as stem density, stem diameters, plant stiffness and the amount of foliage varied temporally (Section 4.3). It is thought that these physical properties will impact on the flow resistance of a canopy. *Spartina anglica* samples collected in August 2006 and February 2007 were used to represent a typical 'summer' and 'winter' vegetation sample. Full details of the experiments repeated using February vegetation were listed in Section 7.1. Experiments were only repeated for a bed gradient of 0.001 and a stem density of 800 stems m^{-2}.

7.5.2 Variation between August and February Vegetation

In Section 3.4.3, quantification of the projected area of the canopy for the vegetation used in the experiments was discussed. The projected area per unit volume was greater above the bed region for the August vegetation due to a greater amount of foliage (Figure 7-48). The projected area for the August canopy was lower in the region near the bed. However, stem diameter measurements on selected sub-samples chosen from the August and February vegetation samples showed that the latter had the smaller plant stems. The average basal stem diameter was 4.12 mm for the February vegetation compared to 5.51 mm for the August vegetation (used for the 800 stems m^{-2} canopy as reported in Section 4.3.2.5 – 'Sample 3' refers to the sample used to construct the 800 stems m^{-2} density canopy).

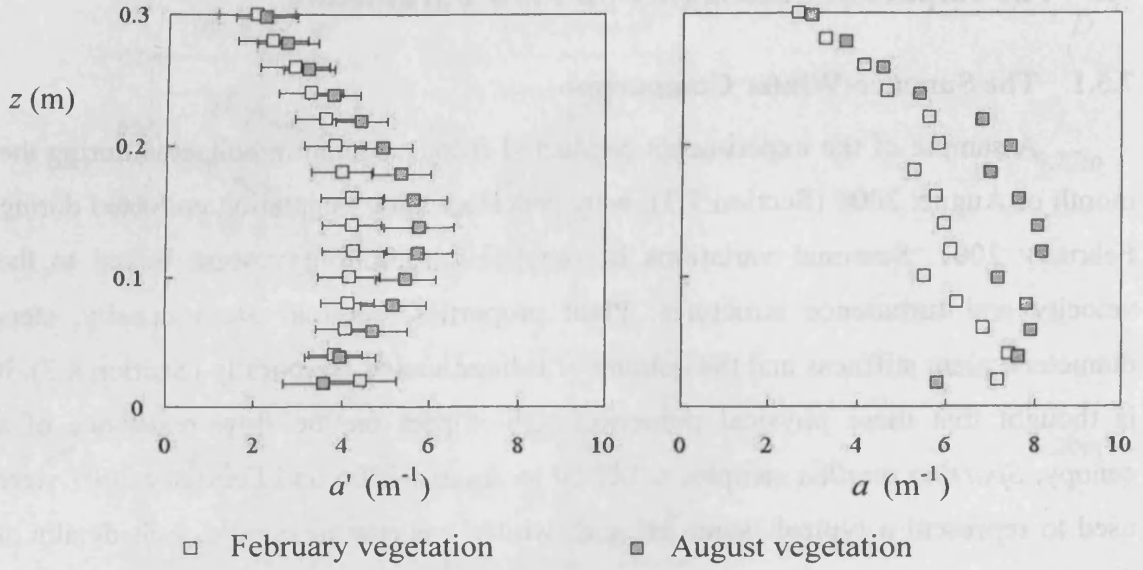

Figure 7-48 [a]: Visible projected area of obstruction per unit volume (a') and [b]: total projected area of obstruction per unit volume (a) for 800 stems m^{-2} canopies of February and August vegetation.

7.5.3 Longitudinal Velocity Profiles

To replicate the previous experiments conducted using vegetation samples collected in August, the same flow depths were used. A higher discharge was necessary to ascertain this flow depth which corresponds to a higher longitudinal velocity for the thinner February canopy experiments.

There was greater spatial variation in the velocity profiles for the February vegetation compared to the August vegetation as indicated by the "form-induced" stress profiles presented later in Section 7.5.5. This may possibly indicate a greater degree of variability in the vegetation, due to individual plants within a canopy "maturing" during the winter at different rates. However, the higher "form-induced" stresses are more likely associated with the higher flow velocities implemented, and the associated higher levels of turbulence in the flow.

The normalised profiles presented in Figure 7-49 for the emergent canopies revealed a contrast between the velocity structure through the February and August vegetation. For the February vegetation, the longitudinal velocity is relatively constant over the flow depth. For the August vegetation, the normalised longitudinal velocity decreases with distance from the bed. Flow resistance was greater in the upper part of the canopy due to a greater projected area of plant foliage compared to the February canopy (see Figure 7-48 and Section 3.4.3).

For submerged conditions, the normalised longitudinal velocity profiles presented in Figure 7-50 for February and August vegetation were similar in shape. This indicates that they were not significantly affected by the differences in plant properties.

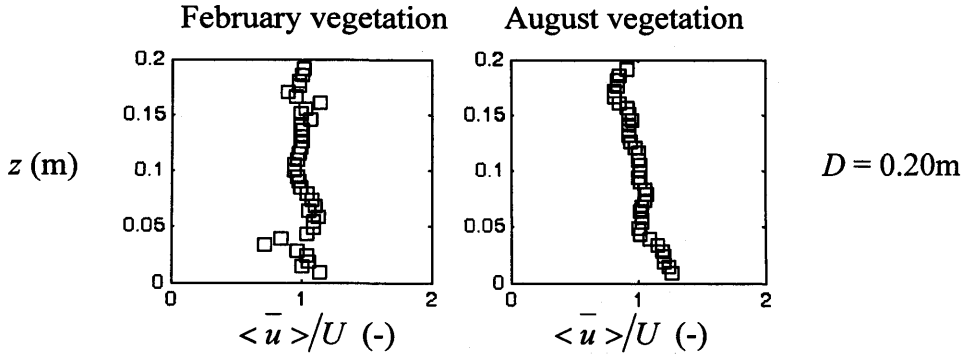

Figure 7-49 Profiles of normalised longitudinal velocity for emergent February and August vegetation canopies, a bed gradient of 1/1000, a stem density of 800 stem m^{-2} and a flow depth of 0.20m. U is the depth-averaged longitudinal velocity.

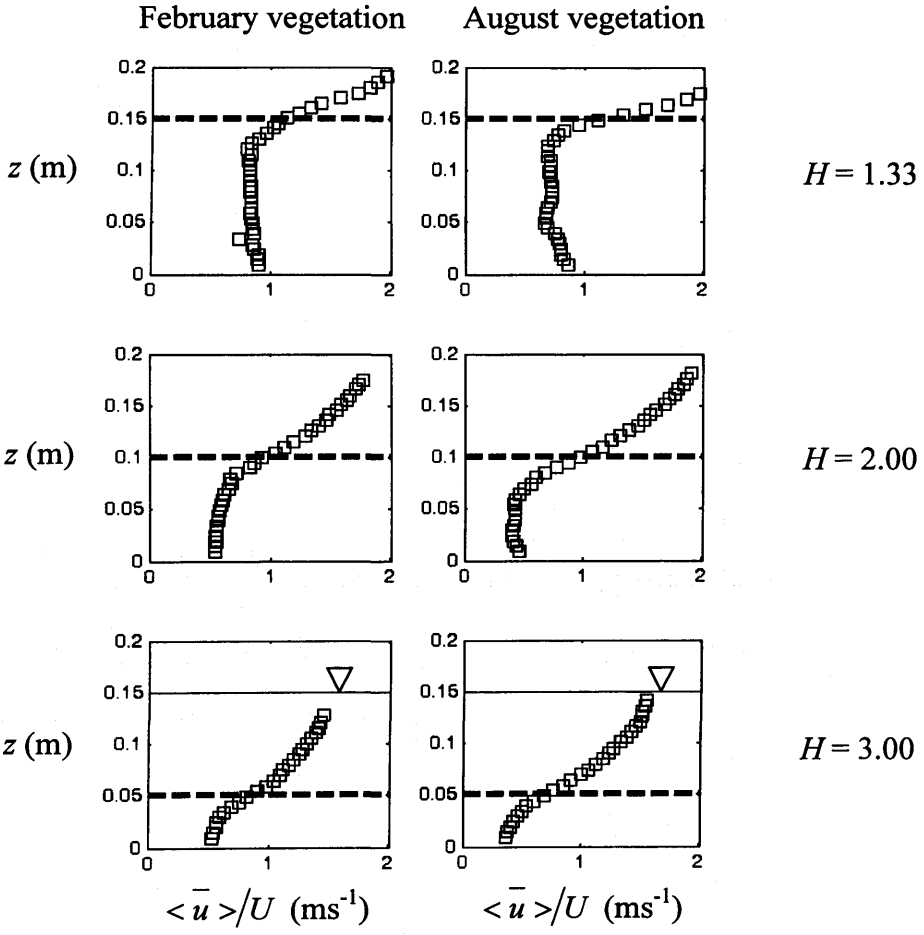

Figure 7-50 Profiles of normalised longitudinal velocity for submerged February and August vegetation canopies, for a bed gradient of 1/1000, a stem density of 800 stem m^{-2} and submergence levels of 1.33, 2.00 and 3.00. The dashed line marks the top of the vegetation. U is the depth-averaged longitudinal velocity.

7.5.4 Reynolds Stress

For emergent conditions, flow through the February canopies was more turbulent than that through the August canopies. The average stem Reynolds numbers over the flow depths for the two canopies were 360 and 250 respectively. For the August canopy, values were generally around a stem Reynolds number of 200 throughout the canopy height (Figure 7-26), above which vortex shedding is thought to be initiated within dense canopies, as observed by Nepf *et al.* (1997b) (Section 2.2.6). The normalised Reynolds stress profiles are presented in Figure 7-51. The Reynolds stress formed a considerably greater proportion of the total stress budget for the February vegetation. Average stem Reynolds numbers over the canopy depth for submergence levels of 1.33, 2.00 and 3.00 were 510, 650 and 960 respectively for the February canopies, compared to 280, 400 and 540 for the August canopies. The higher Reynolds stress values are a result of the changes in gradient of the longitudinal velocity profiles which therefore produce greater spread in the normalised Reynolds stress magnitudes.

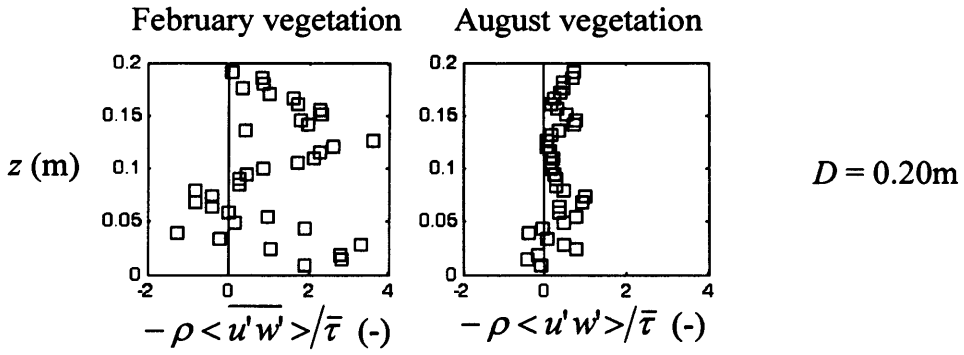

Figure 7-51 Profiles of normalised Reynolds stress (normalised by the depth-averaged total shear stress values) for emergent February and August vegetation canopies, a bed gradient of 1/1000, a stem density of 800 stem m^{-2} and a flow depth of 0.20m. $\bar{\tau}$ is the depth-averaged total shear stress.

The thinner plant stems together with the lower projected area of the plant material has resulted in a greater depth of Reynolds stress penetration for the February canopy (see Figure 7-52).

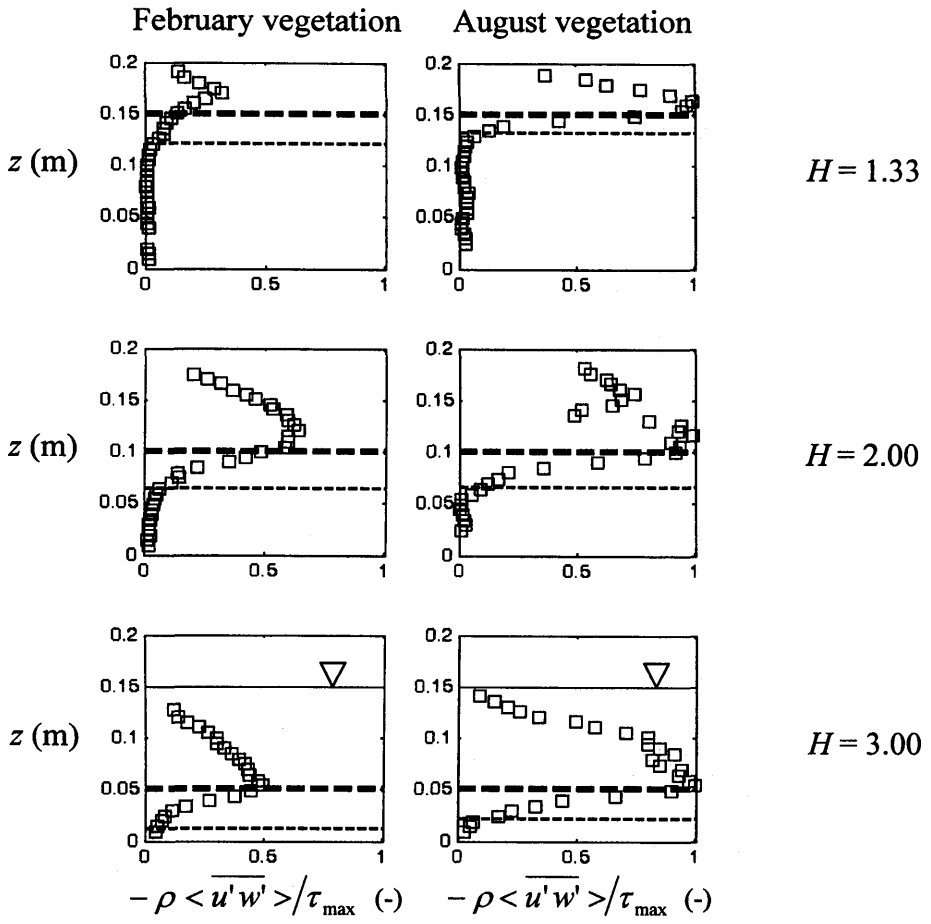

Figure 7-52 Profiles of normalised Reynolds stress (normalised by the maximum shear stress values) for submerged February and August vegetation canopies, a bed gradient of 1/1000, a stem density of 800 stem m^{-2} and submergence levels of 1.33, 2.00 and 3.00. The bold dashed line marks the top of the canopies, the faint dashed line marks the shear penetration depth, and τ_{max} is the peak total shear stress value over the flow depth.

7.5.5 "Form-induced" Stress

"Form-induced" stress profiles were discussed in Section 7.4.6 for three stem densities of August vegetation (800, 1160 and 1850 stems m^{-2}). As discussed previously, a significant "form-induced" stress is indicative of large variations in flow velocities at different locations within the canopy. This may be attributed to variation in the vegetation structure. Compared to an 800 stems m^{-2} canopy of August vegetation, "form-induced" stress magnitudes were greater through February vegetation as shown in Figure 7-53 for emergent conditions, and in Figure 7-54 for submerged conditions. This, in part, may be due to the higher Reynolds number range of the flow through the February vegetation canopies (Section 7.5.4), where the flow was more turbulent due to the higher flow velocities imposed. Variations in flow

velocities due to turbulence production in the wakes of the heterogeneous vegetation may have therefore been amplified compared to the August vegetation canopies. "Form-induced" stresses were also high above the canopies for submerged February canopies in Figure 7-54.

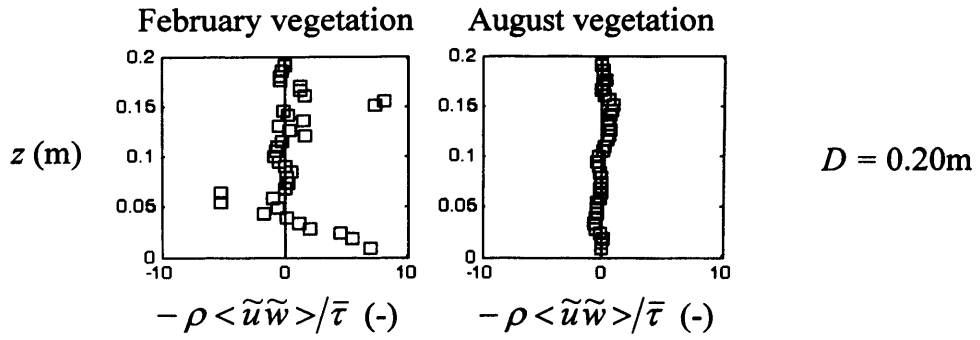

Figure 7-53 Profiles of normalised "form-induced" stress for emergent February and August vegetation canopies, a bed gradient of 1/1000, a stem density of 800 stem m^{-2} and a flow depth of 0.20m. $\bar{\tau}$ is the depth-averaged total fluid stress.

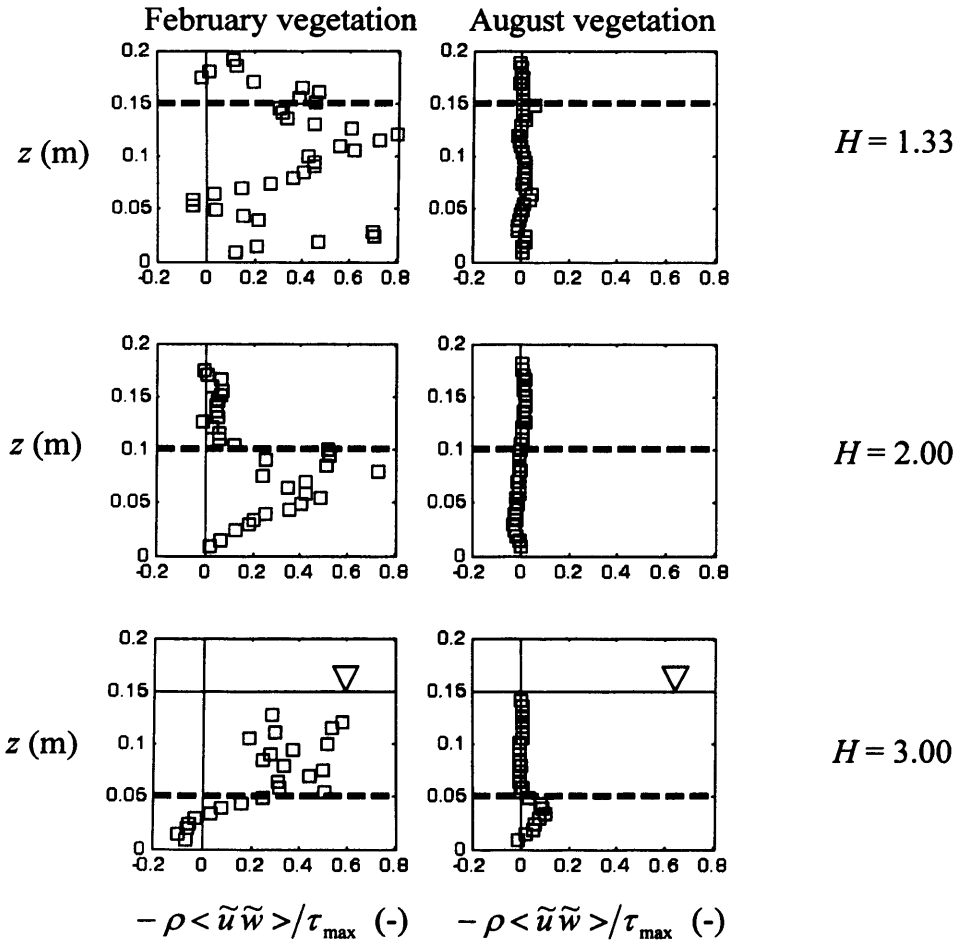

Figure 7-54 Profiles of normalised "form-induced" stress for submerged February and August vegetation canopies, a bed gradient of 1/1000, a stem density of 800 stem m^{-2} and submergence levels of 1.33, 2.00 and 3.00. The bold dashed line marks the top of the canopies. τ_{max} is the peak total fluid stress over the flow depth.

7.6 Two-Dimensional Drag Coefficients

7.6.1 Two-Dimensional Drag Coefficient Definition

In Section 7.2.2, the one-dimensional bulk drag coefficient was determined for the experiments conducted to assess how bed gradient, stem density, Reynolds number, submergence level and seasonality affected canopy flow resistance. A similar comparison is presented here, except the variation in drag coefficients over the height of each canopy was evaluated using a two-dimensional definition of drag coefficient which includes the Reynolds stress term (Section 2.3.7).

Lightbody and Nepf (2006a) highlighted the difficulties in predicting velocity profiles for submerged conditions due to the large magnitudes of Reynolds stress that affect the flow structure within the canopy layer. In Section 7.2.2.1, where the one-dimensional bulk drag coefficient, $\overline{C_D}'$, was calculated for submerged canopies, the shear force at the canopy-surface flow layer interface was included in the force balance to resolve for the magnitude of the drag force due to the canopy. Similarly, to determine the two-dimensional drag coefficient, $C_{D\,2D}$, for a given elevation within the canopy, where the shearing is dominated by the Reynolds stress, the Reynolds stress term must be included in the calculation. The derivation proposed by Dunn *et al.* (1996) has been used in this study where the two-dimensional drag coefficient is given by Equation 2.34, the derivation of which is presented in Appendix I. The derivation is conducted with the assumption of a fully-turbulent uniform, unidirectional flow with negligible sidewall effects and a viscous sublayer. The total shear stress is assumed to follow a linear relationship from a minimum value at the water surface level to a maximum value at the bed level, whereby the Reynolds stress is suppressed wthin the canopy layer due to the drag force created by the vegetation.

The $C_{D\,2D}$ coefficient is used to characterise the magnitude of the hydraulic resistance due to the vegetation at any given elevation within the canopy layer. The coefficient is dependant on the vegetation characteristics, such as the stem size and spacing, and the stiffness of the vegetation, as well as the flow characteristics, namely the velocity and Reynolds stress.

7.6.2 Emergent and Submerged Conditions

For emergent conditions, the variation in Reynolds stress over the canopy height was negligible (Figure 7-29). Hence, there was little variation in the turbulence structure over the flow depth. Profiles of the two-dimentional drag coefficients are presented in Figure 7-55 for a bed gradient of 0.00$\dot{3}$ and in Figure 7-56 for a bed gradient of 0.001. Vertical variation in the coefficients profiles was more likely due to variation in the vegetation structure such as the projected area or the difference in properties between the stem region near the bed and the foliage region higher up in the canopy. For a bed gradient of 0.001, the 1850 stems m^{-2} canopy experienced a smaller range of Reynolds numbers over the flow depth compared to the 800 and 1160 stems m^{-2} canopies (Section 7.4.2). This resulted in less variation in coefficient calues over the canopy height.

Profiles of $C_{D\,2D}$ for submerged conditions are presented in Figure 7-57 for a bed gradient of 0.00$\dot{3}$ and Figure 7-58 for a bed gradient of 0.001. The decrease in the magnitudes of $C_{D\,2D}$ at higher elevations and at the higher submergence level of 3.00 can be in part attributed to the removal of plant foliage in the cropping process to scale the vegetation down as outlined in Section 5.2.4.2. This resulted in a lower projected area of obstruction at the top of the canopy and hence, higher longitudinal velocities and Reynolds numbers.

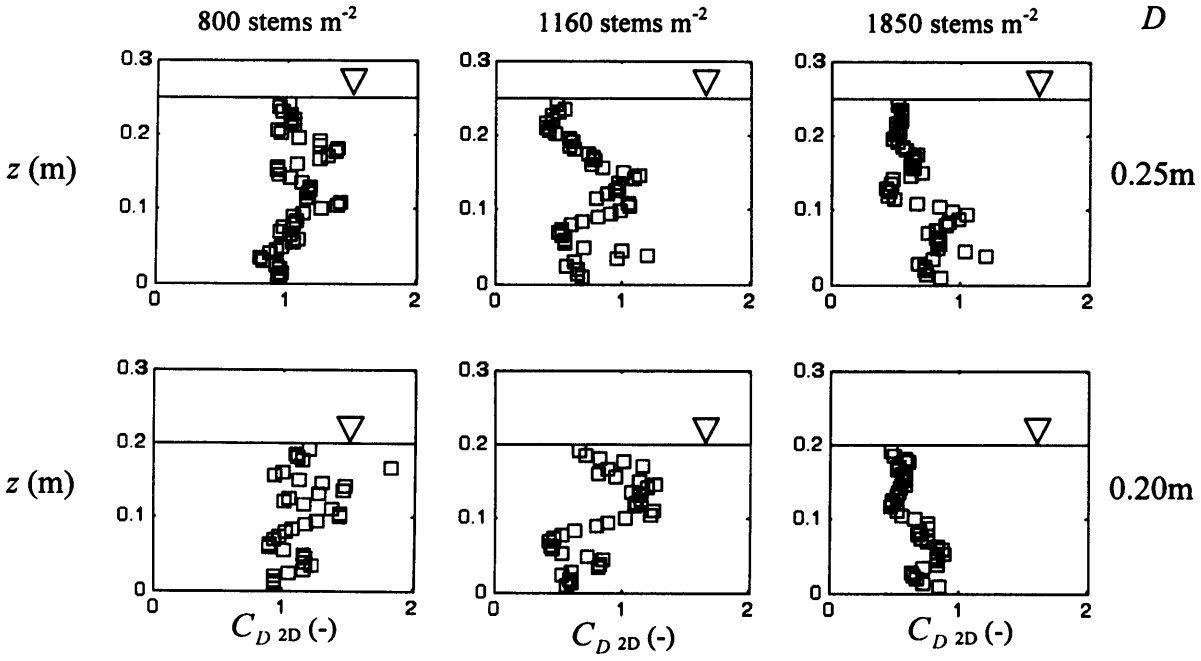

Figure 7-55 $C_{D\,2D}$ profiles for emergent flow conditions and a bed gradient of 1/300 for flow depths, *D*, of 0.20 m and 0.25 m

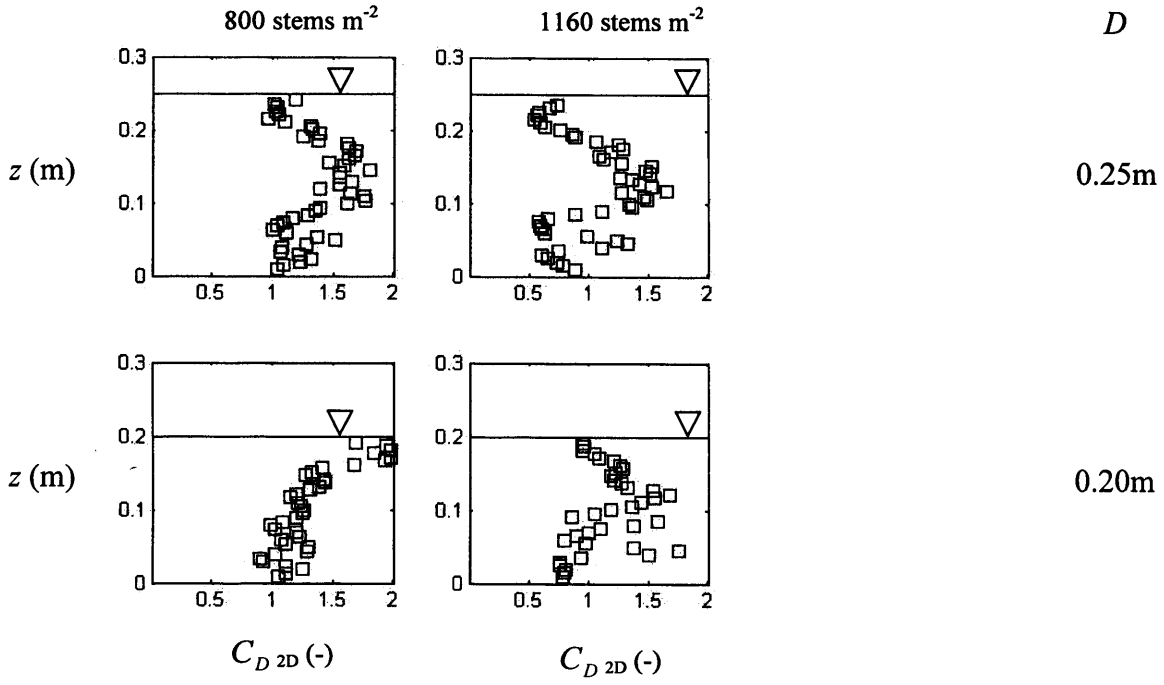

Figure 7-56 $C_{D\,2D}$ profiles for emergent flow conditions and a bed gradient of 1/1000 for flow depths, *D*, of 0.20 m and 0.25 m

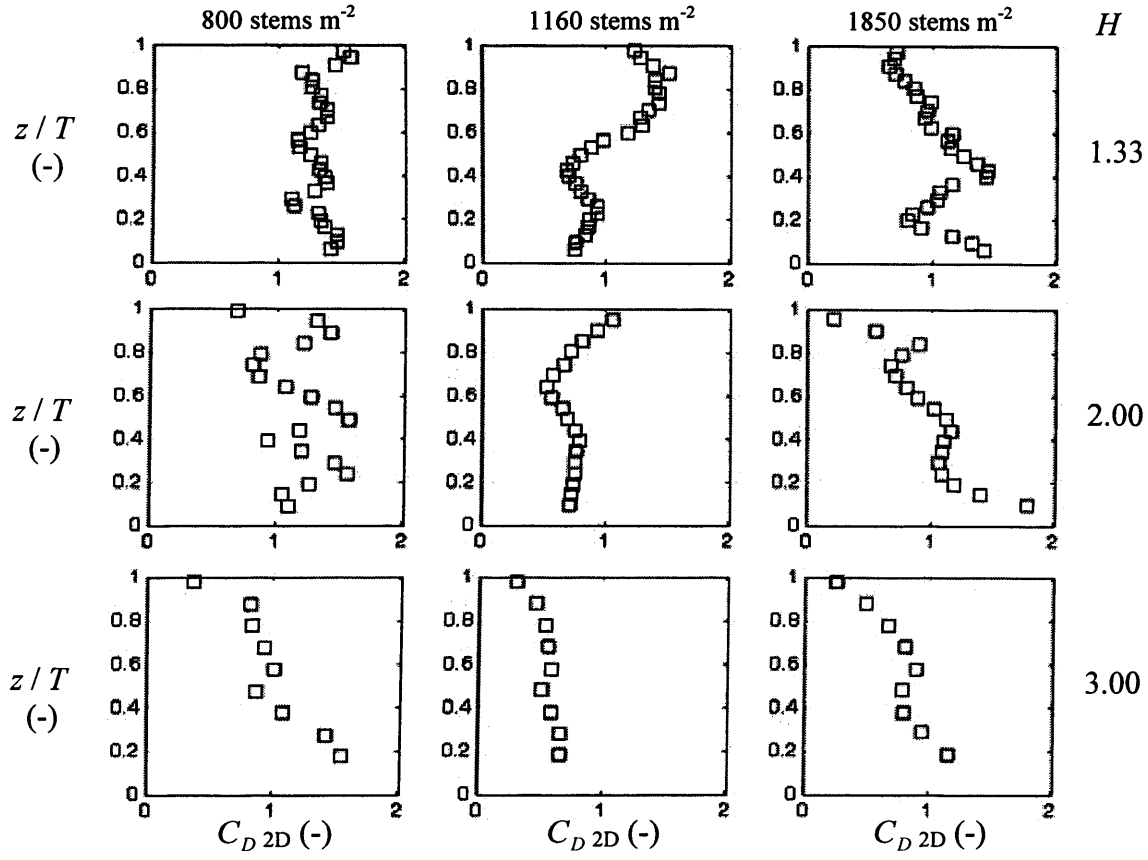

Figure 7-57 $C_{D\,2D}$ profiles for submerged flow conditions and a bed gradient of 1/300 for submergence levels, *H*, of 1.33, 2.00 and 3.00

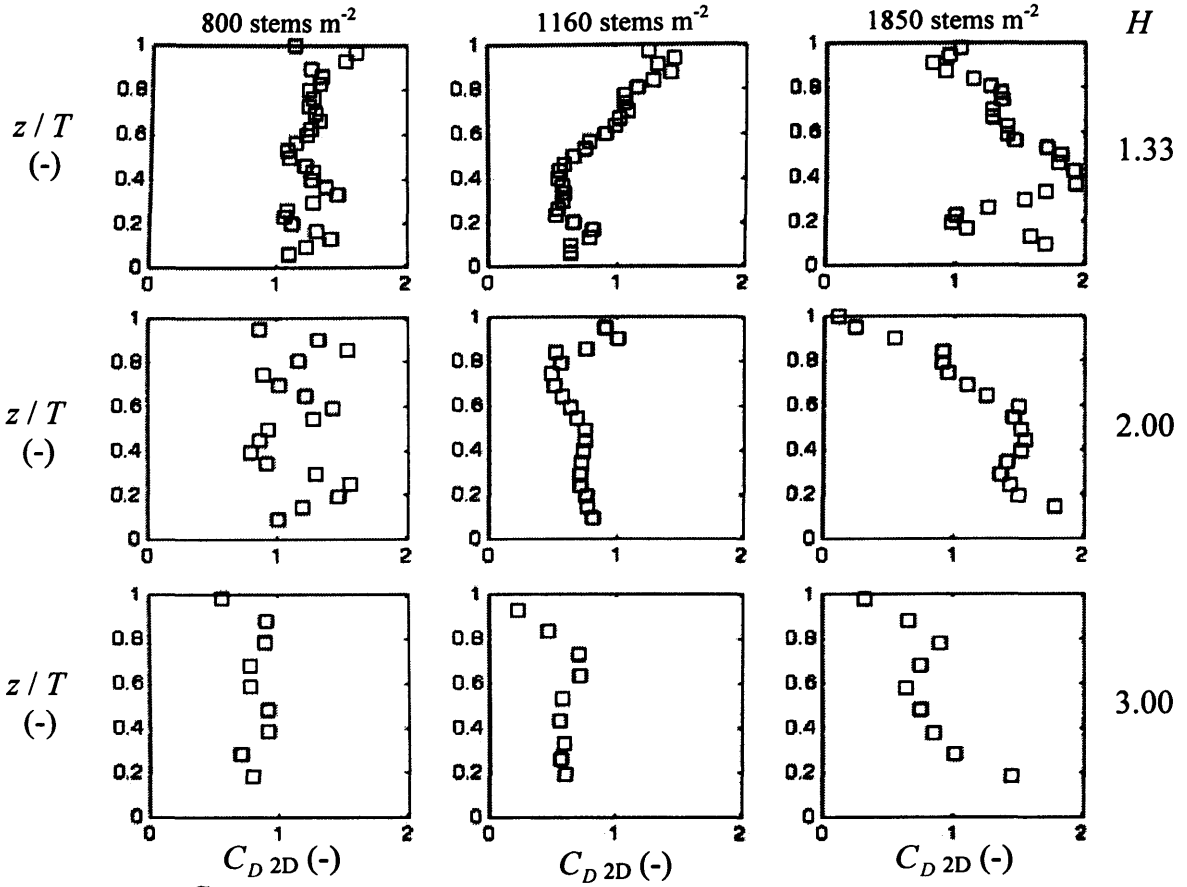

Figure 7-58 $C_{D\,2D}$ profiles for submerged flow conditions and a bed gradient of 1/1000 for submergence levels, *H*, of 1.33, 2.00 and 3.00

In Figure 7-59 and Figure 7-60, the one-dimensional bulk drag coefficient, $\overline{C_D}$ and the depth-averaged two-dimensional drag coefficient, $C_{D\,2D}$, are compared for emergent and submerged conditions respectively. The key difference between the two methods is in the depth of flow over which the water body weight and the vegetation drag force are resolved to determine the drag coefficient. In the one-dimensional approach, which is used to calculate $\overline{C_D}$, the forces are resolved over the entire flow depth meaning that the weight of the surface flow layer is included in the calculation (refer to Section 2.3.5).

In the two-dimensional approach, $C_{D\,2D}$ is calculated for thin horizontal sections of the canopy and averaged over the height of the canopy. By definition, the $C_{D\,2D}$ calculation cannot be used for the surface flow layer where there is no obstruction of flow (refer to Equation 2.34). In theory, inclusion of the Reynolds stress term in the two-dimensional approach compensates for the turbulent stress within the flow in the canopy layer, which to a large extent is influenced by the higher

velocity surface flow layer. This concept was shown through the evaluation of Reynolds stress penetration into submerged canopies in Section 7.4.4. However, the results presented in Figure 7-60 suggest otherwise, and the reason that one-dimensional drag coefficients are usually higher for a given canopy than the two-dimensional counterpart is that the drag force is calculated by resolving against a larger water body which includes the surface flow layer. Hence, for the emergent cases, where $C_{D\,2D}$ was averaged for the entire flow depth in the absence of a surface flow layer, there was very close resemblance between the one-dimensional and two-dimensional coefficients.

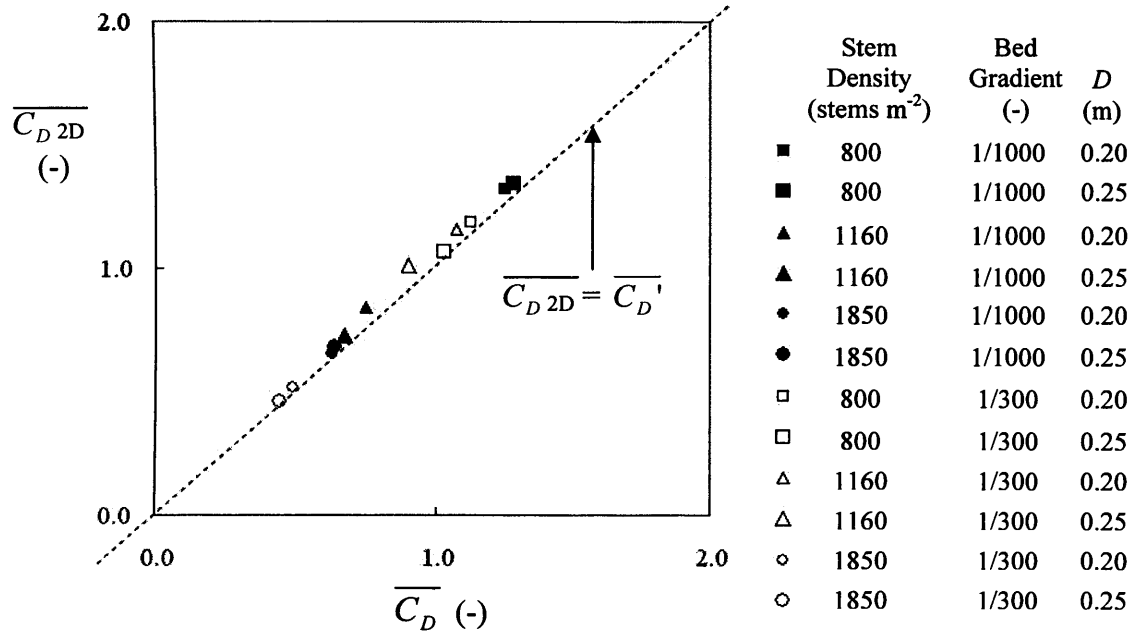

Figure 7-59 A comparison between the bulk drag coefficient, $\overline{C_D}$, and the depth-average of the two-dimensional drag coefficient, $\overline{C_D}'_{2D}$ for emergent *Spartina anglica* canopies for flow depths of 0.20m and 0.25m, and for August and February vegetation canopies.

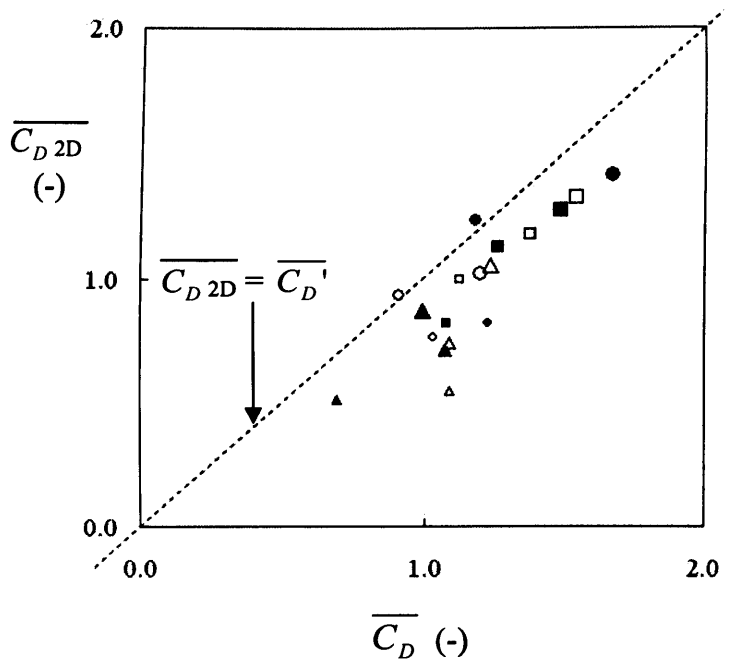

Stem Density (stems m^{-2})	Bed Gradient (-)	H (-)
■ 800	1/1000	1.33
■ 800	1/1000	2.00
■ 800	1/1000	3.00
▲ 1160	1/1000	1.33
▲ 1160	1/1000	2.00
▲ 1160	1/1000	3.00
● 1850	1/1000	1.33
● 1850	1/1000	2.00
◆ 1850	1/1000	3.00
□ 800	1/1000	1.33
□ 800	1/1000	2.00
□ 800	1/1000	3.00
△ 1160	1/1000	1.33
△ 1160	1/1000	2.00
△ 1160	1/1000	3.00
○ 1850	1/1000	1.33
○ 1850	1/1000	2.00
○ 1850	1/1000	3.00

Figure 7-60 A comparison between the bulk drag coefficient, $\overline{C_D}$, and the depth-average of the two-dimensional drag coefficient, $\overline{C_{D\,2D}}$ for submerged *Spartina anglica* canopies for submergence levels of 1.33, 2.00 and 3.00, for August and February vegetation canopies.

7.7 Concluding Remarks

A series of laboratory experiments were performed in which a 10m long laboratory flume was vegetated with a typical saltmarsh species commonly found along coastal saltmarshes in Great Britain, namely *Spartina anglica*. A range of stem densities (800, 1160 and 1850 stems m^{-2}) and bed gradients (0.001 and 0.003) were investigated under both emergent and submerged conditions. The experiments were conducted under uniform flow conditions.

Based on a comparison between the stage-discharge curves for the submerged and emergent canopies for a flow depth of 0.02 m, a reduction in submergence level from 2.00 to an emergent state could result discharge reductions between 20% and 42%. The percentage reduction in discharge increased with increasing stem density and decreased with increasing bed gradient. A reduction in submergence level from 3.00 to an emergent canopy could result in reductions in discharge of between 60% and 74%. However, it should be noted that due to the scaling method applied to the vegetation, the canopy structure was altered significantly with changes to the submergence level.

Longitudinal velocity profile shapes were influenced by the vertical distribution of vegetation material. The magnitudes of longitudinal velocities in the stem region near the bed were often greater than values for higher elevations in the canopy where vegetation foliage results in a greater level of obstruction to the flow.

The flow structure at the canopy-surface flow layer for submerged conditions is complex. Longitudinal velocities were significantly higher in the surface flow layer compared to the canopy layer. The ratio of the depth-averaged velocity of the surface flow layer to the depth-averaged velocity for the total layer, U_S/U, was examined to evaluate the distribution of the flow between the canopy and surface flow layers. For higher submergence levels, where the vegetation was shortened and foliage was removed from the canopy, the hydraulic resistance of the canopy was reduced, velocities through the canopy layer were higher and the U_S/U ratio was smaller. Furthermore, U_S/U increased with increasing stem density as this resulted in an increase of the hydraulic resistance of the canopy.

The interface between the canopy and surface flow layers resulted in a highly turbulent region near the interface between the two layers. Reynolds stress profiles showed a peak a short distance above the interface, and the magnitude was reduced significantly a short distance into the canopy (except where a significant amount of foliage had been removed). Reynolds stress penetration decreased with increasing stem density and with decreasing submergence level because in both cases, the amount of foliage within the canopy increased. Foliage is believed to play a significant role in dissipating turbulence from the interface region and reducing the impact of the higher velocities in the surface flow layer on the velocities near the bed.

Across the canopy-surface flow layer interface, the longitudinal velocity gradient is large and a shear layer is generated which is dominated by vortices acting along the vertical plane. Quadrant analysis was used to show the upward and downward movements of particles and it was found to be significant at the interface region, and to a lesser extent, at the mid-canopy height. The rotational capacity of the vortices increased with the velocity gradient, which was greater for a steeper bed gradient and a higher submergence level. The effects of the shear layer appeared to be effective over a greater depth of the canopy with increasing submergence level, although this was related to the removal of plant foliage by shortening the canopy

since the foliage had been shown to reduce Reynolds stress penetration into the canopy.

The one-dimensional drag coefficient, $\overline{C_D}$, and two-dimensional drag coefficient, $C_{D\,2D}$, provided a quantitative method for characterising the hydraulic resistance of the canopy. $\overline{C_D}$ values ranged between 0.6-1.3 for emergent conditions and increased with decreasing stem density due to a higher level of resistance contributed per unit volume of vegetation. For submerged conditions, values ranged between 0.4-0.6 for the February vegetation (800 stems m^{-2} and a bed gradient of 0.001) and between 0.7-1.7 for August vegetation within the ranges of stem density and bed gradients listed above. Drag coefficients were lower for the February vegetation due to thinner plants within the canopy and higher Reynolds numbers due to the higher velocities that the winter canopy were conducted at. However, for the submerged condition, the correlation between $\overline{C_D}$ and the stem density and bed gradient was weaker compared to the emergent condition due to significant differences in the flow regimes between the submerged canopies. The range of values observed was of a similar order of magnitude to the drag coefficient for a single cylinder ranging between Reynolds numbers of 100 and 100000, which usually ranged between 1.0 and 2.0.

The impact of the Reynolds number on one-dimensional drag coefficients must be accounted for when comparing the drag coefficients calculated for different canopies due to the difference in flow conditions (e.g. flow rates and submergence levels) implemented. It would therefore be convenient to compare the drag coefficients for different canopies at similar Reynolds numbers, and by doing so, the increase in hydraulic resistance, corresponding to an increase in drag coefficient, can be observed with increasing stem density and decreasing bed gradient. However, if the experiments on different canopies were conducted for the same Reynolds numbers, then the flow depth or flow rate would not be the same.

Gradients of the drag coefficient – Reynolds number curves were considerably greater for the submerged canopies indicating that drag coefficient values are strongly dependant on the Reynolds number. For the emergent canopies, despite the average Reynolds numbers of the flows being considerably lower, the curve gradients were considerably smaller indicating that coefficient values were relatively constant over a wide range of Reynolds numbers. The mean Reynolds values for all the experiments

fell within the range that is characteristic of vortex shedding which is shown by zone C in Figures 2-5 and 2-6.

The increase in hydraulic resistance with increasing total amount of vegetation material was observed more clearly for both submerged and emergent conditions when the parameter $\overline{C_D}'$ was considered, which combines the drag coefficient, $\overline{C_D}$, and the projected area of obstruction per unit volume of the canopy, *a*, into a product parameter. The parameter quantifies the total drag force resulting from a vegetation canopy due to both the vegetation characteristics (e.g. stiffness and stem diameter) and the quantity of the vegetation (e.g. the stem density and the projected area of obstruction per unit volume). Values ranged between 5 and 20 m^{-1} for emergent canopies, 7 and 49 m^{-1} for submerged August canopies, and 2 and 4 m^{-1} for submerged February canopies. Magnitudes of $\overline{C_D}'$ consistently increased with the quantity of vegetation material, as characterised by the projected area per unit volume, *a*, regardless of whether the increase was due to a higher stem density, or larger stem diameters, whereby stem diameters were larger for August vegetation compared to February vegetation.

Although there were differences in the material properties of the August and February vegetation, it was the difference in plant sizes that was the main cause for the difference in hydraulic resistance between the two canopies. The August plants were larger (larger stem diameters and a bigger leaf surface area), thus resulting in a greater level of obstruction, and greater hydraulic resistance.

The two-dimensional drag coefficient, $C_{D\,2D}$, which varies over the canopy height, characterises the vertical variation in drag force over the canopy height. This is influenced by the projected area profile which reflects the difference between the stem and foliage regions, and the Reynolds number which is linked to the velocity and turbulence structures and is also variable over the canopy height. For the highest submergence level of 3.00, a decrease in $C_{D\,2D}$ was observed towards the top of the canopy and this was linked to the removal of foliage in the scaling process. With less foliage in the upper part of the canopy, there was less obstruction to the flow and longitudinal velocities were higher which corresponds to higher Reynolds numbers. For the lower subergence levels of 1.33 and 2.00, there was less consistency in the two-dimensional drag coefficient profile shapes and this could be linked to the heterogeneity of the vegetatioon.

Depth-averaged two-dimensional drag coefficient values were of similar magnitudes to the one-dimensional parameter, particularly for the emergent condition where Reynolds stresses were negligible. For submerged canopies, the difference was linked to the treatment of the surface flow layer in the one-dimensional parameter and the Reynolds stresses in the two-dimensional parameter.

8 Velocity and Turbulence Structure Prediction Methods

8.1 Introduction

In this chapter, the data collected in the laboratory experiments presented earlier in Chapter 7 will be used to reveal trends relating the canopy characteristics (e.g. stem density and projected area) to the velocity profiles and turbulence structures of the flow. If such trends can be verified successfully, they may be applied to saltmarsh environments to predict velocity and turbulence structures for cases where the vegetation canopies resemble the constructed vegetation canopies used to develop the relationships. This can be useful considering the difficulty of collecting field data to characterise the flow velocity and turbulence structure through saltmarsh canopies. The relationships are developed from the experiments conducted on non-dormant *Spartina anglica* vegetation collected during August 2006, for stem densities of 800, 1160 and 1850 stems m^{-2}, for both emergent and submerged canopies (refer to Section 7.1 for full details).

The prediction method presented enables the user to predict velocity and Reynolds stress profiles for both emergent and submerged conditions for uniform flow conditions. The profile shapes and magnitudes can be predicted effectively using this method. In the process of predicting the profiles, relationships are presented for calculating mean canopy layer velocities and Reynolds stresses. For the submerged canopies, relationships have also been presented for calculating the mean surface flow layer velocities, peak Reynolds stress over the flow depth and the shape of the Reynolds stress profile in the upper section of the canopy where the increase in Reynolds stress with elevation is significant.

The relationships and formulae will be developed empirically using data presented in Chapter 7. Verification of the formulae will be conducted using data outside the empirical domain. A selection of the dataset for the August vegetation was reserved for the validation process as listed in Figure 8-1 where the datasets used for derivations and validations are listed separately. In this chapter, the data will be presented followed by a working example demonstrating how the relationships developed from the data can be applied to predict velocity and Reynolds stress magnitudes and profile shapes through vegetation canopies. An appropriate regression curve will be fitted to the data in each case.

Figure 8-1 The range of tests from which data was used to derive and verify the relationships presented in this chapter for submerged canopies. $\overline{a}$ is the projected area per unit volume and Re_d is the stem Reynolds number calculated based on the mean canopy layer velocity.

Test No.	Vegetation	Stem Density (stems m^{-2})	Bed Gradient (-)	T (m)	D (m)	$\overline{a}$ (m^{-1})	Re_d (-)
The following canopies were used for deriving the relationships							
*D-T11	August	1850	1/300	Emergent	0.20	29.8	252
S-V10	August	800	1/300	0.05	0.15	6.6	145
S-S11	August	800	1/300	0.10	0.20	7.2	70
S-M11	August	800	1/300	0.15	0.20	7.4	42
S-V20	August	800	1/1000	0.05	0.15	6.6	42
S-S21	August	800	1/1000	0.10	0.20	7.2	24
S-M21	August	800	1/1000	0.15	0.20	7.4	13
**M-V20	August	1160	1/1000	0.05	0.15	14.1	34
**M-S21	August	1160	1/1000	0.10	0.20	16.3	13
**M-M21	August	1160	1/1000	0.15	0.20	17.3	9
D-V10	August	1850	1/300	0.05	0.15	22.1	36
**D-S11	August	1850	1/300	0.10	0.20	25.9	24
D-M11	August	1850	1/300	0.15	0.20	28.9	11
D-V20	August	1850	1/1000	0.05	0.15	22.1	9
D-S21	August	1850	1/1000	0.10	0.20	25.9	5
D-M21	August	1850	1/1000	0.15	0.20	28.9	2
The following canopies were used for verification of the relationships							
S-T21	August	800	1/1000	Emergent	0.20	7.4	252
S-T22	August	800	1/1000	Emergent	0.25	7.3	251
M-T21	August	1160	1/1000	Emergent	0.20	17.7	183
M-T22	August	1160	1/1000	Emergent	0.25	18.3	196
D-T21	August	1850	1/1000	Emergent	0.20	29.8	156
D-T22	August	1850	1/1000	Emergent	0.25	29.9	164
M-V10	August	1160	1/300	0.05	0.15	14.1	103
M-S11	August	1160	1/300	0.10	0.20	16.3	42
***M-M11	August	1160	1/300	0.15	0.20	17.3	23

** Data used for both derivation as well as validation for the 'shape coefficient' in Section 8.6.4.

*** Data used for both derivation as well as validation for mean canopy velocities for submerged canopies in Section 8.5.2.

8.2 Defining a Representative Canopy

Based on the canopies quantified in Section 5.3, the middle density of 1160 stems m^{-2} will be taken as a representative stem density of a *Spartina anglica* canopy. The projected area profile for a stem density of 1160 stems m^{-2} based on 16 profiles is presented in Figure 8-2. The range of projected areas for stem densities between 800

and 1850 stems m^{-2} are also shown. The values were determined from 16 cross-sections for each stem density. The mean basal stem diameter of non-dormant plants, based on measurements on samples collected during August 2006, is 5.2 mm. A mean canopy height of 0.3m is assumed based on the mean 90th percentile height of the vegetation over a twelve-month monitoring period. The quantification parameters used in this chapter and typical values are listed in Table 8-1.

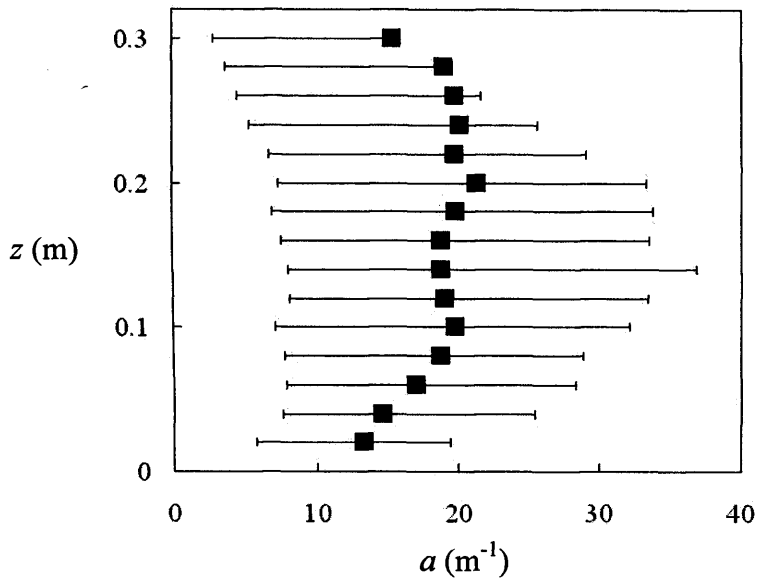

Figure 8-2 A profile of the projected area per unit volume over the canopy height for a stem density of 1160 stems m^{-2}. The error bars show the range of values encompassed by stem densities ranging between 800 and 1850 stems m^{-2}.

Table 8-1 Quantification parameters and suggested values for a typical *Spartina anglica* canopy.

Parameter	Value
Stem density	1160 stems m^{-2}
Canopy Height (T)	0.3 m
Stem spacing (s)	0.0315 m
Stem diameter (d)	5.2 mm
Projected area per unit volume ($\bar{a}$)	18.2 m^{-1}
$\bar{a}s$	0.6

8.3 Velocity Profiles for Emergent Canopies

8.3.1 The Mean Longitudinal Velocity through the Canopy

The one-dimensional drag-force equation (Equation 2.28), can be used to determine the roughness or drag coefficient for uniform flow conditions, can be rearranged for an expression of the mean velocity through the canopy. Consider two different canopies: 'Canopy 1' and 'Canopy 2'. The bed gradients for the canopies are S_1 and S_2 respectively, the projected area per unit volume for each canopy is $\bar{a}_1$ and $\bar{a}_2$ while the respective bulk drag coefficients are $\overline{C_{D1}}$ and $\overline{C_{D2}}$. 'Canopy 1' will be taken as a reference canopy for which the parameters U_1 and a_1 are known for one flow depth, D_1. Rearranging Equation 2.28 for the velocity term and applying it to the two canopies yields:

$$U_{C1}{}^2 = \frac{2gS_1}{\bar{a}_1 \overline{C_{D1}}} \qquad \text{[Equation 8.01]}$$

$$U_{C2}{}^2 = \frac{2gS_2}{\bar{a}_2 \overline{C_{D2}}} \qquad \text{[Equation 8.02]}$$

A plot of the drag coefficient against the Reynolds number for emergent canopies is reproduced from the bulk roughness coefficient, $\overline{C_D}'$, against Reynolds number plot presented in Figure 7-9. For emergent canopies with similar properties, the variation in drag coefficient was relatively small when compared to the variations in roughness coefficients, particularly for stem Reynolds numbers above 100.

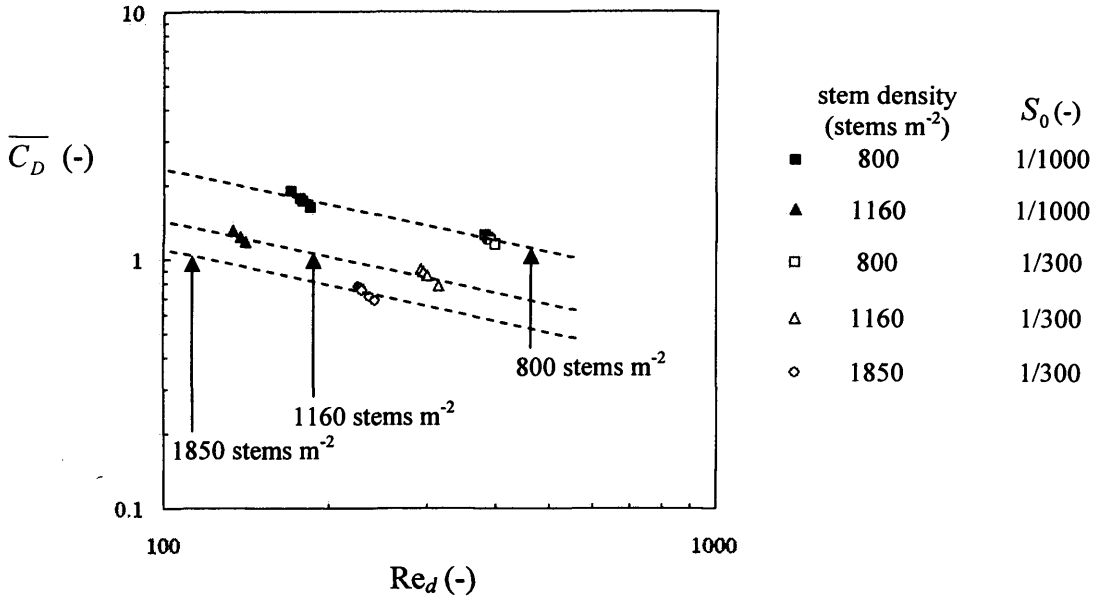

Figure 8-3 Variation in the drag coefficient with the stem Reynolds number for emergent canopies.

Based on these observations, drag coefficient values for emergent canopies with similar stem densities and Reynolds numbers close to or above the transition value of approximately 200 (see Section 2.2.4) are assumed to be similar in magnitude. It has been suggested that the drag coefficient is not a strong function of stem density or Reynolds number for rigid vegetation for stem densities below 3000 stems m^{-2} and Reynolds numbers below 10000 (Koch and Ladd, 1997; Nepf, 1999; Stone and Shen, 2002). The following step is adapted from the Lightbody and Nepf (2006a) method for determining velocity profile shapes through the canopy (see Section 2.4.3). Equation 8.02 is then divided by Equation 8.01 to give:

$$\frac{U_{C2}^{\ 2}}{U_{C1}^{\ 2}} = \frac{2gS_2}{\bar{a}_2\overline{C_{D2}}}\frac{\bar{a}_1\overline{C_{D1}}}{2gS_1} = \frac{\bar{a}_1 S_2 \overline{C_{D1}}}{\bar{a}S_1\overline{C_{D2}}} \approx \frac{\bar{a}_1 S_2}{\bar{a}_2 S_1} \qquad \text{[Equation 8.03]}$$

which can be rearranged to give an expression that can be used to calculate the mean velocity of a uniform flow through an emergent canopy, U_{C2}, if the bed gradient, S_2, and projected area per unit volume, $\bar{a}_2$, are known (Equation 8.04). All values for the reference canopy ($U_{C1}, S_1, \bar{a}_1$) must also be known. The projected area per unit volume can be determined from the photographic method (Section 4.2.2) and bed

gradients can be calculated based on bed levels determined from LiDAR data (Section 3.2.2.2).

$$U_{C2} = U_{C1}\sqrt{\frac{\bar{a}_1 S_2}{\bar{a}_2 S_1}} \qquad \text{[Equation 8.04]}$$

For an emergent canopy with a stem density of 1850 stems m^{-2}, bed gradient of $0.00\dot{3}$ and a flow depth of 0.20m, the depth-averaged projected area per unit volume is 29.8 m^{-1}. From the measured velocity values presented in Section 7.3.1.1, the mean longitudinal velocity was 0.059 ms^{-1}. These values will be used for the reference canopy (Canopy 1). The values are used in Figure 8-4 to implement the method proposed above to predict the depth-averaged velocity through the emergent canopies for which the flow depth is 0.25m. The estimated values are consistently within 10% of the averaged measured values.

Figure 8-4 Prediction of mean longitudinal velocities through emergent canopies. S_0 is the bed gradient, D is the flow depth, $\bar{a}$ is the projected area per unit volume and U_C is the mean velocity through the canopy.

Stem Density (stems m^{-2})	S_0 (-)	D (m)	$\bar{a}$ (m^{-1})	Estimated U_C (ms^{-1})	Measured U_C (ms^{-1})	Error (U_S) (-)
800	1/300	0.25	7.28	0.089	0.093	-4.4%
800	1/1000	0.25	7.28	0.046	0.046	1.2%
1160	1/300	0.25	18.3	0.069	0.073	-5.4%
1160	1/1000	0.25	18.3	0.031	0.034	-8.5%
1850	1/300	0.25	29.9	0.059	0.059	0.9%

8.3.2 Velocity Profile Shapes and Magnitudes

As mentioned in the previous section, Lightbody and Nepf (2006a) proposed a method for predicting the velocity at an elevation within emergent canopies using a reference velocity and reference projected area per unit volume at a reference elevation within each canopy (see Section 2.4.3). The method assumes the projected area of obstruction profiles over the canopy height to be directly linked to the shapes of the longitudinal velocity profiles. Results from the experiments conducted on constructed vegetation canopies and uniform cylinder arrays in Chapters 6 and 7

showed that the vertical distribution of material in the canopy is indeed closely linked to the velocity profile shapes.

The prediction method involves estimating the longitudinal velocity for any elevation based on the fluid momentum balance and on the velocity profile varying inversely with the canopy morphology. The method can then be used to predict the longitudinal velocity at a particular elevation provided that the projected area per unit volume at that particular elevation is known, and as long as the longitudinal velocity and the projected area per unit volume are also known for a reference elevation within the canopy. Lightbody and Nepf (2006a) used a reference elevation of 0.15m above the bed.

A similar concept is applied here, but instead of using values for a reference elevation, the estimated depth-averaged value of the velocity through the canopy, U_C, and the depth-averaged projected area per unit volume, $\overline{a}$, are used and the longitudinal velocity at an elevation within the canopy, u, is given by Equation 8.05. A profile of projected area per unit volume for the canopy and the mean velocity through the canopy must be known.

$$u = U_C \sqrt{\frac{\overline{a}}{a}} \qquad \text{[Equation 8.05]}$$

where a is the projected area per unit volume at the elevation where u is to be determined. The projected area per unit volume profiles are known for the canopies considered in this study (see Section 5.3.3) and can be averaged for the height of the submerged part of the canopy to determine $\overline{a}$. Values of U_C are estimated according to the method outlined in Section 8.3.1 and used to determine the predicted profiles, which are presented in Figure 8-5 for the canopies with stem densities of 800, 1160 and 1850 stems m^{-2}, for a flow depth of 0.25m and a bed gradient of $0.00\dot{3}$. For the application of this method, vertical variation in the drag coefficient is assumed to be insignificant compared to the variation in projected area (see Section 7.6.2). It should be noted that the Reynolds stress term in the two-dimensional drag coefficient equation is negligible in emergent conditions (Equation 2.37).

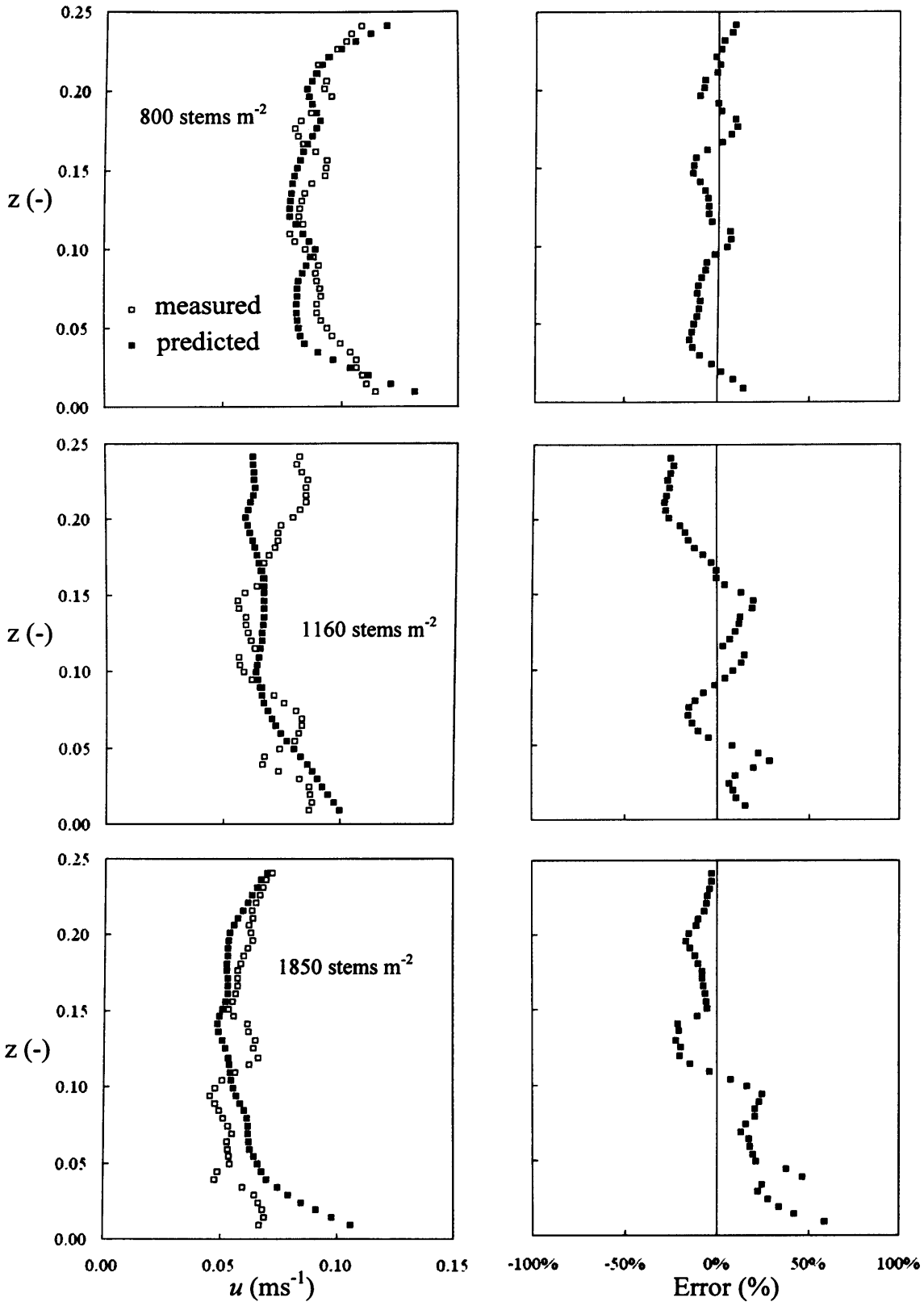

Figure 8-5 Measured (□) and predicted (■) longitudinal velocity profiles and the errors incurred in the predicted values for emergent *Spartina anglica* canopies, for stem densities of 800, 1160 and 1850 stems m^{-2}, a flow depth of 0.25m and a bed gradient of 1/300.

Errors in the predictions are also presented and on average, the predicted values were within 7.4%, 13.9% and 17.1% of the measured values for the three stem densities respectively.

8.4 Reynolds Stress Profiles for Emergent Canopies

It is generally accepted that Reynolds stresses within emergent canopies are negligible in magnitude (e.g. Lightbody and Nepf, 2006a). For the sake of completeness, the magnitude of the mean Reynolds stress over the canopy height, $-\rho u'w'_C$, is related to the mean canopy velocity, U_C, in Figure 8-6.

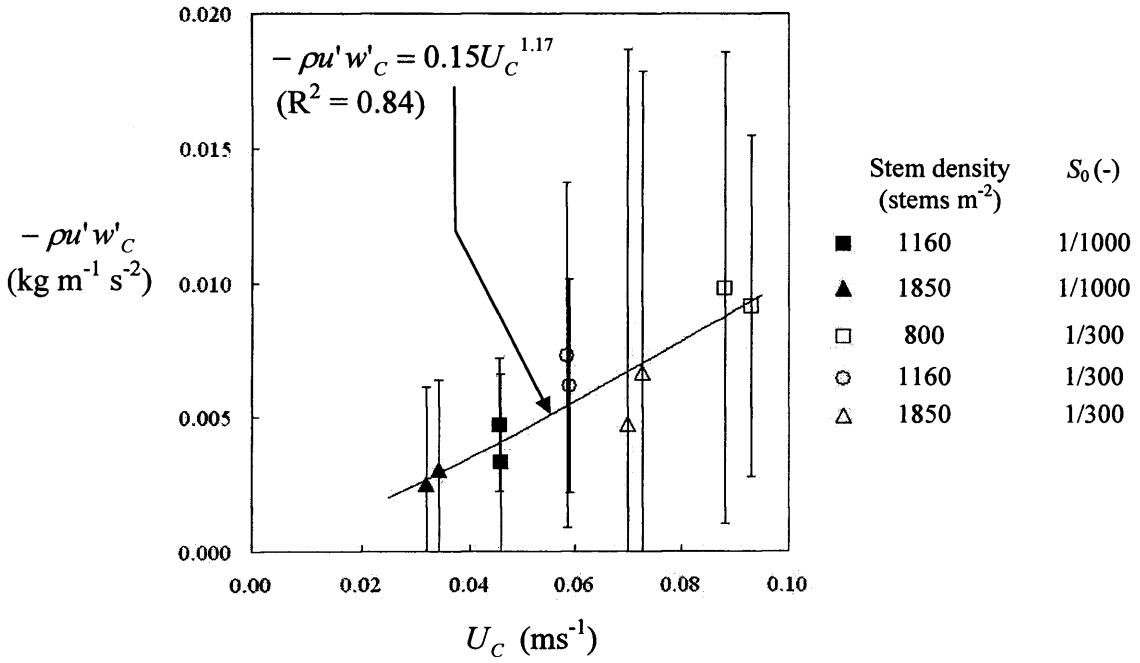

Figure 8-6 The relationship between the mean canopy Reynolds stress, $-\rho u'w'_C$, and the mean velocity, U_C, for emergent canopies with stem densities of 800, 1160 and 1850 stems m^{-2}, flow depths of 0.20m and 0.25m, and bed gradients of 1/1000 and 1/300. For each stem density and bed gradient, the higher mean Reynolds stress value corresponds to a flow depth of 0.20m, and the lower value corresponds to a flow depth of 0.25m. The vertical bars show the standard deviations.

Mean Reynolds stress values for the emergent canopies ranged between 0.002 kg m^{-1}s^{-2} and 0.010 kg m^{-1}s^{-2} and standard deviations were large ranging between 50% and 300%. However, the mean Reynolds stress values observed for the emergent

canopies were significantly smaller than the peak values observed for the submerged canopies which ranged between 0.17 kg $m^{-1}s^{-2}$ and 2.46 kg $m^{-1}s^{-2}$ (see Section 7.4.4). A power function was assigned to the data for the emergent canopies as follows:

$$-\rho u'w'_C = 0.15U_C^{1.17} \qquad \text{[Equation 8.06]}$$

Due to the limited data available, this is verified later in Section 8.6.3 using data from the lower part of the submerged canopies.

8.5 Velocity Profiles for Submerged Canopies

8.5.1 Mean Surface Flow Layer Velocities

Above the canopy, the flow is usually turbulent, and if the surface flow layer is considered separately from the canopy layer, then the roughness, which is caused by the vegetation, does not protrude into the surface flow layer. The Manning's equation is applied to determine values of n_S, the Manning's roughness coefficient specific to the surface flow layer where the top of the vegetation is treated as the bed roughness. Because the sidewalls of the flume are smooth, the surface flow domain is treated as a wide channel and the hydraulic radius is taken to be equal to the depth of the surface flow layer, h_S:

$$n_S = \frac{h_S^{2/3} S_0^{1/2}}{U_S} \qquad \text{[Equation 8.07]}$$

Roughness at the bottom of the surface flow layer is likely to be a function of the density of the vegetation beneath. This is characterised here by the dimensionless product parameter $\bar{a}s$, where $\bar{a}$ is the mean projected area per unit volume of the canopy and s is the stem spacing.

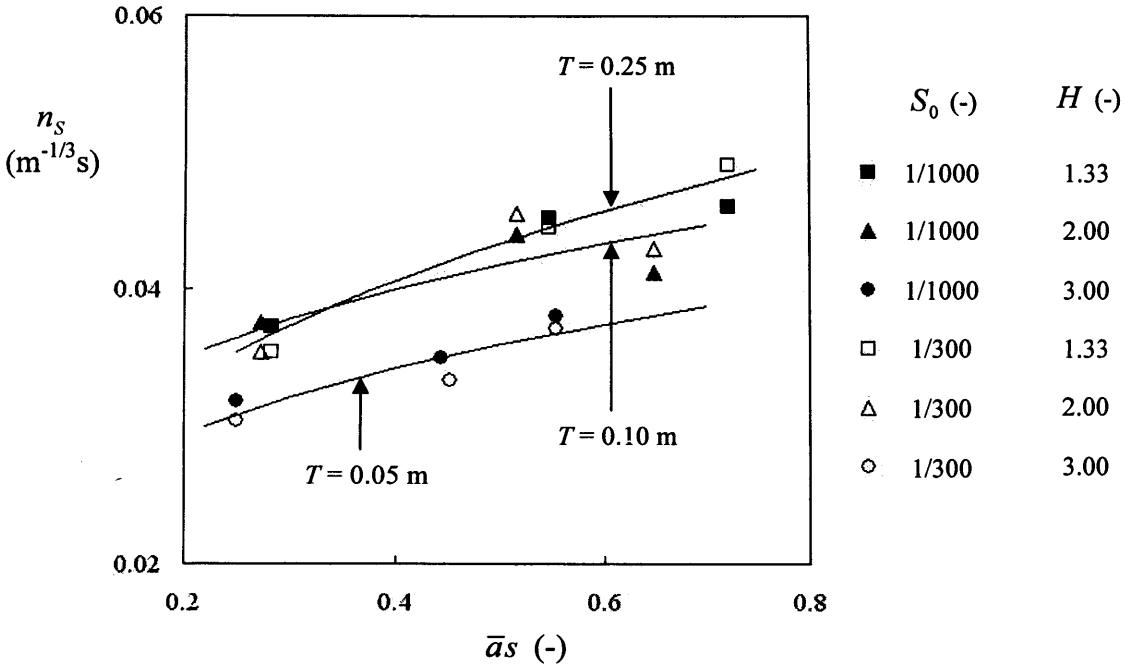

Figure 8-7 The relationship between the Manning's roughness coefficient specific to the surface flow layer, n_S, and the vegetation density parameter, $\bar{a}s$, where $\bar{a}$ is the mean projected area per unit volume of the canopy and s is the stem spacing. S_0 is the bed gradient, T is the canopy height and H is the submergence level. Data is presented for stem densities of 800, 1160 and 1850 stems m^{-2}, submergence levels of 1.33, 2.00 and 3.00, and bed gradients of 1/1000 and 1/300.

The value of n_S decreased for a shorter canopy height, particularly for the shortest canopy (the 0.05m tall canopy). This is most likely due to the cropping of the vegetation which resulted in less foliage with decreasing canopy height. The following relationships were deduced for each canopy height, T:

For $T = 0.05$ m: $n_S = 0.042(\bar{a}s)^{0.22}$ $R^2 = 0.86$ [Equation 8.08]

For $T = 0.10$ m: $n_S = 0.048(\bar{a}s)^{0.20}$ $R^2 = 0.67$ [Equation 8.09]

For $T = 0.15$ m: $n_S = 0.053(\bar{a}s)^{0.29}$ $R^2 = 0.95$ [Equation 8.10]

Substituting into Equation 8.07 gives the following expressions for the mean canopy velocity for each canopy height

:

For $T = 0.05$ m: $$U_S = \frac{h_S^{2/3} S_0^{1/2}}{0.042(\bar{a}s)^{0.22}}$$ [Equation 8.11]

For $T = 0.10$ m: $$U_S = \frac{h_S^{2/3} S_0^{1/2}}{0.048(\bar{a}s)^{0.20}}$$ [Equation 8.12]

For $T = 0.15$ m: $$U_S = \frac{h_S^{2/3} S_0^{1/2}}{0.053(\bar{a}s)^{0.29}}$$ [Equation 8.13]

The data presented in Figure 8-8 was reserved for validation of the relationships developed above. Estimated values of the mean surface flow layer velocity were within 5% of the averaged measured values. Where a value of $\bar{a}s$ is unknown, a value of 0.6 is suggested based on the canopy presented in Section 8.2 (a stem density of 1160 stems m^{-2} and a canopy height of 0.3 m).

Figure 8-8 Prediction of mean longitudinal velocities in the surface flow layer above submerged canopies. s is the stem spacing, S_0 is the bed gradient, T is the canopy height, D is the flow depth, $\bar{a}$ is the projected area per unit volume, n_S is the Manning's roughness coefficient specific to the surface flow layer and U_S is the mean surface flow layer velocity.

Stem Density (stems m^{-2})	s (m)	S_0 (-)	T (m)	D (m)	$\bar{a}$ (m^{-1})	n_S ($m^{-1/3}s$)	Estimated U_S (ms^{-1})	Measured U_S (ms^{-1})	Error (U_S) (-)
1160	0.0315	1/300	0.05	0.15	14.3	0.044	0.355	0.356	0.1%
1160	0.0315	1/300	0.10	0.20	16.3	0.072	0.296	0.283	-4.5%
1160	0.0315	1/300	0.15	0.20	17.3	0.112	0.177	0.174	-2.1%

Based on the available data, it will be assumed that the mean surface flow layer velocity above an uncropped *Spartina anglica* canopy can be characterised by Equation 8.13 for the 0.15 m canopies which contained the greatest surface area of foliage in the upper canopy compared to the 0.05 m and 0.10 m canopies. There is also an indication, according to Figure 8-7, that for cropped canopies with a height of 0.10m or greater, there was relatively little difference in the surface flow layer Manning's roughness coefficient.

8.5.2 Mean Canopy Layer Velocities

For a given vegetation height, the morphology of the vegetation was similar for the different stem densities. Hence, the parameter most likely to affect the ratio of the mean velocity through the canopy, U_C, to the mean velocity through the surface

flow layer, U_S, for uniform flow conditions, is the stem density. The stem density can be characterised by the stem spacing, s, which decreases with increasing stem density. A linear relationship was realised between the mean canopy layer velocity, U_C, and between the product of the mean surface flow layer velocity, U_S, and the stem spacing, s. This is shown in Figure 8-10 and the relationship is defined as follows:

$$U_C = 10.4 s U_S \qquad \text{[Equation 8.14]}$$

The mean surface flow layer velocity, U_S, can be determined as demonstrated in the Section 8.5.1. Using the estimated values of U_S presented in Figure 8-8, the mean canopy layer velocities are estimated within 15% of the averaged measured values (see Figure 8-9).

Figure 8-9 Prediction of mean longitudinal velocities through the canopy for submerged canopies. s is the stem spacing, S_0 is the bed gradient, T is the canopy height, D is the flow depth, U_S is the mean surface flow layer velocity and U_C is the mean velocity through the canopy.

					Estimated		Measured	Error
Stem Density (stems m^{-2})	s (m)	S_0 (-)	T (m)	D (m)	U_S (ms^{-1})	U_C (ms^{-1})	U_C (ms^{-1})	(U_C) (-)
1160	0.0315	1/300	0.05	0.15	0.355	0.116	0.134	-13.3%
1160	0.0315	1/300	0.10	0.20	0.296	0.097	0.086	12.7%
1160	0.0315	1/300	0.15	0.20	0.177	0.058	0.064	-9.2%

Errors in the estimated mean canopy layer velocity values can be reduced by considering the 0.15m canopy separately (see Figure 8-11) and determining a relationship between the canopy and surface flow layer velocities. This is because the difference in morphology between the three vegetation heights considered in Figure 8-10 was significant and grouping them together to produce a comprehensive relationship can lead to larger errors. The new relationship specific to the 0.15m canopy is defined as follows:

$$U_C = 11.2 s U_S \qquad \text{[Equation 8.15]}$$

Equation 8.15 is used to estimate mean canopy layer velocities within 10% of the averaged measured values using mean surface flow layer velocities estimated using Equation 8.13 (see

Figure 8-12).

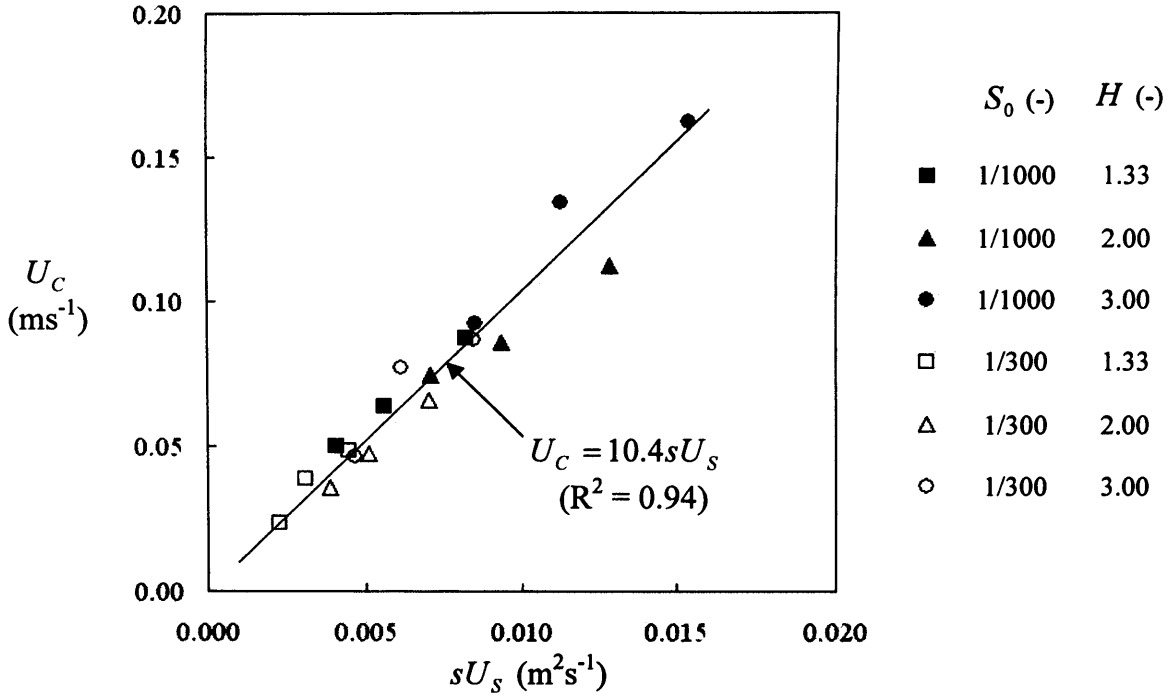

Figure 8-10 The relationship between the mean canopy layer velocity, U_C, and the product parameter sU_S for submerged canopies, where s is the stem spacing and U_S is the mean surface flow layer velocities. Data is presented for stem densities of 800, 1160 and 1850 stems m^{-2}, submergence levels of 1.33, 2.00 and 3.00, and bed gradients of 1/1000 and 1/300.

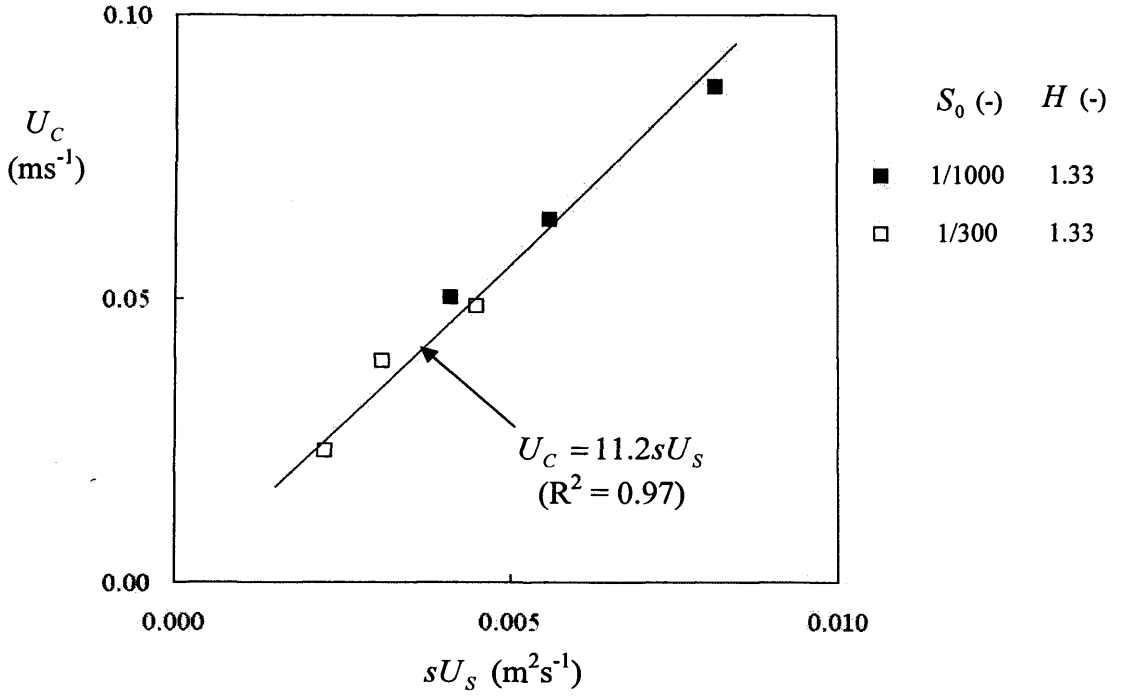

Figure 8-11 The relationship between the mean canopy layer velocity, U_C, and the product parameter sU_S for 0.15m tall submerged canopies, where s is the stem spacing and U_S is the mean surface flow layer velocities. Data is presented for stem densities of 800, 1160 and 1850 stems m^{-2} and bed gradients of 1/1000 and 1/300.

Figure 8-12 Improved predictions of mean longitudinal velocities through the canopy for submerged 0.15m tall canopies. s is the stem spacing, S_0 is the bed gradient, T is the canopy height, D is the flow depth, U_S is the mean surface flow layer velocity and U_C is the mean velocity through the canopy.

Stem Density (stems m^{-2})	s (m)	S_0 (-)	T (m)	D (m)	Estimated U_S (ms^{-1})	Estimated U_C (ms^{-1})	Measured U_C (ms^{-1})	Error (U_C) (-)
800	0.038	1/300	0.15	0.20	0.355	0.091	0.134	4.6%
1160	0.0315	1/300	0.15	0.20	0.296	0.062	0.086	-2.4%
1850	0.025	1/300	0.15	0.20	0.177	0.046	0.064	-9.1%

8.5.3 Velocity Profiles through the Canopy

The adapted version of the Lightbody and Nepf (2006a) method used to predict velocity profiles for the emergent canopies in Section 0 is applied to the submerged canopies. By definition, the approach is inappropriate for submerged conditions since the Reynolds stress term becomes more significant within the upper section of the canopy. However, it was demonstrated in Section 7.4.4 that the foliage

in the upper part of a vegetation canopy plays a significant role in reducing the magnitude of the Reynolds stress within the canopy. Therefore, Reynolds stresses within most of a submerged canopy remain negligible and the approach proposed by Lightbody and Nepf (2006a) may be applicable to submerged canopies.

The predicted profiles are presented in Figure 8-13 for stem densities of 800, 1160 and 1850 stems m^{-2} where the cropped vegetation is 0.15m tall, the flow depth is 0.20m and the bed gradient is $0.00\dot{3}$. Errors in the predictions are also presented and on average, the predicted values were within 13.2%, 9.1% and 16.5% of the measured values for each canopy. Errors in the profile shapes and velocity magnitudes increased for the 0.05m and 0.10m canopies, particularly for the shortest canopy, and it is believed that this is due to the cropping of the vegetation whereby most of the foliage of the vegetation was removed to achieve the shorter canopies (For the sake of brevity, these are not shown here). As explained above, the reason this method was applied successfully to the 0.15m canopies was due to the presence of plant foliage which reduced the Reynolds stress within each canopy significantly. In the absence of foliage, particularly for the 0.05m tall canopies, Reynolds stresses, and consequently drag coefficients, varied significantly within the canopy (see Sections 7.4.4 and 7.6.1).

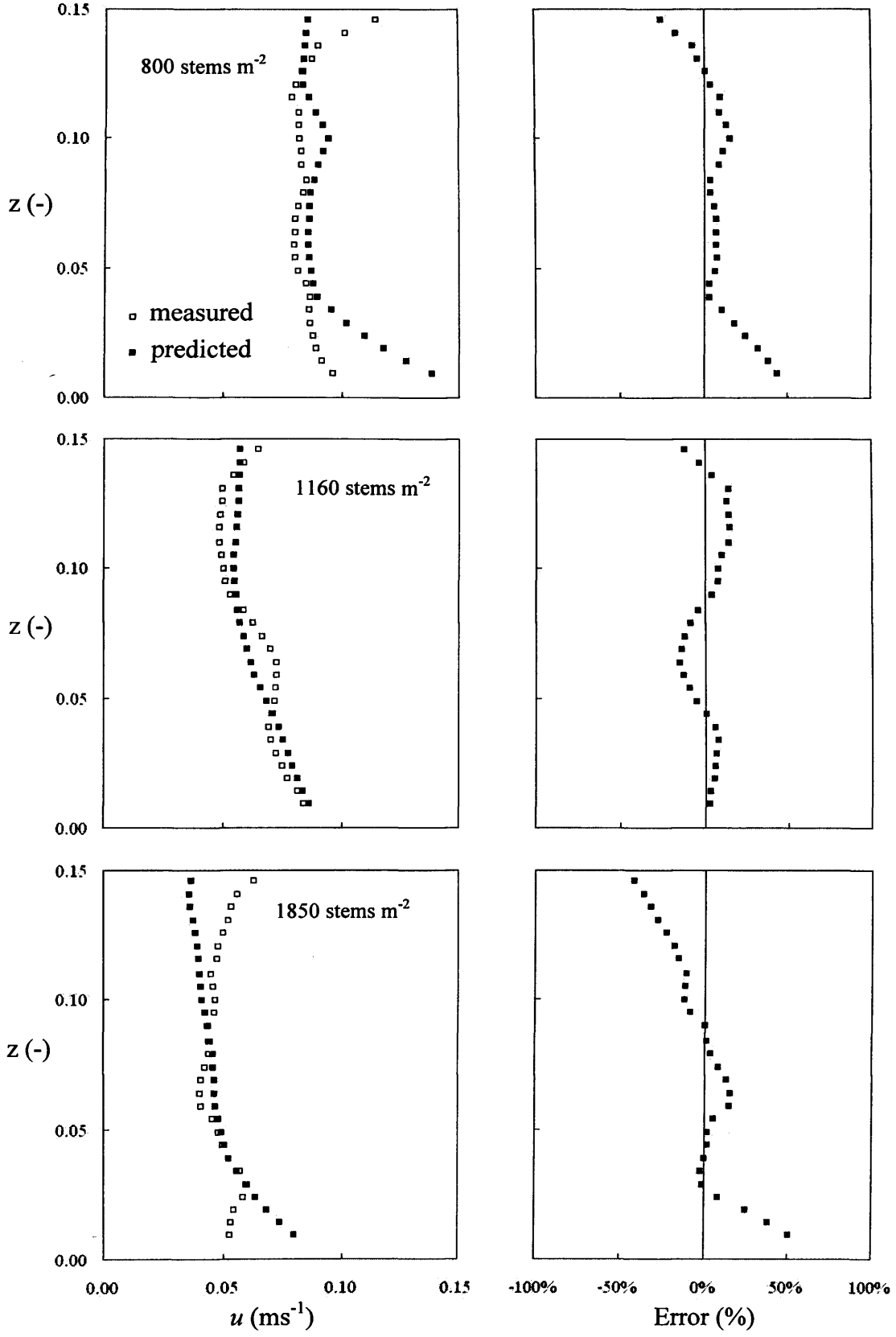

Figure 8-13 Measured (□) and predicted (■) longitudinal velocity profiles and the errors incurred in the predicted values for submerged *Spartina anglica* canopies, for stem densities of 800, 1160 and 1850 stems m^{-2}, a canopy height of 0.15m, a flow depth of 0.20m and a bed gradient of 1/300.

8.6 Reynolds Stresses in Submerged Canopies

8.6.1 Peak Reynolds Stress Magnitudes

The peak in Reynolds stress occurring around the interface between the canopy and surface flow layers is a feature of the mixing layer analogy which characterises the region between two bodies of fluid moving adjacent to each other with different velocities (see Section 2.5.4). To characterise this relationship, the peak Reynolds stress term, $-u'w'_{max}$, was related to the square of the difference between the mean surface flow and canopy layer velocities:

$$-u'w'_{max} = 0.043(U_S - U_C)^2 \qquad \text{[Equation 8.16]}$$

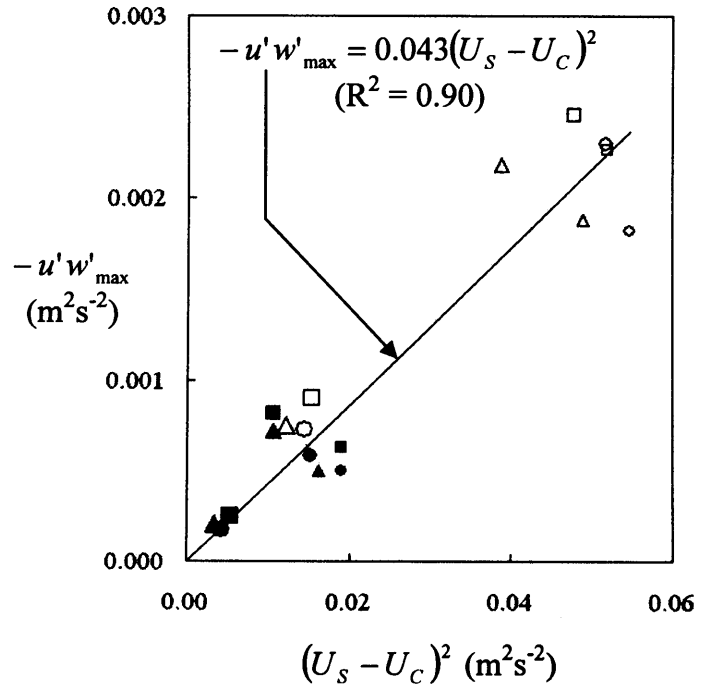

Data used to develop the relationship:

	Stem density (stems m^{-2})	S_0 (-)	T (m)	H (-)
■	800	1/1000	0.05	3.00
■	800	1/1000	0.10	2.00
■	800	1/1000	0.15	1.33
▲	1160	1/1000	0.05	3.00
▲	1160	1/1000	0.10	2.00
▲	1160	1/1000	0.15	1.33
●	1850	1/1000	0.05	3.00
●	1850	1/1000	0.10	2.00
●	1850	1/1000	0.15	1.33
□	800	1/300	0.05	3.00
□	800	1/300	0.10	2.00
□	800	1/300	0.15	1.33
○	1850	1/300	0.05	3.00
○	1850	1/300	0.10	2.00
○	1850	1/300	0.15	1.33

Data used for validation:

	Stem density (stems m^{-2})	S_0 (-)	T (m)	H (-)
△	1160	1/300	0.05	3.00
△	1160	1/300	0.10	2.00
△	1160	1/300	0.15	1.33

Figure 8-14 The relationship between the peak Reynolds stress term above a submerged canopy, $-u'w'_{max}$, and the square of the difference between the mean canopy layer (U_C) and surface flow layer (U_S) velocities. Data is presented for stem densities of 800, 1160 and 1850 stems m^{-2}, submergence levels of 1.33, 2.00 and 3.00, and bed gradients of 1/1000 and 1/300.

The mean surface flow layer velocity, U_S, and canopy layer velocity, U_C, can be estimated from Equations 8.13 and 8.14 respectively. Using the estimated values presented in Sections 8.5.1 and 8.5.2 respectively, the peak Reynolds stress term, $-u'w'_{max}$, was predicted within 30% of the peak values determined from measured results.

Figure 8-15 Prediction of peak Reynolds stress magnitudes above submerged canopies. S_0 is the bed gradient, T is the canopy height, D is the flow depth, U_S is the mean surface flow layer velocity, U_C is the mean velocity through the canopy and $-u'w'_{max}$ is the peak Reynolds stress term.

Stem Density (stems m^{-2})	S_0 (-)	T (m)	D (m)	Estimated U_S (ms^{-1})	Estimated U_C (ms^{-1})	Estimated $-u'w'_{max}$ (m^2 s^{-2})	Measured $-u'w'_{max}$ (m^2 s^{-2})	Error $\left(-u'w'_{max}\right)$ (-)
1160	1/300	0.05	0.15	0.355	0.116	2.45×10^{-3}	1.88×10^{-3}	30.3%
1160	1/300	0.10	0.20	0.296	0.097	1.70×10^{-3}	2.18×10^{-3}	-22.1%
1160	1/300	0.15	0.20	0.177	0.058	6.11×10^{-4}	7.47×10^{-3}	-18.3%

8.6.2 The Reynolds Stress Penetration Elevation

The Reynolds stress penetration depth into the canopy, h_{pen}, is defined as the distance from the top of the canopy to the elevation within the canopy where the Reynolds stress is 10% of the peak Reynolds stress value (Nepf and Vivioni, 2000). Below this level, there was significantly less vertical variation in the Reynolds stress (see Section 7.4.4). The peak Reynolds stress occurs close to the top of the canopy, usually within the surface flow layer. The penetration depth is affected by the strength of the shear layer occurring along the canopy-surface flow layer interface and the density of the vegetation cover. The shear layer strength is characterised here by the ratio of surface layer to canopy layer mean velocity, U_S/U_C, and the canopy density is characterised by the parameter $\bar{a}^2 s$, where $\bar{a}$ is the projected area per unit volume and s is the stem spacing. The following linear relationship is proposed to characterise the depth of penetration:

$$\bar{a}^2 s h_{pen} = 0.156\frac{U_S}{U_C} - 0.334 \qquad \text{[Equation 8.17]}$$

$$h_{pen} = \frac{1}{\bar{a}^2 s}\left(0.156\frac{U_S}{U_C} - 0.334\right) \qquad \text{[Equation 8.18]}$$

The mean surface flow layer velocity, U_S, and canopy layer velocity, U_C, can be estimated from Equations 8.13 and 8.14 respectively. The R-squared value for the relationship described by Equation 8.17 was low ($R^2 = 0.63$) and this may be linked to the high level of uncertainty associated with turbulence prediction. It may also be linked to the significant difference in morphology between the canopies used to develop the relationship. The Reynolds stress penetration elevation, $z_{0.1}$, is defined as the distance from the bed to the location of the Reynolds stress penetration depth:

$$z_{0.1} = T - h_{pen} \qquad \text{[Equation 8.19]}$$

$$z_{0.1} = T - \frac{1}{\bar{a}^2 s}\left(0.156\frac{U_S}{U_C} - 0.334\right) \qquad \text{[Equation 8.20]}$$

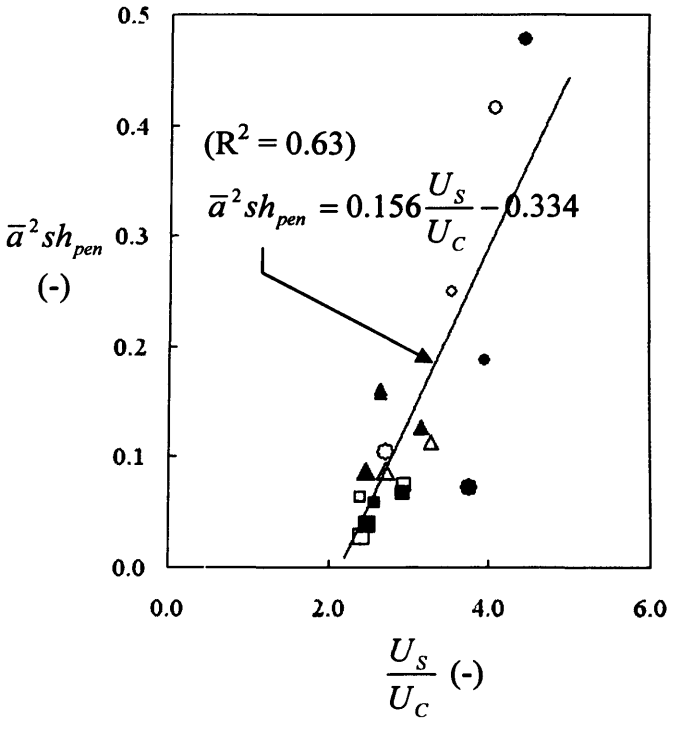

Data used to develop the relationship:

Stem density (stems m^{-2})	S_0 (-)	T (m)	H (-)
■ 800	1/1000	0.05	3.00
■ 800	1/1000	0.10	2.00
■ 800	1/1000	0.15	1.33
▲ 1160	1/1000	0.05	3.00
▲ 1160	1/1000	0.10	2.00
▲ 1160	1/1000	0.15	1.33
● 1850	1/1000	0.05	3.00
● 1850	1/1000	0.10	2.00
● 1850	1/1000	0.15	1.33
□ 800	1/300	0.05	3.00
□ 800	1/300	0.10	2.00
□ 800	1/300	0.15	1.33
○ 1850	1/300	0.05	3.00
○ 1850	1/300	0.10	2.00
○ 1850	1/300	0.15	1.33

Data used for validation:

Stem density (stems m^{-2})	S_0 (-)	T (m)	H (-)
△ 1160	1/300	0.05	3.00
△ 1160	1/300	0.10	2.00
△ 1160	1/300	0.15	1.33

Figure 8-16 The relationship between the dimensionless parameter, $\bar{a}sh_{pen}$, and the ratio of mean surface flow layer (U_S) to canopy layer (U_C) velocity. $\bar{a}$ is the projected area per unit volume, s is the stem spacing and h_{pen} is the Reynolds stress penetration depth. Data is presented for stem densities of 800, 1160 and 1850 stems m^{-2}, submergence levels of 1.33, 2.00 and 3.00, and bed gradients of 1/1000 and 1/300.

Validation of Equation 8.20 is presented in Figure 8-17 for the estimated mean surface flow layer and canopy velocities determined in Sections 8.5.1 and 8.5.2 respectively. A larger error was observed for the 50 mm canopy, although significantly smaller errors were observed for the lesser cropped canopies (100 mm and 150 mm) with the error for the tallest canopy being less than 2%.

Figure 8-17 Prediction of the Reynolds stress penetration elevation for submerged canopies. s is the stem spacing, S_0 is the bed gradient, T is the canopy height, D is the flow depth, U_S is the mean surface flow layer velocity, U_C is the mean velocity through the canopy, h_{pen} is the penetration depth and $(z_{0.1})$ is the penetration elevation.

Stem Density (stems m^{-2})	s (m)	S_0 (-)	T (m)	D (m)	Estimated U_S (ms^{-1})	Estimated U_C (ms^{-1})	Estimated h_{pen} (m)	Estimated $z_{0.1}$ (m)	Measured $z_{0.1}$ (m)	Error $(z_{0.1})$ (-)
1160	0.0315	1/300	0.05	0.15	0.355	0.116	0.018	0.032	0.025	36.5%
1160	0.0315	1/300	0.10	0.20	0.296	0.097	0.024	0.076	0.085	-10.4%
1160	0.0315	1/300	0.15	0.20	0.177	0.058	0.012	0.138	0.141	-1.7%

8.6.3 Reynolds Stresses below the Penetration Depth

Below the Reynolds stress penetration height, Reynolds stress values showed relatively little variation with elevation. Mean values were predicted using Equation 8.06, which was proposed for estimating mean Reynolds stress values for emergent canopies. The predicted values were within 20% of the averaged measured values (see Figure 8-18).

Figure 8-18 Prediction of the mean Reynolds stress below the penetration elevation for submerged canopies. S_0 is the bed gradient, T is the canopy height, D is the flow depth and $-\rho u'w'_C$ is the depth-averaged Reynolds stress term for the section of canopy below the penetration elevation.

Stem Density (stems m^{-2})	S_0 (-)	T (m)	D (-)	Estimated U_C (ms^{-1})	Estimated $-\rho u'w'_C$ (kg m s^{-2})	Measured $-\rho u'w'_C$ (kg m s^{-2})	Error $(-\rho u'w'_C)$ (-)
800	1/1000	0.15	0.20	0.061	0.00452	0.00515	-12.2%
1160	1/1000	0.15	0.20	0.033	0.00290	0.00337	-13.8
1850	1/1000	0.15	0.20	0.025	0.00201	0.00248	-18.7%

8.6.4 Reynolds Stress Profile Shapes

A typical Reynolds stress profile is illustrated in Figure 8-19 for Experiment S-S21 (see Table 5-1 in Section 5.1), where the Reynolds stress penetration elevation (see Section 8.6.2) is marked by a faint dotted line. Below the penetration elevation, there is relatively little variation in the magnitude of Reynolds stress. Above the penetration elevation, there is a large gradient in the Reynolds stress, which increases significantly with elevation towards a peak Reynolds stress value which is often located a small distance above the canopy.

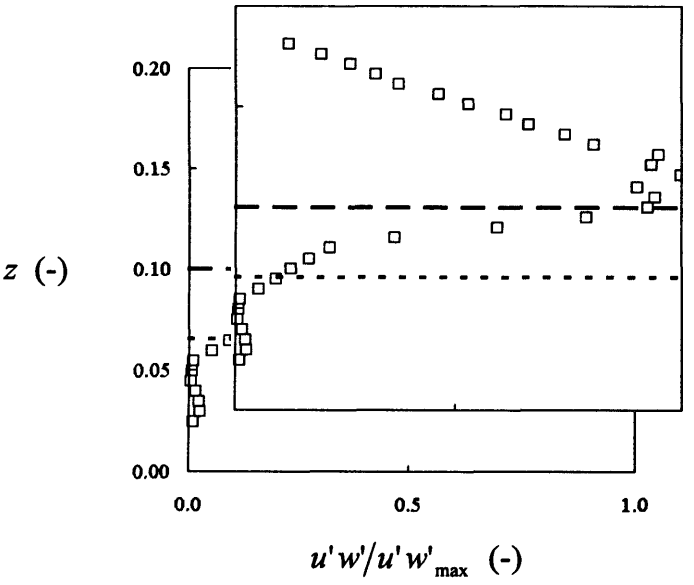

Figure 8-19 A typical normalised Reynolds stress ($u'w'$) profiles for a submerged *Spartina anglica* canopy, where the canopy height is 0.1 m, the flow depth is 0.20 m, the bed gradient is 1/1000 and the stem density id 800 stems m^{-2}. $u'w'_{max}$ is the peak Reynolds stress value, z is the elevation, the bold dotted line denotes the top of the vegetation canopy, and the faint dotted line denotes the Reynolds stress penetration height.

The region between the penetration depth and the canopy top, marked by the bold dotted line, for Experiment S-S21 is shown in Figure 8-20, where the shape of the profile can be approximated to a logarithmic relationship. The penetration elevation, $z_{0.1}$, was taken as the datum, and the elevation was normalised by the canopy height, T.

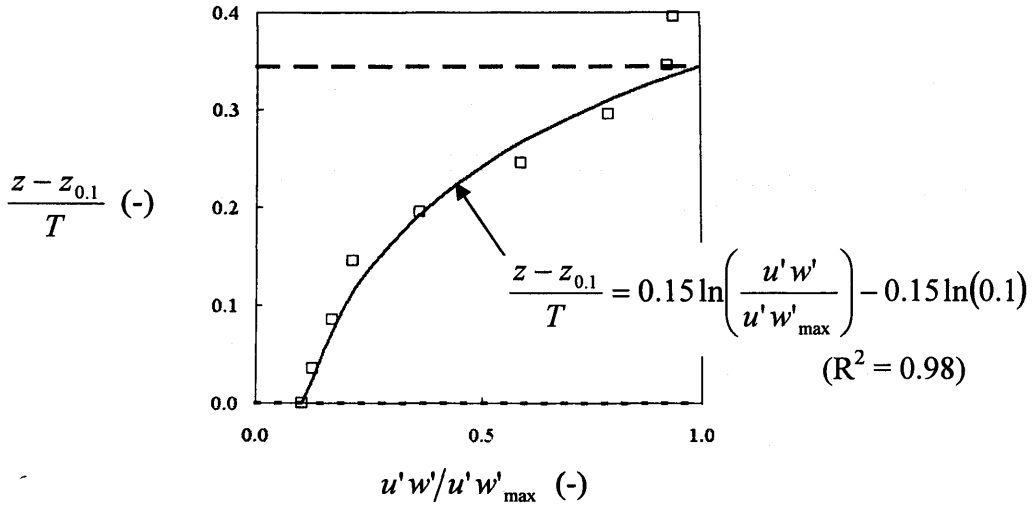

Figure 8-20 The Reynolds stress ($u'w'$) profile shape within the Reynolds stress penetration depth for a submerged *Spartina anglica* canopy, where the canopy height, T, is 0.1 m, the flow depth is 0.20 m, the bed gradient is 1/1000 and the stem density id 800 stems m^{-2}. $u'w'_{max}$ is the peak Reynolds stress value, z is the elevation, $z_{0.1}$ is the Reynolds stress penetration height, the bold dotted line denotes the top of the vegetation canopy, and the faint dotted line denotes the Reynolds penetration depth.

Logarithmic trend lines were fitted to all normalised Reynolds stress plots for the experiments conducted on submerged *Spartina anglica* canopies, where the vegetation was collected during August 2006. The trend lines, which were adjusted to pass through the 0.1 mark along the normalised Reynolds stress axis at the datum level (equivalent to 10% of the peak Reynolds stress), were of the form:

$$\frac{z-z_{0.1}}{T} = \phi\ln\left(\frac{u'w'}{u'w'_{max}}\right) - \phi\ln(0.1) \qquad \text{[Equation 8.21]}$$

where ϕ is a coefficient which varies according to the level of submergence and will be referred to as the 'Reynolds stress profile shape coefficient' or simply the 'shape coefficient' from hereon forth. The values of the shape coefficient, ϕ, can be related to the depth-averaged velocity, U, through a power law relationship as presented in Figure 8-21. Two power law equations are proposed which relate to the bed gradients investigated.

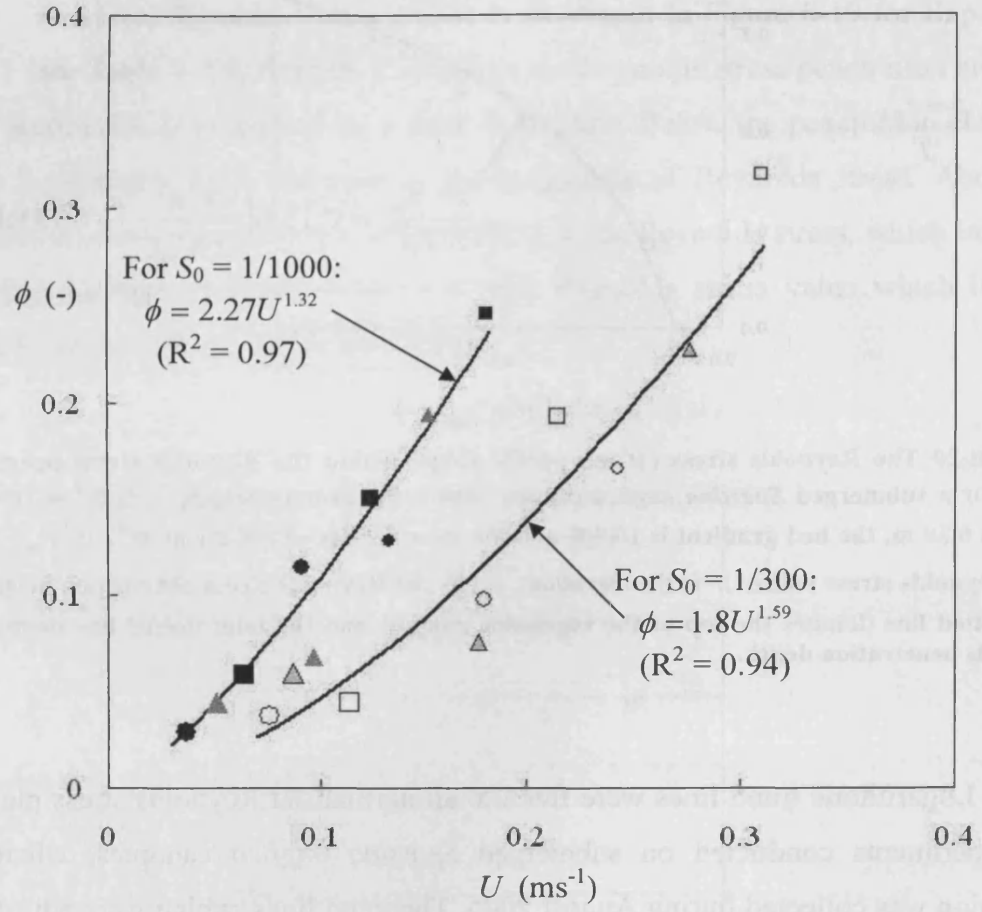

Data used to develop the relationships:

	Stem density (stems m^{-2})	S_0 (-)	T (m)	H (-)
■	800	1/1000	0.05	3.00
■	800	1/1000	0.10	2.00
■	800	1/1000	0.15	1.33
●	1850	1/1000	0.05	3.00
●	1850	1/1000	0.10	2.00
●	1850	1/1000	0.15	1.33
□	800	1/300	0.05	3.00
□	800	1/300	0.10	2.00
□	800	1/300	0.15	1.33
○	1850	1/300	0.05	3.00
○	1850	1/300	0.10	2.00
○	1850	1/300	0.15	1.33

Data used to verify the relationships:

	Stem density (stems m^{-2})	S_0 (-)	T (m)	H (-)
▲	1160	1/1000	0.05	3.00
▲	1160	1/1000	0.10	2.00
▲	1160	1/1000	0.15	1.33
△	1160	1/300	0.10	3.00
△	1160	1/300	0.10	2.00
△	1160	1/300	0.10	1.33

Figure 8-21 The relationship between the shape coefficient, ϕ, and the depth-averaged longitudinal velocity, U for submerged *Spartina anglica* canopies, for stem densities of 800, 1160 and 1850 stems m^{-2}, bed gradients of 1/1000 and 1/300 and submergence levels, H, of 1.33, 2.00 and 3.00. T is the canopy height and R^2 is the goodness of fit for each power trend line.

For bed gradients of 0.001 and $0.00\dot{3}$ respectively, the relationship between the shape coefficient, ϕ, and the mean flow velocity, U, is characterised by the following two equations:

$$\phi = 2.27U^{1.32} \qquad \text{[Equation 8.22]}$$

$$\phi = 1.8U^{1.59} \qquad \text{[Equation 8.23]}$$

According to mass continuity of the fluid, the depth-averaged velocity of the flow can be estimated from predicted values of the mean velocities through the surface flow layer (U_S) and the canopy (U_C) (see Sections 8.5.1 and 8.5.2 as follows:

$$U = \frac{U_S h_S + U_C T}{D} \qquad \text{[Equation 8.24]}$$

where h_S, T and D are the depth of the surface flow layer, the height of the canopy and the total flow depth. Using estimated values of U, the shape function, ϕ, was estimated for the middle density canopies with a stem density of 1160 stems m^{-2} (see Figure 8-22). Errors were significant in some cases, and this may be linked to the accumulated errors in predicting U_S and U_C, the significant difference in morphology between the canopies used to develop the relationships as well as the uncertainty associated with predicting turbulence properties.

Figure 8-22 Prediction of the Reynolds stress profile shape coefficient for submerged canopies. s is the stem spacing, S_0 is the bed gradient, T is the canopy height, D is the flow depth, U is the mean flow velocity and ϕ is the shape coefficient.

Stem Density (stems m^{-2})	S_0 (-)	T (m)	D (m)	Estimated U (ms^{-1})	Estimated ϕ	Measured ϕ	Error (ϕ) (-)
1160	1/300	0.05	0.15	0.276	0.232	0.226	2.4%
1160	1/300	0.10	0.20	0.196	0.135	0.075	79.6%
1160	1/300	0.15	0.20	0.088	0.038	0.059	-36.3%
1160	1/300	0.05	0.15	0.150	0.186	0.193	-3.7%
1160	1/300	0.10	0.20	0.107	0.119	0.068	76.8%
1160	1/300	0.15	0.20	0.048	0.041	0.044	-5.2%

8.7 Worked Example

8.7.1 Scenario

To illustrate the application of the prediction method proposed in this chapter, a worked example is presented. Consider a *Spartina anglica* canopy which experiences inundation during a high tide. A mean 90th percentile height of 0.3m is taken as the height of the vegetation based on a typical *Spartina anglica* canopy (Section 0). The bed gradient is 0.001, and for this example, the problem is simplified by assuming a steady-uniform flow. The velocity and Reynolds stress profiles are to be determined for the canopy at the following two stages of the inundation cycle:

1. when the flow depth is 0.2m and the vegetation is therefore emergent

2. when the flow depth is 0.4m and the vegetation is therefore submerged

8.7.2 The Canopy Characteristics

The canopy is assumed to possess the properties of the mid-range (1160 stems m^{-2}) canopy in this study, including the projected area per unit volume profile presented in Section 8.2. The depth-averaged projected area per unit volume of the canopy is 18.2 m^{-1}, and the 90th percentile height of 0.3m is taken as the height of the vegetation.

8.7.3 Velocities and Reynolds Stresses through the Emergent Canopy

An index canopy was described in Section 8.3.1 for which the projected area per unit volume is 29.8 m^{-1}, the bed gradient is 0.00$\dot{3}$ and the mean velocity is 0.059 ms^{-1}. The same index canopy is used here. For the lower 0.20m of a 1160 stems m^{-2} canopy, the projected area per unit volume, which is determined from the profile presented in Section 0, is 18.2 m^{-1}. From Equation 8.04, the mean velocity can be determined as follows:

$$U_{C2} = U_{C1}\sqrt{\frac{\bar{a}_1 S_2}{\bar{a}_2 S_1}} = 0.059\sqrt{\frac{29.8\times 0.001}{18.2\times 0.003}} = 0.041 \text{ ms}^{-1}$$

The mean velocity ($U_C = 0.041$ ms^{-1}) and projected area per unit volume ($\bar{a} = 18.2$ m^{-1}) are used with the profile of projected area (presented in Section 0) to predict the velocity profile up to an elevation of 0.20m above the bed level using Equation 8.05. The predicted velocity profile is presented in Figure 8-23a.

The mean Reynolds stress, which for an emergent canopy is relatively constant over the flow depth, can be estimated using Equation 8.06:

$$-\rho \overline{u'w'}_C = 0.15 U_C^{1.17} = 3.61\times 10^{-3} \text{ kg m}^{-1} \text{ s}^{-2}$$

The predicted Reynolds stress profile is presented in Figure 8-23b.

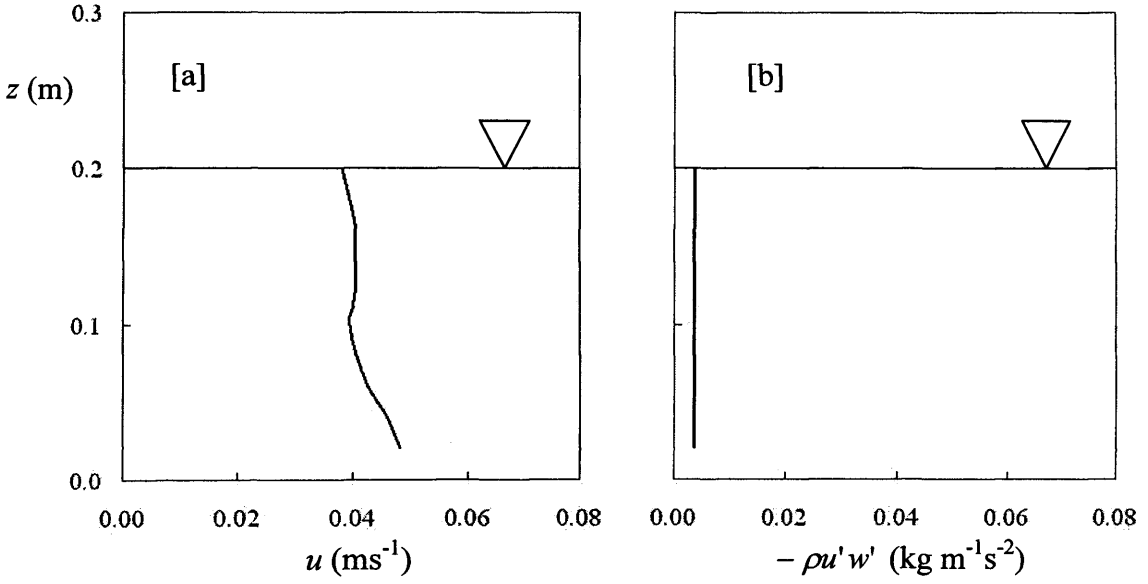

Figure 8-23 Predicted [a]: velocity and [b]: Reynolds stress profiles for a uniform flow through an emergent *Spartina anglica* canopy with a stem density of 1160 stems m^{-2}, for a flow depth of 0.2m and a bed gradient of 1/1000.

8.7.4 Velocities and Reynolds Stresses through the Submerged Canopy

For the stem density of the canopy (1160 stems m^{-2}), the mean stem spacing, s, is 31.5 mm. For the submerged canopy, the projected area per unit volume, $\bar{a}$, for the 0.3m height of the canopy, is 18.4 m^{-1}. Foe a flow depth of 0.4m, the depth of the

surface flow layer, h_S, is 0.1m. First, the surface flow layer velocity is estimated using Equation 8.13:

$$U_S = \frac{h_S^{2/3} S_0^{1/2}}{0.053(\bar{a}s)^{0.29}} = \frac{0.1^{2/3} 0.001^{1/2}}{0.053(18.4 \times 0.0315)^{0.29}} = 0.151 \text{ ms}^{-1}$$

Then the mean canopy layer velocity, U_C, can be estimated using Equation 8.15:

$$U_C = 11.2 s U_S = 11.2 \times 0.0315 \times 0.151 = 0.053 \text{ ms}^{-1}$$

The mean velocity ($U_C = 0.053$ ms^{-1}) and projected area per unit volume ($\bar{a} = 18.4$ m^{-1}) are used with the profile of projected area (presented in Section 0) to predict the velocity profile using Equation 8.05. The predicted velocity profile is presented in Figure 8-24a. The values of U_S and U_C can then be used to estimate the peak Reynolds stress term occurring above the canopy using Equation 8.16:

$$-u'w'_{\max} = 0.43(U_S - U_C)^2 = 0.43(0.151 - 0.027)^2 = 4.12 \times 10^{-3} \text{ m}^2\text{s}^{-2}$$

The Reynolds stress is achieved by multiplying by the fluid density:

$$-\rho u'w'_{\max} = 0.412 \text{ kg m}^{-1}\text{s}^{-2}$$

The Reynolds stress penetration can also be estimated by applying Equation 8.18:

$$h_{pen} = \frac{1}{\bar{a}^2 s}\left(0.156\frac{U_S}{U_C} - 0.334\right)$$

$$= \frac{1}{18.4^2 \times 0.0315}\left(0.156\frac{0.151}{0.053} - 0.334\right)$$

$$= 0.010 \text{ m}$$

The penetration elevation, $z_{0.1}$, is the distance from the penetration depth to the bed:

$$z_{0.1} = T - h_{pen} = 0.3 - 0.01 = 0.29\,\text{m}$$

The Reynolds stress profile is described by Equation 8.21 for which the shape coefficient, ϕ, is required. To determine the shape coefficient, the depth averaged velocity of the flow is required. This can be estimated using estimated values of the mean canopy (U_C) and surface flow layer (U_S) velocities using Equation 8.24 as follows:

$$U = \frac{U_C T + U_S h_S}{D} = \frac{0.053 \times 0.3 + 0.151 \times 0.1}{0.4} = 0.078\,\text{ms}^{-1}$$

The shape coefficient can be calculated using Equation 8.22:

$$\phi = 2.27 \times U^{1.32} = 2.27 \times 0.078^{1.32} = 0.078$$

Substituting values of ϕ, $z_{0.1}$ and $u'w'_{\max}$ into Equation 8.21 facilitates the prediction of the Reynolds stress profile between the penetration elevation and the top of the canopy. Below the penetration elevation, the Reynolds stress is estimated using the estimated mean canopy velocity, U_C, with Equation 8.06:

$$-\rho u'w'_C = 0.15 {U_C}^{1.17} = 4.87 \times 10^{-3}\ \text{kg m}^{-1}\,\text{s}^{-2}$$

The predicted Reynolds stress profile is presented in Figure 8-24b.

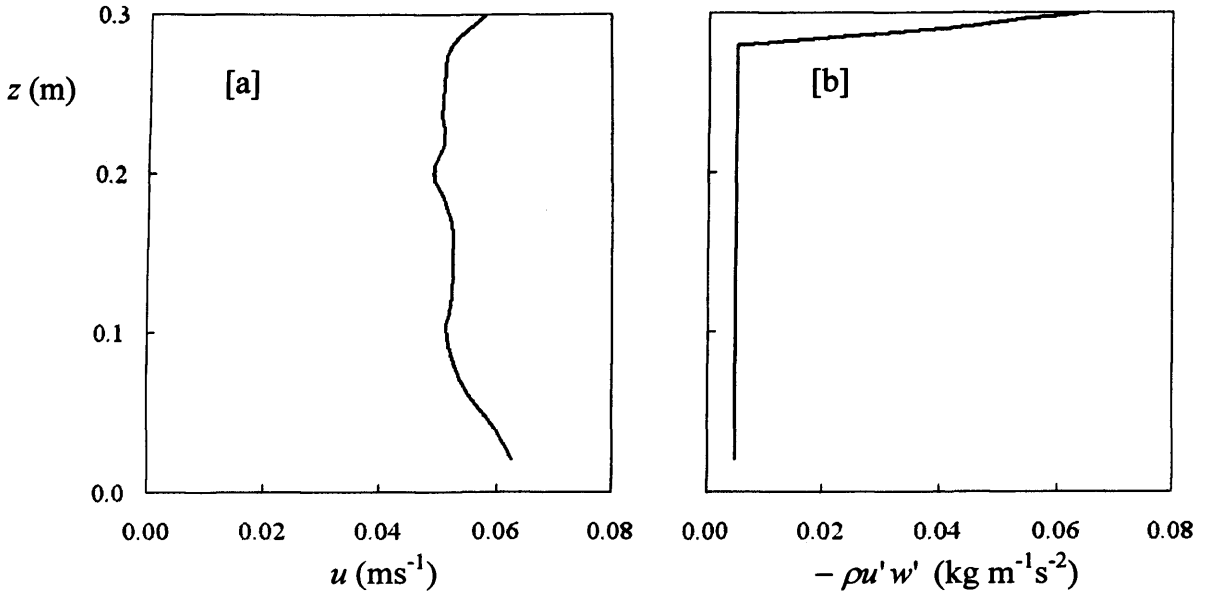

Figure 8-24 Predicted [a]: velocity and [b]: Reynolds stress profiles for a uniform flow through a submerged *Spartina anglica* canopy with a stem density of 1160 stems m^{-2}, for a flow depth of 0.4m and a bed gradient of 1/1000. The canopy is 0.3m tall and the flow depth is 0.4m.

8.8 Concluding Remarks

A method was proposed for the prediction of longitudinal velocity and Reynolds stress profiles for *Spartina anglica* canopies. The method was based on the approach proposed by Lightbody and Nepf (2006a) for emergent vegetation. The longitudinal velocity is assumed to vary inversely with the canopy morphology, thus a greater projected area results in greater obstruction to the flow and in lower longitudinal velocities. The same approach was applied to emergent canopies in this study, and also to the lowest submergence level of 1.33 and resulted in reasonable predictions of the longitudinal velocity in the range of 0.02 to 0.13 ms^{-1}. Reynolds stresses were relatively low for both of these conditions compared to the higher submergence levels of 2.00 and 3.00 investigated in this study.

The Lightbody and Nepf (2006a) approach utilises a reference elevation within a canopy for implementing the prediction method where the projected area per unit volume and velocity are known. However, velocity measurements may not be readily available; hence, a similar concept to the Lightbody and Nepf (2006a) approach was implemented here to estimate the mean velocity through a *Spartina anglica* canopy using a reference canopy for which the mean velocity and obstruction area are known.

For the submerged canopies, an alternative approach was adopted to estimate mean canopy velocities. First, the surface layer was treated as an open channel with a rough bottom, and the bottom roughness, which in fact corresponds to the top of the vegetation canopy, was characterised using a Manning's roughness coefficient. This enabled estimation of the mean surface layer velocity with reasonable accuracy. The mean canopy layer velocity was a linear function of the mean surface layer velocity and the stem density and could therefore be estimated.

The Lightbody and Nepf (2006a) approach, which the authors suggest is only applicable to emergent vegetation where Reynolds stresses are negligible within the canopy, was applied with similar success to the 0.15m submerged canopies as it was to the emergent canopies in this study. Due to the dense foliage cover in the 0.15m canopies, Reynolds stresses remained negligible over most of the canopy height. As with the emergent canopies, the depth-averaged values of projected area and estimated velocity were used as a reference.

For higher submergence levels (2.00 and 3.00), Reynolds stresses through the canopy were more significant, however, it is believed that this is strongly linked to the severely cropped nature of the vegetation at these submergence levels. Large Reynolds stresses affected velocity profiles and drag coefficients, hence the prediction methods which were reasonably successful for the emergent canopies and the 0.15m cropped canopies were not suitable for application to the shorter 0.05m and 0.10m cropped canopies.

A relationship was developed for predicting the shape of the Reynolds stress profile in the region where the Reynolds stress is considered significant. The Reynolds stress profile relationships were specific to each of the two bed gradients implemented because the flow regime, as characterised by the Reynolds number, varied significantly with bed gradient. The peak Reynolds stress above a submerged canopy and the Reynolds stress penetration depth were both functions of the relationship between the mean surface layer and mean canopy velocities. The penetration depth was also a function of the vegetation density.

[*This page has been intentionally left blank*]

9 Conclusions and Recommendations for Further Research

The conclusions presented in this section summarise the findings from the field investigation and the laboratory studies presented in this thesis.

9.1 Conclusions

1. A survey of two saltmarsh sites revealed the complexity of field conditions and identified contrasting vegetation canopy properties with a wide range of bed gradients, stem densities and vegetation species. The saltmarsh sites also contained complex creek networks, and the most significant difference between the two sites was that one of them is part of a bird sanctuary and remains relatively undisturbed throughout the year, whilst the other is used for sheep farming throughout the year. The effects of grazing were evident for the latter site and the vegetation cover was very short with annual monthly average canopy heights ranging between 28 mm and 83 mm (compared to between 260 mm and 390 mm where the vegetation was undisturbed), resulting in considerably less obstruction to tidal flows compared to the undisturbed vegetation.

2. A range of parameters for characterising the physical properties of vegetation canopies were considered to determine how different canopies can influence the hydrodynamics of the flow. Such parameters include stem diameters and densities, the material stiffness of the vegetation, the mass and projected area per unit volume. Determination of projected area per unit volume profiles was achieved using photographs of canopy cross-sections. A linear relationship was established linking the mass per unit volume to stem density of the vegetation. Due to the complex morphology of vegetation, characterisation of the amount of plant material obstructing the flow is difficult to perform using a single parameter. Parameters which have been used for characterising the degree of obstruction for uniform cylinder array models are not appropriate for real vegetation canopies. Profiles of projected area per unit volume and stem densities were considered together for characterising and evaluating the degree of obstruction for the constructed vegetation canopies in this thesis.

3. One limitation of the photographic method is that the projected area determined from the photographs only relates to the plants closest to the camera, and does not represent the total amount of vegetation in the cross section. Hidden plant parts formed a significant proportion of the total obstruction, and there was a greater surface area of hidden vegetation for a greater stem density. Correction for hidden material was possible for the constructed canopies used in the laboratory experiments. This was necessary to relate the total amount of vegetation to its hydraulic resistance and therefore ascertain the impact of the physical properties of a vegetation canopy on the velocity and turbulence structures. The proportion of the total projected area of obstruction that was hidden increased with stem density. For three canopies considered with stem densities of 800, 1160 and 1850 stems m^{-2}, 30.8%, 58.0% and 76.1% of the total projected area was hidden respectively. Furthermore, the photographic method does not account for variations in stem diameter such that two canopies with different stem densities can have similar projected areas due to the difference in the sizes of the plant stems. As one would expect, the turbulence structure can vary significantly between the two canopies as a higher stem density with a smaller average stem diameter will give rise to a greater number of narrower wakes and the stem spacing will be smaller, thus increasing the likelihood of wake interference with downstream stems.

4. Lateral variation in the vegetation was assessed by considering 'local', 'spatial' and 'temporal' variability in the vegetation obstruction. 'Spatial' variability was in part related to the geographical location, such as the elevation above mean sea level or the proximity to creek networks. However, 'spatial' variability was less significant than 'temporal' variability due to the seasonal variation in the vegetation size, and to 'local' variability due to the random variation in the vegetation. The mean 90^{th} percentile *Spartina anglica* canopy height was 308 mm, although minimum and maximum values were 145 mm and 360 mm during the winter and summer periods respectively. 'Local' variability in the projected area per unit volume of the vegetation was demonstrated by applying the photographic method to 16 vertical cross-sections of canopy for three constructed vegetation canopies with stem densities of 800, 1160 and 1850 stems m^{-2}. Average standard

deviations in the projected area per unit volume between the 16 cross-sections for the three canopies were 25.8%, 12.3% and 25.0% respectively.

5. Determination of seasonal variation in vegetation density can depend on the parameters used to quantify the density. Vegetation was quantified in this study according to the mean stem diameter, canopy height, stem density, projected area per unit volume and mass per unit bed area. The vegetation became dormant during the winter period, and young shoots were observed in the spring. The mean stem diameter for a sample of *Spartina anglica* collected during February 2007 was 4.12 mm, compared to 5.16 mm for samples collected during August 2006. Mean moduli of elasticity were up to 2.3 times greater for summer vegetation, reflecting the stiffer nature of the vegetation. Such variation in the physical properties is difficult to recreate in laboratory studies. The seasonal variation in vegetation characteristics can affect the hydraulic resistance properties of the canopy significantly, especially as the largest high tides of the year occur around the months of September and March, for which the canopies show the greatest contrast in terms of stem diameters, stiffness, stem density, canopy height and projected area per unit volume. During September, the vegetation appears green and abundant following the long days of sunlight exposure during the summer months, whereas during March, the vegetation was in the dormant state, whereby stem diameters were smaller and the foliage cover was scarce. For the 800 stems m^{-2}, the average projected area per unit volume for the foliage region between elevations of 0.15 m and 0.20 m above the bed was 35% greater for the summer canopy. Consequently, the level of protection against sediment erosion is considerably less around March.

6. The submergence level of a vegetation canopy is dependant on the height of the vegetation, the bed elevation and the sea level. Submergence levels can therefore vary considerably for a saltmarsh due to a wide range of values encountered for each of these parameters. A predictor was developed to estimate the submergence levels for the saltmarshes considered in the field study. Based on the collected and available data, the mean 90^{th} percentile *Spartina anglica* canopy height was 308 mm and the mean bed elevation for the Llanelli saltmarsh was 2.455 m Above Ordinance Datum (AOD). The mean high tide magnitude for the twelve-month

monitoring period was 3.48 m AOD, for which tidal inundation of the mean bed elevation level would last 1.8 hours and the submergence level during high tide would reach 1.9. For the maximum magnitude high tide of the year (5.26 m AOD), inundation would last 3.9 hours and the submergence level would reach 5.4. 16.7% of high tides during the monitoring period (July 2005 to June 2006) ranged between 8.0 m and 8.5 m AOD in magnitude (this is equivalent to 122 high tides), whilst only 2.7% (equivalent to 20 high tides) fell ranged between 10.0 m and 10.5 m AOD.

7. Flume experiments were conducted to compare the velocity and turbulence structures in submerged vegetation canopies and uniform cylinder arrays for uniform flow conditions. Uniform cylinders with a 6.0 mm diameter were used due to the similarity with the basal diameters of the plants and the same stem densities were implemented for each type of canopy. It was difficult to replicate a similar level of area of obstruction to the flow. There were significant differences in the canopy physical structures between natural canopies *in situ*, constructed canopies in the laboratory using real vegetation stems, and artificial canopies of uniform cylinder arrays. Natural canopies contained loose plant parts near the bed, smaller plants and secondary species of vegetation, which contributed to an increase in the amount of vegetation near the bed. Constructed canopies were primarily composed of larger plant stems of *Spartina anglica*, resulting in clearly distinguishable stem and foliage regions. Plant foliage was abundant in both canopies, but was not represented in the uniform cylinder models, which had considerably lower projected areas per unit volume for similar stem densities compared to the real vegetation. For constructed August vegetation canopies with stem densities of 800, 1160 and 1850 stems m^{-2}, the total projected area per unit volume was 55%, 148% and 161% higher respectively compared to the uniform cylinder arrays.

8. Reynolds stress penetration was considerably greater for the uniform cylinder arrays where foliage was absent compared to the constructed vegetation canopies. Whilst an increase in stem density in the constructed vegetation canopies resulted in a reduction of Reynolds stress penetration, the same increase in stem density resulted in an increase in Reynolds stress penetration for the uniform cylinder

arrays. For the constructed vegetation canopies, an increase in stem density resulted in an increase of plant foliage in the canopy which is believed to reduce the penetration of Reynolds stress into the canopy. However, for the uniform arrays, an increase in stem density resulted in a greater difference in hydraulic resistance between the canopy layer, where the flow resistance increases, and the surface flow layer, where resistance is negligible. Hence, this gave rise to a 'stronger' shear layer along the canopy-surface flow layer interface, and in the absence of plant foliage, the penetrative effect of the shear layer extended deeper into the canopy.

9. Flume experiments were conducted under uniform flow conditions to investigate the influence of the structure of constructed vegetation canopies on hydraulic resistance, velocity and turbulence structures. Some of the experiments were repeated for vegetation samples collected during the summer and winter seasons to assess the significance of the variations in vegetation properties and morphology. The experiments were conducted for a range of stem densities, bed gradients and submergence levels based on measurements conducted during an eighteen month field survey. Stage discharge curves were determined for the different canopies investigated. The curves are useful for quantifying the flow resistance due to the different vegetation canopies. The flow depth for most of the experiments conducted in the laboratory investigation was 200 mm. At this flow depth, a decrease in submergence level (the ratio of flow depth to canopy height) from 2.00 to an emergent condition resulted in a decrease of 20% to 42% in discharge (the percentage reduction increased with increasing stem density). Going from a higher submergence level of 3.00 to an emergent condition may result in a decrease of 60% to 74% in discharge. Increasing the stem density from 800 to 1160 stems m^{-2} resulted in a reductions of 20.5% and 34.1% in discharge for bed gradients of 0.003 and 0.001 respectively. However, a further increase in stem density to 1850 stems m^{-2} did not result in any significant further reduction in discharge.

10. One of the most significant features of real vegetation canopies, which are rarely represented in simulated canopies in the laboratory, is the vertical variation in

projected area associated with the complex structure of the plant canopy. There was a considerable difference in canopy structure between the stem region near the bed and the foliage region higher up in the canopy. This was identified by the photographic method, which was applied to thin horizontal layers of the canopy to quantify the vertical variation in projected plant area per unit volume. Although the vegetation in the foliage region was considerably thinner, and hence, had a much lower mass per unit volume compared to the plant at its base, the surface area of the canopy was significantly higher in the foliage region, resulting in a greater level of obstruction to the flow. This was evaluated by introducing a 'uniformity coefficient' as a measure of vertical variation in the canopy. Standard deviations in the total projected area per unit volume over the canopy height for constructed vegetation canopies were approximately $\pm$ 25% of the depth-averaged value for the canopies considered which ranged between 800 and 1850 stems m^{-2} in stem density. For submerged conditions, it was demonstrated that the magnitude of Reynolds stress remains negligible for vegetation canopies with a relatively dense foliage cover. This was attributed to the influence of plant foliage on reducing the penetration of the Reynolds stress into the canopy.

11. A two-layer flow occurs for submerged conditions whereby the longitudinal velocities within the canopy layer are significantly lower than those in the surface flow layer. The depth-averaged velocity of the canopy layer was between 30% and 42% of the depth-averaged surface flow layer velocity for stem densities of 800 and 1160 stems m^{-2}. For the highest stem density of 1850 stems m^{-2}, depth-averaged canopy layer velocities were even lower ranging between 23% and 30% of the surface flow layer velocity. A large gradient in longitudinal velocity occurs between the two layers as a result. Along the canopy-surface flow layer interface, a shear layer arises that is dominated by rotating vortices indicated by large values of fluctuations in the instantaneous longitudinal and vertical velocity components (u' and w'). Effects of the vortices on the turbulence structure were also evident at the mid-canopy height for the sparser stem densities of 800 and 1160 stems m^{-2} as identified by a quadrant analysis showing a concentration of instantaneous velocity fluctuation measurements within the second and fourth quadrants. For the highest stem density of 1850 stems m^{-2}, a more obstructive foliage cover in the

upper part of the canopy is believed to reduce the penetration of the vortices into the canopy.

12. For submerged conditions, a peak in Reynolds stress was observed a short distance above the top of the canopy. The influence of plant foliage on the turbulence structure in submerged canopies was shown more clearly by evaluating the Reynolds stress penetration into the canopy. The Reynolds stress penetration depth as a proportion of the canopy height was shown to decrease with increasing stem density and decreasing submergence level. With an increase in stem density, the total surface area of foliage naturally increases, and due to the scaling method implemented, for lower submergence levels, the canopy was taller and contained more foliage. The Reynolds stress penetration depth as a proportion of the canopy height ranged between 2% and 12% for a canopy height of 150 mm, and between 30% and 76% for a canopy height of 50 mm.

13. There was more variation in longitudinal velocity profiles through constructed vegetation canopies compared to uniform cylinder arrays. This is attributed to the non-uniform vertical distribution of plant material in the vegetation canopy. For the uniform cylinder arrays, longitudinal velocities through the canopy were more influenced by the 'skimming' flow due to a higher velocity surface flow layer above the canopy layer and a positive gradient was observed in velocity magnitude with elevation above the bed. This was not observed for the vegetation canopies where a dense foliage cover is believed to reduce the effects of the surface flow layer on velocities within the canopy layer.

14. The key species considered in this study (*Spartina anglica*) was relatively stiff and remained upright for the wide range of flow conditions examined. The material stiffness did not seem to be influential in characterising the hydraulic resistance of the plant canopy.

15. The values of $\overline{C_D}$ are dependent on the Reynolds number because the resistance of the canopy is affected by the wake structure, the amount of wake sheltering, and the total amount of turbulence in the flow, which can affect the significance of

turbulence generation in the stem wakes towards energy dissipation. Thus, $\overline{C_D}$ values need to be quoted along with the associated range of Reynolds numbers. For instance, for a stem Reynolds value of 250, $\overline{C_D}$ values for emergent canopies are estimated at 0.622, 0.927 and 1.278 for stem densities of 800, 1160 and 1850 stems m^{-2}. For submerged canopies and a stem Reynolds number of 400, $\overline{C_D}$ values are estimated at 0.886, 1.002 and 1.517 for the respective stem densities.

16. Under certain circumstances, such as where the canopy structure and density are unknown or difficult to determine, or where the Reynolds stress within the canopy is significant (e.g. in submerged canopies), there are advantages to using the bulk roughness coefficient, $\overline{C_D}'$. This is the product of the projected area per unit volume, $\bar{a}$, which quantifies the vegetation density, and the bulk drag coefficient, $\overline{C_D}$. Application of $\overline{C_D}'$ does not require knowledge of the canopy density and had a better correlation with the projected area per unit volume of the canopy than $\overline{C_D}$, which is affected by the influence of the turbulence structure and the contribution of individual stems towards the total resistance of the canopy.

17. A method was proposed for the prediction of longitudinal velocity and Reynolds stress profiles. The velocity prediction was based on the method proposed by Lightbody and Nepf (2006a) for emergent canopies using a reference elevation within the canopy for which the projected area and velocity are known. The method was adapted and the mean projected area and estimated canopy layer velocity were used. For a submerged canopy containing a large amount of foliage, the application of the method produced satisfactory predictions of longitudinal velocity profiles. Where Reynolds stress penetration was significant, longitudinal velocity profiles were more difficult to predict. Relationships were also developed for the Reynolds stress profiles within the penetration depth, however, these were specific to the flow regime. Where experiments were repeated for a different bed gradient and the Reynolds numbers were significantly different, a different relationship was assigned. Furthermore, these relationships, which were developed using constructed canopies from August, were not compatible with constructed

February vegetation canopies or with uniform cylinder arrays due to a significant difference between the morphologies of the three types of canopy.

9.2 Recommendations for Further Research

1. In the flume experiments, variables such as bed gradients, submergence levels and stem densities, were studied for a limited number of values within the range observed on two coastal saltmarshes. This facilitated the consideration of a greater number of variables, and the results were useful for identifying the impact of variations in the aforementioned variables on the velocity and turbulence structures. However, examination of such variables for a greater number of values can be useful for identifying and confirming trends in the data and the effects of these variables on hydraulic resistance.

2. The laboratory experiments in this work were conducted under uniform flow conditions, which was particularly useful where the hydraulic resistance characteristics of the vegetation were unknown. The flow velocities implemented to achieve uniform flow conditions for the range of submergence levels investigated were considerably greater than those observed in saltmarsh environments, which were often below 0.1 ms^{-1} (Section 2.42). Since bulk drag coefficients are strongly influenced by the Reynolds number and are likely to be significantly greater in magnitude for lower flow velocities, it would be useful to determine drag coefficient values at low velocities that are more typical of natural saltmarsh conditions.

3. The flume used for the experiments could only support a maximum flow depth of around 0.25m after installation of the constructed canopies. Therefore, the vegetation had to be trimmed to reduce the canopy height and hence, facilitate greater submergence levels. This scaling method resulted in considerable modification to the morphology of the canopy, due to the significant difference in structure between the lower stem region, which was not affected by any of the scaling conducted, and the upper foliage region, which was gradually removed with the progressive decrease in canopy height. Conducting the experiments in a deeper flume so that the vegetation does not need to be cut down would provide

more representative results of a natural *Spartina anglica* canopy on the hydrodynamics in a coastal environment.

4. Using uniform cylinder arrays to simulate *Spartina anglica* canopies can lead to over simplification of the morphology of the canopy. The use of real vegetation for such studies can produce more realistic results that are representative of the natural environment. However, constructed vegetation canopies can also lead to alteration of the vegetation cover morphology in a natural environment. Firstly, constructed canopies usually consist of neatly organised large plants, whereas natural canopies can consist of plants at various stages of the growth cycle, as well as fallen plant parts accumulating near the bed leading to a significantly different canopy structure. Secondly, the constructed canopies implemented were constructed entirely of *Spartina anglica*, and areas dense in *Halimione portulacoides* were identified adjacent to creek networks during the field survey. For a better understanding of the velocity and turbulence structure, the latter species also needs to be considered. Furthermore, there is often a lack of a clear boundary between the two species on the saltmarshes surveyed. The influence of the different species in various proportions is another recommended area for further study.

5. The relationships relating the vegetation morphology to the velocity and turbulence structure, were developed using the data collected for the August vegetation canopies. Verification of these trends was then attempted using data collected for February canopies and uniform cylinder arrays. This did not always yield good results, and should be conducted using data collected for vegetation samples that are similar in morphology to the original canopies for which the relationships were developed.

6. Determination of the properties and density of the vegetation cover on coastal wetlands from Geographic Information Systems (GIS) data can be useful for evaluating the total protection offered by a saltmarsh to a coastline. This can be achieved by comparing measured vegetation properties (e.g. stem densities, projected areas per unit volume, canopy heights etc.) to the vegetation properties determined from remotely sensed data. Such data can be used to characterise the

boundary conditions in a hydrodynamic numerical model. Although this topic has been explored briefly during the work using LiDAR data supplied by the Environment Agency, higher resolution data was required to differentiate between the bed level and the top of the vegetation. Streutker and Glenn (2006) successfully used LiDAR data to detect and characterise vegetation covers with relatively similar morphologies to the *Spartina anglica* canopies observed at the study sites (e.g. sagebrush, horsebrush wheatgrass, Plain's reedgrass etc.) with a vertical error of $\pm$ 50 mm.

[*This page has been intentionally left blank*]

10 Appendix I: Derivation of the Two-Dimensional Drag Coefficient Equation

This derivation is taken from Dunn *et al.* (1996). It is included for the sake of completeness due to the importance of this equation in the context of this thesis.

For incompressible turbulent flow, the Navier-Stokes equations (momentum equations) for the x, y and z planes are defined as follows:

x-momentum:

$$\rho\frac{\partial u}{\partial t}+\rho\frac{\partial\left(u^2\right)}{\partial x}+\rho\frac{\partial(uv)}{\partial y}+\rho\frac{\partial(uw)}{\partial z}=-\frac{\partial P}{\partial x}+\mu\left(\frac{\partial^2 u}{\partial x^2}+\frac{\partial^2 u}{\partial y^2}+\frac{\partial^2 u}{\partial z^2}\right)+\rho g_x$$

[Equation 10.01]

y-momentum:

$$\rho\frac{\partial v}{\partial t}+\rho\frac{\partial(uv)}{\partial x}+\rho\frac{\partial\left(v^2\right)}{\partial y}+\rho\frac{\partial(vw)}{\partial z}=-\frac{\partial P}{\partial x}+\mu\left(\frac{\partial^2 v}{\partial x^2}+\frac{\partial^2 v}{\partial y^2}+\frac{\partial^2 v}{\partial z^2}\right)+\rho g_y$$

[Equation 10.02]

z-momentum:

$$\rho\frac{\partial w}{\partial t}+\rho\frac{\partial(uw)}{\partial x}+\rho\frac{\partial(vw)}{\partial y}+\rho\frac{\partial\left(w^2\right)}{\partial z}=-\frac{\partial P}{\partial x}+\mu\left(\frac{\partial^2 w}{\partial x^2}+\frac{\partial^2 w}{\partial y^2}+\frac{\partial^2 w}{\partial z^2}\right)+\rho g_z$$

[Equation 10.03]

where g_x, g_y and g_z are the components of the gravitational acceleration in the x, y and z directions, μ is the dynamic viscosity, ρ is the fluid density and P is the hydrostatic pressure. The continuity equation is defined as follows:

$$\frac{\partial u}{\partial x}+\frac{\partial v}{\partial y}+\frac{\partial w}{\partial z}=0$$

[Equation 10.04]

Assuming a uniform, steady, incompressible flow, the time-averaged y-momentum

and z-momentum equations become insignificant. The time-averaged x-momentum equation becomes:

$$0 = \rho g_x + \frac{\partial}{\partial x}\left(\mu\frac{\partial \overline{u}}{\partial x} - \rho\overline{u'^2}\right) + \frac{\partial}{\partial y}\left(\mu\frac{\partial \overline{u}}{\partial y} - \rho\overline{u'v'}\right) + \frac{\partial}{\partial z}\left(\mu\frac{\partial \overline{u}}{\partial z} - \rho\overline{u'w'}\right)$$

[Equation 10.05]

The time-averaging procedure gives rise to a number of mean products of fluctuating velocities that relate to the Reynolds stresses (Section 2.3.1). The $-\rho\overline{u'w'}$ Reynolds stress component associated with the x-z plane normal to the bed is dominant in fully turbulent uniform flow and Equation 10.05 can be approximated with a simpler streamwise momentum equation:

$$0 \cong \rho g_x + \frac{\partial}{\partial z}\left(\mu\frac{\partial \overline{u}}{\partial z} - \rho\overline{u'w'}\right) \qquad \text{[Equation 10.06]}$$

$$0 \cong \rho g_x + \frac{\partial \tau}{\partial z} \qquad \text{[Equation 10.07]}$$

where $$\tau = \mu\frac{\partial \overline{u}}{\partial z} - \rho\overline{u'w'} = \tau_v + \tau_t \qquad \text{[Equation 10.08]}$$

where τ_v is the viscous stress and τ_t is the Reynolds stress. The Reynolds stress profile for a fully turbulent uniform flow in a wide channel is illustrated in Figure 10-1, showing that the mean total shear stress varies linearly and follows the equation:

$$\tau = \tau_b\left(1 - \frac{z}{D}\right) \qquad \text{[Equation 10.09]}$$

where τ_b is the bed shear stress and is given by the following equation:

$$\tau_b = \rho g D S_0 \qquad \text{[Equation 10.10]}$$

Equations 10.09 and 10.10 can be obtained by integrating Equation 10.07 from the bed to the free surface. The total stress at the water surface is negligible.

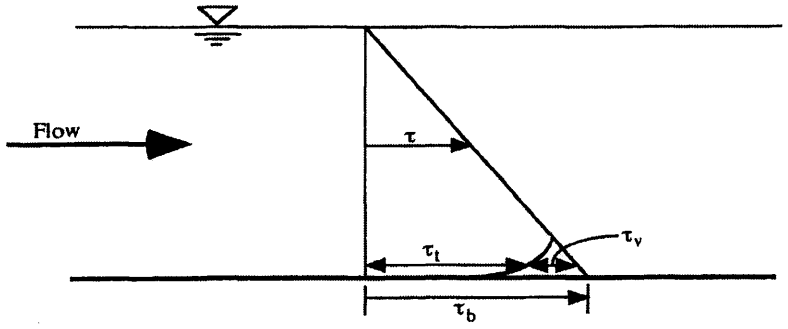

τ_t : Reynolds stress
τ_v : Viscous stress
τ : Total shear stress
τ_b : Total bed shear stress

Figure 10-1 Stress partition for fully turbulent flow with a viscous sublayer in a wide rectangular channel (taken from Dunn *et al.*, 1996)

The viscous stress is negligible for most of the flow depth (except for the region adjacent to the bed) and the turbulent stress dominates such that:

$$\tau = -\rho\overline{u'w'} \qquad \text{[Equation 10.11]}$$

Vertical variation in the total stress outside the viscous region near the bed can therefore be characterised as follows:

$$\frac{\partial \tau}{\partial z} = \frac{\partial}{\partial z}\left(-\rho\overline{u'w'}\right) = -\rho g S_0 \qquad \text{[Equation 10.12]}$$

which is consistent with Figure 10-1. In the presence of a uniform cylinder array, the Reynolds stress profile is illustrated in Figure 10-2, where T is the height of the cylinders. Actual measurements usually indicate lower values of the Reynolds stress than the theoretical values in the surface flow, and this is attributed to secondary currents and other components of the Reynolds stress tensor. The magnitude of these effects is a function of the width-to-depth ratio of the surface flow (Nezu and Nakagawa, 1993).

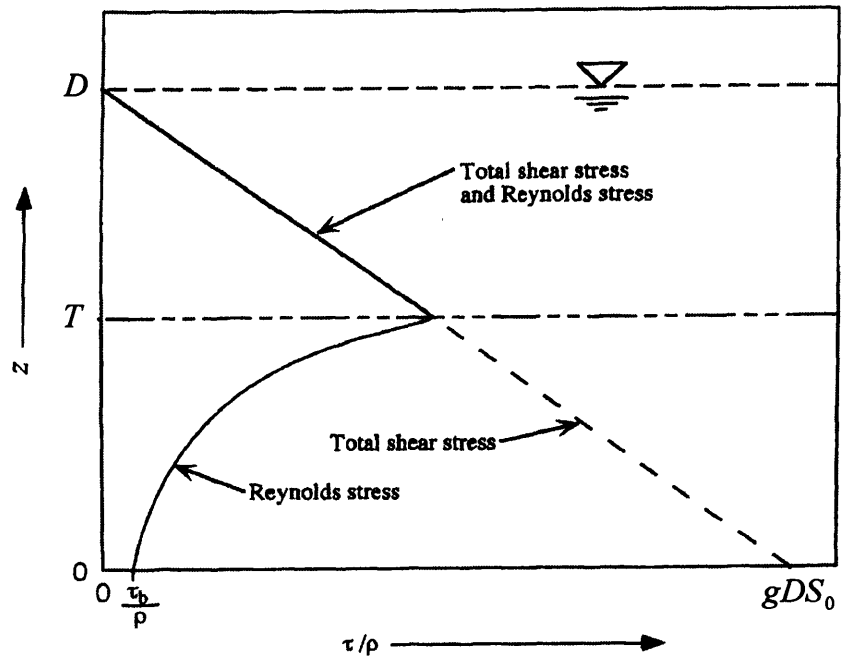

Figure 10-2 Expected effect of canopy on total stress and turbulent shear stress (taken from Dunn *et al.*, 1996)

Within the canopy region, the difference between the total theoretical shear stress and the Reynolds stress is due to the stresses imposed by the form drag of the cylinders. Equation 9.05 is modified to include the stress partitioned to the cylinder drag. This is achieved by longitudinally averaging the Navier-Stokes equations as described by Raupach and Shaw (1982) and results in an additional term for the drag force per unit volume, F_D'. [Equation 9.12] becomes:

$$\frac{\partial \tau}{\partial z} = \frac{\partial}{\partial z}\left(-\rho\overline{u'w'}\right) - F_D' = -\rho g S_0 \qquad \text{[Equation 10.13]}$$

where the drag force per unit volume is defined as:

$$F_D' = \frac{1}{2}\rho C_{D\,2D}\, a u^2 \qquad \text{[Equation 10.14]}$$

where $C_{D\,2D}$ is the vertically-varying drag coefficient, and a is the projected area per unit volume (Section 2.2.6). Substituting Equation 10.14 into Equation 10.13 gives:

$$\frac{\partial}{\partial z}\left(\overline{u'w'}\right)=gS_0-\frac{1}{2}C_{D\,2D}au^2 \qquad \text{[Equation 10.14]}$$

Rearranging Equation 10.14 gives the following expression for the vertically-varying drag coefficient:

$$C_{D\,2D}=\frac{gS_0-\frac{\partial}{\partial z}\left(\overline{u'w'}\right)}{a/2\,\overline{u}^2} \qquad \text{[Equation 10.15]}$$

[*This page is intentionally left blank*]

11 Appendix II: Local, Spatial and Seasonal Variation in Vegetation Obstruction

The different types of variation in the relative vegetation obstruction that have been implemented are described by the equations presented below. Three types of variation are classified: 'spatial' variation, σ_S, and 'temporal' variation, σ_T. The terms are calculated from the obstruction of a vegetation canopy which is defined as the percentage of the flow area A_l, at elevation z, occupied by the projected area of the canopy, A_{pi}. This can be equated as follows:

$$O_p = \frac{A_{pi}}{A_i} \times 100 \qquad \text{[Equation 10.01]}$$

The reader is reminded that along transect A, *Spartina anglica* was monitored at five locations, namely A2, A3, A4, A5 and A6, each of which consists of four sampling points labelled 'a', 'b', 'c' and 'd'. In the following equations, each parameter is proceeded by a pair of brackets, the contents of which refer to the vicinity followed by the time period to which the parameter refers. The vicinity can be a sampling point (e.g. A2a, A2b etc.), a sampling location (e.g. A2, A3 etc.) or a transect (e.g. A, B etc.). The months of the monitoring period (July 2005 to June 2006) were numbered from 1 to 12 such that (A2,1) refers to sampling location A2 during the first month of monitoring (July 2005) and (A,1:12) refers to the twelve-month average for transect A. Now consider the relative vegetation obstruction at location A2 for July 2005. This is the 'local' average of the relative vegetation obstructions at four sampling points (A2a, A2b, A2c and A2d) such that:

$$O_p(A2,1) = \frac{O_p(A2a,1) + O_p(A2b,1) + O_p(A2c,1) + O_p(A2d,1)}{4} \qquad \text{[Equation 10.02]}$$

The 'local' variation of the relative vegetation obstruction at A2 during July 2005 is equivalent to the standard deviation of the four sampling points such that:

$$\sigma_L(A2,1)=\sqrt{\frac{\left(O_p(A2a,1)-O_p(A2,1)\right)^2+\cdots+\left(O_p(A2d,1)-O_p(A2,1)\right)^2}{3}}$$

[Equation 10.03]

The long-term and large-scale effects of the 'local' variations were assessed in two ways. Firstly, the average 'local' variation for a single location were averaged 'temporally', and secondly, they were averaged for the sampling locations across a transect for any given month of sampling. For the first approach, the 'local' variation at location A2 for the twelve-month monitoring period is simply the average of the 'local' variations calculated for each month such that:

$$\bar{\sigma}_L(A2,1:12)=\frac{\sigma_L(A2,1)+\sigma_L(A2,2)+\cdots+\sigma_L(A2,12)}{12}$$

[Equation 10.04]

To assess the amount of 'local' deviation across transect A each month, the values calculated for the five monitoring locations along the transect during July 2005 are averaged as follows:

$$\tilde{\sigma}_L(A,1)=\frac{\sigma_L(A2,1)+\sigma_L(A3,1)+\cdots+\sigma_L(A6,1)}{5}$$

[Equation 10.05]

Now consider the twelve-month average relative vegetation obstruction for a sampling location, in this case, location A2:

$$O_p(A2,1:12)=\frac{O_p(A2,1)+O_p(A2,2)+\cdots+O_p(A2,12)}{12}$$

[Equation 10.06]

This is used to calculate the 'temporal' variation in relative vegetation obstruction at location A2, which is effectively the standard deviation of the monthly values calculated in Equation 4.02 as follows:

$$\sigma_T(A2,1:12)=\sqrt{\frac{\left(O_p(A2,1)-O_p(A2,1:12)\right)^2+\cdots+\left(O_p(A2,12)-O_p(A2,1:12)\right)^2}{11}}$$

[Equation 10.07]

The relative vegetation obstruction for transect A, in this case for July 2005, can be calculated as follows:

$$O_p(A,1)=\frac{O_p(A2,1)+O_p(A3,1)+O_p(A4,1)+O_p(A5,1)+O_p(A6,1)}{5}$$ [Equation 10.08]

This is used to calculate the 'spatial' variation of the relative vegetation obstruction at transect A during July 2005 as follows.

$$\sigma_S(A,1)=\sqrt{\frac{\left(O_p(A2,1)-O_p(A,1)\right)^2+\cdots+\left(O_p(A6,1)-O_p(A,1)\right)^2}{4}}$$ [Equation 10.09]

To summarise the results obtained from the analysis described above, mean 'local', 'temporal' and 'spatial' relative vegetation obstructions were calculated from the data. The mean 'local' relative vegetation obstruction was obtained by averaging the twelve-month average 'local' values calculated for each locations across the transect (from Equation 4.04) as follows.

$$\overline{\sigma_L}(A,1:12)=\frac{\overline{\sigma}_L(A2,1:12)+\overline{\sigma}_L(A3,1:12)+\cdots+\overline{\sigma}_L(A6,1:12)}{5}$$ [Equation 10.10]

The mean 'temporal' relative vegetation obstruction was calculated by averaging the twelve-month average 'temporal' values calculated for each locations across the transect (from Equation 4.07) as follows.

$$\overline{\sigma_T}(A,1:12)=\frac{\sigma_T(A2,1:12)+\sigma_T(A3,1:12)+\cdots+\sigma_T(A6,1:12)}{5}$$ [Equation 10.11]

The mean 'spatial' relative vegetation obstruction was calculated by averaging the twelve-month average 'spatial' values calculated for the transect during each of the monitoring months (from Equation 4.09) as follows:

$$\overline{\sigma_S}(A,1:12)=\frac{\sigma_S(A,1)+\sigma_L(A,2)+\cdots+\sigma_S(A,12)}{12} \qquad \text{[Equation 10.12]}$$

12 References

Ackerman, J.D., and Okubo, A. (1993). "Reduced mixing in a marine macrophyte canopy." *Functional Ecology*, 7, 305-309.

Allen, J.R.L. (2000). "Morphodynamics of Holocene salt marshes: a review sketch from the Atlantic and Southern North Sea coasts of Europe". *Quaternary Science Reviews*, 19, 1155-1231.

Anderson, S.M., and Charters, A.C. (1982). "A fluid dynamics study of seawater flow through *Gelidium nudifrons*." *Limnology and Oceanography*, 27(3), 399-412.

Ashutosh, O., Dhanda, P., and Singh, G. (2002). "Changes in grazing behaviour of native and crossbred sheep in different seasons under semi-arid conditions." *Tropical Animal Health and Production*, 34, 399-404.

Baker, C.J. (1979). "The laminar horseshoe vortex." *Journal of Fluid Mechanics*, 95(2), 347-367.

Beeftink, W.G. (1977). "Salt-Marshes" *In:* Barnes, R.S.K. (Ed.) The Coastline. John Wiley & Sons, 93-121.

Blevins, R.D. (1977). "Flow-induced vibration". Litton Educational Publishing, New York.

Bölscher, J., Ergenzinger, P., Obenauf, P., and Schnauder, I. (2005). "*Conclusions.*" *In:* Bölscher, J., Ergenzinger, P., and Obenauf, P. (Eds). Hydraulic, sedimentological and ecological problems of multifunctional riparian forest management (RIPFOR) (2005). Berliner Geographische Abhandlungen.

Boorman, L.A. (1999). "Salt marshes – present functioning and future change." *Mangroves and Salt Marshes*, 3, 227-241.

Boorman, L.A., Gross-Custard, J.D., and McGrorty, S. (1989). Climate change, rising sea level and the British coast. Her Majesty's Stationary Office, London, UK.

Brampton, A.H. (1992). "Engineering significance of British saltmarshes." *In*: Allen, J.R.L. and Pye, K. (Eds) Saltmarshes: morphodynamics, conservation and engineering significance. Cambridge University Press, Cambridge, UK.

Brown, S.L. (1998). "Sedimentation on a Humber saltmarsh" *In:* Black, K.S., Paterson, D.M. & Cramp, A. (eds.) Sedimentary processes in the intertidal zone. Geological Society, London, Special Publications 139, 207-222.

Brown, G.L., and Roshko, A. (1974). "On density effects and large structure in turbulent mixing layers." *Journal of Fluid Mechanics*, 64(4), 775-816.

BS 1377-2: 1990. "Methods of test for soils for civil engineering purposes – part 2: classification tests."

BS 2782-10: Method 1005:1977, EN 63:1977. "Methods of testing plastics. Determination of flexural properties. Three point method."

Burd, F. (1989). "Saltmarsh survey of Great Britain: an inventory of British saltmarshes." Joint Nature Conservation Committee.

Burke, R.W., and Stolzenbach, K.D. (1983). "Free surface flow through salt marsh grass." *MIT Sea Grant Report MITSG 83-16* Cambridge, Massachusetts, US.

Chadwick, A., and Morfett, J. (1986). "Hydraulics in Civil and Environmental Engineering." HarperCollins Academic, UK.

Chen, C., (1976). "Flow resistance in broad shallow grassed channels." *Journal of the Hydraulics Division,* 102(HY3), 307-322.

Chiew, Y., and Tan, S. (1992). "Frictional resistance of overland flow on tropical turfed slope." *Journal of Hydraulic Engineering,* 118(1), 92-97.

Chow, V.T. (1959). "Open-Channel Hydraulics." McGraw-Hill, Japan.

Christiansen, T., Wiberg, P.L., and Milligan, T.G. (2000). "Flow and sediment transport on a tidal salt marsh surface." *Estuarine, Coastal and Shelf Science,* 50, 315-331.

Church, J.A. and White, N. (2006). "A 20th century acceleration in global sea-level rise." *Geophysical Research Letters,* 33(L01602), 1-4.

Collinson, A.S. (1988). "Introduction to World Vegetation." Springer, USA.

Dargahi, B. (1989). "The turbulent flow field arund a cirular cylinder." *Experiments in Fluids,* 8, 1-12.

Darke, A.K., and Megonigal, J.P. (2003). "Control of sediment deposition rates in two mid-Atlantic Coast tidal freshwater wetlands." *Estuarine, Coastal and Shelf Science,* 57, 255-268.

DEFRA (2006). "Shoreline management plan guidance. Volume 1: Aims and requirements." DEFRA, UK.

DEFRA (2007). "Determining environmentally sustainable and economically viable grazing systems for the restoration and maintenance of heather moorland in England and Wales. BD1228, Annex 2.1 – Sheep Grazing."

Dickerman, J., and Stewart, A.J. (1986). "Estimates of net annual aboveground production: sensitivity to sampling frequency." *Ecology,* 67(3), 650-659.

Douglas, J.F., Gasiorek, J.M., and Swaffield, J.A. (1979). Fluid Mechanics. Longman, UK.

Dunn, C., López, F., and Garcia, M. (1996). "Mean flow and turbulence in a laboratory channel with simulated vegetation." *Hydraulic Engineering Series No.*

51, UILU-ENG-96-2009. Department of Civil Engineering, Univ. of Illinois, Urbana-Champaign.

Edmunds, M., and Robertson, P. (2005). "Working with the sea: the new approach to coastal management." *In*: Conservation Land Management Spring 2005. RSPB, UK, 4-8.

The Environment Agency (1996). "East Anglian salt marshes – The meadows of the sea." The Environment Agency, UK.

Fathi-Maghadam, M., and Kouwen, N. (1997). "Nonrigid, nonsubmerged, vegetative roughness on floodplains." *Journal of Hydraulic Engineering,* 123(1), 51-57.

Fairbanks, J.D.(1998) "Velocity and turbulence characteristics in flows through rigid vegetation." Master's thesis, Virginia Polytechnic Institute & State University.

Fern, K. (1997). Plants for a Future: Edible & Useful Plants for a Healthier World. Permanent Publications.

Fiedler, F.R., and Ramirez, J.A. (2000). "A numerical method for simulating discontinuous shallow flow over an infiltrating surface." *International Journal for Numerical Methods in Fluids*, 32, 219-240.

Finnigan, J.J. (1979). "Turbulence in waving wheat." *Boundary Layer Meteorology*, 16, 181-211.

Finnigan, J.J. (2000). "Turbulence in plant canopies." *Annual Review of Fluid Mechanics*, 32, 519-571.

Fischer-Antze, T., Stoesser, T., Bates, P., and Olsen, N.R.B. (2001). "3D numerical modelling of open-channel flow with submerged vegetation." *Journal of Hydraulic Research*, 39(3), 303-310.

Fitter, R., Fitter, A. & Farrer, A. (1984). Grasses, Sedges, Rushes and Ferns of Britain and Northern Europe. Harper Colins.

Fonseca, M.S., and Kenworthy, W.J. (1987). "Effects of current on photosynthesis and distribution of seagrasses." *Aquatic botany*, 27(1), 59-78.

French, R.H. (1985). "Open-Channel Hydraulics." McGraw-Hill International Editions, Singapore.

French, J.R., Spencer, T., Murray, A.L., and Arnol, N.S. (1995). "Geostatistical analysis of sediment deposition in two small tidal wetlands, Norfolk, U.K." *Journal of Coastal Research*, 11(2), 308-321.

Frey, R.W., and Basan, P.B. (1978). "Coastal salt marshes" *In:* Davis, Jr. R.A. (Ed.) Coastal Sedimentary Environments. Springer-Verlag, New York, 101-169.

Gacia, E., Granata, T.C., and Duarte, C.M. (1999). "An approach to measurement of particle flux and sediment retention within seagrass (*Posidonia oceanica*) meadows." *Aquatic Botany*, 65, 255-268.

Gambi, M.C., Nowell, A.R.M., and Jumars, P.A. (1990). "Flume observations on flow dynamics in *Zostera marina* (eelgrass) beds." *Marine Ecology Progress Series* 61, 159-169.

Gerrard, J.H. (1977). "The wakes of cylindrical bluff bodies at low Reynolds number." *Philosophical Transactions of the Royal Society of London A*, 288, 383-643.

Ghisalberti, M., and Nepf, H.M. (2002). "Mixing layers and coherent structures in vegetated aquatic flows." *Journal of Geophysical Research*, 107(C2), 3.1-3.11.

Gimenez-Curto, L.A. and Corniero Lera, M.A. (1996). "Oscillating turbulent flow over very rough surfaces." *Journal of Geophysical Research*, 101(C9), 20745-20758.

Gray, A.J. (1992). "Saltmarsh plant ecology: zonation and succession revisited" *In:* Allen, J.R.L. & Pye, K. (Eds.) Saltmarshes – Morphodynamics, Conservation, and Engineering Significance. Cambridge University Press, Cambridge, 63-79.

Grizzle, R.E., Short, F.T., Newell, C.R., Hovenc, H., and Kindblom, L. (1996). "Hydrodynamically induced synchronous waving of seagrass: 'monami' and its possible effects on larval mussel settlement." *Journal of Experimental Marine Biology and Ecology*, 206, 165-177.

Hall, B.R., and Freeman, G.E. (1994). "Study of hydraulic roughness in wetland vegetation takes new look at Manning's *n*." *The Wetlands Research Program Bulletin*, U.S. Army Corps of Engineers, Waterway Experiment Station, 4(1), 1-4.

Hammer, D.E., and Kadlec, R.H. (1986). "A model for wetland surface water dynamics." *Water Resources Research*, 22(13), 1951-1958.

Her Majesty's Almanac Office (2000). "The astronomical almanac for the year 2001." Stationary Office. London.

Hulme,M., Jenkins,G.J., Lu,X., Turnpenny,J.R., Mitchell,T.D., Jones,R.G., Lowe,J., Murphy,J.M., Hassell,D., Boorman,P., McDonald,R., and Hill,S. (2002). "Climate change scenarios for the United Kingdom: The UKCIP02 scientific report." Tyndall Centre for Climate Change Research, School of Environmental Sciences, University of East Anglia, Norwich, UK.

Ikeda, S., and Kanazawa, M. (1996). "Three-dimensional organised vortices above flexible water plants." *Journal of Hydraulic Engineering*, 122(11), 634-640.

Intergovernmental Panel on Climate Change (2001). "Climate change 2001: impacts, adaptation and vulnerability." Cambridge Univeristy Press.

Intergovernmental Panel on Climate Change (2008). "Technical paper on climate change and water." World Meteorological Organisation, Geneva, Switzerland.

Järvelä, J. (2005). "Effect of submerged flexible vegetation on flow structure and resistance." *Journal of Hydrology*, 307, 233-241.

Jenkins, G.A., and Greenway, M. (2005). "The hydraulic efficiency of fringing versus banded vegetation in constructed wetlands." *Ecological Engineering*, 25, 61-72

Kang, H., and Choi, S. (2006). "Turbulence modelling of compound open-channel flows with and without vegetation on floodplain using the Reynolds stress model." *Advances in Water Resources*, 29, 1650-1664.

Kadlec, R.H. (1990). "Overland flow in wetlands: vegetation resistance." *Journal of Hydraulic Engineering*, 116(5), 691-706.

Keeble Martin, W. (1965). The Concise British Flora in Colour. Ebury Press.

King, S.E., and Lester, J.N. (1995). "The value of salt marsh as a sea defence." *Marine Pollution Bulletin*, 30(3), 180-189.

Kiya, M., Tamura, H., and Arie, M. (1980). "Vortex shedding from a circular cylinder in moderate-Reynolds-number shear flow." *Journal of Fluid Mechanics*, 141(4), 721-735.

Koch, D.L. and Ladd, A.J.C. (1997). "Moderate Reynolds number flows through periodic and random arrays of aligned cylinders." *Journal of Fluid Mechanics*, 349, 31-66.

Kouwen, N. (1988). "Field estimation of the biomechanical properties of grass." *Journal of Hydraulic Research*, 26(5), 559-568.

Kouwen, N., and Li, R. (1980). "Biomechanics of vegetative channel linings." *Journal of the Hydraulics Division*, 106(HY6), 1085-1103.

Kouwen, N., and Unny, T.E. (1973). "Flexible roughness in open channels." *Journal of the Hydraulics Division*, 99(HY5), 713-728.

Kouwen, N., Unny, T.E., and Hill, H.M. (1969). "Flow retardance in vegetated channels." *Journal of the Irrigation and Drainage Division*, 95(IR2), 329-342.

Leonard, L.A., and Luther, M.E. (1995). "Flow hydrodynamics in tidal marsh canopies." *Limnology and Oceanography*, 40(8), 1474-1484.

Leonard, L.A., and Reed, D.J. (2002). "Hydrodynamics and sediment transport through tidal marsh canopies." *Journal of Coastal Research*, SI 36, 459-469.

Li, R., and Shen, H.W. (1973). "Effect of tall vegetation on flow and sediment." *Journal of the Hydraulics Division*, 99(HY5), 793-814.

Li, C.W., and Yan, K. (2007). "Numerical investigation of wave-current-vegetation interaction." *Journal of Hydraulic Engineering*, 133(7), 794-803.

Linnane, M.I., Brereton, A.J., and Giller, P.S. (2001). "Seasonal changes in circadian grazing patterns of Kerry cows (*Bos Taurus*) in semi-feral conditions in Killarney National Park, Co. Kerry, Ireland." *Applied Animal Behaviour Science*, 71, 277-292.

Lightbody, A.F., and Nepf, H.M. (2006a). "Prediction of velocity profiles and longitudinal dispersion in emergent salt marsh vegetation." *Limnology and Oceanography*, 5(1), 218-228.

Lightbody, A.F., and Nepf, H.M. (2006b). "Prediction of near-field shear dispersion in an emergent canopy with heterogeneous morphology." *Environmental Fluid Mechanics*, 6, 477-488.

López, F., and García, H. (1997). "Open-channel flow through simulated vegetation: Turbulence modelling and sediment transport." *Wetlands Research Program Rep. WRP-CP-10*, U.S. Army Corps of Engineers, Washington, D.C.

Lu, S.S., and Willmarth, W.W. (1973). "Measurement of the structure of the Reynolds stress in a turbulent boundary layer." *Journal of Fluid Mechanics*, 60(3), 481-511.

Luo, S.C., Gan, T.L., and Chew, Y.T. (1996). "Uniform flow past one (or two in tandem) finite length circular cylinder(s)." *Journal of Wind Engineering*, 59, 69-93.

Möller, I., Spencer, T., and French, J.R. (1996). "Wind wave attenuation over saltmarsh surfaces: preliminary results from Norfolk, England." *Journal of Coastal Research*, 12(4), 1009-1016.

Möller, I., Spencer, T., French, J.R., Leggett, D.J., and Dixon, M. (1999). "Wave transformation over salt marshes: a field and numerical modelling study from North Norfolk, England." *Estuarine, Coastal and Shelf Science*, 49, 411-426.

Morris, J.T. (1995). "The mass balance of salt and water in intertidal sediments: results from North Inlet, South Carolina." *Estuaries*, 18, 556-567.

Morris, J.T., and Haskin, B. (1990). "A 5-yr record of aerial primary production and stand characteristics of *Spartina alterniflora*." *Ecology*, 71(6), 2209-2217.

Morris, J.T., Sundareshwar, P.V., Nietch, C.T., Kjerfve, B., and Cahoon, D.R. (2002). "Responses of coastal wetlands to rising sea level." *Ecology*, 83(10), 2869-2877

Nepf, H.M. (1999). "Drag, turbulence, and diffusion in flow through emergent vegetation." *Water Resources Research*, 35(2), 479-489.

Nepf, H.M. and Ghisalberti, M. (2008). "Flow and transport in channels with submerged vegetation." *Acta Geophysica*, 56(3), 753-777.

Nepf, H.M., Mugnier, C.G., and Zavistoski, R.A. (1997a). "The effects of vegetation on longitudinal dispersion." *Estuarine, Coastal and Shelf Science*, 44, 675-684

Nepf, H.M., Sullivan, J.A., and Zavistoski, R.A. (1997b). "A model for diffusion within emergent vegetation." *Limnology and Oceanography*, 42(8), 1735-1745.

Nepf, H.M., and Vivioni, E.R. (2000). "Flow structure in depth-limited, vegetated flow." *Journal of Geophysical Research*, 105(C12), 28547-28557.

Neumeier, U. (2005). "Quantification of vertical density variations of salt-marsh vegetation." *Estuarine, Coastal and Shelf Science*, 63(4), 489-496.

Neumeier, U., and Amos, C.L. (2004). "Turbulence reduction by the canopy of *Spartina* salt-marshes." *Journal of Coastal Research* SI 39/1, pp. 433-439 (Proceedings of the 8th International Coastal Symposium, Itajaí, SC – Brazil)

Neumeier, U., and Ciavola, P. (2004). "Flow resistance and associated sedimentary processes in a *Spartina maritime* salt-marsh." *Journal of Coastal Research*, 20(2), 435-447.

Nezu, I. and Nakagawa, H. (1993). "Turbulence in Open-channel Flows". IAHR Monograph series. A.A. Balkema, Rotterdam, Netherlands.

Niedoroda, A.W. and Dalton, C. (1982). "A review of the fluid mechanics of ocean scour". *Ocean Engineering*, 9, 159-170.

Nortek AS (1997). "ADV Operation Manual."

Pennings, S.C., and R.M. Callaway (1992). "Salt-marsh plant zonation – the relative importance of competition and physical factors." *Ecology*, 73(2), 681-690.

Pethick, J.S. (1992). "Saltmarsh geomorphology." *In:* Allen, J.R.L. & Pye, K. (Eds.) Saltmarshes – morphodynamics, conservation and engineering significance. Cambridge University Press, Cambridge.

Pethick, J., Leggett, D., and Husain, L. (1990). "Boundary layers under salt marsh vegetation developed in tidal currents." *In:* Thornes, J.B. (ed.) Vegetation and erosion. John Wiley & Sons Ltd.

Petryk, S., and Bosmajian III, G. (1975). "Analysis of flow through vegetation." *Journal of the Hydraulics Division*, 101(HY7), 871-884.

Phleger, C.F. (1971). "Effect of salinity on growth of a salt marsh grass." *Ecology*, 52, 571-577.

Plate, E. J., and Quraishi, A. A. (1965). "Modelling of velocity distributions inside and above tall crops." *Journal of Applied Meteorology*, 4, 400-408.

Poggi, D., Porporato, A., Ridolfi, L., Albertson, J.D., and Katul, G.G. (2004). "The effect of vegetation density on canopy sub-layer turbulence." *Boundary-Layer Meteorology*, 111, 565-587.

Prandtl, L. (1935). "The mechanics of viscous fluids" *In*: Durand, F. (Ed) *Aerodynamic Theory, Vol. III.* Springer, Berlin, 57–109.

Raupach, M.R. (1992). "Drag and drag partition on rough surfaces." *Boundary-Layer Meteorology*, 60, 375-395.

Raupach, M.R., Finnigan, J.J., and Brunet, Y. (1989). "Coherent eddies in vegetation canopies." *Heat and Mass Transfer 1989: 4th Australian Conference*, 75-90.

Raupach, M.R., Finnigan, J.J., and Brunet, Y. (1996). "Coherent eddies in vegetation canopies: the mixing-layer analogy." *Boundary-Layer Meteorology*, 78, 351-382.

Raupach, M.R., and Shaw, R.H. (1982). "Averaging procedures for flow within vegetation canopies." *Boundary-Layer Meteorology*, 22, 79-90.

Raupach, M.R., and Thom, A.S. (1981). "Turbulence in and above plant canopies." *Annual Review of Fluid Mechanics*, 13, 97-129.

Ree, W.O., and Palmer, V.J. (1949). "Flow of water in channels protected by vegetative linings." Tech. Bull. No. 967. Soil Conservation Service, US Agriculture, Washington, DC.

Righetti, M., and Armanini, A. (2002). "Flow resistance in open channel flows with sparsely distributed bushes." *Journal of Hydrology*, 269, 55-64.

Rodi, W. (1980). "Turbulence models and their application in hydraulics." International Association for Hydraulics Research, Delft.

Rodwell, J.S. (2000). "British plant communities, vol. 5: maritime communities and vegetation of open habitats." Cambridge University Press, Cambridge, UK.

Sanchez, J.M., Izco, J., and Medrano, M. (1996). "Relationships between vegetation zonation and altitude in a salt-marsh system in northwest Spain." *Journal of Vegetation Science*, 7(5), 695-702.

Schlichting, H. (1955). "Boundary-layer theory." McGraw Hill, US.

Shaw, R. (1977). "Secondary wind speed maxima inside plant canopies." *Journal of Applied Meteorology*, 16, 514-521.

Shi, Z., Pethick, J.S., Burd, F., and Murphy, B. (1996). "Velocity profiles in a salt marsh canopy." *Geo-Marine Letters*, 16, 319-323.

Shi, Z., Pethick, J.S., and Pye, K. (1995). "Flow structure in and above the various heights of a saltmarsh canopy: a laboratory flume study." *Journal of Coastal Research*, 11(4), 1204-1209.

Shih, S.F., and Rahi, G.S. (1982). "Seasonal variations of Manning's roughness coefficient in a subtropical marsh." *Transcriptions of the American Society of Agricultural Engineers*, 25(1), 116-120.

Shimwell, D.W. (1971). "The description and classification of vegetation." Sidgwick & Jackson, London, UK.

Shinde, A.K., Karim, S.A., Patnayak, S.A., and Mann, J.S. (1997). "Dietary preference and grazing behaviour of sheep on *Cenchrus ciliaris* pasture in a semi-arid region of India." *Small Ruminant Research*, 26, 119-122.

Somes, N.L.G., Bishop, W.A., and Wong, T.H.F. (1999). "Numerical simulation of wetland hydrodynamics." *Environment International*, 25(6/7), 773-779.

Stephan, U., and Gutknecht, D. (2002). "Hydraulic resistance of submerged flexible vegetation." *Journal of Hydrology*, 269, 27-43.

Streutker, D.R. and Glenn, N.F. (2006). "LiDAR measurement of sagebrush steppe vegetation heights." *Remote Sensing of Environment*, 102, 135-145.

Stone, B.M., and Shen, H.T. (2002). "Hydraulic resistance of flow in channels with cylindrical roughness." *Journal of Hydraulic Engineering*, 128(5), 500-506.

Sumer, B.M., Christiansen, N., and Fredsoe, J. (1997). "The horseshoe vortex and vortex shedding around a vertical wall-mounted cylinder exposed to waves." *Journal of Fluid Mechanics*, 332, 41-70.

Townsend, A.A. (1961). "Equilibrium layers and wall turbulence." *Journal of Fluid Mechanics*, 11, 97-120.

Tsihrintzis, V.A. Wu, F., Shen, H. W., and Chou, Y. (2001). "Variation of roughness coefficients for unsubmerged and submerged vegetation." *Journal of Hydraulic Engineering*, 127(3), 241-245.

Tsujimoto, T., Shimizu, Y., Kitamura, T., and Okada, T. (1992). "Turbulent open-channel flow over bed covered by rigid vegetation." *Journal of Hydroscience and Hydraulic Engineering*, 10(2), 13-25.

Turner, A.K., and Chanmeesri, N. (1984). "Shallow flow of water through non-submerged vegetation." *Agricultural Water Management*, 8, 375-385.

UK Climate Impacts Programme (2002). Climate Change Scenarios for the United Kingdom – The UKCIP02 Briefing Report.

Vernberg, F. J. (1993). "Salt-marsh processes: a review." *Environmental Toxicology and Chemistry*, 12, 2167-2195.

Vogel, S. (1994). "Life in moving fluids." Willard Grant, Boston, US.

Whittaker, R.H. (1973). "Ordination and classification of communities." Junk, The Hague.

Williams, G.J. (2004). "The spread of *Spartina anglica* on the saltmarshes and mudflat of the Burry Inlet." Master's Thesis, University of Glamorgan, UK.

Williamson, C.H.K. (1992). "The natural and forced formation of spot-like 'vortex dislocations' in the transition of a wake." *Journal of Fluid Mechanics*, 243, 393-441.

Wilson, C.A.M.E., Stoesser, T., Bates, P.D., and Batemann Pinzen, A. (2003). "Open channel flow through different forms of submerged flexible vegetation." *Journal of Hydraulic Engineering*, 129(11), 847-853.

Wilson, C.A.M.E., Yagci, O., Rauch, H., P., and Olsen, N.R.B. (2006a). "3D numerical modelling of a willow vegetated river/floodplain system." *Journal of Hydrology*, 327, 13-21.

Wilson, C.A.M.E., Yagci, O., Rauch, H., P., and Stoesser, T. (2006b). "Application of the drag force approach to model the flow-interaction of natural vegetation." *International Journal of River Basin Management*, 4(2), 137-146.

Wilson, N.R., and Shaw, R.H. (1977). "A higher order closure model for canopy flow." *Journal of Applied Meteorology*, 16(11), 1197-1205.

Wu, F., Shen, H. W., and Chou, Y. (1999). "Variation of roughness coefficients for unsubmerged and submerged vegetation." *Journal of Hydraulic Engineering* 125(9), 934-942.

Yalin, M.S. (1972). "Mechanics of sediment transport." Pergamom Press, Canada.

Zavistoski, R. (1994). "Hydrodynamic effects of surface piercing plants." Master's thesis. Massachusetts Institute of Technology.

Zdravkovich, M.M. (1977). "Review of flow interference between two circular cylinders in various arrangements." *Journal of Fluids Engineering*, 99, 618-633.

Zukauskas, A. (1987). "Heat transfer from tubes in cross flow." *Advances in Heat Transfer*, 18, 87-159.